A Study of Carbonation in Stabilised Peat

by

Alan Richard Duggan

B.E. (Hons) MIEI

A thesis submitted to the College of Engineering and Informatics, National University of Ireland, Galway, in partial fulfilment of the requirements for the degree of Doctor of Philosophy

September 2016

Academic supervisors: Dr. Bryan McCabe
Dr. Eoghan Clifford
Dr. Jamie Goggins

Professor of Civil Engineering: Prof. Padraic O'Donoghue

Declaration

I hereby declare that this thesis has not been submitted in whole or in part to any other University as an exercise for a degree. I further declare that, except where reference is given in the text, it is entirely my own work.

This thesis may be lent or copied by the library.

Signed: .....

Alan Duggan

Date .....

Acknowledgements

Firstly, I want to thank my main project supervisor, Dr. Bryan McCabe, for his leadership, support and wisdom throughout the course of my PhD. Bryan always had time to chat to me about my work, providing encouragement and valued feedback when I needed it. Bryan, I really appreciate it. I would also like to express my gratitude to my other supervisors, Dr. Jamie Goggins and Dr. Eoghan Clifford, for their guidance, suggestions and help over the years.

A special thanks to the members of my Graduate Research Committee, Prof. Padraic O'Donoghue and Dr. Marcus Keane for their direction and comments throughout my work as well as the other staff of the Department of Civil Engineering. I also want to express my appreciation to the College of Engineering and Informatics at the National University of Ireland, Galway for their financial support, which enabled me to enjoy a certain quality of life as a PhD researcher and to attend a geotechnical conference in Edinburgh.

This body of work has benefited greatly, too, from the information provided by various companies and individuals with whom I established contact in order to compile the research. Thank you to all who generously gave of their time and made valuable contributions, especially RPS Group Consulting Engineers, Galway, in particular Mr. Cian McGuinness for the data on the construction of the Pollboy road section. Thank you, too, to David MacLynn, formerly of Allu UK, for keeping me up to date on peat stabilisation internationally.

To Peter Fahy, Dermot McDermott and Mary O'Brien of the civil engineering technical staff at NUI Galway, thank you for your support in my laboratory work. To Dr Andrea Erxleben, fellow PhD researcher, Michael Gurry and the technicians in the chemistry department, thank you for allowing me access to your laboratories over the last three years. Thanks also to Séamus Kellehan for his helpfulness in providing the keys to the X-ray diffractometer room whenever I needed them.

Many thanks to Mark O'Connor for helping me acquire the peat necessary to conduct my experiments and to Dr. Wynette Reddington of the University of Limerick for taking time to advise me in an area vital to the understanding of my work, as well as for doing some laboratory work for me. Thanks, also, to Dr. Jerome Sheahan of the School of Mathematics, Statistics and Applied Mathematics, for advising me on how to analyse my work statistically.

I made some great friends during my years as a postgraduate. Many thanks to the geotechnical researchers' brigade—Brian Sheil, Brian Sexton, Kevin, Martin, Eanna and Eugene for their support, advice and friendship. To my fellow postgraduate friends—Colm, Des, Conan, Maebh, Brendan, Kelly, Emma, Dave, Noelle, William, Karlo, Luka, Edelle, and Conor, merci beaucoup for the memories, craic and tea sessions. I would also like to express my appreciation to the people who played football and tag rugby with me over the past few years, which helped keep me sane and to all my Galway friends who kept my social calendar busy, providing essential destress time.

Finally, I would like to thank my brothers, Dave and Tony; my parents, Deirdre and Tony, and my grandmother, Yvonne, for their unwavering support throughout my PhD time.

Abstract

In addition to the traditional drivers of cost and timely delivery, embodied energy (EE) and embodied carbon (EC) have emerged as major considerations in all aspects of large construction projects. This is due to stricter environmental regulations introduced in Ireland and the European Union, which have resulted in geotechnical engineers beginning to compare the EC/EE associated with various piling and ground improvement options as part of an overall appraisal of scheme feasibility for road construction projects. Where construction involves the modification or removal of peat, these calculations become more challenging as allowances should be made for the impact on the carbon stored within the peat and the gases potentially released. To incorporate these allowances in the EE and EC summations in a life cycle assessment (LCA) for a construction project requires the inclusion of peat-related factors such as peat drainage, drainage systems, slope stability, restoration and clearance of vegetation/forest.

As there is a dearth of methodologies to quantify EC and EE of ground improvement techniques for road construction on peat, new LCA methodologies need to be developed to more accurately quantify emissions and energy consumed in order to produce more sustainable solutions. Traditionally, excavate-and-replace is the most commonly used method in Ireland, but other techniques such as piling and dry soil-mixing can also be considered. In projects employing an excavate-and-replace solution, peat is often removed to disposal areas and the subsequent drying causes a significant release of CO_2 into the atmosphere. To date, however, in dry soil-mixing the impact of stabilising peat on on-site CO_2 emissions has not been considered and is, therefore, the primary focus of this thesis.

A preliminary study of nine columns containing peat and peat mixed with cement was set up in a temperature control room to investigate CO_2 emission rates. Gas samples were collected using the closed chamber method and analysed using a gas chromatograph. The result of the experiment showed that the stabilised peat absorbed CO_2 both from the air and CO_2 released by the oxidised peat due to the carbonation process. Subsequent to this substantial finding, two extensive column studies were undertaken to examine the carbonation potential of stabilised peat whose binders consisted of cement and cement and ground granulated blast slag (GGBS) combinations. As in the first experiment, the CO_2 intake rate decreased with time as the depth of the carbonation front grew. Variables which significantly influenced the CO_2 intake rate included time, initial CO_2 concentration, cement content, GGBS content, water table and surcharge. Besides calculating CO_2 intake rates, the depth of the carbonation front was analysed to produce k-rate factors, representing the rate at which the carbonation front increases. As this was the first time

the carbonation front in stabilised peat was examined, several techniques were used to establish the most suitable procedure to explore this carbonation front: phenolphthalein indicator, pH of stabilised peat slurries, X-ray powder diffraction analysis (XRD), Fourier transform infrared spectroscopy (FTIR), loss on ignition method (LOI), and water evaporation method. From the results, the carbonation front obtained by XRD was similar to those from LOI and FTIR. In contrast, the phenolphthalein method underestimated the carbonation front, while the pH of stabilised peat slurries technique showed a carbonation front greater than the other methods.

The laboratory results provided crucial information on the environmental impact of dry soil-mixing and its on-site impact. Using these results and a novel LCA methodology, an LCA to examine EE and EC was performed on a case study of a section of motorway built on peat. To ascertain the optimum solution for EE and EC, several ground improvement scenarios were studied, including excavate-and-replace, dry soil-mixing and a combination of excavate-and-replace and piling. From laboratory results, it was taken for the dry soil-mixing scenario that emissions from the stabilised peat were zero for the lifetime of the road. The LCA also investigated emissions from peat under various management practices and restoration techniques, assessing their strength in terms of hydrology and carbon storage potential. The results showed that dry soil-mixing had a minimal on-site impact and that the EC of the binder could be lowered markedly if the binder type was changed. On the other hand, even though the EC and EE of materials used in the excavate-and-replace solution were low, the on-site impact was immense due to extensive peat disturbance. In the case study which forms part of the subject of this research, a combination of excavate-and-replace and piling was found to be most favourable solution, but the preferred ground improvement technique in general was found to change according to the project and site location.

In this research, novel laboratory studies were undertaken and a new LCA methodology was developed. Various techniques to understand the carbonation process in stabilised peat were utilised, with advantages and disadvantages found for all of them. The body of work has international implications as it points to dry soil-mixing having a lower environmental impact than previously thought. Additionally, it provides a platform for further studies in this area. From this research, the environmental impact of building on peat can be quantified more accurately and the understanding of stabilised peat enhanced in terms of emissions and carbonation depth and potential.

Table of Contents

Table of Figures

List of Tables

Nomenclature

Abbreviations:

$Ca(OH)_2$	Calcium hydroxide
$CaCO_3$	Calcium carbonate
CaO	Calcium oxide
CH_4	Methane
CO_2	Carbon dioxide
CO_2eq	Carbon dioxide equivalent
CSH	Calcium silicate hydrate
DOC	Dissolved organic carbon
EC	Embodied carbon
EDX	Energy-dispersive X-ray spectroscopy
EE	Embodied energy
ER	Excavate-and-replace
ER + P	Combination of excavate-and-replace and piling
ETS	Emissions Trading Scheme
EU	European Union
FTIR	Fourier transform infrared spectroscopy
GC	Gas Chromatograph
GGBS	Ground granulated blastfurnace slag
GHG	Greenhouse gas
GWP	Global warming potential
IOA	Input-output analysis
ICE (V2.0)	Inventory of Carbon and Energy Version 2.0
ICP-AES	Inductively coupled plasma atomic emission spectroscopy
IPCC	Intergovernmental Panel on Climate Change
IR	Infrared
LCA	Life Cycle Assessment
LCI	Life Cycle Inventory
LOI	Loss on ignition
LULUCF	Land Use, Land Use Change and Forestry
N_2O	Nitrous oxide
NRA	National Roads Authority
NUIG	National University of Ireland Galway
PA	Process analysis
PFCs	Perfluorocarbons
POC	Particulate organic carbon
ppm	Part per million
S	Soil-mixing
SEM	Scanning electron microscopy
SiO_2	Silicon dioxide
TGA	Thermogravimetric analysis
TTI	Transport Infrastructure Ireland
UK	United Kingdom
UNFCCC	United Nations Framework Convention on Climate Change
XRD	X-ray powder diffraction

Symbols:

A	Area (m^2)
C	Mass of CO_2 in sample (g)
C_0	Mass of CO_2 in the uncarbonated sample (g)
C_a	Gas concentration in the chamber (%)
CaO	Percentage of CaO in the cement (%)
Cem	Portland cement content (kg/m^3)
C_f	Final gas concentration (%)
C_i	Initial gas concentration (%)
C_{lost}	Percentage of carbon lost from the excavated peat (%)
$CO_{2\ cd,h}$	Concentration difference in the headspace (mg CO_2eq/m^2/hr)
$CO_{2\ i,h}$	Mass intake of CO_2 from the atmosphere/headspace into the stabilised peat (mg CO_2eq/m^2/hr)
$CO_{2\ i,peat}$	Mass intake of CO_2 from the CO_2 released by the peat (mg CO_2eq/m^2/hr)
$CO_{2\ peat}$	Mass of CO_2 released by the organic matter (mg CO_2eq/m^2/hr)
$CO_{2\ carbonation}$	Sum of $CO_{2\ i,peat}$ and $CO_{2\ i,h}$ (mg CO_2eq/m^2/hr)
C_p	Carbonation potential (g)
c_v	Oedometer coefficient of consolidation (m^2/year)
D	Diffusion coefficient (m^2/s)
d	Distance between lattice planes (m)
D_c	The degree of carbonation (%)
D_{c0}	The degree of carbonation in the uncarbonated zone (%)
D_{CSH}	The degree of carbonation taking into account CSH carbonation between 520 and 650ºC (%)
E	Extent of drainage (m)
ECI	Embodied carbon intensity ($kgCO_2/kg$)
EC_{peat}	Total CO_2 released from the volume of excavated peat (tCO_2eq)
F	Division factor used in calculating EC_{peat}
f	Gas flux (mg CO_2eq/m^2/hr)
h	Gas chamber height (m)
I	Intensity
I_0	Initial intensity
K	Hydraulic conductivity (mm/d)
k	Carbonation rate factor (mm/√year)
M	Mass (kg)
M_{CaO}	Molar weight of CaO (g/mol)
M_{CO2}	Molar weight of CO_2 (g/mol)
m_v	Oedometer coefficient of volume compressibility (m_v)
OC	Organic content percentage (%)
t	Time (hr)
T	Transmittance (%)
V	Volume (m^3)
V_{peat}	Volume of excavated peat (m^3)
V_t	Total volume (cm^3)
V_v	Volume of voids (cm^3)
X_c	Depth of carbonation front (mm)
X_{oc}	Depth at which the organic content becomes constant (mm)
X_p	Depth of carbonation front as measured by the phenolphthalein indicator (mm)

X_{pH}	Depth of carbonation front as measured by the pH of stabilised peat slurries method (mm)
θ	Angle (^{o})
λ	Wavelength (m)
ρ	Density (g/cm^3)
ρ_d	Dry density (g/cm^3)
ϕ	Porosity (%)

Chapter 1: Introduction

1.1 Research background

Ireland has an obligation to reduce its annual non-Emissions Trading Scheme (non-ETS) greenhouse gases (GHGs) emitted to at least 20% below 2005 levels by 2020 or face substantial fines under the legally binding EU's '20-20-20' initiative (EPA, 2012). It is anticipated that Ireland will violate its non-ETS annual GHG commitments from 2016 onwards, exceeding its EU 2020 target by between 4.1 (11%) (With Measures) and 7.8 $MtCO_2eq$ (21%) (With Additional Measures) (EPA, 2012). Each year the construction sector accounts for a large proportion of the annual allowance for GHGs, with the Irish construction sector in 2005, for example, domestically responsible for the emission of 8.11 $MtCO_2eq$ (Acquaye & Duffy, 2010), amounting to 11.7% of the country's emissions of 69.3 $MtCO_2eq$ (EPA, 2012). CO_2 equivalents (CO_2eq) include not only carbon dioxide (CO_2) but other GHGs such as methane (CH_4), nitrous oxide (N_2O) and perfluorocarbons (PFCs) and take account of the global warming potentials (GWPs) of these gases as set out in the Kyoto protocol (UNFCCC, 1998). GWP is based on the relative amounts of heat trapped in the atmosphere by greenhouse gas; for example, CO_2 and CH_4 have GWPs of 1 and 25 respectively (IPCC, 2007).

To combat Ireland's emissions, comply with environmental regulations and increasing demands for sustainable engineering practices, it is vital to be in a position to produce accurate calculations of construction-related energy consumption and emissions, including the geotechnical elements of projects. The geotechnical profession has recently taken steps to quantify energy consumption and emissions for construction projects. Egan & Slocombe (2010) investigated the embodied carbon (EC) of several piling options on a range of construction projects, while Chau et al. (2012) examined the embodied energy (EE) associated with the construction of sections of a UK rail tunnel. Both Milachowski et al. (2011) and Chappat & Bilal (2003) estimated the environmental impact of constructing roads. EE is the total primary energy consumed over a product's life cycle and is measured in joules, while EC is associated with GHG emissions released over the lifetime of a product, measured in CO_2 equivalents. It is usual to consider one or both measures in any environmental Life Cycle Assessment (LCA).

Despite the LCA studies undertaken such as those mentioned above, there remains a dearth of LCA studies and methodologies for geotechnical projects. There is no guidance on how to determine (at planning and design stages) the potential construction-related emissions from road construction in areas of organic soil such as peat. In a country where peatlands account for approximately 20% of the land area (Renou-Wilson et al., 2013), the

improvement of Ireland's road infrastructure has proved challenging. Significant motorway construction projects in the first decade of the 21st century, such as the M6 Athlone to Galway section, have presented geotechnical engineers with difficulties in dealing with the large volumes of peat encountered along these routes. The poor engineering properties of peat compel engineers to resort to ground improvement options such as excavate-and-replace, dry soil-mixing (peat stabilisation) and piling. Therefore, materials, transport and machinery, all produce extensive emissions in these road construction projects and will have to be accounted for in the country's annual emissions.

Construction in peatlands also poses an additional complication. Healthy peatlands continuously sequester carbon and have been doing so for thousands of years. Based on assumptions made by Nayak et al. (2008), peat can contain between 180 and 227 kg CO_2/m^3; disturbing this peat will release much of its carbon into the atmosphere and contribute to global warming. This highlights the need for a robust methodology for performing an LCA to quantify the emissions released and the energy consumed for road construction on peat, thereby enabling engineers to appraise various options with a view to minimising environmental impacts.

Traditionally, excavate-and-replace has been the most commonly used method in Ireland, but other techniques such as piling and dry soil-mixing have also been considered. In projects involving an excavate-and-replace solution, peat is often removed to disposal areas, and the subsequent drying causes a significant release of CO_2 into the atmosphere (Nayak et al., 2008). While it is acknowledged that the binder used in soil-mixing applications can be environmentally costly in terms of carbon emissions, it may be advantageous that peat remains *in situ* despite the sizable reduction in moisture content (often hundreds of percent) that occurs upon stabilisation. However, the impact of stabilising peat on on-site CO_2 emissions has not been considered to date. Although dry soil-mixing has been considered in numerous road construction projects in Ireland, it has rarely been used due to cost implications and the general lack of experience in employing this technique. If doubts about the on-site impact of carbon emissions from the stabilised peat were addressed, geotechnical engineers could perhaps make more informed decisions on the suitability of this technique for road construction projects.

In this study, extensive laboratory experiments are carried out to fill the gap in the LCA inventory on whether stabilised peat is a net source or net sink of carbon. A closed chamber method widely used for quantifying CO_2 fluxes between the soil and the atmosphere and carbonation depth techniques normally associated with concrete are applied to stabilised

peat. The experiments and the application of the experimental techniques to stabilised peat described in this thesis are believed to be the first of their kind ever conducted.

1.2 Aims and objectives

The primary aim of this thesis is to develop an improved understanding of the on-site environmental impact of the stabilisation of peat by carrying out experimental studies in the laboratory on the CO_2 gas flux between the stabilised peat and the atmosphere and on the carbonation process. A literature survey of the factors associated with road construction on peat that contribute to the overall EC identified this as a clear gap in the knowledge. To this end, the following tasks were identified:

(i) Investigate the CO_2 gas flux between stabilised peat and the atmosphere as it is unknown whether stabilised peat is a net source or net sink of carbon.
(ii) Determine the most appropriate techniques to establish the depth of the carbonation front and examine the depth and level of carbonation in stabilised peat.
(iii) Establish the variables that affect the CO_2 gas flux and the depth of the carbonation front in stabilised peat and produce statistical models to reconstruct this flux and depth of carbonation.

Achievement of this specific objective has allowed a broader objective to be met: comparison of the EE and EC associated with various ground improvement/foundation options for road construction in peatlands, including stabilisation. To make these comparisons, the following objectives were identified:

(i) Develop a life-cycle inventory to perform this environmental LCA and a methodology to tackle the problem.
(ii) Incorporate the results of the experiments carried out on stabilised peat into the life-cycle inventory and use the novel LCA methodology to perform an LCA on a road construction case study on peatlands.

1.3 Methodology

In order to investigate the EC and EE of ground improvement techniques for road construction on peat, the elements common to every construction project were examined: materials, transport and machinery, as well as peat-related factors such as peat drainage, drainage systems and peatland restoration techniques. Limitations in how certain peat-related factors are accounted for in an LCA were discovered, and a salient shortcoming was whether stabilised peat, as a land type, was a net source or net sink of carbon. Addressing this issue consequently became the overarching objective of this thesis.

A pilot laboratory study was undertaken to investigate emissions from stabilised peat and from a raw Irish peat, with both high and low water tables modelled. The results were then compared and the implications for soil-mixing assessed. Once the results had been analysed, two extensive studies were carried out on stabilised peat with varying binder types and binder amounts to examine the CO_2 gas flux and the depth and level of carbonation.

A closed gas chamber method was used to calculate the CO_2 flux, and gas samples were taken from stabilised peat columns with a syringe and analysed for CH_4 and CO_2 concentrations using an Agilent 7890A Gas Chromatograph. To evaluate the depth and level of carbonation in stabilised peat, the following techniques were employed: phenolphthalein indicator, X-ray diffraction analysis (XRD), Fourier transform infrared spectroscopy (FTIR), thermogravimetric analysis (TGA), loss on ignition (LOI), pH of stabilised peat slurries and the water evaporation method.

Statistics on the data from the experiments were gathered using Minitab tools such as t-tests, one-way ANOVA and multiple linear regression analysis as well as Monte Carlo sensitivity analyses. Using these tools, the impact of variables such as surcharge, temperature, water table, and binder type and amount were evaluated and the important variables highlighted. Statistical models for stabilised peat were then developed for CO_2 gas fluxes and the depth of the carbonation front.

Comparisons could now be made between the EE and EC associated with various ground improvement/foundation options for road construction in peatlands, including peat stabilisation, excavate-and-replace, and piling. An LCA methodology was developed to quantify the environmental impact and a life cycle inventory was compiled. Databases, reports and previous studies were consulted to quantify the EC and EE intensities of items required in the life cycle inventory. This included retrieving data on machinery and rate of work from piling and stabilising machinery companies. Data from relevant literature were also collected on emission factors for land types such as peatlands, forests and ponds.

Once the inventory was compiled and the novel methodology developed, an LCA was performed. To demonstrate the effectiveness of the LCA methodology, a section of the M6 motorway in Ireland built in drained peatland was chosen as a case study, and RPS Group PLC, who were consultants on the project, supplied the relevant road construction data. In addition to examining the environmental impact of the project as constructed, other scenarios were considered; for instance, the effect on the total environmental impact had other ground improvement techniques and peatland restoration options been

employed. The CO_2 gas flux and carbonation front depth implications from the stabilised peat experiments in this body of research were incorporated into the LCA inventory for a scenario where dry soil-mixing is the ground improvement technique used. As a result, an improved quantification of the total EC of this scenario was possible.

1.4 Structure of thesis

Chapter 2 reviews the relevant literature on factors likely to affect the EC and EE of building roads on peat. It also describes the carbonation process in concrete, the techniques used to investigate the carbonation process and infers how these might be applied to stabilised peat.

Chapter 3 details the experimental methods used in this thesis, starting with information on how the peat was classified and on the laboratory peat stabilisation method. The designs and operations of the three experiments are given, with the chapter also setting out the experimental procedures used to calculate the CO_2 gas fluxes from stabilised peat and the depth of the carbonation front. The statistical tools used to analyse the results of the experiments are presented at the end of the chapter.

Chapter 4 investigates the CO_2 gas flux measurements from both peat and stabilised peat using a closed chamber method and presents and analyses the results of Laboratory Experiments P, A and B by way of statistical tools such as one-way ANOVA and multiple regression analysis. The properties of the raw and stabilised peat are also given in this chapter.

Chapter 5 examines the carbonation depth results from Experiments P, A and B, found by applying several carbonation depth techniques to the stabilised peat specimens; namely, the phenolphthalein indicator, XRD, FTIR, LOI, pH of stabilised peat slurries and the water evaporation method.

Chapter 6 elaborates on the CO_2 flux and carbonation depth results of Experiments A and B and interprets them further statistically. The linearity of the CO_2 flux data is considered, along with the similarities and relationships between the results of several carbonation depth techniques and the advantages and disadvantages of the application of each carbonation depth technique to stabilised peat. Additionally, the chapter includes a hypothesis on why the depth of carbonation results are different from stabilised peat with various binder content and types and under varying environmental conditions.

Chapter 7 describes the environmental LCA carried out on a section of the M6 motorway in Ireland. It contains the development of the novel LCA methodology for road

construction in peatlands and how each factor, including peat-related factors, were incorporated into the life cycle inventory. The LCA quantifies the EC and EE associated with the excavate-and-replace solution chosen for this road section. It also examines the EC and EE of peat stabilisation and a combination of piling and excavate-and-replace as alternative ground improvement scenarios. Arising from the experimental results from stabilised peat presented in Chapters 4, 5, and 6, some relevant information on the peat stabilisation scenario was included in the inventory, thereby enabling a more accurate quantification of EC.

Chapter 8 summarises the conclusions of the research and points to future work on carbonation in stabilised peat and in the area of LCA development for construction in peatlands.

The following additional information is presented in the Appendices:

Appendix A: Review of the effect of some variables on peatland emissions from raised/blanket bogs in a temperate climate.

Appendix B: Notation system for Experiments P, A and B.

Appendix C: Reference plots for XRD and FTIR.

Appendix D: Results from Chapter 4, including some of the output from the Minitab statistical analyses for the CO_2 flux studies.

Appendix E: Some of the results from the carbonation depth technique studies.

Appendix F: Some of the output from the Minitab statistical analyses for the carbonation depth technique studies.

1.5 Publications

The following papers have been published during the course of this research and the development of this thesis:

Journals (peer reviewed journal publications)

- Duggan, A., McCabe, B.A., Goggins, J., and Clifford, E. (2015). An embodied carbon and embodied energy appraisal of a section of Irish motorway constructed in peatlands. *Construction & Building Materials*. 79. 402-419. Chapter 7 is a more developed version of the study reported in this paper.
- Manton, R., Duggan, A., Goggins, J., and Clifford, E. (2014). Carbon costs and savings of Greenways: creating a balance sheet for the sustainable design and

construction of cycling routes. *International Journal of Environment and Sustainable* Development 13(1). 3-19. Some of the LCA methodology used in this paper is presented in Chapter 7 with the results of this LCA greenway study used as a comparison to the results of the LCA road case study.

Peer reviewed conference publications (national and international)

- Duggan, A.R., McCabe, B.A., Goggins, J., and Clifford, E. (2015). Carbonation in stabilised peat. *Proceedings of the 16th European Conference on Soil Mechanics and Geotechnical Engineering* (ECSMGE, 2015), Edinburgh, 13th-17th September, 5, 2383-2388. The results of Experiment P were published in ECSMGE 2015, some of which are presented in Section 4.5.
- Manton, R., Duggan, A., Goggins, J., McCabe, B., Clifford, E. (2012). Use of Carbon Calculation Tools for Sustainable Cycle Network Design. *Proceedings: 7th Conference on Sustainable Development of Energy, Water and Environment Systems.* Ohrid, Macedonia. 1st-7th July.
- Duggan, A.R., McCabe, B.A., Goggins, J.M., Clifford, E. (2012). Factors affecting Embodied Carbon / Embodied Energy associated with ground improvement techniques for construction on peat. *Proceedings: Bridge & Concrete Research in Ireland,* Dublin Institute of Technology, Ireland, 6th-7th September, 147-52. This work is a general review of the factors, especially the peat-related factors that must be incorporated into an environmental LCA for road construction on peat. Some of this paper has been merged into Sections 2.4 to 2.6.

Chapter 2: Literature Review

2.1 Introduction

The context for the research conducted in this thesis is the onset of global warming and resulting environmental regulations that has obliged geotechnical engineers to quantify the environmental impact of geotechnical infrastructure. Existing LCA methodologies for construction projects are reviewed in the chapter, and this review highlights the absence of individual studies that consider all the major factors that should be incorporated in an LCA for road construction on peat. Relevant literature addressing these factors is explored in this chapter.

On investigating the EC and EE of ground improvement or foundation solutions for construction in peatlands, the absence of information on the on-site environmental impact of the mass stabilisation of peat was identified as a major gap and has become the primary objective of this body of work. Carbonation, a process not previously acknowledged in this respect, is discussed by first reviewing the carbonation process in concrete and postulating how it affects stabilised peat. The techniques employed to investigate the carbonation process in concrete are then reviewed with the aim of applying them to stabilised peat in this thesis.

2.2 Background

2.2.1 Climate change and greenhouse gases

The earth's atmosphere plays a pivotal role in our environment; without it global temperature would drop below freezing point. Our atmosphere consists mainly of nitrogen (N_2) and oxygen (O_2), but it is the trace gases such as water vapour, CO_2, and CH_4 that produce the greenhouse effect that enables the earth to be habitable (Brasseur et al., 1999). The greenhouse effect allows heat and radiation to enter the atmosphere and be absorbed by the earth's surface, which then emits energy in the form of infrared radiation to cool down. Before this radiation can enter outer space, some of it is absorbed by GHGs thereby keeping the earth warm.

The release of carbon into the atmosphere is a naturally occurring process whereby a constant amount of carbon is cycled through the world's terrestrial and aquatic ecosystems. Outside the natural carbon cycle, more heat and radiation is being trapped in our atmosphere due to the increases in concentrations of GHGs, which have high radiative properties that prevent heat from escaping the earth's atmosphere and cause global warming (IPCC, 2001). GHG concentrations and temperature are closely correlated in the natural process of climate change, with the earth's climate itself being in a state of change

for at least 420,000 years, as exemplified by the examination of an ice core from Antartica by Petit et al. (1999). However, due to human activities, climate change is widely accepted as the greatest environmental challenge facing the world today.

The effect of human influence on climate change started to occur gradually, with a decrease in annual carbon intake due to deforestation for agricultural purposes some 2000 years ago (Brasseur et al., 1999). Since the industrial revolution, anthropogenic emissions from fossil fuel burning and land use change have dramatically increased the rate of climate change, resulting in an increase in GHG emissions that is unprecedented in the last 420,000 years (IPCC, 2001). By burning fossil fuels, the carbon and GHGs stored in coal, oil and natural gas are released in large amounts into the atmosphere over a short period of time. CO_2 and CH_4 are the most important GHGs; and since 1750, the atmospheric concentrations of these gases have increased by 31% and 151%, respectively (IPCC, 2001). CO_2 concentration levels have increased from pre-industrial age levels of about 280 parts per million (ppm) to 379 ppm in 2005 (Figure 2.1). The average annual CO_2 concentration growth rate during the ten-year period 1995 to 2005 was 1.9 ppm/yr, an upsurge on the period 1960 to 1995 when it averaged 1.4 ppm/yr (IPCC, 2007). Similar trends were recorded by Met Eireann (EPA, 2010a).

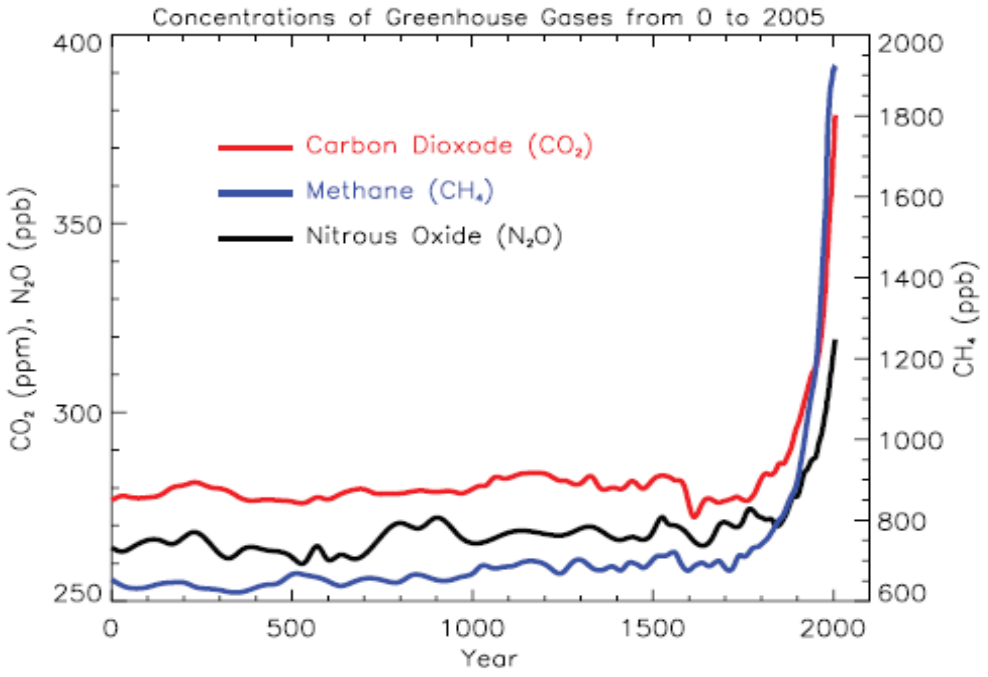

Figure 2.1 - Atmospheric concentrations of important long-lived GHGs over the last 2,000 years Concentration units in parts per million (ppm) or parts per billion (ppb) (IPCC, 2007)

With global temperatures forecast to increase by 1.4 to 5.8°C by 2100 (IPCC, 2007), Holden et al. (2003) predicts temperatures in Ireland will rise by 1.68 °C by 2075. Globally extreme events such as intense precipitation, summer heat waves and gales are also likely

to increase (IPCC, 2007). In Ireland, rainfall in high rainfall sites is expected to become more seasonally severe through a decrease in rainfall in spring and summer and a slightly wetter autumn and winter. Climate change is predicted, therefore, to be detrimental to the earth's ecosystems and the way we live.

2.2.2 Policy for energy and GHG emissions reduction

To combat climate change and reduce emissions, the EU has committed to reducing annual emissions under the Kyoto Protocol and the EU 20-20-20 Initiative. The United Nations Framework Convention on Climate Change (UNFCCC) and its advisory group, the Intergovernmental Panel on Climate Change (IPCC), were set up to deal with the climate change issue. The Kyoto Protocol Agreement, agreed in 1997, was the first major legally binding step to combat global warming. Its objective was to curtail the concentration of CO_2 at 450 ppm by 2020 and limit the global rise in temperature to 2°C (UNFCCC, 1998). Under the Kyoto Agreement, Ireland had an obligation to limit its GHG emissions to 13% above 1990 levels over the period 2008–2012, which translated into limiting total emissions to an average of 62.8 $MtCO_2eq$ per annum (13% above the baseline estimate of 55.6$MtCO_2eq$) in the period 2008–2012 (EPA, 2008). Ireland achieved this target mainly due to the downturn in the economy and the construction industry. In 2011 it was decided to extend this protocol at the Conference of Parties (COP) in Durban, South Africa, where an agreement was reached to begin talks on a new treaty for 2015, with 2020 set as the enforcement date (UNFCCC, 2011).

At European level, in 2007 the EU's Effort Sharing Decision (Decision No 406/2009/EC) set 2020 targets, known as the '20-20-20' initiative, for EU member states including Ireland. It was developed in accordance with Directive 2009/28/EC and coupled with the EU Emissions Trading Scheme (EU ETS), the aim was to reduce GHG emissions by 20% by 2020 based on 1990 levels (European Commission, 2009b). The total effort for GHG reductions by 2020 has been divided among the sectors covered by the EU Emissions Trading Scheme (ETS) and non-ETS sectors. Under the EU Emissions Trading Scheme, ETS emissions cover the main industrial activities such as energy and heavy industry while non-ETS emissions relate to agriculture, transport, residential and waste activities (EPA, 2015). In Ireland, the allocation to the ETS sectors was 22.3 $MtCO_2eq$ and 40.6 $MtCO_2eq$ to non-ETS sectors (EPA, 2012).

For Ireland to reduce its carbon footprint, avoid heavy fines and, more importantly, to combat climate change, it is vital that EU policy strategy is adhered to. It is predicted that Ireland will violate its annual GHG commitments from 2017–2018 onwards, exceeding its EU 2020 target by between 0 and 4 $MtCO_2eq$ (Figure 2.2) (EPA, 2015). The regulating

authority for EU-ETS in Ireland is the EPA, which is responsible for monitoring and reporting Ireland's GHG emissions to the European Commission, a charge that requires methodologies to accurately quantify GHG emissions.

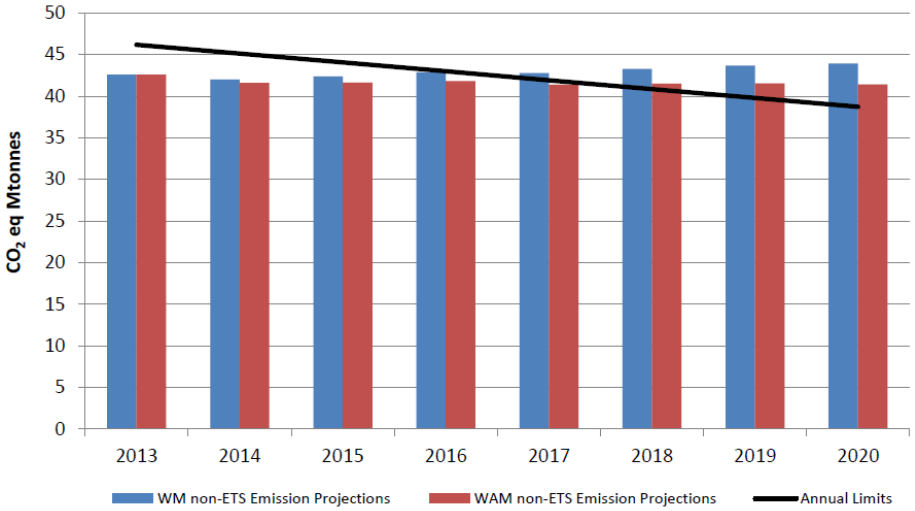

Figure 2.2 - With Measures (worst case) and With Additional Measures (best case) GHG emissions projections and comparison with the linear reduction pathway required between 2013 and 2020 (EPA, 2015)

2.2.3 Carbon credits and sustainability

To incentivise large GHG industrial emitters to reduce their GHG emissions, carbon credits were established in the EU-ETS in accordance with 2003/87/EC (European Commission, 2003) up to and including all amendments 2009/29/EC (European Commission, 2009a). The scheme to allow GHG emission trading within the EU was developed as a response to the Kyoto protocol (UNFCCC, 1998), and the price of tonnes of CO_2eq (€/tCO_2eq) was benchmarked. Manufacturers such as cement producers are allocated allowances, regulated in Ireland by the EPA. All GHG permit holders in Ireland must monitor their operations annually and report to the EPA. If the national allowance, in terms of CO_2eq, allocated to Ireland (i.e. 62.84 MtCO_2eq) is exceeded, then the individual installations responsible for the excess GHG emissions must purchase carbon credits from other countries that have reduced their emissions below their targets. The monitoring and reporting (M&R) guidelines on GHG emissions (European Comission, 2007) for the EU-ETS recommend the IPCC guidelines for use in the calculation of emission factors and emission intensities (IPCC, 2006a).

According to the EPA (2010b), Ireland exceeded its allowances by 3.99 MtCO_2eq in 2008. Carbon credits were sold at prices ranging from €6.22/tCO_2eq to €6.40/tCO_2eq at the start of 2013 (Vitelli, 2013), a decrease from a high in 2008 of €25/tCO_2eq (Sethuraman et al., 2011). In essence, 3.99 MtCO_2eq amounted to €100 million in necessary offset purchases of carbon credits in 2008.

The EPA and the Sustainable Energy Authority of Ireland (SEAI) are required to report carbon sinks such as forest lands and peatlands under the Land Use, Land Use Change and Forestry (LULUCF) category and the Kyoto Protocol. Under the Kyoto Protocol, these sinks are currently unaccounted for in the annual limits for the 2013–2020 period but must be reported. To reflect this, the European Commission has indicated that these sinks will not be allowed under the 20-20-20 Initiative but must be recorded (EPA, 2015). However, this situation is likely to change with the European Council's confirmation in 2014 that LULUCF (forest and peatland carbon sinks) would be included in 2030 targets (Matthews, 2015). Forest sinks could play a vital role in reducing Ireland's emissions and are predicted to remove 4.6 $MtCO_2eq$ by 2020 annually (EPA, 2012). As recognised by LULUCF negotiators, drained peatlands can act as significant contributors of GHG emissions, but the restoration of wetlands and previously drained peatlands can act as both carbon sinks and significant contributors of GHG emissions, the combination of which has the potential to offset annual emissions if included (Wilson & Farrell, 2007). Under the Kyoto Protocol, carbon credits generated from peatland restoration and afforestation can be traded as a commodity and have a mandatory and voluntary market value, with the highest potential sale value being achievable on the voluntary markets.

As a major contributor to GHG emissions, the construction industry must comply with the environmental policies and guidelines of recent years and needs to be proactive in the reduction of emissions. Consequently, detailed research into methods of reducing its impact upon global warming have gained popularity as there is a requirement for more robust and complete methodologies to accurately quantify emissions in construction projects. Furthermore, construction can change land types from carbon sinks to carbon sources, which can have a huge impact on annual emissions, and all road construction projects require vast tracts of land and resources. As stricter environmental regulations are introduced in Ireland, it is imperative that energy and emissions associated with road construction are calculated accurately to mitigate the environmental impact.

The current approach to building roads and motorways in some of our more delicate ecosystems such as peatlands and forests has drastic effects on annual emisisons. To help offset the degradation of land and the environmental impact of these construction projects, it is possible to include forest and peatland carbon rich sinks in the overall environmental impact. To this end, afforestation and peatland restoration can be carried out in conjunction with a road construction project while simultaneously accruing carbon credits. These types of construction projects could, therefore, play a key role in reaching Ireland's emission targets by way of sustainable methods, materials and land type.

2.3 Peat

2.3.1 Formation

Peat is a soft organic soil formed in high water table environments where the supply of organic material to the surface surpasses the rate of decomposition due to anaerobic conditions (Koehler et al., 2011). Peatlands have adapted to severe conditions of high water content, low oxygen content, of high water table and of low availability of plant nutrients (Joosten & Clarke, 2002). Peat usually grows at a rate of one millimetre a year (10 m over 10,000 years); and to a large extent, peat bogs formed in high latitudes after the end of the Ice Age.

There are two distinct layers in a peat profile. The first, varying in depth between 100–600 mm, is the acrotelm (Hobbs, 1986). It is the zone of direct oxygen penetration that can support plant life, has a fluctuating water table, high hydraulic conductivity, and is rich in peat-forming aerobic bacteria (Joosten & Clarke, 2002). The second layer, the catotelm, is the lower anaerobic layer which has a low hydraulic conductivity and a water content that remains constant over time, is free of peat-forming aerobic micro-organisms, and is not subject to air entry. Its permeability decreases with depth and humification, a process which involves the decay of plants and vegetation (Hobbs, 1986).

Von Post (1922) established a peat classification system based on characteristics including degree of decomposition, moisture content, and fibre type and content on a 10-point scale. The scale ranges from H1 (least humified) to H10 (most humified), representing the state of decay. This quick test entails squeezing a small sample in the hand; the colour and form of the expelled fluid (peat) is inspected, together with the nature and structure of the remaining residue; and these are all then used to categorise the peat. The peat in the H1–H4 range is considered fibrous peat, which retains some strength and contains plant remains that are recognisable. The H5–H7 range is named the pseudo-fibrous peat as plant remains are still visible but the peat has lost some of its original strength. Finally, the H8–H10 range, the peat that is amorphous, contains no recognisable plant structures and retains little strength. Hobbs (1986) suggests an extended classification to include tensile strength, plasticity, organic content, smell and acidity, thereby acknowledging the role that soil science can play in characterising a material that is not easily characterised by traditional engineering parameters.

2.3.2 Bog types

Organic soils cover a considerable amount of Europe, with significant peat deposits in Finland (9 m hectares), Sweden (6.6 m ha), and Poland (3 m ha) (Montanarella et al., 2006). Almost one third of Europe's peatlands are in Finland and cover 33.5% of its land

mass, while Ireland's peatlands make up between 13.8% (0.95 m ha) and 18.9% (1.2 m ha) of its land mass, depending on criteria used for defining organic matter and organic content (Connolly et al., 2007; Montanarella et al., 2006). An example of Ireland's peatland distribution is shown in Figure 2.3.

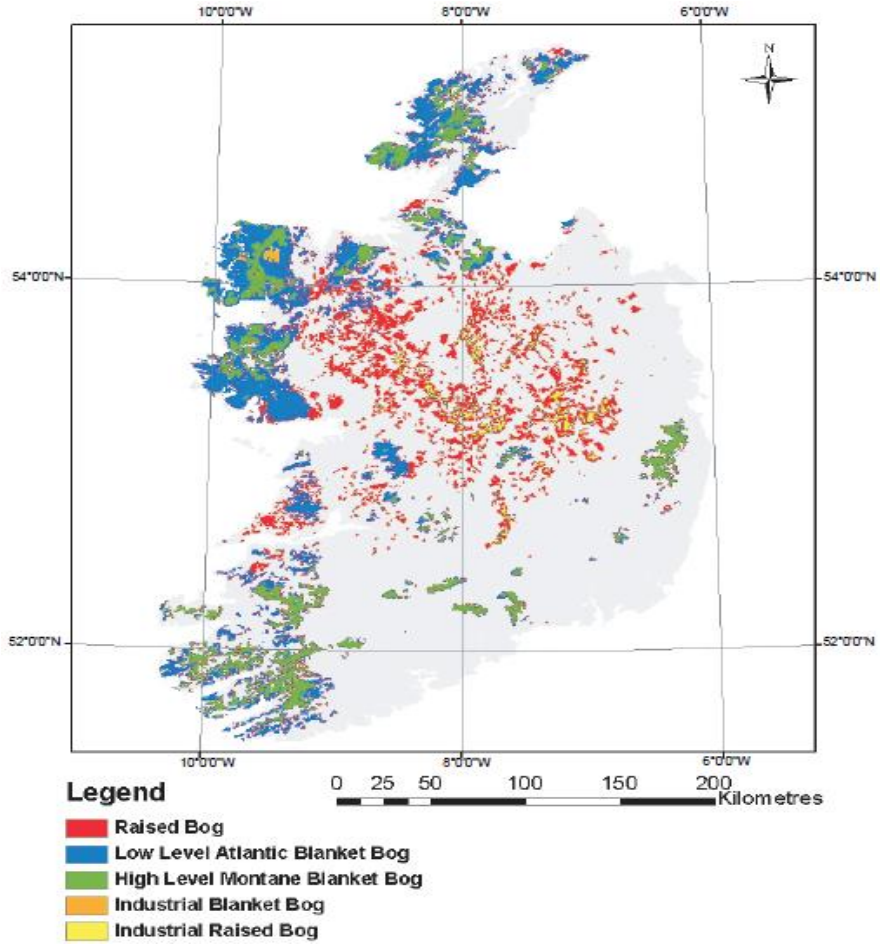

Figure 2.3 - The DIPM peatland map identifying 0.95 Mha of peatland (13.8% of the total land area) (Ward et al., 2006)

Peatlands in Ireland are found in three main forms; namely, raised bogs, blanket bogs and fens. Figure 2.3 shows the extent of raised bogs and blanket bogs across the country. Raised bogs, commonly found in the midlands of Ireland cover 0.31 million hectares and are generally 7.5 m deep on average but can be over 13 m deep (Bord Na Mona, 2015; IPCC, 2015b). They began to develop 10,000 years ago and were usually formed in lakes or basins that were fed by nutrient-rich groundwater or feeding streams (Hammond, 1981). As a consequence, plants and vegetation grew, causing lake filling; and as the bog grew, flow through it became impeded, resulting in swamping. Anaerobic conditions prevailed and organic material built up to the level of the basin to create marshy areas known as fens, which are 2.2 m deep on average and create the base of a raised bog (Figure 2.4) (Munro, 2004). More peat forms in the fen as a result of plants and vegetation dying, eventually accumulating enough materials to rise above the water table to become a raised

bog. The more the bog starts to rise into an upward dome shape, the more it relies on rainwater rather than local groundwater levels (Figure 2.4) (Hammond, 1981). Over time, vegetation relies solely on precipitation for its nutrient supply and becomes an acidic ombrotrophic bog (Munro, 2004).

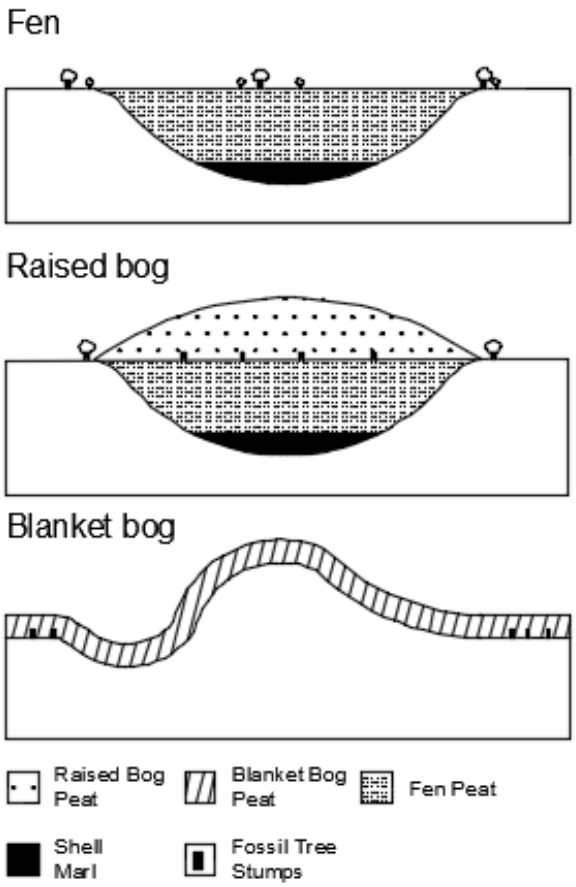

Figure 2.4 - Peatland types (Adapted from Bord Na Mona (2015))

Blanket bogs in the west of Ireland are the most extensive type of bog in the country, originally covering up to 0.77 Mha and range in depth from 1 to 7 m, with an average of 2.6 m (IPCC, 2015a). They are up to 4000 years old and typically form a blanket-like layer over the surface of the underlying mineral soil (Hammond, 1981). These bogs are climate controlled, depend mostly on rainwater to form and survive, require cool summers, precipitation levels of over 1250 mm and slopes of < 20° where poor surface drainage exists (Hammond, 1981). They form in a similar manner to raised bogs and change from open water in shallow hollows or lakes to acidic peat through waterlogging caused by low nutrient precipitation. Heavy rainfall causes minerals to be washed away or leached to the bottom of the peat layer to form an impermeable layer known as an iron pan. Water is unable to move through this layer and, consequently, it becomes waterlogged (IPCC, 2015a). Once the hollow is filled, the accumulation of peat continues, and the bog spreads outwards over the poorly drained land, connecting with similar formations to form a

blanket of peat (Figure 2.4). The variability of these irregular formations causes the underlying peat to vary substantially in thickness and humification.

2.3.3 Some peat properties

Peat is highly organic and acidic, with organic contents typically ranging from 80 to 98% and pH ranging from 3 to 6 (Hobbs, 1986; Munro, 2004). Bogs generally have a pH lying in the range of 3.3 to 4.5, while fens, which tend to be much more nutrient-rich, have a pH above 5 (Hobbs, 1986).

The level of decomposition can indicate the engineering properties of the peat. Moisture contents can range from a few hundred percent to over 2000% and will reduce with increasing humification (Hobbs, 1986) due to lower void ratios and less water held by capillary action. Porosity and pore size distribution influence the flow and water storage in peat (Holden, 2009). Water is present in peat in three ways: (1) within large pores in the peat, (2) within smaller pores but held by capillary action, and (3) water bound physically or chemically (MacFarlane & Radworth, 1964). The water in (1) is removed by drainage and in (2) by compression.

The bulk density of peat is similar to water at 1000 kg/m^3 and can range from as low as 600 kg/m^3 in woody fibrous peat (low degrees of humification) to 1200 kg/m^3 in granular amorphous peats (higher degree of humification) (Hobbs, 1986; Munro, 2004). Its dry density varies from 60 kg/m^3 to 120 kg/m^3 and is an important engineering property because the higher the density, the greater the shear strength (Munro, 2004). In a peat deposit, shear strength decreases with increasing moisture content, decreasing mineral content, and humification (Helenlund, 1980). Frequently, a peat bog will show a strength decrease with depth due to the changing character of the peat, particularly where it becomes less fibrous and more amorphous (Munro, 2004). The acrotelm can have considerable tensile strength depending on the nature of the plant cover and the horizontal orientation of fibres in the peat, which act to provide vertical shear resistance. This layer is more permeable than the deeper peat in the catotelm, which is more humified and more compacted (Hobbs, 1986).

Undrained shear strengths in Ireland have been reported to vary from 20 kPa in fibrous peat to below 4 kPa in more amorphous peats (Long, 2005), the fibres reinforcing the peat vertically. However, their spongy nature and high void ratios result in high compressibility when loaded. Consolidation of peat leads to a reduction in permeability, void ratio and water content (Hobbs, 1986; Hanrahan, 1954).

2.3.4 Stored carbon and carbon cycle

In addition to the poor engineering properties of peat, engineers must now also factor in the economic value of peatlands, which has dramatically increased in recent years due to the recognition of its high carbon storage and valuable water supply. Peat covers only 3% of the world but contains 30% of its carbon (550Gt) (Parish et al., 2007). The peatland carbon cycle, illustrated in Figure 2.5, is explained in the following bullet points:

- The cycle begins with the uptake of CO_2 due to photosynthesis and the release of half of it back into the atmosphere through plant respiration (Ryan, 1991). Peatland vegetation, such as sphagnum moss, grows and sequesters the rest of the CO_2 as carbon.
- When it dies, the high water table prevents aerobic decay, with anaerobic decay occurring instead, which is two to three times slower than aerobic decomposition (Clymo, 1984).
- Consequently, peat accumulates over time, slowly absorbing carbon from the atmosphere (Joosten & Clarke, 2002). While water takes up the majority of the peat volume, the carbon content is part of the dry matter as shown in Figure 2.6.

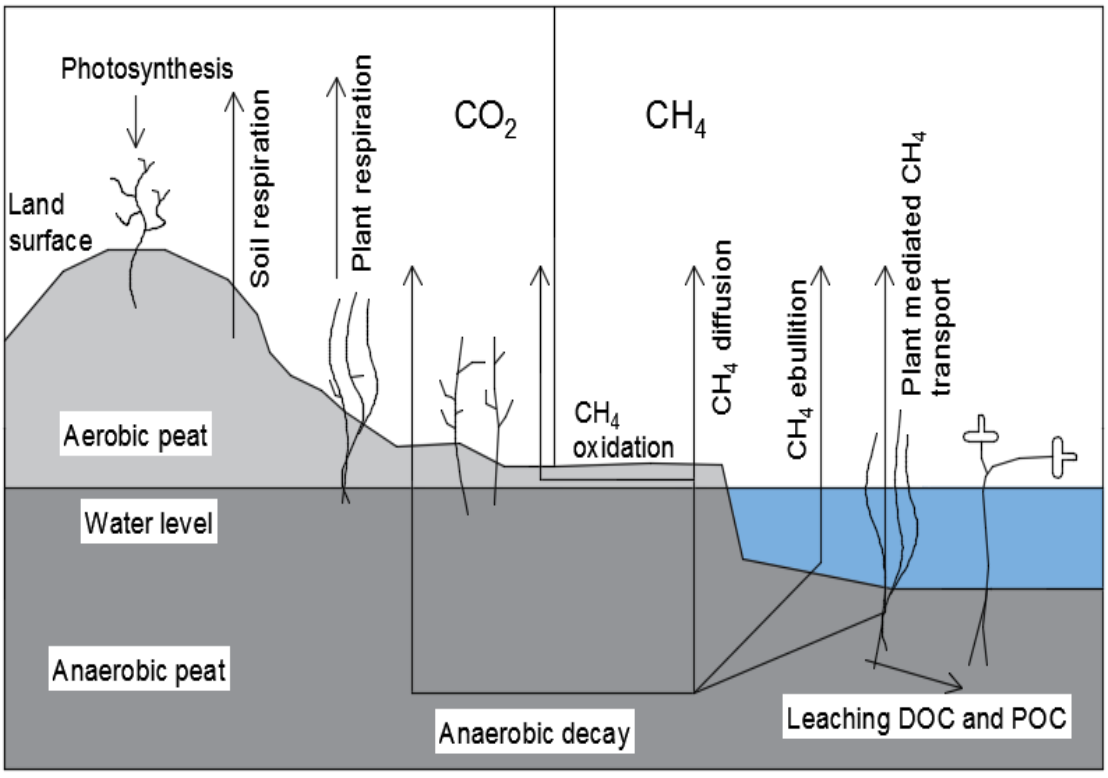

Figure 2.5 - Schematic representation of carbon cycle in peatlands (Laine, 2006)

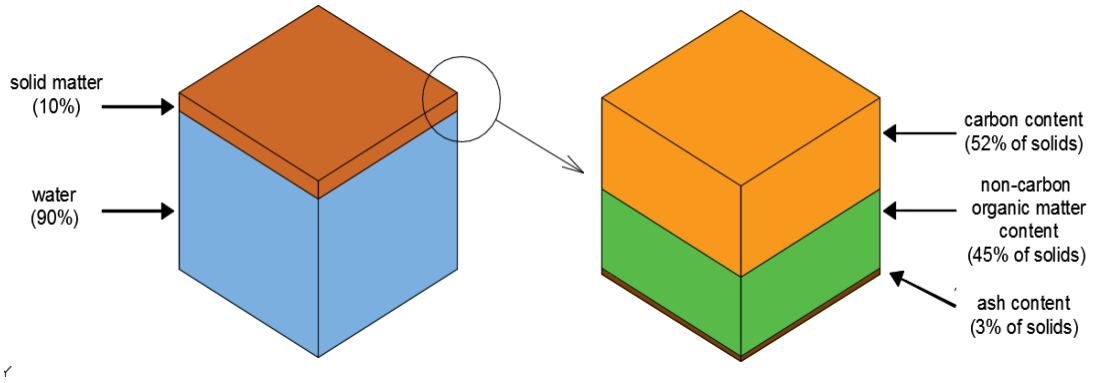

Figure 2.6 - Typical proportion of solid matter and water in peat (left) and typical proportions by weight of solid-matter components in peat (right). Adapted from Lindsay (2010)

Undisturbed peatlands have been sequestering carbon for thousands of years, exerting a net cooling effect on the world's atmosphere. The long-term negative effect of methane emissions from anaerobic decomposition is smaller than the positive effect of CO_2 sequestration (Parish et al., 2007). However, many of these peatlands are now disturbed and are net sources of CO_2. Further disturbance of these carbon sinks by drainage and construction could rapidly release large proportions of the stored carbon as CO_2.

2.4 Construction in peatlands

2.4.1 Peat excavate-and-replace

In the decade 2000–2010, the length of motorway and dual carriageway in the Republic of Ireland approximately quadrupled to a total of 1200 km (NRA, 2010). Given that peatlands account for much of Ireland's land area, it was inevitable that peat would be encountered in large expanses on some of these projects. Not only is it difficult terrain for construction plant to negotiate, peat is challenging because of its low shear strength and high compressibility, especially its propensity for long-term creep settlements.

Road construction on peatlands normally requires some form of ground improvement or foundation solution, with techniques such as excavate-and-replace, piling, dry soil-mixing and surcharging generally considered. The favoured option in Ireland has been to excavate the peat, particularly where the depth is no greater than 3–4 m (Buggy & Farrell, 2012) and to replace it with competent fill to construct the embankment, which may include geogrids and geotextiles for extra tensile strength. Where low permeability soft clays and silts underlie the peat, drains may be installed to accelerate the rate of consolidation under load by draining porewater upwards to a surface drainage blanket or downward to a permeable stratum (Woodward, 2005).

When peat thickness is greater than 4 m, the partial excavation technique is occasionally used (Munro, 2004; Wojtasik et al., 2006). This involves the application of an overload fill to induce a force to 'push out' the low-strength peat. Ideally, peat should have a shear

strength of < 20 kPa and moisture content above 100% (Woijtasik et al., 2006) for this process to be effective. Dredging a manageable depth of peat in front of where the fill material has been replaced reduces the amount of material to be displaced, but pockets of peat can remain, and settlement issues can subsequently occur.

In recent years, the 'green issues' of earthworks construction are becoming increasingly important within the public domain. Peat-left-in-place techniques avoid the heavy earthworks associated with excavate-and-replace, require fewer areas for peat disposal, are more cost effective, and will continue to be explored as environmental regulations become stricter. For example, the UK government in the late 1990s introduced a tax on new quarry materials used in construction works as well as a peat disposal/landfill tax (Soga et al., 2011).

For lower classes of road, a variety of options is available for retaining the peat; surcharging is one such option. Fill is placed on the surface in stages so as not to increase pore water pressures to an extent that will cause embankment failure. Temporary fill is applied over and above final embankment level, which makes it possible to eliminate primary consolidation settlement and reduce secondary settlement (Mesri & Ajlouni, 2007; Sas & Malinowska, 2006). Peat compresses significantly under embankment loads as the free water within the pores is squeezed out into the adjacent unloaded bog. As the load is applied, the inter-colloidal particle attractions increase, with a consequent rapid reduction in the permeability of the peat and an increase in its shear strength (Munro, 2004). Extensive research has been undertaken into surcharging peat by Mesri et al. (1997), Haan (1996), O'Loughlin & Lehane (2003) and others. In Ireland surcharging is not currently permitted by the National Roads Authority (NRA) (recently renamed as Transport Infrastructure Ireland (TII)) for peat soils (Buggy & Farrell, 2012) as settlement is unpredictable and the time required for it to impact significantly on secondary consolidation is excessive. The TII may well change its stance for lower class roads; but for motorway construction where settlement must be minimal, surcharging may remain prohibited.

2.4.2 Dry soil-mixing

In some cases, excavate-and-replace in peat soils may be too expensive due to factors such as peat depth, cost of backfill material and availability of peat disposal areas. Peat-left-in-place techniques such as dry soil-mixing and piling can be used instead. Dry soil-mixing or mass stabilisation of peat is becoming increasingly popular worldwide as a method of ground improvement and is used extensively in Scandinavia and Japan (Hebib & Farrell, 2003). Dry soil-mixing works by injecting suitable, dry cementitious and pozzolanic

binders into the ground using an excavator equipped with a mechanical mixing tool. Stabilisation can be carried out to a depth of 7–8 m (Forsman et al., 2015) and is done in blocks using equipment similar to that shown in Figure 2.7. From a hydraulically operated mixing unit, the dry binder is fed into the mixing head with compressed air where the mixing head rotates vertically and horizontally through the peat mass. Here, the binder interacts with the pore water in the peat, leading to hydration reactions and *in situ* curing over time (Jelisic & Leppänen, 1999). It creates a homogenous mass in the peat structure, which solidifies to strengthen and stiffen the peat, thereby creating a stabilised platform. It is primarily used for road and railway embankments in peatlands and in the stabilisation of dredged materials for land reclamation and erosion control (Axelsson et al., 2002; Allu, 2007).

The stabilised peat block (Figure 2.7(a)) is usually covered with a geotextile, surcharged with 0.5 m to 1 m of fill immediately after the completion of mixing to guarantee consolidation of the stabilised block, increase in strength, decrease in void ratio and permeability, and to provide a working platform for machinery (Hebib & Farrell, 2003; EuroSoilStab, 2002; Axelsson et al., 2002). In Ireland, some projects have considered dry soil-mixing, but in most cases this technique was not deemed commercially viable because of the large amounts of binder required (Hebib & Farrell, 2003).

Lime was the first binder used, but cement, because of its greater potential for strength gain, increased in popularity (Åhnberg, 2006). Nowadays, other cementitious and pozzolanic binders, produced as by-products of industrial processes, can also be used; namely, ground granulated blast furnace slag (GGBS), fly ash and gypsum. These by-products meet the criteria for more environmentally friendly materials and sustainable development but must be activated by some amount of cement, lime or aggregates and so are mixed in combination (Jelisic & Leppänen, 1999). It has been shown that cement binders and combinations of cement and GGBS typically provide the greatest strength gain in peat (Axelsson et al., 2002; Timoney et al. 2012).

The choice of final binder is site-specific, depends on the geotechnical and chemical properties of the unstabilised peat to be improved and requires multiple laboratory tests to discover the right mix (Munro, 2004). Important geotechnical properties include moisture content, density, liquid limit, sensitivity, shear strength, soil type, organic content and degree of humification (Axelsson et al., 2002). The peat after mixing can increase in undrained shear strength by up to two orders of magnitude, ideal for high-standard roads where the demand for high bearing capacity and low settlement are crucial (EuroSoilStab, 2002; Jelisic & Leppänen, 1999). Sometimes, siliceous sand and limestone are used as a

filler to increase the number of solid particles in the peat (Axelsson et al., 2002; Åhnberg, 2006). The inclusion of the filler produces no chemical reaction, but it enhances the strength and stiffness of the stabilised peat by increasing the number of soil particles available to react with the binders. Furthermore, the filler helps to fill the void spaces within the peat during stabilisation.

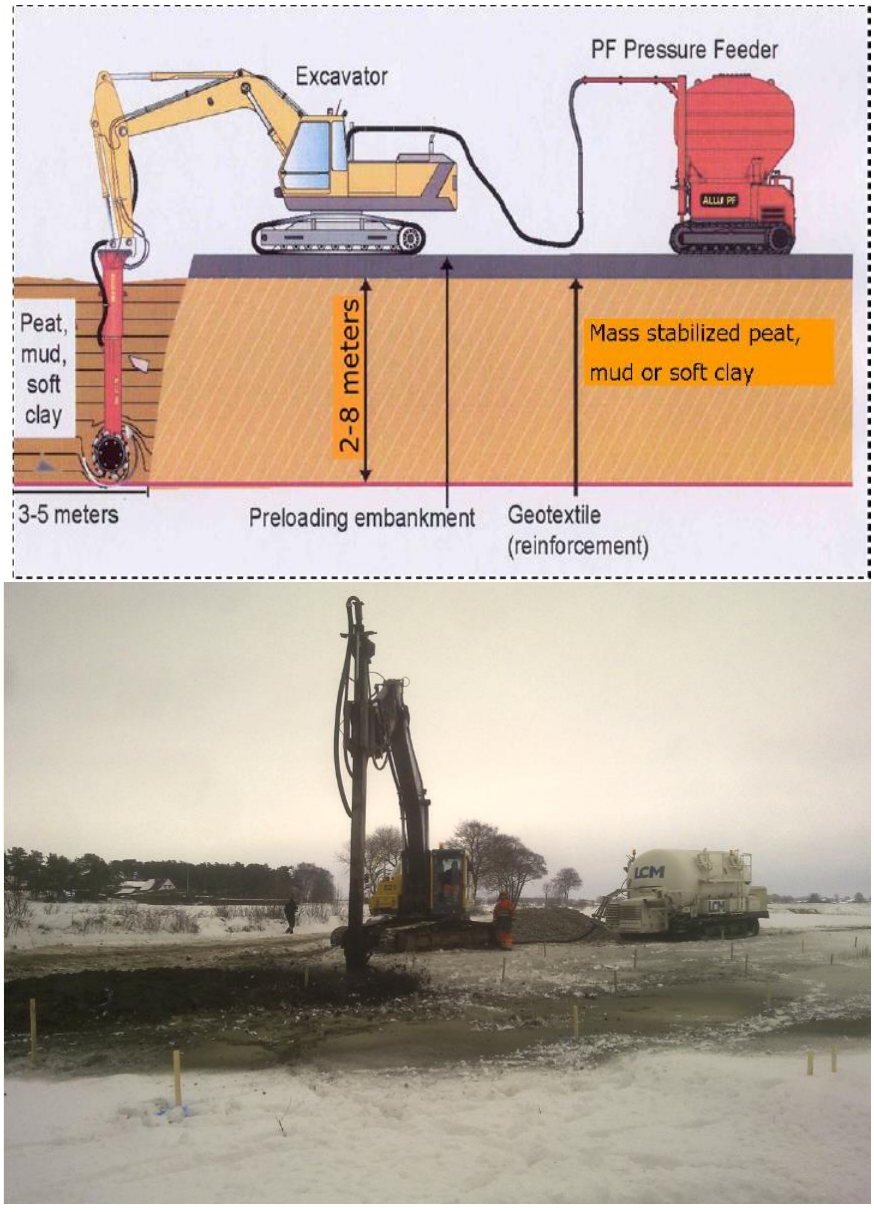

Figure 2.7 - (a) Principle of the mass stabilisation method and equipment (top) (Forsman et al., 2015) and (b) Photo of the rig used in stabilising peat (bottom) (courtesy of LCM)

2.4.3 Piling

In some road projects in Ireland, depths greater than 4 m were excavated, with local excavations reaching depths of up to 13 m (Buggy & Farrell, 2012). Piled embankments have been used on a number of occasions to support roads over significant thicknesses of very soft materials as shown in Figure 2.8.

First used in the late 1960s in Finland (Orsmond, 2012), piled embankments now have many support arrangements. Driven precast concrete piles or continuous flight auger (CFA) piles are installed to depths of up to 30 m (Munro, 2004). They are then usually capped in several ways, including by a rigid continuous concrete slab, individual concrete pile caps or a geotextile pile concrete cap combination (Munro, 2004). Geosynthetic load transfer platforms are popular in Ireland and involve a grid of piles with pile caps, which is overlain by one or more layers of geotextiles, with the embankment constructed on top. An embankment usually includes a piling platform to support machinery over the low-strength peat, which is overlain by the load transform platform. Soil arching occurs within the overlying embankment soil between the pile caps, transferring the embankment load into the pile and down to the firm layer. In peat it is generally assumed in design that the entire vertical load of the embankment is carried by the piles, transferred either by soil arching or by the reinforcement (Orsmond, 2012). The ideal combination of pile and pile cap spacing and the height of the embankment varies and is contingent on cost as well as strength (Orsmond, 2012). As peat holds very little strength, frictional resistance cannot be relied upon, and the piles need to extend to a firm soil or bedrock.

All of the aforementioned ground improvement methods for supporting roads demand a substantial amount of construction materials, leading to the depletion of natural resources, the emission of GHGs and damage to the local environment due to construction operations.

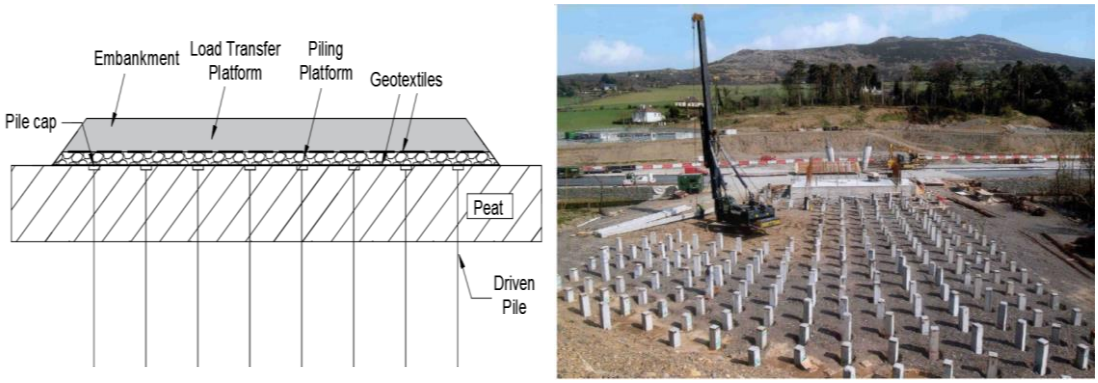

Figure 2.8 - (a) Typical section for piled embankment and (b) pile installation for a piled embankment (Orsmond, 2012)

2.4.4 Drainage and its impact on emissions in peatlands

Peat has a high carbon content, ranging from 49 to 62% of its dry weight (Birnie et al., 1991). Near-intact peatlands take in carbon slowly from the atmosphere, and nationally they may absorb as much as 20,474 tCO_2/yr (57,492 tC/yr) (Renou Wilson et al. 2011). However, when peat soils become aerated or drained, the rate of aerobic decomposition increases to the point where CO_2 emissions usually exceed plant fixation, culminating in

a net release of CO_2 into the atmosphere (Nayak et al., 2008), and the higher the organic content of the peat, the higher the potential loss of carbon as CO_2.

The excavation process and the extent of drainage due to road construction on peatlands negatively impact on the peat's carbon store as drained peatland releases its carbon as CO_2 and other GHGs; thereafter it loses the ability to sequester carbon (Lindsay, 2010). The ground improvement techniques outlined in this chapter all require the removal of some peat, whether for drainage ditches, ponds or the road itself. On removal, it can be dried and burned as fuel, and it can be assumed that it will emit all its carbon as CO_2. Excavated peat can also be dried for agriculture purposes, used to fill in borrow pits, or can be laid on both sides of a road in peat disposal areas. Under anaerobic conditions, it could potentially retain a large percentage of its carbon content, but peat laid on the surface to dry will lose a high proportion of its carbon as CO_2.

Drainage of a peatland drastically alters the hydrological regime, leading to significant water loss, loss of habitat structure and subsidence of the peatland. As well as peat oxidation, major shrinkage of the peat may occur, which on rewetting will not return to its original volume (Regan & Johnston, 2010). The excavate-and-replace technique requires peat to be excavated, allowing ground water flow to enter the excavation, necessitating drainage of some of the surrounding peatland and resulting in a water table drawdown. The embankment itself can act as a linear drain or drainage corridor through the peatland, which can affect the drainage regime and overall hydrology of the area. The drawdown can also be due to the installation of drains along either side of the road, resulting in a permanent lowering of the water table. The extent of drainage can vary from less than a 1.5 m radius to over 50 m (Nayak et al., 2008).

In piling and soil-mixing, little or no peat is removed during the operations, but drainage still occurs because of the drains placed at either side of the road. In soil-mixing, the natural water content of the peat to be stabilised is high prior to mixing, but because of the reaction of water with the binder, the water content reduces (EuroSoilStab, 2002; Duggan et al., 2015). This hydration process may affect the carbon store of the peat, but the extent has not yet been ascertained. Piling, on the other hand, has little impact on peat, apart from initially applying lateral pressures on the upper layers and, consequently, causing possible heave. Some peat may temporarily dry because of this, but the extent is unknown.

The effect of each ground improvement technique on the carbon stored in peat is not well known but is vital in evaluating the environmental impact of road construction. EC and

EE estimates are being used increasingly as indicators to assess this environmental impact as part of an environmental life cycle assessment.

2.5 Overview of Life Cycle Assessment (LCA)

2.5.1 Introduction

Environmental life cycle assessment (LCA) tools quantify and evaluate the environmental burden associated with a product or process by considering the use of resources and the environmental consequences of releases into the environment. These tools can be utilised to devise ways to decrease the environmental cost of engineering projects such as road construction. International standards such as BS ISO 14025:2006, BS ISO 14040:2006 and BS ISO 14044:2006 all provide important standardised approaches to LCA requirements and framework guidelines (BSI, 2006c; BSI, 2006a; BSI, 2006b). An LCA includes four phases: goal and scope definition (Phase 1), life cycle inventory (LCI) (Phase 2), life cycle impact assessment (Phase 3), and interpretation (Phase 4) (Figure 2.9) (BSI, 2006c).

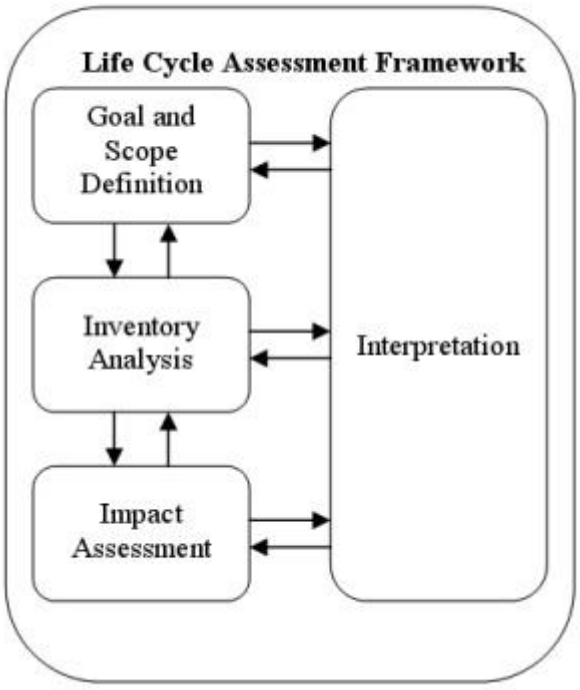

Figure 2.9 - Phases of an LCA (BSI, 2006a)

2.5.2 Goal and scope definition

Having defined the LCA goal, the following are identified in Phase 1: functional unit (e.g. tCO_2eq/m^3, tCO_2eq/t, tCO_2eq/km), system boundary (factors/unit processes involved), data requirements and limitations. The goal and scope must provide the reasons for undertaking the study while the functional unit allows a meaningful comparison of products.

The system boundary determines the range of impacts that are considered directly linked to the product and includes the unit processes or factors to be incorporated into the assessment. A unit process as defined by BSI (2006a) is 'the smallest portion of a product system for which data are collected when performing a life cycle assessment'. Each unit process is provided with inputs and generates output products, by-products and recyclable wastes. The manufacture of all products is comprised of identifiable unit processes; for instance, in the case of a timber product, unit processes include sawing, drying, and gluing. Once these unit processes are defined and the production system identified, the construction of standard flowcharts linking up these unit processes can begin. The system boundary separates the system from its surroundings, allowing inputs to enter the system and outputs to leave the system. It also determines the factors to be included in the life cycle inventory (LCI). A 'cradle-to-grave' assessment examines the whole life of the product from raw material extraction to disposal while a 'cradle-to-gate' assessment examines the product from raw material extraction to the factory gate and is the most commonly used in the UK (Moncaster & Symons, 2013). A 'cradle-to-site' assessment includes the 'cradle-to-gate' result and the transportation of the material or product to its target site.

Decisions and assumptions made are based on the selection of a product or products, selection of manufacturing plants, contacts and meetings with industry, selection of unit process, input/output parameters, and construction of standard process flowcharts (Tucker et al., 2009). It is crucial that a certain level of confidence exists so that decisions can be made based on the conclusions of the LCAs. Data should be taken from the country where the assessment is carried out, and the best sources are government organisations, industries, and internationally recognised databases. The International Organisation for Standardisation (ISO) has defined broadly categorised data quality requirements (BSI, 2006b).

In an environmental LCA, it is usual to examine global warming in terms of EC and EE, although other category indicators such as, but not limited to, impacts from water and land use, acidification, eutrophication and ecotoxicity can be used (BSI, 2006a; BSI, 2006b; BSI, 2006c). In this research, EE and EC are examined. EE is measured in joules and EC in CO_2 equivalents (CO_2eq), the emission metric chosen by the United Nations Framework Convention on Climate Change (UNFCC) in the Kyoto Protocol (UNFCCC, 1998), which includes CO_2, CH_4, N_2O and PFCs (Hammond & Jones, 2011) and is found by multiplying the mass of the GHGs by their associated 100-year GWP (IPCC, 2007). EC and EE calculations are increasingly required to demonstrate compliance with environmental

regulations. The terms energy and carbon are often used interchangeably as they are closely linked, and the use of energy has a certain amount of carbon emissions associated with it, which is dependent, for example, on whether the source of energy is from fossil fuel combustion or not.

2.5.3 Life cycle inventory, impact assessment and interpretation

Once the system boundary and category indicators are defined, Phase 2 involves the collection of information on EE/EC intensities from existing databases such as the Inventory for Carbon and Energy V2.0 and other published material to create a database for materials and processes that lie within the system boundary (Hammond & Jones, 2011). It requires analysts to build their own systems by assembling materials and processes using programmes such as *SimaPro* and *GaBi* that allow them to choose from a wide range of LCI databases (PRé Sustainability, 2015; Thinkstep, 2015). The relevant inputs and outputs are then tabulated and quantified. These inputs relate to the materials used and the energy required, while the outputs are the products and the emissions to air, water and land. Once the computer model is completed, Phase 3 focuses on performing the impact assessment by evaluating the influence of the flows to and from nature, while Phase 4 is concerned with interpreting the results in order to make recommendations and arrive at conclusions.

2.5.4 LCA methodologies

In the case of carbon footprint, all GHG emissions should be accounted for when examining an activity, but this is not possible due to the expense and time required to address all facets of each activity in a 'full cycle perspective'. Three main methods have been established to calculate EE and EC: process analysis (PA), input-output analysis (IOA), and hybrid analysis, which is a combination of both.

PA was developed to understand the environmental impacts of individual products. This method can achieve very accurate results for defined products, but is subject to the problem that a system boundary must be set, leading to truncation errors of unknown size. Due to data requirements, PA is generally cost-intensive.

IOA provides an alternative, economy-wide approach, allowing for the allocation of all impacts along the production and supply chain to the final product, thereby cutting out system cut-offs. This has the advantage of avoiding boundary issues associated with PA. IOA is suitable for larger entities such as companies or countries using economic IOA tables that are unique to each economy, making it feasible to compare environmental performances between similar products (Acquaye & Duffy, 2010). The IOA method saves

money and time as it requires minimum data, but its appropriateness for examining the impacts of single products or processes is limited as it assumes homogeneity of prices, outputs and their carbon emissions at the sector level (Wiedmann, 2010; Acquaye & Duffy, 2010). Another limitation of the method is that when countless individual activities are grouped, it only shows the impact of an industry and not the specific products.

Combining the strength of these two approaches to create a hybrid is the preferred option for a detailed yet comprehensive and robust carbon footprint analysis. Using the hybrid model developed by Treloar (1997), the IOA model can be employed to scope a product's system boundary to establish the most important inputs. This hybrid LCA allows PA to carry out detailed and accurate collection of primary data for important inputs or processes while the less pertinent process stages can be covered by the IOA. Using the PA method leads to the truncation of system boundaries and underestimation of environmental impacts, while a combination of the PA and IOA methods offers more completeness than PA only. It is for this reason that hybrid LCA models are rapidly gaining popularity in industry (Wiedmann, 2010). An example of the application of an IOA hybrid method includes McCaffrey (2011) who used Irish data to calculate EE and EC in reinforced concrete structures and construction materials. The sum of these results gave the total process-based hybrid EE for the different assemblies, and the values then had to be substituted in the overall IOA model to complete the system boundary.

2.5.5 Past LCA studies on geotechnical projects

To combat soaring emissions and comply with regulations, Ireland needs to be in a position to produce accurate calculations of construction-related energy consumption and emissions, including the geotechnical elements of projects. LCAs, therefore, will enable engineers to appraise various options with a view to minimising environmental impacts. Some LCA studies on construction projects have examined EC and EE and have taken a process-based LCA methodology approach, with many authors extending the word 'embodied' and 'cradle-to-site' scenario to include materials, transport and construction impacts but not end-of-life (Pantelidou et al., 2012; Chau et al., 2012).

Recently, the geotechnical profession has taken steps to quantify energy consumption and emissions for geotechnical processes in construction projects. However, according to Shillaber et al. (2015), the level of commitment in time and resources to complete full process-based LCAs is not as realistic for geotechnical designers to deliver as it is for industries manufacturing a product day in day out, where it may be acceptable to implement a full process-based LCA. It makes more sense for geotechnical engineers to simplify LCAs by utilising LCA streamlining, which reduces the system boundary and

chooses only impact factors such as EE and EC that have been shown to be relevant impact factors in streamlined LCAs of geotechnical works (Shillaber et al., 2015).

Examples of moves towards quantifying EE and EC for geotechnical processes in construction projects include Egan & Slocombe (2010) who investigated the EC of several piling options on a range of construction projects, Inui et al. (2011) who calculated the EE and EC of various retaining wall structures and Chau et al. (2012) who examined the EE associated with the construction of sections of a UK rail tunnel. Milachowski et al. (2011), Treloar et al. (2004) and Chappat & Bilal (2003) estimated the environmental impact of constructing roads, while EFFC & DFI (2013) developed a calculator for the CO_2 emissions from several foundation and ground improvement activities. However, even with the aforementioned advances, there is still a major lack of LCA studies and methodologies for geotechnical projects, which probably explains the absence of guidelines to determine the potential construction-related emissions for road construction in areas of organic soil such as peat.

2.5.6 Use of emission and peat-related factors in LCA studies

To understand and quantify the dynamics of gas emissions from peatlands, the Intergovernmental Panel on Climate Change (IPCC) has published basic Tier 1 default emission factors for peatlands in different climates (IPCC, 2006). Hall (2006) and Nayak et al. (2008) used these emission factors and other basic assumptions to estimate the carbon cost of building a windfarm on peat and to investigate the effect of forest removal and peat drainage, establishing new LCA methodologies in the process. Notwithstanding progress to date, only a limited number of peat-related factors have been incorporated into EC studies. Applying these methodologies to quantify the EC of ground improvement techniques for road construction on peat still leaves large gaps, highlighting the need for a robust LCA methodology.

The estimation of EC for a particular method of road construction depends on a wide-range of factors and construction activities such as construction operations, peat drainage, drainage systems, peat stability, restoration of peatlands, clearance of vegetation/forest, and the effect of climate change, some of which are covered in Section 2.6. By combining several LCA methodologies and using Tier 2 country-specific emission factors where possible in addition to established Tier 1 emission factors (IPCC, 2006), better predictions can be arrived at.

2.6 Factors affecting EC and EE for road construction

2.6.1 Introduction to materials, transport and machinery

All road construction operations require materials, transport and machinery, which consume energy and result in emissions. When the quantities of these EC and EE inputs are known, EC intensities (eg. $kgCO_2eq/kg$) and EE intensities (eg. MJ/kg) values are needed to produce totals for emissions and energy for each activity. The following existing databases help to calculate these EE and EC inputs for an LCA:

- The Inventory of Carbon and Energy (ICE V2.0) (Hammond & Jones, 2011): ICE V2.0 is a cradle-to-gate database that gives EC and EE intensities for many products and incorporates the impacts of material extraction, processing, transport, and fabrication of the product.
- The DECC & Defra (2012) database: This database is sufficiently accurate for EC and EE intensities for fuel used by freight transport. Values include the extraction and transport of primary fuels and materials, together with the refining, distribution, storage and retail of finished fuels and materials.

With the aid of the aforementioned databases, EE and EC inputs for materials, transport and some machinery can be quantified for geotechnical solutions for road construction in peatlands, such as excavate-and-replace, dry soil-mixing, and piling.

2.6.2 Materials

Using existing EE and EC methods, it might be expected that the excavate-and-replace option would be less energy/carbon intensive than soil-mixing and piling as replacement of peat with fill such as quarried material is relatively cheap and environmentally friendly. The EE associated with producing the binder in soil-mixing and the cement for the concrete in piles is energy intensive because of the additional manufacturing stage and, in general, high EE activities give rise to high EC (Egan & Slocombe, 2010) (Table 2.1).

Table 2.1 - Some EC and EE intensities for common materials used in road construction on peat

Material	$kgCO_2eq/kg$	MJ/kg
Aggregate	0.0052	0.083
Portland Cement	0.95	5.5
GGBS	0.083	1.6
Precast RC 40/50	0.242	2.33

For dry soil-mixing, the choice of binder is important. Portland cement is responsible for 5% of global CO_2 emissions and is extremely energy intensive (Higgins, 2007). Cement replacements with lower environmental burdens offer opportunities for significant

reductions in energy consumption and CO_2 emissions. For example, GGBS, a by-product of the steel industry, has less than one-tenth of the environmental impact of cement in terms of EC (Table 2.1).

2.6.3 Transport

Transportation of materials to site must be included in EE and EC summations to extend cradle-to-gate figures to cradle-to-site figures. Moreover, for every road construction project, transport of machinery and labour to site and transport of waste to peat disposal areas should be included.

Ireland's transport emissions in 2012 accounted for 19% of the country's total GHG emissions of 58.5 $MtCO_2$ (EPA, 2014). Therefore, planning of haulage is an important aspect of road construction projects. EE and EC intensities of transport can be improved by attention to geographical location, vehicle selection, highway congestion, and distances. Patey et al. (2008) suggested that CO_2 emissions rise steadily when speeds are variable compared to operating at steady speeds.

2.6.4 Machinery

Machinery uses energy and emits unwanted gases, and EC and EE calculations for machinery should account for, if possible, initial manufacture and maintenance. For construction on peat, particularly for excavate-and-replace, machinery primarily includes excavators for peat excavation and loading and dump trucks for haulage and deposition. Dredging of this peat is not particularly energy intensive because of the semi-liquid state of the peat (Woijtasik et al., 2006).

In any construction project, materials usually account for the highest proportion of the total EE and EC, followed by transport and then machinery. Studies such as by Chau et al. (2012), based on constructing a rail tunnel, calculated the EE of materials for one construction scenario to be the highest contributor at 82%, followed by transport and machinery at 10% and 8% respectively.

2.6.5 Drainage

2.6.5.1 Carbon dioxide

In terms of materials, transport and machinery, high EE normally produces high EC in construction projects. Construction in peatlands poses an additional problem. In the excavate-and-replace solution, while the excavation and replacement with more competent fill seems greener than the other methods, the excavation process and extent of drainage due to construction have a detrimental effect on the carbon stored within the peat.

Drainage of the nearby peatland reverses the carbon-storing process into emitting carbon as CO_2 and other GHGs.

Drained peat allows stored carbon to readily decompose due to the aerobic conditions created, releasing a substantial amount of CO_2 that needs to be accounted for. CO_2 emissions vary mostly according to depth to water level, peat depth and temperature (Nayak et al., 2008). Due to peat oxidation in the aerobic layer, intensified by the lowering of the water table, damaged Irish peatlands currently emit an estimated 9.68 $MtCO_2/yr$ (Wilson et al., 2013). Beuving & van den Akker (1996) reported that in drained peatland grasslands, a subsidence rate of almost 0.5 m every 100 years occurs due to oxidation and decomposition. The reason for such a large figure is that up to 100% of organic matter may decompose in the deep aerobic layer, some of which has been stored for many years. It is imperative that this peat-related factor and its likely impact on gas emissions is included in EC calculations as it will dramatically increase the EC total.

To quantify this factor, the extent of the water table reduction around the road needs to be estimated. Without detailed measurements of peat hydrogeology on a level site with uniform soil distribution, the extent of drainage on each side of the road or drainage ditches can be estimated using Equation 2.1 (Nayak et al., 2008), where E (m) is the extent of drainage around the road or ditch and K (mm/d) is the hydraulic conductivity (Figure 2.10).

$$E = 11.958 \times \log(K) - 9.361$$ **Equation 2.1**

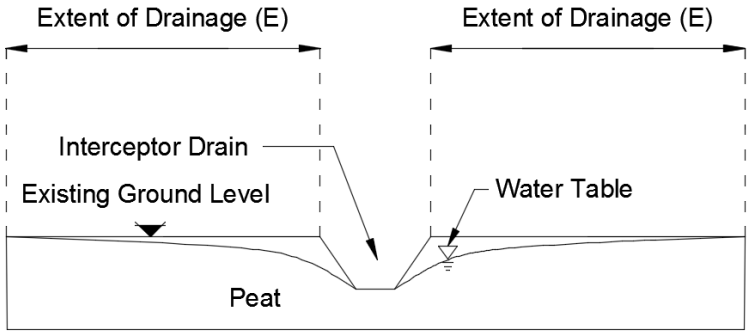

Figure 2.10 - Extent of drainage around interceptor drain

Hydrological modelling in drained peatlands has been examined by Ballard et al. (2011) and could be used to estimate the water table drawdown at any time and distance from the road in the surrounding peatlands. Methods are also available to mitigate the extent of drainage in the surrounding peatlands that lower CO_2 emissions and thus EC; for instance,

the procedure of installing low permeability peat plugs along a road, described by Gill (2010).

Other losses of CO_2 that could be accounted for are dissolved organic carbon (DOC), particulate organic carbon (POC) and dissolved CO_2 leaching from the peatland (fluvial outputs), which will increase due to ditch construction and further drainage (Worrall et al., 2003). However, these losses are difficult to quantify and fluctuate dramatically from site to site. Limited studies have been undertaken, but no emission factors have been published by the IPCC.

2.6.5.2 Methane

CH_4 has a global warming potential (GWP) of 25, meaning a large amount of heat is trapped in the atmosphere relative to that for CO_2, which has a GWP of 1 (IPCC, 2007). CH_4 emissions are released in an intact peatland by three processes: diffusion across the air-water interface, bubble emissions, and transport via vascular plants (Strack et al., 2004; IPCC, 2006) (Figure 2.11).

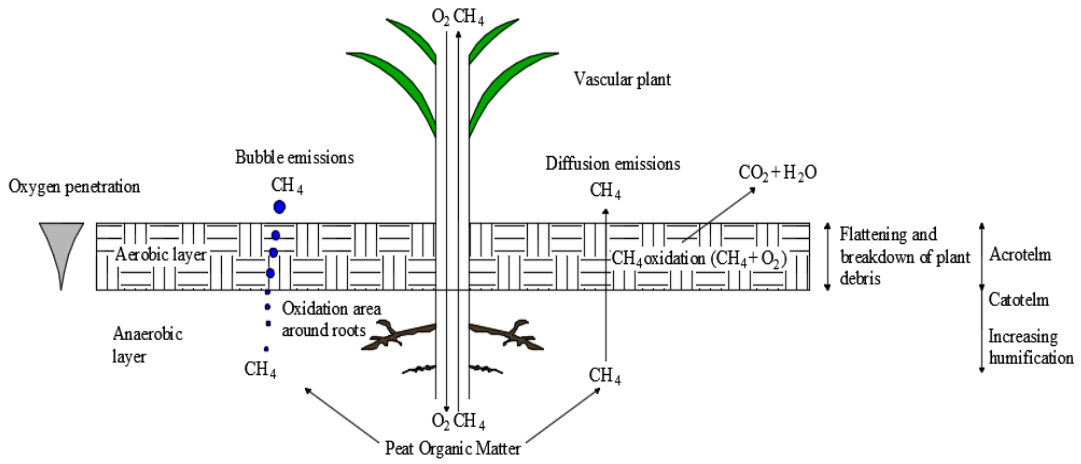

Figure 2.11 - CH_4 release from a peatland site (Couwenberg, 2009; Lindsay, 2010)

The IPCC (2006) suggests that for a basic calculation of CH_4 emissions, it is satisfactory to count diffusive emissions only, but it has not released guidelines for calculating CH_4 emissions because pristine peatlands are not anthropogenic and, as such, are not relevant under the United Nations Framework Convention on Climate Change (UNFCCC) (Couwenberg, 2009). Restoration of a peatland after road construction is, however, anthropogenic and must be reported.

The emission factors in Table 2.2 produced by Couwenberg (2009) are based on climate, water table, and vegetation. These factors illustrate the importance of incorporating CH_4 transport via vascular plants into calculations as emissions average 170 kg CH_4/ha/yr in a

wet peatland. CH_4 travels straight into the atmosphere through the aerenchymous shunts (air channels in the roots) bypassing the aerobic zone (Couwenberg, 2009; Laine et al., 2007). Frequently, the majority of CH_4 transported through diffusion is lost in the upper aerobic zone due to oxidisation by methanotrophic bacteria, producing CO_2 in the process (Strack et al., 2004; Segers, 1998). This aerobic zone decreases in thickness at higher water levels, leading to reduced CH_4 oxidation and increased CH_4 production and vice versa (Whalen, 2005). It must be remembered, however, that CH_4 production is offset by the amount of carbon sequestered by peat. In any case, Table 2.2 shows the need to calculate CH_4 released from restored peatlands as part of road construction.

Table 2.2 - Emission factors (Dry = mean annual water level -20 cm, Wet = above -20 cm) (Couwenberg, 2009)

kg CH_4/ha/yr mean (range)			
Climate	**Dry**	**Wet**	
Temperate		Without shunts	With shunts
	0.2(-4 to 9)	50(-0.2 to 250)	170(0 to 763)

2.6.5.3 Nitrous oxide

N_2O is even more harmful to the atmosphere than CH_4 as it has a GWP of 298. N_2O emissions depend on many factors, not just on the water table position. Factors influencing N_2O emissions include the presence of organic nitrogen, the degree of humification, the presence of vascular vegetation and pH (Regina et al., 1996). Drainage permits bacteria to convert the organic nitrogen in peat to nitrates, which are then carried by leaching to the surface where they are finally reduced to N_2O (IPCC, 2006). According to Glatzel et al. (2008), only cultivated or drained peatlands release more than 100 μg $N_2O/m^2/hr$. It may seem, therefore, that N_2O release should peak in summer because of drier weather but is negligible due to competition among plants for uptake of excess nitrogen and NO_3 (Silvan et al., 2005; Rückauf et al., 2004).

N_2O emissions from Irish oligotrophic (nutrient-poor) peatlands are small or negligible because of their low nitrogen concentration (Martikainen et al., 1993). Consequently, it is not a significant factor in emissions from road construction in Ireland, unless the site is a nutrient-rich fen. Klemedtsson et al. (2005) reports that significant N_2O emissions can occur if the C/N ratio drops below 25; otherwise, they should be considered negligible in calculations.

In addition to the water table depth, other variables such as peat properties, vegetation, weather and temperature influence emissions. Appendix A lists some research findings

from several authors that shows how each variable influences CO_2, CH_4 and N_2O emissions.

2.6.6 Drainage systems

Depending on the peatland type, peat depth, slope and type of ditch/pond, drainage ditches and ponds constructed in tandem with road construction on peatlands may stay functional for decades or deteriorate and fill with vegetation within 10 years of installation (Minkkinen & Laine, 2006). High CH_4 fluxes from drainage ditches and ponds in a temperate climate have been reported by Hendriks et al. (2007), particularly in nutrient-rich ponds and ditches. Ditches clogged with algae and other vegetation that are not regularly maintained tend to produce higher CH_4 emissions (Minkkinen & Laine, 2006). Emissions can also be high from turbulent water due to the thinner boundary layer between the water and air interface (Minkkinen & Laine, 2006). These CH_4 emissions depend primarily on air temperature, water level, speed of the moving water and vegetation (Minkkinen & Laine, 2006; Schrier-Uijl et al., 2008).

Studies of gas emissions from ditches and ponds in temperate, boreal and Mediterranean climates reported in the literature were examined. The highest emissions, 61.5 $tCO_2eq/ha/yr$, were from a site in a Mediterranean climate because of higher temperatures and a higher decomposition rate (Teh et al., 2011). In comparison, emission rates in a temperate climate ranged from 12.7 to 27.3 $tCO_2eq/ha/yr$ (Hendriks et al., 2007; Schrier-Uijl et al., 2011).

2.6.7 Slope stability

Soil disturbance should be minimised to prevent the development of aerobic conditions, which are ideal for decomposition and, therefore, the release of CO_2. Many factors may reduce the stability of the peat and impact on EC summations. Water is the main cause of slope instability and acts in reducing the shear resistance of the underlying layer. Loading of the underlying material by saturation of the overlying layer may exceed the frictional resistance of the soil, causing it to fail. In peat excavate-and-replace, the water content of the peat on the excavation slope may exceed its liquid limit, causing the peat to collapse. Peat translational slides tend to occur where the slide's base meets the peat-substrate interface because natural lines of drainage exist along this interface (Boylan et al., 2008).

Artificial drainage lines may induce shear stresses and cause potential failures; so, too, can the presence of water in cracks, which are indicative of compression and tension (Wilson & Hegarty, 1993; Scottish Executive, 2006). As a result of drying, cracks start to appear that potentially can cause failure in heavy rainfall, as shown in Figure 2.12. The loss of

surface vegetation due to construction leaves the peat surface fragile and without sufficient tensile strength (Scottish Executive, 2006). Furthermore, loading of the peat mass by heavy machinery, structures, or overburden increases the shear stress. Until pore pressures dissipate, peat stability is at its most vulnerable (MacCulloch, 2006).

Blanket bogs are more prone to peat collapses than raised bogs because of their formation on slopes. Most slides occur in slope angles of 2° to 20°, where 20° appears to be the limiting gradient for deep peat (MacCulloch, 2006). Peat erosion has in the past decade been cited as a significant factor in losses of carbon due to drying out of the dislodged material, which can be from a few hundred cubic metres to greater than 100,000 m^3 of peat (Dykes & Warburton, 2007). In summating emissions and EC, it may be necessary to include a factor for peat erosion collapses because of peat debris drying out and releasing CO_2. Protecting this peat carbon store must become a priority in construction management (Warburton et al., 2004), hence peat stability may become a major factor in choosing the ground improvement or foundation technique.

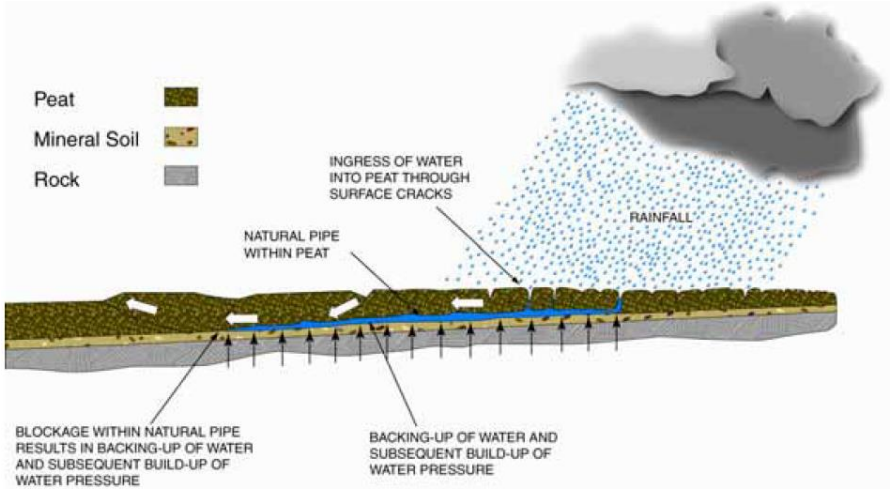

Figure 2.12 - Typical water ingress through peat matrix (MacCulloch, 2006)

2.6.8 Peatland restoration

Restoration techniques can be applied to reduce the overall EC of a construction project. For instance, peatland restoration can be carried out on drained peatlands or peat disposal areas that can alter overall EC. Any improvement plan for restoring a peatland that has suffered because of road construction should demonstrate a high probability that peat hydrology will be restored, disturbance of peat minimised, and subsidence stopped (Regan & Johnston, 2010). Peatlands often have complex modes of water transport, and identifying these pathways is crucial if saturated conditions in the peat and its dependent ecology are to be restored to their original status of sequestering carbon.

To restore peatlands, simple techniques are used. Drains can be blocked to promote rewetting after construction (Gill, 2010). Soft rushes and sphagnum can be planted to bind the peat together, which leads to a complete cover and stabilisation of the introduced peat (Bord na Móna, 2005). Shade can be provided to lower the temperature and increase relative humidity near the surface, impacting on CO_2 and CH_4 emissions and thus EC.

2.6.9 Forest and vegetation

Another common practice after road construction is to continue drainage on disposal sites and drained lands and to plant Sitka spruce. During the first few years, a net CO_2 release occurs due to the exposure of soil carbon to aerobic conditions, but the uptake of carbon in vegetation and trees will somewhat offset oxidation losses. Furthermore, CH_4 emissions will cease due to increasing aerobic conditions in the peat profile. In 4 to 12 years after restoration, the site will become a net sink, the changeover time depending on vegetation dynamics, climate, peat depth and type, and site productivity (Black & Gallagher, 2010). The timeframe for emissions is shown in Figure 2.13. In addition to this positive EC impact, the average carbon loss due to decomposition decreases from a value of between 1 and 14.6 tCO_2/ha/yr in the first rotation to a smaller value after two or three rotations, signifying that more carbon will be stored in the peatland forest annually (Hargreaves et al., 2003). During the first few rotations, though, some subsidence takes place, depending on the bulk density of the peatland. Lindsay (2010) found that this occurrence may extend up to 50 to 60 m around the forest with time, somewhat draining the adjacent land and, inevitably, increasing GHG emissions.

As part of construction, it may be necessary to clear a forest, resulting in a CO_2 loss, although the amount of carbon loss depends on the type of tree, the age of crop on felling and the end use of the timber. A drained peatland cleared of forest continues to release CO_2. Moreover, there is no carbon uptake from trees, which means a net loss of CO_2 is taking place and must be accounted for (Black & Gallagher, 2010).

It is essential, also, to evaluate the carbon and nitrogen content of the biomass layer as well as the peat (Lindsay, 2010). The clearance of vegetation such as sphagnum and vascular plants due to road construction can lead to GHG emissions. Vegetation is a source of carbon and nitrogen and, if destroyed, harmful gases are released (Schiller & Hastie, 1996; IMCES, 2011). Lindsay (2010) suggested that a 15 cm sphagnum layer has a carbon content of 183.3 tCO_2/ha, while a damaged peatland dominated by vascular plants is thought to have a lower carbon content of 36.7 tCO_2/ha. The reason for the difference is that sphagnum has a greater resistance to decay than vascular plants and allows undecayed material to pass to the anaerobic zone, where the decomposition is so slow that peat

accumulates carbon (Lindsay, 2010). As part of peatland restoration, it would be advisable, therefore, to plant sphagnum rather than vascular plants to reduce EC.

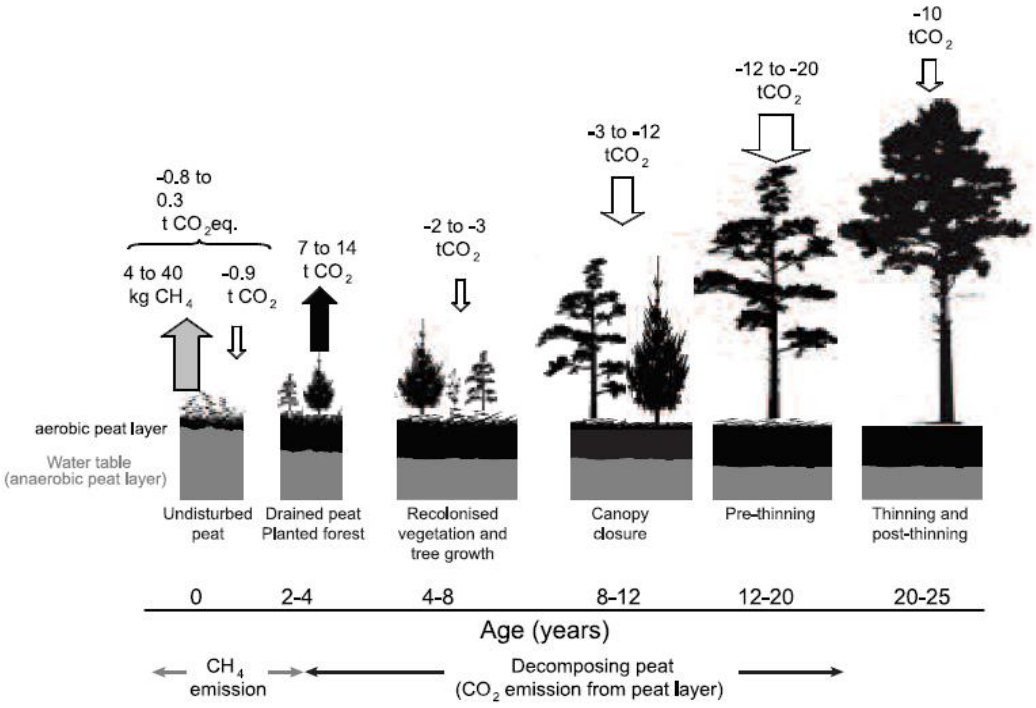

Figure 2.13 - GHG balance of peatlands after afforestation. Values represent an annual flux of CO_2/ha (Black & Gallagher, 2010)

2.6.10 Variability in peat and uncertainty of emissions

Each peat site is different in its climate, landscape, properties and characteristics. Aggregated emission factors from the IPCC estimate emissions only from an undrained or drained peatland and nothing in between; consequently, there is little guidance for calculating emissions from a near-intact peatland. Site-specific equations developed by Nayak et al. (2008) can be used to estimate GHG emissions from peat more accurately. Even with these, there are substantial inaccuracies in relation to emissions. For example, CH_4 takes at least a month to revert to producing emissions after restoration because of suppression of CH_4 due to methanogens requiring a long regeneration period following exposition to aerobic conditions (Glatzel et al., 2008; Tuittila et al., 2000).

It is significant that peatland restoration over a short period of time may lead to higher GHG emissions than if it were in a drained state. The peatland may still be releasing CO_2 through the aerobic layer and simultaneously releasing CH_4 from rewetting areas, though CH_4 emissions do not normally exceed the emission levels of the original natural state (Lindsay, 2010). A rising water table then stimulates growth of sphagnum and other vegetation, increasing carbon accumulation, raising the surface of the peatland and, in essence, increases the depth to the water table, which leads to a slight decrease in CH_4

release. A near-intact peatland may be mildly contributing to climate change or global cooling on a 100-year timeframe (Lindsay, 2010). It would appear crucial, therefore, that new published EC summation models take the above factors into account.

As mentioned in Section 2.4.4, the emissions in peatlands subjected to dry soil-mixing and piling are unknown. The major focus of this research is the environmental impact of the ground improvement technique, dry soil-mixing, which, when better understood, will be crucial in filling gaps in the LCA inventory needed to complete an LCA for road construction on peat. To explain the likely carbon response of peat mixed *in situ*, a process called carbonation is discussed in the following sections.

2.7 Carbonation

2.7.1 Carbonation in concrete

2.7.1.1 Hydration process

Ordinary Portland cement (CEM I) is composed of between 90 and 95% cement clinker (Irish Cement, 2010), which consists of four main cement minerals, alite (C_3S), belite (C_2S), aluminate and ferrite (Table 2.3). C_3S and C_2S mix with water, leading to the formation of calcium silicate hydrate (CSH) gel and a corresponding increase in strength (Equation 2.2 and Equation 2.3) (Kazemian et al., 2011). The strength gain varies depending on the ratio of C_3S to C_2S and other parameters such as temperature; the higher the ratio and the temperature, the greater the CSH production and, consequently, the greater the strength. Some calcium hydroxide (CH/ $Ca(OH_2)$), also known as hydrated lime, is produced by the reaction.

Table 2.3 - Representative weights of main chemical components in Portland cement clinker (Taylor, 1997)

Chemical Name	Oxide Formula	Cement Notation	Mineral Name	Weight (%)
Tricalcium silicate	$3CaOSiO_2$	C_3S	Alite	50–70
Dicalcium silicate	$2CaOSiO_2$	C_2S	Belite	15–30
Tricalcium Aluminate	$3CaOAl_2O_3$	C_3A	Aluminate	5–10
Tetracalcium aluminoferrite	$4CaOAl_2O_3Fe_2O_3$	C_4AF:	Ferrite	5–15

Short $2C_3S+6H \rightarrow C_3S_2H_3+3CH$

Full form $2Ca_3SiO_5+6H_2O \rightarrow 3CaOSiO.2SiO_2.3H_2O+3CaO.H_2O$ **Equation 2.2**

Short $2C_2S+4H \rightarrow C_3S_2H_3+CH$

Full form $2Ca_3SiO_5+4H_2O \rightarrow 3CaOSiO.2SiO_2.3H_2O+CaO.H_2O$ **Equation 2.3**

2.7.1.2 Carbonation process

The calcination of limestone represents about half the CO_2 emissions from the cement production process, with cement consuming about the same amount in its lifetime in a process called carbonation (Engelson et al., 2005). Carbonation is a well-known reaction in concrete. For the reaction to take place, gaseous CO_2 from the atmosphere must first dissolve in water to form carbonate (CO_3^{2-}) ions, their type depending on the pH. Bicarbonate (HCO_3^-) ions are the main ones in the carbonated zone of the concrete (Equation 2.4) (low pH), while CO_3^{2-} ions are present in the uncarbonated zone (high pH) (Engelson et al., 2005) (Equation 2.5). The CO_3^{2-} ions then react with calcium ions (Ca^{2+}) in the pore solution to form the calcium carbonate ($CaCO_3$) precipitate (Equation 2.6).

$$CO_2(g)+H_2O \rightarrow HCO_3^-(\text{bicarbonate ion})+H^+ \qquad \textbf{Equation 2.4}$$

$$HCO_3^- \rightarrow CO_3^{2-}(\text{carbonate ion})+H^+ \qquad \textbf{Equation 2.5}$$

$$Ca^{2+}+CO_3^{2-} \rightarrow CaCO_3 \qquad \textbf{Equation 2.6}$$

Separately, calcium oxide (CaO), from calcium silicate compounds contained in the cement paste, reacts with water (H_2O) to form CSH and $Ca(OH)_2$ due to hydration (Equation 2.2 and Equation 2.3). Consequently, due the lower concentration of Ca^{2+} as a result of carbonation, dissolution of $Ca(OH)_2$ occurs (Equation 2.7). Once again, the carbonate ions react with Ca ions in the pore solution to form $CaCO_3$ (Equation 2.6). The solubility of $CaCO_3$ is much lower than that of $Ca(OH)_2$. Equation 2.8 combines Equation 2.7 and Equation 2.6.

$$Ca(OH)_2 \rightarrow Ca^{2+}+2OH^- \qquad \textbf{Equation 2.7}$$

$$Ca(OH)_2+CO_2 \rightarrow CaCO_3+H_2O \qquad \textbf{Equation 2.8}$$

The chemistry of carbonation involves the neutralisation of the alkaline compounds in cementitious materials by carbonic acid in the pore solution of the concrete (McPolin et al., 2007). Since $Ca(OH)_2$ has a pH of 12.5 and $CaCO_3$ has a pH of 9.4, carbonation reduces the pH of the concrete, destroying the passivity (the protective oxide layer) of the embedded steel reinforcement bars, rendering it susceptible to corrosion (Papadakis et al., 1991a). CO_2 must diffuse through an ever-thickening carbonated surface to reach

uncarbonated or fresh concrete. Figure 2.14 is an example of a carbonation profile which identifies a carbonation front depth.

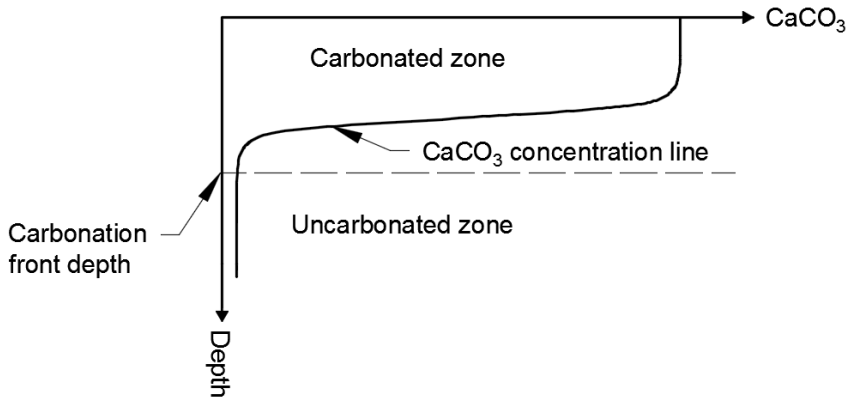

Figure 2.14 - Typical schematic $CaCO_3$ depth profile in concrete

$CaCO_3$ exists in the three crystallographic forms, aragonite, vaterite and calcite. Calcite is the most stable polymorph of $CaCO_3$. Transformation of $Ca(OH)_2$ to calcite gives a volume change of 12%; to vaterite, 19%; and to aragonite, 3% (Houst, 1996). It is this surplus volume of calcite and vaterite precipitation that mainly fills empty space in the capillary system, densifying and strengthening the concrete. The volume change in the transformation of the CSH is, however, more uncertain and depends on the water content of the silica gel. The volume changes affect the porosity in the carbonated layer and, consequently, the diffusion speed. The change in porosity due to carbonation will be examined in the stabilised peat experiments carried out in this body of work.

2.7.1.3 Decomposition of CSH and ettringite/monosulphate due to carbonation

Components in the cement paste such as CSH and ettringite/monosulphate (Aft/AFm) are in equilibrium as a result of high pH and Ca^{2+} in the pore solution. As $Ca(OH)_2$ is consumed, the pH of the cement paste/pore solution drops, resulting in all Ca compounds such as CSH dissolving over time and finally forming $CaCO_3$ along with other carbonates as well as ferrite, silicate and aluminium-hydroxide phases (Table 2.4) (Lagerblad, 2005). As soon as the pH drops, CSH dissolves, followed by AFm, which decomposes at a pH of around 11.6. Aft then decomposes at a pH of around 10.6. At a pH of less than 9.2, none of the original calcium-bearing cement hydrates remain. These phase changes are summarised in Table 2.5.

When carbonation lowers the Ca^{2+} content in the pore solution due to depletion of $Ca(OH)_2$, it is compensated for by the release of Ca^{2+} from CSH. The Ca/Si ratio of the CSH falls, changing its composition. Eventually, when the Ca/Si ratio drops below 1 and the pH is around 10, it transforms/decomposes into a silica gel (Stronach & Glasser, 1997),

which is more porous and permeable than CSH (Bier et al., 1989). Some Ca will always remain in the silica gel. Most of the Ca^{2+} from the aluminate phases form carbonates, and the aluminate and ferrite phases form stable metal hydroxides (Lagerblad, 2005).

Table 2.4 - Concrete carbonation products (Lee et al., 2012)

Portland cement hydration product	Carbonation products
Calcium hydroxide	Calcite and water
Calcium silicate hydrate	Calcite, silica gel, and water
Calcium aluminate hydrate	Calcite, alumina gel, and water
Hydrated ferrite phases	Calcite, ferric oxide, alumina gel, and water
Ettringite and calcium monosulfoaluminate	Gypsum, alumina gel, and water

Table 2.5 - Phase changes in the carbonation process (Chen et al., 2004) (CC = calcite, $Al(OH)_3$ = alumina gel, SH = silica gel, $Fe(OH)_3$ = hydrated iron oxide)

Intact cement	First stage	Second stage	Third Stage	Carbonated
CH	----------	----------	----------	----------
C-S-H(1)	C-S-H (1)	C-S-H (2)	C-S-H (3)	SH (with some CaO)
	CC	CC	CC	CC
AFm	AFm	Aft/Al $(OH)_3$	$Al(OH)_3$	$Al(OH)_3$
AFt	AFt	AFt	$Fe(OH)_3$	$Fe(OH)_3$
pH > 12.5	pH < 12.5	pH < 11.6	pH < 10.5	pH < 10

2.7.1.4 Factors affecting carbonation

The factors most likely to affect the carbonation speed in concrete include degree of hydration, relative humidity, moisture content, temperature, concrete quality (porosity), external environment, concentration of CO_2 and additives (Engelson et al., 2005).

Humidity: The maximum speed of carbonation occurs when relative humidity is somewhere between 60 and 80% (Lagerblad, 2005). Meland (1985) proved through accelerated experiments that a porous stabilised block carbonates faster at a higher relative humidity than less porous concrete as a narrow capillary system blocks more easily with water. In a concrete with very low relative humidity, the CO_2 gas diffusion is rapid, but lack of water leads to a slow carbonation rate. Furthermore, the degree of hydration is low, which in turn affects the porosity. When humidity is too high, the pores become blocked, and the path for CO_2 is more restricted, curtailing carbonation. It must be borne in mind that cyclical wetting and drying seem to accelerate carbonation (Lee et al., 2012). A porous cement paste with capillary condensation is shown in Figure 2.15.

Water content: Water is not consumed in the carbonation reaction but is needed in the carbonation process (Section 2.7.1.2). In concrete, mixes with the highest water to cement (w/c) ratios create large pores; and as carbon ions can penetrate deeply into the larger pore

volume available, the depth of carbonation was found to grow with increasing w/c ratios (Lee et al., 2012; AI-Khaiat et al., 2004; Loo et al., 1994; Houst, 2002) (Figure 2.16).

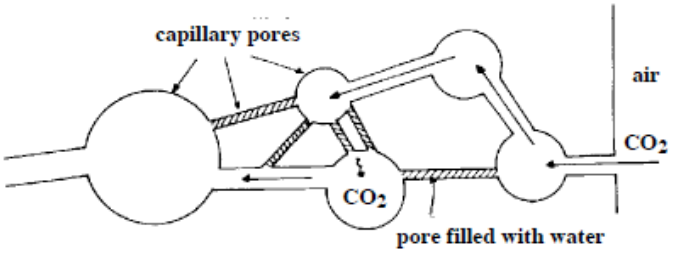

Figure 2.15 - Capillary system in the porous cement paste (Houst, 1996)

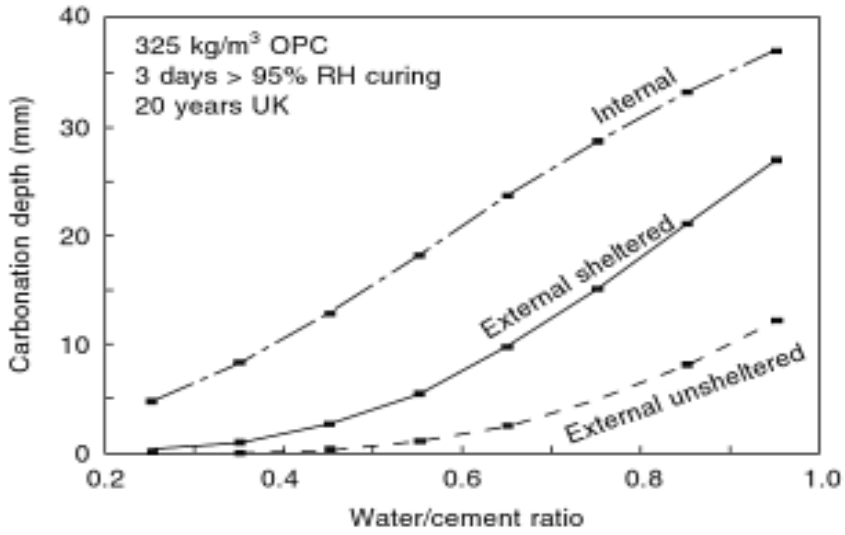

Figure 2.16 - The effect of water/cement ratio and external exposure environment on the depth of carbonation in concrete (Hassanein, 1997)

Temperature: The carbonation rate increases with temperature; therefore, exposure to warmer regions leads to faster carbonation if all other factors remain constant (Liang et al. 2000).

Porosity: Lower w/c ratios and higher quality concrete slow down carbonation due a reduced connective porosity. With a finer porosity, CO_2 has more difficulty penetrating the cement paste, thereby decreasing the rate of carbonation (Figure 2.15). Lo & Lee (2002) suggest that the reduction of carbonation with time is due to the volume of capillary pores decreasing with cement hydration, thereby making CO_2 diffusion into the hardened concrete more difficult. Furthermore, carbonation leads to reduced total porosity and affects all pore sizes (Houst 1996).

CO_2 concentration: A higher amount of CO_2 in the atmosphere increases the carbonation rate (Loo et al., 1994; Fukushima, 1988); and according to Fukushima's (1988) calculations, a rise in CO_2 concentration from 300 to 600 ppm increases the carbonation

rate fivefold. The rate is elevated in suburban areas and indoors in general because the partial pressure of CO_2 is higher (Figure 2.16 and Figure 2.17) and is at its lowest in coastal areas because water absorbs CO_2. As atmospheric CO_2 rises globally, the carbonation rate is increasing simultaneously.

External environment: The carbonation rate in concrete depends on whether it is located above or below ground. Under saturated conditions below the water table, carbonation is slow due to low CO_2 diffusivity. However, the leaching of $Ca(OH)_2$ into ground water and to the carbonation front is another possible way for carbonation to occur as the dissolved $Ca(OH)_2$ eventually reacts with carbonate ions. The extent of this leaching process depends on the ground water speed and its chemistry (Engelson et al., 2005).

2.7.1.5 Effect of cements and GGBS on carbonation

According to Schubert (1987), pozzolanic materials in concrete involve the consumption of $Ca(OH)_2$ in the pozzolanic reaction, substantially reducing the alkaline reserves in hydrated cement by forming more CSH. Consequently, the pH in concrete drops, increasing the carbonation rate while at the same time producing CSH, which blocks pores and reduces the carbonation rate. However, as suggested by Park (1995) and confirmed by Glass (2003), an increase in the quantity of pozzolanic materials deepens the carbonation front. Studies have shown somewhat increased carbonation rates for concrete with PFA or silica fume (Nagataki et al., 1986; Lagerblad, 2005; Matthews, 2012; Matthews, 1984; McPolin et al., 2007), and replacement of cement with GGBS in concrete has also been found to lead to an increase in carbonation depth (Parrot, 1987; Matthews, 2012; Houst, 1996; McPolin et al., 2007). Results demonstrate that Ordinary Portland Cement (OPC) matrices are more resistant to carbonation than those containing combinations of OPC and GGBS, as illustrated in Figure 2.17.

For the same w/c ratio, pozzolanic cement concrete has a remarkably higher carbonation depth due to its greater porosity and its smaller concentration of carbonated constituents (Papadakis et al., 1992). When these pozzolanic materials are used to partially replace the cement proportion, the extent of hydration tends to decrease, resulting in increased permeability and facilitating the ingress of atmospheric CO_2 (Torgal et al. 2012). The amount of calcium to be carbonated is also less, thus the carbonate ions can penetrate deeper.

Torii & Kawamura (1992) and Nakamoto & Togawa (1995) found that concrete with cement containing above 50% GGBS displayed higher carbonation depths than OPC concrete (Figure 2.18). Bouikni et al. (2009) discovered that cement replacement with

GGBS of 65% consistently showed higher carbonation penetration than concrete whose cement content was 50% slag. Similarly, Bier (1987) found that for cements with a slag content exceeding 50% by mass, a coarser capillary pore system was formed during carbonation, which enhanced the speed of diffusion (Stark & Ludwig, 1997; Utgenant, 2004). Ngala (1997) concluded that the proportion of large capillary pores (diameter > 30 nm) due to carbonation increased significantly for PFA and slag pastes compared to cement paste. According to Häkkinen (1993), however, concrete with GGBS in the binder carbonates faster initially, but this rate is similar to pure OPC in old concrete.

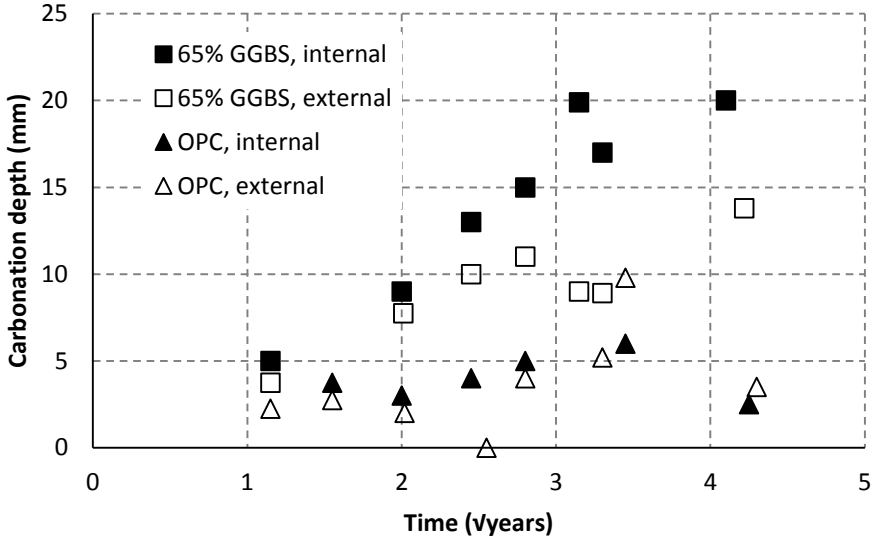

Figure 2.17 - Measured natural carbonation depths over a 20-year period in 65% GGBS and OPC concretes plotted as a function of the root of time. Adapted from Hassanein (1997)

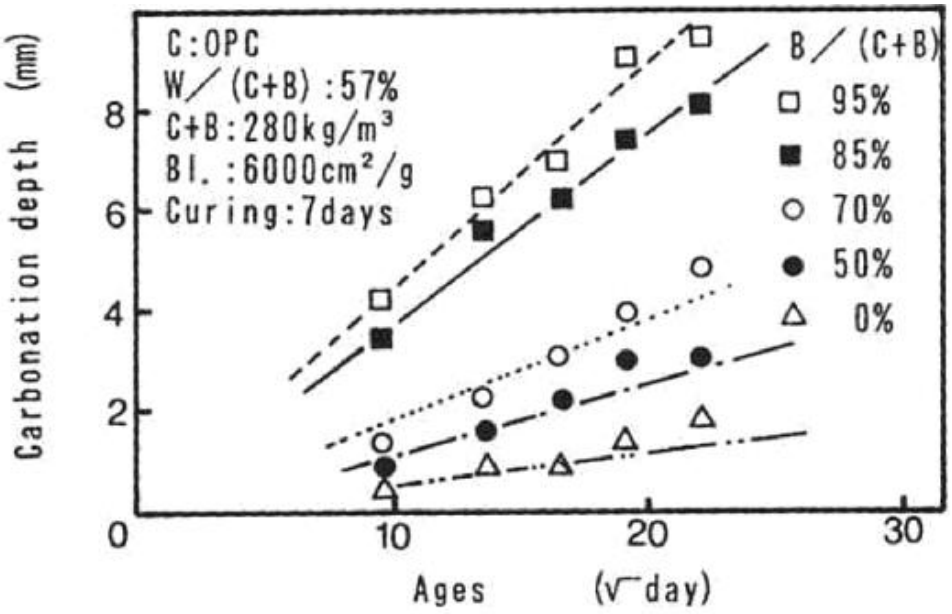

Figure 2.18 - Depth of carbonation with time in the field tests for high ratios of GGBS (B) to OPC (C), (Nakamoto & Togawa, 1995)

The coarser pore system is also attributed to a considerable decomposition of the CSH gel. Lagerblad (2005) suggests that a GGBS cement paste contains less $Ca(OH)_2$ and more CSH, which causes the slow release of Ca^{2+} from CSH to occur sooner as a result of a drop in the concentration of Ca^{2+} in the pore solution due to carbonation. Ca^{2+} diffusion is then slower, but the concentration of CO_3^{2-} remains the same. It can be presumed, therefore, that $CaCO_3$ precipitates close to CSH, affecting the CSH gel porosity rather than the capillary porosity. The coarser capillary pore system may also be a consequence of the different form of carbonation in slag concretes as more vaterite is formed than calcite. Furthermore, the CSH contains more aluminium and magnesium, which changes the carbonation process and the structure of the carbonated paste.

2.7.1.6 Models employed

Numerous models have been developed to understand the carbonation process in concrete, many of which were devised by assuming that the process is controlled by CO_2 diffusion through concrete and reaction hydrated cement products. CO_2 diffusion is examined using simple laws such as Fick's first law of diffusion (Equation 2.9) where J is a quantity of a component passing through unit area per unit time (in this case net transport of CO_2 and carbonate ions), $\delta c/\delta x$ is the concentration gradient (c is concentration, x is length), and D is the diffusion coefficient. The diffusion coefficient for CO_2 is difficult to measure as the carbonation process is slow and results in a change in the pore structure. The simplest model or relationship derived from this law assumes that the carbonation depth (X_c) is proportional to the square root of time (t) where k is the rate factor (Equation 2.10).

$$J = D\frac{\partial c}{\partial x} \qquad \textbf{Equation 2.9}$$

$$X_c = k\sqrt{t} \qquad \textbf{Equation 2.10}$$

Equation 2.10 assumes that carbonation penetration corresponds to CO_2 diffusion. The carbonation process, however, is more complex as it involves gas and liquid transport. This approximation is not rigorous because Fick's law assumes diffusion through a uniform homogeneous porous material and is not appropriate for any changes in properties over time or in the presence of chemical reactions (carbonation in this case). In practice, the law or variations of this law have been extensively applied to concrete (AI-Khaiat et al., 2004; Lagerblad, 2005; Memorandum, 2005; Khunthongkeaw et al., 2006; McPolin et al., 2007). k-rate factors have been determined for numerous concrete/environment combinations. k-rate factors suggested by Lagerblad (2005) for concrete surfaces with Portland cement range from 0.5 mm/√yr in wet/submerged concrete (> 35 MPa) to

15 mm/√yr in concrete indoors (< 15 MPa). Correction factors for binders are 1.1 for 20% GGBS replacement and 1.2 for 40%.

The analytical carbonation model developed by Papadakis et al. (1991b) is more comprehensive and can be extended to two and three dimensional geometry. It provides a theoretical basis for predicting k and incorporates some of the chemical reactions, calculating the carbonation depth by factoring in time, w/c ratio, aggregate-cement ratio, CO_2 atmospheric concentration, temperature, and humidity above 50%. Rezagholilou & Nikraz (2012) successfully applied their model to cement-treated base material for pavements.

2.7.2 Carbonation in stabilised peat

2.7.2.1 Process

Based on analogies with carbonation in concrete, stabilised peat is also susceptible to carbonation as CO_2 and water are present in almost every environment. A carbonation process for stabilised peat is postulated in this section, and Figure 2.19 is a schematic of the process. Carbonation in stabilised peat is likely to comprise a more intricate gas diffusion process than in concrete, involving diffusion from a carbonated surface to freshly stabilised peat (C), not only by atmospheric CO_2 (A) but also by CO_2 released by peat oxidation (B). It is unknown whether stabilised peat is a net source or sink of CO_2 (D).

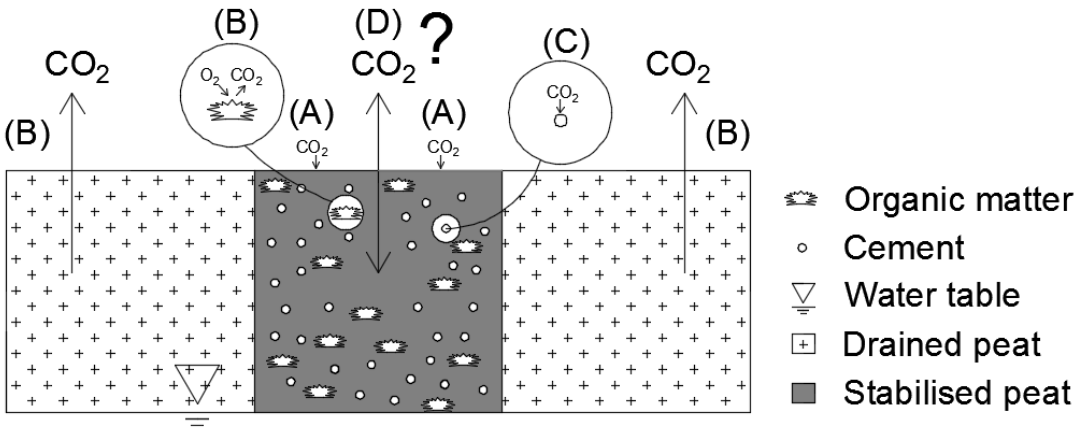

Figure 2.19 - Schematic of gas diffusion process in stabilised peat

In stabilised peat, dead plant and animal decomposition occurs rapidly in the aerobic layer (above the water table) where organic compounds ($C_xH_xO_x$) are oxidised, releasing CO_2 (Lindsay, 2010) (Equation 2.11). Decay also takes place at a lesser rate in the anaerobic layer (under the water table) where CH_4 is produced. CH_4 may then diffuse into the aerobic

layer where it comes into contact with oxygen (O_2), producing further CO_2 and water (Couwenberg, 2009) (Equation 2.12).

$$C_xH_xO_x+O_2 \rightarrow CO_2+H_2O$$ **Equation 2.11**

$$CH_4+O_2 \rightarrow CO_2+H_2O$$ **Equation 2.12**

Carbonation may occur in the aqueous phase, either at the stabilised peat surface that is exposed to precipitation or anywhere in the stabilised mass where groundwater is present. It is highly probable that the majority of the stabilised block will be submerged under the water table. Most of the factors affecting carbonation cited in Sections 2.7.1.4 and 2.7.1.5 are also relevant to stabilised peat; however, instead of concrete quality, the amount/type of binder and the gas diffusion coefficient of peat are influential. The higher the porosity of the peat, the greater its gas diffusion coefficient, hence the greater the carbonation rate if other variables remain constant. Peat decomposition seems to increase soil gas diffusivity (Iiyama & Hasegawa, 2010); therefore, in stabilised peat the CO_2 concentration and the carbonation rate are increased in the aerobic layer (Appelo & Postmas, 1993). In organic soils, Appelo & Postmas (1993) suggested that organic matter decomposition can increase the CO_2 concentration up to 50000 ppm. It must be remembered that the rate of peat decomposition will also increase with higher temperatures (Nayak et al., 2008).

The pH of the stabilised peat after mixing is likely to increase due to the high alkalinity of the cement paste. As the stabilised peat ages and more $CaCO_3$ is produced, the pH of the peat drops as carbonation neutralises the cement. Microbial activity in peatlands is retarded by high acidity and is apparent when examining a nutrient-rich fen peat and an acid fen peat, the former is alkaline and more likely to decompose (Hobbs, 1986). Similarly, with stabilised peat, a high pH may lead to a higher decomposition rate and hence a higher carbonation rate. The dry soil-mixing process breaks down organic matter to some degree and may also lead to an increase in peat decomposition. Furthermore, the rise in temperature due to hydraulic reactions in the stabilised peat may lead to increased peat decomposition for a time.

2.7.2.2 CO_2, Ca and O_2 diffusion

In concrete, carbonation is a reaction whereby CO_2 or carbonate ions must pass through a carbonated surface into the material to reach fresh concrete. It is a diffusion process either by CO_2 or by carbonate ions, which in turn is controlled by the water saturation of the capillary system. In stabilised peat, O_2 to oxidise the peat and CO_2 must diffuse through a

carbonated surface to reach fresh stabilised peat. The carbonation rate will decelerate over time as O_2 and CO_2 must pass through an ever-thickening carbonated layer as well as a potentially high water table. CO_2 released from the peat may also have to diffuse through some of the stabilised peat to react with calcium ions.

Houst (1996) proved that the diffusivity of CO_2 is always lower than that of O_2 (Figure 2.20), suggesting that peat oxidation may occur before CO_2 from the atmosphere diffuses to the same level, which is significant in carbonation. The process of passing through already carbonated stabilised peat whose connectivity porosity has changed is even more complex than in concrete as CO_2 is released from peat in the presence of O_2. Consequently, the effect of decomposition on the connective porosity is as important as the altering properties of the cement paste in the stabilised peat.

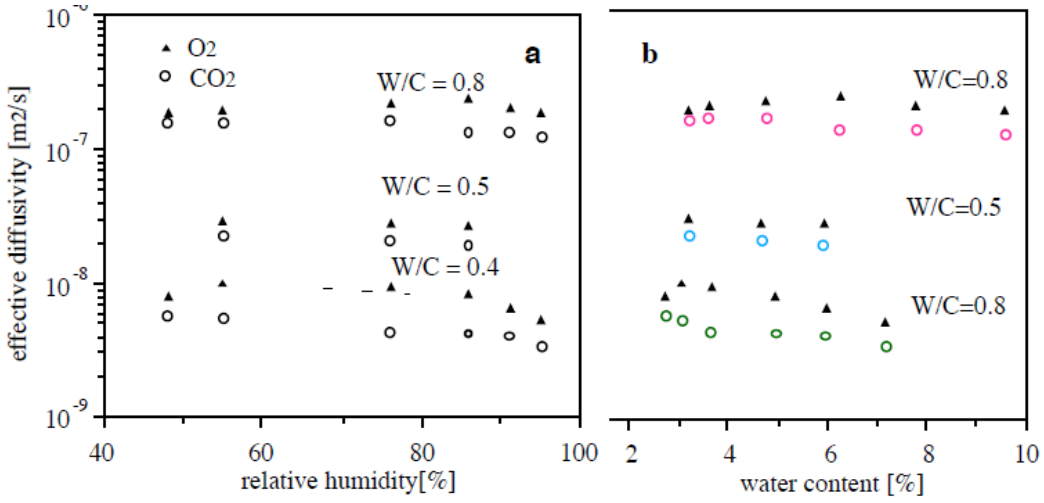

..

Figure 2.20 - Effective diffusivity of carbonated hydrated cement paste versus: (a) relative humidity and (b) water content: W/C is given as a parameter (Houst, 1996)

The availability of CO_2 released from the peat is limited as the capillary system may be blocked with water, and CO_2 and O_2 will encounter difficulty diffusing into the cement. Stabilised peat submerged in water carbonates more slowly as diffusion in a liquid is about 10,000 times slower than in air (Houst, 1996). The carbonation speed, therefore, depends on the humidity in the stabilised peat. In saturated stabilised peat, only carbonate ions can move, making carbonation slow, whereas in dry stabilised peat the CO_2 can penetrate deeply, but there is not enough water for the carbonation reaction. In essence, there is an optimum relative humidity where the speed of carbonation is at a maximum. Papadakis et al. (1991a) showed that where the humidity in concrete was above 50% there was a sharp carbonation front, a likely scenario for stabilised peat due its high moisture content.

When the concentration of carbonate ions and Ca^{2+} are low in the pore solution, the carbonation rate is controlled to a large extent by outward diffusion of Ca^{2+} from the

interior of the stabilised peat to the carbonation front, otherwise known as leaching, a process sometimes found in concrete if the internal humidity is high enough (Lagerblad, 2001). Initially, when the diffusion speed of the Ca^{2+} is high, $CaCO_3$ precipitates at the surface; but when the diffusion speed of Ca^{2+} decreases over time, calcite will precipitate in the stabilised peat, causing it to become dense and to strengthen.

The decelerating carbonation rate is related to a volume increase associated with the transformation of $Ca(OH)_2$ to crystallographic forms such as calcite ($CaCO_3$) (Equation 2.8). This in turn fills empty pore space, densifying and strengthening the stabilised peat. The cement paste over time will revert to its basic components in cement production (carbonate minerals form rock types such as limestone). It can be concluded, therefore, that stabilised peat carbonates; and while the duration of the process is unknown, it may be within the structure's lifecycle that it supports.

2.7.2.3 Binder-soil reactions in peat

In addition to lime and cement, the traditional binders, many cementitious and pozzolanic binders are currently used in soil stabilisation. These include various cements, gypsum, latent hydraulic admixtures such as GGBS, pozzolanic admixtures such as PFA, and silica fume, and even inert fillers such as silica sand, limestone, and geosynthetic fibres. Several authors such as Timoney et al. (2012) have examined the use of each binder for stabilising peat and concur that cement and cement-GGBS combinations produce the greatest strengths. This thesis, therefore, focuses on these binders and are the subject of this section.

Latent hydraulic materials have to be activated with $Ca(OH)_2$ to react as they contain large amounts of pozzolanic materials (siliceous or aluminous materials), which require the availability of $Ca(OH)_2$ throughout the reaction. The reactivity of cement, latent hydraulic and pozzolanic materials depend, among other factors, on the ratio of calcium oxide to silicon dioxide, $CaO{:}SiO_2$. The larger this ratio is, the more hydraulic the material (EuroSoilStab, 2002). A hydraulic binder like cement can react with water, but a non-hydraulic binder requires a catalyst to start curing (Allu, 2007).

Ordinary Portland cement (OPC)

Cement is manufactured by combining cement clinker with gypsum. Unlike lime, cement contains a lot of SiO_2 and primarily forms CSH gel upon hydration. The reactions that create CSH involve minerals contained in the binder itself and are, generally, more rapid than pozzolanic reactions with the soil (Åhnberg, 2006). Similar to hydration processes in concrete explained in Section 2.7.1.1, dry cement reacts with the water in the pore solution in the organic soil to form mostly CSH and some $Ca(OH)_2$ (Kazemian et al., 2011; Janz &

Johansson, 2002). The CSH binds the soil particles and become denser and stronger over time. The $Ca(OH)_2$ may react with minerals in the soil, contributing to an increase in long-term strength by forming calcium aluminate silicate hydrate (CASH) and CSH/calcium aluminate hydrate (CAH). Other products of cement reaction that may contribute to a strength increase but to a lesser degree are various aluminate ferrite tri phases (Aft/AFm) (Åhnberg, 2006). Since the hydraulic reaction happens much faster than the pozzolanic reaction, cement-stabilised soil normally attains high strength in the first few months (Axelsson et al., 2002).

GGBS and cement-GGBS combinations

GGBS, a latent hydraulic cement, is a by-product of the steel industry and contains a ratio of CaO to SiO_2 significantly lower than cement, as illustrated in Figure 2.21, which shows high CaO binders such as lime and cement in the lower left of the triangle. Higher up and further to the right in the triangle shows materials like GGBS with less CaO content and more SiO_2. Consequently, the build-up of reaction products in GGBS is normally slower than in cement, but the products formed are similar (Axelsson et al., 2002; Åhnberg, 2006). The chemical composition of GGBS includes a higher amount of C_2S and less C_3S than cement, the former usually generating a higher long-term strength following hydration (Åhnberg, 2006). Initial strengths can be lower than mixes using other binders, but long-term strengths (years) can be significant. This is due to the low temperatures generated, resulting in slow strength gains, with changes in the temperature of the soil mass affecting the rate of reactions (Timoney et al., 2011). GGBS contains some lime but produces only low quantities of $Ca(OH)_2$ and so requires activation by some form of alkali, normally cement or lime. A stabilised peat in Timoney et al. (2012) containing 85% GGBS showed that lack of activation can result in poor strength gains.

As well as achieving substantial cost savings, cement and GGBS combinations are used in stabilising peat to provide greater strength improvements for organic soils than cement alone as shown by Timoney et al. (2011) and Axelsson et al. (2002). When GGBS is mixed with cement in peat, the slag containing silica, alumina and reactive lime is activated, accelerating the chemical reactions and improving the stabilisation effect (Åhnberg, 2006; EuroSoilStab, 2002; Axelsson et al., 2002).

In stabilised peat whose binder type is solely cement, cement reactions can be retarded due to insufficient silica (SiO_2) and alumina (Al_2O_3) in the peat that would otherwise react with the $Ca(OH)_2$ generated from cement hydration to form secondary calcium silicates and aluminates, which are responsible for the long-term strength of the stabilised peat. These are provided, however, by pozzolanic minerals contained in the latent hydraulic and

pozzolanic additives like GGBS which can form strength-enhancing products with $CaOH_2$ (Axelsson et al., 2002).

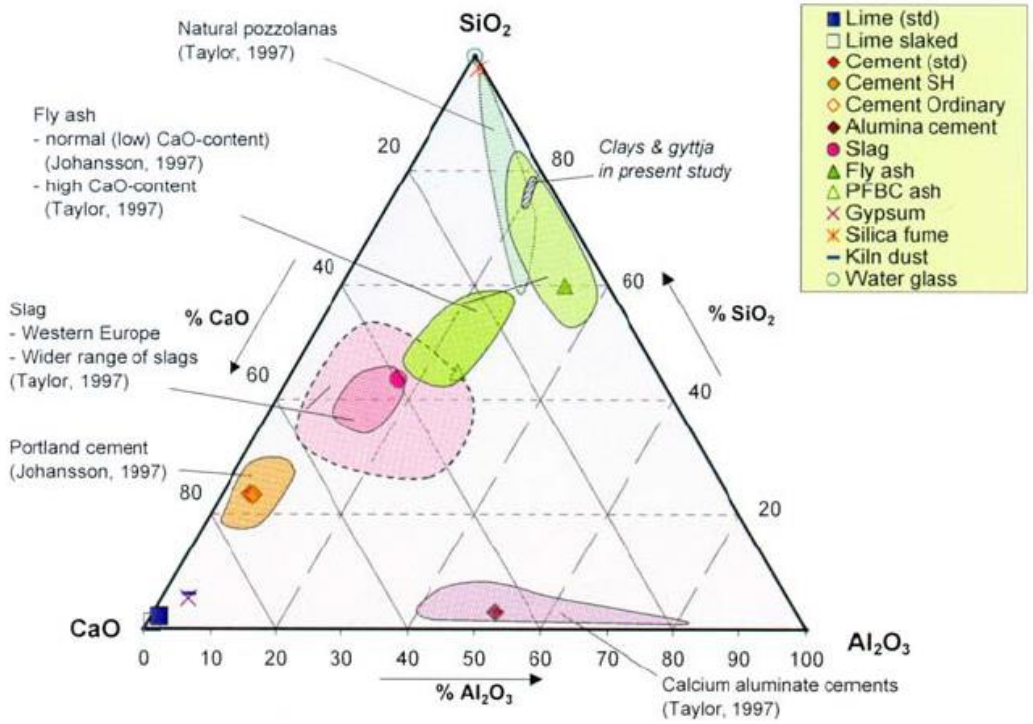

Figure 2.21 - Relative percentages of CaO, SiO_2 and Al_2O_3 in the materials used in the field (see legend) (Åhnberg, 2006)

Binder threshold

Organic soils such as peat require greater binder content than inorganic soils for stabilisation and to achieve the requisite strength. The low pH and humic acid in peat interferes with the hydration process and the reactions required for strength development as the acid tends to react with calcium that is free from cement hydrolysis to form insoluble products that coat the soil particles, preventing them from binding properly and delaying calcium crystallization, which is responsible for the strength increase in stabilised peat (Ali et al., 2010; Chen & Wang, 2006; Timoney et al., 2012; Axelsson et al., 2002). Tremblay et al. (2002) found strong acids in stabilised cement soil prevented the pore water from reaching a sufficiently high pH to allow strength development. $Ca(OH)_2$ reacts with humic acids to form insoluble products, leaving only part of the calcium released during hydration for the pozzolanic reaction, and this is believed to be the reason for the difficulty encountered in stabilising organic soils (Hebib & Farrell, 2003). Work quoted in Stevenson (1994) shows that maximum binding capacity of the humic acids increases with humification of the organic matter. This finding corresponds to studies undertaken by Hebib & Farrell (2003), Huttunen & Kujala (1996) and Timoney et al. (2011), who reported that the strength achieved by stabilisation for a given binder type and content weakened with increasing humification in all types of peats tested.

Axelsson et al., (2002) concluded that a binder threshold exists below which no strengthening occurs. Once this threshold is passed, there is enough binder to produce a pH increase, neutralising the acids present (Timoney et al., 2011; Axelsson et al., 2002). Hebib & Farrell (2003) inspected stabilised peat samples under an electron microscope and observed that there was no interaction between the hydrated cementation products and the organic matter under a threshold, which was found to be 150 kg/m^3 for two Irish peats. The stabilised peat experiments conducted in this research, therefore, have a minimum binder content of 150 kg/m^3.

2.7.2.4 Modelling carbonation in stabilised peat

The basic and more comprehensive calculations described in Section 2.7.1.6 could be used for stabilised peat to provide estimates of the carbonation rate but do not, however, allow for the CO_2 released from peat. The application of the basic model in Equation 2.9 may be a good starting point, calculating k-rate factors for stabilised peat for various scenarios and examining variables such as binder type, location and climate. By choosing the binder type and content, the climate and the peatland type, it may be possible to get a good estimate of the rate of CO_2 uptake for EC calculations. Subsequently, a theoretical basis for k-rate factors could be developed from further experiments.

The need to understand and model the carbonation process in stabilised peat is vital. From this study, the identification of the carbonation front will help estimate CO_2 intake. Identifying the depth of the carbonated zone will show the depth at which properties of the stabilised peat have been altered, which is important in modelling and design. Though properties of carbonated stabilised peat have not been examined to date, research on cement-stabilised contaminated soil has confirmed that hydration reactions are acclerated when waste is exposed to high CO_2 conentrations, and geotechnical properties enhanced by carbonation include an increase in stiffness, compressive strength, impermeability and density as well as a decrease in porosity (Lange et al., 1996) (Fernández Bertos et al., 2004). For clayey soil stabilised with olvine sand and exposed to carbonation, a stronger and stiffer matrix was found than in the uncarbonated stabilised soil (Fasihnikoutalab et al., 2016). In addition to benefiting the environment through the sequestration of CO_2, carbonation may also strengthen the stabilised peat.

2.7.2.5 Carbonation potential of binders and organic content of peat

Binders with varying levels of cement, lime, GGBS and PFA all have varying carbonation potentials and rates. The carbonation potential (C_p) of a cement binder can be estimated by assuming that it is equal to half the EC of cement (Engelson et al. 2005) as shown in

Equation 2.13 where, in this instance, M is the mass of cement and ECI is the EC intensity measured in kg CO_2/kg.

$$C_p = 0.5 \times M \times ECI$$ **Equation 2.13**

A better estimation of C_p or CO_2 uptake of a cement binder can be performed by using an equation developed by (Lagerblad, 2005) (Equation 2.14), where 0.75 is the proportion of CaO carbonated, Cem is the amount of Portland cement in the stabilised peat (kg/m^3), CaO is the amount of CaO in the cement (%), M_{CO2} is the molar weight of CO_2 and M_{CaO} is the molar weight of CaO. Engelson et al. (2005) and Lagerblad (2005) assumed that 75% of the calcium oxide (CaO) in the Portland clinker undergoes carbonation, taking into account that all the CaO in the $Ca(OH)_2$, Aft and AFm are transformed into $CaCO_3$ and that half of the CaO in the CSH is transformed into $CaCO_3$ (Section 2.7.1.3). It also assumes that all remaining unhydrated cement grains have reacted and are carbonated. The basis for the CSH assumption is that the ratio CaO/SiO_2 in uncarbonated concrete cement pastes is between 1.6 and 2.0 (Shui et al., 2015), while in a carbonated state, this ratio is halved and is between 0.8 (Bary & Sellier, 2004) and 1.0 (Stronach & Glasser, 1997). These assumptions are also based on work done by Taylor (1997) who found that in cement paste with 65.3 weight % CaO, 31.4 weight % is bound to CSH. CSH makes up around 60% of the cement hydration products, while the other 40% is attributed to $Ca(OH)_2$ and Aft and AFm.

$$C_p = 0.75 \times Cem \times CaO \times \frac{M_{CO_2}}{M_{CaO}}$$ **Equation 2.14**

Equation 2.14 can be applied to other binders but may not be as accurate because the amount of $Ca(OH)_2$ and the composition of the CSH depend on the amount of pozzolans. For example, in concrete with GGBS, the CaO/SiO_2 ratio will be lower, and there will be relatively more CSH in the cement paste and thus relatively more Ca in the remaining silica gel. Typical CaO values for binders are displayed in Table 2.6, and the average values are used to plot Figure 2.22, which shows a graph of C_p (from Equation 2.14) against binder content for various binders. For the CaO content values for cement and GGBS, figures from an Irish company are used that give the average CaO content for cement and GGBS they produce as 65% and 40% respectively (Ecocem, 2015).

Table 2.6 - Typical CaO contents of several binders

Binder	CaO content (%)			References
	Max.	Min.	Average	
Portland Cement	66	60	63	Kosmatka et al. (2002)
Hydrated lime	74	72	73	AWWA (2011)
GGBS	42	30	36	GGBS Review Group (2009)
Class F PFA	5	1	3	Sear & Coombs, (2001), GGBS Review Group (2009)

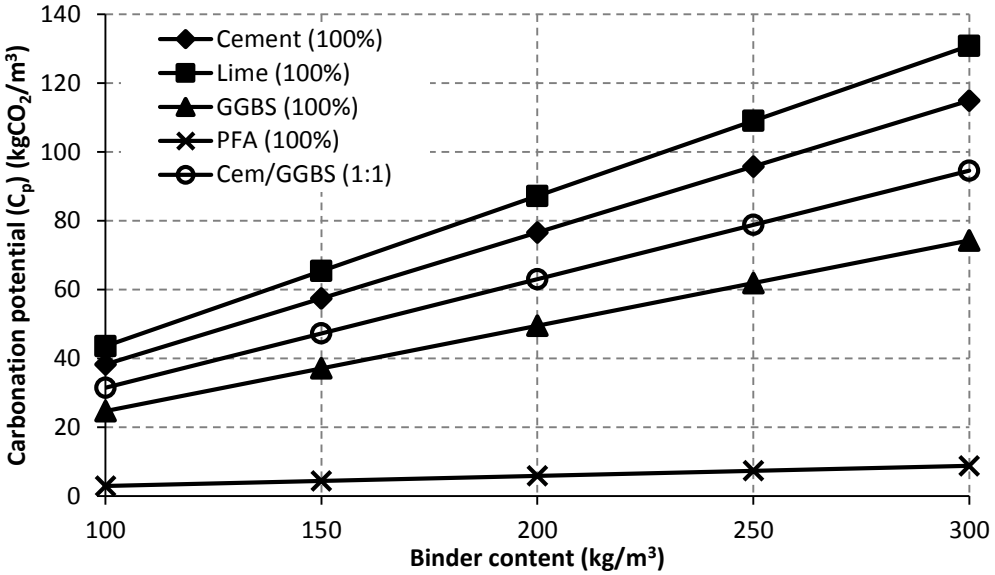

Figure 2.22 - Graph of binder content versus carbonation potential for several binders

The binders have the potential to take up some of the peat's carbon as described in Section 2.7.2.1; therefore, to calculate how much the C_p values of the binders offset the carbon in peat, methods to calculate this carbon are described. The organic content of the peat is important as the higher the organic content, the higher the potential for loss of carbon as CO_2. The carbon content in peat can be measured directly by elemental analysis or a combination of acidification and dry combustion (Chambers, et al., 2011). However, it is more practicable to estimate the carbon content indirectly using its dry density and the relationship between organic matter and carbon content. In the absence of organic content values, the SNH (2000) proposed that the carbon content of peat may be estimated at between 49% and 62% of its dry weight. Using this method, the carbon content of peat with a typical dry density value of 0.1 g/cm^3 lies between 0.18 and 0.23 t CO_2eq/m^3. However, it is preferable to quantify the organic content of the peat by the loss-on-ignition method (ASTM, 2007). Schumacher (2002) suggests finding carbon content by dividing the organic content values by a factor, which has been derived by experiment and ranges between 1.724 (representing 58% carbon) and 2.5 (representing 40% carbon). In general, the range of organic contents found in peat soils is greater than the range of carbon contents found in the organic matter, thereby justifying the latter approach (Schumacher, 2002).

The graph below was plotted using Equation 2.14 for C_p and assuming the peat has a dry density of 0.1 g/cm^3 and carbon content of 50% of its dry weight.

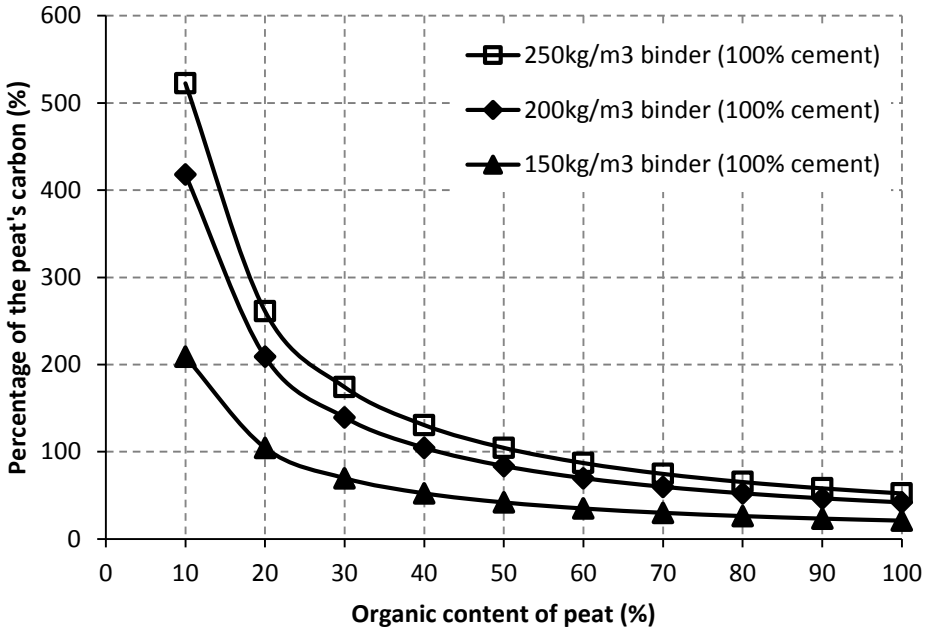

Figure 2.23 - Organic content of peat versus the percentage of the peat's carbon contained in the binder's carbonation potential

2.8 Closed chamber method

2.8.1 Introduction

Soil cover methods are employed extensively to estimate CO_2, CH_4 and N_2O fluxes from peatlands, grasslands, crops, ponds, woodlands and other land types. An example of a soil cover method is the closed chamber method, which has been applied in studies by Wagner et al. (1997), Wilson et al. (2009); Tuittila et al. (2000), Glatzel et al. (2008) and Koehler et al. (2011).

A collar constructed of non-reactive materials such as stainless steel, aluminium or polypropylene is inserted into the ground on the target area of interest prior to the start of the study (Figure 2.24(a)) (Parkin and Venterea, 2010). A chamber acting as a lid is placed over the collar during gas sampling. On top of the collar, a small channel is filled with water to provide an airtight seal between the collar and the chamber during gas measurements. Typical chambers will have two holes, one for a vent and the other for a sampling port, which is used for taking gas samples (Figure 2.24(b)).

Gas samples are retrieved over a short period of time to analyse the gas flux. A flux can be defined as the rate of flow of a property per unit area which has the dimensions: $[\text{quantity}][\text{time}]^{-1}[\text{area}]^{-1}$.

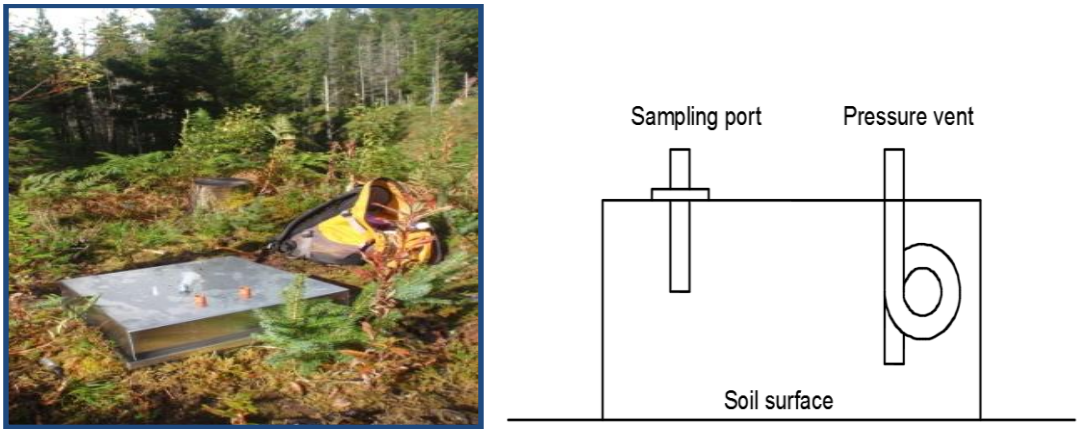

Figure 2.24 - Closed chambers (a) photograph (left) and (b) schematic diagram (right)

The closed chamber method is also employed in the laboratory where soil cores are extracted from site and placed in columns with the base capped (Moore & Dalva, 1993; Regina, et al., 1999; Jansen, 2008). The advantage of this scenario is that environmental conditions can be regulated. During a gas sampling event, a removable bung with two holes, a vent and a sampling port, is placed on the column through which headspace air can be sampled. This laboratory version of the closed chamber method is applied in this thesis to investigate how binder type and content and environmental conditions affect the CO_2 gas flux and carbonation process in stabilised peat.

2.8.2 CO_2 and CH_4 flux

2.8.2.1 Linear regression methods

Using a closed chamber method, gas fluxes are calculated by examining the rate of change in the gas concentration of interest in the chamber headspace (Parkin & Venterea, 2010). If this rate is constant, the slope of the regression line ($\partial C_a/\partial t$) over the chamber deployment time can be used to calculate the flux f(t) where h is the effective chamber height, C_a is the gas concentration in the chamber and t is time (Equation 2.15).

$$f(t) = h\frac{\partial C_a}{\partial t}$$ **Equation 2.15**

The slope ($\partial C_a/\partial t$) is calculated as $(C_f - C_i)/t$ where C_f and C_i (% of air) are the final and initial gas concentrations respectively and t is the chamber deployment time t (hr). By multiplying the rate or slope by $V\rho/A$, where V is the chamber volume (m^3), ρ is the density of the trace gas (kg/m^3) and A is the area (m^2), the flux (f) is obtained in units of mg $CO_2/m^2/hr$ as shown in Equation 2.16.

$$f = 10^6 \times \frac{\rho V(C_f - C_i)}{At}$$ **Equation 2.16**

However, the rate of change in gas concentration may not be constant, hence linear regression may be unsuitable and may underestimate the true flux. In work by Matthias et al. (1978), linear regression underestimated curvilinear data by about 55%. Livingston et al. (2005) suggests that the application of a linear model to this non-linear diffusion process ensures that the exchange rate in most applications is often substantially underestimated. Even when a plot of gas concentration versus time is of high linearity $R^2 = 0.99$, it may still underestimate the flux according to Nakanoa et al. (2004). Their results suggest that linearity by itself should not be regarded as an indicator of measurement accuracy, though it is widely accepted that linearity of the rate of change of gas concentration over time is desirable. Nevertheless, in recent studies, linear regression is used continually for calculating gas fluxes (Forbrich et al., 2010; Alm et al., 2007; Saarnio et al., 1997). By keeping the chamber deployment time brief to minimise error and by assuming the concentration change over time to be in the linear range, the linear regression approach has been justified (Kutzbach et al., 2007). In some instances, a linear model may be better than a non-linear model; for example, in Forbrich et al. (2010), a linear model provided a better fit to the data than an exponential model.

2.8.2.2 Non-linear regression methods

Non-linear regression methods exist that are based on diffusion theory and may be more appropriate than linear regression. The steady flux of gas is described by Fick's law of diffusion in Equation 2.10. Across the soil-atmosphere interface, the exchange rate of a trace gas is generally a function of its diffusion coefficient and the concentration gradient between the depth at which the gases are emitted or consumed and the earth surface. However, natural gas fluxes are disturbed during closed-chamber deployment as the concentration gradient immediately changes and continues to worsen the longer the chamber is deployed (Nakanoa, et al., 2004). A linear model assumes the rate of gas exchange is constant across the soil-atmosphere boundary, but diffusion theory predicts that this is not constant as the rate of gas exchange continuously declines as the soil concentration changes and the driving force for diffusion decreases.

An overview of the methods developed to estimate fluxes more accurately for closed chamber methods over time is given in Table 2.7. To account for diffusion theory and the curvilinear shape due to the build-up of the gas in question in the chamber, Matthias et al. (1978) devised an exponential model based on one-dimensional diffusion theory that required continuous data measurement and was an iterative process to calculate a flux. Subsequently, Hutchinson & Mosier (1981) proposed a non-linear regression model (the

HM method) a special case of the exponential method, which is again based on one-dimensional diffusion theory and requires three equally spaced points (Equation 2.17).

$$f = \frac{(C_2 - C_1)^2}{0.5t \times (2 \times C_2 - C_3 - C_1)} \times \ln\left(\frac{C_2 - C_1}{C_3 - C_2}\right) \times \frac{V\rho}{A}$$ **Equation 2.17**

C_1, C_2 and C_3 are the chamber headspace gas concentrations at times 0, 0.5t and t respectively. This is, however, highly sensitive to random variations in the trace gas concentrations, in particular if the condition $(C_2\text{-}C_1)/(C_3\text{-}C_2) > 1$ is not reached, the flux cannot be estimated. Anthony et al. (1995) reported a 45% failure rate when the method was applied 2,224 times.

Table 2.7 - Methods that been used to evaluate the gas flux for the closed chamber method

Method	Fit	Advantage	Disadvantage
Linear regression	• Linear	• Accommodates measurement variability	• Underestimates flux • Depends if change in gas concentration is constant
Matthias (1978)	• 1st exponential method	• Good for bare soils • Based on simplified diffusion theory	• Requires continuous data measurement • Iterative process to find some parameters
Hutchinson and Mosier (1981) (HM method)	• Special case of exponential model	• Based on diffusion theory • For curvilinear data • Requires three equally spaced points	• Assumes steady state conditions • Highly sensitive to random fluctuations in concentration measurements
Wagner et al. (1997) (Quad)	• Form of quadratic determined empirically	• Accounts for non-linear disturbances by the chamber deployment	• Not based on physiology and diffusion physics
(Pedersen, 2000) (H-M-P model)	• Stochastic diffusion model, extension of HM method	• Does not require equi-spaced data points and can accommodate more than three data points	• Continuous measurement needed
Livingston et al. (2005) (NDFE model)	• Non-steady-state diffusive flux estimator • Physically-based time dependent diffusion model	• Three-parameter model estimated by iteratively fitting equation (most advanced method)	• Need soil gas diffusion coefficient and the soil's air filled porosity • Restricted to gas sources in bare soils
Pederson et al 2010 (HMR model)	• Modification of the HM method	• Can account for three or more points • Accounts for horizontal gas transport • Includes methods for analysis of linear data	• More studies are required to see if this method is robust

Wagner et al. (1997) proposed a quadratic model, which extended the linear model to account for non-linear disturbances by the chamber deployment but is not based on diffusion physics. Even with a short closure time of 60 seconds, they proved that fluxes derived from quadratic regression were 10% to 40% greater than those calculated with linear regression.

Pedersen (2000) devised a stochastic diffusion method that is an extension of the HM method, does not require equi-spaced data points, and can accommodate more than three data points. Livingston et al. (2005) introduced the non-steady-state diffusive flux estimator (NDFE) function, which is derived from time-dependent diffusion theory and can be fitted by non-linear regression to gas concentration over time data from closed chamber experiments. However, the air-filled porosity and diffusion coefficient of the soil are required inputs. They demonstrated for numerical model simulations that only the NDFE model was able to accurately determine the natural gas fluxes whereas quadratic and exponential regression still underestimated them. The NDFE model, though, is restricted to gas sources in bare soils whereas vegetation and gas sinks are not considered. The most recent method by Pedersen et al. (2010) accounts for horizontal gas diffusion and/or chamber leaks.

With seemingly linear trace-gas accumulation or depletion, non-linear models are often over-parameterised so linear regression is applied. Furthermore, non-linear models may not take proper account of random variation in concentration data and, consequently, may estimate a large flux from sites with little or no gas flux. Procedures are needed to identify such data sets and treat them appropriately. Adopting a linear regression approach offers many advantages according to Anthony et al. (1995), including the accommodation of measurement variability and facilitation of goodness of fit testing to the observed exchange rate (Livingston & Hutchinson, 1995).

2.9 Determining the depth and level of carbonation in concrete

2.9.1 Introduction

In addition to examining the carbonation process in stabilised peat by way of CO_2 gas flux calculation, the depth of carbonation reveals the speed of the carbonation process. Experimental methods have been used to determine the depth of the carbonation front in reinforced concrete, among which is the phenolphthalein indicator method, the traditional and quickest method. New techniques including XRD, FTIR, TGA and the pH of slurries technique produce better estimates of true carbonation depth, and a review of these methods is discussed in the following sections, with a view to applying them to help identify the carbonation front in stabilised peat.

2.9.2 Phenolphthalein indicator

The phenolphthalein indicator technique is a well-established and extensively used means of determining carbonation depth in concrete (Chang & Chen, 2006; Parrott & Killoh, 1989; Torgal et al., 2012; AI-Khaiat et al., 2004; Lo & Lee, 2002). This method enables the reduction of the pH value as a result of carbonation in concrete to be visually examined

by colour change. Normally, a concrete specimen is split along its vertical axis, and the indicator is sprayed on the surface of the split specimen. It turns purple when the pH of the specimen is greater than 9 (uncarbonated zone) and remains colourless when the pH is below 9 (carbonated zone), as in the example in Figure 2.25. In the carbonated zone, Chang & Chen (2006) believed the carbonation degree to be greater than 50%. A pink region may sometimes be identifiable and represents partially carbonated concrete.

The phenolphthalein indicator method is a useful technique because it shows the carbonation front visually, but it has several disadvantages as it works by pH only. Carbonation occurs below the colourless region as the partially carbonated zone may have a pH in the pore solution of between 9 and 12.5 (Lo & Lee, 2002), which is not shown by the indicator (Herrera, 2011). Underestimating the carbonation depth can overestimate the lifespan of reinforced concrete structures. Furthermore, the indicator may not recognise carbonation depth in concrete with non-cementitious materials that have a pH of less than 9, hence the limitation of this indicator.

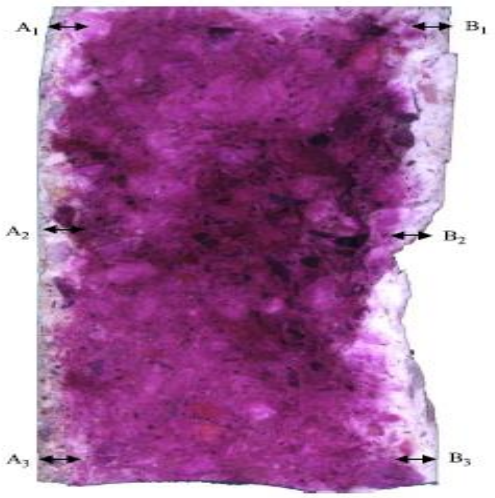

Figure 2.25 - Cross-section of a split concrete cylinder specimen after application of phenolphthalein indicator (Chang & Chen, 2006)

2.9.3 X-ray diffraction analysis (XRD)

X-ray powder diffraction analysis has been extensively used to classify cement and concrete by analysing the considerable number of crystals in a powder sample and identifying their atomic and molecular structure. It works by sending an X-ray beam to the sample, causing the beam to diffract into many specific directions due to the different lattice planes of atoms. For each possible diffraction angle θ, a lattice plane can be detected when the X-ray source, the sample and the detector are correctly oriented for Bragg diffraction, thereby producing a diffraction peak as shown in Figure 2.26 (Klug & Alexander, 1974). Based on Bragg's Law, where d is the distance between the lattice

planes, diffraction occurs only when the distance travelled by parallel X-rays are an integer (n) multiple of the wavelength (λ), causing constructive interference (Equation 2.18).

$$n\lambda = 2d\sin\theta$$ **Equation 2.18**

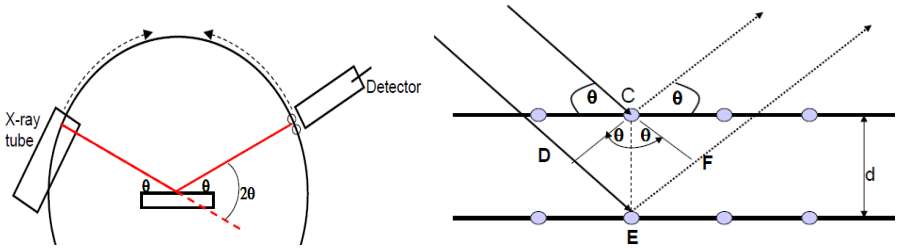

Figure 2.26 - (a) Diffraction of X-rays in powder diffractometer (Speakman, n.d.) (left) (b) X-rays diffracting off two lattice planes (Speakman, n.d.) (right)

Using X-rays of a fixed wavelength and rotating the sample so that the angle of diffraction changes, data are collected. By measuring the angles (2θ) and intensities of recorded peaks, the crystals present and their intensity in the sample are revealed. Graphs of 2θ (on the x-axis) against intensity (on the y-axis) are obtained, as exemplified in Figure 2.27, where calcite is identified by a peak at 29.4° and portlandite ($Ca(OH)_2$) at 18.04° and 34.07°. The mineralogy database (Barthelmy, 2014) and databases developed by the International Centre for Diffraction Data (ICDD) contain many powder diffraction patterns to help XRD users identify phases and minerals. A guide written by Stutzman (1996) on X-ray analysis of Portland cement and clinker as well as the mineralogy database have been used to draw up Table 2.8.

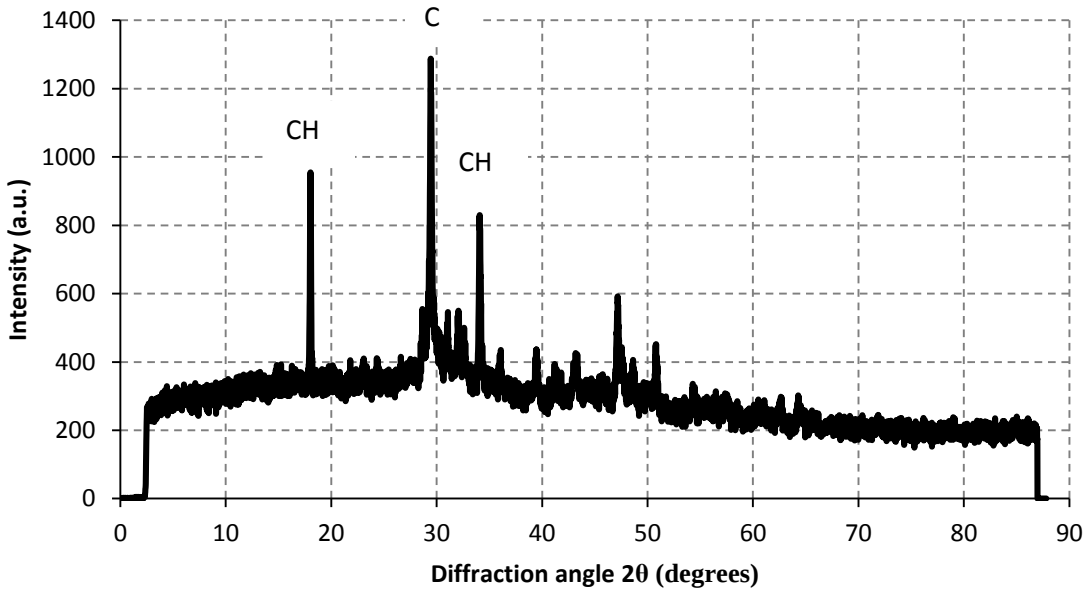

Figure 2.27 - Typical XRD graph of stabilised peat (C = calcite, CH = portlandite)

Table 2.8 - Some typical phases identified in cement at various diffraction angles using XRD (Stutzman, 1996; Barthelmy, 2014)

Minerals	XRD diffraction angles (2θ)			
Calcite	29.41	39.4	43.15	47.49
Vaterite	24.9	27.05	32.78	50.08
Aragonite	26.21	33.13	45.86	27.22
Calcium hydroxide	18.09	28.66	34.09	47.12
Ettringite	9.16	15.87	27.77	
Tobermorite (C-S-H)	6.31	23.99	29.75	
C_3S (Alite)	29.37	32.22	34.36	51.72
C_2S (Belite)	32.14	32.05	34.33	41.21
Tricalcium aluminate (C_3A)	33.17	47.63	59.27	21.76
Ferrite (C_4AF) (Calcium aluminoferrite)	12.1	24.4	33.9	44.34
Gypsum (calcium sulphate dihydrate)	11.59	20.72	29.11	31.1
Free lime (CaO)	32.2	37.35	53.86	64.15

By examining the peak positions and intensities, some authors have used XRD to investigate carbonation in concrete and even to calculate its carbonation depth in qualitative and semi-quantitative manners. Sauman (1971) used it to examine carbonation of porous concrete and CSH and investigated the types of $CaCO_3$ (aragonite, vaterite and calcite) and their intensities, which were formed at different humidities and CO_2 concentrations. Matsushita et al. (2000) identified carbonation in concrete over time by increased peaks for calcite and vaterite and decreased peaks for tobermorite (a type of CSH mineral). Similarly, Slegers & Rouxhet (1976) investigated the products obtained after hydration of C_3S over time and showed with XRD that portlandite decreased and aragonite and vaterite increased. Ševula et al. (1994) examined the hydration products of cement, GGBS and cement/GGBS pastes, and after one year identified portlandite, calcite, ettringite and CSH phases. These phases are easier to identify in cement than GGBS because cement mineralogy is crystalline and GGBS amorphous (Axelsson et al., 2002).

By examining the intensity distribution of $Ca(OH)_2$ and $CaCO_3$ in XRD, Fukushima et al. (1998) and Chang & Chen (2006) found the depth of the carbonation front in concrete to be twice that of the phenolphthalein indicator. By analysing powder samples extracted at 5 mm intervals from the specimen surface, Chang & Chen (2006) plotted the relative intensities (%) of $Ca(OH)_2$ and $CaCO_3$ with depth and took the carbonation front depth from where the intensity distribution approached the horizontal. Their method is applied later to stabilised peat and is discussed in Section 3.5.4.4. The front can be either visually identified by examining the XRD graph changes in $Ca(OH)_2$ and $CaCO_3$ with depth or by using an analysis method such as the one used by Chang & Chen (2006).

2.9.4 Fourier transform infrared spectroscopy (FTIR)

Fourier transform infrared spectroscopy (FTIR) is a powerful tool for finding the structure of the functional groups that build up molecules in a sample and hence has been used to identify these groups and levels of carbonation in concrete and cement. It works by passing infrared (IR) light through a powder sample, with each functional group in the sample resonating to its characteristic absorption frequencies in the infrared region of the electromagnetic spectrum (Lo & Lee, 2002). IR light intensity decreases with the absorption or transmittance of a functional group, with transmittance (T) representing the ratio of IR light intensity before (I_0) and after (I) passing through the sample as in Equation 2.19. Graphs of T (%) against wavenumber (cm^{-1}) (the number of wavelengths per unit distance) can be produced from a FTIR detector, as shown in Figure 2.28. Each trough is caused by energy absorption at that particular frequency of IR radiation, which identifies particular bonds in a molecule. The big trough to the left in Figure 2.28 is used to identify the presence of $Ca(OH)_2$ by an oxygen-hydrogen bond and can be confirmed by Table 2.9, which shows the range of typical bands found in concrete.

$$T = \frac{I}{I_0}$$ **Equation 2.19**

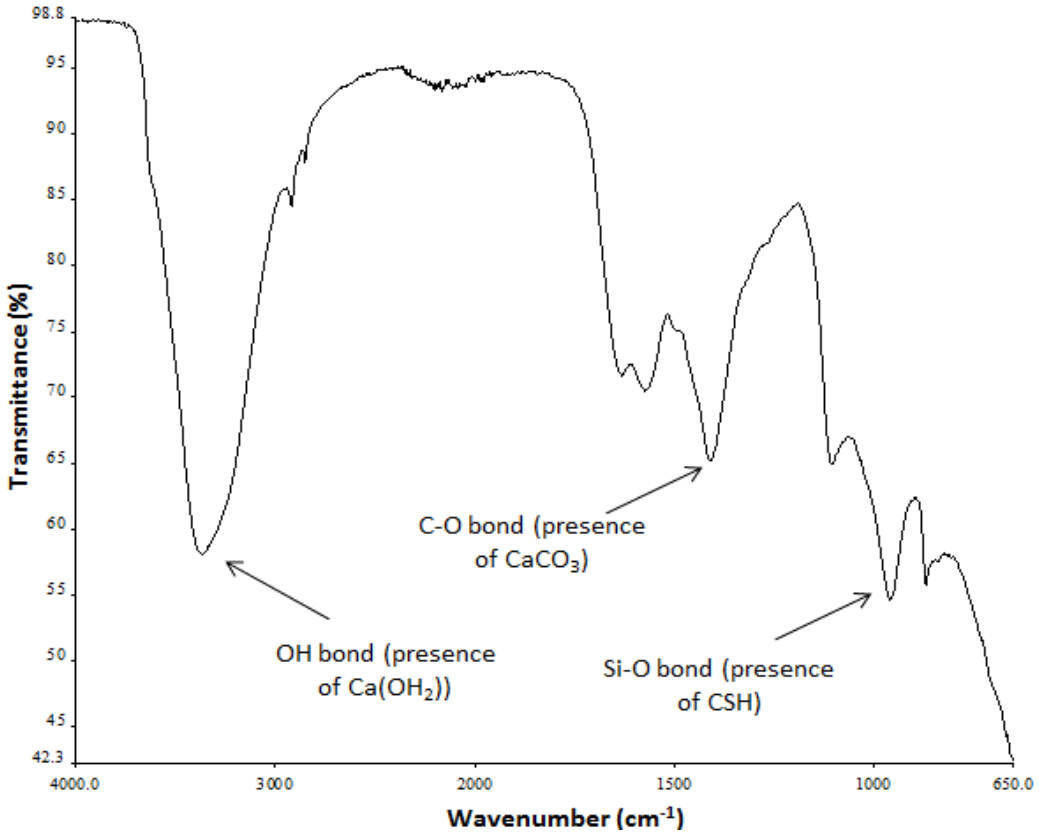

Figure 2.28 - Typical FTIR graph of stabilised peat

Table 2.9 - Range of typical concrete bands between 650 and 4000 cm^{-1} (Adapted from Lee et al. (2012))

FTIR Identification Bands			
cm^{-1}	**group**	**cm^{-1}**	**group**
3640	OH	3696	OH
3402	S-O	3620	CH_2
1622	S-O	3380–3450	OH
1426	CO_3^{2-}	2940–2864	CH_2, CH_3
1136	S-O	1740	C-O
920	Si-O	1442	CH_2,CH_3, CO_3^{2-}
880	Si-O;Al-O, CO_3	1378	C-CH_3
748	CH_2, CO_3^{2-}	1244	C-O
746	Al-O	1102	C-O, OH
712	CO_3^{2-}	1022	C-O, CH_3
660	S-O	882	CO_3^{2-}

Carbonation is represented by the transformation of the C=O bonds of CO_2 into C-O bonds in the $CaCO_3$ (Lo & Lee, 2002; Chang & Chen, 2006). Ševula et al. (1994) used FTIR to inspect the products in year-old hydrated cement and GGBS pastes by examining bonds such as C-O for $CaCO_3$ and Si-O for CSH. Similarly, Ylmén & Jäglid (2013) and Slegers & Rouxhet (1976) studied carbonation of hydrated cement and C_3S pastes respectively, identifying the absorbance of the C-O range and Si-O range over time. FTIR can also be used to find the carbonation front in concrete by visually inspecting and comparing the functional groups associated with $CaCO_3$ and $Ca(OH)_2$ on FTIR graphs of samples taken at regular depth intervals from the concrete surface. Lee et al. (2012), Chang & Chen (2006) and Lo & Lee (2002) observed that the trough peak for $CaCO_3$ decreases while the peak representing $Ca(OH)_2$ increases with depth in concrete until a constant baseline is reached, which is the carbonation front. The spectra obtained beyond this depth overlap and fluctuate within noise limits. In these studies, paste powder was extracted at regular depth intervals; for instance, every 5 mm, starting at the specimen surface.

Lee et al. (2012) used the peak intensity ratio of calcite and portlandite of each sample analysed to ascertain the carbonation progress over time and with depth. The method produces encouraging results as it gives a precise analysis rather than a visual depth measurement. According to Chang & Chen (2006), FTIR can be used to measure the presence of $CaCO_3$ from a level at which the pH is 11.5 to saturation with $CaCO_3$ at pH 8.3, while Lo & Lee (2002) suggests that the presence of $CaCO_3$ can be measured from a pH of 12.5. They determined the carbonation rate by FTIR to be 23.9% higher than that obtained by the phenolphthalein indicator, while Chang & Chen (2006) found FTIR

carbonation results to be on average twice that of the phenolphthalein indicator. IR spectrum analysis based on a study of C-O bonding and/or calcite/portlandite ratios produces a scientific measurement of carbonation depth, providing a quick and convenient tool for cross-examination with other experimental methods.

2.9.5 Thermogravimetry analysis (TGA) and loss on ignition (LOI)

2.9.5.1 Overview

Another widely used method to establish the carbonation front in concrete and cement pastes is thermogravimetry analysis (TGA), a method that can be interpreted either qualitatively and quantitatively (Chang & Chen, 2006; Matsushita et al., 2000; Sauman, 1971; Villain & Platret, 2006; Parrott & Killoh, 1989; Dweck et al., 2000). This method involves using a TGA instrument that continuously measures the mass of a concrete powder sample subjected to a steady increase in temperature. For instance, the temperature could be set to increase by 10°C or 20°C every minute from room temperature to 1000°C. The concentrations of $Ca(OH)_2$ and $CaCO_3$ are measured by mass losses at different temperature ranges, losses that are a result of the dehydration of $Ca(OH)_2$ and thermal decomposition of $CaCO_3$. Temperature ranges where these processes occur are difficult to pinpoint because of the chemical composition of the concrete or cement, but attempts have been made by several authors. In this thesis, with the help of some TGA analyses carried out on stabilised peat, the temperature ranges where $Ca(OH)_2$ and $CaCO_3$ decompose are identified in Section 3.5.4.6. Consequently, it is then possible to measure the $Ca(OH)_2$ and $CaCO_3$ mass losses at the identified temperature ranges using a muffle furnace (loss on ignition (LOI) technique).

A typical TGA/TG curve on a concrete sample from Chang & Chen (2006) is displayed in Figure 2.29. In addition to mass changes (mg), the TGA records the temperature difference in units of heat flow (mW) between the sample and a reference sample, which is indicated by the differential thermal analysis curve (DTA curve) in Figure 2.29. Using this curve, it is possible to locate where the various hydrated and carbonated products decompose. Figure 2.29 shows three troughs in the DTA curve, representing the loss of water molecules, the loss of H_2O from $Ca(OH)_2$ and the loss of CO_2 from calcite.

2.9.5.2 Stage 1

A summary of some of the studies that establish the temperature ranges at which the hydrates and carbonated products decompose in concrete and cement as well as other materials, such as CSH gel and $CaCO_3$, is provided in Table 2.10. The first endothermic peak in a TGA plot for concrete exists generally between 0°C and 200°C, which is due to

the removal of water molecules from Aft and gypsum (Singh & Singh, 2007; Huntzinger et al., 2009). An endothermic reaction absorbs heat as opposed to exothermic which releases it and can be identified by troughs in the DTA curve. Other free and absorbed H_2O, H_2O from CSH and AFm, and CO_2 absorbed between the layers of CSH decompose between 25°C and 430°C, but the CO_2 loss was found to be small (Villain & Platret, 2006).

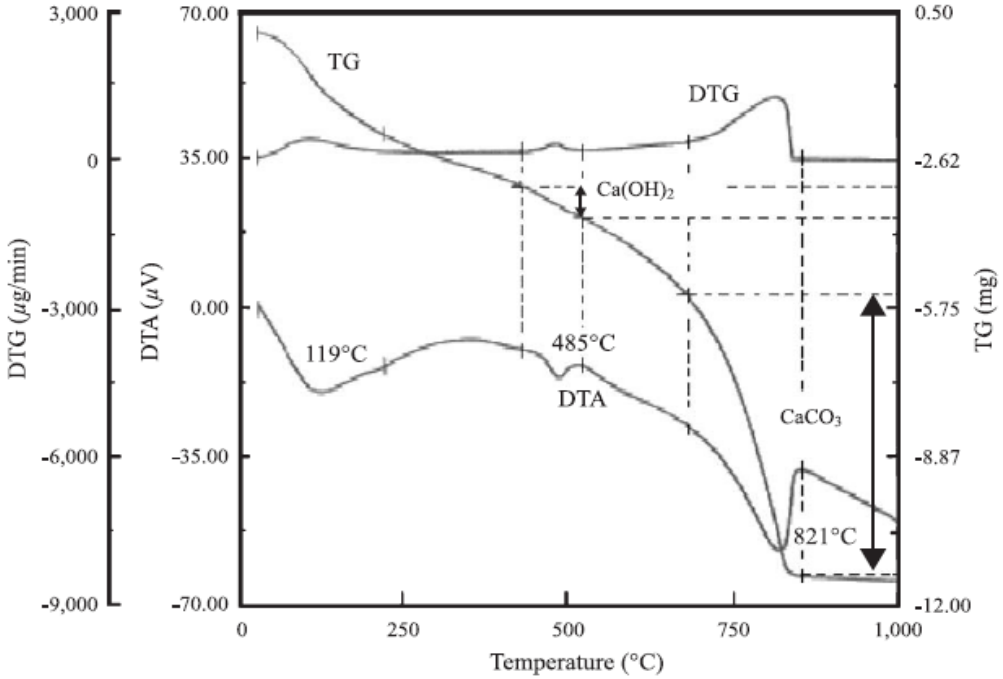

Figure 2.29 - The concrete characteristic curves of thermogravimetric and differential thermogravimetric analysis with temperature (Chang & Chen, 2006)

2.9.5.3 Stage 2

The second main endothermic peak identifies the dehydration of $Ca(OH)_2$. Villain et al. (2007) observed that $Ca(OH)_2$ dehydrates at temperatures of 430°C to 530°C, while Chang & Chen (2006) noted that it occurred between 425°C and 550°C in concrete (Figure 2.29). However, in cement kiln dust, Huntzinger et al. (2009) found that it occurred between 300°C and 400°C. Based on studies in Table 2.10, the likely range for this peak is between 300°C and 550°C.

2.9.5.4 Stage 3

Between 520°C and 680°C, mass loss is mostly due to the unstable $CaCO_3$ products aragonite and vaterite emanating from CSH carbonation (Villain et al., 2007; Thiery et al., 2007) (Table 2.10). Before decomposing at a low temperature range of between 500°C and 700°C, aragonite and vaterite transform into calcite. Sauman (1971) discovered vaterite transformed into calcite at approximately 440°C to 470°C. Opinions differ on the

interpretation of the mass loss between 520°C and 650°C as there is an overlap between mass loss due to hydrates and CSH carbonation (Villain et al., 2007). It is, therefore, hard to specify a precise temperature that would separate CSH and portlandite decomposition (Villain et al., 2007). Nonetheless, using a TGA coupled with a mass spectrometry analysis, Villain & Platret (2006) showed that mass loss between 520°C and 650°C corresponded chiefly to CO_2 emissions whereas H_2O loss was negligible. From an FTIR analysis, this CO_2 emission originated from vaterite at a peak of 876 cm^{-1}. If it is assumed that all mass loss between 520°C and 650°C stems from CSH carbonation, carbon sequestration will be underestimated if this mass loss is not taken into account (Villain & Platret, 2006).

Table 2.10 - Summary of research on temperature ranges of decomposition of hydrates and carbonated products during TGA measurements

References	Temperature ranges of decomposition of hydrates and carbonated products (°C)					Material
	1	2	3	4	5	
Sauman, 1971	50–300		650–750	750–850		Porous concrete
Sauman, 1971	50–200		500–700	800–900		CSH gel
Rahman & Glasser, 1989	20–425	425–550	550–650	650–800		OPC cement paste
Parrott & Killoh, 1989	100–375	375–425		550–750		Concrete
Papadakis et al., 1991		400–500		650–800		Concrete
Dweck et al., 2000	0–450	410–460	520–730			Cement blended with $CaCO_3$
Matsushita et al., 2000			600–800			AAC*
Sanders & Gallagher, 2002				600–800 600–775 600–900		$CaCO_3$
Chang & Chen, 2006		425–550	550–820			Concrete
Villain & Platret, 2006	25–430	430–520	520–620	650–720	720–900	Concrete
Villain et al., 2007		430–530		650–950		Concrete
Thiery et al., 2007			550–680	680–990		OPC cement paste
Singh & Singh, 2007	< 200			700–850		$CaCO_3$
Huntzinger et al., 2009	0–200	300–500	500–800		800–1000 (unidentified)	Cement kiln dust

*** AAC = Autoclaved aerate concrete**
Stage 1 - Free and adsorbed H_2O, H_2O from CSH, Aft, AFm and gypsum, and CO_2 adsorbed in CSH
Stage 2 - H_2O from $Ca(OH)_2$
Stage 3 - $CaCO_3$ Calcite of CSH carbonation
Stage 4 - $CaCO_3$ Calcite of carbonation
Stage 5 - Calcite of aggregates

2.9.5.5 Stage 4

Sauman (1971) found that calcite in porous concrete decomposed from 500°C to 950°C in an environment with 1% to 30% CO_2, and the first peak he observed in TGA testing was between 500°C and 700°C, which was mostly from CSH carbonation and vaterite. Peaks

detected between 750°C and 950°C were from calcite decomposition from carbonation and aggregate. Similarly, Villain & Platret (2006) found a peak between 650°C and 720°C from CO_2 carbonation and a peak between 720°C and 850°C, representing an overlap of CO_2 from carbonation and CO_2 from calcite in limestone aggregates. In contrast, Chang & Chen (2006) noted only one peak from 550°C to 820°C for concrete (Figure 2.29). DTA curves from Matsushita et al. (2000) show endothermic peaks at 700°C for the non-carbonated concrete sample and 790°C for the sample cured for 50 days. These authors proposed the weight loss from 600°C to 800°C as the temperature range to represent the mass of CO_2 from carbonation. CO_2 mass loss can also be converted into mass losses of $CaCO_3$ and moles of $CaCO_3$ per m^3.

Rahman & Glasser (1989) found that the peak for $CaCO_3$ decomposition, tested after 80 days, was between 650°C and 800°C for OPC pastes. Dweck et al. (2000) found the peak to lie at the lower range of between 520°C and 730°C for CEM II pastes (contains hydrated calcium sulphates and $CaCO_3$). These were, however, tested from one hour to one week after hydration, hence the lower range which may indicate unstable $CaCO_3$. Cole & Kroone (1959) demonstrated by X-ray diffraction that CO_2 in cement mortars cured in air, chemically bonded largely as poorly crystallised vaterite, aragonite and calcite, with an endothermic peak between 650°C and 750°C. A peak at 800°C was attributed to the decomposition of well-crystallised calcite. Because the thermal dissociation of $CaCO_3$ is influenced by grain size, the calcite from carbonation is of finer granulometry and breaks up before the calcite contained in the limestone aggregates (Villain et al., 2007). Although the temperature at which calcite in limestone decomposes is debatable and depends on the type and quantity of impurities present, Singh & Singh (2007) suggest that it decomposes at about 900°C.

2.9.5.6 Degree of carbonation

From a concrete or cement powder sample analysed using a TGA system, the percentage of carbonation that has taken place (D_c) can be found using Equation 2.20, which was used by Iwasaki & Tada (1985), Huntzinger et al. (2009) and Matsushita et al. (2000). C is the mass of CO_2 in the sample, C_p is the theoretical maximum mass of CO_2 needed to combine with the total calcium oxide in the sample to form $CaCO_3$, and C_0 is the initial CO_2 concentration in the uncarbonated sample which may differ from sample to sample. The mass of CO_2 is calculated by the CO_2 mass loss from calcite at the relevant temperature ranges.

$$D_c(\%) = \frac{C - C_0}{C_p - C_0} \times 100$$ **Equation 2.20**

For concrete, Dapkus & Stankevičius (1985) estimated C_0 to be 2% and C_p to be 16% of the mass, while Matsushita et al. (2000) found C_0 in autoclaved aerated concrete to be 0.9%. An estimate of C_p can be obtained using Equation 2.14.

According to Villain et al. (2007), TGA should be supplemented with chemical analysis (CA) to give accurate quantitative carbonation profiles. CA is undertaken to determine the cement content of powder samples from concrete specimens, which are also tested by TGA. CA allows for comparison of the overall cement content of the specimens with the local sample used for TGA tests, which may give different results. Thiery et al. (2007) and Villain et al. (2007) extracted pieces of concrete from specimens and crushed them to quantify $Ca(OH)_2$ and $CaCO_3$ by TGA coupled with CA. Mindful of the large variability in stabilised peat, TGA-CA may be a worthwhile technique to create an accurate carbonation-depth profile.

2.9.6 pH of slurries technique

Measuring the pH in the pore solution of concrete at regular depth intervals from the surface gives a pH profile with depth that is used to examine carbonation and could be applied to obtain a carbonation profile in stabilised peat. Chang & Chen (2006) investigated the relationship between degree of carbonation (found using TGA and Equation 2.20) and pH. To determine pH, crumbled pieces of concrete mortar were mixed with distilled water in a solid to liquid ratio of 1:10 and placed in a sealed container for 20 days at 15°C after which time the pH of the pore solution was measured with a pH probe. Results showed that when the pH is between 7.5 and 9, the degree of carbonation is 50–100%; and when the pH is between 9 and 11.5, the degree of carbonation is 0–50%.

A variation of this technique called the dust digestion method was applied to calculate the carbonation front depth by Herrera (2011) and McPolin et al. (2007). Herrera (2011) collected mortar powder samples at 2 mm depth intervals from the surface, mixed them with distilled water in a 1:20 ratio and placed them in containers whose air was replaced with nitrogen gas to avoid the reaction of environmental CO_2 with the alkaline slurry. The pH was found to increase from the surface with depth until a baseline was reached. McPolin et al. (2007) prepared dust slurries similarly with distilled water and were able to measure the pH over time as well as with depth. This was done by extracting dust samples from the specimen starting at a depth of 0 mm and increasing in 2-mm increments. The specimens were drilled to the first depth, the dust was removed, the same hole was drilled further to the next depth until the final sample was collected, and the entire hole was then

filled with cement. A new hole starting at the surface could be drilled at a later time and the pH measured.

Profiles of pH depend on the binder type and content and the timespan for which the concrete has been exposed to the atmospheric/environmental CO_2. Though simple and inexpensive, the pH of slurries methods are destructive (Herrera, 2011) but can be used as an indicator of the level of carbonation. However, it is harder to recognise partial carbonation and the depth of the carbonation front in concretes whose cement content has high levels of GGBS or low levels of cement as the pH difference between carbonated and uncarbonated concrete may be a lot lower, making it harder to observe a change. The alkalinity of the slurries depends mainly on the concentration of alkaline compounds such as $Ca(OH)_2$ and CSH in the mortar. Due to the conversion of these compounds into $CaCO_3$ as a result of carbonation, the slurry has a lower pH than those with non-carbonated material.

2.9.7 Porosity

Porosity change in concrete due to carbonation provides more information about the level and type of carbonation, but it has not been used in previous studies to determine the depth of carbonation. As explained in Section 2.7.1.2, carbonation leads to a decrease in porosity as a result of the volume increase in carbonated products in the concrete. A similar outcome could be expected from stabilised peat.

Several techniques are employed to find the porosity of materials such as concrete, cement paste or peat. These include mercury intrusion porosimetry, helium pycnometry, and the water evaporation method. Information on these techniques and their application to cement is available in Anstice et al. (2005) and Unosson et al. (2015). The main drawbacks of mercury intrusion porosimetry and helium pycnometry are their destructiveness, long analysis times and the need for special equipment (Unosson et al., 2015). The focus of this research is on the water evaporation technique, a non-destructive method, which means samples can be used for other tests. It is a fast and reliable method to measure porosity (Unosson et al., 2015) and is based on total porosity being equal to the water content at saturation (Walczak et al., 2002).

Besides the binder type and content and the level of carbonation in stabilised peat, the properties of natural peat may affect the porosity of stabilised peat. Total porosity for blanket and raised bog peatlands have been reported to be in the range of 85% to 98%, depending on whether the peat is slightly, moderately or highly decomposed (Holden,

2009; Bozkurt, et al., 2001). This is because an increase in the organic content of peat results in an increase in its porosity (Hobbs, 1986).

2.9.8 Other techniques

Additional techniques have been used to broaden the understanding of the carbonation process in concrete, which may also be applied to stabilised peat. Some of these include: Inductively Coupled Plasma-Atomic Emission Spectroscopy (ICP-AES), Scanning Electron Microscope (SEM) and Energy Dispersive X-Ray Spectrometer (EDX). The ICP-AES analyses can obtain the chemical properties of cement, GGBS and concrete in terms of major oxides such as calcium oxide (CaO), silicon dioxide (SiO_2), and aluminium oxide (Al_2O_3). The chemical composition of materials in the form of major oxides contained are generally tabulated in publications on carbonation in concretes and cement, examples include Chang & Chen (2006), Houst (2002) and Anstice et al. (2005).

SEM gives highly magnified images and has been used to examine hydration and carbonation products in concretes and cement; examples of this work are presented by Ševula et al. (1994) and Sauman (1971). EDX analyses give the elemental composition of cement and concrete samples in terms of elements such as carbon, oxygen and silicon.

2.10 Context for literature review

A review was carried out of the environmental policies introduced in the last three decades and the steps taken by the construction industry to comply with these. In addition to being a challenging material to build on, peat is also a carbon sink; therefore, disturbance or alteration has major implications for EC and EE studies. Unfortunately, as identified in the literature review, there is a major lack of LCA studies, methodologies and guidelines to determine the potential construction-related and peat-related emissions associated with ground improvement/foundation techniques for road construction in peatlands. A literature survey on the peat-related factors affecting the EC associated with road construction on peat was undertaken, which identified the impact that stabilising peat has on emissions as a major knowledge gap.

The carbonation process in concrete was then discussed as a framework to help understand the carbonation process in stabilised peat, and a review of measurement techniques used in other fields of engineering was provided. The closed chamber method, which calculates CO_2 fluxes between soil and the atmosphere, was examined, as were methods to calculate the depth of the carbonation front in concrete. This review informed the choice of experiments to apply to stabilised peat in Chapter 3.

The goal of this research is to determine the on-site carbon impact of stabilised peat (ascertain whether stabilised peat is a net sink or source of carbon) and to use the results/outcomes of the experiments to develop a new LCA methodology specifically to quantify the EE and EC associated with ground improvement/foundation techniques (including peat stabilisation) applied in road construction on peat.

Chapter 3: Experimental Procedures

3.1 Introduction

The experimental procedures for investigating carbonation in stabilised peat are described in this chapter. Firstly, standard methods and procedures used to classify both raw and stabilised peat are outlined. It was unknown at the outset of the research whether peat mixed *in situ* was a net source or sink of carbon, prompting a pilot laboratory carbonation study, Experiment P. This was then followed by two more extensive experiments, Experiments A and B (Table 3.1). The objective of these experiments was to determine the gas flux from stabilised peat and to examine the depth and level of the carbonation front for various conditions. It was envisaged that these results would be useful in quantifying the on-site environmental impact of dry soil-mixing in peat.

Experiment P: Gas fluxes from a raw Irish peat (with both high and low water tables modelled) and stabilised peat are compared, and the implications for dry soil-mixing are assessed. Temperature, time and initial CO_2 concentration were the stabilised peat variables examined (Table 3.1).

Experiment A: From the results of the pilot carbonation study performed in Experiment P, it was decided to further explore the gas fluxes from stabilised peat. Varying levels of peat oxidation rendered it impossible to quantify accurately the depth and level of carbonation solely from CO_2 gas flux results. To solve this problem, several methods used to determine the depth of the carbonation front in concrete were applied to the stabilised peat: XRDA, FTIR, LOI, pH of stabilised peat slurries, and the phenolphthalein indicator. Variables examined in this experiment were time, cement, GGBS, surcharge, and initial CO_2 concentration in the headspace (Table 3.1). Large stabilised peat specimens were used to measure gas fluxes and the carbonation front depth, while small specimens were used to measure the depth of the carbonation front only. The number of small and large specimens is shown in Table 3.2.

Experiment B: While binder type, surcharge, initial CO_2 concentration and binder amount were the principal variables tested in Experiment A, water table depth was an additional variable examined in Experiment B (Table 3.1). Furthermore, in this experiment three (A3, A4, A8) of the eight types (A1–A8) of stabilised peat columns from Experiment A were reproduced to validate the reliability of the results obtained from Experiment A. The same techniques used in Experiment A to calculate the CO_2 fluxes from stabilised peat and to measure the depth of the carbonation front were also used for Experiment B. Once again, large stabilised peat specimens were made to measure gas fluxes and the carbonation front

depth, while small specimens were made to measure the depth of the carbonation front only. The number of small and large specimens is shown in Table 3.2.

After describing the experiments, there is a review of the techniques applied to calculate the CO_2 gas flux from stabilised peat and the depth of its carbonation front, and statistical tools employed to interpret the experimental data are outlined.

Table 3.1 - Variables examined in Experiments P, A and B

Experiment	Date	Variables examined
P	Nov. 2012 to July 2013	Temperature, time and initial CO_2 concentration
A	Nov. 2013 to May 2014	Time, initial CO_2 concentration, cement content, GGBS content and surcharge
B	Mar. 2015 to Aug. 2015	Time, initial CO_2 concentration, cement content, surcharge and water table depth (high or low)

Table 3.2 - Number of specimens analysed and techniques used in Experiments P, A and B

Experiment	Duration (days)	Number of specimens		Gas flux technique	Carbonation depth techniques
		Large specimens	Small specimens		
P	228	9	0	✓	
A	180	24	66	✓	✓
B	180	24	72	✓	✓

3.2 Peat sampling and classification

3.2.1 Study region and on-site soil sampling

Peat required for Experiments P, A and B was obtained from a cutover upland blanket bog at Raheen Bar Windfarm, about 10 km northwest of Castlebar, Co. Mayo, Ireland (53º53′50″N, 9º21′03″W). According to Met Eireann (2015), the mean annual temperature at the nearest weather station in Newport, Co. Mayo is 10.4°C, and the mean annual precipitation is 1607 mm. Peat cores were collected from the bog by securing a hollow acrylic cylindrical tube (10 cm in outer diameter, 9.3 cm in inner diameter, 65 cm in height) into a 10 cm diameter core sampler. The peat sampler was then slowly screwed clockwise into the catotelm of the peat bog to a depth of 50–60 cm and was pulled up by unscrewing it in an anti-clockwise motion. This operation was performed very carefully to ensure minimal disturbance of the *in-situ* peat and to prevent water from being squeezed from the peat core (Landva et al., 1983). Both ends of the peat-filled tube columns were covered with strong plastic bags, which were sealed and secured with thick rubber bands and then transported to NUI Galway in large, sealed plastic bags. On examination of the outside of the bags and the peat-filled tube columns in the laboratory, no moisture was lost between

sampling and mixing as the outside was dry. The tubes used to hold both the peat cores and later the stabilised peat, were supplied by Amari Ireland Ltd.

3.2.2 Peat classification

The peat retrieved was classified according to moisture content, organic content, density, degree of humification and pH, following standard procedures:

- Peat moisture contents were obtained according to ASTM D2974–07a (ASTM, 2007) by drying the samples in an oven at 105°C.
- Using Method C of the same standard ASTM D2974–07a (ASTM, 2007), organic contents tests were carried out by using loss-on-ignition methods at a temperature of 440°C.
- Peat bulk densities were determined in accordance with Method A in ASTM D4531-86 (ASTM, 2008) using linear measurement methods.
- The degree of decomposition or humification was estimated based on the von Post scale (von Post, 1922), supplemented by the work of Hobbs (1986).
- All pH tests were carried out with guidance from BS 1377–3: 1990 (BSI, 1996).

3.3 Laboratory stabilisation method

Laboratory stabilisation trials were undertaken to assess carbonation in stabilised peat under varying surcharges, environmental factors, and binder types and amounts. The procedure for carrying out the binder trials in this research is explained in this section.

3.3.1 Fresh peat homogenisation process

(i) Three raw peat cores from three tubes were placed in a large soil pan mixer (Figure 3.1). In accordance with design guidance in EuroSoilStab (2002), isolated roots, large fibres and coarse material were removed from the natural peat before its mass was determined.

(ii) To homogenise the peat, it was mixed for a duration not exceeding 5 minutes to avoid breakup of the fibre structure (Pousette et al., 1999).

(iii) Any peat that adhered to the wall of the mixer was returned to the mix.

(iv) For each peat core placed into the mixer, a subsample was removed to determine the moisture and organic content of the parent peat.

Figure 3.1 - NUIG soil pan mixer

3.3.2 Addition of binder

The mass of the binder to be added to the homogenised peat is determined using Equation 3.1.

$$\text{Binder required (kg)} = \frac{\text{mass of fresh peat (kg) x binder content (kg/m}^3\text{)}}{\text{bulk density of fresh peat (kg/m}^3\text{)}} \quad \textbf{Equation 3.1}$$

The peat was stabilised with either one or two binders of varying binder amounts. Cement and GGBS were used in Experiment A, whereas cement alone was used in Experiments P and B. The cement was CEM II A/L 32.5N from Irish Cement and came in 25 kg bags while the GGBS was sourced from Ecocem Ireland. The average chemical and physical properties of the binders in Experiments A and B are displayed in Table 3.3 and were obtained by Inductively Coupled Plasma—Atomic Emission Spectroscopy (ICP-AES) analyses carried out by ALS Geochemistry, Loughrea, for this research.

If two binders were used for one mix, they were weighed out according to their selected proportions and mixed together manually. The binder was added to the peat gradually and mixed until a visually homogeneous stabilised mixture was obtained, a process limited to five minutes (EuroSoilStab, 2002; Åhnberg, 2006). As in the raw peat homogenisation process, for each peat core added to the mixer, a stabilised peat sample was taken to determine its moisture and organic contents.

3.3.3 Sample compaction

In keeping with techniques used by Åhnberg (2006) and Timoney (2015), the mix was placed into cylindrical acrylic columns (Figure 3.2) (described in Section 3.2.1) in 50 mm-

high layers and each one compacted 30 times with a tamping bar to eliminate voids in the stabilised peat. The columns were filled to a height of approximately 0.5 m, and an air gap of > 0.1 m was left at the top of the column. Mix was also placed in small cylindrical plastic piping moulds (6.3 cm in inner diameter x 12 cm in height) to make up the small specimens in Experiments A and B. Due to the high moisture content of the mixes, distinct layering did not occur.

Table 3.3 - Chemical and physical properties of cement and GGBS

Results of chemical analysis	Cement (Exp. A) (%)	Cement (Exp. B) (%)	GGBS (%)
Silicon dioxide, SiO_2	18.55	19.81	37.5
Aluminium oxide, Al_2O_3	4.66	4.9	11.43
Ferric oxide, Fe_2O_3	2.74	2.82	0.8
Calcium oxide, CaO	62.50	64.74	42.8
Magnesium oxide, MgO	2.26	2.39	6.61
Sodium oxide, Na_2O	0.15	0.21	0.21
Potassium oxide, K_2O	0.75	0.74	0.41
Chromium oxide, Cr_2O_3	0.01	0.01	<0.01
Titanium dioxide, TiO_2	0.23	0.23	0.22
Manganese oxide, MnO	0.03	0.03	0.03
Phosphorus pentoxide, P_2O_5	0.05	0.07	0.06
Strontium oxide, SrO	0.04	0.04	0.04
Barium oxide, BaO	0.03	0.03	0.02
Loss on ignition at 1000°C	7.86	4.18	-0.71

3.4 Experiments P, A and B: Notation, Setup and Conditions

3.4.1 Notation for experiments

In Appendix B, two A3 fold-out pages, the notation used to describe the small and large specimens in Experiments P, A and B is provided. The following is the notation system for the large specimens:

- Each large specimen has the following notation: Capital letter_Number(Number)
- The capital letters, P, A, B, represent Experiments P, A and B respectively, while the first number after the letter corresponds to the column or specimen type (1 to 8), which reflects a particular binder type, content and environmental conditions.
- The number in brackets represents the replica specimen numbers (1 to 3). Replica specimens indicate the specimens were made with the same binder type and content and were subject to the same environmental conditions.

The large cylindrical specimens examined were labelled: P1(1) to P3(3) (n = 9) for Experiment P, A1(1) to A8(3) (n = 24) for Experiment A, and B1(1) to B8(8) (n = 24) for Experiment B.

For each large specimen in Experiments A and B, three small cylindrical specimens were made with the same binder type and content and subject to the same environmental

conditions as their large specimen counterparts. The following is the notation system for the small specimens:

- Each small specimen has the following notation Small letter_Number (Number_Small letter).
- A lower case letter ‘a’ at the start of a small specimen name indicates Experiment A and a lower case ‘b’, Experiment B.
- The first number after the letter corresponds to the column or specimen type (1 to 8), and the second number (in brackets) again stands for the replica specimen number (1 to 3).
- The letter at the end of the specimen name (a, b, c) indicates the day the specimen was analysed during the experiment. ‘a’ stands for 20 days, while ‘b’ stands for 94 days for Experiment A and 90 days for Experiment B. ‘c’ stands for 180 days.

The small cylindrical specimens examined were therefore labelled a1(1a) to a8(3c) (n = 72) for Experiment A and b1(1a) to b8(3c) (n = 72) for Experiment B.

3.4.2 Experiment P (Pilot laboratory carbonation study)

3.4.2.1 Laboratory setup and initial experimental conditions

The 228-day study ran from 25 November 2012 to 11 July 2013 and involved setting up nine hollow acrylic cylindrical columns containing peat to an average height of 50 ± 5 cm (± 1 standard deviation) as shown in Figure 3.2(a). Three sets P1, P2 and P3 were established, each comprising three intended replicates, albeit within the limitations of peat and mixing variability. The columns were kept in a temperature-controlled room with an initial temperature of 15°C and a relative humidity in the range 60% to 90%. Water levels were monitored and adjusted when necessary. To monitor the water table of each column, standpipes were constructed using plastic tubing attached to holes in plastic cylindrical lids, and these lids were sealed with silicone to the bottom of the columns (Figure 3.2).

As shown in Figure 3.2(a), columns P1 contained raw peat with the water table at the surface. To keep the water table at the surface, the samples were topped up daily with rainwater collected from harvesting systems used to gather rainwater for the toilet flush system in the building where the tests were carried out. Columns P2 contained raw peat with the water table at the bottom (P2(1)–P2(3)). Columns P2(1) and P2(2) were replicates, while the peat in P2(3) was mixed for 10 minutes to simulate the mixing element of the mass stabilisation of peat, but binder was not added. Columns P3 contained stabilised peat (P3(1)–P3(3)) with the water table at the bottom. Each time immediately

after mixing 250 kg/m^3 of cement binder with peat in a mixer, the mixture was placed into the acrylic columns.

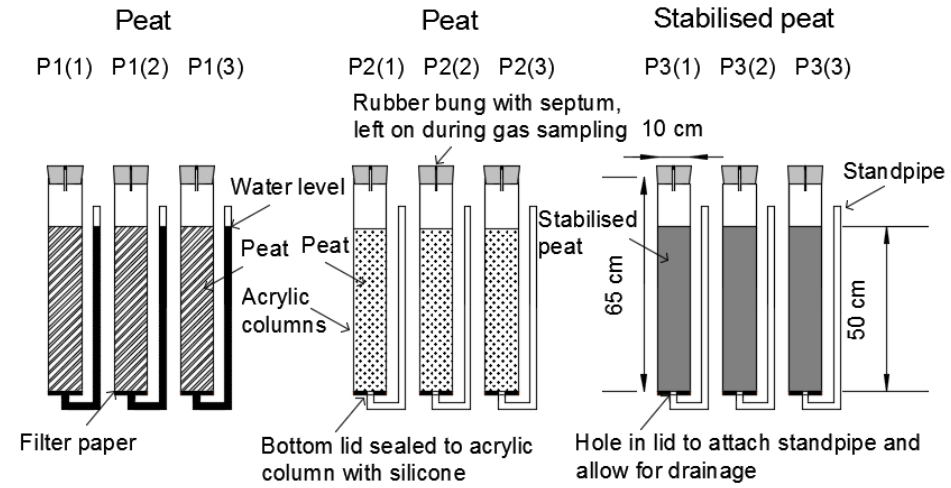

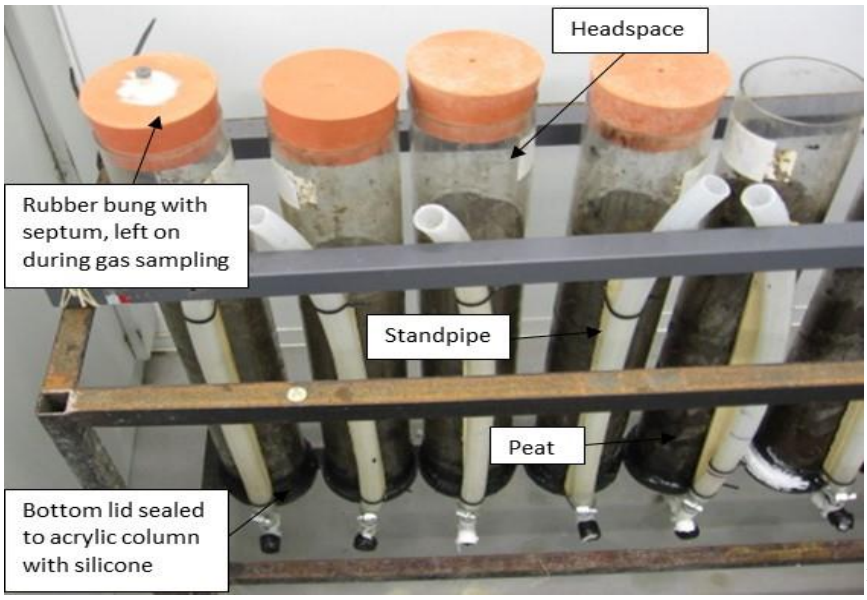

[1]

Figure 3.2 - (a) Schematic layout of experiment (top) (b) Photo of columns during gas sampling (bottom)

The gas chamber method outlined in Section 2.8 was used to analyse gas fluxes, which required rubber bungs (orange in colour) (102 mm in top diameter, 92 mm in bottom diameter and 54 mm high) from Vwr International Ltd to plug the columns during gas sampling. A 6 mm diameter hole was drilled into the bungs, and a butyl septum from Supcelo Ltd placed inside. Tubing, 6 mm in outer diameter and 4 mm in inner diameter, was attached to the bottom of the bungs. When these bungs were placed on the columns

[1] Average height of columns 50 ± 5 cm (± 1 standard deviation). Heights fluctuated over the duration of experiment (see Section 4.5.1).

during gas sampling, air could be retrieved from closer to the centre of the headspace as the tubing extended 2 cm downwards from the underside of the bung.

With the exception of the period required for gas sampling, the columns were in darkness, thereby minimising plant growth. The average CO_2 concentration in the room was 803 ± 96 ppm (± 1 standard deviation), which is closer to underground CO_2 concentration conditions than atmospheric CO_2 concentrations as underground CO_2 concentration conditions can be up to 50000 ppm (Appelo & Postmas, 1993). The high temperatures and relatively high CO_2 levels in addition to the exclusion of a surcharge in the case of the stabilised columns (leaving the structure more porous) were conditions that were deliberately imposed with a view to accelerating the carbonation process.

3.4.2.2 Subsequent modifications

On day 90, specimens P1 were drained by removing the standpipe from the bottom lids of the acrylic columns to allow the water to flow out of the columns, while the water table in P2 was restored to the peat surface to simulate a peatland restoration scenario. This 'reversal' was intended as an additional check on the effect of water level on emissions assessed over the first 90 days. It was suspected that columns P3 would become a CO_2 source due to the lack of water available (due to evaporation) for carbonation to occur. Consequently, after day 90, it was decided that these columns would receive 20 ml/day of rainwater, equivalent to 2.94 mm/day, in keeping with average rainfall in the west of Ireland of 2.7–3.4 mm/day (Eireann, 2015b). The room temperature was changed three times to investigate the impact of temperature: on day 137, from 15 to 20°C; on day 194, from 20 to 10°C; and on day 227, from 10 to 20°C. These changes were also imposed due to a separate experiment taking place in the room. All events are summarised in Table 3.4. The gas sampling process is discussed later in Section 3.5.3.

Table 3.4 - Experimental conditions summary table

Day	**Temp. (°C)**	**Water Conditions**		
		P1 (n = 3) (Peat)	**P2 (n = 3) (Peat, P2(3) mixed)**	**P3 (n = 3) (stabilised)**
1–90	**15**	**Waterlogged**	**Drained**	**Drained**
90–137	15	Drained	Waterlogged	Water added daily
137–194	20	Drained	Waterlogged	Water added daily
194–227	10	Drained	Waterlogged	Water added daily
227–228	20	Drained	Waterlogged	Water added daily

3.4.3 Experiment A

3.4.3.1 Laboratory setup and experimental conditions

This laboratory experiment ran for 180 days, from 05 November 2013 to 03 May 2014. Additional bungs (blue in colour) were acquired for Experiments A and B to plug the

columns during gas sampling but were different in size to the ones used in Experiment P in that they had a top diameter of 102 mm, bottom diameter of 80 mm and a height of 67 mm. A 6 mm diameter hole was drilled into these bungs, similar to Experiment P, and a septum was placed inside. This time, to maintain pressure equilibrium and avoid pressure perturbations during gas sampling, a vent was drilled into the bungs. The vent tube length and diameter were designed based on work done by Hutchinson & Mosier (1981). Since the enclosure (chamber) volume was < 1.1 litres and there was no wind present in the chamber, the minimum vent tube diameter needed and length required was approximately 2 mm and 2 cm respectively (Figure 3.3). The vent tube diameter in Experiments A and B was consequently 4 mm and the length was ≥ 5.4 cm.

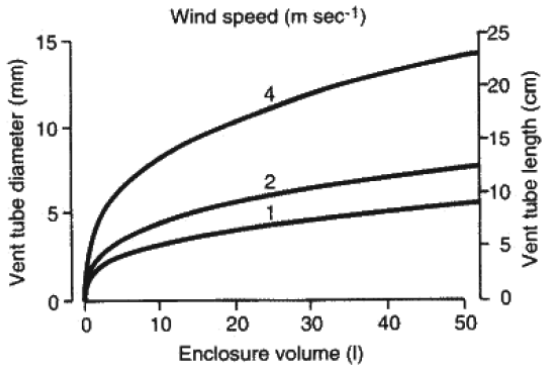

Figure 3.3 - Vent tube length as a function of chamber volume and vent tube diameter (Hutchinson & Mosier, 1981)

Plug-in reducers from Radionics Ltd. were placed into the vents and some of the gas sample slots. The gas sampling holes were closed with septums, and the vents were loosely closed with 4 mm plug fittings from Radionics Ltd. Tubing, 6 mm in outer diameter and 4 mm in inner diameter, was again attached to the bottom of the bungs. Figure 3.4(a) shows the bungs, syringes and vials required to carry out gas sampling, while Figure 3.4(b) shows a schematic of a typical bung used in Experiments A and B.

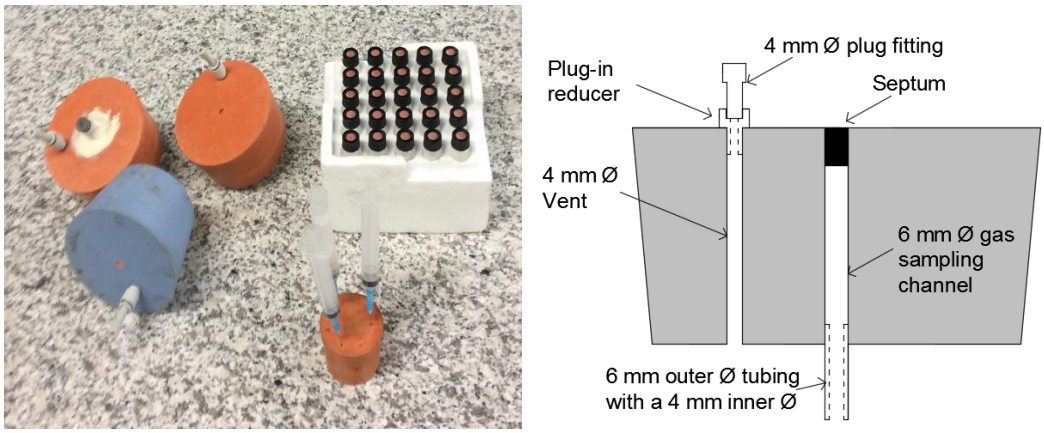

Figure 3.4 - (a) Photo of bungs, syringe and vials (b) Typical bung

Once in the laboratory, 24 of the 27 peat cores were mixed with different binder types and contents, and 24 large specimens in total were formed (Figure 3.5). These consisted of three replicates of each of eight scenarios with different binder types and contents and different environmental conditions (Appendix B):

- A1, A2 and A3 had varying amounts of cement to ascertain the effect cement had on carbonation: A1, 148 kg/m^3 [2]; A2, 200 kg/m^3; A3, 250 kg/m^3. Three separate mixes were made for A3(1), A3(2) and A3(3), but only one mix was made for stabilised peat column types A1, A2 and A4–A7 when it became apparent that the mixer could hold this volume of peat and binder satisfactorily.
- To explore surcharge and its effects, A4 and A5 were subjected to surcharges of 6 kPa and 12 kPa respectively for 21 days. Three-inch (76.2 mm) grey sewer pipes were cut to appropriate sizes (0.5 to 1 m), filled with gravel and stones and used as surcharges (Figure 3.6(a)). Plastic connections were devised to distribute the load evenly across the specimens, and holes were drilled into the connections so that atmospheric O_2 and CO_2 could reach the stabilised peat during the first 21 days for which the surcharge was applied. For example, sixteen 3 mm holes were drilled into the plastic connections for the large specimens between the inner and outer ring (Figure 3.6(b)).
- To discover the influence of another binder constituent, varying levels of cement and GGBS were trialled. A6 and A7 both had 250 kg/m^3 of binder, but A6 had a ratio of 3:1 cement to GGBS, while A7 had a ratio of 1:3 cement to GGBS.
- A8 contained only peat and acted as a control.

For each large specimen, using the excess stabilised peat, it was intended to produce three smaller cylindrical specimens (diameter of 63.5 mm and maximum height of 120 mm) that had the same binder type and content as their large specimen equivalent. Two-and-a-half inch (63.5 mm) black pipes were cut to one size (63.5 mm in inner diameter x 120 mm in height) to hold 72 small stabilised peat specimens (Figure 3.6(a)). However, there was insufficient excess stabilised peat material for this purpose, so some smaller mixes were made to provide more small specimens. Notwithstanding these additional mixes, a4(3b), a1(3c), a2(2c), a3(1c), a4(3c) and a5(1c) were not produced. All small specimens were also subject to the same environmental conditions as their large specimen counterparts. As surcharges, two-inch (50.8 mm) white pipes were cut, filled with gravel and stones and applied to the relevant small specimens (Figure 3.6(a)).

[2] Due to a measurement error, A1 was mixed with 148 kg/m^3 of cement binder instead of 150 kg/m^3.

Figure 3.5 - (a) Laboratory setup for Experiment A (b) Surcharged small specimens behind rack and columns with lids for gas sampling

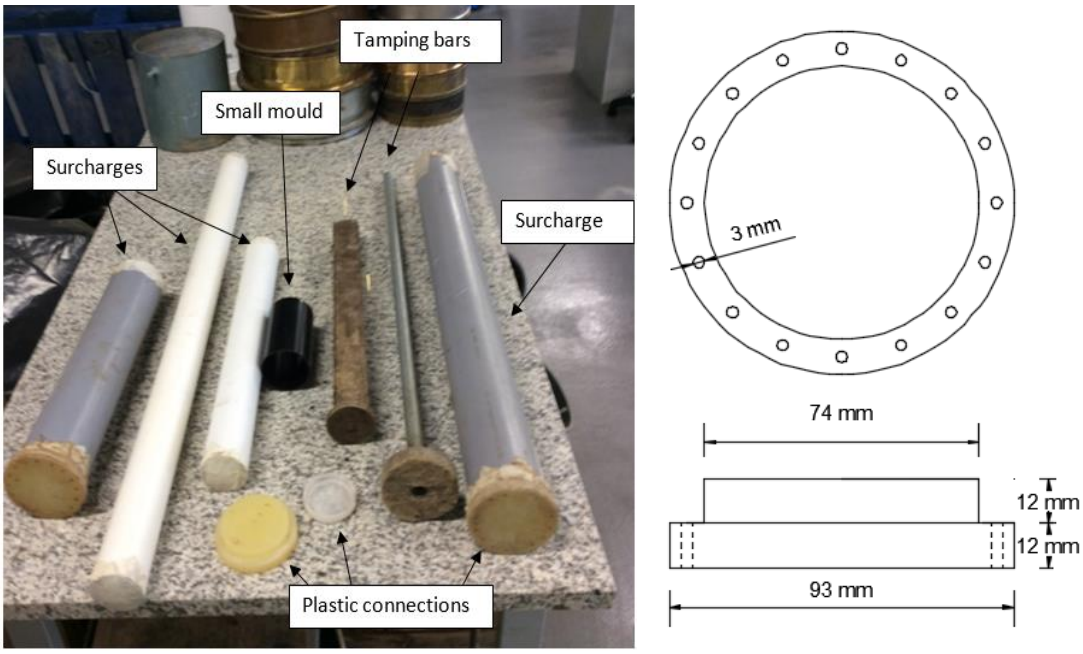

Figure 3.6 - (a) Items used in Experiments A and B (b) Plastic connection

Every fourth day, 20 ml of water was sprayed onto the large specimens, the equivalent of 0.74 mm/day of rainfall, while 9 ml of water was sprayed onto the smaller specimens, the equivalent of 0.74 mm/day of rainfall. Large specimens, A1(1)–A8(3), and the small specimens a1(1a)–a8(3c) were set up in a temperature-controlled room, the temperature maintained at 20°C and the humidity at 70% by using a dehumidifier (the maximum carbonation speed occurs when humidity is between 60 and 80% (Section 2.7.1.4)).

3.4.4 Experiment B

3.4.4.1 Laboratory setup and experimental conditions

This experiment ran for 180 days, from 03 March 2015 to 29 August 2015; and of the 28 peat cores retrieved, 24 large specimens were set up in the temperature controlled room

(Figure 3.7). These consisted of three replicates of each of eight scenarios with different binder types and contents and different environmental conditions (Appendix B):

- Specimens B1 (150 kg/m^3), B2 (200 kg/m^3) and B3 (250 kg/m^3) had varying amounts of cement and were subjected to 6 kPa of surcharge.
- To explore water table and its effects, two different water table conditions were tested: B4 with its water table at the bottom and B5 with its water table at the surface. Both B4 and B5 were mixed with 250kg/m^3 of cement binder.
- Acting as controls, B6 (water table at surface) and B7 (water table at bottom) contained peat only.
- B8 contained 250 kg/m^3 of cement binder and was subjected to 12 kPa of surcharge.
- The surcharged specimens were subjected to a pressure for only 21 days.

For each large specimen, three smaller replica cylindrical columns of 63.5 mm in diameter and a maximum height of 120 mm were filled with excess stabilised peat as well as stabilised peat from mixes made using the three left-over tubes of peat. Environmental conditions such as temperature, humidity and precipitation were kept the same as in Experiment A.

Figure 3.7 - Lab setup for Experiment B

3.5 Experimental measurements

3.5.1 Environmental measurements

Temperature and CO_2 concentrations were automatically measured every hour in the temperature control room by the Building Management System (BMS). In Experiment P,

the temperature was changed several times, dictated by the presence of another experiment, but in Experiments A and B the temperature was held constant throughout. Since the room did not have humidity control, humidity was maintained using a dehumidifier in Experiments A and B. A humidity reading was taken every two to four days using a digital reader on the outside of the temperature control room. In addition to the automatic recordings of CO_2 concentrations, the initial CO_2 concentrations in the chamber headspace taken at the start of each gas sampling event at t = 0 minutes gave more localised CO_2 concentrations for each of the columns (Section 3.5.3).

3.5.2 Heights

In Experiments P, A and B, the heights of the peat and stabilised peat in the columns were recorded to the nearest 0.25 cm from the outside of the acrylic pipes, and the heights of the water tables in the columns were measured to the nearest 0.25 cm from the outside of the standpipes attached to each column. The heights of the water table, peat and stabilised peat were noted at each gas sampling event as changes would affect the size of the chamber headspace, which in turn would affect the fluxes.

3.5.3 Gas exchange measurement technique: closed chamber method

3.5.3.1 Introduction

Gas fluxes were calculated in Experiments P, A and B using the static closed chamber method described in Section 2.8. To initiate gas sampling, a bung was placed slowly on each column to equalise pressure. As recommended by Parkin and Venterea (2010), these bungs were left on the columns for a maximum deployment time of 60 minutes. For Experiments P and A, the deployment time was 60 minutes, while for Experiment B it was only 40 minutes when it became apparent that the closed chamber effect (Section 2.8.2.1) for the 0–60 minute flux was sometimes quite large for some of the specimens in Experiments P and A.

For Experiment P for each gas sampling event, gas samples were retrieved at 0, 20, 40, and 60 minutes, inserted into 3.7 ml pre-evacuated vials from Labco Ltd and their constituents examined for CO_2 and CH_4 concentrations using an Agilent 7890A gas chromatograph from Agilent Technologies Ireland Ltd. Initially, gas sampling events took place every 1 to 3 days but later to maximum intervals of 29 days. When a change in a variable such as water level or temperature occurred, a gas emission event took place shortly before and after. These samples were analysed within a 48-hour period to avoid gas leakage, and the septa were pierced a maximum of 12 times, the equivalent of four gas sampling events. The vials were over pressurised by an extra millilitre of air so that any gas leakage would be evident when analysing samples.

For Experiments A and B, 4 ml screw-neck vials and septum screw caps purchased from VWR International Ltd were used to store gas samples. At each gas sampling event in Experiment A, samples were retrieved at 0, 20, 40, and 60 minutes; however, an extra sample was taken at 10 minutes from day 15 onwards due to the need for more data points for linear regression and the high non-linearity in the time versus gas concentration results displayed by some of the specimens. During the first 21 days while the surcharge was being applied, the surcharge was removed temporarily when gas sampling. Initially, gas sampling events took place every 2 to 3 days, but later to maximum intervals of 4 to 5 days. At each gas sampling event in Experiment B, samples were retrieved at 0, 5, 10, 20, and 40 minutes, and surcharges were again removed during the gas sampling period. Initially, sampling events took place every 1 to 3 days, but later to maximum intervals of 10 days. Intervals of four to five days were normally used; but due to problems with the gas chromatograph, there were several periods of time that gas flux readings could not be taken. For Experiments A and B, the gas samples were inserted into 4 ml pre-evacuated vials. As there were only 12 bungs available, the first 12 columns were measured in the first chamber deployment time and the second 12 columns in the second deployment time.

When a gas sample was removed from the headspace in Experiments A and B, air entered the chamber through the 4 mm vent tube, resulting in a dilution of the analyte in the chamber headspace. The error associated with this dilution effect is a function of both the sample volume withdrawn and the chamber volume to surface area ratio (Figure 3.8) (Parkin & Venterea, 2010). The red and blue bungs extended 1.5 cm and 4 cm respectively into the chamber headspace, and the chamber volume to area ratio in the columns remained between 8.5 and 16. As recommended by Parkin & Venterea (2010), correction for this dilution effect was unnecessary for chamber volume to surface area ratios > 10 and sample volumes < 30 ml. Although 3 of 48 columns had a chamber volume to surface area ratio < 10, no correction was needed for dilution as the maximum sample volume was only 25 ml, hence the percentage error was too small to have any significant effect.

3.5.3.2 Gas analysing procedure for CH_4 and CO_2 analysis

Gas samples were taken from the air in the closed chambers with a 5 ml syringe and injected into the pre-evacuated vials. The samples were removed from the vials using a 500 µl SGE gastight syringe from Supelco and injected into an Agilent 7890A Gas Chromatograph (GC). CH_4 and CO_2 were both analysed using the Agilent 7890A GC equipped with a 1/8-inch (3.2 mm) stainless steel packed column (HayeSep Q 80/100) and a thermal conductivity detector (TCD). CO_2 and CH_4 were identified by separate peaks on each plot obtained. The GC configuration was based on method 2 (SP1 7890–0467) of

Simultaneous Analysis of Greenhouse Gases by Gas Chromatography (Wang, 2010). The error of the GC had a relative standard deviation (RSD) of < 1%. High levels of CO_2 were analysed by a TCD, and the minimum detectable level of CO_2 was 50 ppm.

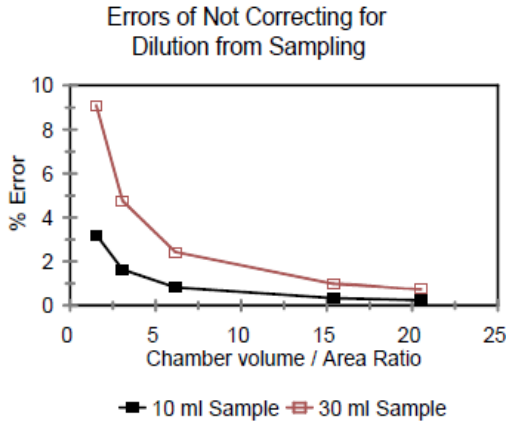

Figure 3.8 - Percentage underestimation of flux due to headspace dilution as a result of sampling

3.5.3.3 CO_2 flux measurements

Depending on the experiment, gas fluxes were calculated over the following periods of time: 0 to 5, 0 to 10, 0 to 20, 0 to 40 and 0 to 60 minutes by examining the rate of change in gas concentration in the closed chambers over those periods. As described in Section 2.8.2.1, this rate was calculated using linear regression on the gas concentration data points and substituting the slope of this line for $\partial C_a/\partial t$ in Equation 2.15. Multiplying this rate by the chamber volume V (m^3) and dividing it by the area A (m^2) results in a gas flux (mg CO_2eq/m^2/hr) (Equation 3.2) where C_i is the initial gas concentration (%); C_f is the final gas concentration (%); ρ is the density of CO_2 (kg/m^3); and the flux is calculated over a period of time, t (minutes). A positive gas flux represents a CO_2 release, and a negative gas flux represents a CO_2 intake. This calculated flux is the average flux over that time period t.

$$f = \frac{10000\rho V\left(C_f - C_i\right)}{A} \times \left(\frac{60}{t}\right)$$ **Equation 3.2**

The density of CO_2 changes according to the temperature of the room which was taken into account in the gas flux calculations, a list of the densities of CO_2 between 0 and 30°C is displayed in Table 3.5. When no CO_2 concentrations were detected in a gas sample, it was assumed the concentration was 50 ppm, the minimum CO_2 detection threshold of the GC.

Table 3.5 - Densities of CO_2 and CH_4 at temperatures of 0 to 30°C calculated using the Ideal Gas Law

Temperature of room (°C)	0	5	10	15	20	25	30
Density of CO_2 (kg/m^3)	1.96	1.93	1.89	1.86	1.83	1.80	1.77
Density of CH_4 (kg/m^3)	0.72	0.70	0.69	0.68	0.67	0.66	0.64

3.5.3.4 CH_4 flux measurements

Gas fluxes for CH_4 were calculated similarly to fluxes for CO_2 using Equation 3.2, but ρ in this case was the density of CH_4 (kg/m^3) which also changes according to temperature (Table 3.5). The minimum CH_4 detection threshold of the GC was also 50 ppm, but as no CH_4 was detected from stabilised peat at any point during the experiments it was taken that the CH_4 concentraton was zero when none was detected in a gas sample. CH_4 fluxes had to be converted to CO_2 equivalent fluxes, and this was done by multiplying the gas flux from Equation 3.2 by 25, the 100-year GWP for methane (Forster et al., 2007). CO_2 and CH_4 measurements were combined to give an overall flux measured in CO_2 equivalents (CO_2eq).

3.5.3.5 Regression modelling

At each gas sampling event, the 0 to 10, 0 to 20, 0 to 40 and 0 to 60 minute fluxes, calculated using linear regression and Equation 3.2, were inspected for linearity to discover the most appropriate time over which a gas flux should be calculated. Linearity, though, cannot be accurately detected by means of R^2 when only two measurement points are used (Pedersen et al., 2001). The goodness-of-fit of linear regression was also studied to see if there were any changes or patterns in the linearity of the gas concentration data at gas sampling events over the duration of Experiments A and B (0 to 180 days).

Linearity was examined in Experiments A and B due to the large differences in the linearity of the gas concentration data over which the fluxes were calculated. These differences are exemplified in Figure 3.9 where plots of gas concentration versus time for two separate specimens on different days in Experiment A are shown. For the 60-minute flux, the goodness-of-fit of linear regression on the gas concentration data in Figure 3.9(a) is strong as the data is highly linear ($R^2 = 0.9839$), while the data in Figure 3.9(b) is very non-linear ($R^2 = 0.1583$), highlighting the range in difference in linearity in Experiment A.

According to Kutzbach et al. (2007), the use of a linear model is justified if the chamber deployment is kept relatively short, hence the maximum chamber deployment time was kept to ≤ 60 minutes. While non-linear methods have been employed to certain soil types to calculate gas fluxes, little is known about CO_2 fluxes from stabilised peat. In stabilised peat, chemical and bacterial reactions occur, thereby making it difficult to predict gas

fluxes from past non-linear models. Non-linear models, NDFE and HMR use factors such as soil-porosity, diffusivity and vegetation, and were developed for N_2O emissions, not for CO_2 emissions from stabilised peat (see Section 2.8.2.2). Until the non-linear models, NDFE and HMR, can be evaluated further, Parkin & Venterea (2010) recommend that the investigator apply linear regression or the Quad method when the HM model fails. Linear regression was used, therefore, in this study, but the non-linear HM model (described in Section 2.8.2.2) was also tested.

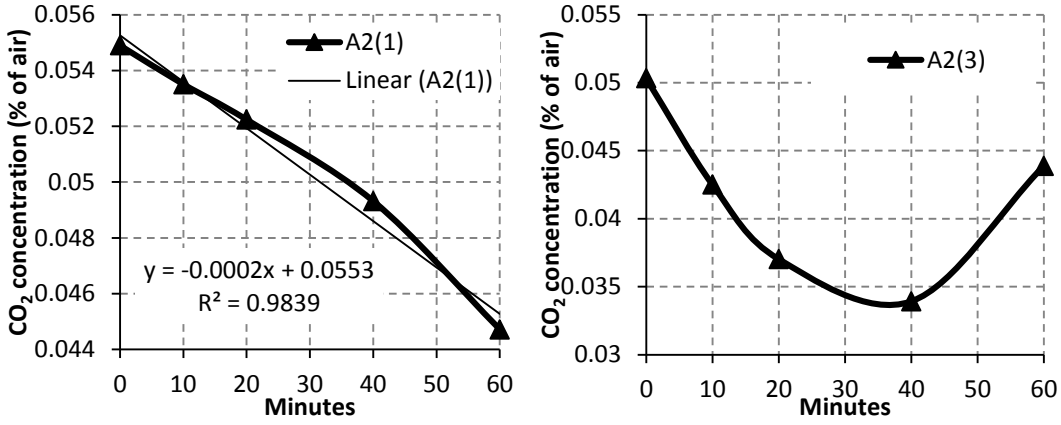

Figure 3.9 - (a) CO_2 flux for A1(2) on day 170 and (b) A2(3) on day 91

3.5.4 Measurement of carbonation front depth

3.5.4.1 Procedure

The carbonation front depth (X_c) was determined for the small specimens and the large specimens in Experiments A and B. The three sets of small specimens a, b and c in each experiment were measured for their carbonation front depth on days 20, 94, and 180 respectively. However, in Experiment B, small specimens b were examined on day 90. X_c values were measured in large specimens A and B at the end of the experiments on day 180. The procedure for measuring X_c is outlined below.

(i) Small specimens a, b and c were removed from their moulds and their heights measured before being saturated for 48 hours. ASTM (2010) recommends 24 hours; however, it is recognised for some materials that not all of the pore space may be saturated after 24 hours. Saturation does not affect the depth and level of carbonation as little carbonation occurs under water (see Section 2.7.2.2). The large specimens were similarly handled; but because of their height, they were cut horizontally in 100 mm sections to fit them in the ovens.

(ii) The saturated specimens were weighed and then split vertically using a saw or knife.

(iii) Both split surfaces for each specimen were placed in tinfoil and dried in an oven at 105°C for at least 48 hours, more depending on the size of the sample.

(iv) The mass of the specimens was again recorded; then, using the water evaporation method, their porosity was measured (see Section 3.5.4.8).

(v) All samples were covered with cling film to deprive them of oxygen and CO_2 and placed in a dry room to minimise carbonation (Chang & Chen, 2006).

(vi) One of the freshly split surfaces of each specimen was then cleaned and sprayed with a phenolphthalein indicator to measure X_c (Figure 3.10). This side was also used for determining the pH of stabilised peat slurries method. The other split surface was used for XRD, FTIR and LOI analyses (Figure 3.10).

(vii) For XRD, FTIR, LOI, and other chemical analyses, powder samples were taken from the designated half of the stabilised peat specimens at depth intervals of 2.5 to 10 mm from the top surface.

(viii) Once the XRD and FTIR samples had been obtained and analysed, the destructive technique LOI was performed on sections of the designated half of the stabilised peat specimens.

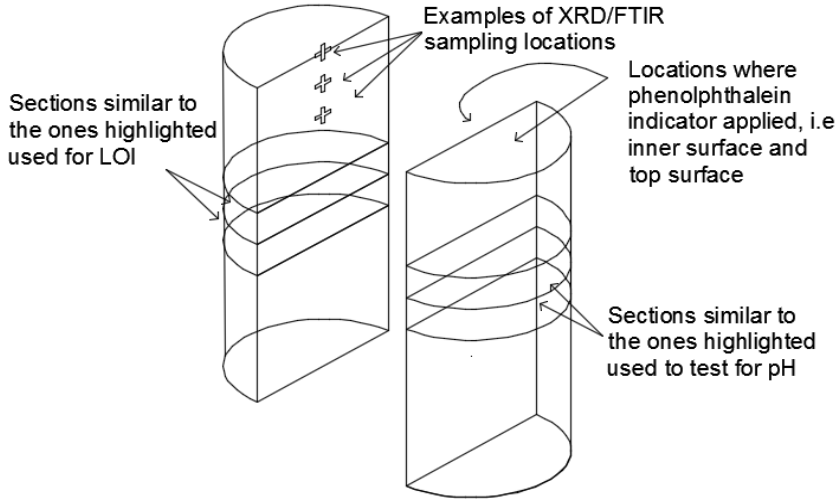

Figure 3.10 - Diagram depicting the purpose of each split surface of the small and large specimens in Experiments A and B

3.5.4.2 Intercept method

A series of steps was followed to interpret the carbonation front depth from the results of the XRD, FTIR, LOI, and pH of stabilised slurries tests. Each plot had depth on one axis and test output on the other. A technique, hereafter referred to as the intercept method, was followed to ascertain the carbonation front depth for each plot. Using a plot from results of the pH of stabilised peat slurries method as an example (Figure 3.11), the following procedure exemplifies how this method was implemented.

(i) Using the average value of the baseline points, the horizontal average line (a_1) was drawn. This baseline (a_1) represents the uncarbonated material.

(ii) pH measurements away from the baseline were fitted by a line (a_2).

(iii) The point at which a_1 and a_2 intercept was interpreted as the carbonation front depth (X_c) (Figure 3.11).

(iv) The locations of the last point on the a_2 line and the first point of the baseline (see Figure 3.11) are noteworthy since the estimated X_c cannot be below the a_2 point or exceed the baseline point. In the event of the intercept point being below the a_2 point or exceeding the baseline point, the first point on the baseline was assumed to be X_c.

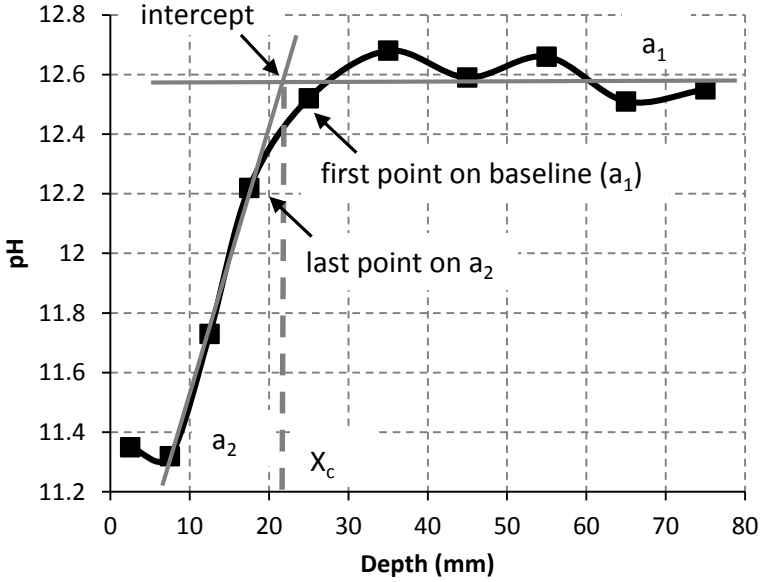

Figure 3.11 - Assessment of the depth of the carbonation front for pH of stabilised peat slurries method

3.5.4.3 Phenolphthalein indicator

The indicator used in Experiments P, A and B was made up of 1% phenolphthalein solution in 99% ethanol from Panreac AppliChem. It was applied on the top and inner surface of the split specimen, and measurements were taken immediately (Figure 3.10). The carbonated zone was indicated by the region where the indicator remains colourless, showing a pH of less than 9.0. A pink region indicated partial carbonation, while the purple region showed the uncarbonated layer (Figure 2.25) (Section 2.9.2). Using a measuring tape, the average depth of carbonation (X_c) of the region where the indicator remained colourless to the nearest millimetre was determined by taking an average of three measurements from the top surface to the colour change boundary (Equation 3.3) (Figure 3.12). If the indicator remained colourless only on the top surface of the specimen, it was assumed X_c was 1 mm.

Equation 3.3

$$X_c = \frac{\sum_{i=1}^{3} X_{ci}}{3}$$

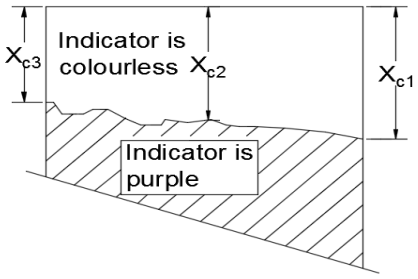

Figure 3.12 - X_c measurements using the phenolphthalein indicator on stabilised peat

3.5.4.4 X-ray diffraction analysis (XRD)

The powder method of XRD was conducted on an Inel Equinox 6000 powder X-Ray diffractometer where powder samples were analysed for 15 minutes in Experiment A and only 10 minutes in Experiment B. The reason for the time difference was that in Experiment A there were stabilised peat specimens containing GGBS; and because the mineralogy of GGBS is amorphous compared to that of cement which is crystalline, peaks are harder to identify in stabilised peat with GGBS. Therefore, the stabilised peat with GGBS required further analysis time. In both experiments, the generator settings were CuKα radiation (wavelength $\lambda = 1.54056$ m) with an X-ray tube voltage and current fixed at 35 kV and 25 mA respectively. The scan was in the range 2θ from 2–88°. To verify that the diffractometer was working satisfactorily, an X-ray diffractometer in the University of Limerick was used for some samples. The following subheadings explain the preparation of the samples, the examination of the reference curves required before analysing a stabilised peat sample and the analysis method.

Sample preparation: This was key to obtaining a homogeneous representative sample for analysis (Stutzman, 1996). As identified by Klug & Alexander (1974), items demanding thorough inspection are: particle and crystallite size, sample thickness, preferred orientation, strain, and surface planarity. Even though most of the stabilised peat was close to powder form, it was ground further with a pestle and mortar to reduce the particle size to between 1 and 10 μm to minimise peak intensity error and then made up into 10 and 40 mg samples for test purposes. If the crystallites in the sample were too large, it would lead to peak intensity variation. A small particle size sample also produces strong intensity diffraction patterns while minimising the influence of problems such as microabsorption, extinction, preferred orientation and sample homogeneity.

Reference curves: The background intensity curve (Appendix C1) was examined before analysing a stabilised peat sample as the samples were to be placed on aluminium objects which could interfere with the intensities and phases produced. Reference XRD plots were also created for cement, GGBS and peat (Appendix C1). As $CaCO_3$ appears in a

carbonated specimen and $Ca(OH)_2$ in an uncarbonated specimen, the pure phases of calcite and portlandite were also evaluated (Figure 3.13(a) and (b)). The highest $CaCO_3$ peak is at 29.4° in (a), and the highest peaks in the pure $Ca(OH)_2$ in (b) are at 18.09°, 34.09° and 47.12°.

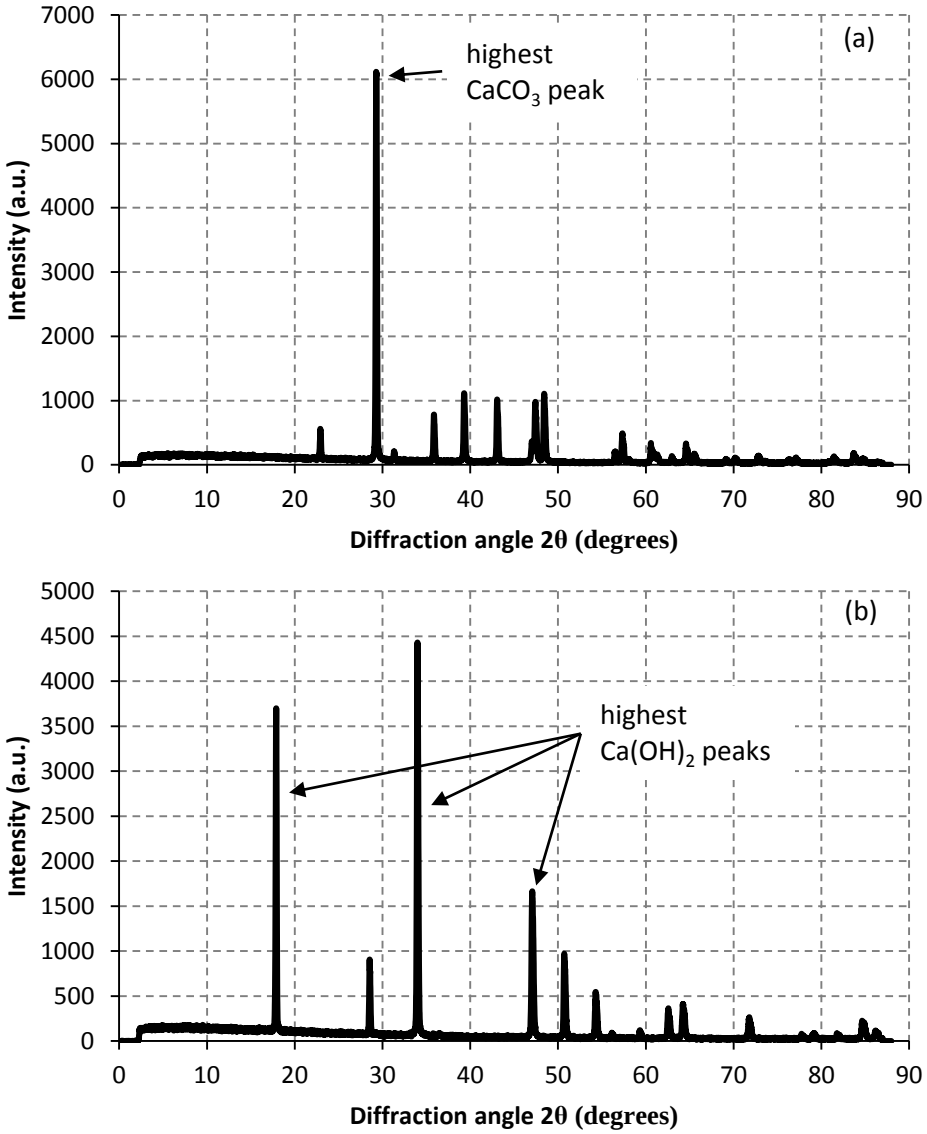

Figure 3.13 - Diffractogram of (a) pure calcite ($CaCO_3$) and (b) pure portlandite ($Ca(OH)_2$)

Analysis: In Experiment A, powder samples were taken at 10 mm intervals for a1(1a) to a8(3a). In general, for samples a1(1b) to a8(3b) and a1(1c) to a8(3c), powder samples were taken at 5 mm intervals for XRD. For the large specimens, X_c values were measured to the nearest 2.5 mm. With a greater understanding of techniques and carbonation, in Experiment B, X_c values were measured to the nearest 5 mm for the small specimens b1(1a) to b8(3a), b1(1b) to b8(3b) and b1(1c) to b8(3c) (Figure 3.14), and 2.5 mm for the large specimens B1(1) to B8(3).

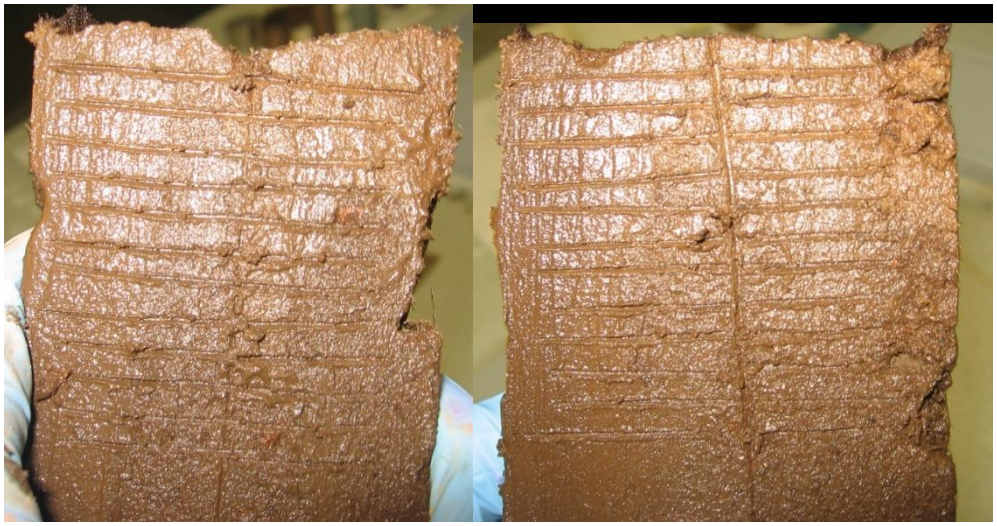

Figure 3.14 - Stabilised peat specimens with 5 mm depth intervals lined out for (a) b3(2c) and (b) b8(3c)

XRD graphs such as Figure 3.15 were plotted to find the dominant peaks, and the highest intensities of $CaCO_3$ and $Ca(OH)_2$ at the correct phases were identified. Figure 3.15(a) shows a stabilised peat sample that is considered carbonated as it is identical to the pure calcite graph (Figure 3.13 (a)) whose maximum phase occurs at 29.4°. Both peaks, $CaCO_3$ and $Ca(OH)_2$, exist in Figure 3.15(b), pointing to partial carbonation of the sample. A non-carbonated sample, Figure 3.15(c), shows high $Ca(OH)_2$ peaks in addition to the phase at 29.4°, which could represent either the original cement constituents or calcite as both phases overlap.

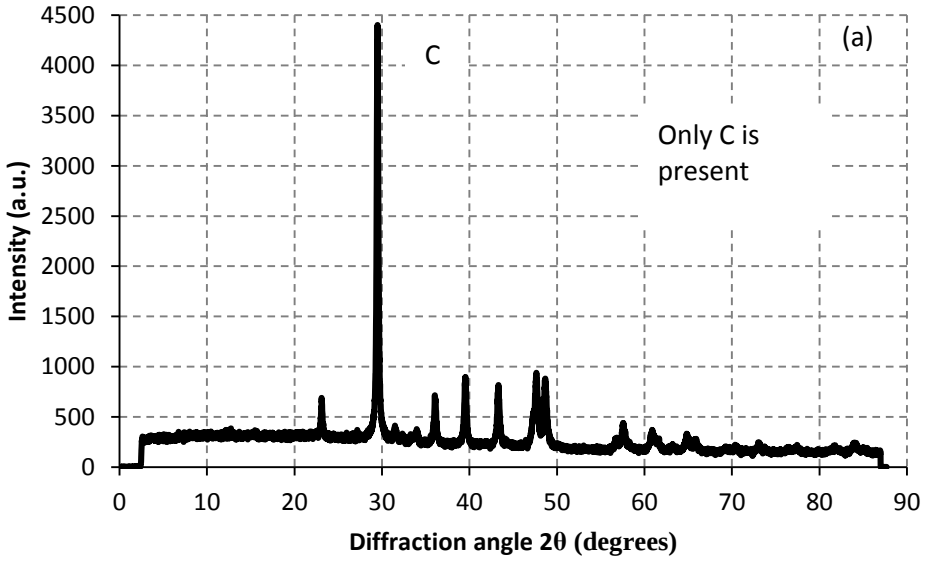

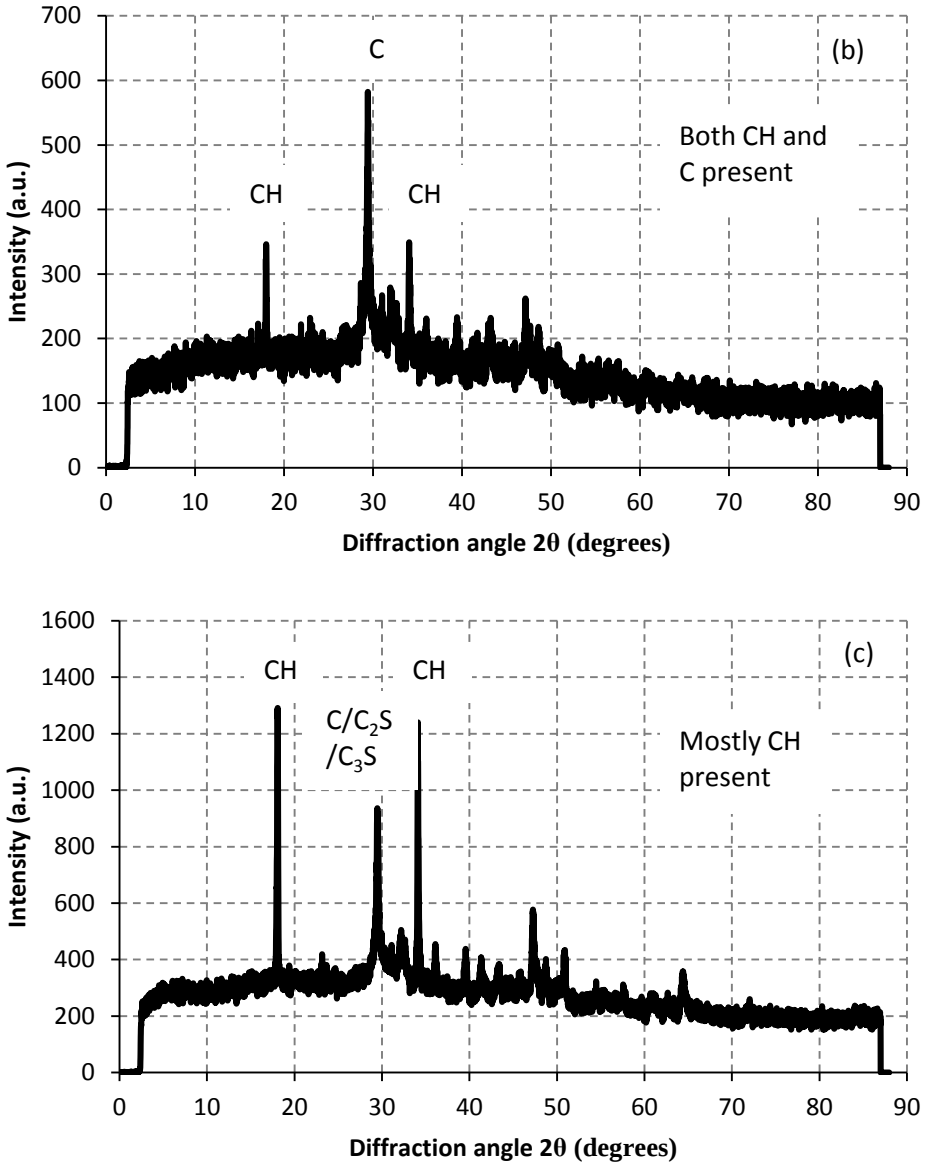

C: $CaCO_3$, CH: $Ca(OH)_2$

Figure 3.15 - (a) Carbonated a5(2c) d = 0 (b) Partly carbonated a4(1b) d = 5 (c) Uncarbonated a3(3a) d = 60

For each specimen analysed, a depth profile of the relative intensities of the diffraction peaks of $CaCO_3$ and $Ca(OH)_2$ was then produced (Section 2.9.3) (Figure 3.16). The intercept method explained in Section 3.5.4.2 was subsequently applied to plots such as Figure 3.16 on the relative intensity distribution of $CaCO_3$. As explained in Section 5.3.2.2, $Ca(OH)_2$ peaks might not be visible in some samples so the $CaCO_3$ relative intensity line is used to calculate X_c.

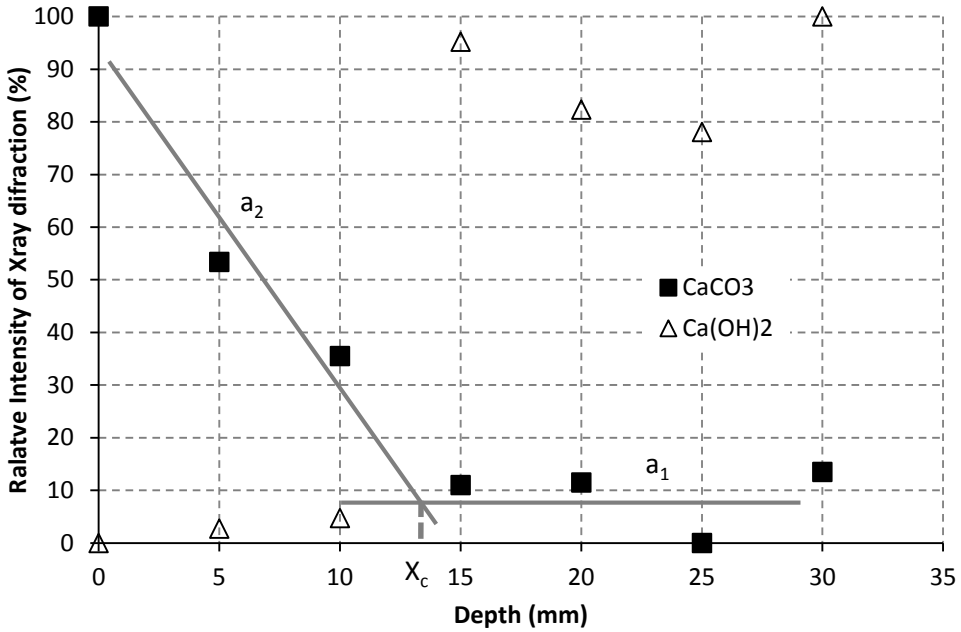

Figure 3.16 - Relative intensity of X-ray diffraction versus depth for b4(3c)

3.5.4.5 Fourier transform infrared spectroscopy (FTIR)

A Perkin Elmer Spectrum 400 FT-IR Spectometer was used to perform the FTIR analysis of stabilised peat samples. Grinding of the samples was done with a mortar and pestle to reduce the particle size to between 1 and 10 μm to minimise measurement error. The background spectrum of the laboratory environment was also scanned before scanning the dry powder samples. Each sample was scanned four times with a 4 cm^{-1} resolution in the range of 650–4000 cm^{-1}. Spectra for cement, GGBS, peat, pure $CaCO_3$ and pure $Ca(OH)_2$ were obtained as references before analysing any stabilised peat samples (Appendix C2).

In Experiment A, dry powder samples were primarily taken at 5 mm intervals from the top surface to a depth of 20 mm, thereafter increasing to 10 mm intervals for the small specimens. For the large specimens, carbonation front depths were measured to the nearest 2.5 mm. From the experience acquired in conducting Experiment A, X_c in Experiment B was measured to the nearest 5 mm for the small specimens and 2.5 mm for the large ones.

The FTIR test detects the C-O bonds and OH bonds in samples, which indicate the presence of $CaCO_3$ and $Ca(OH)_2$ respectively. Carbonation is represented by the transformation of the C=O bonds of CO_2 into C-O bonds in the $CaCO_3$. Therefore, a study of the C-O functional group in the wave number range of 1410–1510 cm^{-1} identified carbonation (Chang & Chen, 2006). The OH bond representing $Ca(OH)_2$ was found to be between 3640 and 3696 cm^{-1} (Lo & Lee, 2002). For each sample analysed, graphs such as Figure 3.17 were obtained, and the percentage of transmittance of the dominant $CaCO_3$ and $Ca(OH)_2$ peaks were measured to the nearest 0.25%. Calcite/portlandite ratios, such

as the one in Figure 3.17, were calculated to two decimal places for each sample analysed from their respective FTIR plot.

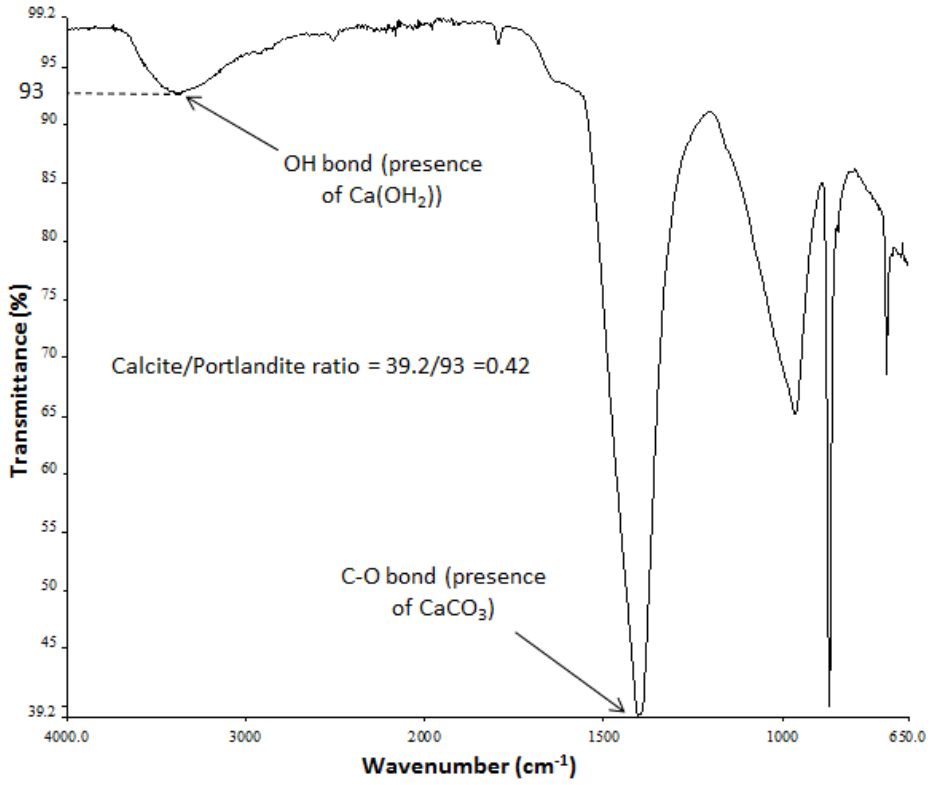

Figure 3.17 - FTIR plot showing calcite/portlandite ratio

A depth profile for each specimen of the calcite/portlandite ratios was then developed (Figure 3.18). With increasing depth from the surface, there was a corresponding increase in the calcite/portlandite ratios. X_c was calculated using the intercept method (Section 3.5.4.2) on the calcite/portlandite ($CaCO_3/Ca(OH)_2$) peak ratios such as those in Figure 3.18 for a5(3b).

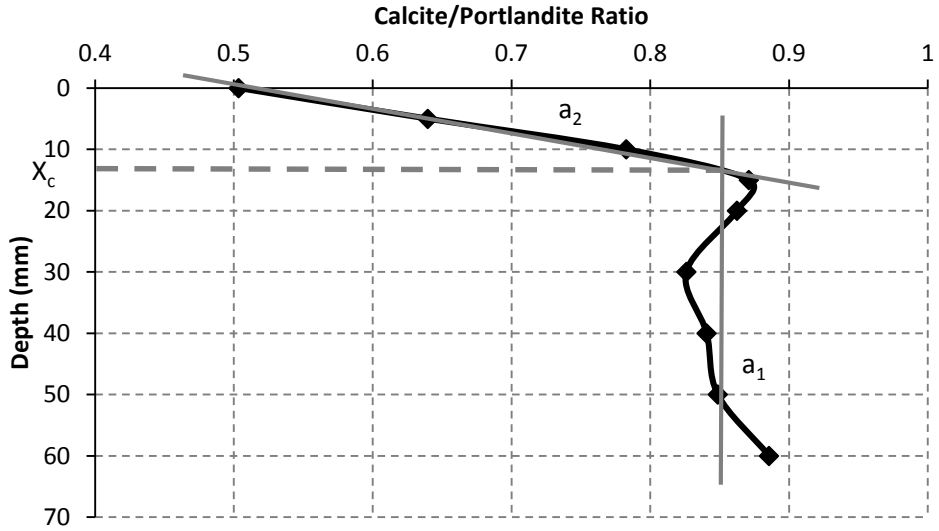

Figure 3.18 - Calcite/portlandite ratio versus depth for FTIR analysis on a5(3b)

3.5.4.6 Thermogravimetric analysis (TGA) and Loss on Ignition (LOI)

The TGA method, described in Section 2.9.5.1, is a suitable technique for determining the depth and level of carbonation but is a costly process and requires a TGA analyser that can hold typically only between 10 and 30 mg of sample, Although TGA was trialled, a muffle furnace (LOI technique) was found to be more practicable to calculate the degree of carbonation and carbonation depth as muffle furnaces are more readily available and a larger sample (0–10g) could be used, which is more representative of the stabilised peat at the sampling depth.

To help develop and calibrate the temperature ranges at which $Ca(OH)_2$ and $CaCO_3$ decomposition occurs in stabilised peat, several samples were taken to the University of Limerick for TGA analyses. The TGA model was a Setaram Labsys DTA/DSC/TGA simultaneous thermal analyser that had a maximum temperature capability of 1400°C. Due to the time needed and the expense associated with each analysis, only two samples were analysed. These were taken at depths (d) of 0 mm (25.3 mg) and 50 mm (11.7 mg) from a5(3c). Of all the small and large specimens analysed, a5(3c) had the greatest carbonation depth and lowest pH at the surface, showing the d = 0 mm sample to be ideal for measuring the maximum temperatures at which $CaCO_3$ decomposition can occur. The d = 50 mm sample was shown by XRD and FTIR to be in the uncarbonated zone with plenty of $Ca(OH)_2$ present, making this sample an ideal candidate for showing the temperature at which $CaCO_3$ decomposition occurs in the uncarbonated zone, if any. More stable calcite exists in the carbonated zone than in the uncarbonated zone and decomposes at a higher temperature.

The samples were analysed from room temperature to 1000°C, with the temperature ramped up 10°C/min. For the sample at d = 0 mm, $CaCO_3$ decomposed between 700°C and 850°C (to the nearest 50°C) as shown by the endothermic peak on the TG-DTA curve (Figure 3.19 (a)), but the d = 50 mm curve showed $CaCO_3$ to decompose sooner at between 650°C and 800°C (to the nearest 50°C) (Figure 3.19(b)). This is because the $CaCO_3$ is not as stable in the d = 50 mm sample. An endothermic $Ca(OH)_2$ peak is also observed between 440°C and 480°C (to the nearest 10°C) in this sample.

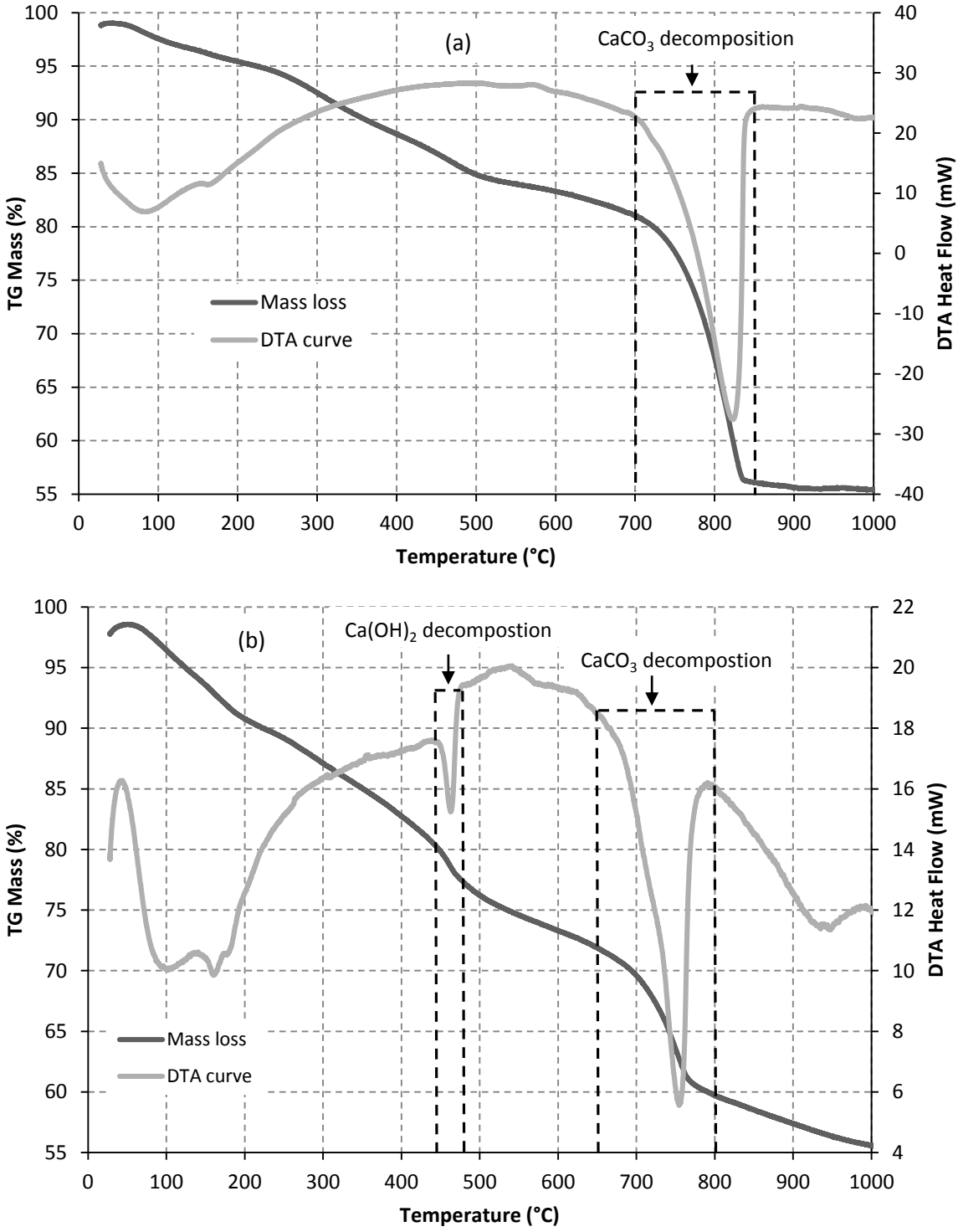

Figure 3.19 - TGA analysis with mass against temperature (a) a5(3c) d = 0 and (b) a5(3c) d = 50

By applying the knowledge gleaned from the literature on measuring carbonation in concrete and cement pastes using TGA (Table 2.10) combined with the TGA results from stabilised peat in Figure 3.19, a procedure for the use of the furnace was devised (Table 3.6). Appropriate temperature ranges displayed in Table 3.6 were developed to quantify organic matter, $Ca(OH)_2$ and $CaCO_3$. The table shows the temperature ranges for the LOI procedure, except for the first range which had already taken place prior to these analyses.

The dry samples were put in the oven for a minimum of one hour, removed, and weighed at 440°C, 520°C, 650°C and 850°C. From 0°C to 440°C and 650°C to 850°C, a minimum two-hour period in the furnace was allowed. It was assumed that losses above 850°C would be negligible as the calcite present would be small in granular size and would decompose quickly.

Table 3.6 - Temperature ranges for LOI technique

Number	Temperature Range (°C)	Decomposition of hydrates or carbonated products
1	0–105	Water (ASTM, 2007)
2	105–440	Organics (ASTM, 2007)
3	440–520	H_2O from portlandite ($Ca(OH)_2$)
4	520–650	OH^- from structure of hydrates, structure H_2O or CO_2 from vaterite, and C-S-H carbonation
5	650–850	CO_2 from calcite of carbonation

In Experiment A, only the small 'c' specimens (i.e. a1(1c) to a8(3c)) and the large specimens A1–A8 were analysed using the LOI technique. In the majority of cases, 5 mm depths of oven-dried stabilised peat from the stabilised peat surface, starting at 0–5 mm and extending to 45–50 mm, were placed in the muffle furnace. Samples were between 2 and 6 grams depending on the mass of the 5 mm sections. For Experiment B, the small and large specimens were used, taking 5 mm thicknesses, starting at 0–5 mm and extending to depths of 45–50 mm.

Using a modified version of Equation 2.20, Equation 3.4, to find the percentage carbonated (D_c) for each depth, taking C as the CO_2 mass loss between 650 and 850°C, the temperature range where $CaCO_3$ primarily decomposes, graphs of D_c against depth were plotted for each specimen as exemplified in Figure 3.20. The reasons for omitting C_0 (initial CO_2 concentration in the uncarbonated sample) from Equation 3.4 will be become apparent in Chapter 5. From the stabilised peat surface, the amount of $CaCO_3$ or CO_2 released decreased to a point where D_c was relatively constant, points beyond this are part of the D_{c0} line or baseline. X_c was again calculated using the intercept method defined in Section 3.5.4.2.

$$D_c(\%) = \frac{C}{C_p} \qquad \textbf{Equation 3.4}$$

The mass loss at 520 to 650°C was not accounted for initially in calculating X_c because there is an overlap between $Ca(OH)_2$ and $CaCO_3$ decomposition (see Section 2.9.5.4). Some vaterite and CSH decomposition was anticipated at this temperature range, especially in the stabilised peat containing GGBS, which produces more vaterite than in stabilised peat with cement only. To see if there was a change in X_c, D_c was calculated

differently for all the stabilised peat specimens by assuming C to be a combination of the mass losses between 520 and 650°C and 650 and 850°C. If there was a difference in X_c, this alternative depth was used if it could be proved by XRD and FTIR that the sample contained vaterite and no $Ca(OH)_2$, as this would mean the decomposition occurring between 520 and 650°C was solely due to unstable $CaCO_3$ decomposition (vaterite). This will be discussed further in Section 5.3.4.3.

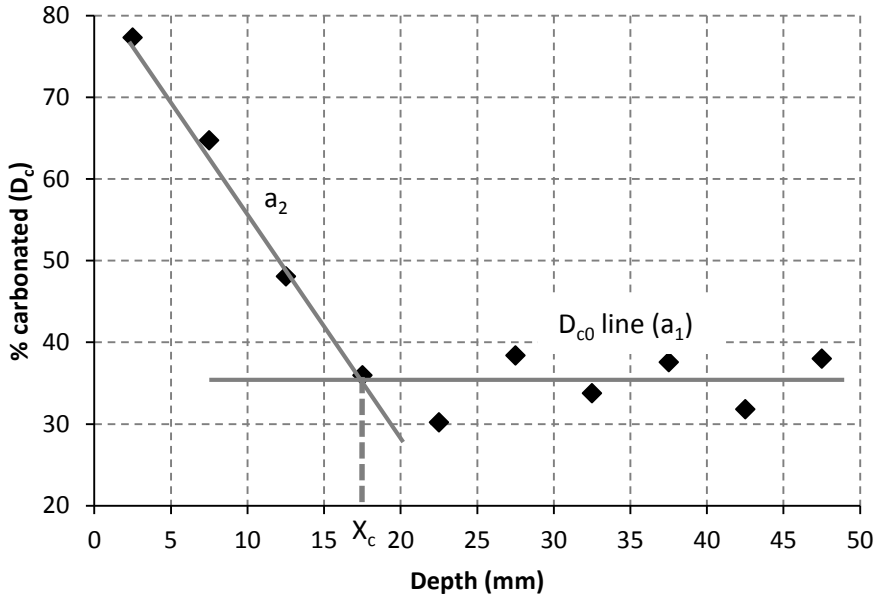

Figure 3.20 - LOI analysis plot of percentage carbonated against depth for A4(3)

To confirm that the mass loss between 520 and 650°C was not due to organics, two peat controls, A8(1) and A8(2), were studied. Results revealed that less than 2% of the mass loss in the controls occurred between 440°C and 850°C, with the mass loss between 520°C and 650°C averaging less than 0.3%. These results proved that the mass loss due to peat was negligible.

3.5.4.7 pH of stabilised peat slurries

The pH meter in this test had an electrode and temperature probe [HI-83141] with an accuracy of ± 0.01 pH / ± 1 mV / ± 0.4°C at 20°C and a typical EMC deviation ± 0.07 pH / ± 5 mV / ± 1°C (Figure 3.21). The stabilised peat was crushed and placed in containers. The pH of stabilised peat slurries technique was performed using BS 1377-3:1990 for the electrometric method of pH determination for Experiment P (BSI, 1996). However, for Experiments A and B, only 2 to 6 grams of material was available so a 1:10 solid to liquid ratio (Chang & Chen, 2006) was used to facilitate the insertion of the pH probe into the solution. The mass of material available depended on the density and volume of the stabilised peat.

Figure 3.21 - pH meter, probe and containers used

In Experiment A, the small specimens were not used to calculate X_c as an inadequate number of data points was retrieved for each specimen with section intervals of only 20 mm, 0–20, 20–40 and 0–60 mm tested for pH. Instead, statistical analyses were carried out to see if there were any relationships between pH, time and depth. For the small specimens in Experiment B, however, the pH of 10 mm section intervals from a depth of 0 to 50 mm was measured, giving enough points to infer a carbonation front depth. For the large specimens in Experiments A and B, section intervals of 5 mm were taken to a depth of 20 mm, thereafter 10 mm sections were taken to a depth of at least 80 mm. Section 3.5.4.2 explains the method for determining X_c and includes Figure 3.11, which shows pH against depth. The pH increases with depth from the surface as the degree of carbonation decreases.

3.5.4.8 Porosity

As discussed in the Section 2.9.7, it was thought that if the porosity decreased over time, it may indicate carbonation. Using the water evaporation method to calculate porosity, described briefly in Section 3.5.4.1, the small and large specimens were saturated by leaving them in water for 48 hours, bearing in mind that the large specimens were cut horizontally in 100 mm sections so that they could fit into the ovens. The specimens were removed from the water, split in half, placed in tinfoil, and put in the oven at 105°C for at least 48 hours. The mass of the specimen was measured before and after drying, and the pore volume (V_v) corresponded to the water content of the specimen at saturation (Equation 3.5). The porosity (ϕ) was then calculated by dividing the pore volume (V_v) by the total volume of the sample (V_t) (Equation 3.6).

$$\text{Pore Volume } (V_v)\ (cm^3) = \frac{\text{mass of saturated sample (g) - mass of dried sample (g)}}{\text{density of water } (g/cm^3)} \quad \textbf{Equation 3.5}$$

$$\text{Porosity } \Phi = \frac{V_v \times 100}{V_t} \quad \textbf{Equation 3.6}$$

3.5.4.9 Other techniques

Additional techniques were used to enhance the understanding of stabilised peat and the carbonation process and contributed to supporting some of the carbonation depth techniques. These included ICP-AES, SEM and EDX. The ICP-AES analyses were carried out by ALS Geochemistry to obtain the chemical properties of cement, GGBS and some stabilised peat in terms of major oxides such as calcium oxide (CaO), silicon dioxide (SiO_2), and aluminium oxide (Al_2O_3). The quantity of these oxides in stabilised peat can be adopted as tracers of cement and were used to determine the cement content of some samples. SEM and EDX analyses were performed in Athlone Institute of Technology and NUIG. The SEM provided some highly magnified images of stabilised peat, while the EDX analyses gave the elemental composition of stabilised peat samples in terms of elements such as carbon, oxygen and silicon.

3.6 Minitab statistical analysis methods

3.6.1 One-way analysis of variance (ANOVA)

For the gas fluxes, one-way analysis of variance (ANOVA) was carried out using Minitab 16 to see if replica specimens such as A1(1), A1(2) and A1(3) had similar means and if two specimen types such as A1 and A2 behaved similarly. A significant difference was evident between the means of the specimens when the p-value was less than 0.05. P-values < 0.05 were highlighted in bold. For the results on the carbonation front depths, ANOVA was applied to discover if results from the carbonation depth techniques examined were similar or significantly different from each other and to see if replica specimens had similar or significantly different carbonation fronts for each technique. Obtaining p-values of less than 0.001 indicated a highly significant difference; a p-value of less than 0.2 meant there was a slight encouraging trend towards a difference; a p-value of greater than 0.2 showed that there was no difference.

3.6.2 Reconstruction of gas flux and depth of carbonation front

3.6.2.1 Correlation statistics

The effect of variables (predictors) such as time, surcharge and cement content on the CO_2 flux from stabilised peat and on the depth of the carbonation front (X_c) was examined initially using correlation statistics. Bivariate correlation analyses were performed to indicate if independent variables had an effect on or a relationship with the dependent variable and were judged by their significances, interpreted by p-values. The same level of significance was used as for one-way ANOVA (Section 3.6.1), where a p-value of less than 0.05 was considered significant, showing a significant correlation between the independent and dependent variable examined. Correlation statistics and linear regression models were an important first step an understanding the carbonation process in stabilised peat.

3.6.2.2 Multiple linear regression analysis

To expand on the linear relationships found between the dependent variables CO_2 flux and X_c and the independent variables, multiple linear regression analysis, a more powerful extension of linear regression, was carried out using Minitab 16 to produce best-fit statistical models/equations for CO_2 flux and X_c, models that were developed using a backward elimination method. Backward elimination started with all the predictors in the model, including interaction variables. The least significant variable, that is, the one with the largest p-value, was removed and the model refitted. This process was continued, removing the least significant variable in the model until all remaining variables had individual p-values smaller than 0.05. P-values < 0.05 are highlighted in bold.

Each model produced by Minitab gives descriptive statistics, including the coefficients of the variables included in the model along with their standard error. Four residual graphs were also produced to visually analyse the model constructed and are used to examine the goodness-of-fit of regression:

- Normal probability plot of the residuals: verifies the assumption that the residuals are normally distributed, which follows a straight line if normal.
- Residual values versus fitted values: verifies the assumption that the residuals have a constant variance. It is used to check for independence and similar variance. Residuals should behave like white noise, and the variance of the error terms must have a mean of zero.
- Histogram of the residuals: shows if there is a violation of normality of the underlying random response at each combination of the covariates.

- Residuals versus the order of the data: verifies the assumption that the residuals are uncorrelated. The residuals in the plot should fluctuate in a random pattern around the centre line.

Models were not judged merely on their R^2 values but were used along with the above graphs and other values such as the variance inflation factor (VIF), lack-of-fit value, adjusted R^2 and predicted R^2 as well as the sample size to assess the quality of the model. For explanations on these terms, see Appendix D2. Plots of the actual observations versus the predicted or fitted values were also plotted to discover how well the model predicted the experimental data and individual observations.

In a first attempt to assess the correlation between the predictors or variables, a correlation analysis using Pearson correlation was performed to indicate predictors that may have a possible effect on each other and their significances. A significance value of greater than 0.05 indicated some sort of correlation. A high/strong correlation has a Pearson correlation coefficient of between 0.5 and 1, a medium/moderate correlation of between 0.3 and 0.5, and a low/weak correlation of between 0.1 and 0.3. This helped to identify multicollinearity and interaction between variables. For each model constructed, multicollinearity was checked by examining the VIF values, and interaction between variables was also checked by creating interaction plots.

Cross-validation was also carried out on the final statistical models/equations produced by taking a subset of the data and performing multiple linear regression analysis. How well the model predicted all the data (subset and removed data) was then determined. If the statistical model still produced an R^2 adjusted value similar to the original model; if the same variables were significant; and if the coefficients and signs for the significant variables were similar to the original model, the original model was considered to be a good predictive model.

After producing best-fit models for the CO_2 flux and carbonation depth results for Experiments A and B separately, a meta-analysis was carried out to increase the sample size. A meta-analysis is a statistical technique for combining the findings from independent studies, which in this case involved combining the CO_2 flux results from Experiments A and B and combining the carbonation front depth results from both experiments. Multiple linear regression analyses were then performed on these larger data sets.

3.6.2.3 Sensitivity analysis

The sensitivity of the final equations/statistical models, developed from the CO_2 gas flux results, to changes in the input variables was examined using Excel. The global sensitivity analysis performed adjusted more than one variable at a time, and the Monte Carlo simulation was run for multiple combinations of inputs to find the sensitivity of the final equations/statistical models and to discern to which variables the final equation/model was most sensitive. Each simulation was run 1000 times with the help of the random function, normdist function and the data table tools in Excel.

Chapter 4: Gas Fluxes

4.1 Introduction

This chapter first describes the properties of the raw and stabilised peat used in Experiments P, A and B and the environmental conditions to which they were subjected in the laboratory. The gas flux measurements (i.e. the change in CO_2 concentrations in the headspace of each column) derived using the closed chamber method are then presented and analysed; the results of Experiment P are presented in Section 4.5 and the results of Experiments A and B in Section 4.6.

One-way ANOVA and multiple linear regression analysis are statistical tools used to identify the significant variables determining the gas fluxes in Experiments P, A and B. Best-fit regression models are produced for each experiment, and cross validation and sensitivity analyses are performed on the best-fit models. A meta-analysis is then carried out, which combines the CO_2 flux results from stabilised peat in Experiments A and B to produce a more powerful regression model.

Finally, Section 4.7 discusses the linearity of the gas flux calculations and the test time that gives the best-fit flux-time relationship, whether it is 10, 20, 40 or 60 minutes.

4.2 Properties of raw and stabilised peat

4.2.1 Raw peat

Immediately after the peat cores were brought to the laboratory, the properties of the raw peat were examined and are summarised in Table 4.1. The peat retrieved for Experiments P, A and B was acidic and classified to be at a H2–H4 stage of degradation (von Post, 1922; Hobbs, 1986). The lower organic and moisture content in Experiment P were due to one of the nine samples having a much lower moisture and organic contents of 552% and 55% respectively. Excluding this sample, the organic content and moisture content were 998 ± 175% and 93 ± 4% respectively, and were more consistent with averages in Experiments A and B.

Table 4.1 - Average values for the raw peat properties for Experiments P, A and B (± referring to one standard deviation from the mean)

Properties	Experiment P	Experiment A	Experiment B
pH	5.07 ± 0.06 (n = 6)	4.90 ± 0.69 (n = 9)	4.99 ± 0.54 (n = 6)
Humification degree	H2–H4	H2–H4	H2–H4
Bulk density (kg/m^3)	955 ± 23 (n = 5)	1037 ± 16 (n = 9)	992 ± 32 (n = 6)
Organic content (%)	88.36 ± 13.25 (n = 9)	96.97 ± 1.96 (n = 21)	96.18 ± 6.31 (n = 24)
Moisture content (%)	949 ± 221 (n = 9)	1195 ± 208 (n = 21)	1039 ± 146 (n = 24)

4.2.2 Stabilised peat

Table 4.2 summarises the properties of mixes in each experiment used to create the large specimens. The average organic contents of the stabilised peat for each specimen type ranged from 19.4% in B5 to 36.9% in B1, while the average moisture content ranged from 203% in B5 to 412% in A1.

Table 4.2 - Average values for the raw peat and stabilised peat properties for Experiments P, A and B (± referring to one standard deviation from the mean)

Columns	Peat			Stabilised peat	
	Bulk density (kg/m^3)	**Moisture Content (%) n = 3**	**Organic Content (%) n = 3**	**Moisture Content (%) n = 3**	**Organic Content (%) n = 3**
			Experiment P		
P1-P3	955 ± 23 (n = 5)	949 ± 221 (n = 9)	88 ± 13 (n = 9)	237 ± 28	24.1 ± 3.4
			Experiment A		
A1	1028	1176 ± 129	96.5 ± 1.1	412 ± 32	36.6 ± 3.5
A2	1020	1031 ± 69	97.3 ± 1.1	325 ± 10	29.6 ± 1.2
A3	1053 ± 19 (n = 3)*	1094 ± 127	96.9 ± 0.9	321 ± 6	28.8 ± 1.0
A4	1031	1108 ± 120	92.9 ± 2.8	271 ± 7	24.3 ± 0.3
A5	1037	1430 ± 352	98.1 ± 0.7	264 ± 1	26.2 ± 1.0
A6	1037	1285 ± 135	98.1 ± 0.3	288 ± 6	26.2 ± 0.6
A7	1023	1375 ± 221	98.0 ± 0.6	271 ± 3	26.0 ± 1.0
A8			Natural peat		
			Experiment B		
B1	1002	991 ± 57	97.2 ± 0.4	358 ± 5	36.9 ± 2.3
B2	933	1135 ± 204	97.9 ± 0.8	324 ± 3	29.0 ± 0.2
B3	989	986 ± 52	98.4 ± 1.1	258 ± 4	23.7 ± 0.3
B4	1032	1046 ± 74	97.9 ± 1.0	315 ± 77	29.2 ± 7.1
B5	1000	1156 ± 213	97.6 ± 2.0	203 ±29	19.4 ± 3.3
B6		929 ± 240	86.9 ± 17.2		
B7		1069 ± 129	97.5 ± 1.4		
B8	998	947 ± 48	96.1 ± 1.3	273 ± 10	26.5 ± 1.4

* See Section 3.4.3.1: three identical mixes done for A3, i.e. one for A3(1), A3(2) and A3(3).

4.2.3 Comparison

All individual organic and moisture content values for the peat determined before and after stabilisation are plotted in Figure 4.1, which includes samples from mixes used to create both large and small specimens in each of the Experiments P, A and B. Figure 4.1 shows that after peat stabilisation the moisture and organic contents decreased significantly. For example, in Experiment P the moisture content of the stabilised material was measured immediately after mixing and was found to have decreased from 767% to 206% in P3(1), 1157% to 258% in P3(2), and 1036% to 247% in P3(3). After 228 days these moisture

contents had reduced further but marginally, suggesting additional cementitious reactions and/or evaporation.

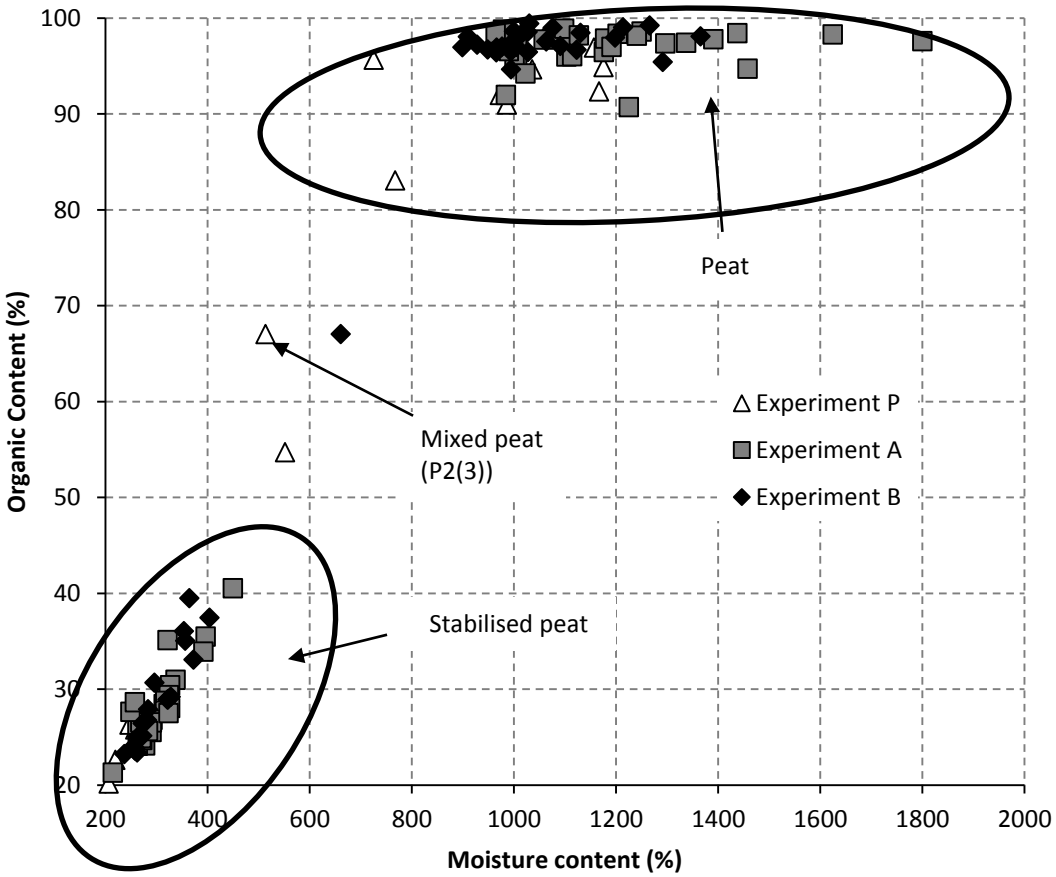

Figure 4.1 - Organic versus moisture content for the peat and stabilised peat columns in Experiments P, A and B

There is no correlation (p = 0.325) between the ratio of initial to final moisture content with binder content (Appendix D1). However, a significant correlation (p = 0.000) between organic and moisture content for the stabilised peat, reflecting binder content, is apparent in Figure 4.2, which is a close-up of the relevant section of Figure 4.1. Figure 4.2 shows that a mix with a higher binder content generally has a lower moisture and organic content. The data are represented alternatively as plots of binder content against moisture content (Figure 4.3(a)) and binder content against organic content (Figure 4.3(b)), also showing significant relationships (p = 0.000). These figures give confidence in the quality of the process for producing stabilised column samples.

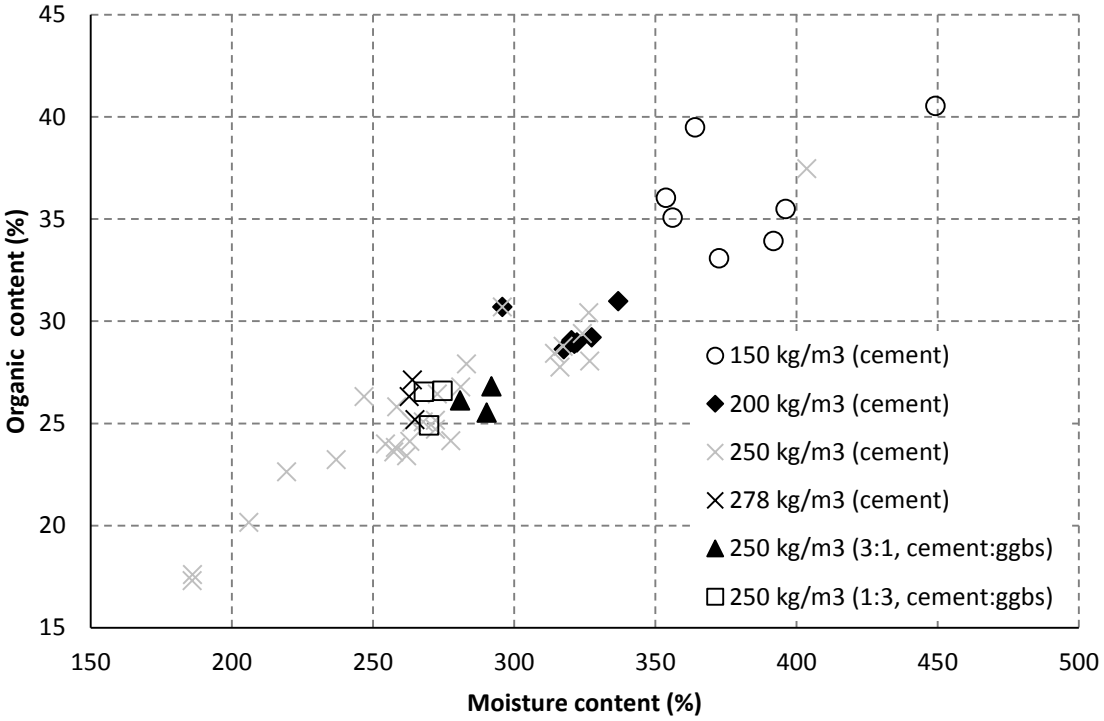

Figure 4.2 - Variation in organic content with moisture content for stabilised peat columns in Experiments P, A and B (close-up of stabilised peat in Figure 4.1)

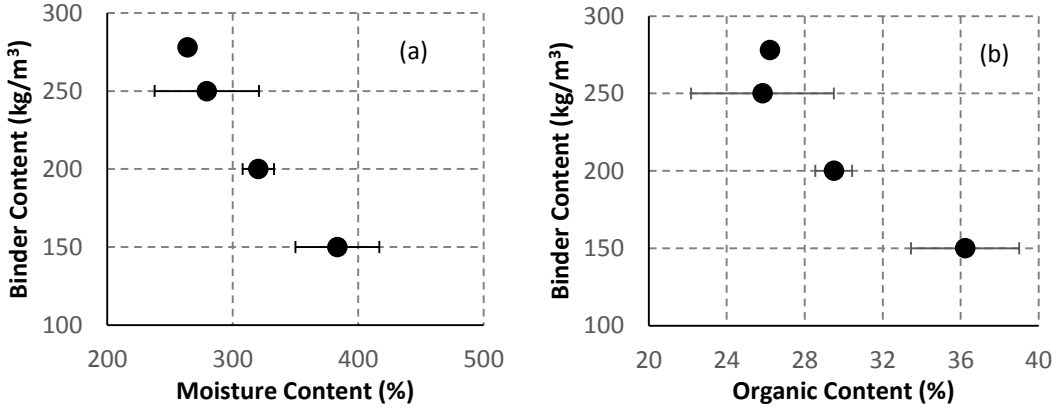

Figure 4.3 - Relationship in stabilised peat between (a) binder and moisture content and (b) binder and organic content (means with standard error bars)

4.3 Environmental measurements

In Experiment P, the CO_2 concentration in the control room averaged 803 ± 96 ppm (n = 5495), and the humidity ranged from 60 to 90%. The temperature was changed three times, dictated by another experiment taking place in the room, and the average temperatures and their standard deviations are shown in Table 4.3.

Table 4.3 - Measured temperatures from day 1 to 228 in Experiment P

Time (Day)	Set temperature (°C)	Actual temperature (°C)
1–137	15	15.9 ± 0.4
137–194	20	20.9 ± 0.4
194–227	10	11.2 ± 0.3
227–228	20	19.7 ± 0.6

For Experiments A and B, the temperature and humidity were kept nominally constant, and the CO_2 concentration and temperature readings were taken every hour. In Experiment A, the CO_2 concentration in the control room averaged 741 ± 74 ppm (n = 3151), the temperature 20.7 ± 0.4°C (n = 3151), and the humidity 70.1 ± 4% (n = 62). In Experiment B, the CO_2 concentration in the control room averaged 701 ± 52 ppm (n = 4060), the temperature 20.8 ± 0.4°C (n = 4060), and the humidity 69.8 ± 1.5% (n = 43). These data indicate that Experiments A and B were conducted under comparable conditions.

4.4 CO_2 concentration difference in the headspace

Before examining the CO_2 flux results from stabilised peat, the various contributors to the CO_2 flux are discussed. The gas flux, which is the concentration difference in the headspace ($CO_{2\ cd,h}$) (4) over the chamber deployment time, can be broken into sub parts, highlighted by numbers 1–3 in Figure 4.4 and shown in Equation 4.1.

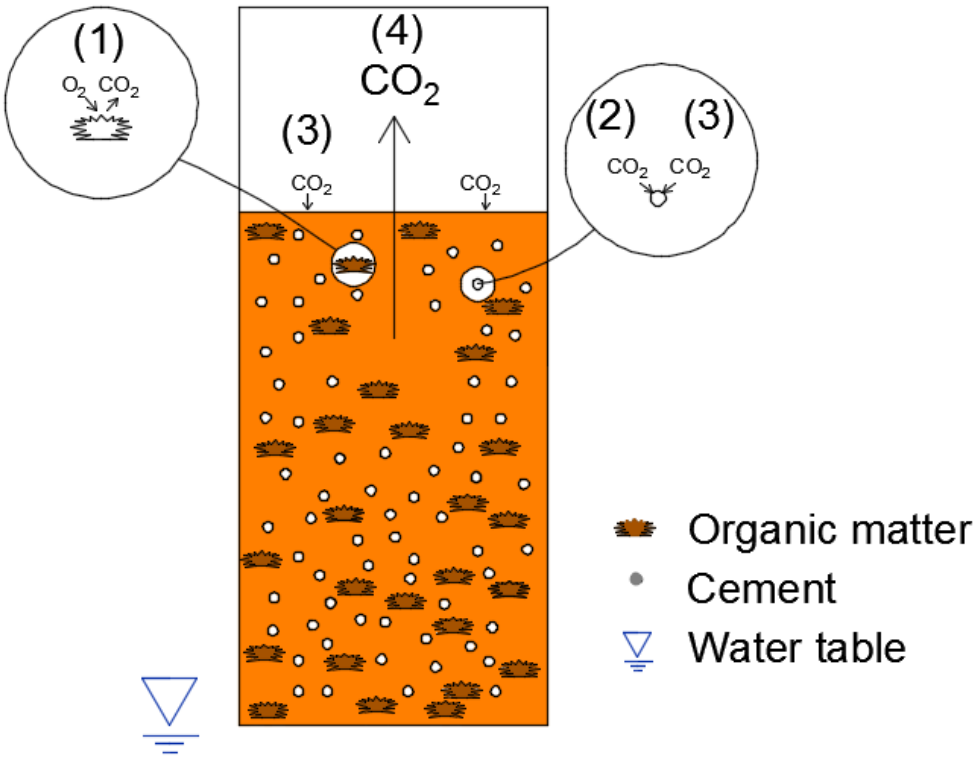

Figure 4.4 - The carbonation process in stabilised peat

$$CO_{2\ cd,h}\ (4) = CO_{2\ peat}\ (1) + CO_{2\ i,peat}\ (2) + CO_{2\ i,h}\ (3) \qquad \textbf{Equation 4.1}$$

where:

- $CO_{2\ peat}$ (1) (mg CO_2eq/m^2/hr) is the mass of CO_2 released by the organic matter in the stabilised peat as a result of oxygen in the aerobic layer oxidising the organic matter. This is a positive term as it is a source of CO_2.
- $CO_{2\ i,peat}$ (2) (mg CO_2eq/m^2/hr) is the mass intake of CO_2 from the CO_2 released by the peat, which reacts with calcium ions (Ca^{2+}) from the cement due to carbonation. This is a negative term as it is a CO_2 sink.
- $CO_{2\ i,h}$ (3) (mg CO_2eq/m^2/hr) is the mass intake of CO_2 from the atmosphere/headspace into the stabilised peat due to a CO_2 diffusion gradient caused by carbonation. This CO_2 reacts with Ca^{2+} and is another negative term as it, too, is a CO_2 sink. $CO_{2\ carbonation}$ is the sum of (2) and (3) and is the net intake of CO_2 due to carbonation.
- $CO_{2\ cd,h}$ (4) (mg CO_2eq/m^2/hr) can be a positive or negative term depending on the net CO_2 flux, which is contingent on the strength of the carbonation and peat oxidation rates.

4.5 Experiment P

4.5.1 Height changes in peat and stabilised peat

The column heights in Experiment P changed slightly over time. In P1 they dropped when the water level was lowered and then gradually decreased for the remainder of the experiment due to a combination of self-weight settlement and peat oxidation. P2 responded to the rise in water level by increasing in height, after which the heights became constant. The height of the stabilised peat columns P3 decreased initially due to compression under their own weight and then marginally decreased over time due to further compression and peat oxidation. All these changes are illustrated in Figure 4.5 and are relevant to determination of headspace volumes.

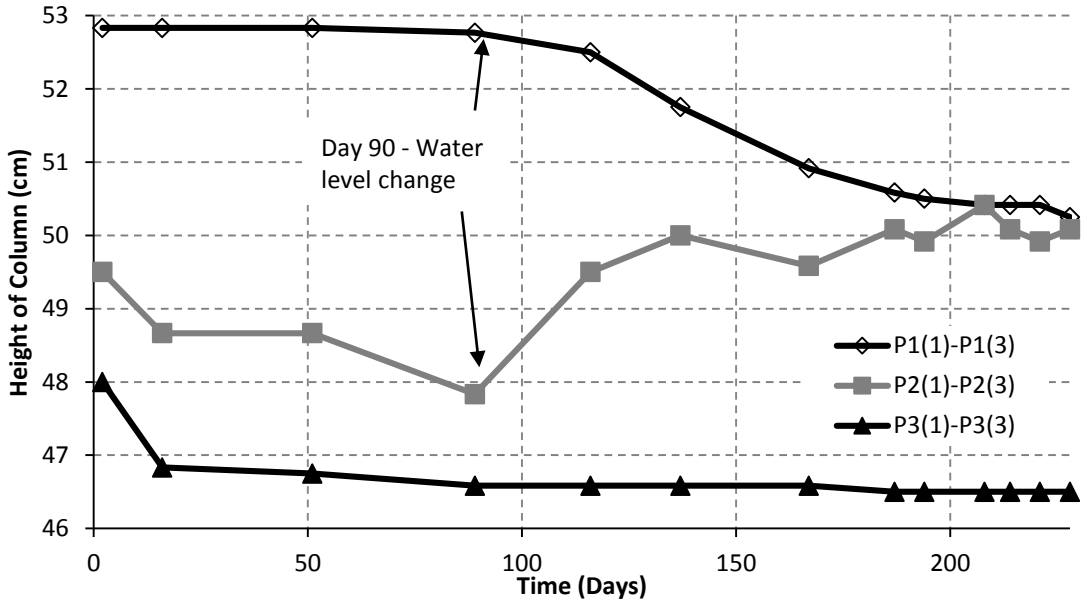

Figure 4.5 - Average heights for columns P1, P2 and P3 over the duration of Experiment P

4.5.2 CO_2 and CH_4 flux

4.5.2.1 Introduction

Over the 228-day duration of Experiment P, 22 gas sampling events took place. As the relationships between gas concentration change and chamber deployment time at each gas sampling event were mostly linear for unstabilised columns P1 and P2 in Experiment P, the results are discussed using the 0–60 minute flux, which is the average flux over this time period. However, for stabilised peat columns P3 in Experiment P, the 0–20, 0–40 and 0–60 minute CO_2 fluxes are calculated because of evidence of non-linearity in the gas concentration change against time plots. On day 1, for example, the gas concentration with time plots for all raw peat columns P1 and P2 (n = 6) had an R^2 of 0.99 ± 0.01 over 60 minutes, while the stabilised peat columns (P3) (n = 3) plots had an R^2 of only 0.72 ± 0.1.

4.5.2.2 Peat columns P1

Specimens P1, where the water table was at the surface initially, experienced high short-term fluxes of CO_2 and CH_4 release at the outset. Emissions then stabilised, reducing from an average of 477 ± 496 mg $CO_2eq/m^2/hr$ (±1 standard deviation) over the first four days to 49 ± 33 mg$CO_2eq/m_2/hr$ from day 6 to day 89 (Figure 4.6).

On day 90 after water levels were lowered, short-term high fluxes of CH_4 gas were again noted, which is consistent with observations made in wetlands where major fluxes of CH_4 occurred after a drop in the water table due to drought (Couwenberg, 2009). Gas emissions then decreased to drained peat flux levels, consistent with gas fluxes in specimens P2(1)–P2(2) before day 90 (see Section 4.5.2.3). Thereafter, in specimens P1, emissions fluctuated according to temperature, first increasing to an average of 223 ± 61 mg

$CO_2eq/m^2/hr$ at 20°C, then decreasing to 68 ± 46 mg $CO_2eq/m^2/hr$ at 10°C, and finally increasing on day 228 at 20°C. For a more in-depth analysis of the results, individual graphs of CO_2 and CH_4 are presented in Appendix D2 for P1(1)–P1(3).

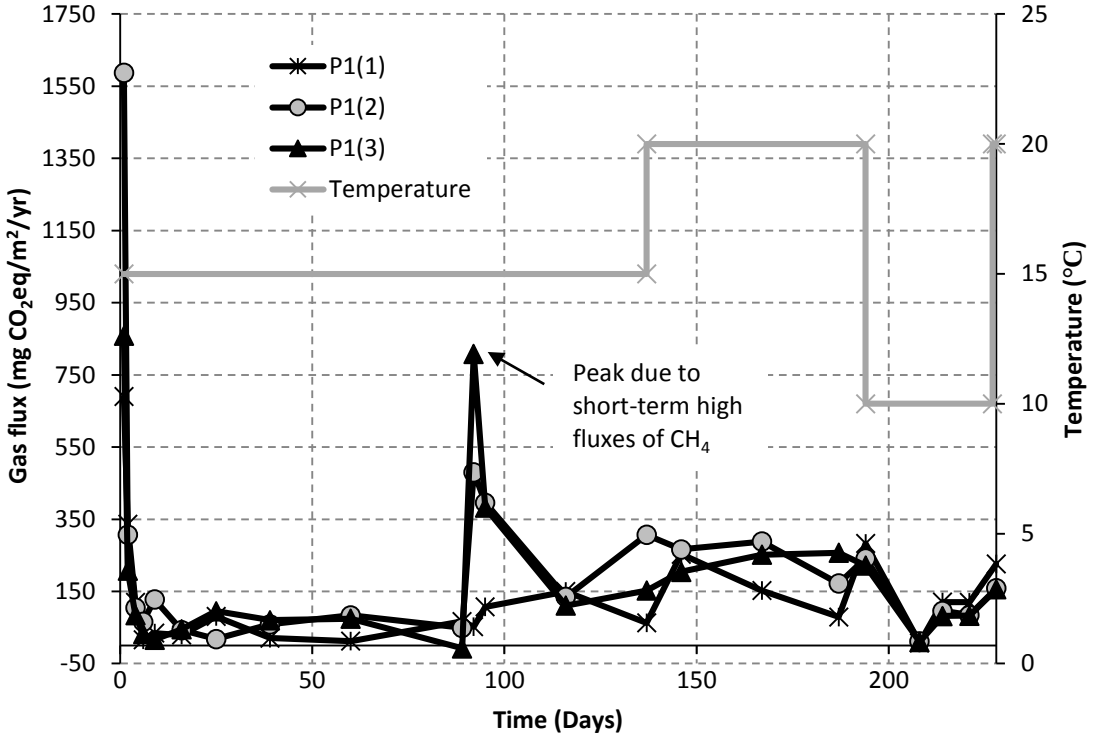

Figure 4.6 - 60-minute gas fluxes for P1(1)–P1(3)

4.5.2.3 Peat columns P2

As described in Section 3.4.2, the raw peat columns P2(1)–P2(3) were initially drained, with the water table at the bottom of the columns. In keeping with P1, specimens P2(1)–P2(2) also experienced high CO_2 emissions in the first four days but decreased to 224 ± 28 mg $CO_2eq/m^2/hr$ from day 6 to day 89 (Figure 4.7). The mixed peat specimen P2(3) behaved differently in that it was at first a small source of emissions compared to specimens P2(1)–P2(2); nonetheless, between days 16 and 89 it acted similarly to specimens P2(1)–P2(2) (Figure 4.8). On day 90, water levels were restored to the surface in P2, and emissions immediately decreased to emissions comparable with P1 up to day 90 (Section 4.5.2.2). No CH_4 was detected during the first 137 days.

Following the change of temperature on day 137 in specimens P2, emissions increased dramatically. Notably in P2(3), overall emissions increased 82 fold due to high CH_4 fluxes (Figure 4.8); evidently, the disturbed peat was more sensitive to temperature change than P1(1)–P1(3) and P2(1)–P2(2). Even when the temperature was decreased from 20°C to 10°C on day 194, emissions remained relatively high (except for the anomalous point at day 208), suggesting that time might have been required for the microbes in the peat to

readjust. It is likely that mixing the peat caused organic components to be broken down into more readily biodegradable material by generating a larger surface area for methanogens to digest. This resulted in high levels of anaerobic decomposition occurring when water levels were changed and temperatures increased, which led to high CH_4 and CO_2 production (Couwenberg, 2009). For a more in-depth analysis of the results, individual graphs of CO_2 and CH_4 are presented in Appendix D2 for P2(1)–P2(3).

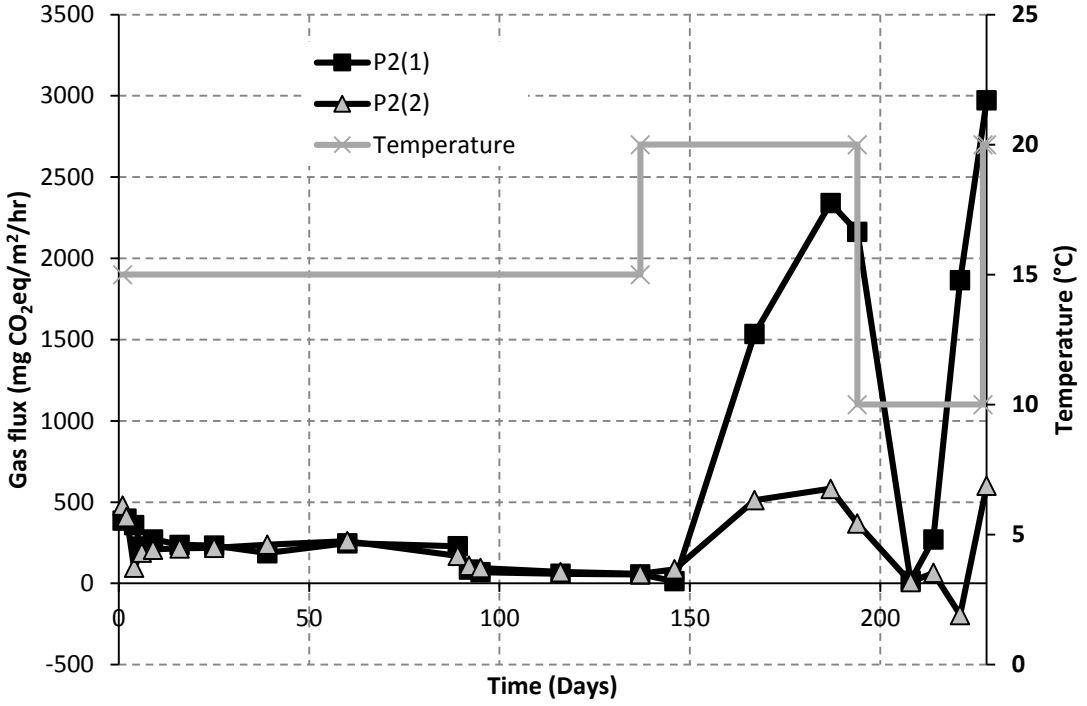

Figure 4.7 - 60-minute gas fluxes for P2(1)–P2(2)

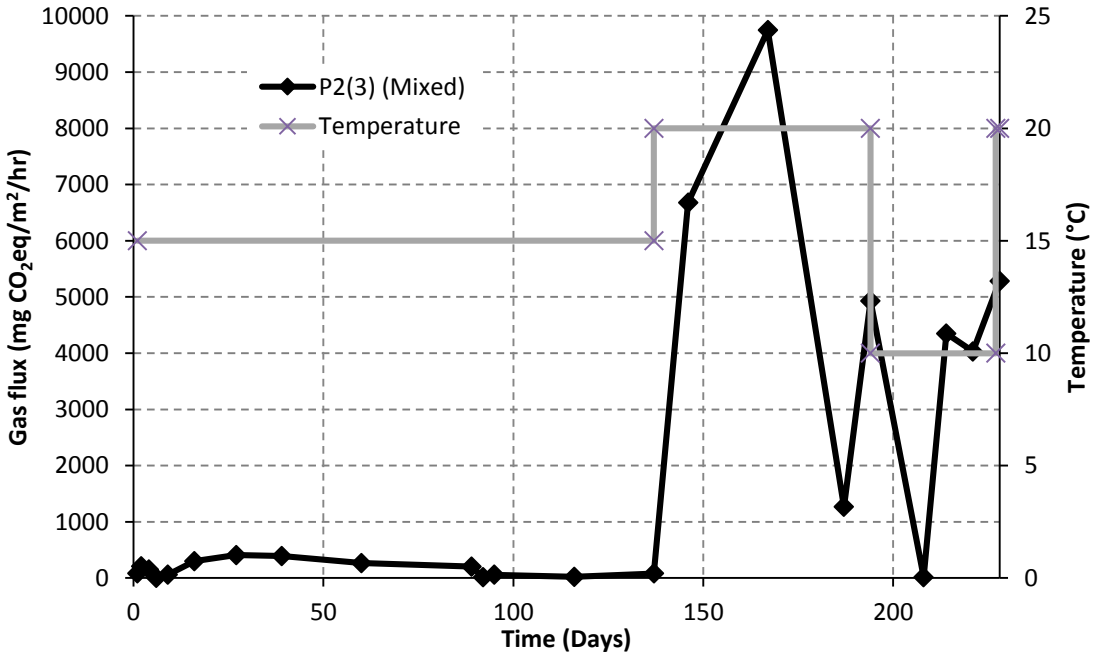

Figure 4.8 - 60-minute gas flux for P2(3)

4.5.2.4 Stabilised peat columns P3

The 60-minute flux results for P3 are calculated in order to compare them with the results of P1 and P2, but the 20 and 40-minute fluxes are also calculated because of evidence of non-linearity in the relationship between gas concentration data and chamber deployment time. In contrast to P1 and P2, the stabilised peat in P3(1)–P3(3) acted as a carbon sink, with average fluxes recorded in the first 4 days of -196 ± 69 mg CO_2eq/m^2/hr. As expected, in keeping with the argument in Section 2.7.2, the carbonation rate gradually declined to a steady carbon intake of 55 ± 41 mg CO_2eq/m^2/hr between day 6 and day 89 (Figure 4.9). Despite adding rainwater on and after day 90 (the reasons for which have been explained in Section 3.4.2.2), it was observed that the columns could be a CO_2 source (see day 116 in Figure 4.9 where P3(2) emitted 17 mg CO_2/m^2/hr and P3(1) emitted 0.2 mg CO_2/m^2/hr). P3 specimens also reacted to the temperature increase and produced a higher carbonation rate, averaging -38 ± 24 mg CO_2eq/m^2/hr after day 137, but this then decreased slightly to -35 ± 21 mg CO_2eq/m^2/hr from day 194 onwards. CH_4 emissions were not detected from the stabilised peat. The average fluxes along with their standard deviations for P3(1)–P3(3) over 0 to 20, 40 and 60 minutes are shown in Table 4.4. Confidence intervals are also given in Table 4.4 as the spread of flux values are skewed and standard deviation values may be misleading.

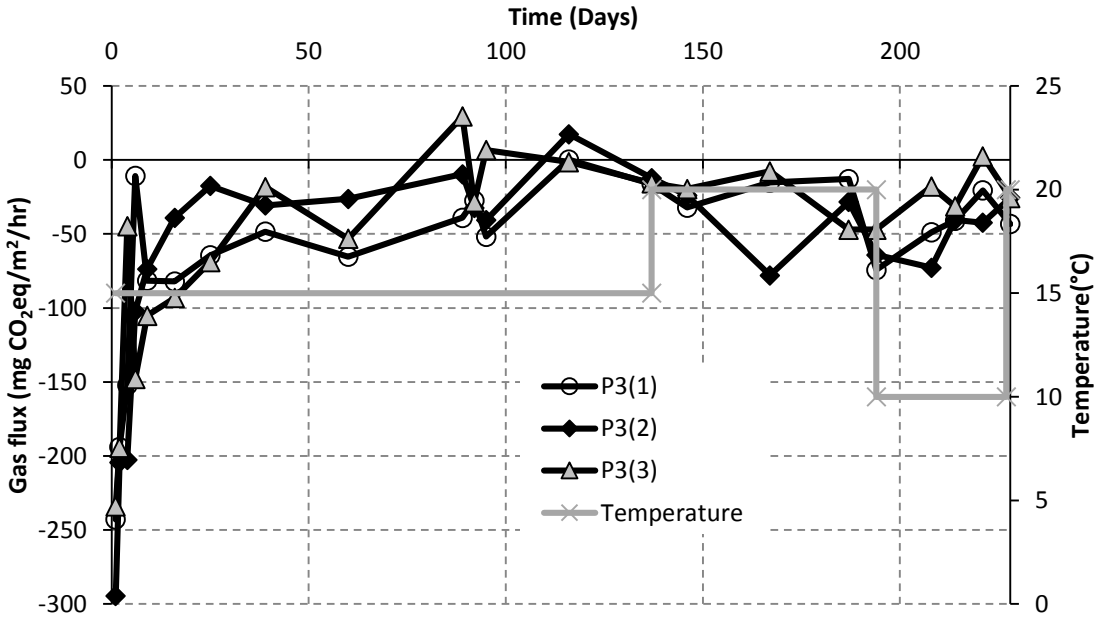

Figure 4.9 - 60-minute gas fluxes for P3(1)–P3(3)

Table 4.4 - Average gas fluxes (± 1 standard deviation) and 95% confidence intervals for P3(1)–P3(3) over 0 to 20, 40 and 60 minutes

Columns	Gas flux (mg CO_2eq/m^2/hr)					
	0–60		0–40		0–20	
	Average	95% CI	Average	95% CI	Average	95% CI
P3(1)	-62 ± 61	(-91, -33)	-68 ± 194	(-108, -27)	-79 ± 160	(-146, -13)
P3(2)	-66 ±75	(-94, -37)	-70 ± 101	(-110, -29)	-92 ± 146	(-158, -26)
P3(3)	-53 ± 66	(-82, -24)	-61 ± 89	(-101, -20)	-88 ± 160	(-157, -19)

The combined CO_2 and CH_4 emission levels averaged for each column category (P1, P2 and P3) plus their standard deviations on each day of measurement are presented as 60-minute fluxes in Figure 4.10 for days 1 to 228. To show the difference in fluxes with temperature and water level, the average 60-minute flux for each period of constant environmental conditions is shown in Table 4.5.

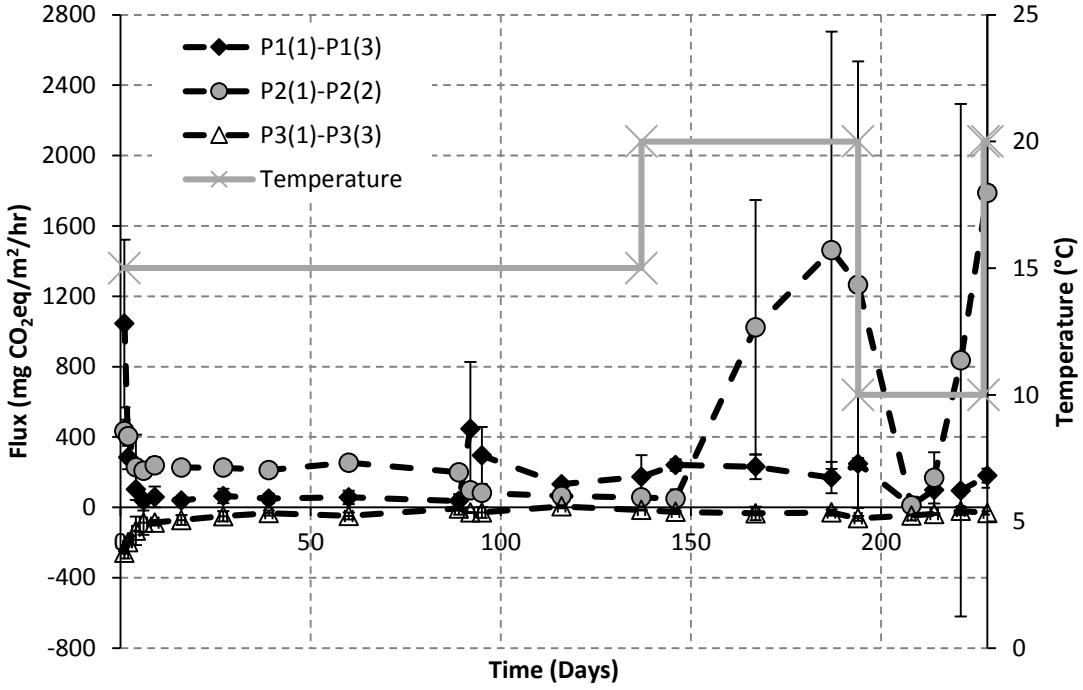

Figure 4.10 - Average 60-minute fluxes (with standard error bars) for day 1 to 228 for specimens P1, P2 (P2(1) and P2(2)) and P3

Table 4.5 - Average 60-minute fluxes (mg CO_2eq/m^2/hr) (± 1 standard deviation) for each period of constant environmental conditions in Experiment P

Days	Temperature (°C)	Columns			
		P1	P2(1)–P2(2)	P2(3)	P3
1–89	15	178 ± 329	263 ± 95	207 ± 137	-97 ± 82
90–137	15	262 ± 224	75 ± 19	44 ± 31	-17 ± 20
138–194	20	223 ± 61	950 ± 928	5654 ± 3540	-38 ± 24
195–221	10	68 ± 46	339 ± 763	2797 ± 2416	-35 ± 21
228	20	180 ± 40	1787 ± 1676	5283	-31 ± 10

4.5.3 Replicate analysis

Before multiple regression was applied to ascertain the variables that were significant predictors of the carbonation rate, one-way ANOVA was used to see if a significant difference existed between the replicates. ANOVA is relatively robust for non-normal data and hence was deemed to be an adequate tool in this instance. ANOVA demands variance homogeneity to some extent; if the variances are not homogeneous, there is a risk of overlooking a significant difference in means. However, ANOVA is sufficiently robust to variance if the sample size is ample. The number of gas sampling events (n = 22) examined is large and satisfies the guidelines that each group examined comprises more than 15 samples (Frost, 2015).

From the p-value results of ANOVA in Table 4.6, the CO_2 fluxes in the three replicates for each of P1 and P3 behaved similarly ($p > 0.05$). However, for columns P2, due to the variability in the high emissions observed at 20ºC for the 0–20, 40 and 60 minute fluxes, the fluxes in nearly all cases were significantly different from each other.

Table 4.6 - One-way ANOVA p-values for comparing specimens P1, P2 and P3

Flux	P1 (n = 3)	P2 (n = 3)	P2(1) and P2(2)	P3 (n = 3)
(0–60)	0.458	**0.011**	**0.034**	0.812
(0–40)	0.286	0.055	**0.010**	0.947
(0–20)	0.593	0.240	**0.040**	0.962
	> 0.05		< 0.05	> 0.05

4.5.4 Multiple linear regression analysis

4.5.4.1 Variables controlling CO_2 flux in peat

Multiple linear regression analysis was performed on the gas fluxes from peat in P1 and P2, with goodness-of-fit values (R^2 adjusted values) shown in Table 4.7 for each model developed and the significant variables by way of p-values highlighted in bold. The peat emission rates for P1 and P2 were found to be strongly related to the temperature and water table, as established by Nayak et al. (2008). Time (days) was a significant variable, mainly only because of the water table and temperature changes at specific times but is not a true factor in its own right. No relationship was found between the gas flux and initial CO_2 concentration.

Table 4.7 - Multiple linear regression analyses showing the effects of the variables examined on the gas fluxes for specimens P1 and P2

	60-min. flux		40-min. flux		20-min. flux	
Analysis	1	2	1	2	1	2
R^2 (adjusted) %	15.16	15.65	10.14	10.4	9.5	10.21
Variables			**p-values**			
Intercept	**0.011**	**0.003**	**0.027**	**0.024**	**0.029**	**0.004**
Time	**0.006**	**0.003**	**0.022**	**0.024**	0.177	0.1
Temperature	**0.013**	**0.006**	0.056	**0.025**	**0.006**	**0.004**
Water table	**0.003**	**0.003**	**0.007**	**0.009**	**0.018**	**0.018**
Initial CO_2 conc.	0.605	-	0.433	-	0.999	-

4.5.4.2 Variables controlling CO_2 flux in stabilised peat

Multiple linear regression was applied to reconstruct the 0–20, 40 and 60 minute fluxes individually for stabilised specimens P3 using the variables: temperature, initial CO_2 concentration, and the natural logarithm of time. The natural logarithm of time as opposed to time gave better relationships as shown in Table 4.8. The CO_2 gas flux was significantly related to the initial CO_2 concentration ($p < 0.05$), and the natural logarithm of time ($p < 0.05$), except for the 20-minute flux where there was no relationship with ln(time) ($p = 0.192$) (Table 4.8). As there were no water table changes in P3 and temperature was not a significant variable, time was a true variable in this case for stabilised peat, as it is well established from carbonation in concrete that the carbonation rate decreases with time and that time in the short term is not a variable for peat alone.

Insufficient gas sampling readings were taken at each temperature setting to establish the full effect of the temperature change for stabilised peat. Some evidence of temperature sensitivity was found for P3 from these data but not to the same extent as for P1 and P2.

Table 4.8 - Multiple linear regression analyses showing the effects of the variables examined on the fluxes for specimens P3

	60-min. flux		40-min. flux		20-min. flux	
Analysis	1	2	1	2	1	2
R^2 (adjusted) %	62.22	69.34	59.32	65.08	61.18	61.28
Lack-of-fit	0.401	0.441	0.133	0.143	-	-
Variables			**p-values**			
Intercept	**0.006**	0.486	**0.006**	0.634	**0.000**	0.215
Time	0.570	-	0.995	-	0.212	-
Ln(time)	-	**0.000**	-	**0.002**	-	0.192
Initial CO_2 conc.	**0.000**	**0.002**	**0.000**	**0.002**	**0.000**	**0.000**
Temperature	0.306	0.794	0.107	0.348	0.117	0.334

Using backward elimination, the statistical model (Equation 4.2) that provided the best fit to the stabilised peat data was the one produced using the 60-minute flux, which accounted for 69.8% (R^2 adj) of the variation in the CO_2 flux data in this study (Table 4.9). The parameters given in Table 4.9 are explained in Appendix D3. The results of the multiple regression analysis, including the residual plots, are shown in Appendix D4, as well as a

plot of the predicted fluxes against the measured fluxes. Residuals from the analysis are not distributed normally; but because there are greater than 15 data points, the test results can be deemed reliable (Frost, 2014).

$$\text{Gas flux} = b_0 + b_1 \times \text{initial } CO_2 + b_2 \times \ln(\text{time}) \qquad \textbf{Equation 4.2}$$

Table 4.9 - Parameters for the CO_2 flux reconstruction model for Experiment P

Parameters	Coefficient	Standard error	p-value
b_0 (constant)	-32.2	48.7	0.511
b_1 (initial CO_2)	-1278.5	390.4	0.002
b_2 (ln(time))	19.71	4.855	0.000
R^2 (adj.)	69.8		
R^2 (pred.)	67.1		
SE	36.6869		
d.f (reg, res)	2,63		
F-value	76.08		
P-value	0.000		

4.6 Experiments A and B

4.6.1 Introduction

In this section, the CO_2 flux results from Experiments A and B are presented, as well as the statistical analyses undertaken. Over the 180-day durations of Experiments A and B, 52 gas sampling events took place in Experiment A and 44 in B. Changes in the height of the stabilised peat were accounted for in flux measurements as heights decreased slightly, increasing the closed chamber volume. For Experiment A there were no changes in heights from day 36 onwards, while in Experiment B the stabilised peat column heights decreased slightly over time, with a maximum change of 1.5 cm (3% of the initial height of the column) recorded over 180 days.

4.6.2 Minimum CO_2 detection level

The low CO_2 concentrations (0 and 50 ppm) in some of the gas collected could not be measured using the gas chromatograph as they fell below the 50 ppm minimum detection threshold. Gas fluxes in this instance were calculated using both 0 and 50 ppm values to discover if there were any major differences. The maximum percentage change in the mean flux in Experiment A was only a 3.9% difference for A5(3) for the 60-minute flux, and in Experiment B there was a 5.3% difference recorded for the 40-minute flux in B3(2); further detail is provided in Appendix D5. However, readings below 50 ppm only arose in 6, 12 and 43 readings of the 1248 data points in Experiment A for the 20, 40 and 60-minute fluxes respectively, and 31, 75 and 106 readings of 1056 data points in Experiment B for the 10, 20 and 40-minute fluxes respectively. It was concluded, therefore, that it was appropriate to use either value for one-way ANOVA and multiple linear regression, so the results presented in the following sections are based on the 50 ppm assumption.

4.6.3 CO_2 fluxes

4.6.3.1 Linear regression method

As established in the preliminary study (Experiment P), the average CO_2 fluxes from each of the stabilised peat columns in Experiments A and B were negative, indicating that the carbonation rate was greater than the peat oxidation rate in contrast to the raw peat columns A8, B6 and B7 which released CO_2. In Experiment A, the maximum CO_2 intake rate or lowest CO_2 flux measured for the 0–20, 0–40 and 0–60 minute fluxes from the stabilised peat columns was -499 mg CO_2eq/m^2/hr, and the maximum CO_2 release was 81 mg CO_2eq/m^2/hr. In Experiment B, the maximum intake rate measured from the stabilised peat columns for the 0–10, 0–20 and 0–40 CO_2 fluxes was -1046 mg CO_2eq/m^2/hr, and the maximum CO_2 release was 221 mg CO_2eq/m^2/hr.

By way of example, a histogram of the 40-minute flux data is shown in Figure 4.11 for Experiment A and in Figure 4.12 for Experiment B. Given the skew, the 95% confidence interval of the mean was determined and found to lie between -60 mg CO_2eq/m^2/hr and -54 mg CO_2eq/m^2/hr in Experiment A and between -87 mg CO_2eq/m^2/hr and -78 mg CO_2eq/m^2/hr in Experiment B. Corresponding summary reports for the 20, 40 and 60-minute fluxes for Experiment A and for the 10, 20 and 40 minute fluxes for Experiment B are provided in Appendix D6.

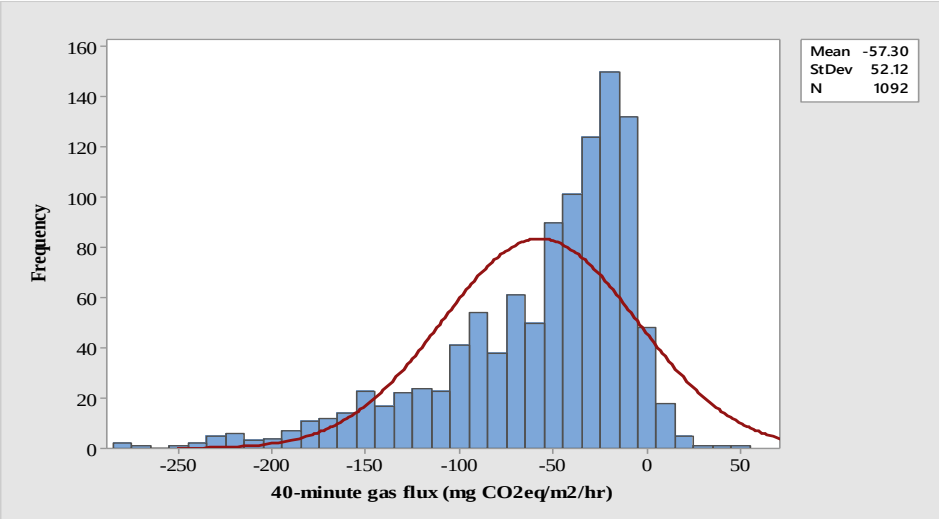

Figure 4.11 - Histogram (with normal curve) of 40-minute gas fluxes (mg CO_2eq/m^2/hr) from stabilised peat in Experiment A

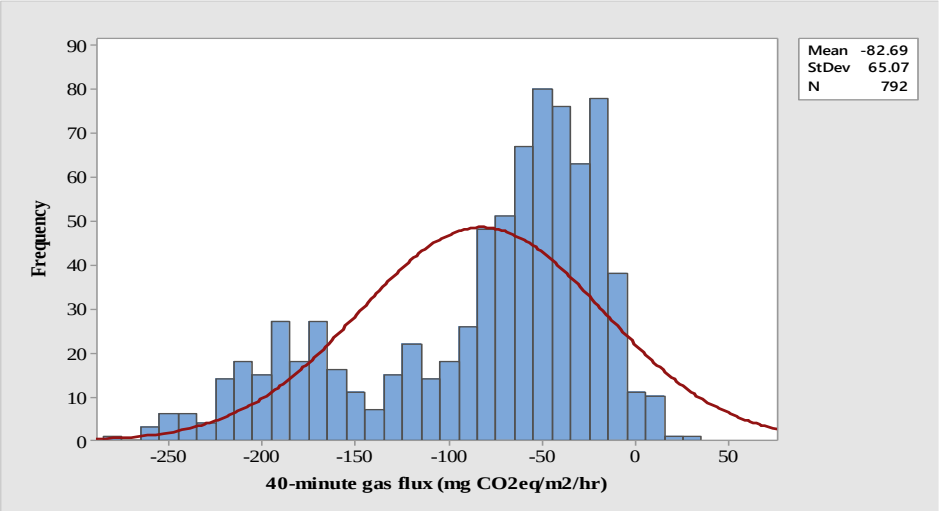

Figure 4.12 - Histogram (with normal curve) of 40-minute gas fluxes (mg CO_2eq/m^2/hr) from stabilised peat in Experiment B

Similar to Experiment P, the carbonation rate in the stabilised peat columns in Experiments A and B decreased over the 180 days as the carbonation depth increased ($p < 0.001$). A typical graph of the change in CO_2 flux from stabilised peat over the duration of the experiments is given in Figure 4.13. Again, in keeping with the results from Experiment P, CH_4 was not detected in emissions from the stabilised peat, even from the stabilised peat B5 whose water table was at the surface.

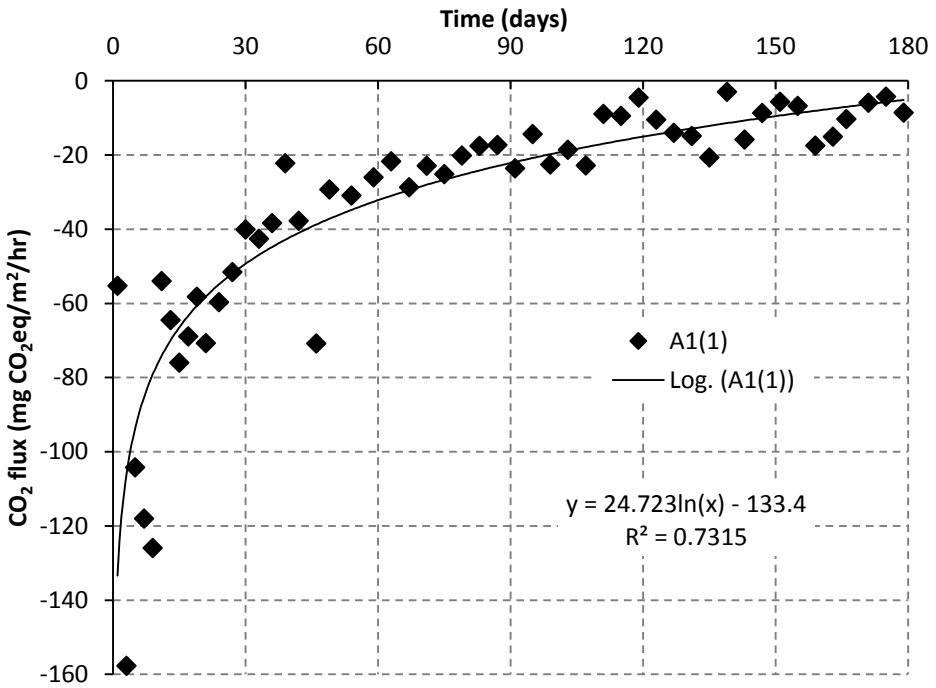

Figure 4.13 - 60-minute CO_2 flux for A1(1) over 180 days

The individual stabilised peat columns in Experiment A can be compared by examining Figure 4.14, an interval plot showing the mean 40-minute fluxes for A1(1) to A7(3), as well as examining intervals plots in Appendix D7 for the 20 and 60-minute fluxes. The

mean value of CO_2 fluxes for Experiment A together with their standard errors as estimated by linear regression are provided in Appendix D8.

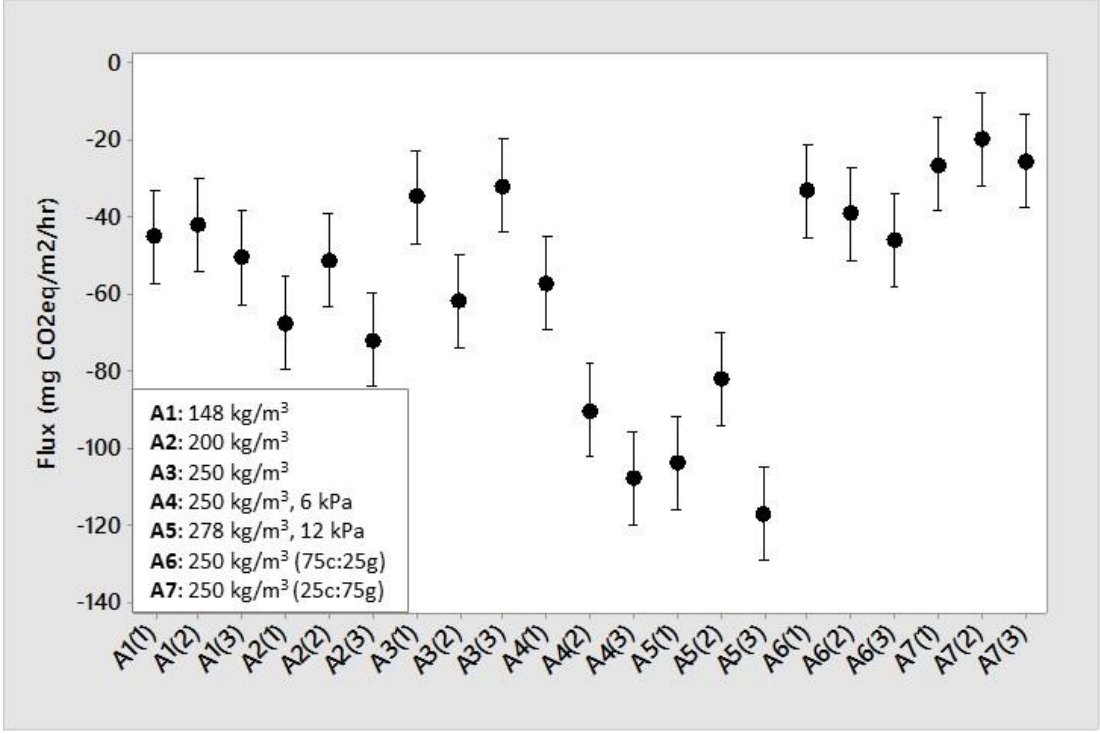

Figure 4.14 - Interval plot showing mean 40-minute flux for A1–A7 over 180 days with 95% confidence interval bars for the mean for Experiment A based on a pooled standard deviation

In advance of the more insightful one-way ANOVA results in Section 4.6.4, preliminary observations from Figure 4.14 and Appendices D6 and D7 were made:

- On examination of columns A1 (148 kg/m^3), A2 (200 kg/m^3), and A3 (250 kg/m^3) in Figure 4.14, there does not seem to be a relationship between cement content and the CO_2 flux.
- In general, the surcharged columns had higher CO_2 intake rates than the other A columns. The surcharged columns A5(3), A4(3) and A5(1) had the highest CO_2 intake rates among the surcharged columns. A4(2) and A5(2) had a higher CO_2 intake rate than the rest of the columns, but their means were not significantly greater than some of the cement-only unsurcharged columns. A4(1) had the lowest CO_2 intake rates of the surcharged columns, with significantly different means to the rest of the surcharged columns and behaved like an unsurcharged column. The possible reasons for this outlier will be discussed in Section 6.3.
- The columns with the most GGBS (A7) had the lowest CO_2 intake rates.

The individual stabilised peat columns in Experiment B can be compared by examining Figure 4.15, an interval plot showing the mean 40-minute fluxes for B1–B5 and B8, as

well as examining the intervals plots in Appendix D7 for the 10 and 20 minute fluxes. The mean value of CO_2 fluxes for Experiment B together with their standard errors as estimated by linear regression are provided in Appendix D8.

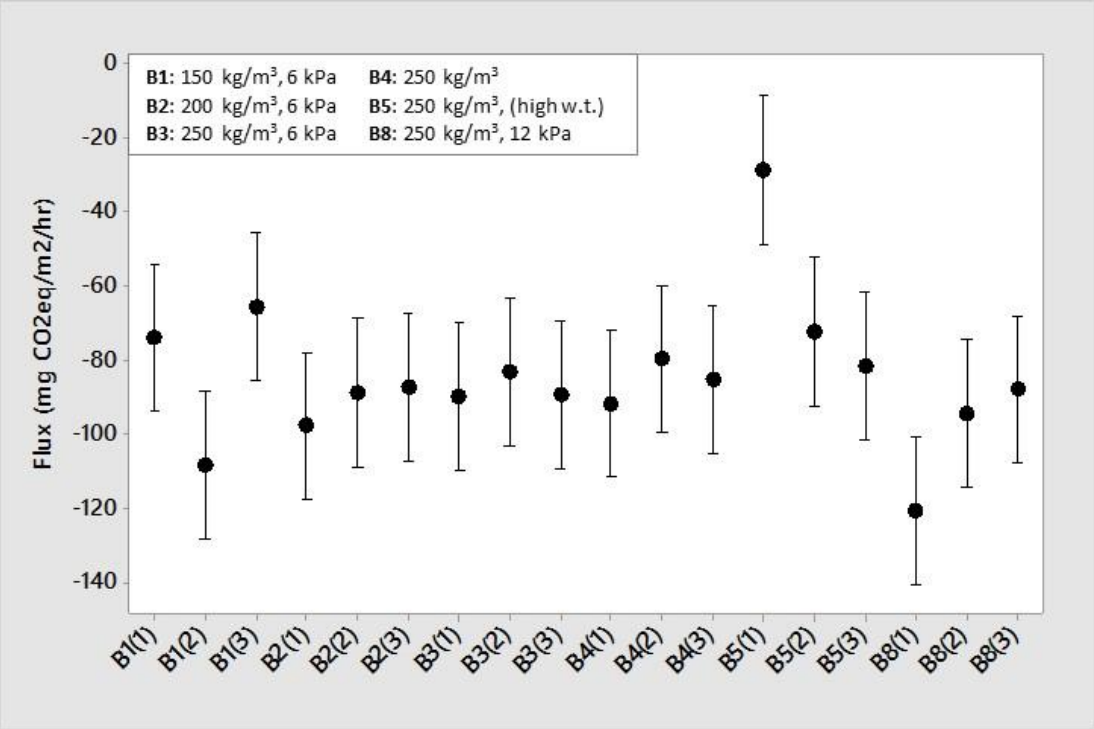

Figure 4.15 - Interval plot showing mean 40-minute flux for B1–B5, B8 over 180 days with 95% confidence interval bars for the mean for Experiment B based on a pooled standard deviation

Results in Figure 4.15 and Appendices D6 and D7 showed that:

- Similar to findings in Experiment A, there was no obvious relationship in B1 (150 kg/m^3), B2 (200 kg/m^3), and B3 (250 kg/m^3) between CO_2 flux and cement content even with a 6 kPa surcharge imposed for 21 days. However, two of the columns B1(1) and B1(3) had lower CO_2 intake rates than B2 and B3 which had higher cement contents.
- Like results in Experiment A, the greatest mean CO_2 intake rate was from a column which had been surcharged with 12 kPa, B8(1).
- The highest CO_2 flux or lowest CO_2 intake rate was from the unsurcharged column B5(1) whose water table was at the surface. This was expected as carbonation in concrete is slowest in water (Section 2.7.1.4)
- In contrast to Experiment A, there does not seem to be much difference between surcharged (B1, B2, B3 and B8) and unsurcharged columns (B4 and B5).
- The high laboratory temperature of 20°C produced high CH_4 emissions in the raw peat columns (high water table) B6(1) and B6(2) and, consequently, large emissions

(Appendix D7), and like in Experiment P signify the impact climate change will have on peatlands.

4.6.3.2 Non-linear methods

The non-linear methods described in Section 2.8.2.2 were considered in Experiment A, but it is important to note that they were not developed with the intention of using them for stabilised peat and required additional parameters such as soil gas diffusion coefficients. Nonetheless, the HM method described in Section 2.8.2.2 was tested in Experiment A with data points at 0, 20, and 40 minutes for the first 13 days; thereafter, data points were taken at 0, 10 and 20 minutes. The method failed to give a flux value in 26.4% of 1248 cases, and some carbonation rates calculated were considered unrealistic; for instance, the rates of over -2,000,000 mg $CO_2/m^2/hr$ for the stabilised peat. It was concluded, therefore, that this method was highly sensitive to random fluctuations in concentration measurements and could not be applied to stabilised peat.

4.6.4 Assessment of specimen similarities and differences

4.6.4.1 Replicate analysis

Before multiple regression was carried out to find the variables that were significant predictors of the carbonation rate, one-way ANOVA was used on each group of specimens for the fluxes to see if there was a significant difference between the replicates. Due to the variability of peat, it was anticipated that some specimens with the same binder mix and under the same environmental conditions (replicates) could have different results. In Experiment A, no substantial difference was found between the replicates A1(1)–A1(3), A6(1)–A6(3) and A7(1)–A7(3) ($p > 0.05$) for all flux times (Table 4.10). There was, however, a significant difference between the means of A2(1)–A2(3), A3(1)–A3(3), A4(1)–A4(3), A5(1)–A5(3) and A8(1)–A8(3).

Table 4.10 - One-way ANOVA p-values for comparing replicas in Experiment A

Flux	A1	A2	A3	A4	A5	A6	A7	A8
(0–60)	0.833	**0.029**	**0.000**	**0.000**	**0.000**	0.618	0.659	**0.000**
(0–40)	0.696	**0.037**	**0.000**	**0.000**	**0.004**	0.270	0.440	**0.000**
(0–20)	0.460	**0.023**	**0.001**	**0.000**	**0.031**	0.550	0.766	**0.000**
	> 0.05	**< 0.05**	**< 0.05**	**< 0.05**	**< 0.05**	> 0.05	> 0.05	**< 0.05**

The results from Experiment B revealed no substantial difference between the replicas B2(1)–B2(3), B3(1)–B3(3), B4(1)–B4(3) and B8(1)–B8(3) ($p > 0.05$) (Table 4.11). There was, however, a significant difference between the means of B5(1)–B5(3) and B6(1)–B6(3). For B1 and B7, there was no difference between the means for the 10 and 20-minute fluxes, but a difference did exist for the 40-minute flux.

Table 4.11 - One-way ANOVA p-values for comparing replicas in Experiment B

Flux	B1	B2	B3	B4	B5	B6	B7	B8
(0–40)	**0.013**	0.735	0.914	0.488	**0.000**	**0.001**	**0.042**	0.068
(0–20)	0.053	0.562	0.871	0.710	**0.001**	**0.001**	0.086	0.176
(0–10)	0.186	0.838	0.988	0.575	**0.001**	**0.004**	0.076	0.423
	> 0.05	> 0.05	> 0.05	> 0.05	**< 0.05**	**< 0.05**	> 0.05	> 0.05

Closer inspection of the fluxes for specimens A2, A3, A4, B5 and B6 shows that in all cases one out of three columns was different (Figure 4.14; Figure 4.15; Appendix D8). To verify the similarities between the other two columns in these cases, p-values using one-way ANOVA were calculated and are shown in Table 4.12 and Table 4.13. Similar fluxes were observed for A2(1) and A2(3), A3(1) and A3(3), and A4(2) and A4(3). In Experiment B, similar fluxes were witnessed for B5(2) and B5(3), and B6(1) and B6(2). Though not significant over all 20, 40 and 60 minute fluxes; average fluxes in A5(3) were always higher than for A5(1) and A5(2); and the average gas flux in B1(2) was always higher than for B1(1) and B1(3).

Table 4.12 - One-way ANOVA p-values for comparing two replicas in Experiment A

Flux	A2(1) vs A2(3)	A3(1) vs A3(3)	A4(2) vs A4(3)	A5(1) vs A5(2)	A5(1) vs A5(3)	A8(1) vs A8(3)
0–60	0.412	0.612	0.213	0.056	**0.002**	**0.011**
0–40	0.598	0.727	0.097	**0.043**	0.177	**0.041**
0–20	0.866	0.869	0.277	0.308	0.091	0.093
	> 0.05	> 0.05	> 0.05			

Table 4.13 - One-way ANOVA p-values for comparing two replicas in Experiment B

Flux	B5(2) vs B5(3)	B6(1) vs B6(2)	B1(1) vs B1(3)	B7(2) vs B7(3)
0–40	0.517	0.315	0.535	0.783
0–20	0.564	0.556	0.679	0.933
0–10	0.452	0.782	0.902	0.753
	> 0.05	> 0.05	> 0.05	> 0.05

4.6.4.2 Comparisons of groups of specimens

In each experiment, the gas flux results from replicates (eg. A1(1), A1(2) and A1(3)) were combined in order to compare each group (A1, A2, A3 etc.) The following are the conclusions from the ANOVA analyses of Experiment A:

(i) The hypothesis was that an increase in cement content would lead to an increase in the CO_2 intake rate. This was the case for A1 (148 kg/m^3) which had means lower than A2 (200 kg/m^3) but was not the case for A3, which had 250 kg/m^3 of cement binder and behaved like A1 ($p > 0.05$) (Figure 4.16;

(iii) Table 4.14; Appendix D9). No evident relationship was found between cement content and CO_2 intake rate using one-way ANOVA but one is found in Section 4.6.5.4 where cement content is examined in more detail using multiple linear regression analysis.

(iv) Surcharged specimens had a greater CO_2 intake rate than the unsurcharged specimens ($p = 0.000$). Importantly, there was a significant difference ($p = 0.001$) between the mean 60-minute flux of A4 which had the lowest CO_2 intake rates among the surcharged columns and the means of A2 which had the highest rates from unsurcharged columns.

(v) For the 40 and 60-minute fluxes, a comparison of A4 (6 kPa) and A5 (12 kPa) revealed that when a greater surcharge was applied there was a significantly higher CO_2 intake ($p = 0.000$).

(vi) Substituting GGBS for cement had a negative effect on the CO_2 intake rate, a logical outcome since the carbonation potential of GGBS is lower than cement due to its lower CaO content. The 60-minute flux in A3, which had the lowest CO_2 intake rate among the cement columns, had a higher CO_2 intake rate than in A6 but was not significant ($p = 0.214$). However, in A7, which had a GGBS to cement ratio of 75:25, the difference was significant ($p < 0.001$).

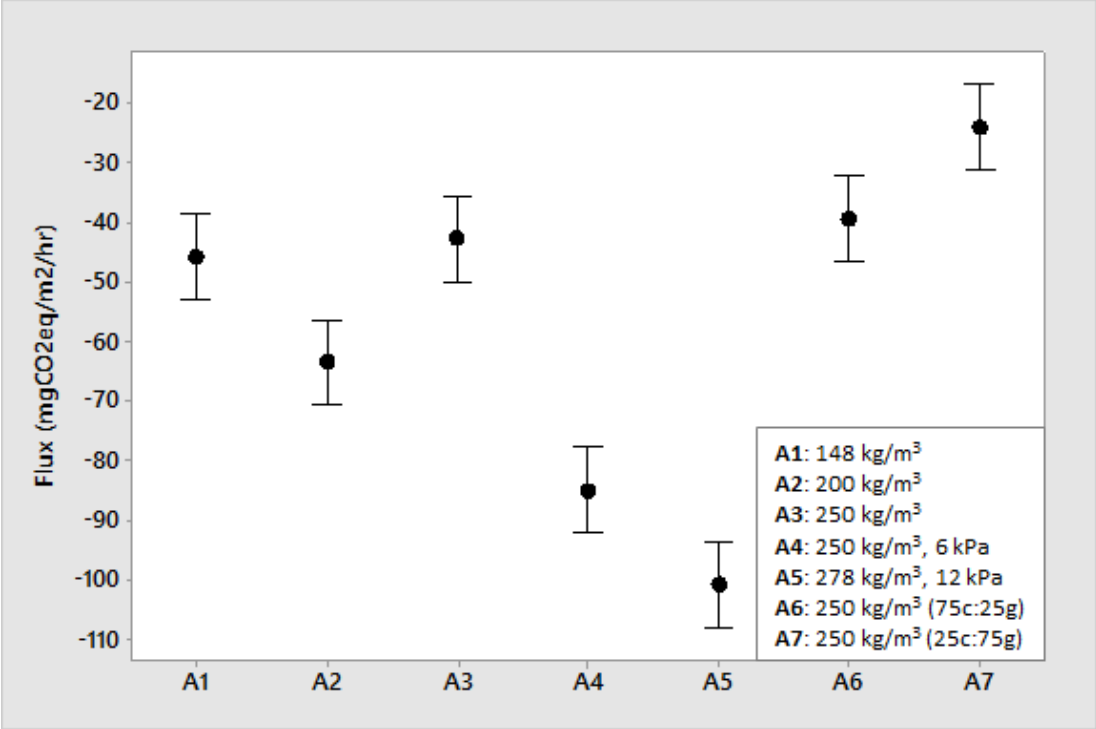

Figure 4.16 - Interval plot showing the mean for each column type with 95% confidence interval bars for the 40-minute flux for Experiment A based on a pooled standard deviation

Table 4.14 - One-way ANOVA p-values for comparing groups of specimens in Experiment A

Flux	A4 vs A5 (iii)*	A1 vs A2 (i)*	A1 vs A3 (i)*	A1 vs A3 vs A6	A6 vs A7 (iv)*	A3 vs A6 (iv)*
0–60	**0.000**	**0.000**	0.596	0.234	**0.000**	0.214
0–40	**0.010**	**0.001**	0.571	0.458	**0.000**	0.480
0–20	0.187	**0.001**	0.725	0.209	**0.001**	0.160
	< 0.05	**< 0.05**	> 0.05	> 0.05	**< 0.05**	> 0.05

* (i), (iii), (iv) are cross referenced with the numbering above.

The following are the conclusions from the ANOVA analyses of Experiment B:

(i) The hypothesis was that an increase in cement content combined with a surcharge would lead to an increase in the CO_2 intake rate. However, B1 (150 kg/m^3), B2 (200 kg/m^3) and B3 (250 kg/m^3) were statistically similar for the 10, 20 and 40-minute fluxes (Table 4.15). This is evident in Figure 4.17 for the 40-minute fluxes and in Appendix D9 for the 10 and 20-minute fluxes.

(ii) The unsurcharged columns B4 in Experiment B had a similar CO_2 intake rate to the surcharged columns B3 for the 40-minute flux but had a lower CO_2 intake rate for the 10 and 20-minute fluxes ($p < 0.05$) (Table 4.15)

(iii) There was no difference in the means of the 6 kPa columns B3 and the 12 kPa columns B8, but there was however, a larger difference between B8 and the unsurcharged column B4 compared to between B3 and B4.

(iv) The high water table in B5 gave a lower CO_2 intake rate than the other columns. This was mainly due to B5(1), which had a much lower rate than B5(2) and B5(3) (Figure 4.15). A reason why B5(2) and B5(3) were similar to the unsurcharged columns may be that less CO_2 was released from peat oxidation due to the high water table, leaving less CO_2 available for carbonation, hence more CO_2 was taken from the chamber headspace for carbonation. The low levels of CO_2 emissions in high water table peat had already been demonstrated in Experiment P and in specimens B6, where in place of high CO_2 emissions, high CH_4 emissions increased the peat emission rate substantially.

(v) As expected, the peat specimens B6, whose water table was at the surface, had significantly higher emissions than the drained specimens B7 ($p \leq 0.001$) due to the high CH_4 emissions released by B6.

Table 4.15 - One-way ANOVA p-values for comparing groups of specimens in Experiment B

Flux	B1 vs B2 vs B3 (i)*	B3 vs B4 (ii), (iii)*	B4 vs B8 (iii)*	B3 vs B8 (iii)*	B4 vs B5 (iv)*	B1 vs B2 vs B3 vs B8	B6 vs B7 (v)*
0–40	0.593	0.856	0.060	0.101	**0.000**	0.163	**0.001**
0–20	0.615	**0.011**	**0.001**	0.851	0.052	0.657	**0.000**
0–10	0.477	**0.001**	**0.000**	0.581	0.173	0.647	**0.000**
	> 0.5			> 0.5		> 0.5	< **0.5**

* (i)–(v) are cross referenced with the numbering above.

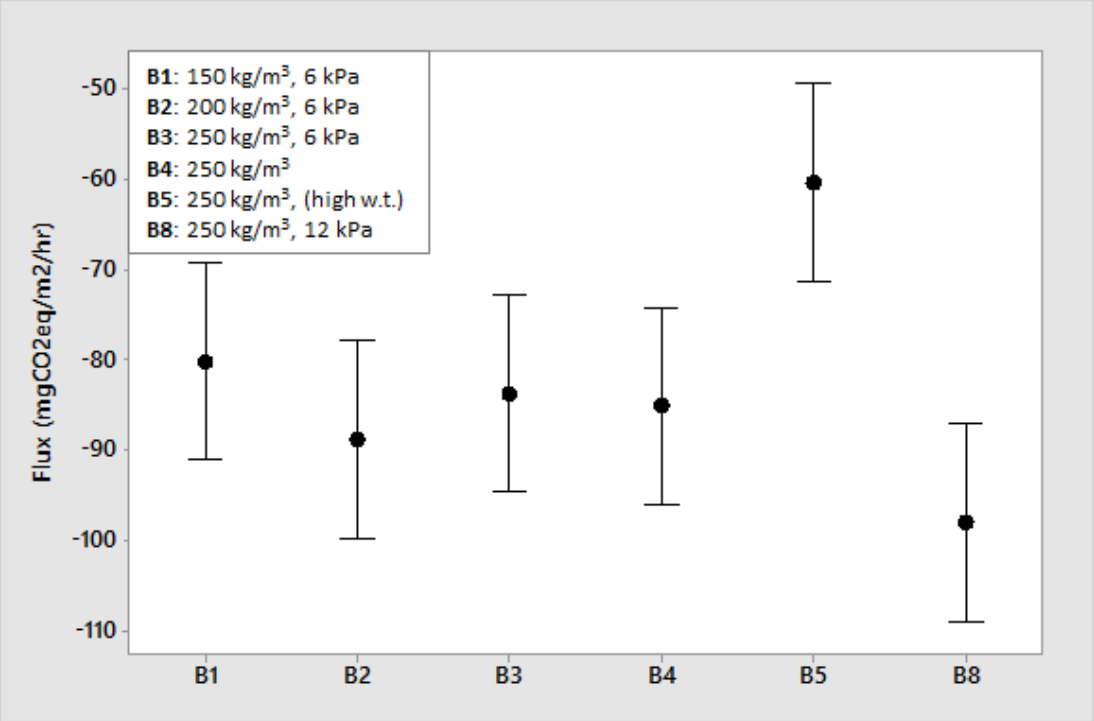

Figure 4.17 - Interval plot showing the mean for each column type with 95% confidence interval bars for the 40-minute flux for Experiment B based on a pooled standard deviation

4.6.5 Multiple linear regression analysis

4.6.5.1 Introduction

For an in-depth analysis of the variables that strongly affected the carbonation rate, multiple linear regression analysis was undertaken. Based on the variables that were significant, best-fit models were then developed individually for Experiments A and B in order to reconstruct the observed fluxes. As temperature and humidity were kept constant, these factors were not examined. At least three data points are required for gas flux analysis, so the 0–10 minute flux in Experiment A and the 0–5 minute flux in Experiment B, both based only on two data points, were disregarded.

The variables examined in Experiment A were: initial CO_2 concentration (% CO_2 in air), cement content (kg/m^3), GGBS content (kg/m^3), surcharge (kPa), and time (days), and in Experiment B the variables examined were: initial CO_2 concentration, cement content, water table, surcharge, and time. For the multiple regression analysis, a ‘dummy’ variable

was assigned to the water table variable. A low water table was scored as 0 and a high water table as 1.

4.6.5.2 Correlations in experimental design

Multicollinearity (defined in Appendix D3) was checked in the experiments at two stages. Check 1 took place before multiple linear regression analysis and involved performing correlation statistics between the various dependent variables (predictors), while Check 2 examined multicollinearity in the results of the multiple regression analyses by studying the variance inflation factors (VIFs). These factors capture how much multicollinearity exists in a regression analysis. The following paragraph briefly explains the results of Check 1.

Strong correlations existed between some variables, which necessitated extra attention in the multiple regression analyses. GGBS content (-0.818) and surcharge (0.620) were found to be highly correlated with cement content, and time was highly correlated with CO_2 concentration (-0.682) in Experiment A (Table 4.16). In Experiment B, there were low correlations in the experimental design between surcharge and cement (-0.159) and water table and cement (0.293), and a strong correlation existed between surcharge and water table (-0.542) (Table 4.17).

Table 4.16 - Correlation and p-value table for the variables considered in Experiment A

	Cement	GGBS	Surcharge	Time
GGBS	**-0.818**			
	0.000			
Surcharge	**0.620**	**-0.320**		
	0.000	0.000		
Time	0.000	0.000	0.000	
	1.000	1.000	1.000	
Initial CO_2 concentration	**-0.122**	**0.067**	**-0.098**	**-0.682**
	0.000	0.027	0.001	0.000

Cell content: Pearson correlation
p-value

Table 4.17 - Correlation and p-value table for the variables considered in Experiment B

	Cement	Water table	Surcharge	Initial CO_2 concentration
Water table	**0.293**			
	0.000			
Surcharge	**-0.159**	**-0.542**		
	0.000	0.000		
Initial CO_2 concentration	**0.076**	0.013	-0.022	
	0.032	0.721	0.534	
Time	0.000	0.000	-0.000	-0.029
	1.000	1.000	1.000	0.416

Cell content: Pearson correlation
p-value

4.6.5.3 Variables controlling CO_2 flux in stabilised peat

Table 4.18 and Table 4.19 show the multiple regression analyses performed for the 40-minute flux for Experiments A and B respectively, while the analyses of the other fluxes are in Appendix D10.

It was discovered in Experiment A that the CO_2 flux in stabilised peat was significantly related to the initial CO_2 concentration, the natural logarithm of time, surcharge, GGBS content and cement content for the 20, 40 and 60-minute fluxes. However, when cement and GGBS were analysed together, cement was not a significant variable due to multicollinearity which causes some variables to be statistically insignificant when they should be significant (Appendix D3). To account for cement and GGBS, GGBS was removed from the model, and a significant interaction between cement and GGBS was included, which was only moderately correlated with other variables (1<VIF<5). A significant interaction also exists between surcharge and time, which is only moderately correlated to surcharge (1<VIF<5). Interactions between cement and surcharge, initial CO_2 concentration and time, and cement and time were tested but were either not significant or highly correlated with other variables. The initial moisture content of the peat was also tested but, as anticipated, due to the relatively high moisture content of the all the peat specimens, it was not a significant variable. From the first to last analysis, overall R^2 values increased from 58% to 66% for the 40-minute flux.

Table 4.18 - Multiple linear regression analyses showing the effects of the variables examined on the fluxes for stabilised peat specimens in Experiment A

	40-min. flux					
Analysis	1	2	3	4	5	6
R^2 (adj) %	58.30	65.24	64.32	66.27	66.1	66.29
Lack-of-fit	0.410	0.469	0.461	0.48	0.478	0.48
Variables	**p-values**					
Intercept	0.334	**0.000**	0.918	**0.002**	0.337	**0.002**
Time	**0.000**	-	-	-	-	-
Ln (time)	-	**0.000**	**0.000**	**0.000**	**0.000**	**0.000**
Initial CO_2 conc.	**0.000**	**0.000**	**0.000**	**0.000**	**0.000**	**0.000**
Cement	0.666	-	**0.000**	-	**0.000**	-
GGBS	**0.000**	**0.000**	-	**0.000**	-	**0.000**
Surcharge	**0.000**	**0.000**	**0.000**	**0.000**	**0.000**	**0.000**
Surcharge*time	-	-	-	**0.000**	**0.000**	**0.000**
Cement*GGBS	-	-	-	0.423	**0.000**	-

The analysis of gas fluxes in Experiment B revealed the CO_2 flux in stabilised peat to be significantly related to the natural logarithm of time, surcharge and water table in the 10, 20 and 40-minute fluxes. Cement was only significant for the 40-minute fluxes. As in Experiment A, a significant interaction existed between surcharge and time which was only moderately correlated to surcharge (1<VIF<5). Interactions between cement and

surcharge, water table and time, and cement and time were tested and found to be either not significant or highly correlated with other variables under VIF guidelines (Appendix D3). The initial moisture content of the peat was also tested as a variable but was found not to be significant. From the first to last analysis, overall R^2 values increased from 61% to 68% for the 40-minute flux.

Table 4.19 - Multiple linear regression analyses showing the effects of the variables examined on the fluxes for stabilised peat specimens in Experiment B

	40-minute flux				
Analysis	1	2	3	4	5
R^2 (adj) %	60.95	65.99	68.75	68.41	68.42
Lack-of-fit	0.943	0.959	0.967	0.966	0.000
Variables	**p-values**				
Intercept	**0.000**	**0.000**	**0.000**	**0.000**	**0.000**
Time	**0.000**	-	-	-	-
Ln (time)	-	**0.000**	**0.000**	**0.000**	**0.000**
Initial CO_2 conc.	0.457	0.331	0.385	0.371	-
Cement	0.060	**0.045**	**0.006**	**0.037**	**0.031**
Water table	**0.000**	**0.000**	**0.049**	**0.000**	**0.000**
Surcharge	**0.010**	**0.005**	**0.000**	**0.000**	**0.000**
Surcharge*time	-	-	**0.000**	**0.000**	**0.000**
Water table*time	-	-	0.214	-	-
Cement*time	-	-	0.057	-	-

4.6.5.4 Best-fit models

Only the variables contributing significantly to the CO_2 fluxes were included in the final equations/models for stabilised peat. The 1092 data points for the 20, 40 and 60-minute fluxes were used to derive the best-fit model/equation for the 21 stabilised peat columns in Experiment A (Equation 4.3). The 40-minute fluxes provided the best-fit statistical model, the reasons for which are discussed in Section 4.7.2.4, and included the natural logarithm of time, initial CO_2 concentration, surcharge, cement content, and two interaction variables, cement*GGBS and surcharge*time (where * denotes an interaction).

The 792 data points for each flux were used to derive the best-fit model/equation for the 18 stabilised peat columns in Experiment B (Equation 4.4). The best-fit statistical model was again developed using the 40-minute flux which included the variables: cement content, natural logarithm of time, water table, surcharge, and an interaction variable, surcharge*time. The variable cement was not highly significant.

$$\text{Gas flux} = b_0 + b_1 \times \text{initial } CO_2 + b_2 \times \ln(\text{time}) + b_3 \times \text{cement} + b_4 \times \text{surcharge} + b_5 \times \text{surcharge*time} + b_6 \times \text{GGBS*cement} \quad \textbf{Equation 4.3}$$

$$\text{Gas flux} = b_0 + b_2 \times \ln(\text{time}) + b_3 \times \text{cement} + b_4 \times \text{surcharge} + b_5 \times \text{surcharge*time} + b_7 \times \text{water table} \quad \textbf{Equation 4.4}$$

The significant variables identified in Experiments A and B were discovered to be the driving variables for the best-fit statistical models and explained 66.3% and 68.6% of the variability for the 40-minute fluxes respectively (Table 4.20; Table 4.21). The results of the multiple regression analysis, including the residual plots, are shown in Appendix D11 as well as a plot of the predicted fluxes against the measured fluxes. Using the best-fit models in both Experiments A and B, the slopes and R^2 values for the relationship between the observed 40-minute fluxes and the predicted values for the individual columns are shown in Appendix D12.

Table 4.20 - Parameters for the CO_2 flux reconstruction model for stabilised peat in Experiment A

Parameters	Coefficient	Standard error	p-value
b_0 (constant)	-11.0	11.4	0.337
b_1 (initial CO_2)	-1488	116	0.000
b_2 (ln(time))	18.87	1.02	0.000
b_3 (cement)	-0.0957	0.0213	0.000
b_4 (surcharge)	-5.751	0.399	0.000
b_5 (surcharge*time)	0.02157	0.00368	0.000
b_6 (GGBS*cement)	0.001152	0.000232	0.000
R^2 (adj)	66.1		
R^2 (pred)	65.68		
SE	30.3498		
d.f (reg, res)	6,1085		
F-value	355.5		
P-value	0.000		

Table 4.21 - Parameters for the CO_2 flux reconstruction model for stabilised peat in Experiment B

Parameters	Coefficient	Standard error	p-value
b_0 (constant)	-202.7	10.1	0.000
b_2 (ln(time)))	35.03	1.46	0.000
b_3 (cement)	-0.0770	0.0356	0.031
b_4 (surcharge)	-4.209	0.548	0.000
b_5 (surcharge*time)	0.03770	0.00481	0.000
b_7 (water table)	22.7	4.29	0.000
R^2 (adj)	68.42		
R^2 (pred)	68.04		
SE	36.5679		
d.f (reg, res)	5,786		
F-value	343.71		
P-value	0.000		

The flux data were non-normal and negatively skewed in both experiments (Figure 4.11; Figure 4.12); consequently, the residuals of the best-fit statistical models were not generally distributed normally. The histograms of the residuals, however, seemed to follow a normal distribution, and the residuals versus the order of data plots appeared to follow a random pattern around the centre line. Nevertheless, like in Experiment P, as there were greater than 15 data points, the test results were deemed reliable (Frost, 2014).

The significant variables in the best-fit models for Experiments A and B had either positive or negative effects on the CO_2 flux. The following is a summary of these effects:

- The replacement of cement with GGBS had a negative effect on the CO_2 intake rate, which is reflected in the interaction variable, cement*GGBS in Experiment A.
- While cement content and surcharge increased the CO_2 intake rate in both Equation 4.3 and Equation 4.4, time was predicted to decrease the CO_2 intake rate in both models.
- The surcharge*time variable in both equations also had a negative effect on the CO_2 intake rate and improved the modelling of the surcharged columns as shown in Appendix D13 for the surcharged columns in Experiment A. The effect surcharge had on the CO_2 flux became less over the duration of the experiments, hence the difference between the CO_2 intake rate for the surcharged columns and the unsurcharged columns became smaller; the interaction variable surcharge*time accounts for this change.
- The initial CO_2 concentration, proven significant in Experiment A only, increased the CO_2 intake rate, while a high water table decreased the CO_2 intake rate in Experiment B.

The lack-of-fit value, defined in Appendix D3, was zero for the best-fit model in Experiment B. The reason for this was by leaving out the insignificant variable initial CO_2 concentration, multiple observations had identical x values/inputs. Identical x value inputs represent 'pure error' because only random variation can cause differences between the observed response values (Minitab, 2016a). To avoid overfitting, a large set of gas samples was collected and cross-validation carried out (Section 4.6.5.5).

4.6.5.5 Cross validation

In addition to R^2 predicted and the lack-of -fit values, more extensive cross-validation was done to validate both models. The following two scenarios were examined using subsets of the data and fitting models to these subsets:

- Scenario 1: Removed data from day 115 to 179 for Experiment A (31% of data taken out) and Experiment B (32% of data taken out).
- Scenario 2: Removed every third gas sampling event for Experiment A (35% of data taken out) and removed every fourth gas sampling event for Experiment B (25% of data taken out). The reason for removing only every fourth gas sampling event in Experiment B was because there were several periods of time in Experiment B with intervals of 10 days between sampling events, whereas in Experiment A, the maximum

interval was only 5 days. If every third sampling event was removed from Experiment B, there would have been long periods of time with no sampling event.

The cross-validation models produced for both scenarios were similar to the best-fit model in Section 4.6.5.4 in that they remained powerful predictive models, explaining over 64.8% of the variability of the subset data. The models for Scenario 1 are shown in Table 4.22 for Experiment A and Table 4.23 for Experiment B, while the models for Scenario 2 are in Appendix D14. Most of the significant variables in the overall models were significant in the cross-validation models and had the same positive or negative signs as the overall ones. The cross-validation models were fitted to all the data, which included the removed observations. The results were satisfactory as the cross-validation models for Scenario 1 for Experiments A and B accounted for 64.8% and 66.2% of the variability respectively, while the models for Scenario 2 accounted for 66.3% and 68.6% of the variability. These outcomes signalled that due to the large number of data points, the lack-of-fit and R^2 predicted values may have been sufficient for cross-validation.

Table 4.22 - Cross-validation model for Scenario 1 using data from Experiment A

Parameters	Coefficient	Standard error	p-value
b_0 (constant)	-10.6	13.7	0.442
b_1 (initial CO_2)	-1588	141	0.000
b_2 (ln(time))	21.79	1.18	0.000
b_3 (cement)	-0.1137	0.0286	0.000
b_4 (surcharge)	-4.722	0.359	0.000
b_6 (GGBS*cement)	0.001525	0.000311	0.000
R^2 (adj.)	62.9		
R^2 (pred.)	61.91		
SE	33.7784		
d.f (reg, res)	5,750		
F-value	251.49		
P-value	0.000		

Table 4.23 - Cross-validation model for Scenario 1 using data from Experiment B

Parameters	Coefficient	Standard error	p-value
b_0 (constant)	-207.09	8.16	0.000
b_2 (ln(time))	31.31	2.09	0.000
b_4 (surcharge)	-5.657	0.743	0.000
b_5 (surcharge*time)	0.0716	0.0104	0.000
b_7 (water table)	18.38	3.20	0.001
R^2 (adj.)	60.29		
R^2 (pred.)	59.76		
SE	41.8360		
d.f (reg, res)	4,535		
F-value	205.57		
P-value	0.000		

Examining the cross-validation models individually, surcharge*time was not significant for Scenario 1 in Experiment A ($p = 0.815$), and cement was not significant for Scenario 1

in Experiment B ($p = 0.121$), though cement showed an encouraging trend towards significance ($p < 0.2$). Surcharge*time was not significant as the effect of surcharge on the CO_2 flux became less over time; consequently, surcharge*time was not as dominant a variable in the first 115 days as over the full experimental time (180 days). Cement content, on the other hand, was barely significant ($p = 0.031$) in Experiment B when the full dataset was examined, so for Scenario 1 it is not surprising that cement was not significant for a smaller sample size. The relatively small influence cement had on the CO_2 flux in Experiment B is evident in the sensitivity analysis carried out in Section 4.6.5.6.

Similar findings to the best-fit models for Experiments A and B were found when 0 ppm was assumed instead of 50 ppm for undetectable gas readings (Appendix D14). The models fitted for the 0 ppm scenario in Experiments A and B were statistically powerful predictive models that accounted for 66.2% and 68.6% of the variability of the flux data respectively. The same variables were significant, and the coefficients were of similar magnitude and had the same positive or negative signs as the best-fit model in Section 4.6.5.4.

4.6.5.6 Sensitivity analysis of best-fit models

The sensitivity of the derived equation/models (Equation 4.3 and Equation 4.4) to changes in the input variables was checked to see if the CO_2 fluxes calculated were realistic. Through a sensitivity analysis which involves adjusting a single variable or multiple variables at a time, a Monte Carlo simulation was set up to perform multiple runs. The boundary conditions in Table 4.24 were applied to the input variables for these analyses.

Table 4.24 - Boundary conditions for input variables for sensitivity analysis for Experiments A and B

Experiment A	Experiment B
Cement content = 62.5 to 278 kg/m^3	Cement content = 150 to 250 kg/m^3
GGBS content = 0 to 187.5 kg/m^3	Water table = 0 or 1
Time = 1 to 179 days	Time = 1 to 179 days
CO_2 concentration = 0.04485 to 0.1086 CO_2% in air	Surcharge = 0 to 12 kPa
Surcharge 0 to 12 kPa	

All input factors were sampled from the probability density functions defined for each input. For Equation 4.3 derived from Experiment A data, the cement*GGBS term was not counted if the value was above 187.5*62.5 = 11719, as values above this were not present in the experiment.

The analysis was run 1000 times on Excel and the normal distribution curve for the 40-minute flux for Equation 4.3 from Experiment A was found to have a mean of -83 mg

$CO_2eq/m^2/hr$ and standard deviation of 38 mg $CO_2eq/m^2/hr$, while the normal distribution curve produced by Equation 4.4 for Experiment B was found to have a mean of -64 mg $CO_2eq/m^2/hr$ and standard deviation of 45 mg $CO_2eq/m^2/hr$. The maximum and minimum CO_2 flux were 28 mg $CO_2eq/m^2/hr$ and -268 mg $CO_2eq/m^2/hr$ for Equation 4.3 and 21 mg $CO_2eq/m^2/hr$ and -272 mg $CO_2eq/m^2/hr$ for Equation 4.4. This shows that the models developed for each experiment were producing realistic flux values as they were in the range of values obtained during the experiments.

The Monte Carlo simulation was then repeated several times for each statistical model, holding selected inputs constant at default maximum and minimum values whilst allowing all others inputs to vary within the pre-defined ranges. This showed the percentage change each variable had on the average fluxes stated in the previous paragraph. Figure 4.18 and Figure 4.19 show sensitivity of the statistical models for Experiments A and B to each input variable. As expected, the average flux was most sensitive to time for both experiments, changing the average flux by -108% in Experiment A and -260% in Experiment B. Surcharge is seen to be a much more significant variable in Experiment A than in Experiment B, which was first evident in an examination of the flux values for the unsurcharged and surcharged specimens in Figure 4.14 and Figure 4.15. A maximum percentage change in the average flux of 30% was recorded in Experiment A while in Experiment B a percentage change of only 9% was calculated.

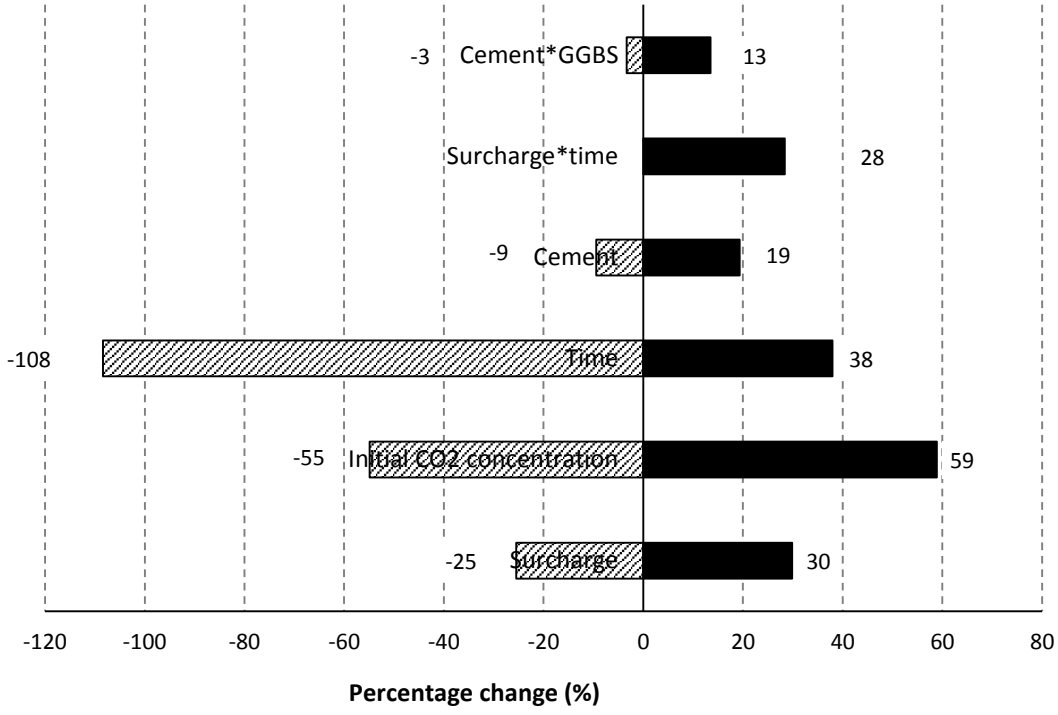

Figure 4.18 - Sensitivity of statistical model produced for Experiment A to changes in input variables

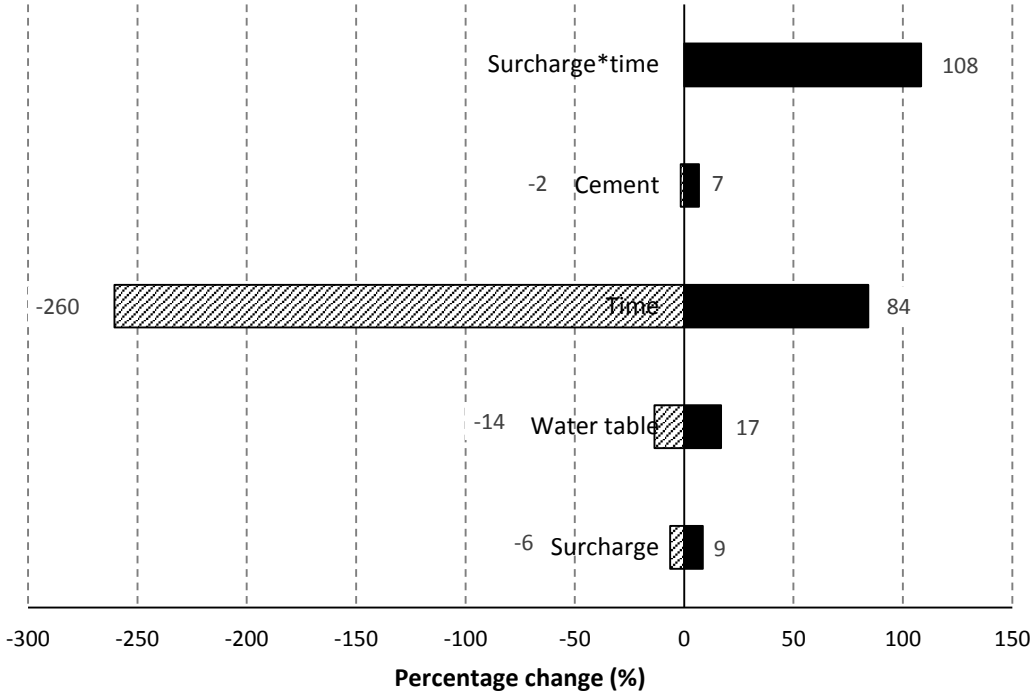

Figure 4.19 - Sensitivity of statistical model produced for Experiment B to changes in input variables

4.6.6 Comparisons of CO_2 fluxes between Experiments A and B

The initial CO_2 concentration for sampling events in Experiments A and B at the same point in time during the experiment was different, thereby affecting the fluxes. Additionally, more measurements were taken in Experiment A than in B, especially in the first fifty days, which affected the mean and standard deviation of the fluxes. Furthermore, gas sampling events for Experiments A and B took place on different days. The aforementioned effects on the fluxes are relevant to making a fair comparison of the two sets of data.

Nonetheless, similar mixes were used in Experiments A and B to discover if they would produce the same gas flux results. The 40-minute flux data from each column type in Experiments A and B were compiled in Figure 4.20. Appendix D15 gives the equivalent plot for the 20-minute fluxes and also shows the interval plots for the 20 and 40-minute fluxes of all individual columns. From these plots and the one-way ANOVA table, Table 4.25, it was found that:

(i) The identical mixes B3 and A4 had similar CO_2 flux values ($p > 0.05$).

(ii) The 12 kPa surcharged specimens B8 and A5 also had similar CO_2 intake rates ($p > 0.05$) (Table 4.25), the largest rates of all the specimens.

(iii) Identical mixes A3 and B4 (unsurcharged) were significantly different from each other. It was thought that this difference may have been due to the higher CaO

content of the cement used in Experiment B, which meant the cement had a greater carbonation potential and the ability to take in more CO_2 due to carbonation. In Experiment A, the CaO content of the cement was only 62.5 ± 1.37 (n = 3) while in Experiment B it was 64.74 ± 0.64 (n = 5), indicating a difference between the two, though not significant (p = 0.117).

(iv) Drained peat columns B7 and A8 were significantly different from each other, but this was mainly due to one column A8(2) in A8 and one column B7(1) in B7 having average CO_2 flux values significantly smaller than the rest (Appendix D8). When A8(2) and B7(1) were omitted from the analysis, the rest of the drained peat columns had similar CO_2 emission rates for the 20-minute flux (p = 0.138) and the 40-minute flux (p = 0.139).

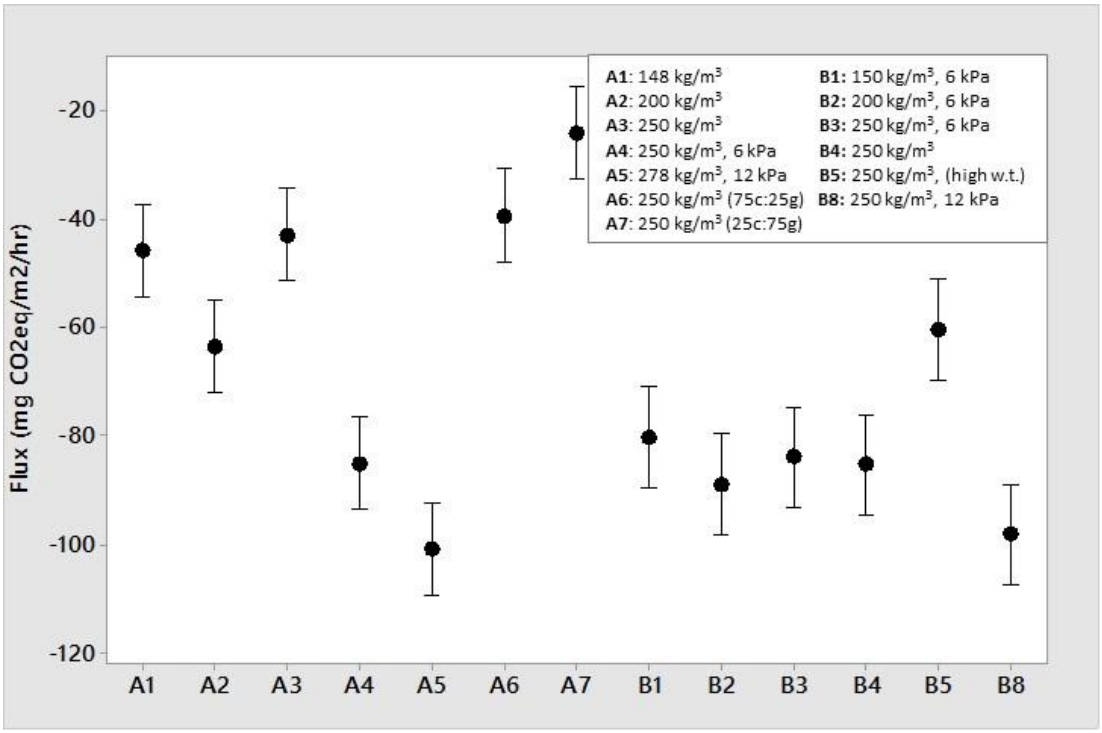

Figure 4.20 - Interval plot of mean 40-minute fluxes for each stabilised peat column type in Experiments A and B with 95% confidence interval bars for the mean, based on a pooled standard deviation

Table 4.25 - One-way ANOVA p-values for comparing similar groups of specimens in Experiments A and B

Minute fluxes	Specimen Numbers			
	B3 vs A4[(i)*]	**B8 vs A5[(ii)*]**	**B4 vs A3 [(iii)*]**	**B7 vs A8 [(iv)*]**
0–40	0.876	0.696	**0.000**	**0.002**
0–20	0.284	0.762	**0.000**	**0.002**
	> 0.05	**> 0.05**	**< 0.05**	**< 0.05**

* (i)–(iv) are cross referenced with the numbering above.

4.6.7 Meta-analysis

4.6.7.1 Variables controlling CO_2 flux in stabilised peat

A meta-analysis (Section 3.6.2.2) was performed on the data from Experiments A and B combined to increase the statistical power over individual studies with a view to improving the precision of estimates of the relationships between the gas flux and its influencing factors. Generally, a meta-analysis provides stronger evidence for the hypotheses, enables results to be generalised to a larger population, and helps determines if further studies are needed to investigate an issue.

The variables examined were initial CO_2 concentration (% CO_2 in air), cement content (kg/m^3), GGBS content (kg/m^3), water table, surcharge (kPa), and time (days). Only the 20 and 40-minute fluxes were used in the meta-analysis; the chamber deployment time in Experiment B was only 40 minutes (thereby excluding the 60-minute flux), and no 10-minute gas sample was retrieved in Experiment A until day 15 (thereby excluding the 10-minute flux). Before undertaking this analysis, variables were checked for multicollinearity: while a low correlation existed between some variables, there was a strong correlation between cement and GGBS (-0.756) and moderate correlations between surcharge and cement (0.432) and GGBS and surcharge (-0.317) (Table 4.26). These correlations were again checked in the meta-analysis using VIF factors, where action may be taken if the VIF value is high.

Table 4.26 - Correlation and p-values for the variables in the meta-analysis

	Cement	GGBS	Water table	Surcharge	Time
GGBS	-0.756 0.000				
Water table	**0.192** 0.000	**-0.107** 0.000			
Surcharge	**0.432** 0.000	**-0.317** 0.000	**-0.222** 0.000		
Time	0.005 0.823	-0.007 0.753	-0.007 0.760	0.006 0.798	
Initial CO_2 concentration	0.004 0.872	0.009 0.710	0.023 0.318	-0.027 0.244	**-0.185** 0.000

Cell content: Pearson correlation
p-value

Table 4.27 and Table 4.28 show the analyses for the 40 and 20-minute fluxes respectively. For these fluxes, 1884 data points were used to produce each model for the 39 stabilised peat columns. From the meta-analysis, the CO_2 flux was found to be significantly related to the natural logarithm of time, surcharge, cement, GGBS and initial CO_2 concentration. Cement, however, was not significant on its own for the 20-minute flux. Like in Experiment A, when cement and GGBS were analysed together for the 40-minute flux, cement was not a significant variable due to multicollinearity. To account for cement and

GGBS, GGBS was removed from the model, and a significant interaction variable was substituted (cement*GGBS). A significant interaction was also present between surcharge and time. By performing multiple regression analyses and examining VIF values, interactions between cement and surcharge, water table and time, cement and time were tested and found to be either not significant or highly correlated with other variables (Table 4.27). From the first to last analysis, overall R^2 adjusted values increased from 56% to 64% for the 40-minute flux and from 48% to 62% for the 20-minute flux.

Table 4.27 - Meta-analyses showing the effects of variables examined on the 40-minute fluxes for stabilised peat specimens in Experiments A and B

	40-minute flux					
Analysis	1	2	3	4	5	6
R^2 (adj)	55.55	60.99	61.01	64.67	63.77	63.74
Lack-of-fit	0.797	0.845	0.752	0.878	0.87	0.791
Variables	**p-values**					
Intercept	**0.000**	**0.000**	**0.000**	**0.000**	**0.000**	**0.000**
Time	**0.000**	-	-	-	-	-
Ln (Time)	-	**0.000**	**0.000**	**0.000**	**0.000**	**0.000**
Initial CO_2	0.067	**0.001**	**0.001**	**0.002**	**0.001**	**0.001**
GGBS	**0.000**	**0.000**	**0.000**	**0.002**	0.110	-
Cement	0.095	0.054	**0.049**	0.976	**0.011**	**0.000**
Water table	0.822	0.901	-	0.002	0.508	-
Surcharge	**0.000**	**0.000**	**0.000**	**0.000**	**0.000**	**0.000**
Surcharge*time	-	-	-	**0.000**	**0.000**	**0.000**
Water table*time	-	-	-	**0.000**	-	-
Cement*time	-	-	-	0.623	-	-
Cement*GGBS	-	-	-	**0.004**	**0.002**	**0.000**
Cement*surcharge	-	-	-	**0.000**	-	-

Table 4.28 - Meta-analyses showing the effects of variables examined on the 20-minute fluxes for stabilised peat specimens in Experiments A and B

	20-minute flux					
Analysis	1	2	3	4	5	6
R^2 (adj)	48.49	57.85	62.3	61.93	61.9	61.97
Lack-of-fit	0.449	0.538	0.589	0.584	0.431	0.737
Variables	**p-values**					
Intercept	**0.000**	**0.000**	**0.000**	**0.000**	**0.000**	**0.000**
Time	**0.000**	-	-	-	-	-
Ln (Time)	-	**0.000**	**0.000**	**0.000**	**0.000**	**0.000**
Initial CO_2	0.236	**0.035**	**0.008**	**0.028**	**0.032**	**0.027**
GGBS	**0.000**	**0.000**	0.083	0.051	-	**0.007**
Cement	0.791	0.874	0.422	0.722	0.053	-
Water table	0.306	0.417	**0.000**	0.722	-	-
Surcharge	**0.000**	**0.000**	**0.000**	**0.000**	**0.000**	**0.000**
Surcharge*time	-	-	**0.000**	**0.000**	**0.000**	**0.000**
Water table*time	-	-	**0.000**	-	-	-
Cement*time	-	-	**0.003**	-	-	-
Cement*GGBS	-	-	**0.004**	**0.004**	**0.000**	**0.003**
Cement*surcharge	-	-	0.646	-	-	-

Water table was not significant as the unsurcharged columns in Experiment A had lower CO_2 intake rates than the unsurcharged columns in Experiment B and two of the unsurcharged columns whose water table was at the surface. In addition to the reason given in Section 4.6.4.2, it was again thought that the difference in CaO contents of the cements was the reason for water table not being a significant variable as the CO_2 intake rate was generally lower in Experiment A.

4.6.7.2 Best-fit model

Only parameters that contributed significantly to the gas flux in stabilised peat were included in the final equation/model. The 40-minute fluxes provided the best-fit statistical model and included the natural logarithm of time, cement content, initial CO_2 concentration, surcharge, and interaction variables, surcharge*time and cement*GGBS. These were recognised to be the driving variables and explained 63.85% of the variability for the 40-minute fluxes (Equation 4.5) (Table 4.29). The results of the multiple regression analysis, including the residual plots, are shown in Appendix D16 as well as a plot of the predicted fluxes against the measured fluxes. The residuals were not distributed normally; however, the histogram of the residuals follows a normal distribution, and the residuals versus the order of data plot seemed to follow white noise (a random pattern). Using the best fit model, the slopes and R^2 values for the relationship between the observed 40-minute fluxes and the predicted values for the individual columns are shown in Appendix D17.

$$\text{Gas flux} = b_0 + b_1 \times \text{initial } CO_2 \text{ conc.} + b_2 \times \ln(\text{time}) + b_3 \times \text{cement} + b_4 \times \text{surcharge} + b_5 \times \text{surcharge*time} + b_6 \times \text{cement*GGBS} \quad \textbf{Equation 4.5}$$

Table 4.29 - Parameters for the CO_2 flux reconstruction model for Experiments A and B

Parameters	Coefficient	Standard error	p-value
b_0 (constant)	-149.11	5.98	0.000
b_1 (initial CO_2)	-121.5	37.1	0.001
b_2 (ln(time)))	28.719	0.848	0.000
b_3 (cement)	-0.0784	0.0185	0.000
b_4 (surcharge)	-6.287	0.328	0.000
b_5 (surcharge*time)	0.03607	0.00310	0.000
b_6 (cement*GGBS)	0.001821	0.000244	0.000
R^2 (adj)	63.74		
R^2 (pred)	63.18		
SE	35.6768		
d.f (reg, res)	6,1877		
F-value	552.59		
P-value	0.000		

4.6.7.3 Cross-validation

Further cross-validation was carried out to validate the best-fit model. The following two scenarios were examined using subsets of the data and fitting models to these subsets.

- Scenario 1: Removed data from day 115 to day179 (31% of data taken out).
- Scenario 2: Removed every third gas sampling event from Experiment A and every fourth gas sampling event from Experiment B (29% of data taken out) (for reason discussed in Section 4.6.5.5).

The cross-validation model produced for both scenarios were similar to the best-fit model in Section 4.6.7.2 in that they remained powerful predictive models, explaining over 58 % of the variability of the subset data. The model for Scenario 1 is shown in Table 4.30, while the model for Scenario 2 is in Appendix D18. All significant variables in the overall models were significant in the cross-validation models and had the same positive or negative signs as the overall models. The cross-validation models were fitted to all the data, which included the removed observations. The results were satisfactory as the cross-validation models for Scenarios 1 and 2 accounted for over 53% of the variability.

Table 4.30 - Cross-validation model for Scenario 1 using data from Experiments A and B

Parameters	Coefficient	Standard error	P-value
b_0 (constant)	-150.83	7.66	0.000
b_1 (initial CO_2)	-109.4	42.9	0.011
b_2 (ln(time))	28.66	1.2	0.000
b_3 (cement)	-0.0821	0.0254	0.001
b_4 (surcharge)	-6.312	0.442	0.000
b_5 (surcharge*time)	0.04206	0.00666	0.000
b_6 (cement*GGBS)	0.002453	0.000334	0.000
R^2 (adj)	57.59		
R^2 (pred)	56.89		
SE	40.5799		
d.f (reg, res)	6,1289		
F-value	294.04		
P-value	0.000		

4.6.7.4 Sensitivity analysis of best-fit meta-analysis model

The sensitivity of the derived equation/model (Equation 4.5) to changes in the input variables was checked to ascertain if the gas fluxes calculated were realistic. The boundary conditions applied to the input variables for the analysis were the same as for Experiment A in Table 4.24. The cement*GGBS term was excluded if the value was above 187.5*62.5 = 11719 as it had not been examined in the experiment.

The Monte Carlo analysis was run 1000 times on Excel, and the normal distribution curve for the 40-minute flux was found to have a mean of -64 mg CO_2eq/m^2/hr and standard deviation of 40 mg CO_2eq/m^2/hr. The maximum and minimum CO_2 flux were found to be

6 mg CO_2eq/m^2/hr and -224 mg CO_2eq/m^2/hr respectively, a smaller range than in Experiments A and B individually, showing that a larger sample size leads to less variation than a smaller sample size. Figure 4.21 shows the sensitivity of the meta-analysis model to each input variable. As expected, the average flux was again most sensitive to time, changing the average flux by -221%. The gas flux is also quite sensitive to the interaction variables surcharge*time and cement*GGBS, with maximum percentage changes in the average flux of 75% and 43% respectively.

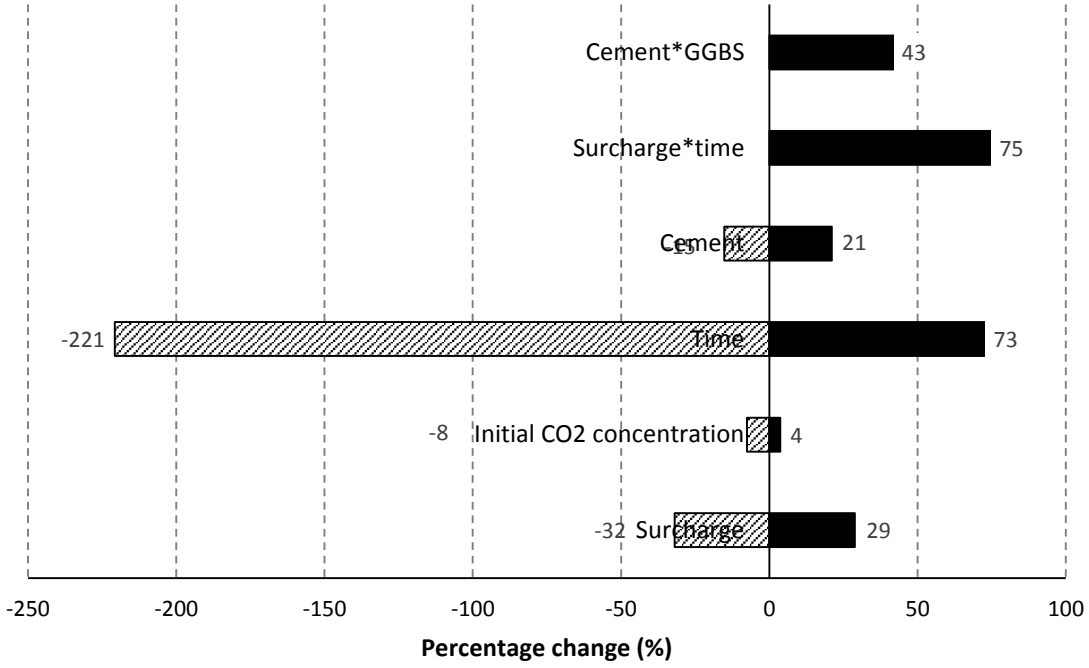

Figure 4.21 - Sensitivity of meta-analysis model to changes in input variables

4.6.8 Summary

The best-fit statistical models of Experiments A and B both revealed cement, surcharge, the natural logarithm of time, and an interaction variable surcharge*time to be significant variables in predicting the CO_2 gas flux in stabilised peat. An increased cement content and a larger surcharge contributed to a rise in the CO_2 intake flux. As in Experiment P, the CO_2 intake flux decreased logarithmically with time. It is noteworthy that the significant variable surcharge*time was responsible for decreasing the CO_2 intake rate, showing surcharge to be a less significant variable over time.

Experiment A also revealed initial CO_2 concentration and cement replacement with GGBS to be significantly related to the CO_2 flux in stabilised peat. The more cement that is replaced with GGBS, the smaller the CO_2 intake rate became. As anticipated, Experiment B showed water table to be a significant variable, decreasing the CO_2 intake or carbonation rate as it does for carbonation in concrete.

The best-fit models for the meta-analysis revealed the natural logarithm of time, surcharge, cement, initial CO_2 concentration, and the interaction variables cement*GGBS and surcharge*time to be significant variables, all of which had the same positive and negative signs as the variables in the individual best-fit models for Experiments A and B. Surprisingly, water table depth (high or low) was not significantly related to CO_2 flux, and it is thought that the reason may be due to the difference in the CaO contents of the cements used in the two experiments. Sensitivity analyses were performed that showed this model to be statistically powerful in predicting stabilised peat CO_2 fluxes.

4.7 Discussion on CO_2 gas fluxes from stabilised peat

4.7.1 Underestimating the true gas flux

In keeping with the CO_2 flux data from stabilised peat in Experiment P, there was not a strong linear relationship between the CO_2 concentration data and time for most of the gas sampling events in Experiments A and B. The slope of the best-fit relationship in Figure 4.22 shows that the 0–60 minute flux is less than the 0–40 minute flux; and when considered with data for other flux times in Appendix D19, it can be concluded that the longer the deployment time, the smaller the flux. Therefore, the 0–60 minute flux is likely to underestimate the true flux. As explained in Section 2.8.2.1, the true flux is the one that would have occurred in the stabilised peat had it not been restricted by the closed chamber. It is noteworthy that the 0–10 minute flux in Experiment A and 0–5 minute flux in Experiment B were not of major relevance as only two data points are used to derive the fluxes, so R^2 is always 1.

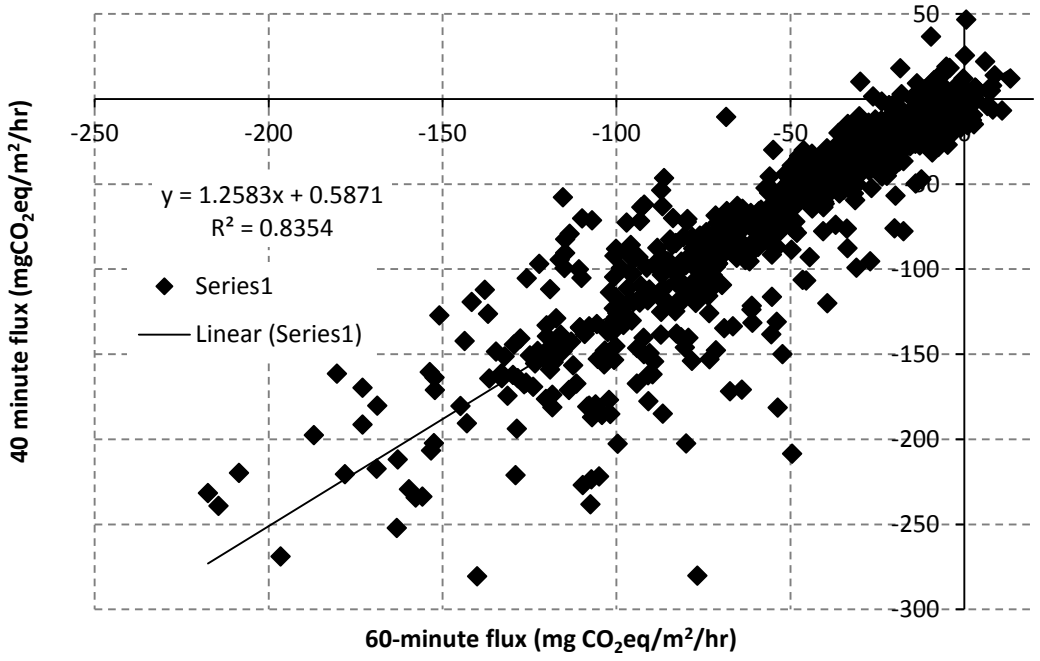

Figure 4.22 - 40-minute versus 60-minute flux for stabilised peat in Experiment A

4.7.2 Goodness-of-fit of linear regression

4.7.2.1 Introduction

Each CO_2 flux result from the stabilised peat was obtained by calculating the concentration difference in the headspace over a time period, t, (5, 10, 20, 40 or 60 minutes). Linear regression was applied to the gas concentration against time plots, and the slope of the regression line was then used to calculate the average CO_2 flux over t (Section 3.5.3.3). Though the 40-minute flux gave the best-fit statistical models, it had to be considered if it was the most appropriate flux time or if a different one should be used, say the 10 or 20-minute flux. For future studies, it important to know the period of time over which a flux should be calculated, 10, 20, 40 or 60 minutes. While multiple linear regression analyses were the first indicators of the appropriate flux times and showed that both the 20 and 40-minute fluxes gave good predictive models, an examination of the application of linear regression to the gas concentration data shows the appropriateness of each flux time.

4.7.2.2 Stages 1, 2, and 3

The goodness-of-fit of the linear regression (R^2 values) was calculated for each CO_2 flux at each gas sampling event. This involved examining the goodness-of-fit for 1248 CO_2 flux results in each of the 20, 40 and 60 minute fluxes for Experiment A and 1056 for 10, 20 and 40 minute fluxes for Experiment B. These results suggested that for Experiments A and B there was an 'evolution' in the goodness-of-fit over the course of the experiment, which could be broken down into three stages: Stage 1, Stage 2 and Stage 3. The duration of each stage depended on the binder type and content and the environmental conditions of the stabilised peat. Figure 4.23 shows typical examples of these stages.

Stage 1 corresponded to when the carbonation rate or CO_2 intake rate was at its highest. For a gas flux calculated using a shorter chamber deployment time, a better goodness-of-fit of linear regression was recorded (Figure 4.23(a)). This was primarily due to the chamber deployment having more of an effect on the gas flux the longer the deployment time, which in turn is because diffusion theory is not linear (Section 2.8.2). The effect of the chamber deployment is evident in Figure 4.23(a) as the gas concentration remains relatively constant after 20 minutes.

In Stage 2, the goodness-of-fit of linear regression on the CO_2 concentration data was much better than in Stage 1, as demonstrated by R^2 values that were closer to one (Figure 4.23(b)). This was due to the lower carbonation intake or CO_2 intake, which decreased over time and resulted in the effect of the chamber deployment being less influential on the gas flux.

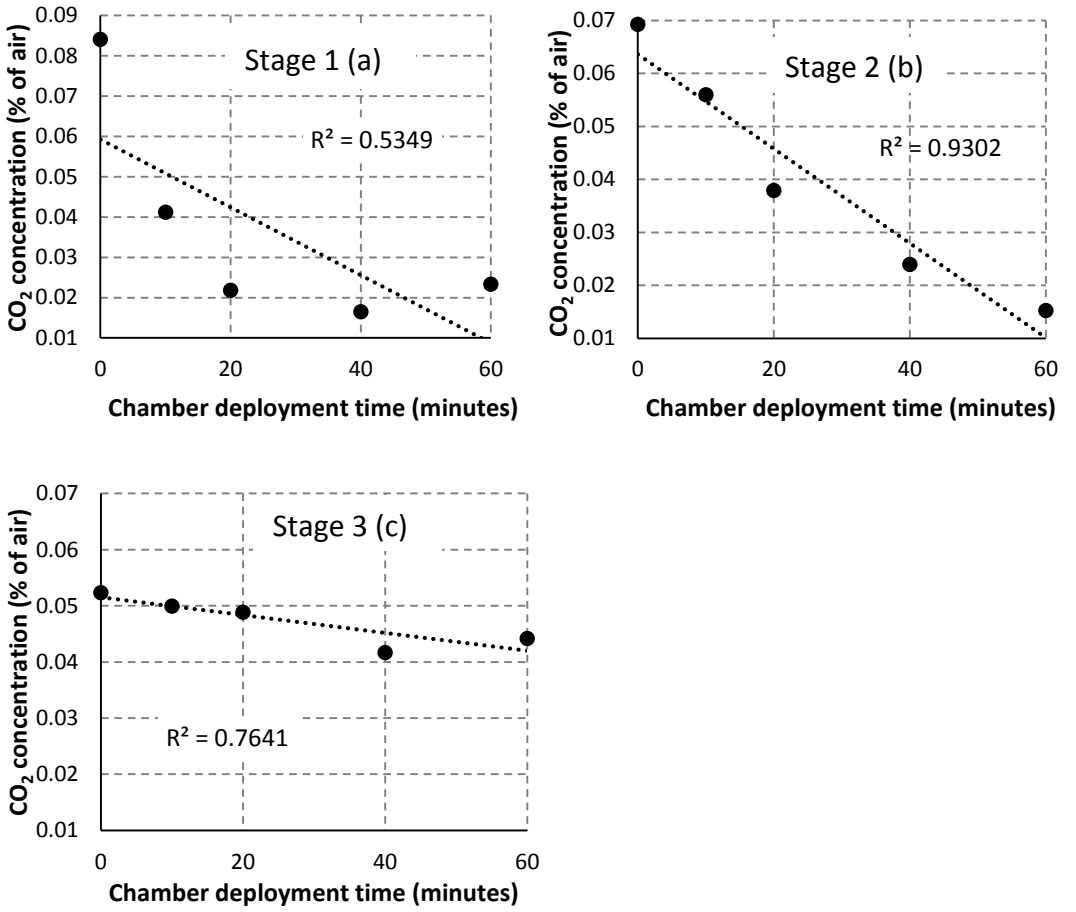

Figure 4.23 - Change in CO_2 gas concentration with time for (a) Stage 1 (A5(1) at day 15), (b) Stage 2 (A5(1) at day 46), and (c) Stage 3 (A5(1)) on day 179)

In Stage 3, the carbonation rate decreased to a point where the effects of the small variability in the peat emission rate and the carbonation process became more prevalent as did the error of the gas chromatograph (GC) (Section 4.7.2.4) (Figure 4.24). As shown in Figure 4.23(c), the concentration drop over 60 minutes was less than only 0.01% compared to Figure 4.23(a) and Figure 4.23(b) where the drops were approximately 0.06%. In addition to the error in the GC measurements, the carbonation process and emissions-from-peat rates (Equation 4.1) were not constant due to their dependence on many variables (Sections 2.6.5 and 2.7.1.4). Carbonation depends primarily on time but also on other factors. The stabilised peat is part of a biological and chemical environment whose gas flux fluctuates during chamber deployment, its variability having a greater effect as the carbonation intake rate lessens over time.

4.7.2.3 Duration of Stages 1, 2 and 3

The effects that specimen type and the gas sampling event time (0–180 days) have on the appropriateness of the chamber deployment time over which a gas flux is calculated is explored in this section. This is achieved through a rough guide that shows the start and end times of Stages 1, 2 and 3 for surcharged and unsurcharged stabilised peat. Defining

the start and the end of the stages is difficult; therefore, a criterion for R^2 values was set. A change in the goodness-of-fit of linear regression that goes above or below an R^2 value of 0.85 is chosen arbitrarily to indicate a change in stages. The length of these stages is discussed primarily using the results of Experiment A.

Stage 1 lasted between 3 and 36 days in Experiment A, 3 days for the unsurcharged specimens and between 24 and 36 days for the surcharged specimens, the difference being due to the higher CO_2 intake rate of the surcharged specimens. Stage 1 was evident in the surcharged specimens in Experiment A for the first 36 days from examination of the goodness-of-fit of linear regression on the gas concentration data for the 40 and 60-minute fluxes, which had mean R^2 values (± 1 standard deviation) of 0.795 ± 0.151 and 0.669 ± 0.194, respectively. As stated above, a gas flux calculated using a shorter chamber deployment time shows higher linearity in the relationship between gas concentration data and time. Similar trends were found in Experiment B, where average R^2 values for the 20 and 40-minute fluxes for the surcharged specimens for the same period were 0.83 ± 0.125 and 0.66 ± 0.196 respectively.

Stage 2 started between days 3 and 36 in Experiment A and lasted, with odd exceptions, for the unsurcharged specimens until between days 54 and 107 and between days 139 and 171 for the surcharged specimens. The difference in the end time of Stage 2 was due to the higher CO_2 intake rate in the surcharged specimens. In Stage 2, the goodness-of-fit of linear regression was much better than in Stage 1, demonstrated by R^2 values that were closer to one (Table 4.31).

Table 4.31 - Mean R^2 values (± 1 standard deviation) representing the goodness-of-fit of linear regression on CO_2 concentration with time plots for Experiments A and B

Flux time (mins)	Experiment A			Experiment B		
	Day 1–60	Day 60–120	Day 120–180	Day 1–60	Day 60–120	Day 120–180
10				0.89 ± 0.21	0.81 ± 0.29	0.76 ± 0.29
20	0.87 ± 0.22	0.83 ± 0.26	0.64 ± 0.35	0.83 ± 0.20	0.84 ± 0.27	0.74 ± 0.30
40	0.88 ± 0.17	0.81 ± 0.27	0.67 ± 0.32	0.76 ± 0.22	0.87 ± 0.21	0.79 ± 0.27
60	0.84 ± 0.19	0.81 ± 0.24	0.66 ± 0.32			

Stage 3 continued until the end of Experiment A, representing the time when the relationship between gas concentration data and chamber deployment time became more non-linear and the error of the GC became problematic (Section 4.7.2.4). The higher non-linearity is reflected in Table 4.31 between days 120 and 180 for both Experiments A and B as linear regression was not as good a fit for the gas concentration data between days 1 and 120. Taking into account that Stage 3 generally occurs later for surcharged specimens, the higher R^2 values between days 120 and 180 in Experiment B compared to in

Experiment A are primarily due to 15 of the 21 specimens in Experiment A being unsurcharged whereas only 6 of the 18 were unsurcharged in Experiment B.

4.7.2.4 The period of time over which a gas flux should be calculated

As discussed in Section 2.8.2, a smaller chamber deployment time is recommended for calculation of gas fluxes from peat, but this appears not to be the case for stabilised peat as illustrated in Figure 4.24. In the experiments for the first 36 days in general, the goodness-of-fit of linear regression on gas concentration data was quite good for the 20-minute flux due to a high CO_2 intake (Figure 4.23 (a)); but due to the lower CO_2 intake rate over the full duration of the experiments, the relationship between gas concentration and time at each gas sampling event for the 20-minute flux became more non-linear, with the error of the GC having a greater effect (Table 4.31). For example, if the 20-minute flux was used for A1(2) on day 151, the error of the GC would have been high, whereas for the 0–40 minute flux the error was much lower (Figure 4.24).

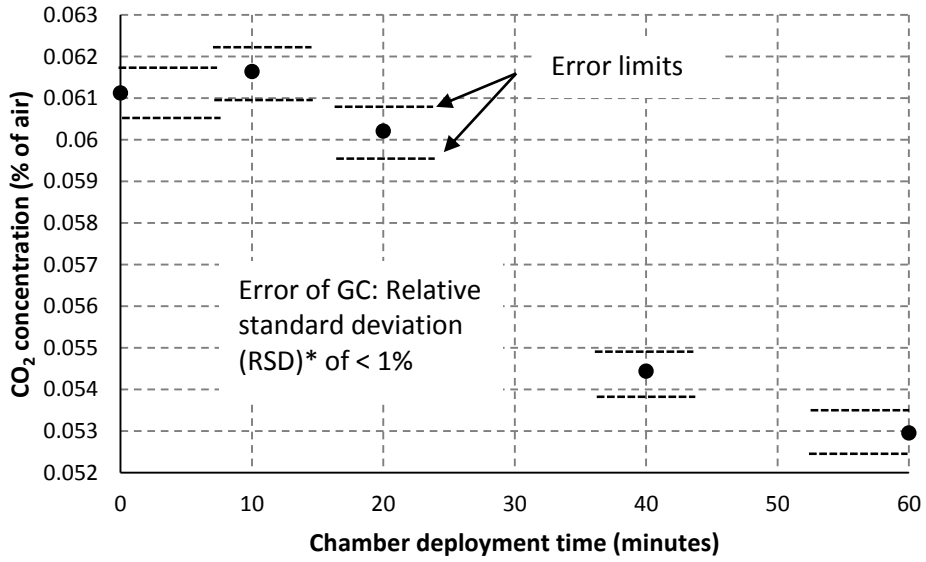

*** RSD is defined as the ratio of the standard deviation σ to the mean μ**

Figure 4.24 - Variation in CO_2 concentration with time for A1(2) on day 151

The 0–60 minute flux in Figure 4.24 and Figure 4.23(a) may not be appropriate as the effect of the chamber deployment time increases as the CO_2 concentration in the chamber decreases. Due probably to the reasons outlined in this section, the 40-minute flux provided the best-fit statistical models for Experiments A and B. The 20-minute flux provided the next best-fit models but were always slightly lower in goodness-of-fit to the 40-minute flux. This is evident in Table 4.31 for both experiments as only one of the three average goodness-of-fit values (R^2 values) for the 20-minute flux is greater than one of three for the 40-minute flux.

In the case of experiments conducted over 180 days on stabilised peat with similar binder types and contents and environmental conditions, the use of the 40-minute flux is recommended, followed by the 20-minute flux. If the CO_2 gas flux from stabilised peat were examined over a longer time period, say 1 to 2 years, the CO_2 intake rate would decrease further, which may require a longer chamber deployment time, maybe 60 minutes or longer, to witness the full effect of the gas flux. Otherwise, the sensitivity of the GC measurements and the variability in peat emissions and carbonation process become a greater issue when determining the accuracy of the gas fluxes calculated.

4.8 Summary

While the raw peat in Experiments P, A, and B, was found to be a source of CO_2, influenced by water levels and temperature, stabilised peat acted as a net carbon sink, its CO_2 flux varying according to time, surcharge, cement and GGBS content, water table depth, and initial CO_2 concentration. Appropriate statistical techniques were used to investigate the significance of these relationships.

These findings are important for carbon calculations relevant to soil-mixing applications as the variables that influence the CO_2 flux from stabilised peat have been identified. The best-fit statistical model/equation for CO_2 fluxes from stabilised peat produced by the meta-analysis in this chapter will be used in Chapter 7 to account for the on-site environmental impact of stabilising peat in an environmental LCA.

Chapter 5: Depth of Carbonation Front

5.1 Introduction

In this chapter, the results from the experimental methods employed to establish the depth of the carbonation front (X_c) are presented and discussed. The methods employed are (i) phenolphthalein indicator, (ii) X-ray powder diffraction analysis (XRD), (iii) Fourier transform infrared spectroscopy (FTIR), (vi) loss on ignition (LOI), (vii) pH of stabilised peat slurries and (viii) water evaporation method. The results of Experiment P are presented in Section 5.2 and those of Experiments A and B in Section 5.3.

None of the stabilised peat specimens in Experiment P are tested for their carbonation depths, but one is analysed for signs of carbonation. Four sets of specimens are analysed for their depth of carbonation in each of Experiments A and B. In Experiment A, small specimens a(a) are tested at day 20, small specimens a(b) at day 94, and small specimens a(c) and the large specimens (A) at day 180. In Experiment B, small specimens b(a) are tested at day 20, small specimens b(b) at day 90, and small specimens b(c) and the large specimens (B) at day 180. This chapter aims to demonstrate the applicability of the various carbonation depth techniques to stabilised peat and to discover which variables influence carbonation depth.

In Section 5.4, statistical analyses are carried out on the X_c results by way of correlation statistics, one-way ANOVA and multiple linear regression. One-way ANOVA is used to compare the carbonation depths calculated from each experimental technique, while for each experiment, multiple linear regression analysis is undertaken to identify the significant variables in predicting X_c. The data from each experiment are then combined to perform a meta-analysis.

5.2 Experiment P

5.2.1 A preliminary investigation of carbonation

In Experiment P, the depth of carbonation was not formally investigated, but the stabilised peat columns were inspected for signs of carbonation on completion of the gas chamber study. After dismantling the columns by taking the stabilised peat cores gently from their respective hollow acrylic columns, crystals on the surface of the cylindrical stabilised peat samples were observed as depicted in Figure 5.1(a), and residue was taken from P3(3) to investigate if these crystals were $CaCO_3$ or $Ca(OH)_2$. Exhalation (breathing out air) into a diluted solution of the residue did not result in a milky-coloured solution, indicating the absence of $Ca(OH)_2$. In a second test, the residue was mixed with 37% dilute hydrochloric

acid that extinguished a lit match held over the test tube due to the release of CO_2 from the tube, thereby indicating the presence of $CaCO_3$ (Kennedy, 2000).

Figure 5.1 - (a) Crystals on P3(3) (b) P3(3) after phenolphthalein indicator application

On establishing that some $CaCO_3$ was present, the phenolphthalein indicator was applied on the cylindrical surface and top surface of the stabilised peat column P3(3). The indicator was applied on random locations on the cylindrical surface which turned purple (Figure 5.1(b)), showing that no carbonation had taken place; however, the top surface turned bright pink, signifying that some carbonation had occurred. Samples were then taken from the interior of one of the stabilised peat columns at a depth of 250 mm and tested for pH. The results showed the stabilised peat to have a pH of 12.65 ± 0.03 (n = 5), also suggesting that the cement in this location was uncarbonated.

5.3 Experiments A and B

5.3.1 Phenolphthalein indicator

5.3.1.1 Results

Measurements of the carbonation front using the phenolphthalein indicator are summarised in Table 5.1 for Experiments A and B; X_c is renamed X_p for the phenolphthalein method. These were obtained using the method described in Section 3.5.4.3. Regions where the indicator remained colourless were observed to increase in size over time in most cases, from specimens a (tested on day 20) to specimens c (tested on day 180), thereby confirming an increase in X_p over time ($p = 0.000$).

In specimens a for Experiments A and B, the indicator turned pink/purple on the majority of the specimens; however, the indicator remained colourless (carbonated) on the top surface in a1(2a), a6(1a), a6(3a) and a7(3a), none of which displayed colourless regions with depth. In the second set of small specimens b tested on days 90 and 94, the indicator was not colourless at the surface in only two specimens in Experiment A and one in Experiment B, indicating that carbonation was manifesting at this time. The maximum X_p

recorded or the maximum depth at which the indicator remained colourless was 3 mm in b3(3b).

Table 5.1 - Carbonation depths (X_p) measured by the phenolphthalein indicator for Experiments A and B

X_p values in Experiment A (mm)					**X_p values in Experiment B (mm)**				
Test day	**20**	**94**	**180**	**180**		**20**	**90**	**180**	**180**
Specimen	**a**	**b**	**c**	**A**		**a**	**b**	**c**	**B**
A1(1)	0	1	2	2	B1(1)	0	1	21	0
A1(2)	1	1	2	1	B1(2)	0	2	27	0
A1(3)	0	1		0	B1(3)	0	1	1	1
A2(1)	0	1	1	1	B2(1)	0	1	2	1
A2(2)	0	0		0	B2(2)	0	3	17	1
A2(3)	0	1	1	1	B2(3)	0	1	22	1
A3(1)	0	1		1	B3(1)	0	1	12	2
A3(2)	0	1	1	1	B3(2)	0	1	7	1
A3(3)	0	1	2	1	B3(3)	0	3	5	1
A4(1)	0	1	14	1	B4(1)	0	1	1	1
A4(2)	0	1	1	0	B4(2)	0	1	2	1
A4(3)	0			0	B4(3)	0	1	1	1
A5(1)	0	2		0	B5(1)	0	0	0	0
A5(2)	0	1	12	0	B5(2)	0	1	0	0
A5(3)	0	1	31	1	B5(3)	0	0	0	0
A6(1)	1	1	4	1	B8(1)	0	2	10	0
A6(2)	0	0	6	1	B8(2)	0	1	5	0
A6(3)	1	1	6	1	B8(3)	0	1	15	1
A7(1)	0	1	5	0					
A7(2)	0	1	2	1					
A7(3)	1	1	14	0					

Noteworthy X_p values were recorded in specimens c (Figure 5.2), which show that:

- All specimens were carbonated at the surface (Figure 5.3(a)) except for b5(c) (n = 3) (i.e. X_p = 0 mm), which was anticipated, as minimal carbonation occurs under the water table (see Section 2.7.2.2).
- By examining the results from the unsurcharged specimens with 250 kg/m^3 of cement binder; namely, a3 (low water table), b4 (low water table), and b5 (high water table), a high water table was confirmed to decrease X_p ($p = 0.005$).

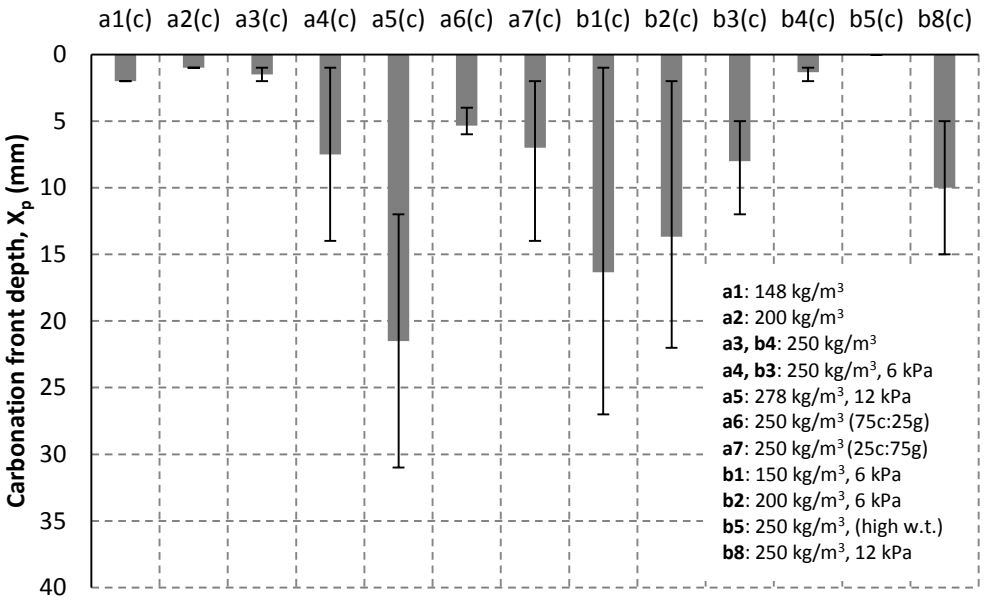

Figure 5.2 - Average X_p for each group of replicates for specimens c (180 days) in Experiments A and B using the phenolphthalein indicator with error bars showing range of values

Figure 5.3 - (a) No colour change on top surface of a4(1c) (b) Carbonation depth profile for a5(3c) (c) Pink region on top of surface of B5(1)

- On average, a5(c) had the greatest X_p values, with a depth of 31 mm recorded for a5(3c) (Figure 5.3(b)). For specimens having 250 kg/m^3 or greater of cement binder; namely, a3(c) and b4(c), (0 kPa surcharge), a4(c) and b3(c) (6 kPa surcharge) and a5(c) and b8(c) (12 kPa surcharge), X_p increased with surcharge ($p = 0.000$) (Figure 5.4). There were plausible relationships between X_p and surcharge for specimens with 150 kg/m^3 of binder ($p = 0.253$) and 200 kg/m^3 of binder ($p = 0.201$), but more data points were needed for confirmation.

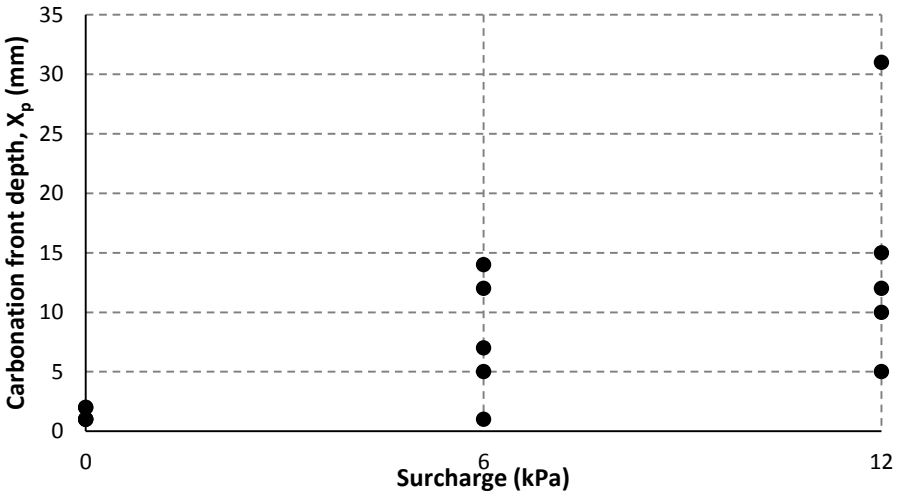

Figure 5.4 - Relationship between X_p and surcharge for phenolphthalein indicator results for specimens c with a cement binder content ≥ 250 kg/m^3

- In unsurcharged specimens, increasing GGBS content resulted in greater carbonation depths ($p = 0.042$).
- While cement content was not an important variable for X_p in the unsurcharged specimens a1(c), a2(c), a3(c) and b4(c) ($p = 0.326$), there was a weak association between cement and X_p in the surcharged specimens b1(c), b2(c), b3(c) and a4(c) ($p = 0.204$). On average, greater carbonation depths were recorded in surcharged specimens with a lower cement content.

After 180 days, 15 of the 39 large stabilised peat specimens A and B were not carbonated at the surface, an example of which is shown in Figure 5.3(c). No conclusions could be drawn from these results as a maximum carbonation depth of only 2 mm was recorded (where carbonation was observed). The possible reasons for the difference in results from small specimens c and large specimens, both of which were analysed at 180 days, will be discussed in Section 6.3.

5.3.1.2 Unusual carbonation fronts

The phenolphthalein test provided important information on the profile of the colour change front (carbonation front). In 13% of specimens tested, the front did not resemble a horizontal line as would be generally found in above-ground concrete structures. For example, the fronts for a5(2c) and b2(2c), shown in Figure 5.5 (a) and (b) respectively, are not horizontal. In a5(2c) the indicator remained colourless for depths of 1 and 20 mm at each edge and 16 mm in the centre, from which an X_p value of 12 mm was derived from Equation 3.3. Unusual carbonation fronts can sometimes be present in underground structures (Broomfield, 2007) where carbonation by a combination of groundwater and

CO_2 released by organic soil does not always produce a consistent carbonation profile like that created by atmospheric CO_2 ingress (see Section 2.7.1.2).

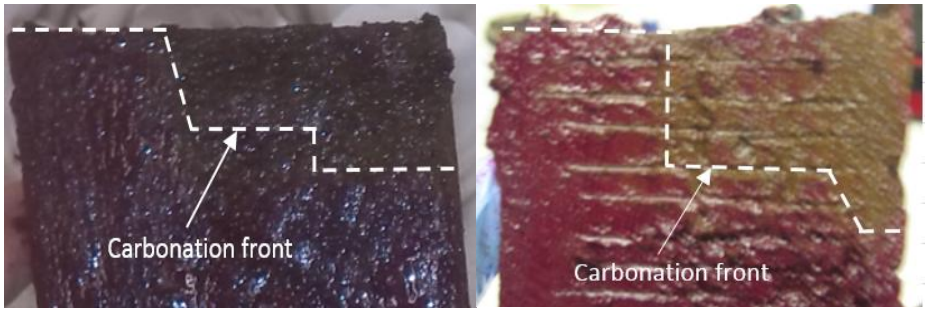

Figure 5.5 - Carbonation depth of (a) 12 mm in a5(2c) (left) and (b) 17 mm in b2(2c) (right)

5.3.2 X-ray powder diffraction (XRD)

5.3.2.1 Results

The majority of the X_c results determined by XRD were calculated using the XRD method discussed in Section 3.5.4.4 and the intercept method in Section 3.5.4.2. However, there were exceptions, and these are discussed in Section 5.3.2.2. The X_c results from XRD are shown in Table 5.2, where the carbonation front depth X_c is generally seen to extend deeper over time ($p = 0.000$).

Table 5.2 - X_c values measured by XRD for Experiments A and B

X_c values in Experiment A (mm)					**X_c values in Experiment B (mm)**				
Test day	**20**	**94**	**180**	**180**		**20**	**90**	**180**	**180**
Specimen	**a**	**b**	**c**	**A**		**a**	**b**	**c**	**B**
A1(1)	0	5	5	16	B1(1)	7	5	26	7.5
A1(2)	0	5	5	2.5	B1(2)	5	20	25	20
A1(3)	5	5		16	B1(3)	0	5	5	3
A2(1)	5	5	10	2.5	B2(1)	5	5	5	5
A2(2)	5	10		6	B2(2)	5	5	30	2.5
A2(3)	5	10	35	6	B2(3)	5	10	24	2.5
A3(1)	0	5		3	B3(1)	6	5	17	8
A3(2)	5	5	12	11	B3(2)	8	5	20	8
A3(3)	5	5	5	11	B3(3)	5	5	17	10
A4(1)	0	5	30	12.5	B4(1)	5	5	5	3
A4(2)	5	10	20	5	B4(2)	5	5	8	2.5
A4(3)	5			30	B4(3)	10	5	13	3
A5(1)	5	25		14	B5(1)	5	6	5	2.5
A5(2)	5	20	40	13	B5(2)	5	5	5	7.5
A5(3)	0	15	40	20	B5(3)	6	5	5	2.5
A6(1)	5	5	5	7	B8(1)	5	12	20	12.5
A6(2)	5	11	12	2.5	B8(2)	9	5	29	3
A6(3)	5	5	5	2.5	B8(3)	5	5	25	2.5
A7(1)	5	5	20	2.5					
A7(2)	5	5	10	3					
A7(3)	5	5	25	3					

The variations in $CaCO_3$ and $Ca(OH)_2$ content with depth and time and the variations in X_c can be summarised as follows:

(i) The general trend in the XRD plots (intensity against degrees) for the small specimens was a decrease in $CaCO_3$ content from the stabilised peat top surface to the interior while the $Ca(OH)_2$ content increased.

(ii) As the carbonation time increased, $CaCO_3$ content also increased, and the $Ca(OH)_2$ content diminished. An example of carbonation progression is shown in Figure 5.6 where low constant $CaCO_3$ intensities are evident in samples a5(3a), tested at day 20; but by day 180, samples a5(3c) and the large specimens A5(3) record high $CaCO_3$ intensities to depths of 10 and 30 mm respectively.

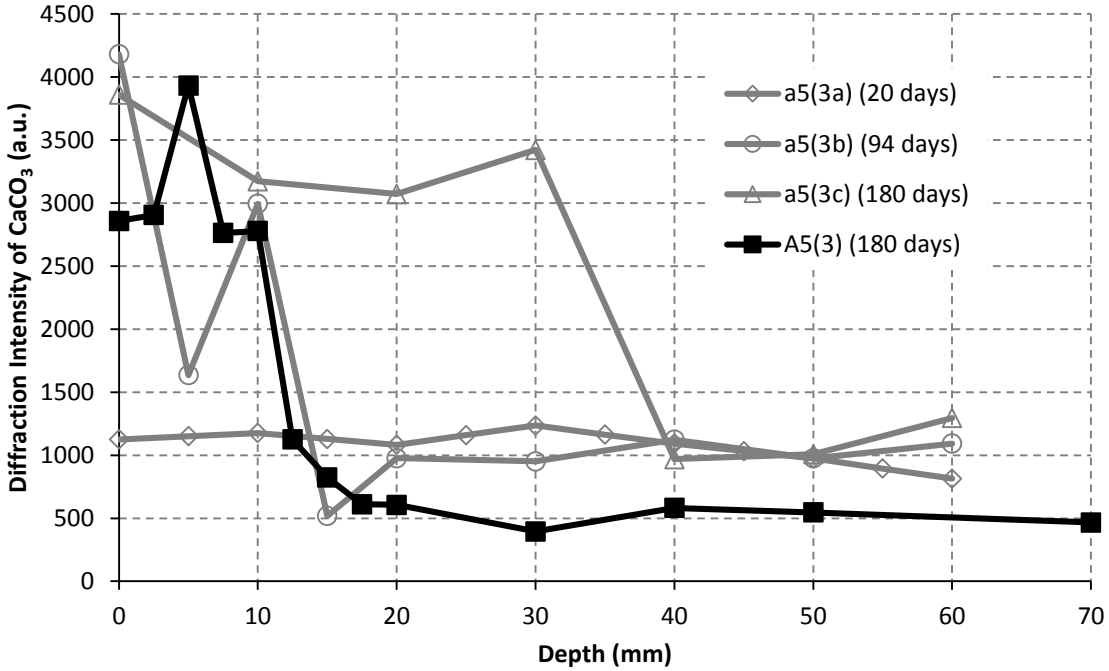

Figure 5.6 - Variation in $CaCO_3$ diffraction intensity with depth for a5(3a), a5(3b), a5(3c) and A5(3)

(iii) For each specimen analysed, a depth profile of the relative magnitudes (intensity/maximum intensity) of the diffraction peaks of $CaCO_3$ and $Ca(OH)_2$ was produced. Up to ten XRD plots were used to develop each relative intensity distribution plot (eg. Figure 5.7) which then enabled a carbonation front to be inferred. Appendix E1 shows some of the relative intensity plots used to calculate X_c for specimens c and the large specimens in both Experiments A and B.

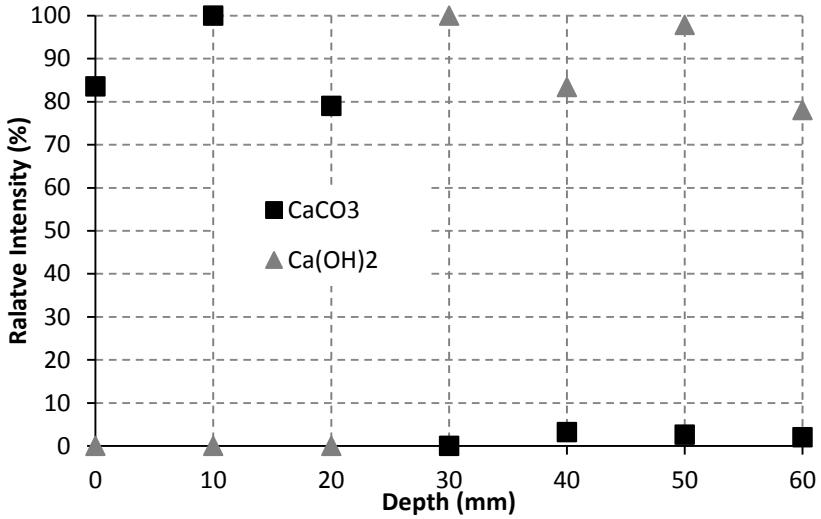

Figure 5.7 - Variation in relatively diffraction intensity for $CaCO_3$ and $Ca(OH)_2$ with depth

Besides the peaks for $CaCO_3$ and $Ca(OH)_2$, other peaks such as for allite, ettringite and CSH were identified in XRD plots. Lowry (2008) found that the high levels of organic matter in the stabilised peat were, however, undetectable by X-ray diffraction.

For both experiments, average X_c values are shown in Figure 5.8 for each group of specimens under the same conditions (A1–A7, B1–B5, B8) and for their small specimen equivalents (a, b and c). Similar to the phenolphthalein results, more obvious relationships are evident in the small specimens than in the large ones. The results in Figure 5.8 show that:

- In keeping with the phenolphthalein results, specimens a5 with 12 kPa had the deepest carbonation fronts, with a5(2c) and a5(3c) having X_c values of 40 mm.
- In line with expectations, the small specimens b5 (water table at the surface) had the smallest average carbonation depths after 180 days: b5(1c), b5(2c) and b5(3c) had individual X_c values of 5 mm. Examining the unsurcharged specimens with 250 kg/m^3, b5(c) (n = 3) had slightly shallower carbonation depths than the drained specimens a3(c) (n = 3) and b4(c) (n = 3) (p = 0.161).
- For the drained specimens with ≥ 250 kg/m^3 of cement binder, a3(c), a4(c), a5(c), b3(c), b4(c) and b8(c), there was a strong relationship between surcharge level and X_c (p = 0.000) as depicted in Figure 5.9. The specimens with 12 kPa of surcharge had the largest X_c values in each experiment, followed by the specimens with 6 kPa of surcharge. There was no evident relationship between X_c and surcharge for specimens c with 150 kg/m^3 of binder (p = 0.219) and specimens c with 200 kg/m^3 of binder (p = 0.847).
- Cement binder content and GGBS content did not affect X_c (p ≥ 0.05).

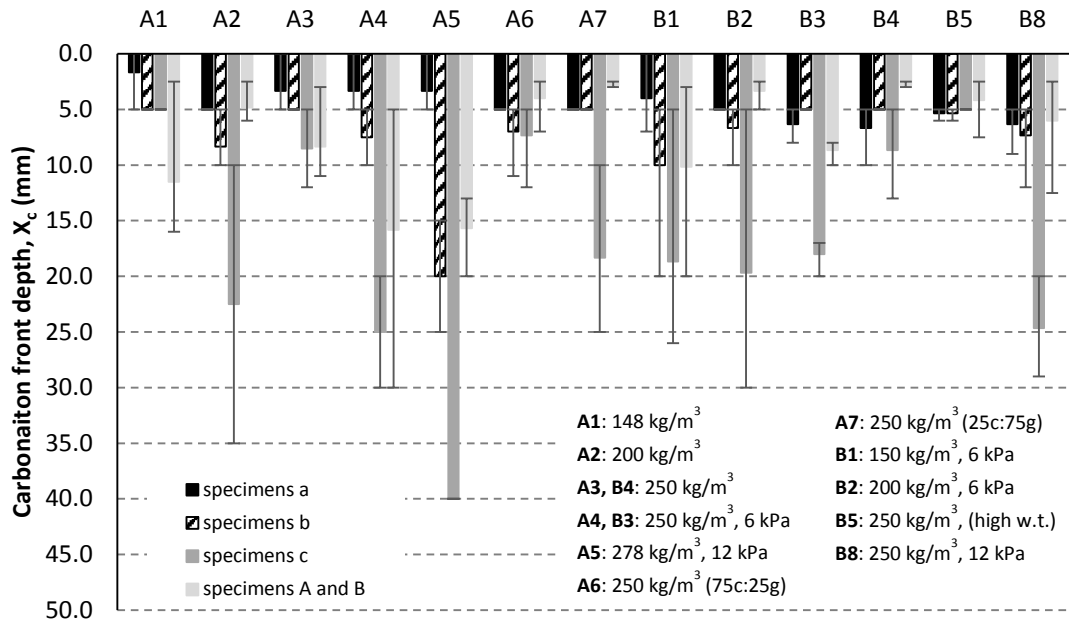

Figure 5.8 - Average X_c for each group of replicates in Experiments A and B using XRD, with error bars showing range of values

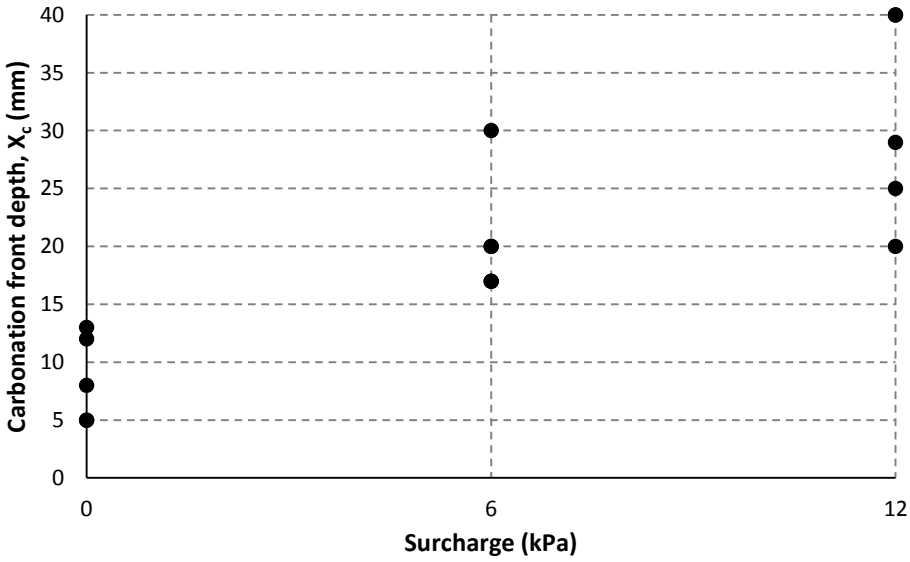

Figure 5.9 - Relationship between X_c and surcharge for XRD results for specimens c with a cement binder content ≥ 250kg/m^3

5.3.2.2 Application of the intercept method

While the intercept method was applied to the $CaCO_3$ and $Ca(OH)_2$ relative intensity distributions, X_c was generally calculated solely from the $CaCO_3$ relative intensity distribution (Section 3.5.4.4). The relative $Ca(OH)_2$ intensities could not be relied on to calculate X_c as $Ca(OH)_2$ was not always detected/present in specimens, especially in unsurcharged specimens with GGBS or low levels of cement. This was due either to the small amounts of $Ca(OH)_2$ produced or to the conversion of $Ca(OH)_2$ to CSH and $CaCO_3$. Conversion of $Ca(OH)_2$ to CSH (identified by a peak at 29°) in specimens with GGBS is

more likely than in cement due to the pozzolanic properties of GGBS (Section 2.7.2.3). For instance, no $Ca(OH)_2$ was visible in XRD plots for the large specimen A7(3) at d = 70 mm (Figure 5.10 (a)) but was visible in the solely cement specimen A3(2) at d = 70 mm (Figure 5.10 (b)). It was also found that the higher the GGBS content, the harder it was to distinguish the important peaks as GGBS is more amorphous than cement, thereby producing fewer peaks. Those that were present were of a much lower intensity than the equivalent peaks in solely cement binder specimens (Figure 5.10).

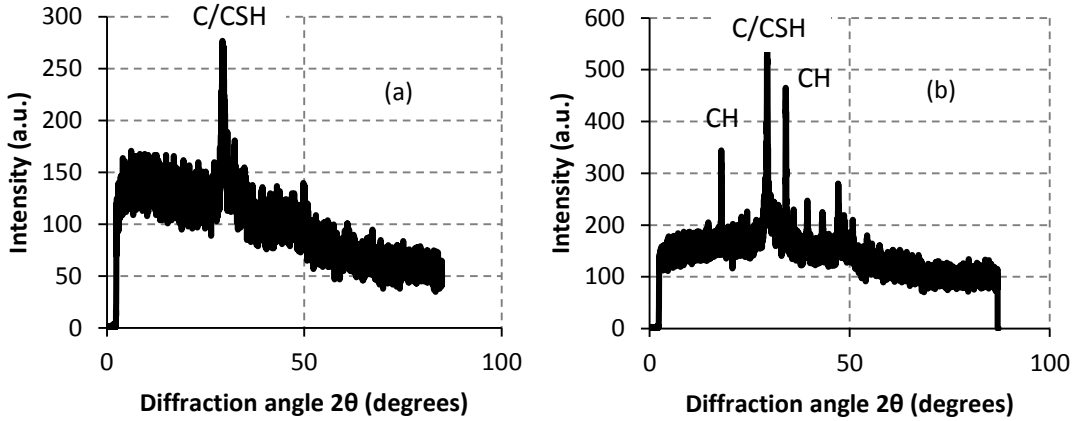

Figure 5.10 - Intensity at various diffraction angles at d = 70 mm for (a) A7(3) and (b) A3(2) (C: $CaCO_3$, CH: $Ca(OH)_2$)

The intercept method used to calculate X_c worked best for the surcharged specimens because the a_2 line (defined in Section 3.5.4.2) was more likely to have a shallow slope, making the carbonation front depth easier to identify as exemplified in Figure 5.11(a) for a5(3c). In this case, X_c was assumed to be the first point on a_1 at 40 mm.

Occasional difficulty was encountered with the intercept method on some of the unsurcharged specimens as the data points near the carbonation front were more scattered, which did not facilitate its identification. It was unclear where the transition between the a_1 and a_2 lines arose, rendering interpretation of the carbonation depth uncertain. Consequently, more information was gathered from the individual XRD plots. For instance, in Figure 5.11(b), the first data point on the baseline (uncarbonated zone) could be interpreted as either at 20 or 30 mm; therefore, to confirm which one was the first point on a_1, the $Ca(OH)_2$ relative intensity line was examined (also shown on this plot). The first point on the baseline for $Ca(OH)_2$ was at 20 mm; therefore, the first point on the baseline for $CaCO_3$ was also taken as 20 mm. In this case, an X_c value of 16 mm was interpreted.

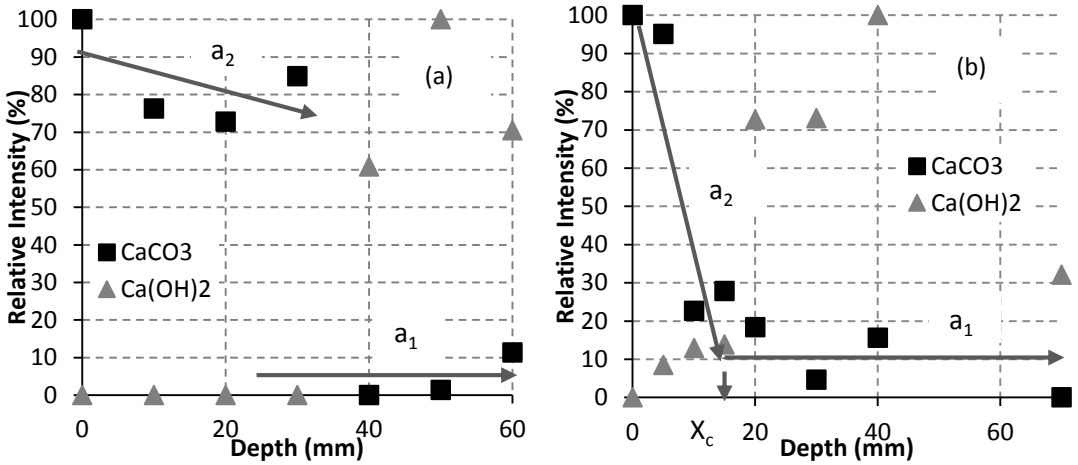

Figure 5.11 - Variation in relative intensity of XRD with depth for (a) a5(3c) and (b) A1(1)

While the XRD settings remained the same throughout testing, the beam optics were changed slightly in September 2014 due to problems with the diffractometer. XRD plots after this date gave lower intensities than before for important phases (peaks), but peak positions remained the same. In Experiment A, most samples were analysed before September 2014; however, some were revisited after this date to sample at a greater resolution. This had implications for the interpretation of some of the results of Experiment A but not for tests in Experiment B, all of which were analysed after September 2014.

For example, in a6(1c) the maximum $CaCO_3$ intensity recorded was 4400 at d = 0 mm, and the average $CaCO_3$ intensity below this depth ($d \geq 10$ mm) was 980 ± 45. After September 2014, a sample at d = 5 mm was analysed which had an intensity of only 538, where a value between 980 and 4400 might have been expected based on values obtained before September 2014. Figure 5.12 shows two XRD plots for a6(1c) that highlight the difference in intensities, one plot before September 2014 (Figure 5.12(a)) and one after (Figure 5.12(b)).

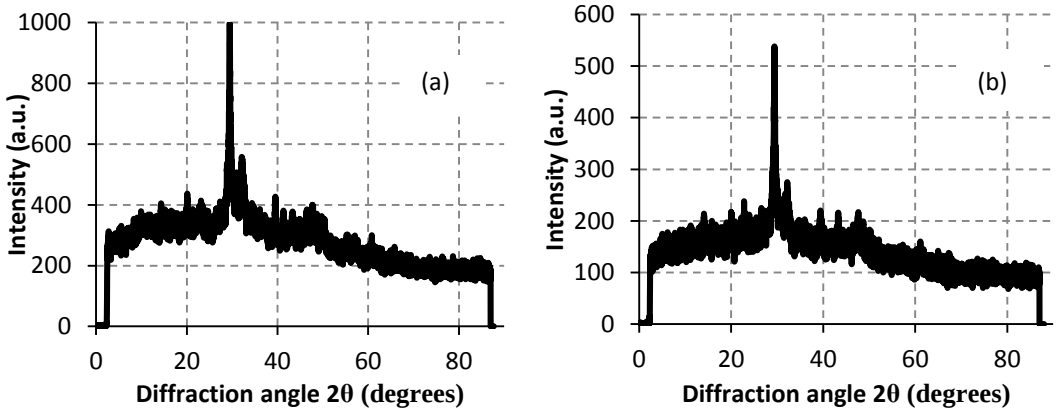

Figure 5.12 - XRD plot for a6(1c) at (a) d = 20 mm and (b) d = 5 mm analysed after September 2014

The ramifications and steps devised to overcome this issue were:

(i) The intensities from XRD plots after September 2014 were smaller on average, rendering these data points unusable for the intercept method. An alternative interpretation was sought so that new data points could be used.

(ii) The alternative interpretation is explained by examining the results of A5(2). Figure 5.13 shows a relative intensity plot for A5(2), with all data points plotted analysed before September 2014. Before the extra analyses, the carbonation front was known to lie between 10 and 15 mm, with the intercept method giving an X_c value of 13 mm.

(iii) To identify the carbonation front more accurately to the nearest 2.5 mm, after September 2014 three extra samples at d = 2.5, 7.5 and 12.5 mm were analysed that were based on a different calibration to the others. In this case, the XRD plots for the data points at d = 2.5, 7.5 and 12.5 mm showed an absence of $Ca(OH)_2$ and so were in the carbonated zone.

(iv) After the extra analyses, X_c was known to lie between 12.5 and 15 mm, with 15 mm being the first data point on the baseline due to its low $CaCO_3$ and high $Ca(OH)_2$ content.

(v) If the 12.5 mm sample had shown the presence of $Ca(OH)_2$, then X_c would have been between 10 and 12.5 mm; and because the intercept point was greater than 12.5 mm, X_c would have been 12.5 mm (Section 3.5.4.2).

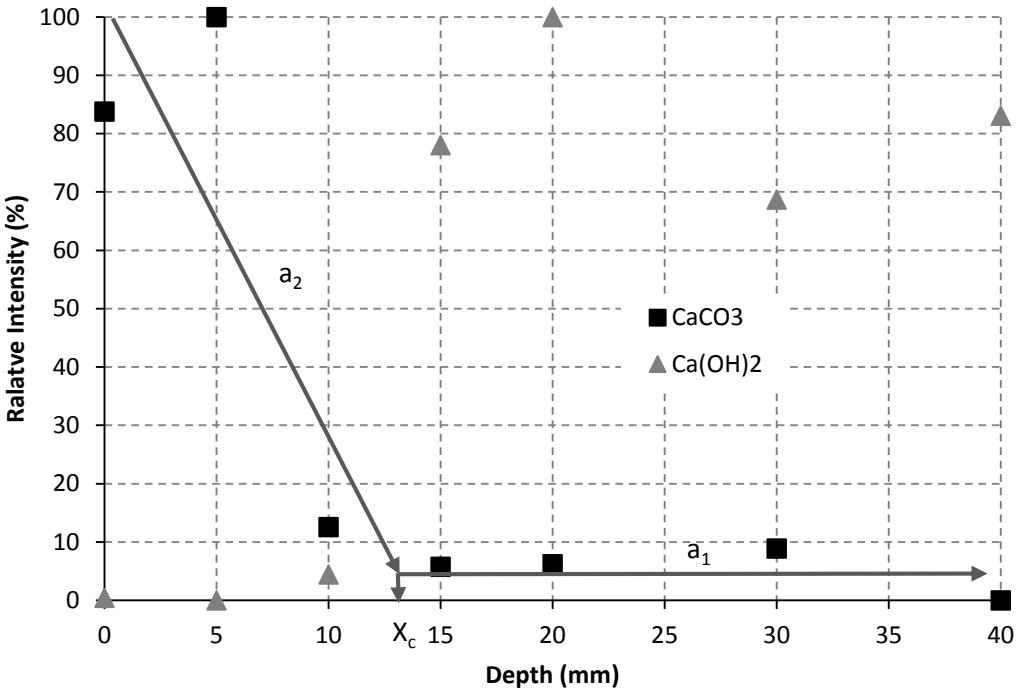

Figure 5.13 - Variation in relative diffraction intensity with depth for A5(2)

To verify results, some XRD analyses were performed using a diffractometer at the University of Limerick (UL) where the X-ray tube voltage and current were fixed at 40 kV and 40 mA respectively. Samples from A1(2), A5(2) and A7(2) were analysed and produced the same peak patterns and positions; examples are shown in Figure 5.14 and Appendix E2 for A7(2) d = 0 and d = 40 mm. The shape of the baselines is influenced by the incident beam optics and does not affect peak positions and the presence of peaks.

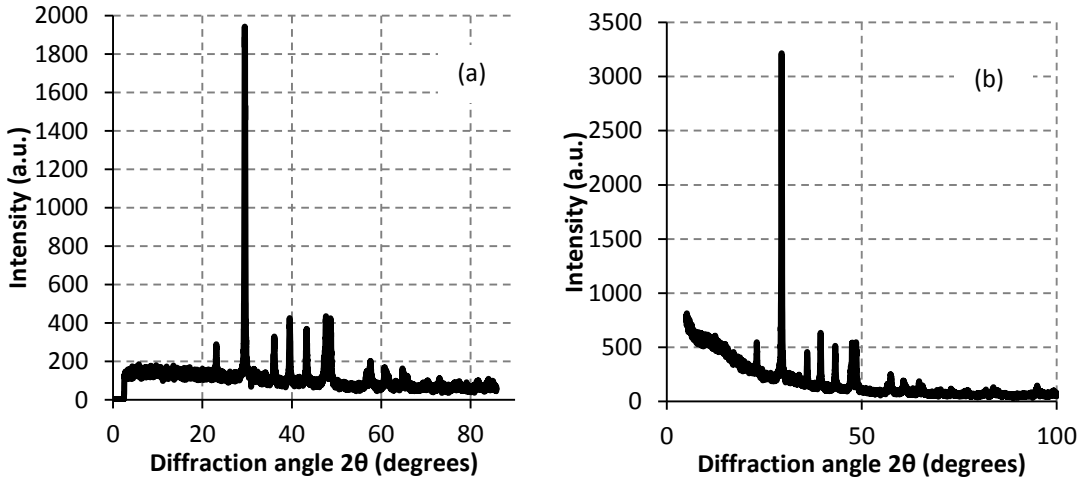

Figure 5.14 - XRD plot for A7(2) d = 0 mm for (a) NUIG (b) UL

5.3.3 Fourier transform infrared spectroscopy (FTIR)

5.3.3.1 Results

Figure 5.15 comprises two FTIR graph, one for an uncarbonated sample from a depth of 60 mm for a5(1a) (Figure 5.15(a)) and the other for a carbonated sample from a depth of 0 mm for a5(1a) (Figure 5.15(b)). The $Ca(OH)_2$ spectrum shows a prominent O-H peak in Figure 5.15(a), at a depth of 60 mm in this instance. As the $CaCO_3$ content increases towards the surface due to carbonation, the C-O peak representing $CaCO_3$ increases, while the O-H peak weakens (as shown in Figure 5.15 (b) at 0 mm depth). This O-H peak also diminished over time as the $CaCO_3$ content increased due to carbonation. Other bands of interest identified in the FTIR plots included Si-O bands, representing CSH at 920 cm^{-1} and CO_3 bands representing vaterite at 880 cm^{-1}.

Using the intercept method, X_c values were calculated from the calcite/portlandite ($CaCO_3/Ca(OH)_2$) peak ratios from FTIR plots such as those in Figure 5.15. Calcite/portlandite ratios decreased with time and increased with depth as exemplified in Figure 5.16 for a4 and A4. Some more examples of these calcite/portlandite ratio with time plots for the small specimens c and large specimens are contained in Appendix E3. Table 5.3 displays the X_c results using FTIR, with X_c generally increasing over time ($p = 0.000$).

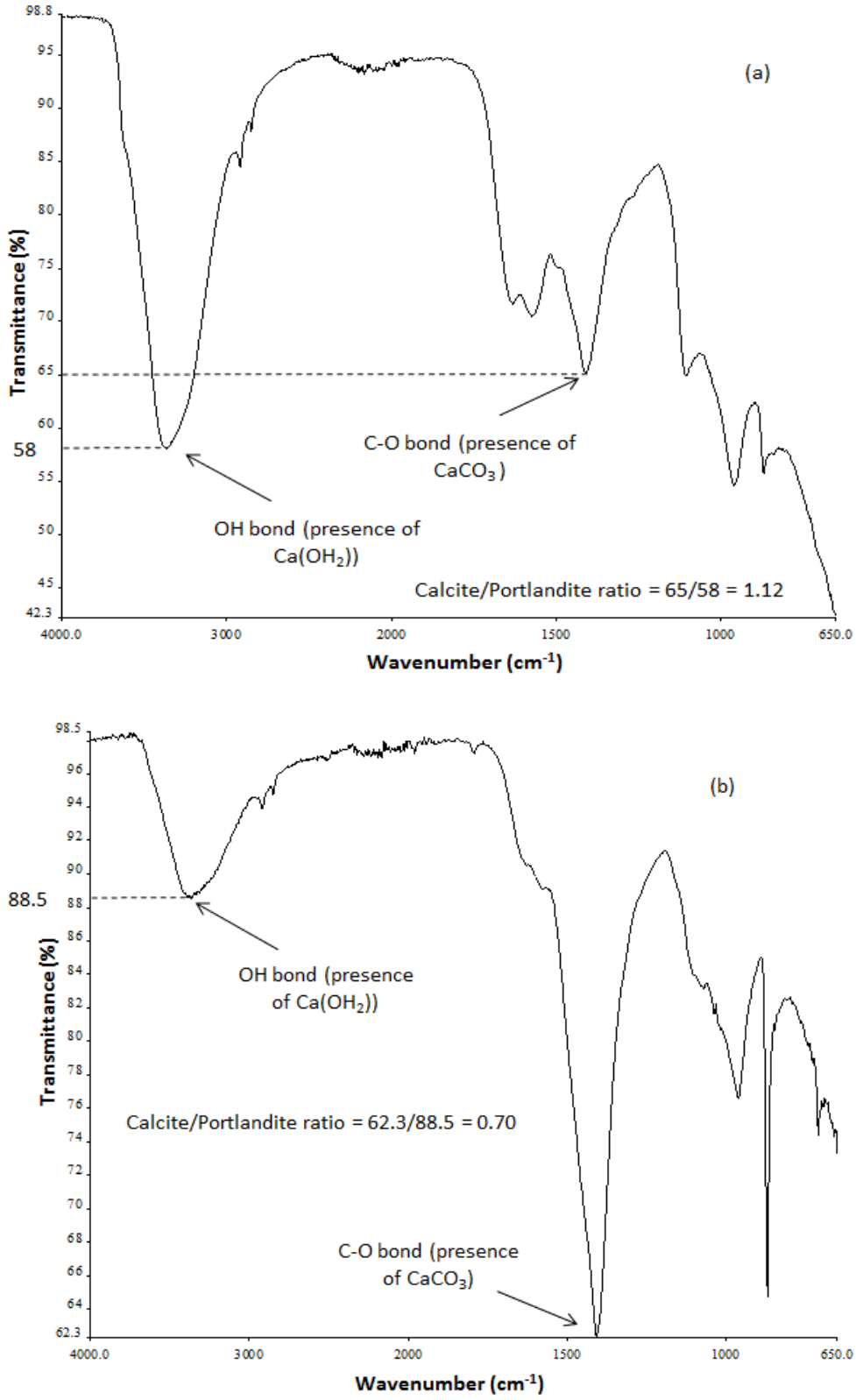

Figure 5.15 - FTIR analysis result for (a) a5(1a) d = 60 mm and (b) d = 0 mm

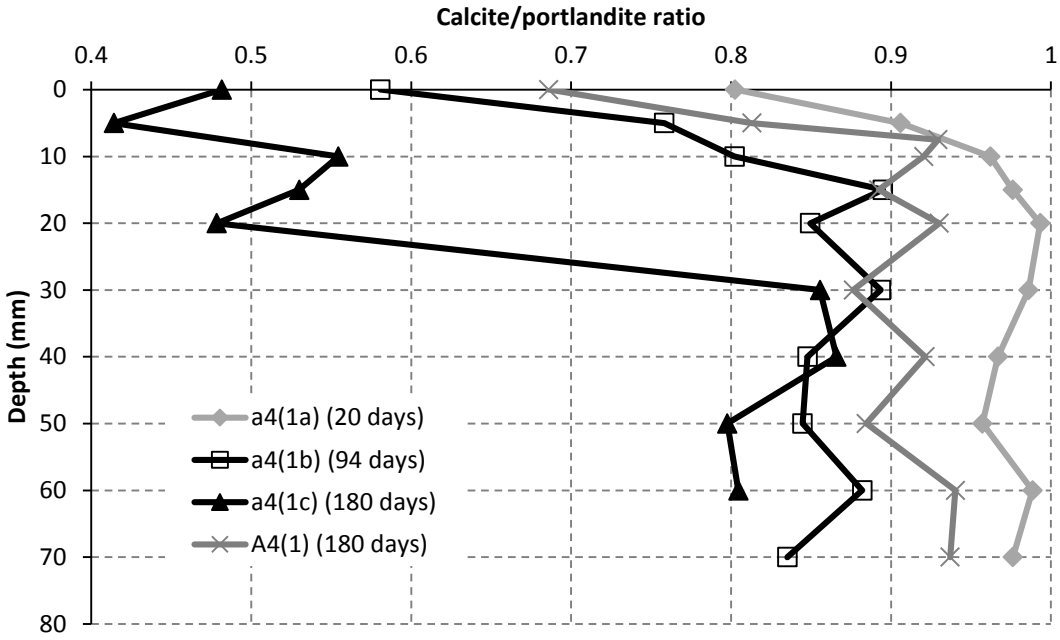

Figure 5.16 - Influence of depth upon calcite/portlandite ratios for a4(1) and A4(1)

Table 5.3 - X_c values measured by FTIR for Experiments A and B

X_c values in Experiment A (mm)					**X_c values in Experiment B (mm)**				
Test day	**20**	**94**	**180**	**180**		**20**	**90**	**180**	**180**
Specimen	**a**	**b**	**c**	**A**		**a**	**b**	**c**	**B**
A1(1)	5	0	5	27	B1(1)	5	5	20	6
A1(2)	5	5	5	7.5	B1(2)	5	15	25	16
A1(3)	20	0		2.5	B1(3)	5	5	10	2.5
A2(1)	5	0	10	5	B2(1)	15	0	30	5
A2(2)	5	5		15	B2(2)	5	25	30	10
A2(3)	5	5	5	7.5	B2(3)	10	5	26	12.5
A3(1)	5	5		2.5	B3(1)	10	5	15	6
A3(2)	5	5	5	7	B3(2)	8	5	30	5
A3(3)	0	5	15	2.5	B3(3)	15	5	15	7.5
A4(1)	8	11	30	7.5	B4(1)	5	6	7	2.5
A4(2)	0	5	20	5	B4(2)	0	0	6	2.5
A4(3)	5			13	B4(3)	10	5	12	4
A5(1)	5	20		12.5	B5(1)	0	7	5	2.5
A5(2)	0	40	40	8	B5(2)	5	5	5	5
A5(3)	0	13	40	20	B5(3)	10	10	5	3
A6(1)	5	5	15	0	B8(1)	0	20	23	6
A6(2)	5	5	15	3	B8(2)	0	15	36	10
A6(3)	5	5	5	2.5	B8(3)	0	15	22	5
A7(1)	10	5	5	2.5					
A7(2)	5	5	11	5					
A7(3)	5	5	26	2.5					

Average X_c values for each class of specimen in Experiments A and B using FTIR are shown in Figure 5.17. In tandem with Table 5.3, the following findings can be deduced:

- Similar to the phenolphthalein and XRD results, specimens a5 (278 kg/m^3 of cement binder, 12 kPa of surcharge) had the greatest carbonation depths on average with a5(2c), a5(2b), a5(3c) all having X_c values of 40 mm in Experiment A. Specimen b8(2c) (250 kg/m^3, 12 kPa) had the greatest X_c value in Experiment B at 36 mm.
- The surcharged specimens showed greater average X_c values than the unsurcharged specimens. As in the XRD results, for the drained specimens with ≥ 250kg/m^3 of cement binder, a3(c), a4(c), a5(c), b3(c), b4(c) and b8(c), a strong relationship was found between surcharge and X_c ($p = 0.000$) (Figure 5.18). There was also a significant relationship between X_c and surcharge for specimens c with 200 kg/m^3 of binder ($p = 0.004$) and a notable trend for the specimens c with 150 kg/m^3 of binder ($p = 0.101$), but more data points would be needed for confirmation.
- Neither GGBS nor cement contents had an effect on X_c ($p \geq 0.32$).

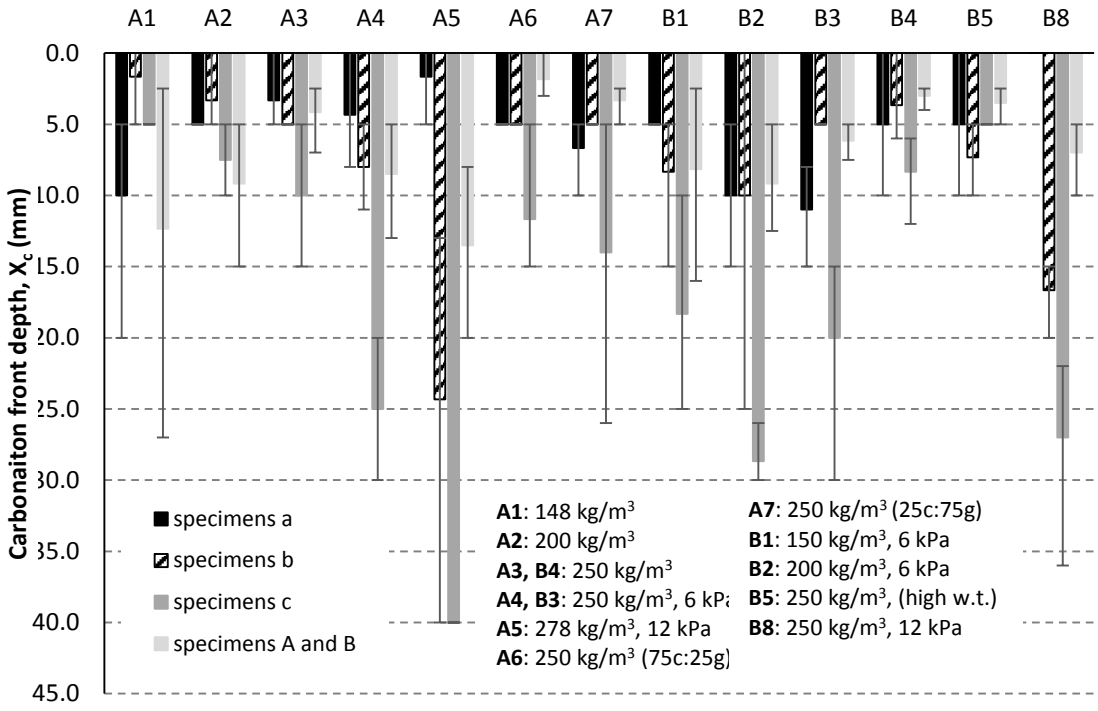

Figure 5.17 - Average X_c for each group of replicates in Experiments A and B using FTIR, with standard error bars showing the range of values

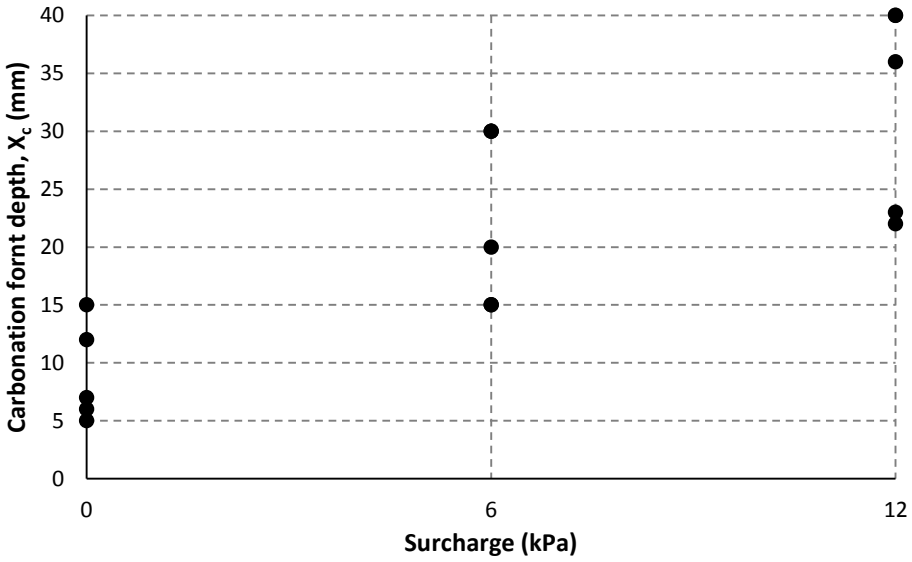

Figure 5.18 - Relationship between X_c and surcharge for FTIR results for specimens c with a cement binder content ≥ 250 kg/m^3

5.3.4 Loss on Ignition (LOI)

5.3.4.1 Results

The LOI method outlined in Section 3.5.4.6 was performed only on small specimens c and the large specimens in Experiment A but was used extensively in Experiment B. Table 5.4 shows the carbonation front depths in Experiments A and B calculated using the intercept method on plots of percentage carbonated (D_c) with depth for each specimen. An example of this type of plot is Figure 5.19, with some more examples for the small specimens c and large specimens contained in Appendix E4. On studying the results from the small specimens, X_c and D_c were found to increase over time ($p = 0.000$). D_c was calculated using a modified version of Equation 2.20, Equation 3.4, where C_0, the initial CO_2 concentration in the uncarbonated sample, was removed from Equation 2.20 for reasons discussed in Section 5.3.4.4, leaving D_c to be evaluated as C/C_p. The C term in Equation 3.4 was taken as the mass loss between 650 and 850°C, the temperature range where $CaCO_3$ primarily decomposes. Nevertheless, in certain circumstances discussed in Sections 5.3.4.2 and 5.3.4.3, the mass loss between 520 and 650°C was combined with the mass loss between 650 and 850°C to calculate C and thus X_c.

Table 5.4 - X_c values measured by LOI for Experiments A and B

Carbonation depths (X_c) (mm)							
Experiment A			**Experiment B**				
Test day	**180**	**180**		**20**	**90**	**180**	**180**
Specimen	**c**	**A**		**a**	**b**	**c**	**B**
A1(1)	7.5	0	B1(1)	0	7.5	32.5	12.5
A1(2)	12.5	7.5	B1(2)	22.5	7.5	27.5	22.5
A1(3)		7.5	B1(3)	0	17.5	32.5	16
A2(1)	22.5*	12.5	B2(1)	17.5	15*	30	22.5
A2(2)		7.5	B2(2)	0	12.5	32.5	7.5
A2(3)	22.5	16	B2(3)	12.5	12.5	37.5*	21
A3(1)		7.5	B3(1)	0	7.5	26*	12.5
A3(2)	15	7.5	B3(2)	0	11	24	22.5
A3(3)	12.5	7.5	B3(3)	22.5	12.5	15	16
A4(1)	30	7.5	B4(1)	7.5	7.5	17	8
A4(2)	25	7.5*	B4(2)	0	7.5	25	7.5
A4(3)		17	B4(3)	0	0	23	9*
A5(1)		12	B5(1)	0	7.5	10	0
A5(2)	40	9	B5(2)	0	0	7.5	7.5
A5(3)	45	17	B5(3)	0	7.5	12.5	7.5*
A6(1)	12	0	B8(1)	0	10	29*	12
A6(2)	31	0	B8(2)	0	15	27	11
A6(3)	18	7.5	B8(3)	0	11	37.5	17.5
A7(1)	0	7.5					
A7(2)	17.5	7.5					
A7(3)	27.5	7.5					

* X_c calculated using the temperature range 520 to 850°C.

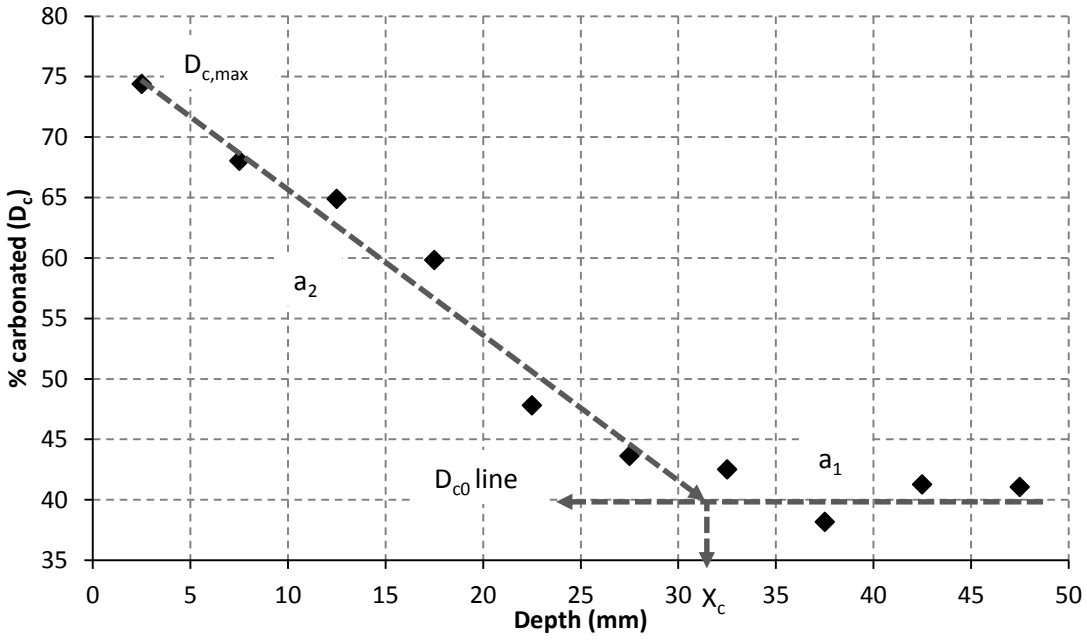

Figure 5.19 - Variation in percentage carbonated (D_c) with depth for b8(3c)

Figure 5.20 shows the average X_c values for each group of replicates for Experiments A and B using LOI. Coupled with the results in Table 5.4, it can be seen that:

- Once again, the surcharged specimens had greater X_c values than the unsurcharged specimens with a5(3c), a5(2c), b8(3c) and b2(3c) recording the maximum X_c values of 45, 40, 37.5 and 37.5 mm respectively.
- The surcharged specimens with cement binder had significantly greater X_c values than the unsurcharged specimens for small specimens c ($p = 0.000$) and the large specimens ($p = 0.001$).
- For the drained specimens with 250 kg/m^3 or more of cement binder, a3(c), a4(c), a5(c), b3(c), b4(c) and b8(c), there was a significant relationship between surcharge and X_c ($p = 0.001$) as illustrated in Figure 5.21. The equivalent large specimens also displayed a significant relationship between surcharge and X_c ($p = 0.044$).
- A significant relationship was observed between X_c and surcharge for samples with 150 kg/m^3 of cement binder in the small specimens c ($p = 0.005$) and the large specimens ($p = 0.036$). This relationship was significant, too, for samples with 200 kg/m^3 of cement binder for small specimens c ($p = 0.032$) but not significant for the large specimens ($p = 0.404$).
- By exploring the results from the unsurcharged specimens c with 250 kg/m^3 of cement binder; namely, a3 (low water table), b4 (low water table), and b5 (high water table), a high water table was confirmed to decrease X_c ($p = 0.044$).
- There was no strong relationship between either cement content and X_c or GGBS content and X_c.

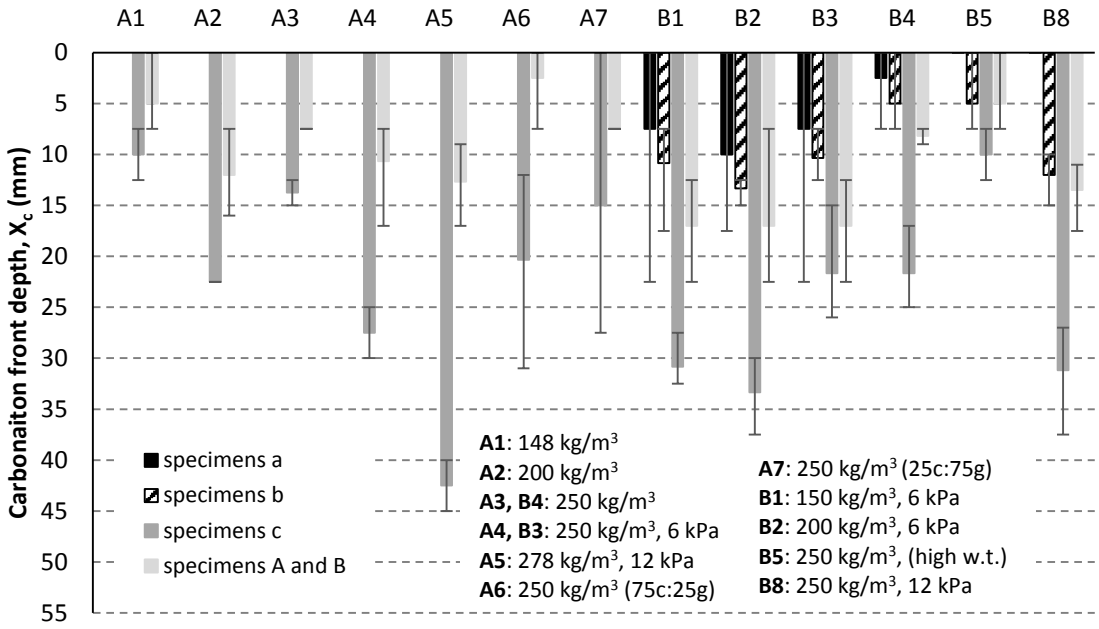

Figure 5.20 - Average X_c values for each group of replicates in Experiments A and B using LOI, with standard error bars showing range of values

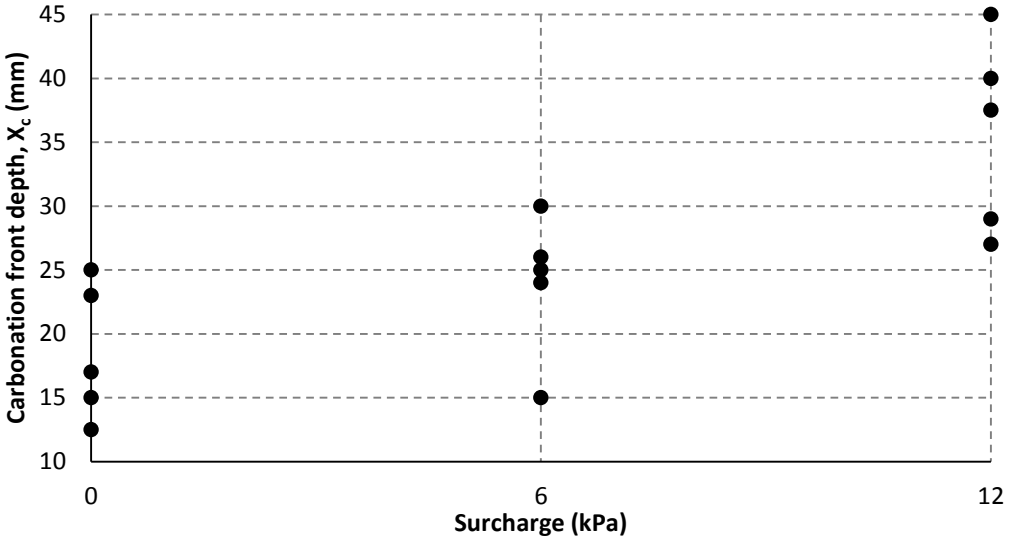

Figure 5.21 - Relationship between X_c and surcharge for LOI results for specimens c with a cement binder content ≥ 250 kg/m^3

5.3.4.2 The importance of a fixed time for temperature ranges

In some specimens, low amounts of $CaCO_3$ decomposition (mass loss) between 650°C and 850°C were noticed. This was discovered to be due to the samples being left in the furnace at 650°C for more than an hour, the minimum set time stated in the LOI procedure in Section 3.5.4.6. For instance, some samples were left in for more than three hours or overnight at 520 to 650°C on the basis that the mass loss would remain relatively constant after one hour. The ramifications and steps devised to address this issue were the following:

- The prolonged exposure to this temperature range resulted in some of the $CaCO_3$ decomposing at the lower range of 520 to 650°C instead of normally decomposing at 650°C to 850°C. Minimal $CaCO_3$ decomposition therefore occurred between 650°C and 850°C.
- In these instances, it was necessary to combine the mass losses at the temperatures ranges of 520°C to 650°C and 650°C to 850°C in order to calculate C and then D_c and X_c. This procedure was adopted in 13.8% (n = 15) of specimens, but X_c was different in only 7 of these specimens.
- While C and D_c results change marginally if a sample is left for 5 minutes more or less than the set time, X_c is less likely to change, assuming that all samples for each specimen are analysed together. This is because all data points on the LOI plots (D_c versus depth) for a specimen are likely to remain at the same relative heights to each other, meaning little or no change to X_c. Nevertheless, a fixed ignition time

should be allocated to avoid differences in D_c results and potential differences to X_c results.

A lengthy duration is needed for this LOI method as the tester must be available to weigh the samples at several intervals over the six hours required for each batch of samples (n = 10). $CaCO_3$ decomposition also cannot be assumed to occur at temperature ranges stated by previous TGA studies in the literature as the range at which $CaCO_3$ decomposes not only depends on the material examined but also on the rate of temperature change; that is, 10°C/min to 20°C/min.

5.3.4.3 Incorporation of 520 to 650°C temperature range

The mass loss at 520 to 650°C was not initially accounted for in calculating X_c because some overlap exists between $Ca(OH)_2$ and $CaCO_3$ decomposition (see Section 2.9.5.4). However, by excluding this temperature range, carbon sequestration may be slightly underestimated if not taken into account as shown by Villain & Platret (2006). For samples a (tested at 20 days) in each experiment, it was anticipated that some $Ca(OH)_2$ and unstable carbonate products such as vaterite (from CSH carbonation) would decompose in the lower temperature range of 520 to 650°C. After 180 days, XRD plots on a lot of samples showed little or no $Ca(OH)_2$ present; therefore, it was expected that the majority of the decomposition occurring in these samples in the temperature range of 520°C to 650°C was from CSH carbonation.

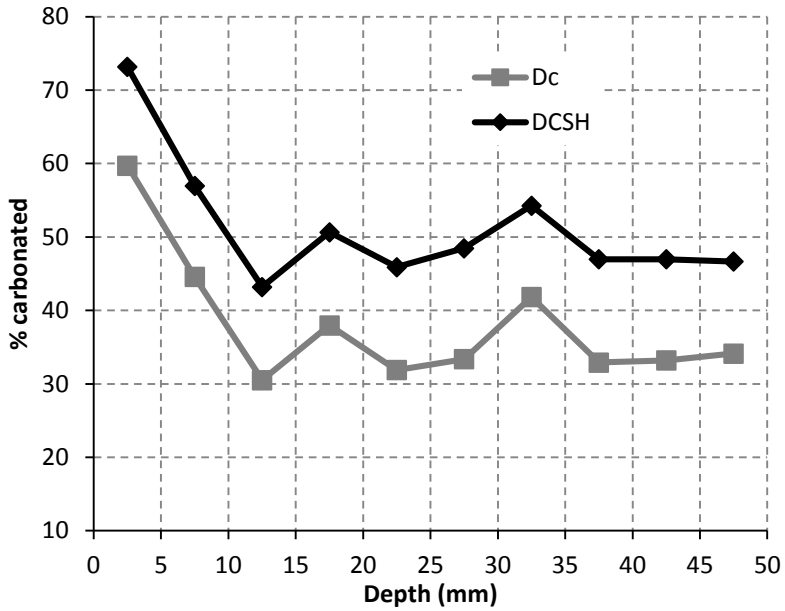

Figure 5.22 - D_c and D_{CSH} lines for A5(2)

Due to the concern about underestimating D_c, both D_c values and the percentage carbonated (D_{CSH}) values were reported. D_{CSH} values are similar to D_c values in that they

were calculated using Equation 3.4, but C in this instance was the combination of the mass losses between 520 and 650°C and 650 and 850°C. In the majority of specimens, the D_{CSH} line (line connecting D_{CSH} data points) replicated the D_c line but at a higher percentage carbonated level as exemplified in Figure 5.22; therefore, X_c was similar. However, discounting the samples left in the furnace for a prolonged period of time discussed in Section 5.3.4.2, 7.4% (n = 7) of the remaining specimens recorded very different D_c and D_{CSH} lines, hence X_c was markedly different.

This alternative depth was used for two of the specimens as they met at least two of the following criteria, the minimum required:

(i) Vaterite (unstable $CaCO_3$) was present in the FTIR plots. This indicated some $CaCO_3$ decomposition occurred between 520 and 650°C.

(ii) $Ca(OH)_2$ was not detected in the XRD plots in the depths above the alternative X_c. This showed that most of the mass loss between 520 and 650°C was from CSH carbonation.

(iii) There was a decrease in mass loss in the temperature range 520 to 650°C with depth. In small specimens c and large specimens tested at day 180, the general trend was a decrease in mass loss with depth (Figure 5.23), which was often in keeping with the D_c line, and when examined more closely was more likely due to a decrease in CSH carbonation with depth and not to $Ca(OH)_2$. With the samples tested at day 20, however, the mass loss at this temperature range often increased with depth. This was as a result of an increase in $Ca(OH)_2$ and not from CSH carbonation (Figure 5.23).

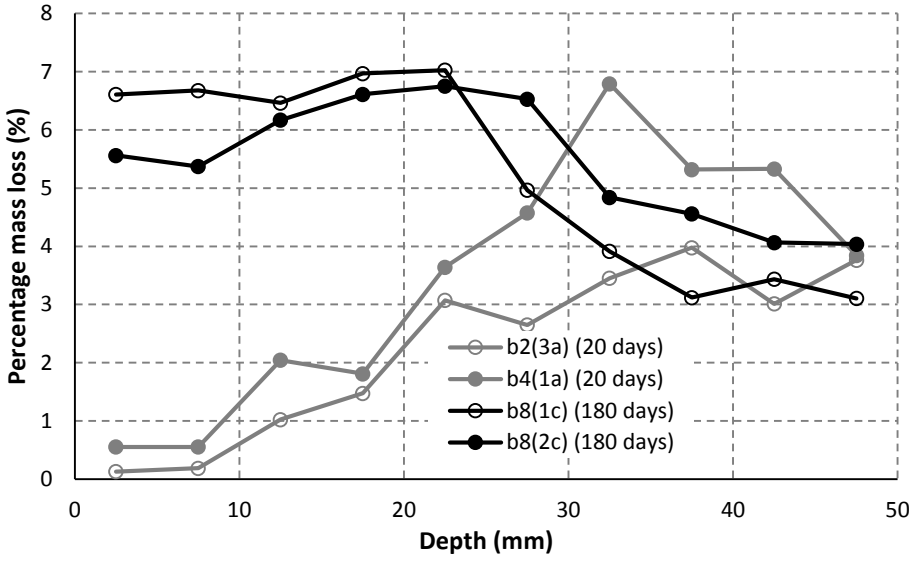

Figure 5.23 - Influence of depth on percentage mass loss at temperature range 520°C to 650°C

5.3.4.4 C_0 and D_{c0}

A fully uncarbonated sample in stabilised peat was difficult to obtain as all the stabilised peat samples analysed, including the purportedly uncarbonated samples, showed an initial degree of carbonation. Villain & Platret (2006) and Rahman & Glasser (1989) also found an initial degree of carbonation in concrete and hydrated cement paste samples retrieved from zones that were supposedly uncarbonated. Villain & Platret (2006) suggested that some of the carbonation of the cement could have taken place before mixing. In the case of stabilised peat, it was expected that carbonation in the supposedly uncarbonated zone could be a lot higher than in concrete on account of additional CO_2 released by peat due to oxidation during the mixing process, the dissolved CO_2 present in the groundwater, and CO_2 trapped in the mix, all of which would react with the cement as soon as it was mixed with the peat.

The results showed that the percentage carbonated in the supposedly uncarbonated zone (D_{c0}) for the cement-only columns was on average 36 ± 3% for the large specimens in Experiment A and 39 ± 4% in Experiment B. Specimens with GGBS A6 and A7 had an average D_{c0} of 28% and 17 ± 1% respectively. In contrast, in concrete D_{c0} is on average a much smaller percentage; for instance, Dapkus & Stankevičius (1985) showed it to be 12.5%. Furthermore, C_0 is a much smaller percentage of the mass of the sample, estimated to be 2% by Dapkus & Stankevičius (1985) and 0.9% by Matsushita et al. (2000). In dry stabilised peat, this was generally between 5 and 10%. As a result of this high initial carbonation in the uncarbonated zone, it was decided to remove C_0 from Equation 2.20 to highlight the percentage carbonated (D_{c0}) and the amount of CO_2 absorbed by the cement. In Figure 5.19 for instance, D_{c0} is around 40%. If C_0 had remained in the equation, this would not be visible in the plot as data points in the uncarbonated zone would have been near zero. Removing C_0 does not affect the calculation of X_c. After this initial carbonation had taken place, it was assumed that CO_2 was only absorbed from atmospheric CO_2 and from CO_2 released from peat oxidation near the peat surface.

Table 5.5 shows the values for D_{c0}, C_0 and $D_{c,max}$ for the large specimens in Experiment A, and Appendix E5 contains a similar table for the large specimens in Experiment B. As expected, C_0 and $D_{c,max}$ values were generally highest in the surcharged specimens, with A5(1) and A5(3) recording $D_{c,max}$ values at the surface of 97% and 92% respectively. The lowest $D_{c,max}$ values were recorded in A7, the specimens with the greatest amount of GGBS. One of the main reasons for these low values is that Equation 2.14 applies to cement and not GGBS as more CaO is kept in the CSH than in cement, only half of which will transform into $CaCO_3$ as estimated by Lagerblad (2005).

The specimens highlighted with an asterisk in Table 5.5 were left in the furnace for longer than the set hour. In order to compare parameters with other specimens, $D_{CSH,0}$ and $D_{CSH,max}$ values are given. Similar to the D_{c0} values, the average $D_{CSH,0}$ values were higher in cement-only columns than in columns with GGBS. The average $D_{CSH,0}$ in Experiment A for cement-only columns was 51 ± 6% and in Experiment B was 51 ± 6%.

Table 5.5 - Results from LOI study on A1(1) to A7(3)

Specimen	C_0 (g)	C_p (g)	D_{c0} (%)	$D_{c,max}$ (%)	$D_{CSH,0}$ (%)	$D_{CSH,max}$ (%)
A1(1)	0.63	1.85	34	40	55	60
A1(2)	0.69	1.85	37	58	58	76
A1(3)*	0.35	1.85	19	28	53	59
A2(1)	0.91	2.50	36	54	56	73
A2(2)	0.97	2.50	39	49	55	64
A2(3)	0.92	2.50	37	75	55	93
A3(1)	1.15	3.13	37	51	55	70
A3(2)	1.15	3.13	37	48	46	56
A3(3)	0.96	3.13	31	36	39	43
A4(1)	1.09	3.13	35	55	56	79
A4(2)*	0.60	3.13	22	32	47	55
A4(3)	1.10	3.13	35	77	49	91
A5(1)	1.13	3.48	39	97	44	100
A5(2)	1.20	3.48	41	66	48	73
A5(3)	1.14	3.48	33	92	47	109
A6(1)*	0.19	2.88	7	13	36	41
A6(2)	0.82	2.88	28	33	41	47
A6(3)*	0.66	2.88	23	29	38	43
A7(1)	0.42	2.39	18	29	28	36
A7(2)	0.38	2.39	16	22	27	32
A7(3)	0.40	2.39	17	22	31	34

* Specimens left in oven for more than an hour at 520 to 650°C.

As illustrated in Figure 5.24, a strong relationship exists between C_0 and cement content ($p = 0.000$), showing that initial carbonation in the uncarbonated zone increases as cement content increases. It is noteworthy that C_0 values for the large specimens with ≥ 250 kg/m^3 of cement binder are higher in Experiment B at 1.3 ± 0.13% than in Experiment A at 1.12 ± 0.07% ($p = 0.002$). Similar trends are evident for the small specimens c in each experiment. The chief reason for the difference is the higher CaO content of the cement in Experiment B which has a higher carbonation potential; the higher CaO content also means that less CaO is locked in CSH as the higher the CaO content, the lower CSH produced. The values presented in Table 5.5 and Appendix E5 give more information about the specimens which will contribute to the discussion in Chapter 6.

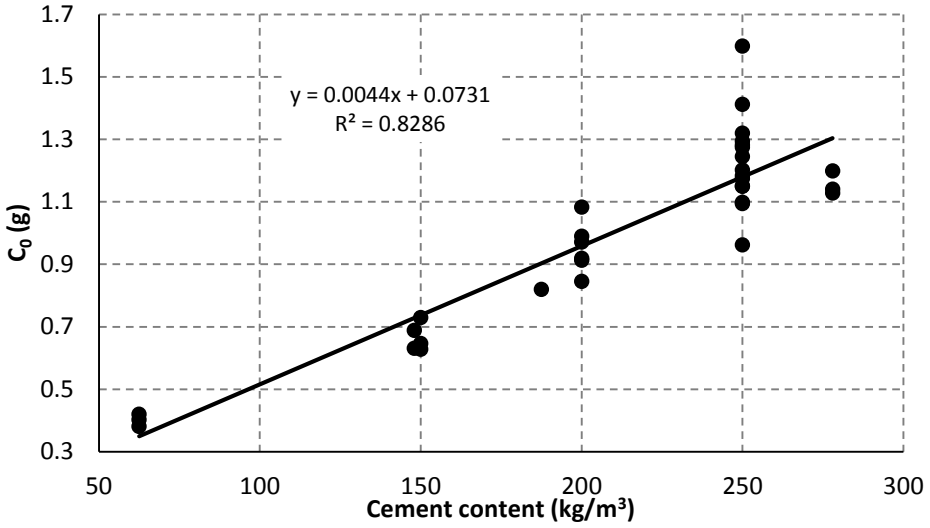

Figure 5.24 - Relationship between C_0 and cement content

5.3.4.5 Relationship between X_c and organic content

Figure 5.25(a) and (b) illustrate that organic content is lowest at the surface and increases with depth until it becomes constant, a trend replicated in most specimens. The $CaCO_3$ lines in Figure 5.25(a) and (b) are roughly mirror images of the organic content lines. While not alike, a strong relationship exists between the carbonation depth and the depth at which the organic content becomes constant (X_{oc}) for the small specimens c and large specimens ($p = 0.000$). This relationship implies that the peat's organic matter is decomposing, releasing CO_2 which is then absorbed by the cement. For the small specimens c, the depth at which the peat oxidises correlates with the depth CO_2 reacts with the stabilised peat, and the depth at which the organic content stabilises (X_{oc}) is on average $0.68X_c$ for Experiment A and $0.63X_c$ for Experiment B.

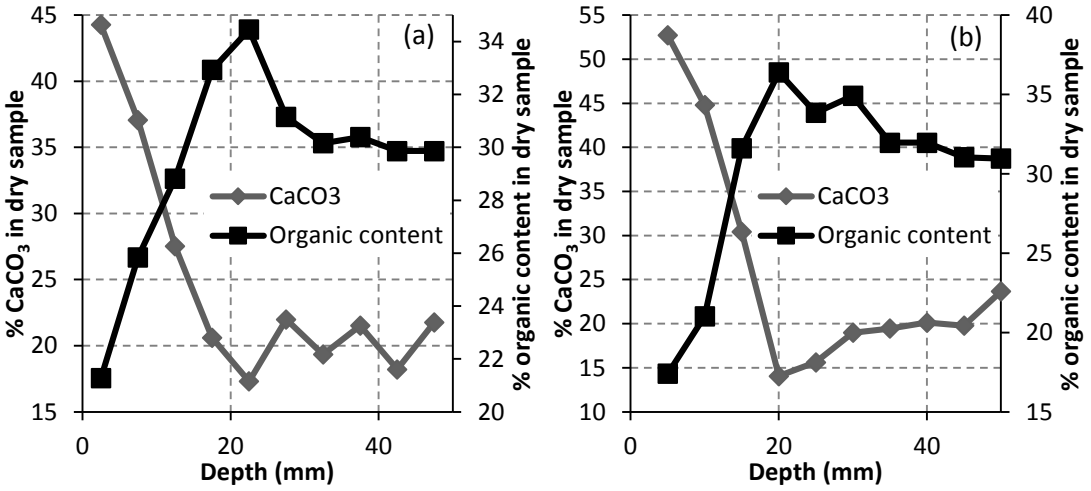

Figure 5.25 - Depth versus % $CaCO_3$ and % organic content in (a) A4(3) and (b) A5(3)

5.3.5 pH of stabilised peat slurries

5.3.5.1 Results

The acidic peat increased in pH after peat stabilisation from between 4 and 6 to between 11 and 13. As illustrated in Figure 5.26, the general trend observed in the specimens tested was an increase in pH from the surface to the interior due to carbonation whereby alkaline compounds such as $Ca(OH)_2$ and CSH were converted to $CaCO_3$. After increasing with depth, the pH then reached a depth where it became relatively constant, suggesting no noticeable carbonation had occurred at this depth. Discussed further in Sections 5.3.5.2 and 5.4.2.3, the pH of stabilised peat slurries technique was found not to give a carbonation depth but the depth at which leaching of $Ca(OH)_2$ and calcium ions to the carbonation front occurs; therefore, this depth is more appropriately referred to as X_{pH} values to distinguish them from X_c values. For comparison purposes later, X_{pH} is still considered a carbonation depth technique. The intercept method was again used but in this case to calculate X_{pH} on plots such as Figure 5.26. Corresponding plots for the large specimens in Experiments A and B are presented in Appendix E6.

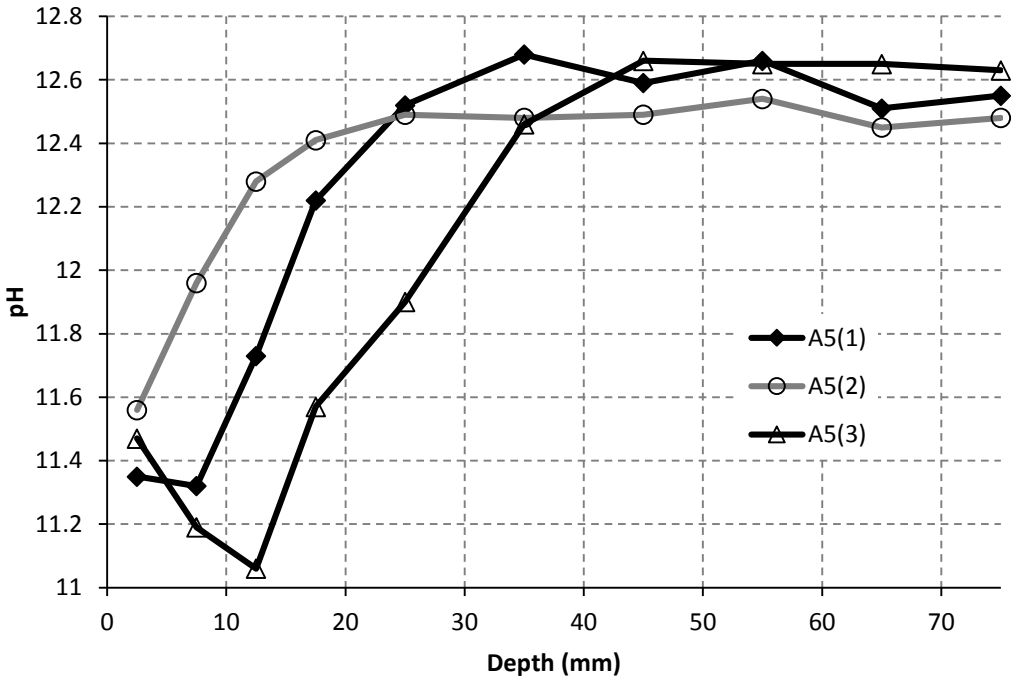

Figure 5.26 - Variation in pH with depth for A5(1), A5(2) and A5(3)

Table 5.6 lists the X_{pH} values observed in Experiments A and B, and their average values are shown in Figure 5.27 for each group of specimens under the same conditions (A1–A7, B1–B5, B8) and for their small specimen equivalents (a, b and c).

Table 5.6 - X_{pH} values measured by pH for stabilised peat slurries technique for Experiments A and B

Carbonation depths (X_{pH}) (mm)						
Experiment A		**Experiment B**				
Test day	**180**		**20**	**90**	**180**	**180**
Specimen	**A**		**a**	**b**	**c**	**B**
A1(1)	12.5	B1(1)	27	44	55	30
A1(2)	0	B1(2)	23	25	39	55
A1(3)	25	B1(3)	31	41	35	32
A2(1)	45	B2(1)	15	45	35	35
A2(2)	75	B2(2)	15	32	45	30
A2(3)	45	B2(3)	35	45	39	45
A3(1)	67	B3(1)	45	16	31	32
A3(2)	51	B3(2)	19	25	28	27
A3(3)	30	B3(3)	15	35	26	34
A4(1)	18	B4(1)	26	45	23	7.5
A4(2)	21	B4(2)	25	25	19	8
A4(3)	40	B4(3)	15	35	45	7.5
A5(1)	22	B5(1)	26	27	15	14
A5(2)	18	B5(2)	15	25	0	15
A5(3)	45	B5(3)	18	37	22	35
A6(1)	0	B8(1)	15	45	35	35
A6(2)	48	B8(2)	17	17	35	18
A6(3)	37	B8(3)	17	45	35	13
A7(1)	0					
A7(2)	0					
A7(3)	22					

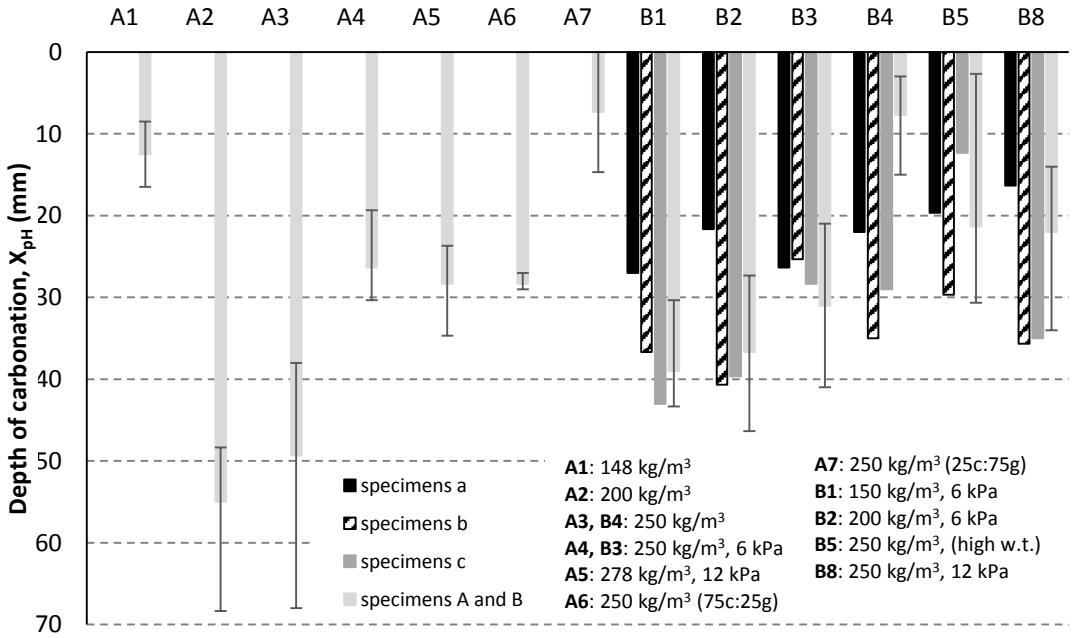

Figure 5.27 - Average X_{pH} values for each group of replicates in Experiments A and B using pH of stabilised peat slurries technique, with standard error bars showing the range of values

Table 5.6 and Figure 5.27 show that:

- X_{pH} values increased over time for the small specimens in Experiment B ($p = 0.027$).
- Water table depth was not a significant variable for the large specimens ($p = 0.667$). There was a slight trend towards significance between a high water table and low X_{pH} for specimens c in Experiment B ($p = 0.183$), but more data points would be needed to confirm this correlation.
- There was no difference between the surcharged and unsurcharged specimens ($p = 0.933$) for the large specimens, but the highest carbonation depths were observed in unsurcharged columns A2(2) and A3(1) at 75 mm and 67 mm respectively. This was at odds with the results of the other techniques where surcharged specimens exhibited the greatest depths.
- There was a small negative correlation between surcharge and X_{pH} for the unsurcharged and surcharged large specimens with 200 kg/m^3 of binder ($p = 0.169$); surcharged specimens gave lower X_{pH} values than unsurcharged specimens.
- X_{pH} values were generally greater than the X_c values recorded by the other carbonation depth techniques.

No X_{pH} values were calculated for the small specimens in Experiment A due to the availability of only three data points. Instead, by analysing the pH results of the small specimens at 20, 94 and 180 days it was proven statistically that the pH decreased with time and increased with depth. The pH decreased with time in the top 20 mm as evident in Table 5.7, which shows a significant difference ($p < 0.05$) between specimens a measured at 20 days and specimens b measured at 94 days. There was also a significant difference between the pH results of the 0–20 mm samples for specimens b and c measured at 180 days.

Table 5.7 - p-value results of two-sample t-tests for pH versus time for Experiment A

Comparison	0–20 mm	20–40 mm	40–60 mm
Specimens a (20 day) vs b (94 days)	**0.000**	0.245	0.452
Specimens b (94 day) vs c (180 days)	**0.028**	0.377	0.724
Specimens a (20 day) vs c (180 days)	**0.000**	0.085	0.735

No significant difference ($p > 0.268$) existed among the pH results of the 0–20 mm, 20–40 mm and 40–60 mm samples after 20 days, proving that the pH of specimens was relatively constant at this time (Table 5.8). However, by day 180 in specimens c, the difference was significant between the 0–20 mm and 20–40 mm samples ($p = 0.004$) as the 0–20 mm samples were significantly lower in pH. The average pH for the 0–20 mm data points for the cement-only specimens dropped from 11.97 in specimens a to 10.68 in

specimens c (Figure 5.28). For specimens c with some GGBS, the average pH dropped from 11.46 to 10.44.

Table 5.8 - p-value results of two-sample t-tests for pH versus depth for Experiment A

Comparison	Specimens a	Specimens b	Specimens c
0–20 mm vs 20–40 mm	0.495	**0.001**	**0.004**
20–40 mm vs 40–60 mm	0.673	0.450	0.099
0–20 mm vs 40–60 mm	0.268	**0.000**	**0.000**

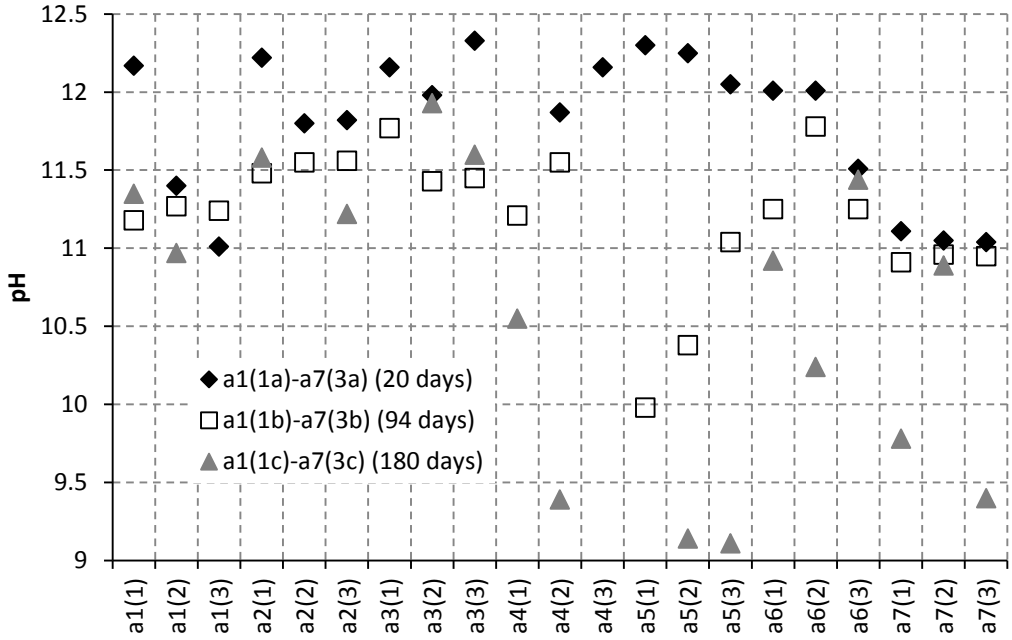

Figure 5.28 - pH values of the 0–20 mm samples for specimens a, b, c in Experiment A

Average pH values for the large specimens for Experiments A and B are given in Appendix E7. These values and pH plots in Appendix E6 show that the pH for the cement-only stabilised peat columns in Experiment A were in general lower than in Experiment B. This was due to the lower CaO content of the cement used in Experiment A, which did not cause the pH of the stabilised peat after stabilisation to rise to the level of the stabilised peat specimens in Experiment B.

5.3.5.2 Application of technique to specimens with GGBS or low levels of cement

Three of the specimens in Table 5.6 containing GGBS recorded an X_{pH} value of 0 mm. Similar to observations in concrete with a high GGBS content (see Section 2.9.6), the pH front or X_{pH} was difficult to recognise in stabilised peat whose binder contained a high GGBS content (Figure 5.29(a)). The GGBS used had an average pH of 11.96 ± 0.03 (n = 3) while cement, due to its higher CaO content, had a pH of 13.01 ± 0.01 (n = 3). Therefore, a smaller range of pH existed between carbonated and uncarbonated stabilised peat with

high GGBS content, which renders it more difficult to distinguish between the carbonated and uncarbonated stabilised peat.

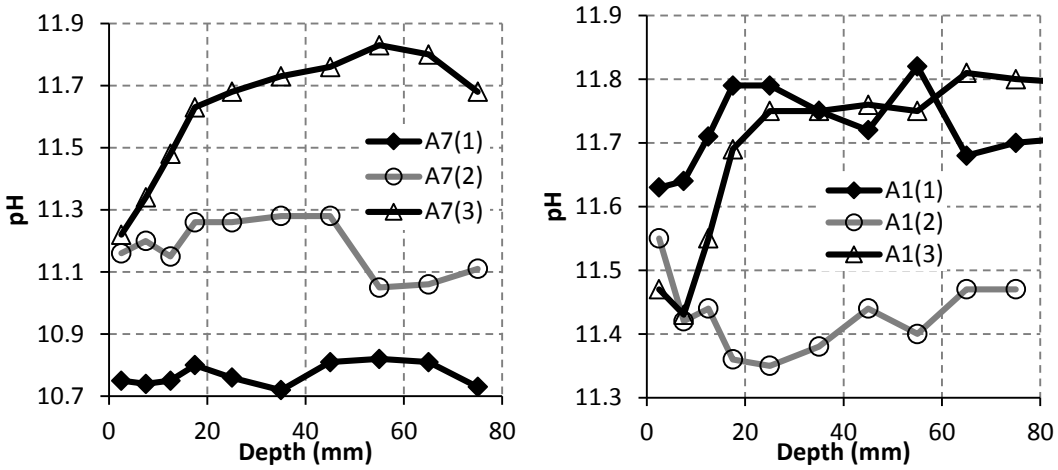

Figure 5.29 - Variation in pH with depth for (a) A7 (n = 3) and (b) A1(n = 3)

The intercept method was effective in determining X_{pH} in both surcharged specimens and specimens with 250 kg/m^3 of binder as steep slopes to the uncarbonated material were visible in the pH plots, making it easier to identify X_{pH} (Figure 5.26) (Appendix E6). However, a decrease in cement content in unsurcharged specimens to 200 kg/m^3 and 150 kg/m^3 in Experiment A made it increasingly difficult to locate X_{pH} as there was a smaller range of pH from uncarbonated to carbonated stabilised peat, a problem also encountered in concrete (see Section 2.9.6). Lower cement content produces stabilised peat with a lower pH, and the homogeneity of the cement and the deviation from the norm becomes more problematic as evidenced by Figure 5.29(b) for A1(n = 3).

However, adding a surcharge to stabilised peat with 150 kg/m^3 and 200 kg/m^3 of cement binder increased the pH to more than those without a surcharge (see Appendix E5 for pH plots for B1, B2, A2, A1). This was probably due to an increased cement content per m^3 as a result of the surcharge compressing the porous stabilised peat, but it may also be simply due to the higher CaO content of the cement used in Experiment B. Consequently, the range of pH between carbonated and uncarbonated stabilised peat increased, making it easier to distinguish X_{pH}. The X_{pH} fronts in these surcharged specimens were similar to those created by the specimens with 250 kg/m^3 of cement binder in that they both had sharp pH fronts. Leaching of $Ca(OH)_2$ and Ca^{2+} ions to the carbonation front (separate to CO_2 and O_2 diffusion) in surcharged specimens is more difficult than in unsurcharged specimens due to higher dry densities and lower porosities, hence the front is sharper. Dry density and porosity values are discussed in Sections 5.3.6 and 6.3 Another leaching effect was that some of the pH profiles of the specimens showed a higher pH reading for 5–10

mm than for 0–5 mm. McPolin et al. (2007) also observed this in concrete and attributed it to leaching of $Ca(OH)_2$ to the surface, which would increase the pH.

5.3.6 Porosity

A reduction in porosity over time is an indicator of carbonation as it reduces the pore volume by over 10% (see Section 2.7.1.3). Figure 5.30 depicts the decrease in porosities found for the small specimens in Experiments A and B using the water evaporation method, which estimates the porosity of the whole specimen. Results of one-way ANOVA tests on the porosities readings of the stabilised peat in Experiments A and B indicate a significant difference between specimens a and specimens c in both experiments ($p = 0.000$) (Table 5.9), which may indicate carbonation. In Experiment A, however, the peat specimens also decreased in porosity due to these specimens being in close proximity to a dehumidifier, which dried the peat samples somewhat. In addition to peat oxidation, shrinkage of the peat was visually observed, which upon rewetting (in this case saturating) did not retain as much water as initially and did not return to its original volume (see Section 2.4.4), hence the lower porosity readings. This issue with the raw peat specimens did not occur to the same extent in Experiment B.

The three largest percentage decreases in porosities, however, for the stabilised and raw peat from specimens tested at day 20 to specimens tested at day 180 were in surcharged specimens a4(2c), a5(2c) and a5(3c) in Experiment A, specimens that recorded large carbonation depths. The three largest percentage drops in stabilised and raw peat in Experiment B were also in surcharged specimens; namely, b1(1c), b1(2c) and b3(3c). There was a strong but not significant association between surcharge and a decrease in porosity over the 180 days ($p = 0.058$), suggesting that the porosity decreases were due to carbonation and not shrinkage.

As only one data point over time was available for the large specimens, no conclusions on carbonation could be made on their porosity readings. Nevertheless, using the water evaporation method, other parameters were calculated, such as dry density, saturated moisture content and void ratio, all of which contribute to identifying stabilised peat properties and to the discussion in Chapter 6.

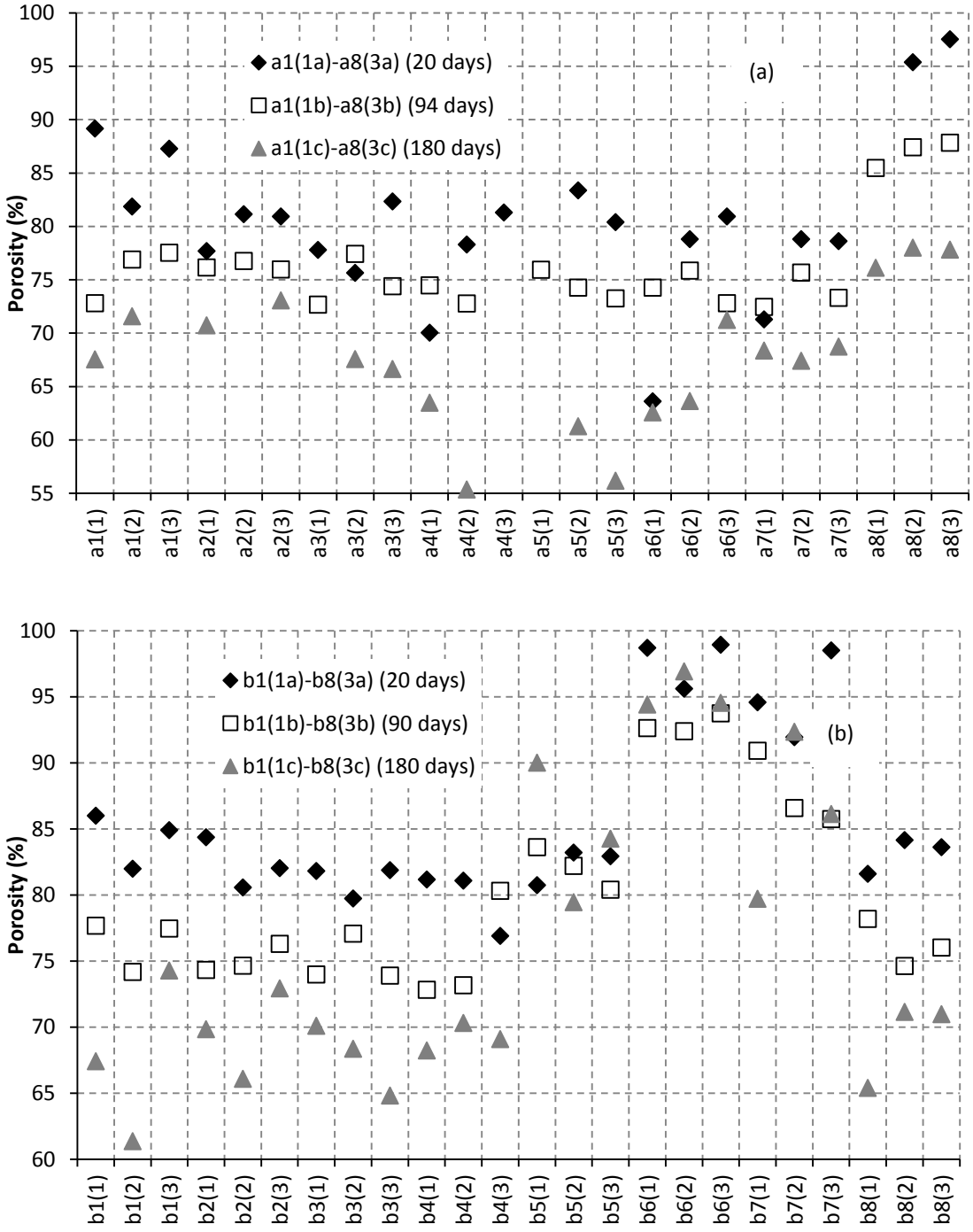

Figure 5.30 - Porosity readings for small specimens in (a) Experiment A and (b) Experiment B

Table 5.9 - p-value table for porosity readings in Experiments A and B

	Experiment A	Experiment B
Specimen a vs b	0.074	0.000
Specimens b vs c	0.000	0.006
Specimen a vs c	0.000	0.000

5.4 Statistical analysis

5.4.1 Introduction

Results of statistical analyses carried out on the X_c results are presented in this section. One-way ANOVA was used to compare the carbonation depths calculated from each experimental technique. Correlation statistics were used to see if there were any relationships between X_c values obtained using the various carbonation depth techniques, while for Experiments A and B, multiple linear regression analyses were undertaken to identify the significant variables in predicting X_c. The data from each experiment were then combined to perform a meta-analysis.

5.4.2 Comparing carbonation depth techniques

5.4.2.1 One-way ANOVA

Carbonation depths for each of the methods are compared on the interval plots in Figure 5.31 and Appendix F1. One-way ANOVA tables, Table 5.10 and Table 5.11, give p-values for the small specimens c and large specimens in Experiment A respectively, from which it can be seen that the XRD, FTIR and LOI techniques generally gave similar carbonation front depths ($p > 0.2$). The equivalent p-value tables for Experiment B are in Appendix F1, where the X_c results of XRD, FTIR and LOI were again similar for the small specimens b ($p > 0.05$), but the X_c results from LOI were significantly larger ($p < 0.05$) than those from XRD and FTIR for the small specimens c and large specimens. It is suggested that the reason for this difference is the higher average pH in the stabilised peat in Experiment B (Appendix E6). For instance, the average pH for the stabilised peat specimens with ≥ 250 kg/m^3 of cement binder for the large specimens is 12.21 in Experiment A and 12.74 in Experiment B. The higher pH may have inhibited the ability of XRD and FTIR to detect small changes in $CaCO_3$ concentrations, especially at the carbonation front. LOI, on the other hand, records the $CaCO_3$ concentration difference directly by measuring the extra mass CO_2 loss due to carbonation.

Table 5.10 - One-way ANOVA table showing p-values for X_c values obtained using carbonation depth techniques for small specimens c in Experiment A

	XRD	FTIR	LOI
FTIR	0.707		
LOI	0.402	0.213	
Phenol.	**0.007**	**0.017**	**0.000**

Table 5.11 - One-way ANOVA table showing p-values for X_c, X_p and X_{pH} values obtained using carbonation depth techniques for large specimens in Experiment A

Technique	XRD	FTIR	LOI	Phenol.
FTIR	0.506			
LOI	0.702	0.692		
Phenol.	**0.000**	**0.000**	**0.000**	
pH of slurries	**0.000**	**0.000**	**0.000**	**0.000**

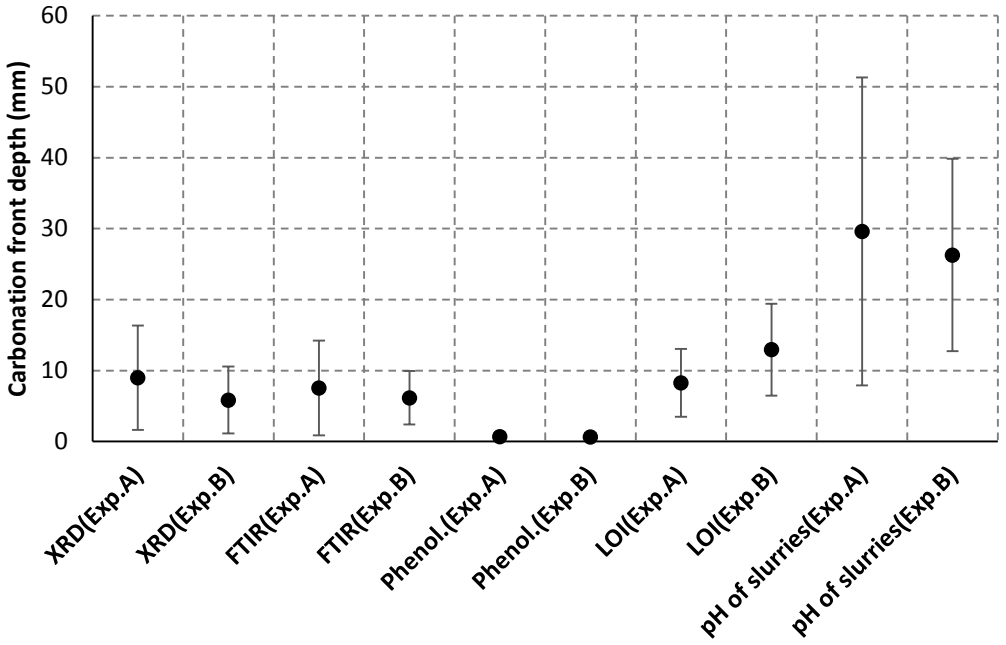

Figure 5.31 - Average X_c, X_p and X_{pH} values with standard deviation bars for the large specimens in Experiments A and B

In both experiments, the phenolphthalein indicator results led to estimated carbonation depths significantly less than the other methods ($p < 0.05$). The lowest depths were recorded by the phenolphthalein indicator (which turns colourless at a pH below 9) because it is based on pH only. In concrete with cement binder, the front measured by this indicator was described by Chang & Chen (2006) as the front at which the concrete is more than 50% carbonated. As described in Sections 2.9.2 and 2.9.4, carbonation first occurs at a pH much greater than 9, which can be detected by XRD, FTIR and LOI by examining the presence of $CaCO_3$.

The pH of stabilised peat slurries technique on the other hand gave significantly greater X_c results than the other techniques in Experiments A and B, except for the LOI technique in the small specimens c in Experiment B where the results were greater but not significant ($p = 0.087$). The relationship between X_c results from the pH of stabilised peat slurries technique and other methods is further discussed in Section 5.4.2.3.

5.4.2.2 XRD, FTIR and LOI comparison

While it has been established for concrete that the FTIR and XRDA methods give carbonations fronts between 1.2 times and twice those of the phenolphthalein method (X_c/X_p = 1.2–2) (Sections 2.9.2 and 2.9.4), this ratio was found to be higher for stabilised peat. The average X_c result for XRD, FTIR and LOI was divided by the average X_p result. X_p/X_c was between 4.7 for FTIR and 8.1 for LOI for small specimens c in Experiment A and between 3.7 for XRD and 7.8 for LOI for small specimens c in Experiment B.

The XRD, FTIR and LOI methods all define the carbonation depth as the depth where the $CaCO_3$ concentration is elevated with respect to the baseline and measures the maximum advancement of the carbonation front. As well as normally giving similar depths (Section 5.4.2.1), there are significant relationships (p = 0.000) between X_c values obtained for XRD, FTIR and LOI as shown in Table 5.12 and Table 5.13. Therefore, the X_c results from these three techniques are combined in Section 5.4.3 as they measure changes in $CaCO_3$ concentration compared to the phenolphthalein and pH of stabilised peat slurries techniques which measure pH. Converting the LOI results to relative percentage carbonated intensities, it is possible to show the similarities of XRD, FTIR and LOI techniques on one plot, as exemplified in Figure 5.32 for A5(3).

Table 5.12 - Investigation of relationships between results of carbonation depth techniques for all small specimens and large specimens in Experiment A

Technique	XRD	FTIR	LOI	Phenol.
FTIR	**0.000***			
	0.521**			
LOI	**0.000**	**0.000**		
	0.496	**0.552**		
Phenolphthalein	**0.000**	**0.000**	**0.000**	
	0.403	**0.426**	**0.540**	
pH of slurries	0.057	0.138	0.193	0.885
	0.650	0.303	0.088	-0.001

* p-value
** R^2 value

Table 5.13 - Investigation of relationships between results of carbonation depth techniques for all small specimens and large specimens in Experiment B

Technique	XRD	FTIR	LOI	Phenol.
FTIR	**0.000**			
	0.542			
LOI	**0.000**	**0.000**		
	0.372	**0.440**		
Phenolphthalein	**0.000**	**0.000**	**0.000**	
	0.610	**0.392**	**0.408**	
pH of slurries	**0.000**	**0.001**	**0.000**	**0.002**
	0.172	**0.150**	**0.177**	**0.130**

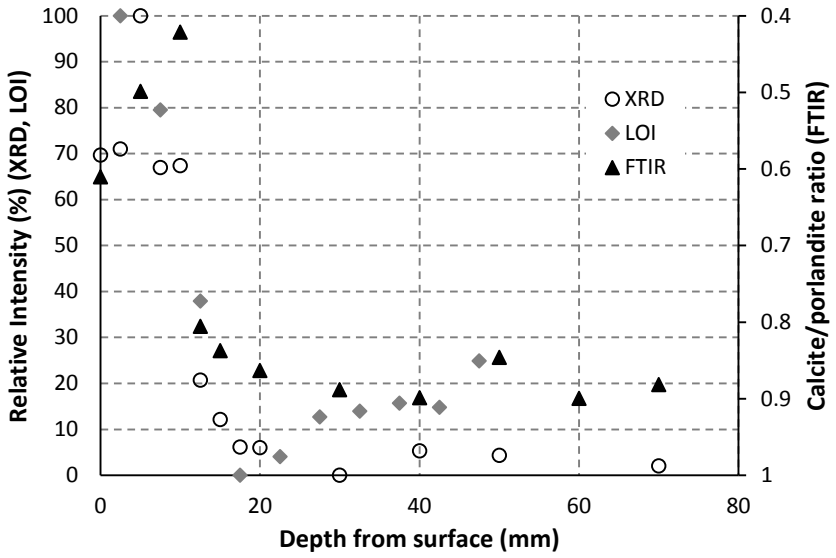

Figure 5.32 - Variation in relatively intensity and calcite/portlandite ratio with depth for A5(3)

5.4.2.3 Relationship between pH of stabilised peat slurries and other techniques

For the large specimens, the pH of stabilised slurries technique largely revealed a carbonation depth greater than the other methods ($p = 0.000$) (Figure 5.31) because it does not indicate a carbonation front depth, but rather a depth X_{pH} that shows the position where the pH drops due to the decrease in concentration of Ca^{2+} and $Ca(OH)_2$ in the pore solution and the dissolution of components such as CSH. X_{pH} indicates the depth at which leaching of Ca^{2+} and $Ca(OH)_2$ occurs, from areas in the uncarbonated zone to the carbonation front (Section 2.7.2.2).

The ratio of X_c/X_{pH} for the large specimens with ≥ 250 kg/m^3 of cement binder was on average between 3.8 for LOI and 6.4 for FTIR for Experiment A and between 1.7 for LOI and 4.6 for XRD for Experiment B. The primary difference between Experiments A and B was due to a slower leaching process in Experiment B as a result of the higher average pH of the stabilised peat specimens and thus the larger number of Ca^{2+} in the pore solution. The cement used in Experiment B had a greater CaO content than in Experiment A ($p = 0.117$), which allowed the cement hydration products to remain in equilibrium longer, thus delaying the dissolution process and the release of Ca^{2+} (Section 2.7.1.3).

Significant relationships ($p = 0.000$) were found between pH and the degree of carbonation (D_c) for the large specimens in Experiments A and B with 250 kg/m^3 or more of cement binder where a decrease in pH meant an increase in D_c (Figure 5.33).

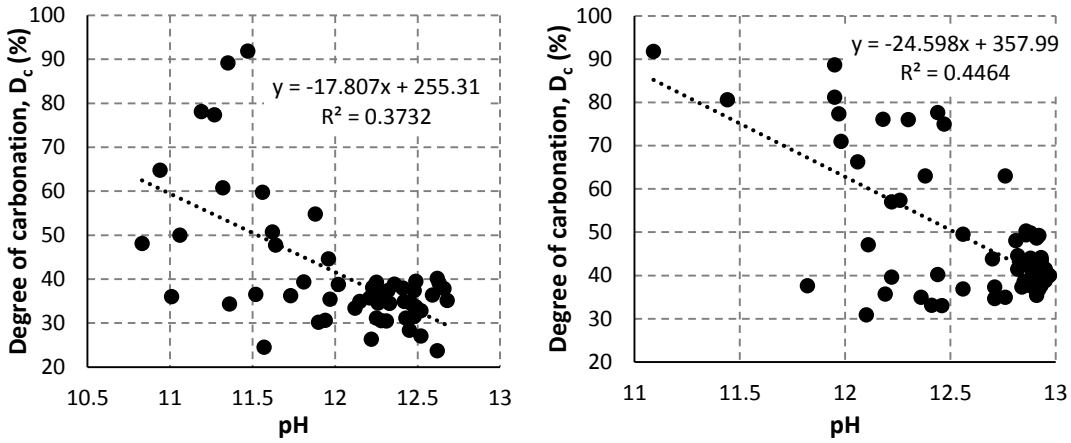

Figure 5.33 - Relationship between pH and degree of carbonation for large specimens with a cement binder content of ≥ 250kg/m^3 in (a) Experiment A and (b) Experiment B

5.4.2.4 Relationship between porosity and X_c

From the water evaporation method results, it was discovered that both weak and significant relationships existed between porosity and individual X_c values calculated using LOI, XRD and FTIR for the small specimens c in both experiments (Table 5.14) ($p < 0.165$). An instance of the relationship between porosity and individual X_c values measured using FTIR is shown in Figure 5.34. The higher the porosity, the lower the X_c value, which is the opposite to what occurs in concrete; a hypothesis is provided in Section 6.5 on this topic as part of a broader hypothesis on carbonation in stabilised peat.

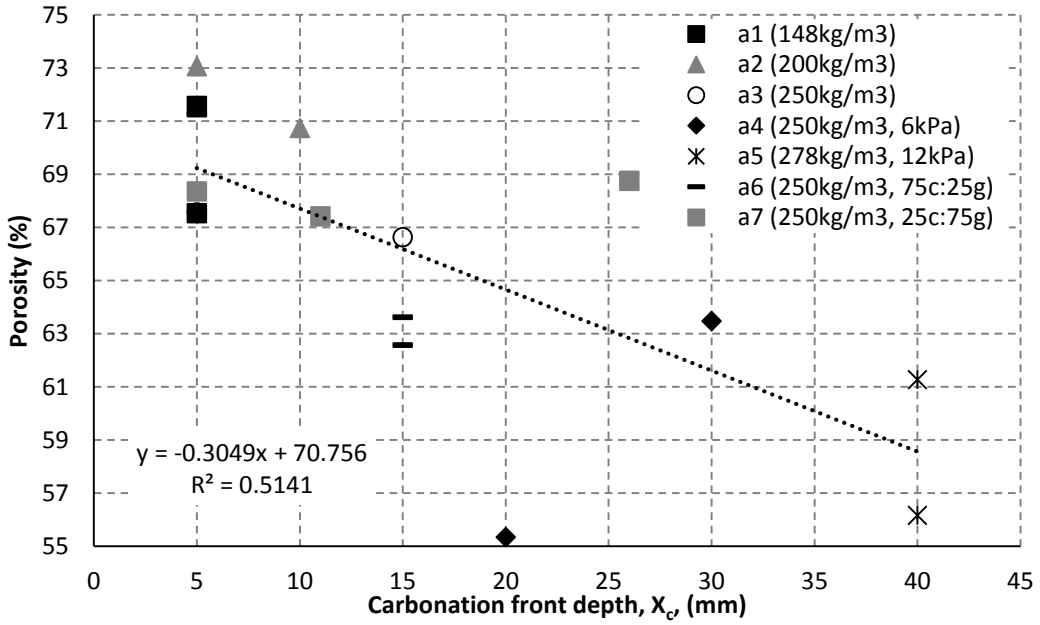

Figure 5.34 - Variation in FTIR X_c values with porosity for small specimens c in Experiment A

Table 5.14 - p-values for X_c with porosity reading for small specimens c in Experiments A and B

Porosity versus X_c results from:	Experiment A	Experiment B
LOI	**0.029**	0.05
XRD	0.132	0.165
FTIR	**0.002**	0.081

5.4.2.5 Postulated relationship between percentage carbonated and depth for stabilised peat

Analysis of the X_c, X_p and X_{pH} results to date suggests that the relationship between percentage carbonated (D_c) and depth can be postulated for stabilised peat. Figure 5.35 shows this new relationship and also highlights the measure of carbonation that each technique is interpreted to produce. The uncarbonated zone now refers to the zone where initial carbonation has taken place but has remained unaffected by atmospheric CO_2 and CO_2 from oxidised peat, assuming that O_2, CO_2 and Ca diffusion are one dimensional (vertical).

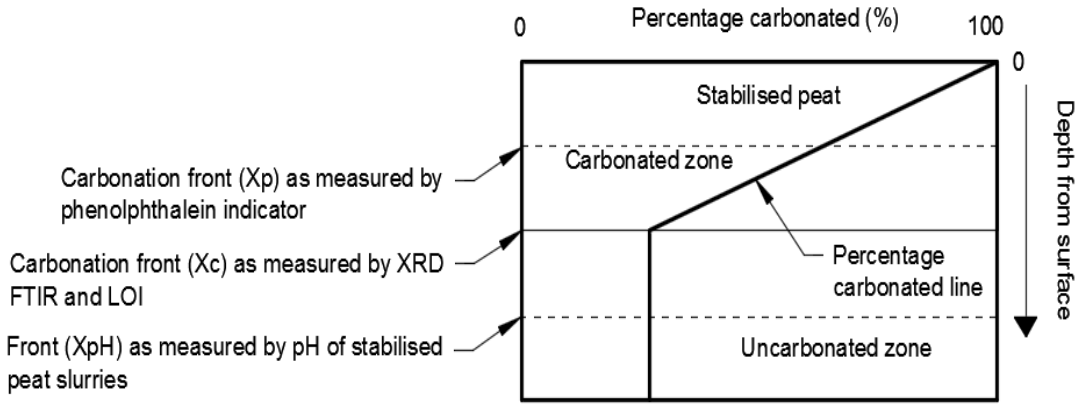

Figure 5.35 - Carbonation front in stabilised peat as measured by phenolphthalein indicator, XRD, FTIR, LOI and pH of stabilised peat slurries

5.4.3 Reconstruction of depth of carbonation fronts in Experiments A and B

5.4.3.1 Small specimens

For an in-depth analysis of the variables that strongly affected X_c, multiple linear regression analysis was undertaken. The variables examined in Experiment A were cement content (kg/m^3), GGBS content (kg/m^3), surcharge (kPa), and time (days), while in Experiment B the variables examined were cement content, water table, surcharge, and time. Time was not considered for LOI in Experiment A as only the small specimens c (tested at 180 days) and large specimens (also tested at 180 days) were analysed. Table 5.15 and Table 5.16 show the results of the multiple linear regression analyses performed for the small specimens in Experiments A and B.

In Experiment A, X_c and X_p proved to be strongly related to surcharge and time, except for LOI which had no time variable. In the multiple regression analysis for Experiment B, a 'dummy' variable was assigned to the water table variable as was done in Chapter 4 for the CO_2 fluxes (Section 4.6.5.1). In Experiment B, X_c, X_p and X_{pH} were strongly related to time for all techniques: the longer the time, the larger X_c, X_p and X_{pH}. Surcharge was a significant variable in only XRD, FTIR and LOI, and cement content was a significant variable in LOI, phenolphthalein indicator and pH of slurries. Where significant, surcharge increased X_c, X_p and X_{pH}, while an increase in cement content decreased X_c, X_p and X_{pH}. It was not possible to prove GGBS and water table to be significant variables in either experiment, except in Experiment B for results of the pH of slurries technique where water table was significant. A high water table meant low X_{pH} values as carbonation under the water table is slow, consequently leaching of Ca^{2+} is slow.

Table 5.15 - Multiple linear regression analyses showing the effects of the variables examined on X_c, X_p and X_{pH} for the carbonation depth techniques for small stabilised peat specimens in Experiment A

	XRD		**FTIR**		**LOI***		**Phenol.**	
Analysis	1	2	1	2	1	2	1	2
R^2 (adj)	50.77	51.95	40.06	41.74	51.98*	56.58	32.04	32.99
Lack-of-fit	0.000	0.000	0.000	0.000	0.000	0.759	0.000	0.000
Variables	**p-values**							
Intercept	0.716	0.511	0.467	0.978	0.780	**0.000**	0.505	0.027
Time	**0.000**	**0.000**	**0.016**	**0.000**	-	-	**0.000**	**0.000**
Cement	0.905	-	0.823	-	0.432	-	0.985	-
GGBS	0.586	-	0.850	-	0.504	-	0.561	-
Surcharge	**0.001**	**0.000**	**0.001**	**0.000**	**0.024**	**0.000**	**0.024**	**0.006**

* No time variable for LOI as only specimens c tested.

Table 5.16 - Multiple linear regression analyses showing the effects of the variables examined on X_c, X_p and X_{pH} for the carbonation depth techniques for small stabilised peat specimens in Experiment B

	XRD		**FTIR**		**LOI**		**Phenol.**		**pH**	
Analysis	1	2	1	2	1	2	1	2	1	2
R^2 (adj)	40.37	41.71	39.95	41.74	66.57	64.81	38.33	36.3	20.81	22.39
Lack-of-fit	0.052	0.001	0.001	0.000	0.067	0.065	0.051	0.016	0.110	0.05
Variables	**p-values**									
Intercept	0.522	0.987	0.670	0.766	0.068	0.065	0.262	0.071	0.000	0.000
Time	**0.000**	**0.000**	**0.000**	**0.000**	**0.000**	**0.000**	**0.000**	**0.000**	**0.017**	**0.016**
Cement	0.601	-	0.649	-	**0.044**	**0.014**	0.058	**0.019**	**0.042**	**0.040**
Water table	0.549	-	0.704	-	0.062	-	0.619	-	0.102	**0.049**
Surcharge	**0.033**	**0.003**	**0.010**	**0.001**	0.140	**0.006**	0.196	-	0.945	-

Since XRD, LOI and FTIR techniques measure X_c similarly (i.e. by examining changes in $CaCO_3$ concentration—see Section 5.4.2.2) and there is similarity ($p > 0.05$) in X_c results for these techniques in Experiment A and specimens b in Experiment B, the results of the three techniques were combined to increase the sample size before undertaking the

multiple regression analysis. Table 5.17 displays the results of the analyses, which show time and surcharge to be highly significant variables ($p < 0.01$) for Experiments A and B, and in Experiment B, cement and water table were also significant if analysed independently.

Table 5.17 - Multiple linear regression analyses showing the effects of the variables examined on X_c (XRD, FTIR and LOI combined) for small stabilised peat specimens in Experiments A and B

	Experiment A		**Experiment B**		
	XRD, FTIR and LOI		**XRD, FTIR and LOI**		
Analysis	1	2	1	2	3
R^2 (adj)	51.81	52.09	48.83	48.23	48.34
Lack-of-fit	0.000	0.000	0.000	0.000	0.000
Variables			**p-values**		
Intercept	0.454	0.301	0.108	0.878	0.098
Time	**0.000**	**0.000**	**0.000**	**0.000**	**0.000**
Cement	0.698	-	0.094	-	**0.034**
GGBS	0.374	-	-	-	-
Surcharge	**0.000**	**0.000**	**0.001**	**0.000**	**0.000**
Water table	-	-	0.114	**0.041**	-

The larger sample size for these analyses produced higher R^2 predicted values that increased the capability of the regression model to predict new observations. Final equations/models, Equation 5.1 for Experiment A and Equation 5.2 for Experiment B are therefore presented with the coefficients for each variable in Table 5.18 and Table 5.19 respectively, with only parameters that contributed significantly to X_c included in the final equations/models. The best-fit models for Experiments A and B explained 52.8% and 49.3% of the variability in the X_c values respectively. The results of the multiple regression analyses, including the residual plots, are shown in Appendix F2.

$$X_c = b_0 + b_2 \times \text{time (days)} + b_4 \times \text{surcharge (kPa)} \quad \textbf{Equation 5.1}$$

$$X_c = b_0 + b_2 \times \text{time (days)} + b_3 \times \text{cement (kg/m}^3\text{)} + b_4 \times \text{surcharge (kPa)} \quad \textbf{Equation 5.2}$$

Table 5.18 - Parameters for the X_c reconstruction model for small specimens in Experiment A

Parameters	**Coefficient**	**Standard error**	**p-value**
b_0 (constant)	1.23	1.23	0.301
b_2 (time)	0.08912	0.00959	0.000
b_4 (surcharge)	1.149	0.148	0.000
R^2 (adj)	52.09		
R^2 (pred)	49.64		
SE	7.27922		
d.f (reg, res)	2,127		
F-value	71.13		
P-value	0.000		

Table 5.19 - Parameters for the X_c reconstruction model for small specimens in Experiment B

Parameters	Coefficient	Standard error	p-value
b_0 (constant)	5.85	3.52	0.098
b_2 (time)	0.08978	0.00823	0.000
b_3 (cement)	-0.0306	0.0143	0.034
b_4 (surcharge)	0.673	0.132	0.000
R^2 (adj)	48.34		
R^2 (pred)	46.53		
SE	6.86206		
d.f (reg, res)	3,158		
F-value	51.21		
P-value	0.000		

5.4.3.2 Large specimens

Multiple linear regression was similarly carried out on the X_c, X_p and X_{pH} results of the large specimens, but it was already known from preliminary analyses done in Section 5.3 that relationships in general between all variables examined and X_c, X_p and X_{pH} were not strong because of reasons discussed in Section 6.3. Moreover, only one data point in time (d = 180 days) and a small sample size were available. The results of these analyses are in Appendix F3, showing low R^2 values for each statistical model produced. Surcharge was significant for XRD, FTIR and LOI in Experiment A, while in Experiment B water table was significant for LOI and phenolphthalein, and cement was significant for the pH of stabilised peat slurries technique. When the XRD, FTIR and LOI results were combined for each experiment, the multiple regression analysis showed GGBS and surcharge to be significant variables in Experiment A and cement and surcharge in Experiment B (Appendix F3).

5.4.4 Meta-analysis on data from Experiments A and B

A meta-analysis was performed on the data from Experiments A and B to increase the statistical power over individual studies. The results of XRD, LOI and FTIR were also put together for Experiments A and B and then combined to enlarge the sample size before undertaking this analysis. The variables examined were cement content (kg/m^3), GGBS content (kg/m^3), depth of water table, surcharge (kPa), and time (days). From the meta-analysis, X_c was found to be significantly related to time and surcharge (Table 5.20).

The best-fit statistical model for X_c is the same as Equation 5.1 but with different parameter coefficients (Table 5.21). The model recognises time and surcharge to be the driving variables, explaining 49% of the variability in the X_c values obtained by XRD, FTIR and LOI for the small specimens. The results of the multiple regression analysis and a plot of the predicted X_c values against the measured X_c values are shown in Appendix F4.

Table 5.20 - Multiple linear regression analyses showing the effects of the variables examined on X_c (XRD, FTIR and LOI combined) and X_p for meta-analysis on small stabilised peat specimens in Experiments A and B

	XRD, FTIR and LOI			Phenol.		
Analysis	1	2	3	1	2	3
R^2 (adj)	48.63	48.65	45.54	35.51	35.17	31.63
Lack-of-fit	0.000	0.000	0.000	0.000	0.000	0.000
Variables	**p-values**					
Intercept	0.554	0.097	**0.000**	0.865	**0.001**	**0.000**
Time	**0.000**	**0.000**	-	**0.000**	**0.000**	-
√Time	-	-	**0.000**	-	-	**0.000**
GGBS	0.539	-	-	0.687	-	-
Cement	0.901	-	-	0.173	-	-
Water table	0.192	-	-	0.681	-	-
Surcharge	**0.000**	**0.000**	**0.000**	**0.001**	**0.000**	**0.001**

Table 5.21 - X_c regression model parameters for meta-analysis for XRD, FTIR and LOI results combined for small specimens in Experiments A and B

Parameters	Coefficient	Standard error	p-value
b_0 (constant)	-1.405	0.844	0.097
b_2 (time)	0.08962	0.00634	0.000
b_4 (surcharge)	0.8705	0.0950	0.000
R^2 (adj)	48.65		
R^2 (pred)	47.74		
SE	7.14823		
d.f (reg, res)	2,289		
F-value	138.84		
P-value	0.000		

The parameters in Table 5.21 and Equation 5.1 can be used to calculate X_c in stabilised peat for the first 180 days (duration of Experiments A and B) after peat stabilisation. However, use of this equation for time periods up to 120 years after stabilisation gives unrealistic results. X_c in concrete has been found to increase with the square root of time (Section 2.7.1.6) and not linearly as in Equation 5.1. This is because the rate at which X_c increases in concrete drops over time, a scenario also likely to be replicated in stabilised peat. In Equation 5.3, an alternative model is shown incorporating the square root of time. The statistical power of this model is slightly lower than that of Equation 5.1 (see Table 5.22), and the results of the multiple regression analysis in Appendix F4. However, it can be used to estimate X_c over a long period of time (used in Chapter 7 to produce an estimate of X_c over 120 years).

$$X_c = b_0 + b_2 \times \sqrt{\text{time (days)}} + b_4 \times \text{surcharge (kPa)} \qquad \textbf{Equation 5.3}$$

Table 5.22 - X_c regression model parameters for meta-analysis for XRD, FTIR and LOI results combined for small specimens in Experiments A and B using √time

Parameters	Coefficient	Standard error	p-value
b_0 (constant)	-6.69	1.23	0.000
b_2 (√time)	1.533	0.117	0.000
b_4 (surcharge)	0.8673	0.0979	0.000
R^2 (adj)	45.54		
R^2 (pred)	44.62		
SE	7.36132		
d.f (reg, res)	2,289		
F-value	122.68		
P-value	0.000		

For the reasons outlined in Section 6.3, low R^2 adjusted values were once again obtained for the meta-analysis for the large specimens (R^2 adjusted values < 20%). These analyses can be found in Appendix F5, where it is of note that for the combined X_c values of XRD, LOI and FTIR, the variables GGBS, cement and surcharge were significant. An increase in GGBS and cement content decreased X_c whereas surcharge increased it.

5.4.5 Summary of statistical results

The statistical analysis showed that XRD, FTIR and LOI techniques generally produced similar X_c values, while the phenolphthalein indicator produced significantly smaller values than the other techniques, and the pH of stabilised peat slurries gave significantly greater values than the other methods.

Similar to the results for CO_2 fluxes in Chapter 4, time and surcharge were highly significant variables that increased X_c. Cement and water table were significant variables for some techniques, especially in Experiment B, cement content decreasing X_c and a high water table decreasing X_c. The meta-analysis showed, however, only time and surcharge to be significant variables in predicting X_c for the small specimens.

5.5 Summary

In this chapter, the carbonation depth results for each technique were presented and their applicability to stabilised peat was discussed. The pH of slurries method was found not to give a carbonation depth; instead, it gave the depth at which leaching of $Ca(OH)_2$ and Ca^{2+} to the carbonation front occurs. Excluding this technique, surcharge and time were found to be two variables that significantly affected the carbonation depth.

The pH of slurries techniques gave the greatest front depths and the phenolphthalein method the smallest carbonation front depths, while XRD, FTIR and LOI techniques generally gave similar carbonation depths. Each technique provided different information on the depth and level of carbonation and the properties of the stabilised peat. Employing a combination of these techniques gives a clearer picture of the carbonation front and

enhances the understanding of the carbonation process in stabilised peat. Table 5.23 gives the approximate number of samples analysed for each carbonation depth technique and includes the number of gas samples analysed for the CO_2 flux studies in Chapter 4.

Table 5.23 - Number of samples analysed using closed chamber method and carbonation depth techniques

Exp.	Gas flux technique	Carbonation depth techniques					
	Closed chamber method	Phenolphthalein indicator	XRD	FTIR	LOI	pH of slurries technique	Water saturation method
P	792	0	0	0	0	0	0
A	6240	90	525	744	390	240	186
B	5280	96	360	684	720	508	192

A comparison of the results from each technique was presented, and a meta-analysis on carbonation depth results showed time and surcharge to be highly significant variables in predicting X_c. These findings are important for carbon calculations relevant to soil-mixing applications as the variables that influence the carbonation depth from stabilised peat have been identified. The best-fit statistical model/equation for X_c from stabilised peat produced by the meta-analysis in this chapter will be used in Chapter 7 to calculate X_c for the stabilised peat in an environmental LCA.

Chapter 6: Discussion

6.1 Introduction

This chapter expands on the analysis and discussion on the CO_2 flux results presented in Chapter 4 and the carbonation front depth (X_c) results in Chapter 5, beginning in Section 6.2 with the relationships discovered between gas flux results, X_c results and the stabilised peat properties.

Section 6.3 focuses on the reasons for the differences in X_c results between the small and large specimens, which are explained by examining the properties of the stabilised peat obtained using the water evaporation method. These properties also contribute to the understanding of other aspects of the results presented in Chapters 4 and 5. From the X_c results of the small and large specimens, k-rate factors, defined in Section 2.7.1.6, are developed in Section 6.4 for comparison with k-rate factors in concrete.

Based on the CO_2 fluxes and X_c results, Section 6.6 outlines a hypothesis of why k-rate factors and X_c values in stabilised peat vary with binder content, binder type(s) and environmental conditions. In the final section, there is further deliberation on some of the carbonation depth techniques and on their advantages and disadvantages. Techniques not examined in depth in this research are also briefly discussed as they can further contribute to understanding the carbonation process in stabilised peat.

6.2 Relationship between gas fluxes and X_c, D_c and pH

Some strong relationships were found between CO_2 gas fluxes and X_c for Experiments A and B. The relationships between X_c obtained using XRD, FTIR and LOI and the average 40-minute fluxes (over 180 days) for the specimens with 250 kg/m^3 or greater of cement binder are shown in Table 6.1 for Experiments A and B by way of p-values and R^2 values, and the significant correlations are highlighted in bold.

In Experiment A, for the large specimens with a cement content of 250 kg/m^3 or more (A3, A4, A5), a greater carbonation depth generally corresponded to a larger average CO_2 intake rate over the duration of the experiment ($p < 0.066$). The surcharged specimens had the greatest CO_2 intake rates and X_c values, and the unsurcharged specimens had the lowest, as exemplified in Figure 6.1 for the significant relationship between average CO_2 flux and X_c as measured by FTIR ($p = 0.003$). The average CO_2 flux value for each data point in this figure is the average gas flux of 52 gas sampling events that were carried out over 180 days. Experiment B produced similar findings for specimens with 250 kg/m^3 (B3, B4, B5, B8); however, the associations were not as strong as in Experiment A as

evidenced by the higher p-values of $0.097 \leq p \leq 0.159$ in Table 6.1, which was likely due to the smaller variability in CO_2 fluxes shown in Experiment B.

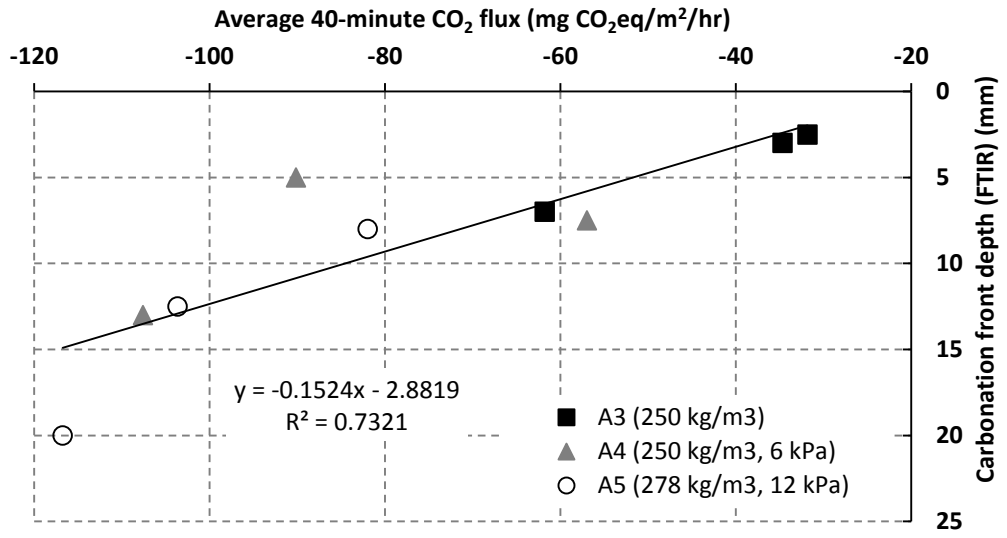

Figure 6.1 - Relationship between X_c and average 40-minute CO_2 flux for FTIR for Experiment A for stabilised peat with ≥ 250 kg/m³ of cement binder

Table 6.1 - Relationship between average 40-minute CO_2 flux and X_c values for XRD, FTIR and LOI

Experiment	Technique	Large specimens with ≥ 250 kg/m³ of cement binder		All large specimens	
		p-value	R^2	p-value	R^2
Exp. A	**XRD**	0.066	0.4046	**0.001**	0.4258
	FTIR	**0.003**	0.7321	**0.025**	0.2387
	LOI	**0.010**	0.6338	**0.001**	0.4715
Exp. B	**XRD**	0.137	0.207	0.052	0.2153
	FTIR	0.159	0.1878	0.06	0.2034
	LOI	0.097	0.2507	**0.048**	0.2229
Exp. A + B combined	**XRD**	0.068	0.1641	**0.012**	0.1594
	FTIR	**0.004**	0.3593	**0.025**	0.1293
	LOI	**0.005**	0.3451	**0.000**	0.4056

Table 6.1 also shows the relationships between X_c and the average CO_2 intake flux, where the data points for all the large specimens (A and B) are combined. Figure 6.2 exemplifies one of the significant relationships found when the X_c (LOI) and CO_2 flux data from all large specimens in Experiments A and B are combined. When the specimens in Experiment A are analysed together, correlations are not as strong as when only specimens with similar binder type and content are examined. However, p-values are lower, but this is simply due to the greater number of data points. The primary reason for weaker correlations was the large X_c values shown by some unsurcharged specimens, which also had a small average CO_2 intake rate as a result of their smaller carbonation potential (C_p).

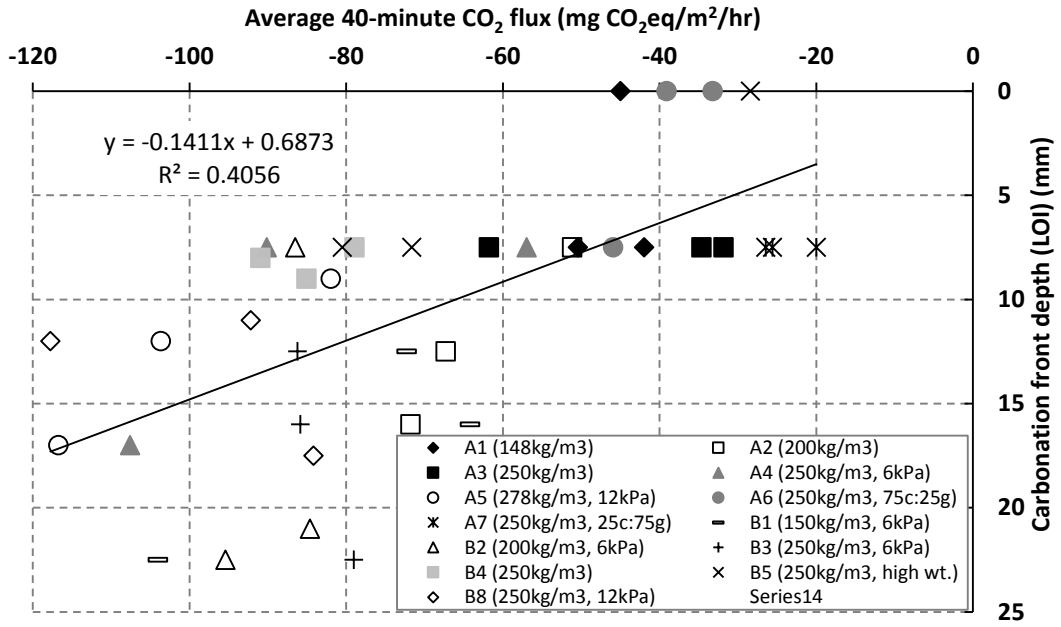

Figure 6.2 - Relationship between X_c (LOI) and average 40-minute CO_2 flux for Experiments A and B

On examination of a set of replicates (e.g. A7(1), A7(2), A7(3)), X_c also correlated with average CO_2 intake flux for the majority of the large specimens. The following are three examples of this correlation:

- Out of A5(1), A5(2) and A5(3), A5(3) had the highest average flux in Experiment A. A5(3) also had the highest X_c and X_{pH} values and the highest percentage carbonated (D_c) at the surface.
- A4(3) had a much higher average CO_2 flux than A4(1) and A4(2) and also had higher X_c, X_{pH} and D_c values at the surface.
- Similar trends were found in Experiment B: the average CO_2 flux for B1(2); for example, was higher than in B1(1) and B1(3). The greatest X_c, X_{pH} and D_c values at the surface were also found in B1(2).

From these analyses, it was evident that there was not only a relationship between X_c and average CO_2 gas flux values but also between average CO_2 flux and D_c at the surface. The relationship between D_c at the surface and average CO_2 fluxes was particularly strong ($p = 0.000$) for all the large specimens (Figure 6.3).

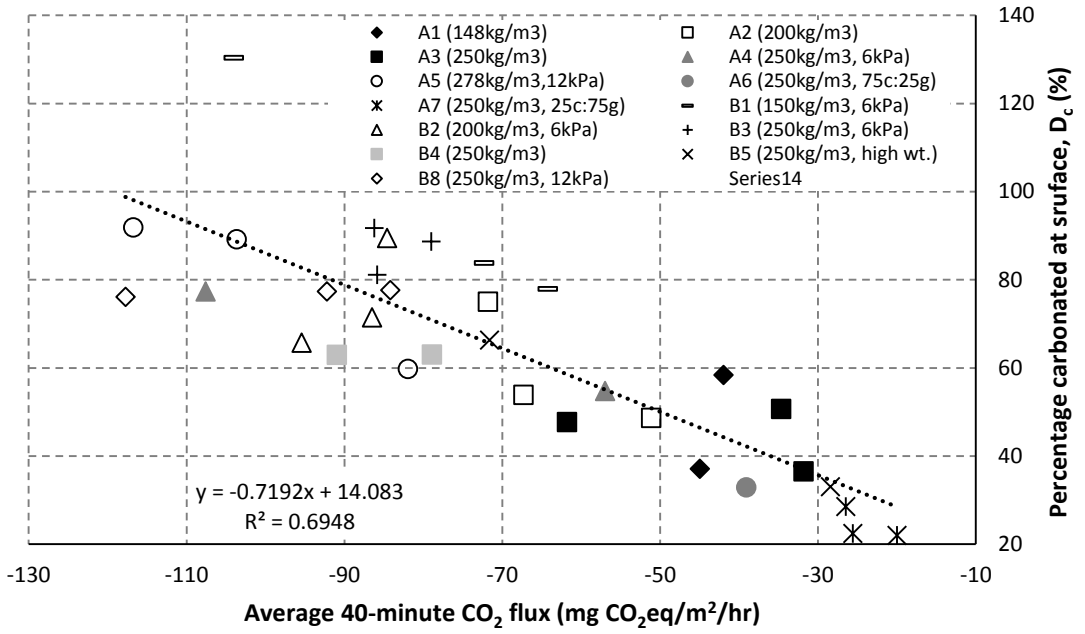

Figure 6.3 - Relationship between D_c at surface and average 40-minute CO_2 flux for the large specimens in Experiments A and B

While there was no significant relationship between pH and average gas flux values for Experiment B due to the higher resistance of the stabilised peat to pH change as a result of the higher CaO content of the cement, there was a weak relationship ($p = 0.116$) between pH and average gas flux for specimens having 250 kg/m^3 or greater of cement binder in Experiment A (Figure 6.4). If gas fluxes and pH were measured over a longer duration, it is suggested that this relationship would be stronger in Experiment B as there would be less resistance to pH change over time.

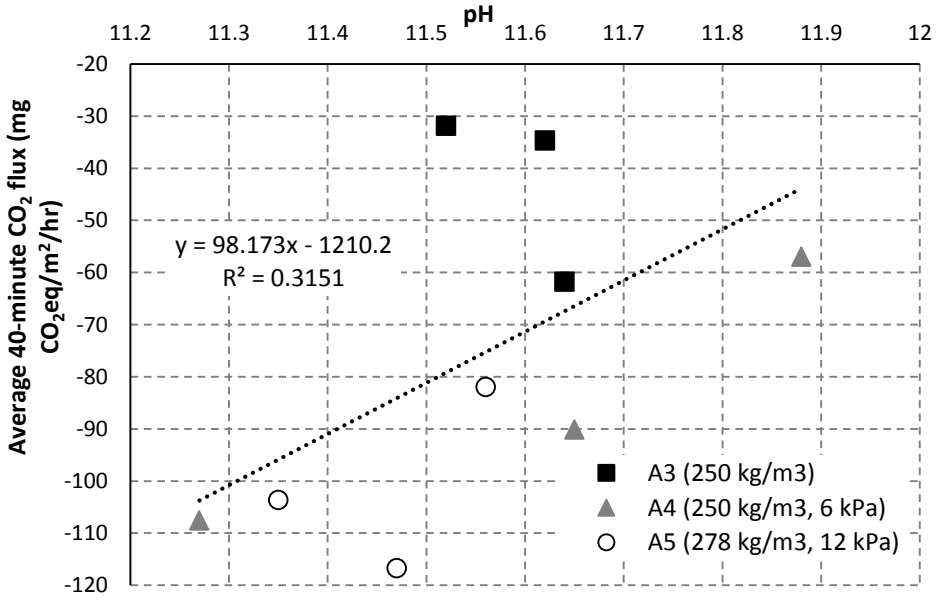

Figure 6.4 - Variation in pH with average 40-minute CO_2 flux for specimens with ≥ 250 kg/m^3 of cement binder in Experiment A

6.3 Difference between the small and large specimens

Better-fit statistical models and stronger relationships between X_c and the variables examined such as surcharge and cement were found for the small specimens than for the large ones. The smaller specimens also returned greater X_c values after 180 days. These differences were due to the small specimens being drier and hence more affected by O_2 and CO_2 ingress, which gave clearer and more identifiable carbonation fronts than the wetter and more porous large specimens (Sections 2.7.1.2 and 5.3.1.2). Similar differences were found between overground and submerged concrete (Section 2.7.1.4).

The drier nature of the small specimens was proven on examination of the properties of the stabilised peat at day 180 using the water evaporation method: the large specimens were discovered to have higher saturated moisture contents and porosity values and lower dry densities than the small specimens in both Experiments A and B ($p = 0.000$). The average saturated moisture content and dry density for the large specimens was 246 ± 42% and 335 ± 40 kg/m^3 respectively while for the small specimens c it was 183 ± 30% and 382 ± 48 kg/m^3. Some of the reasons for the differences were:

- Even though equal amounts of precipitation were added to the small and large specimens, the same loss of water per m^2 occurred (due to evaporation), but was, as a percentage, higher for the small specimens.

- The small specimens were unconfined on the ground, so some drainage occurred around the bottom circumference, especially on application of a surcharge, where water flowed horizontally across the floor. The large specimens, on the other hand, had a lid attached at the bottom to prevent drainage. Standpipes were attached to a hole in the bottom lid of the large specimens, which allowed a small amount of water to flow into the standpipe but against gravity. Water also seeped to the surface and evaporated in both large and small specimens. Overall, it was believed that more drainage occurred in the small specimens than in the large ones due to the greater drainage restriction of the large specimens.

- Furthermore, based on observations the permeability seemed to be lower for the large specimens: when water was added to them, it remained on top for longer than in the small specimens, suggesting that the large specimens were closer to saturation than the small ones.

The applied surcharges also did not affect the large specimens as much as the small ones due to the difference in height and the greater drainage restriction of the large specimens. Higher porewater pressures in the large specimens somewhat suppressed the volume

change that should occur on application of a surcharge as excess porewater pressures were not allowed to dissipate, whereas these pressures were allowed to dissipate in the small specimens. This is evident from Figure 6.5(a) and (b) as it is more difficult in (b) to distinguish between the specimen types A3–A5 that have a binder content ≥ 250 kg/m^3 based solely on surcharge, dry density and saturated moisture content than to distinguish between the corresponding a3–a5 data in (a). Similar plots for all the small specimens and large specimens in Experiments A and B are in Appendix E8.

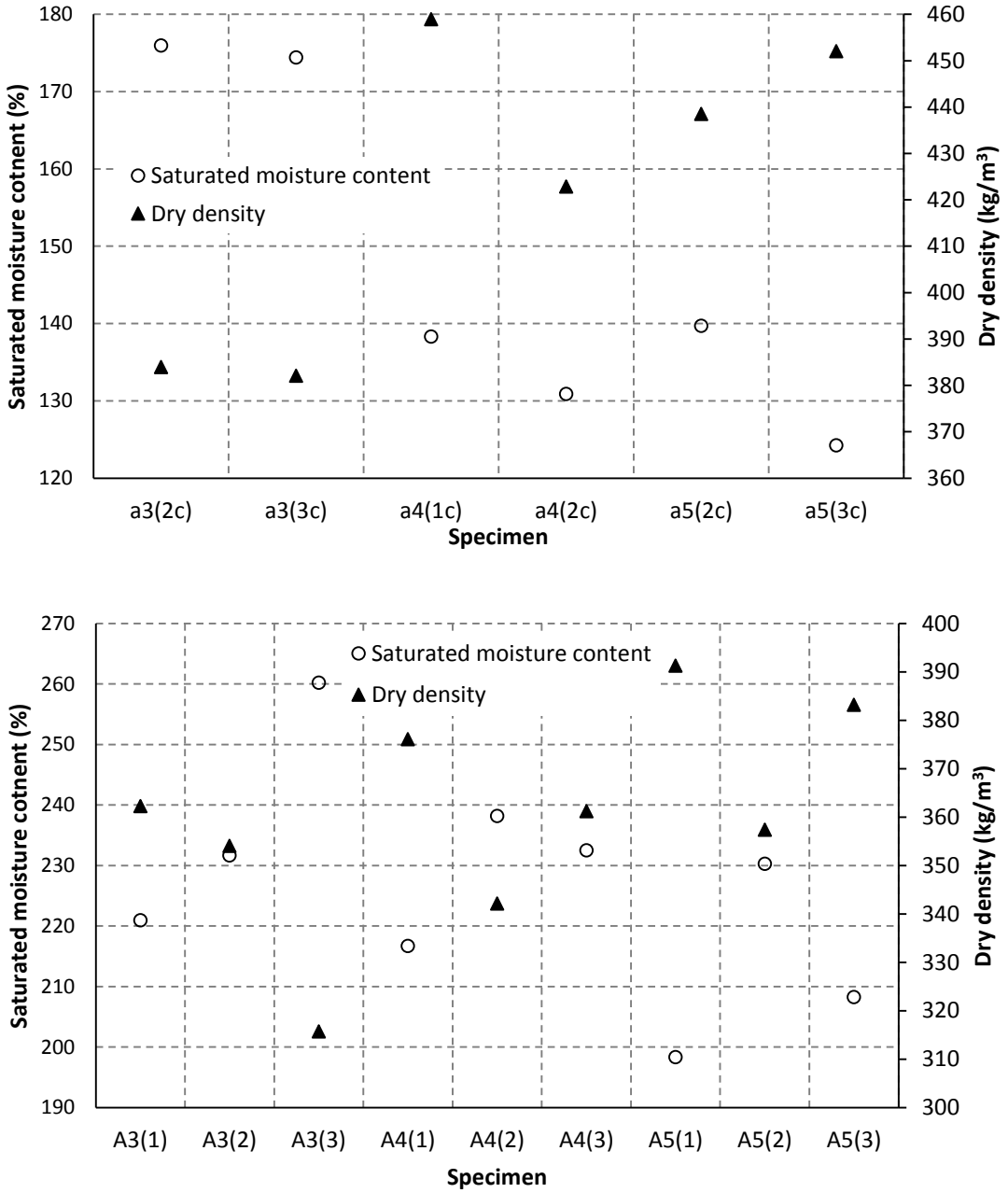

Figure 6.5 - Saturated moisture contents and dry densities in Experiment A for (a) specimens c (a3, a4, a5) and (b) large specimens (A3, A4, A5)

For the small specimens (a3(b)–a5(b)) and (a3(c)-a5(c)) with ≥ 250 kg/m^3 of cement binder, there were significant relationships between dry density and surcharge (p = 0.000 for specimens b, p = 0.039 for specimens c) and saturated moisture content and surcharge (p = 0.002 for specimens b, p = 0.026 for specimens c), but only weak relationships were found between their equivalent large specimens (A3–A5) (p ≥ 0.065). Small specimens b3, b4 and b8 and large specimens B3, B4, B8 in Experiment B produced similar findings, demonstrating again that the applied surcharges had a greater impact on the small specimens than the large ones.

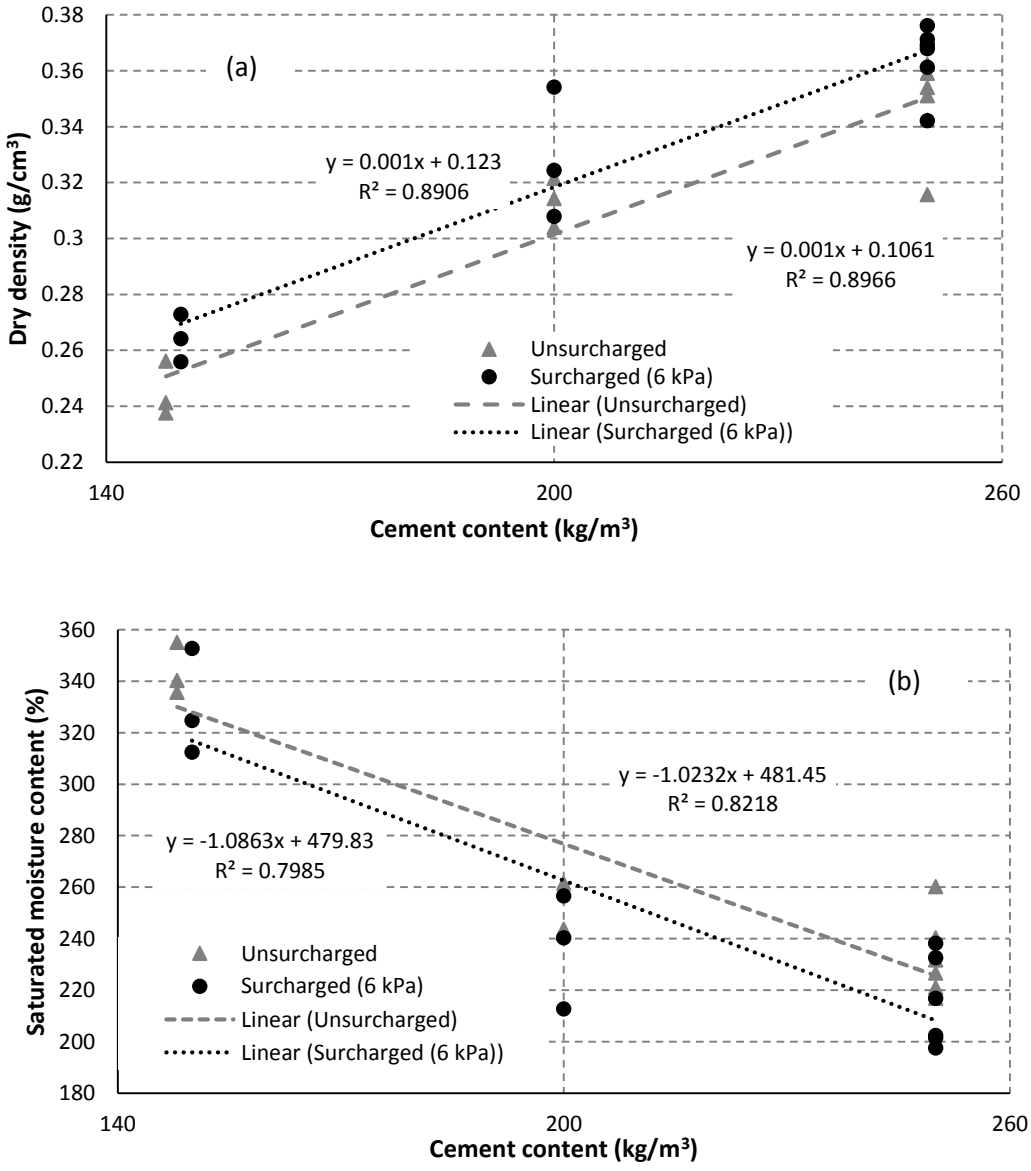

Figure 6.6 - Relationship in large specimens between cement content and (a) dry density and (b) saturated moisture contents

When the results of the large specimens in Experiments A and B were combined, however, there were significant relationships between surcharge and dry density (p = 0.002) and

almost a significant relationship between surcharge and saturated moisture content ($p = 0.053$), showing that the surcharge still had an effect on the large specimens. There were also highly significant relationships ($p < 0.01$) between cement content and dry density (Figure 6.6(a)), and cement content and saturated moisture contents (Figure 6.6(b)) for unsurcharged cement specimens and cement specimens with 6 kPa of surcharge in the large specimens. Both plots illustrate the difference between the unsurcharged and surcharged specimens, again showing the effect of surcharge on the large specimens.

6.4 k-rate factors

While the equations developed in Sections 5.4.3 and 5.4.4 to estimate X_c using time and other variables could be used in other studies and real-life scenarios, the universal equation to calculate X_c for concrete is Equation 2.10 ($X_c = k\sqrt{t}$), hence k-rate factors were developed for stabilised peat for comparison purposes. The X_c results from XRD, FTIR and LOI were combined in order to calculate k for stabilised peat for several binder types and binder contents and for several environmental conditions. The X_c results were plotted against the square root of time with the intercept set at zero. The slope of the regression line is the k-rate factor, where in the case of b8 for example, k is 33 mm/√yr (Figure 6.7).

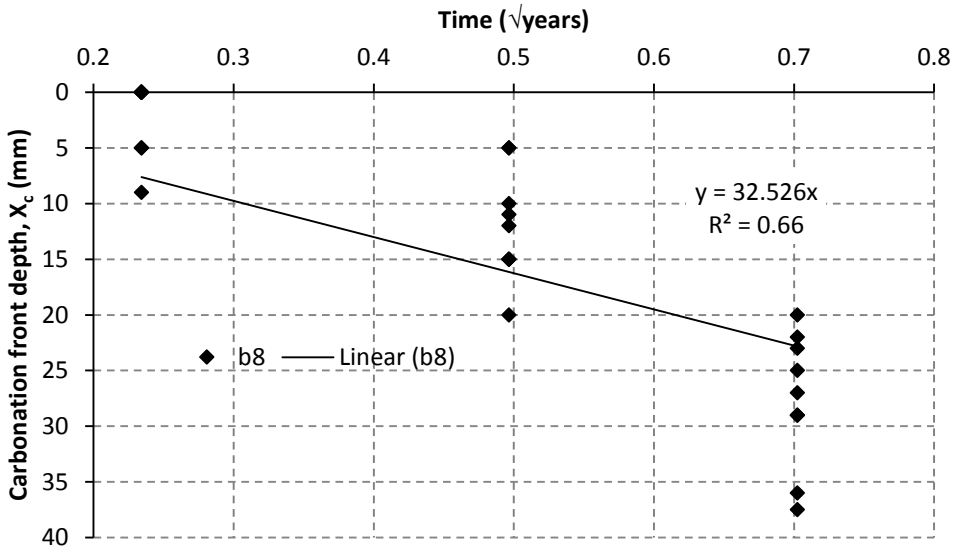

Figure 6.7 - Influence of time on carbonation front depth X_c for small specimens b8

k-rate factors were produced from the small and large specimens; however, for the large specimens, only data points at 180 days were available. The k-rate factors are provided in Table 6.2 along with their fit and significance values. Summary tables with the k-rate factors are also given in Table 6.3 and Table 6.4. For the unsurcharged specimens, R^2 values were generally lower and p-values generally higher than those of the surcharged specimens due to the larger variability in the X_c results of these specimens and the lower

X_c values achieved. The k-rate factors for the small specimens are more reliable on account of the larger number of data points and the availability of three data points over time. P-values for the k-rate factors developed show only one poor/non-significant relationship ($p > 0.05$) for the small specimens, a1. The k-rate factors for the large specimens, on the other hand, are developed based on poor relationships ($p > 0.05$), except for A5 ($p = 0.016$). However, there is a significant relationship ($p = 0.014$) between k-rate factors for the small specimens and for the large specimens as illustrated in Figure 6.8, showing that variables such as cement content and surcharge affected the X_c results of the small and large specimens similarly.

Table 6.2 - k-rate factors for the small and large specimens

Specimen No.	Small specimens			Specimen No.	Large specimens		
	k-rate factor	R^2 value	p-value		k-rate factor	R^2 value	p-value
a1	10	-0.14	0.855	A1	14	0.12	0.320
a2	20	0.31	0.013	A2	12	0.28	0.119
a3, b4	15	0.31	0.000	A3, B4	8	0.16	0.090
a4, b3	26	0.48	0.000	A4, B3	16	0.13	0.124
a5	50	0.73	0.000	A5	20	0.54	0.016
a6	17	0.27	0.015	A6	4	0.10	0.377
a7	19	0.27	0.015	A7	6	0.30	0.102
b1	28	0.42	0.000	A1	17	0.22	0.168
b2	33	0.43	0.000	B2	14	0.16	0.250
b5	11	0.12	0.030	B5	6	0.21	0.185
b8	33	0.66	0.000	B8	13	0.26	0.134

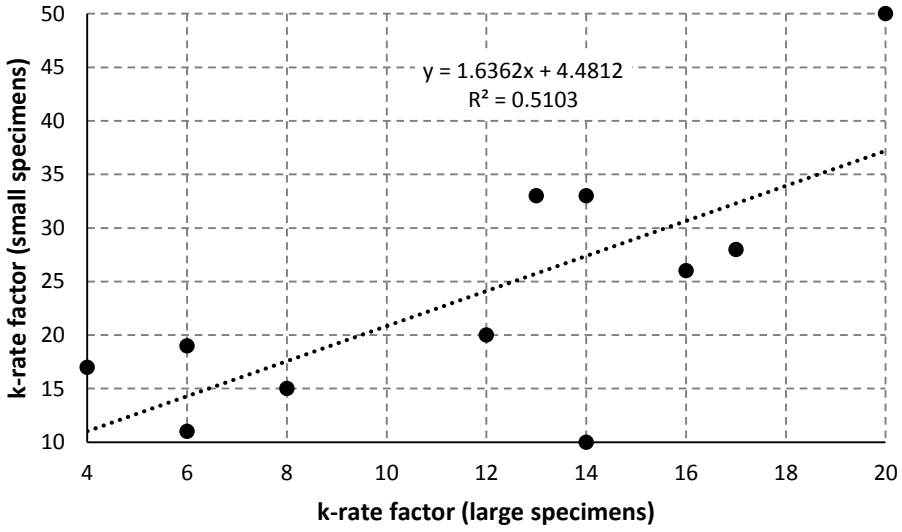

Figure 6.8 - Relationship between k-rate factors (large specimens) and k-rate factors (small specimens)

Table 6.3 - Carbonation k-rate factors (mm/√year) for various stabilised peat types in various conditions developed from the results of the small specimens in Experiments A and B

Stabilised peat properties and environmental conditions	Binder content (kg/m^3)			
	150	**200**	**250**	**278**
No surcharge	10	20	15	
Surcharge (6 kPa)	28	33	26	
Surcharge (12 kPa)			33	50
Cement:GGBS (75:25)			17	
Cement:GGBS (25:75)			19	
No surcharge (high water table)			11	

Table 6.4 - Carbonation k-rate factors (mm/√year) for various stabilised peat types in various conditions developed from the results of the large specimens in Experiments A and B

Stabilised peat properties and environmental conditions	Binder content (kg/m^3)			
	150	**200**	**250**	**278**
No surcharge	14	12	8	
Surcharge (6 kPa)	17	14	16	
Surcharge (12 kPa)			13	20
Cement:GGBS (75:25)			4	
Cement:GGBS (25:75)			6	
No surcharge (high water table)			6	

The highest k-rate factors for the small specimens measured were for the surcharged ones a5 at a value of 50 mm/√yr and the lowest at 10 mm/√yr for the unsurcharged specimens a1. These values prove that carbonation in stabilised peat is significantly higher than in concrete with Portland cement, where k ranges from 0.5 mm/√yr in wet/submerged concrete (> 35 MPa) to 15 mm/√yr in concrete indoors (< 15 MPa) (Lagerblad, 2005).

6.5 Hypothesis on CO_2 fluxes and carbonation depths in stabilised peat

This section outlines a hypothesis based on the X_c and gas flux results for why X_c values are different in stabilised peat with various binder content and types and under varying environmental conditions.

6.5.1 Effect of surcharge

While denser concrete has been shown to have smaller X_c values than more porous concrete, the stabilised peat specimens with the largest surcharge and dry densities and the lowest porosities had the greatest X_c values and k-rate factors. The key difference between the stabilised peat and concrete is the lower porosity in concrete, which is usually below 20% (Safiuddin & Hearn, 2005), whereas even after surcharging stabilised peat, porosity remained over 50%, thereby not heavily impeding Ca^{2+} and CO_2 diffusion. In unsurcharged specimens, the porosity was much higher than 50%, with the pores assumed to be comprised mostly of water. For Ca^{2+} ions from the cement and CO_2 to meet, they

must diffuse through a lot of water; and as diffusion in a liquid is about 10,000 times slower than in air, the reactions between Ca^{2+} and CO_2 are slow.

As is apparent in Figure 6.9, in surcharged stabilised peat, on the other hand, consolidation decreases the distance for the Ca^{2+} and CO_2 to meet as there is a greater cement content per m^3 due to decreases in porosity and saturated moisture contents and increases in dry density. Carbonation, therefore, occurs more quickly, increasing the speed of Ca^{2+} and CO_2 diffusion due to the lowering of the concentration of Ca^{2+} and CO_2 in the pore solution. Although there is more cement content per m^3 to be carbonated, the carbonation rate is high enough to increase X_c quicker than in the unsurcharged specimens due to the abundant availability of CO_2 released by oxidised peat. The diffusivity of CO_2 is always lower than that of O_2 as described in Section 2.7.2.2, which means the majority of the CO_2 intake is from CO_2 released by peat oxidation. In drained peat with a moisture content above 100%, considerable oxygen concentrations were measured as far down as 2 m below the water table (Matthiesen et al., 2004).

O_2 is not impeded by greater density as porosity is still above 50%, thus peat near the surface is oxidised and releases CO_2. This was evident when comparing X_c with X_{oc} (depth at which organic content becomes constant) in Section 5.3.4.5, which showed that the high carbonation depths recorded by the surcharged specimens also registered a high X_{oc} value.

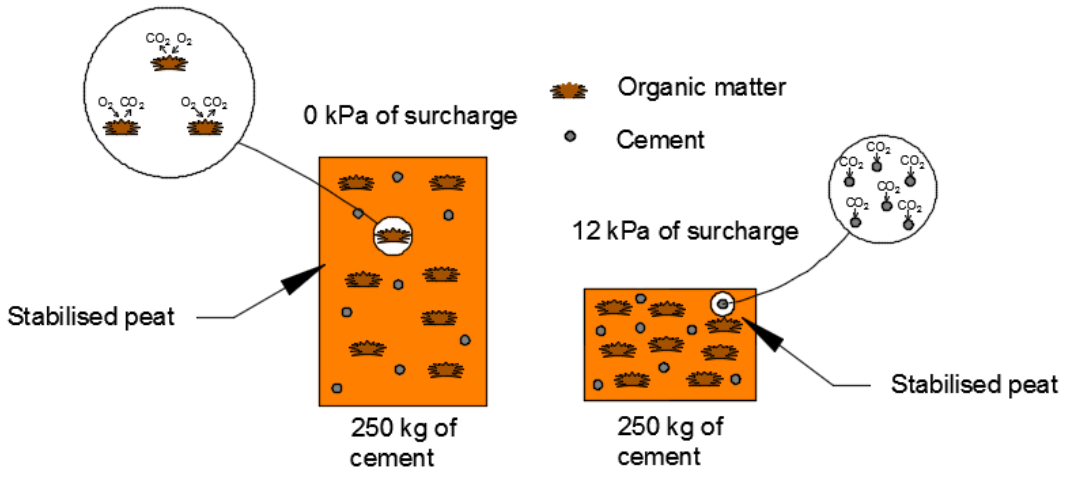

Figure 6.9 - Schematic of unsurcharged and surcharged peat

In addition to their high X_c results and k-rate factors (see Section 6.2), the greatest CO_2 intake flux was also from the surcharged specimens. Surcharged specimens had the highest CO_2 intake rate due to a more rapid intake of CO_2 into the cement as a result of their lower porosity and saturated moisture content and, consequently, there was a shorter distance for

Ca^{2+} and CO_2 to meet, creating a higher diffusion concentration gradient that requires more atmospheric CO_2.

6.5.2 Effect of cement content

There was no trend for increasing X_c (see Equation 5.3) and increasing k-rate factors with cement, although for the CO_2 fluxes discussed in Chapter 4 an increase in cement content led to an increase in CO_2 intake due to a greater carbonation potential. The absence of a difference in X_c may be as a consequence of two opposing effects: (i) Ca^{2+} and CO_2 having to travel further to meet each other in specimens with 150 kg/m^3 of cement binder compared to specimens with 250 kg/m^3 and (ii) in specimens with 250 kg/m^3, there are more calcium ions to carbonate.

6.5.3 Effect of GGBS content

While GGBS content was not a significant variable in reconstructing X_c, the higher GGBS content specimens a7 and A7 (75% GGBS, 25% cement) had greater k-rate factors than the lower GGBS content specimens a6 and A6 (25% GGBS, 75% cement) for the small and large specimens even though the large specimens A7 had a lower CO_2 intake rate than A6 due to their smaller carbonation potential. It is this difference in carbonation potential that gives specimens a7 and A7 greater carbonation depths. The same binder content (250 kg/m^3) was added to a6, a7, A6 and A7, but the carbonation depth front increased faster in a7 and A7 due to the lower availability of Ca^{2+} to be carbonated.

6.5.4 Effect of a high water table

Water table is an established factor in the carbonation process (Section 2.7.1.4): a high water table decreases the rate of carbonation. In stabilised peat, a high water table was shown in Experiment B to lower the CO_2 intake flux and decrease X_c.

6.5.5 Effect of a high pH on the peat emission rate

As a result of the high pH of the stabilised peat, it is likely that the peat emission rate was slightly different than in raw peat. Microbial activity in peatlands is retarded by high acidity which is why rich fen peat is more likely to be highly decomposed than acid bog peat (Hobbs, 1986). The former is alkaline, hence it has a greater emission rate. According to Wardwell et al. (1983), decomposers are most active over the pH range 7.0–7.5. It was suggested by Pichan & O'Kelly (2012) that a pH greater than 7.5 would inhibit the growth of microorganisms and microbial activity, but this did not seem to be the case as highlighted by the X_{oc} values in the stabilised peat, which were in the range of X_{oc} values obtained from two drained raw peat specimens. It is possible that the bacteria involved in decomposition in stabilised peat are different to the kind involved in raw peat.

6.6 The use of carbonation depth techniques on stabilised peat

6.6.1 Advantages and disadvantages of carbonation depth techniques

The carbonation depth techniques and the intercept method worked best on the surcharged specimens for all the techniques, primarily due to their carbonation front being much sharper and hence easier to identify than the unsurcharged specimens. The fronts in these specimens were similar to those in concrete due to the higher densities and lower saturated moisture contents.

There were advantages and disadvantages to the carbonation depth techniques examined in this study, some of which are displayed in Table 6.5. The phenolphthalein indicator test, unlike XRD and FTIR, is a quick and cheap way of examining X_c in stabilised peat and shows the carbonation front across the whole specimen but underestimates X_c and is based only on visual inspection. Due to the colour of stabilised peat, differentiating between colour changes at the carbonation front was sometimes problematic, making it difficult to pinpoint. This problem can also be encountered in concrete where dark-coloured aggregates can create dark concrete mixes, hence colour differences can be less obvious (Broomfield, 2007).

XRD and FTIR measure X_c by examining $CaCO_3$ indirectly and are, therefore, appropriate techniques to calculate X_c: XRD measures X_c by examining the relative intensities of $CaCO_3$ and $Ca(OH)_2$ and FTIR by examining the calcite/portlandite ratios. The LOI technique proved more suitable than either XRD or FTIR as it pinpoints the first signs of carbonation directly by measuring the difference in $CaCO_3$ mass loss and gives the initial degree of carbonation in the supposedly uncarbonated zone. However, in addition to being a destructive technique, another downfall is its inability to locate the temperature range where $CaCO_3$ decomposes.

On the other hand, the pH of stabilised peat slurries technique was found not to give X_c but a depth at which leaching of Ca^{2+} to the carbonation front occurs. It may give an X_c value in dry stabilised peat where carbonation is more to do with O_2 and CO_2 ingress than Ca^{2+} leaching due to lack of water available for leaching. As explained in Section 5.3.5, this method does not work well for stabilised peat with a low binder content or for stabilised peat containing GGBS.

While porosity readings revealed little information about the carbonation front, the water evaporation method helps highlight changes in the properties of the stabilised peat under hydration and carbonation. These properties are good representations of the specimens because the whole specimen is being used. On a smaller scale, porosity could be used to

show X_c if specimens were cut in 10 or 20 mm sections before being used in the water evaporation method, but this was not attempted. A difference in porosity with depth would indicate a carbonation front. This method may work better in older stabilised peat where a large X_c is expected. Otherwise, the water evaporation method can be used only as an indicator of carbonation over time.

Table 6.5 - Advantages and disadvantages of each carbonation front depth technique

Technique	Advantage	Disadvantage
Phenolphthalein indicator	• Quick • Cheap • Readily available • Can see full carbonation front • Not destructive	• Underestimates X_c • Does not work well on stabilised peat specimens with GGBS or low levels of cement • Only based on pH
XRD	• Shows the crystalline material makeup of the specimen • Can use the relative intensities of $Ca(OH)_2$ as a backup to locate X_c • Not destructive as only small sample used	• Expensive • Not readily available • Small sample analysed (may not be representative of the level of carbonation at this depth)
FTIR	• Quick • Shows the makeup of the specimen by way of chemical bonds • Not destructive as only small sample used	• Not readily available • Small sample analysed (may not be representative of level of carbonation at this depth)
LOI	• Readily available in most labs • Directly records increases in $CaCO_3$ concentrations by CO_2 mass loss • Shows initial carbonation in supposed uncarbonated zone	• Difficult to pinpoint temperature range at which $CaCO_3$ decomposes • Destructive technique
pH of stabilised peat slurries	• Quick • Cheap • Shows depth at which Ca^{2+} ions are leaching to the carbonation front	• Does not give X_c value • Does not work well with stabilised peat specimens that contain GGBS • Does not work well with stabilised peat specimens that have a cement content of < 200 kg/m^3
Porosity (Water evaporation method)	• Cheap • Shows stabilised peat properties such as dry density, porosity and saturated moisture contents • Can show signs of carbonation	• Poor estimator of X_c (may be a good technique in older stabilised peat with a large X_c value)

In summary, with the exception of the phenolphthalein indicator technique, the XRD, FTIR, LOI and pH of stabilised peat slurries techniques are more expensive in terms of time, skill and cost. The use of the phenolphthalein indicator as a carbonation depth technique and the use of ratios for FTIR and relative intensities for XRD have been applied to concrete by several authors (Sections 2.9.2, 2.9.3 and 2.9.4) but were applied to stabilised peat for the first time in this body of work. These proven techniques for concrete and the LOI and pH of stabilised peat slurries techniques are as of yet unproven for

stabilised peat, and only their continual application to stabilised peat will confirm their robustness.

6.6.2 Incorporation of the mass loss between 520 and 650ºC in LOI

As stated in Table 6.5, it is difficult to pinpoint the temperature range at which $CaCO_3$ decomposes as $CaCO_3$ in stabilised peat decomposes at slightly different temperature ranges from sample to sample. The more conservative option of using only the mass loss between 650 and 850ºC is recommended to calculate D_c and thus X_c, but this range may underestimate the amount of carbonation. However, if other techniques such as FTIR and XRD are used in tandem with LOI, combining the mass loss between 520 and 650ºC with the mass loss between 650 and 850ºC to calculate X_c is recommended, but only if two of the three criteria outlined in Section 5.3.4.3 are met. For instance, many of the samples analysed after 20 days contained an amount of $Ca(OH)_2$; therefore, the mass loss between 520 and 650ºC should be excluded in these instances in case of an overlap between $Ca(OH)_2$ and $CaCO_3$ decomposition.

It is more likely in stabilised peat containing GGBS than in cement-only specimens that carbonation will be underestimated if the mass loss between 520°C and 650°C is not included as more vaterite (less stable than calcite) is produced in specimens with GGBS and decomposes at a lower temperature range than calcite.

It is noteworthy that the long-term effect of CO_2 on stabilised peat is the likely formation of calcite that is more stable than the calcite formed in the short term, which may require temperatures of up to 950°C to fully decompose the $CaCO_3$ (Section 2.9.5.5). Nevertheless, for the stabilised peat analysed in experiments in this research, the mass loss between 850 and 950°C was negligible. This is evident in Figure 3.19 in Chapter 3 where a5(3c) was one of the most carbonated specimens analysed. Future use of the LOI technique on stabilised peat may require more TGA analyses, especially if the stabilised peat is older than 180 days (the duration of Experiments A and B).

6.6.3 Future use of XRD and FTIR

One downside to the XRD and FTIR technique is the small amount of sample needed for the analysis (Table 6.5), which may result in incorrectly identifying the position of the carbonation front as the front may not be horizontal. For instance, samples analysed may have been taken from an uncarbonated portion in a mostly carbonated zone or vice versa. This was noticeable when using the phenolphthalein indicator as pink and purple spots were sometimes visible in a region where the indicator remained mainly colourless. Based on observations made during the experiments, it is advisable, therefore, in future stabilised

peat studies to analyse at least three samples from positions evenly spaced across the carbonation front to guarantee a more comprehensive examination of the front.

Quantitative XRD methods, such as the external or internal method could be applied to stabilised peat to quantify the $CaCO_3$ concentration, which could then be used to calculate X_c. The external method compares the $CaCO_3$ experimental line intensity from the material in question (stabilised peat) to a line from a pure phase (pure $CaCO_3$). However, the application of this method necessitates many TGA analyses to calculate mass absorption coefficients for each type of stabilised peat at certain points in time, which was beyond the scope of this study.

6.6.4 Future use of the phenolphthalein indicator

Prompted by experience from work carried out in this research, two modifications to the phenolphthalein indicator techniques are proposed. As a result of the variability of peat and the inhomogeneity of the cement in the peat, the carbonation front may vary in depth from one side of a specimen to the other. Due to the non-horizontal, uneven carbonation front displayed in 13% of the specimens, it is proposed for stabilised peat that five measurements should be taken across the front instead of three.

Another option is the use of weighted averages that would account for the different carbonation front depths and the different widths of the carbonation front at these depths and would, as a consequence, enhance the representation of the carbonation depth. In the two carbonation fronts highlighted in Figure 5.5, employing a weighted average system, X_p remains the same for a5(2c), but X_p changes from 17 mm to 13 mm for b2(2c), a difference of 24%.

6.6.5 Other techniques used to assist in carbonation recognition

6.6.5.1 Introduction

A more precise method of evaluating the degree of carbonation is a combination of TGA and chemical analysis (TGA-CA) discussed in Section 2.9.5.6, but a suitable TGA machine was not available at NUIG to examine this method in depth. These analyses also have sizeable cost implications, and the method is inefficient for large-scale work due to the time it takes to process samples. Acid digestion is another method that may be employed to calculate the carbonate content but was not used because it was also thought not to be an efficient method for large-scale work. In this research, TGA-CA and SEM-EDX were examined briefly to discover how they could be employed to help to in carbonation recognition and provide extra information on the stabilised peat specimens:

TGA-CA can be used to calculate quantitative carbonation depth profiles, and SEM-EDX gives more information on the properties of the stabilised peat.

6.6.5.2 TGA-CA

Besides employing TGA to find the appropriate temperature range for the decomposition of $CaCO_3$ (Section 3.5.4.6), it can also be used to calculate the $CaCO_3$ concentration of a sample. On using the TGA graphs displayed in Figure 3.19 to develop the temperature ranges, it was possible to calculate the $CaCO_3$ concentration at d = 0 mm and d = 50 mm for a5(3c) (chosen for reasons discussed in Section 3.5.4.6). Using the mass loss between 650 and 850ºC and molecular proportions, the $CaCO_3$ concentration of samples at d = 0 mm was 2692 moles/m^3 and at d = 50 mm was 1372 moles/m^3.

TGA-CA, described in Section 2.9.5.6, was then undertaken to find the cement content at each depth and thus determine relatively accurate D_c values in the samples at d = 0 and d = 50 for a5(3c). Chemical analysis by Inductively Coupled Plasma – Atomic Emission Spectroscopy (ICP-AES) was performed on a replicate specimen a5(3b) with 200 mg samples taken at 0, 5 and 10 mm in the carbonated zone and 20 mm in the uncarbonated zone (Table 6.6). Ideally, the analyses would have been performed on a5(3c) at d = 0 mm and d = 50 mm, but at the time of the analyses, the only reason for the chemical analysis was to find the general chemical properties of stabilised peat. This section is only a guide to how TGA-CA can be applied as a method to get accurate quantitative carbonation profiles in stabilised peat and was not used to obtain X_c values in this research.

Table 6.6 - Chemical and physical properties of a5(3b)

Results of chemical analysis (%)	D = 0	D = 5	D = 10	D = 20
Silicon dioxide, SiO_2	7.88	11.2	11.75	12.25
Aluminium oxide, Al_2O_3	2.14	2.68	2.8	2.96
Ferric oxide, Fe_2O_3	1.3	1.62	1.7	1.75
Calcium oxide, CaO	39.7	34	36	39.8
Magnesium oxide, MgO	1.13	1.32	1.44	1.44
Sodium oxide, Na_2O	0.28	0.13	0.02	0.02
Potassium oxide, K_2O	1.07	0.78	0.16	0.1
Chromium oxide, Cr_2O_3	<0.01	<0.01	<0.01	0.01
Titanium dioxide, TiO_2	0.11	0.13	0.14	0.15
Manganese oxide, MnO	0.02	0.02	0.02	0.02
Phosphorus pentoxide, P_2O_5	0.03	0.04	0.05	0.04
Strontium oxide, SrO	0.06	0.03	0.02	0.02
Barium oxide, BaO	0.02	0.01	0.01	0.02
Loss on ignition at 1000°C	47.4	47.2	42.9	41.1

As described by Villain et al. (2007), the following main tracers of cement can be used to determine the cement content in an uncarbonated material: SiO_2, CaO, and Al_2O_3. In the carbonated material, SiO_2 cannot act as a tracer as it forms insoluble products such as silica gels produced by CSH carbonation which are not detectable by ICP-AES. This is evident

in Table 6.6 for a5(3b) as SiO_2 increases with depth as carbonation decreases with depth. Villain et al. (2007) advises not to use CaO as a tracer in carbonated material in concrete because of the presence of $CaCO_3$ in the aggregates. Since there are no aggregates in the stabilised peat, CaO can be used as a tracer. Al_2O_3 is another potential tracer for concrete because no other product contains Al_2O_3, but in stabilised peat Al_2O_3 is present in relatively small amounts, so CaO is the preferred tracer.

Adopting CaO as a tracer, the CaO content of the sample at d = 0 mm in a5(3b) (39.7%) (Table 6.6) was divided by the CaO content of the cement used in Experiment A (62.5%) to get the cement content at the surface (d = 0 mm), which in this case was 63.5%. Applying Equation 2.14 and molecular proportions, the maximum $CaCO_3$ concentration that can occur at the surface was 2400 moles/m^3. The difference between the TGA result of 2692 moles/m^3 for a5(3c) and the ICP-AES result of 2400 moles/m^3 for a5(3b) was 12%, showing the sample at 0 mm in a5(3c) to be 112% carbonated. The reason for the carbonation level to be above 100% is likely due to the difference in cement content at the surface between a5(3c) and a5(3b). Regardless, it can be assumed that the stabilised peat in a5(3c) was nearly or fully carbonated as a5(3b) and a5(3c) were made from the same mix and were under the same environmental conditions. From the LOI technique that assumes homogeneity of the cement in the stabilised peat and by including the $CaCO_3$ mass loss between 520ºC and 650ºC, the percentage carbonated (D_{CSH}) for a5(3c) was 99% for the 0–5 mm sample which concurs with the TGA and ICP-AES result.

For the sample at d = 50 mm for a5(3c), the CaO content was taken as the average of CaO values from the samples analysed under ICP-AES for a5(3b) which was 37.4%. Using Equation 2.14, the maximum $CaCO_3$ concentration that could occur was 2260 moles/m^3. Dividing the $CaCO_3$ concentration at this depth (1372 moles/m^3) by the maximum concentration, the sample was found to be 60.7% carbonated, assuming that the cement content in a5(3b) and a5(3c) were the same at this depth. From the LOI technique, the average D_{CSH} for the 40–50 and 50–60 mm samples was 60.7%, showing a difference of less than 0.1% between the TGA-CA and the LOI result.

In summary, it is recommended that future application of this technique uses CaO as a tracer as long as there is no aggregate present. A combination of TGA and CA can produce accurate quantitative carbonation depth profiles, calculating D_c at a higher degree of precision than the LOI technique. X_c is then calculated in the same way as for the LOI technique, the only difference being the use of a more accurate D_c with depth plot.

6.6.5.3 SEM-EDX

Scanning Electron Microscope (SEM) and Energy Dispersive X-Ray Spectrometer (EDX) techniques were used to look more closely at the carbonated and uncarbonated stabilised peat. SEM-EDX was performed on a5(3b) at d = 0, 5, 10, 20 and 50 mm and for samples between 0 and 20 mm for some of the large specimens in Experiment A. Figure 6.10 shows SEM-EDX images for a5(3b) at d = 5, d = 20 and d = 50 mm, with the products of hydration and carbonation and the organic material clearly visible. It may also be possible to see insoluble reaction products on the organic material, products that precipitate on the organic material after humic acids react with $Ca(OH)_2$ (see Figure 6.10(a)) (Section 2.7.2.3).

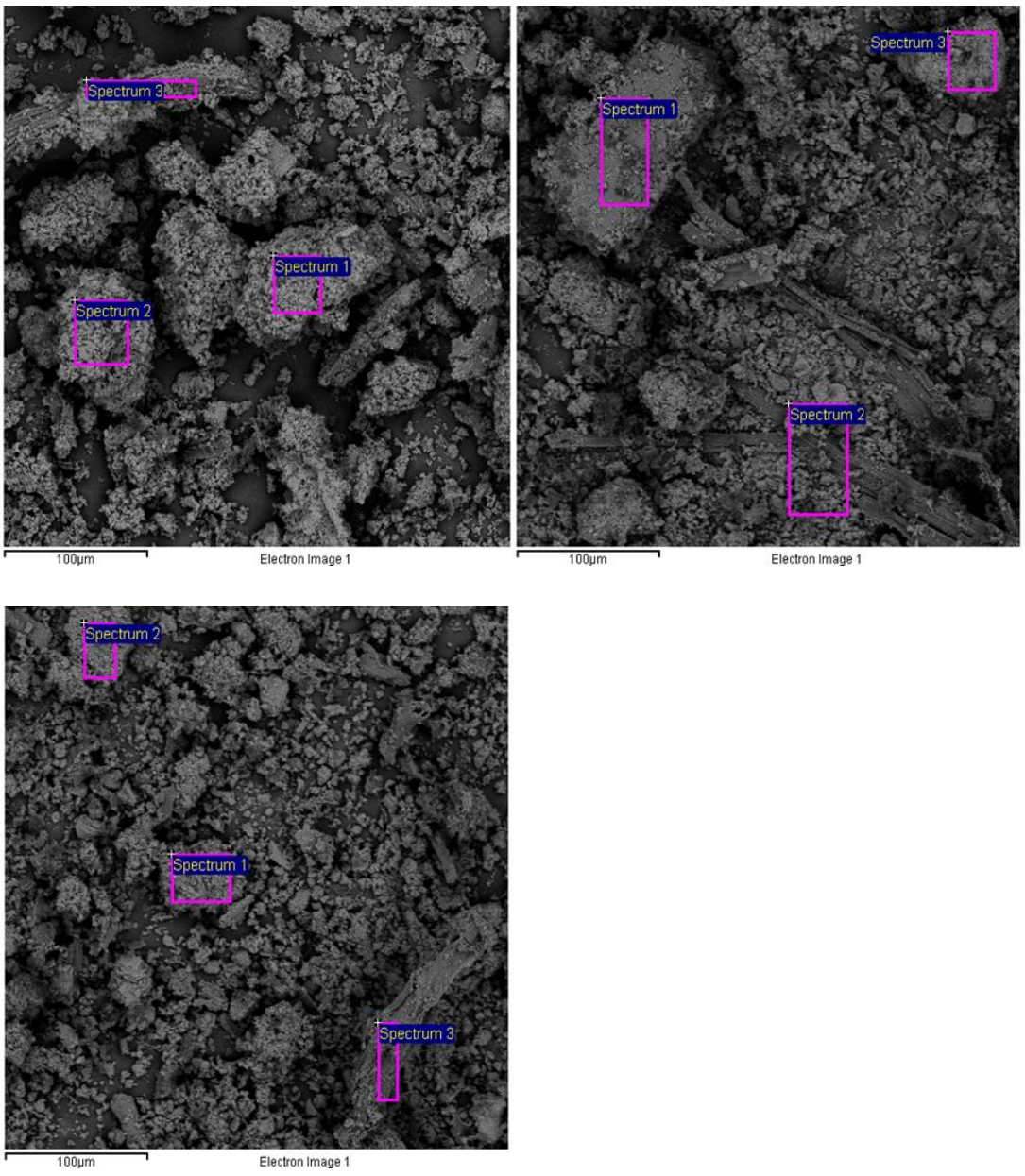

Figure 6.10 - SEM photos for a5(3b) (a) d = 5, (top left) (b) d = 20 (top right) and (c) d = 50 (bottom left)

The elemental properties (% by weight) of some of the hydrated and carbonated products and the organic material were obtained (Table 6.7) and are highlighted by the spectrum squares in Figure 6.10. Spectrum positions on organic matter had higher carbon values and lower calcium values than the large hydrated and carbonated products. The organic matter, however, exhibited higher calcium values than anticipated, which may strengthen the argument that humic acids were reacting with $Ca(OH)_2$ in the organic matter (Section 2.7.2.3). Higher calcium values were observed near the surface of the specimens, which may indicate leaching of Ca^{2+}, a trend also present in the results of the analyses performed on the large specimens. Besides the reported values for C, Ca, O, Mg, Al in Table 6.7, other elements found in the stabilised peat were Fe and S.

The elemental composition of some of the stabilised peat in the first 0–20 mm of some of the large specimens in Experiment A are available in Appendix E9. For the carbonated and hydrated products, there were significantly higher silica values ($p = 0.000$) for the specimens with GGBS. SEM-EDX is cheaper than ICP-AES, but the main disadvantage of EDX compared to ICP-AES is that due to the tiny samples analysed for EDX and the variability of the elemental composition, the elemental composition is not representative of the whole material at that depth, hence a cement and CaO content cannot be accurately inferred.

Table 6.7 - Elemental composition of spectrums highlighted in Figure 6.10 for a5(2b) (Weight percentages)

Spectrum No.	Elements					
	C	**O**	**Mg**	**Al**	**Si**	**Ca**
Depth = 5 mm						
1	14.03	43.21	0.69	1.42	5.23	43.21
2	9.76	40.56	0.61	1.69	7.24	40.56
3	18.60	47.13	0.61	1.07	4.86	47.13
Depth = 20 mm						
1	39.77	42.28	0.25	0.59	1.44	15.68
2	33.16	41.67	0.24	0.81	3.53	19.49
3	21.10	44.35	1.00	1.63	6.34	21.81
Depth = 50 mm						
1	24.05	43.87	0.29	1.12	6.21	22.53
2	22.97	42.76	0.34	1.17	6.51	22.79
3	33.11	37.69	0.48	1.06	3.12	22.68

6.7 Summary

The CO_2 flux results and X_c results first presented in Chapters 4 and 5 respectively were analysed and discussed further in this chapter by examining the relationships between CO_2 flux results and X_c results. Significant relationships were found between average CO_2 fluxes and X_c for the specimens with the same binder type and content. This was

particularly evident for the specimens with greater than 250 kg/m^3 of cement binder. The percentage carbonated (D_c) at the surface was also significantly related to the CO_2 flux.

The drier nature of the small specimens than that of their large specimen counterparts was the primary reason for the difference in X_c results. k-rate factors were then developed in order to estimate X_c at any point in time. The CO_2 flux and X_c results will now be incorporated into an LCA on a case study of a road construction project on peatlands in Chapters 7.

A hypothesis for the reasons for the varying carbonation depths was outlined to assist in understanding the carbonation process in stabilised peat under various binder types and contents and environmental conditions. Finally, the advantages and disadvantages of each carbonation depth technique were discussed, and a method of applying the carbonation depth technique TGA-CA to stabilised peat was also presented.

Chapter 7: Life Cycle Assessment (LCA)

7.1 Introduction

7.1.1 Overview

This chapter outlines a novel life cycle assessment (LCA) methodology that allows a quantitative comparison of the potential environmental impacts of various ground improvement and foundation options for road construction on peat, including excavate-and-replace (ER), dry soil-mixing (S) and piling (P). The methodology incorporates some peat-related factors not examined previously in this type of environmental assessment and is applied to a case study on a section of a recent Irish motorway project for which the excavation and replacement of peaty soil was the chosen solution (Scenario ER). Section 7.1.2 gives details of the scheme layout, the geology of the site and of the road construction. Results are presented for total embodied energy (EE) and embodied carbon (EC) for the case study (Scenario ER) and for the alternative ground improvement and foundation scenarios, soil mixing (Scenario S) and a combination of excavate-and-replace and piling (Scenario ER + P).

Section 7.2 describes how EC and EE intensity values are produced for each factor affecting the carbon and energy calculations needed to compile the life cycle inventories for Scenario ER, S and ER + P. These factors include: materials, transport, machinery and the peat-related factors of peat drainage, drainage systems, slope stability, peatland restoration techniques, and forest and vegetation. The results from Chapters 4, 5 and 6 are integrated into developing the novel methodology and to completing the life cycle inventory for Scenario S, which allows a more accurate quantification of the environmental impact of peat stabilisation.

The bulk of the content of this chapter has been published in Duggan et al. (2015); but by incorporating the results from Chapters 4, 5 and 6 into Scenario S, this chapter represents a more developed version of the published work.

7.1.2 Case study: M6, Pollboy section

7.1.2.1 Introduction

The M6 Galway to East Ballinasloe motorway scheme in the West of Ireland was the final stage of an overall route, approximately 190 km long, connecting Dublin to Galway. The scheme comprised of 56 km of motorway, a 7 km link road to Loughrea and 32 km of side and link roads (RPS Group, 2004). The mainline is a four-lane dual carriageway with a pavement width of 22 m and verges of 2 m in accordance with National Roads Authority guidelines in Ireland (NRA, 2013). Peat underlay approximately 4% of the route. The

study section considered in this chapter is 2.14 km long, in an area of predominantly peaty soil at Pollboy, south of Ballinasloe (approximately 53º18′59″N, 8º13′55″W to 53º18′49″N, 8º12′01″W; Chainage (Ch.) 52,210–54,350, see Figure 7.1). Peat excavate-and-replace (henceforth referred to as Scenario ER) was chosen as the ground improvement technique.

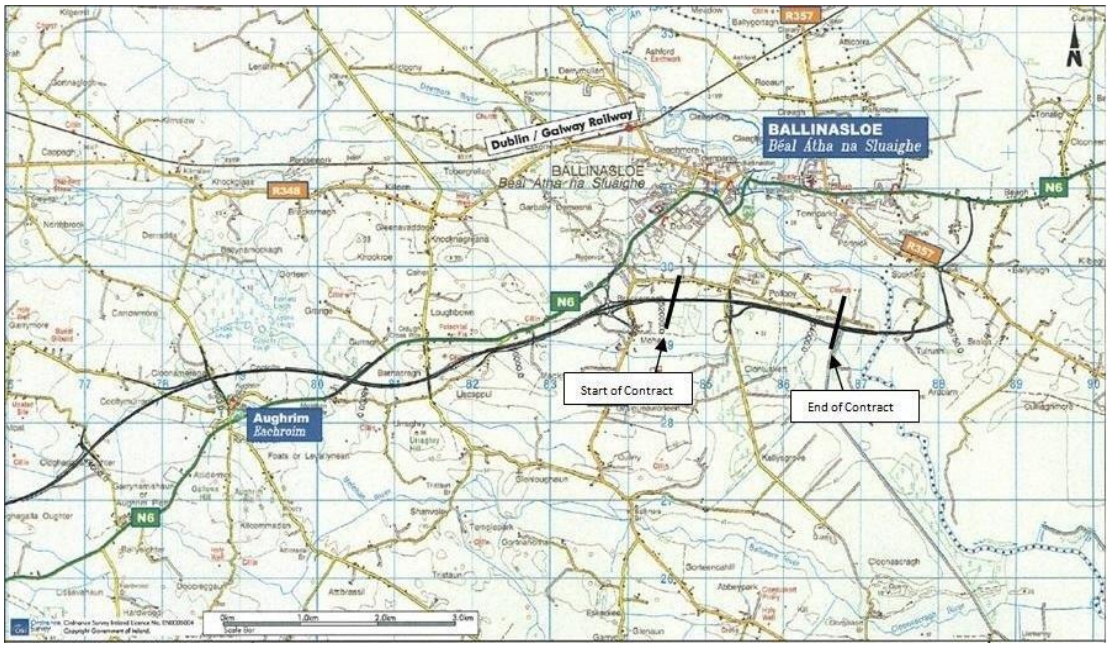

Figure 7.1 - Location of the M6 motorway and the Pollboy Contract, adapted from RPS (2004)

7.1.2.2 Geology

The road section lies in the River Suck catchment, with the River Suck about 2 km to the east. The mean annual rainfall is approximately 1150 mm; the mean annual evaporation loss is 460 mm; and the average annual temperature is 9.8ºC (RPS, 2004). The site has a slope of around 0.5º from north to south and is located in wet land that includes a mixture of drained reclaimed and unreclaimed fields with an underlying layer of peat and peaty clay, hereafter referred to collectively as peat. This site also borders the Pollboy cutover bog (Ch. 52,930–53,530). The peatlands had previously been drained, leaving the water table level below the peat layer (Figure 7.2). Between the start of the section and the River Suck, a significant thickness of alluvial material overlain by peat deposits prevails. In general, good ground conditions exist north of the road alignment and poorer conditions to the south. Peat in the area was found to have moisture contents ranging between 500% and 1000%, organic contents from 25% to 80%, oedometer coefficients of volume compressibility (m_v) values of approximately 2–4 m^2/MN, and oedometer coefficients of consolidation (c_v) values of 0.9–1.5 m^2/year.

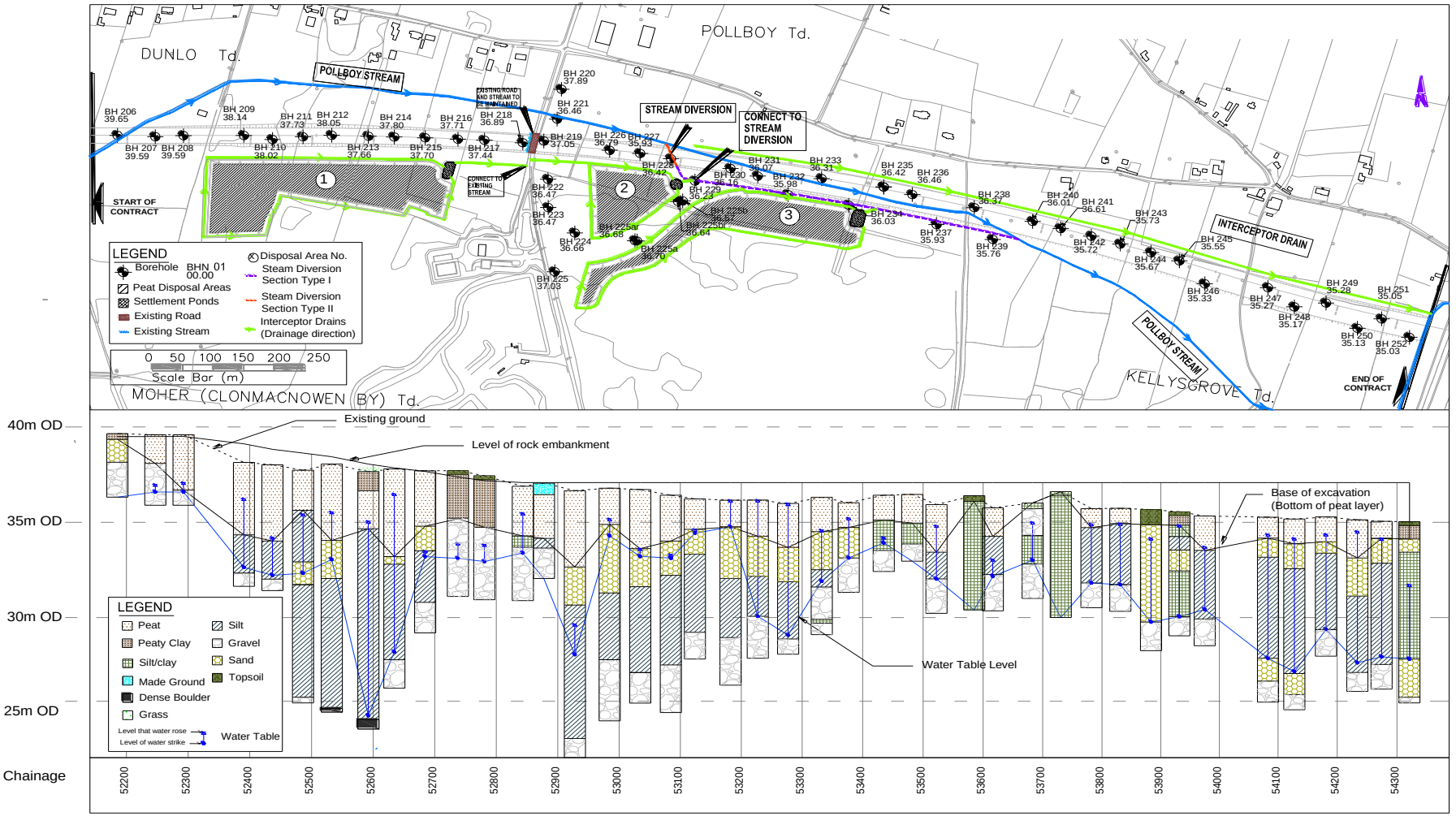

Figure 7.2 - Plan and cross section of contract

7.1.2.3 Road construction and ancillary details

An estimated 115,000 m^3 of peat was excavated for the motorway mainline and replaced with 170,000 m^3 of engineered-fill material from nearby quarries (the extra 55,000 m^3 was used to establish a higher foundation level for the sub-base). The excavated volumes necessitated three peat disposal areas along with drainage works comprising of ponds and infiltration ditches. These additional excavations as well as a stream diversion accounted for an additional 20,173 m^3 of excavated peat. Two wet fields and an open area of moor grass-covered bog south of the alignment were chosen to site the embankments, which have side slopes of 1:4 and a maximum height of 2 m. A plan identifying these elements of the scheme is shown in Figure 7.2. A birch/willow woodland was subsequently planted on the peat disposal areas to blend in with the surrounding landscape.

The road embankment has a maximum height of 4.2 m and incorporates a geogrid for extra strength (Figure 7.3(a)). Deep deposits of soft silt/clay underlay the peat layer in three zones located at the following chainages: Ch. 52,400–52,700, Ch. 53,000–53,350, and Ch. 53,770–54,430 (Figure 7.2). Since the soft silt/clay has c_v values ranging from 2 to 5 m^2/year, prefabricated vertical drains (band drains) were required to accelerate drainage under embankment loading. A drainage blanket of 1.5 m in height was employed to lay the band drains in these three parts of the section (Figure 7.3(b)).

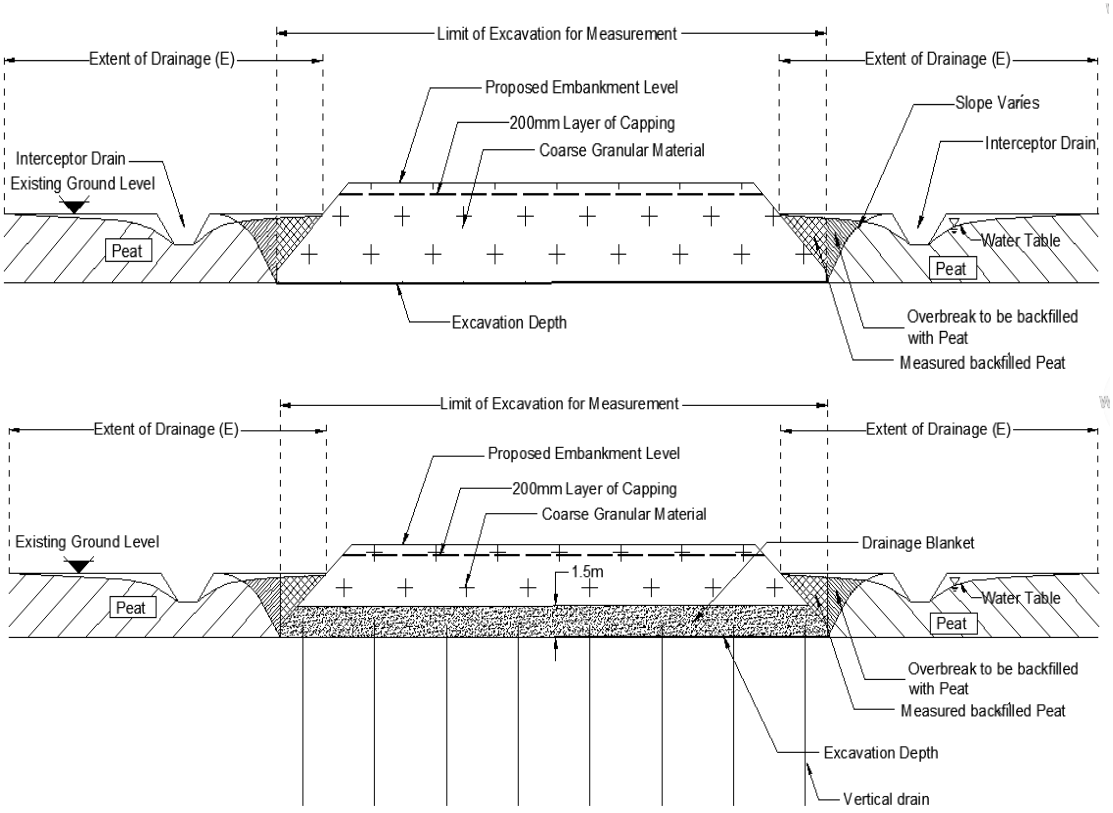

Figure 7.3 - Typical cross sections of (a) rock embankment (top) and (b) rock embankment with vertical drains (bottom) (Courtesy of RPS Group)

The drainage system consists of retention ponds, infiltration ditches and two types of stream diversion. The retention ponds are 0.5 m deep, with a 1:4 side slope and are lined with a permeable geotextile and a 150 mm depth of rockfill. The infiltration ditches around the peat disposal areas have a base width of 1 m, are 1 m in depth and have a 1:1 side slope. As the road alignment crossed a stream, two types of stream diversion had to be built, requiring the excavation of peat to a depth of 2 m in the first type and to 2.5 m in the second. Both types have side slopes of 1:2, with the latter requiring the laying of an impermeable geomembrane and a 150 mm depth of rockfill lining.

7.1.3 Goal and scope definition of LCA

The goal of the study is to present a methodology that geotechnical engineers can deploy on projects to determine the environmental impact of road construction in areas of highly organic soils, where EE and EC are used as indicators. To this end, the construction of a control segment of the aforementioned M6 scheme is utilised as a case study to highlight the key considerations in performing environmental LCAs for this application. While excavate-and-replace was adopted in the contract, the study has been extended by also considering potential EE/EC associated with alternatives, such as dry soil-mixing and piling, and other ancillary activities. For the purposes of this study, the entire 2.14 km section was examined, but a functional 1 km unit was also considered. The calculations have been performed using LCA methodology conforming to ISO 14040 (BSI, 2006a).

The function of the scheme is to support pavement layers and vehicular traffic, while meeting the engineering specifications set out by the NRA in Ireland (NRA, 2013). The functional unit is defined in this study as a kilometre of motorway operational for 120 years. According to the HA (1991), the design lifetime of geotechnical structures such as embankments should range from 60 to 120 years. Based on the upper limit of this standard, the boundary of the LCA study starts at the extraction of raw materials and ends when the design lifetime of the road foundation expires after 120 years.

By LCA streamlining (defined in Section 2.5.5), the system boundary was reduced to examine primarily the difference in environmental impact between ground improvement techniques using the indicators EE and EC. Only aspects of the road construction to the subbase level and related implications were included in the calculations. Pavement layers were common to all ground improvement scenarios considered and were, therefore, excluded in the interests of clarity.

This study adopts the process analysis approach utilising a range of published EE and EC intensities, much of which come from the Inventory of Carbon and Energy Version 2.0

(ICE V2.0) (Hammond & Jones, 2011; DECC & Defra, 2012). The system boundaries employed in the study for an excavation and replacement approach (Scenario ER) for road construction on highly organic soil are given in Figure 7.4, where the dotted line represents the system boundary and the solid black arrows indicate transport. Recurring EC and EE in the form of maintenance, such as resurfacing roads, line painting and new signage, were not taken into account as the pavement layers were excluded. Materials, transport and machinery all have cradle-to-site boundary conditions, while direct and indirect emissions on site are taken into account for the full life cycle. Direct emissions originate from the excavated peat, while indirect emissions come from land construction activities such as emissions from ponds, drainage systems, peat disposal areas and roads, some of which may go into direct emissions and some into the restoration category.

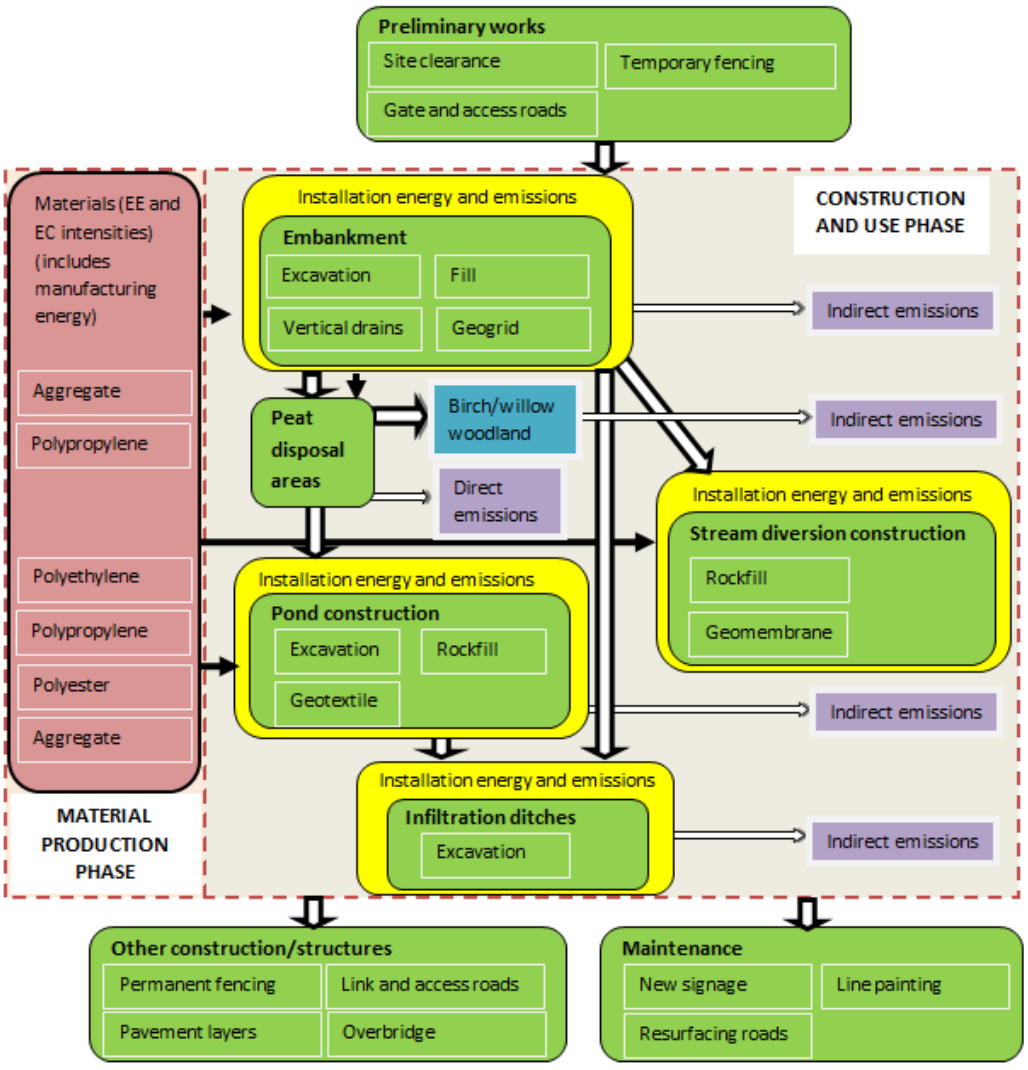

Figure 7.4 - Process flowchart of Scenario ER

Following the establishment of the goals and study boundaries, a methodical examination of the construction stages shown in Figure 7.4 above was undertaken. Once the key processes were identified, data were obtained to quantify each individual process. The box

on the left of Figure 7.4 contains the EE and EC intensities for raw materials used in producing the materials needed for the embankment, stream diversion and ponds. Direct and indirect emissions are illustrated leaving these main unit processes.

7.2 Life cycle inventory

7.2.1 Introduction

This section presents the collection of data for each process included in the product system, as defined in Section 7.1.3 and summarised in Figure 7.4 for Scenario ER. Where possible, data were validated by comparing them with other sources. Data were also collected to compile the life cycle inventories for two alternative ground improvement scenarios which were examined to evaluate the potential environmental impact of using these approaches in the case study. Scenario S used peat stabilisation to support a road embankment (Figure 7.5(a)), while Scenario ER + P involved a combination of peat excavate-and-replace and some piling (Figure 7.5(b)). In Scenario ER + P, piling is only incorporated in the zone Ch. 52,300–52,600, where the depth of peat is greater than 3 m along a significant stretch of road, and peat excavate-and replace was used for the remainder of the section. In this sense, it is a hybrid scenario and should not be considered as exclusively representative of piling. Neither scenario required as many peat disposal areas, retention ponds or ditches as was needed during construction in Scenario ER, as reduced quantities of peat were removed during operations.

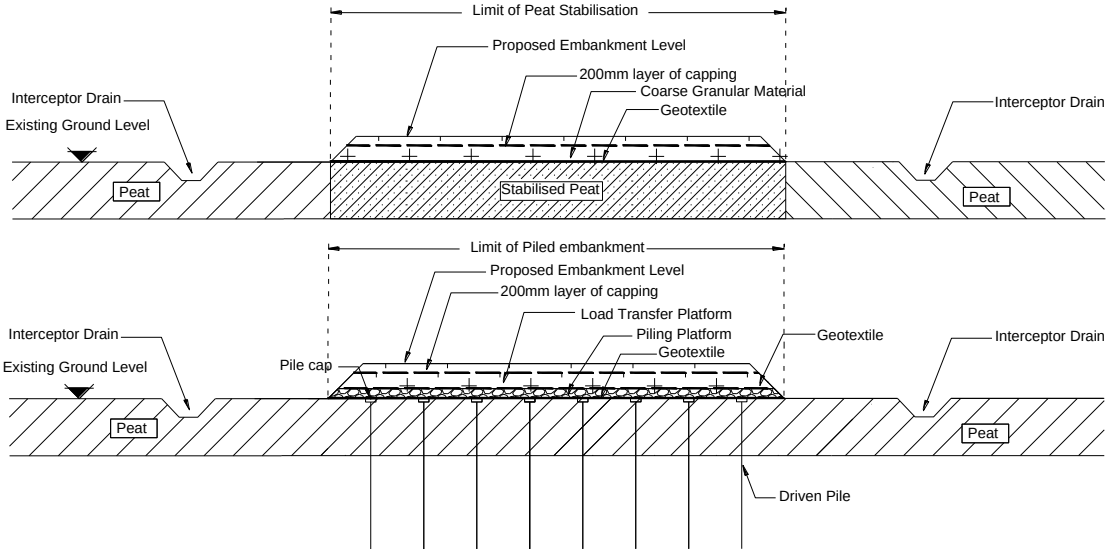

Figure 7.5 - (a) Typical cross sections of a stabilised embankment and (b) typical cross sections of a piled embankment

7.2.2 Scenario ER: excavate-and-replace

7.2.2.1 Materials, transport and machinery

Table 7.1 contains the life cycle inventory (LCI) of the relevant properties of the materials needed for the study. Resulting from uncertainties after product manufacture, it has become common practice to calculate EC and EE intensities for materials right up to when the product leaves the factory (Hammond & Jones, 2011). The aforementioned life cycle profile was adopted in this LCA, using intensities from V2.0 of the inventory (Hammond & Jones, 2011).

The materials employed in Scenario ER (i.e. as constructed) include aggregate, vertical drains, and a geogrid. The 8 m long, 100 mm by 4 mm polypropylene band drains (permeable plastic cores wrapped in filter membranes), installed in a triangular pattern with a centre-to-centre spacing of 1.75 m were imported from the Netherlands via the UK on average weight laden transport (Table 7.1). A polypropylene geogrid was used for the embankment, a polyester geotextile employed for the permeable separating pond liner, and a linear low-density polyethylene (LLDPE) impermeable geomembrane for the stream diversion. These geosynthetics were assumed to have been imported from UK by road and sea over distances given in Table 7.1. A bulk density of 1000 kg/m^3 was adopted for the peat, which was assumed to be transported an average distance of 1.07 km on a rigid truck (> 17 tonnes), a distance equal to half the contract length. The trucks were fully loaded to the peat disposal area and empty on the way back. Table 7.2 gives fuel consumption rates for the use of diesel (UK average biofuel blend), which has an EE intensity of 38.3 MJ/l (DECC & Defra, 2012). Transport distances were kept to a minimum, thereby minimising the environmental cost of transport. All transport by sea was assumed to involve average weight-laden cargo ships.

Since the top pavement layers are not being considered part of the study, machinery such as pavers and compactors were excluded. The EC and EE of machinery are difficult to estimate due to the large variety required in building a motorway. For the purpose of this scenario, only the EC and EE of excavators and band drain rigs were examined (Table 7.3). Transport of machinery to site was not calculated as these values would be similar regardless of the ground improvement method considered.

Table 7.1 - Materials required for Scenario ER

Materials	Density (kg/m^3)	EC intensity ($kgCO_2eq/kg$)	EE intensity (MJ/kg)	Distance on land one way (km)	Transport Vehicle	% Weight Laden	Distance by sea (km)	One or two-way transport	Volume (m^3)
Aggregate	2240	0.0052	0.083	15	Rigid	100, 0*	0	Two	170000
Rockfill	2240	0.0052	0.083	15	Rigid	100, 0*	0	Two	405
	(kg/m^2)								**(m^2)**
Geogrid (PP)	0.4	3.43	99.2	204	Articulated	62	226	One	80000
Geotextile (PE)	0.3	2.54	83.1	204	Articulated	62	226	One	1969
Geocomposite (LLDPE)	0.939	2.08	78.1	204	Articulated	62	226	One	728
Vertical drain	1	3.43	99.2	486	Articulated	62	626	One	10111

* The trucks were 100% loaded from quarry to site and returned to the quarry empty.

Table 7.2 - Fuel consumption rates for heavy goods vehicles and cargo ships (DECC & Defra, 2012)

Transport	% Weight Laden	Payload (t)	Fuel consumption ($kgCO_2eq/t.km$)	Fuel consumption (l/t.km)
Rigid truck (> 17t)	100	9.41	0.146	0.046
Articulated truck (> 33t)	62	11.78	0.103	0.032
Articulated truck (> 33t)	100	19	0.075	0.024
Concrete mixer (> 17t)	100	14.4 (6 m^3)	0.096	0.030
Average cargo ship	60		0.016	0.005
			Fuel consumption ($kgCO_2eq/km$)	**Fuel consumption (l/km)**
Rigid truck (> 17t)	0	0	0.959	0.303
Articulated truck (> 33t)	0	0	0.860	0.272

Table 7.3 - Fuel consumption rates and rates of work for Scenario ER

Machinery	Fuel consumption (l/hr)	Rate (m^3, drains/hr)	Amount (m^3) (drains)
21 tonne excavator	16	100	135173
Band drain rig	45	87.5	16852

7.2.2.2 Drainage and drainage systems

The lateral extent of drainage (E) due to road construction (demarcated in Figure 7.3) was calculated by using Equation 7.1, which was based on 16 previous studies relating E to hydraulic conductivity (K) (Figure 7.6). The equation represents an update by the author of this thesis on a linear fit proposed by Nayak et al. (2008) to eight of these studies:

$$E = 1.527\log^2(K) + 2.84\log(K) \quad \textbf{Equation 7.1}$$

In Equation 7.1, the units of E and K are m and mm/d respectively. Using Equation 7.1 and an average hydraulic conductivity of 200 mm/d (calculated from site investigation data), the extent of drainage was estimated to be 14.6 m from ditches, ponds and any other excavations. However, the extent of drainage has limited relevance for already-drained bogland, and the area will continue to be a net source of greenhouse gases regardless of construction. This drainage equation will, nonetheless, be used in Section 7.4.7 to calculate the environmental impact if the drained bogland had been undisturbed. CO_2 and CH_4 are accounted for in EC calculations, but not N_2O emissions as these are deemed negligible from oligotrophic peatlands (Martikainen et al., 1993).

As discussed in Section 2.6.6, ponds and clogged drainage ditches consisting of algae and other vegetation not regularly maintained tend to produce high CH_4 emissions (Minkkinen & Laine, 2006), exemplified by the ditches at Pollboy (Figure 7.7). Table 7.4 summarises previous studies, some of which include fens which tend to have higher emissions than ombrotrophic peatlands. As the Pollboy section contained plants that are considered a fen species (due to the underlying marl soil), the studies were deemed adequate for use. Emission rates in a temperate climate ranged from 12.7 to 27.3 $tCO_2eq\ ha^{-1}\ yr^{-1}$ (Table 7.4). Thus, an average emission rate of 20 $tCO_2eq\ ha^{-1}\ yr^{-1}$ was assumed for the ditches and ponds at Pollboy for the 120-year life cycle.

For this study, it is assumed only the base of infiltration ditches is covered with water all year round, which will compensate for periods when higher levels are recorded in winter or when lower or no water levels are recorded in summer. In contrast, the ponds are assumed to have a 0.25 m head of water all year round.

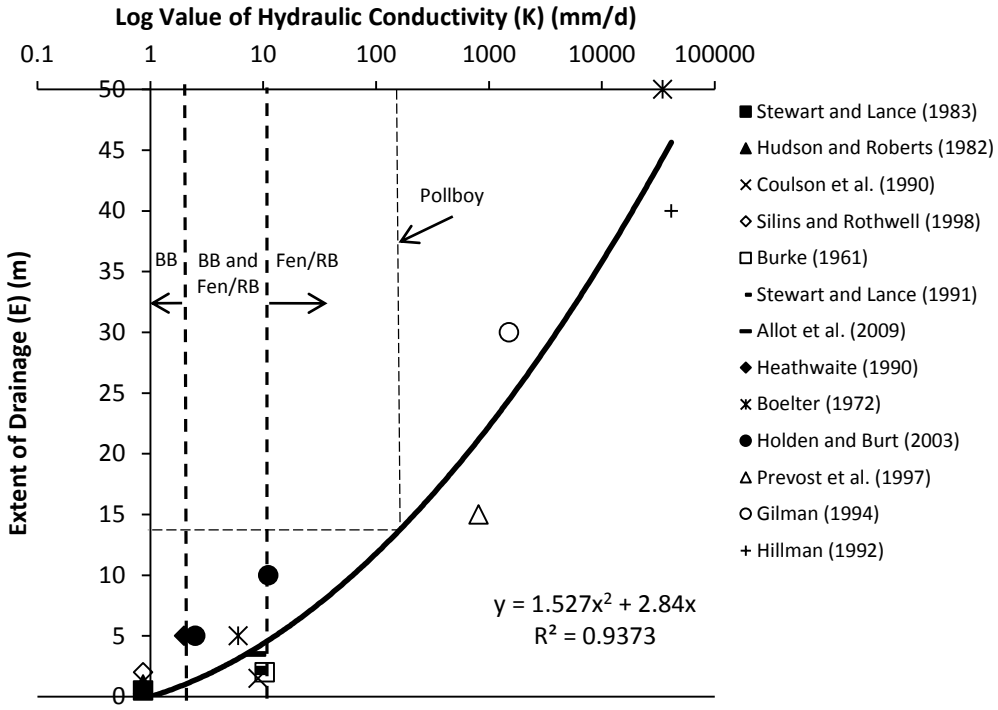

* BB = Blanket bog, RB = Raised bog

Figure 7.6 - Plot of extent of drainage against hydraulic conductivity

Figure 7.7 - Clogged stream diversion shown at front and peat disposal area in background at Pollboy 3 years after construction

Table 7.4 - Emissions from drainage ditches in a temperate climate

Study	Peatland (Nutrient status)	Total ($tCO_2eq\ ha^{-1}\ yr^{-1}$)
Schrier-Uijl et al. (2011)	Mesotropic/eurotrophic status	27.3
Schrier-Uijl et al. (2008)	Eutrophic fen (intensive)	25.4
Schrier-Uijl et al. (2008)	Eutrophic fen (less intensive)	12.3
Hendriks et al. (2007)	Restored agricultural peat meadow	12.7
	Average	**19.4 (~20)**

7.2.2.3 Direct emissions

The loss of carbon as CO_2 from excavated peat is considered a direct emission and should be included in EC calculations (Nayak et al., 2008). Excavated peat that has been under anaerobic conditions starts releasing CO_2 and other gases when exposed to the atmosphere and aerobic conditions (Lindsay, 2010). In this LCA, the percentage of carbon lost from the peat as CO_2 (C_{lost}) was assumed to be 100% as the embankments and their sides are exposed to aerobic conditions, in addition to the high probability that the excavated peat will remain above the water table for the lifetime of the road. The volume of this peat will reduce as a result of primary and secondary consolidation and peat oxidation (Lindsay, 2010). Using the average dry density (ρ_d) of 0.121 g/cm^3 and organic content (OC) of 41%, it was found that the peat had an organic matter density of 0.05 t/m^3, which when divided by a factor (F) of 2.11 gave an embodied carbon content of 0.024 tC/m^3 (0.086 tCO_2eq/m^3). The aforementioned factor refers to the mean of the range of division factors quoted by Schumacher (2002) and is explained in more detail in Section 2.7.2.5. The total CO_2 released EC_{peat} (tCO_2eq) from the volume of excavated peat (V_{peat}) for the 120 years was estimated as 11,670 tCO_2eq using the following equation:

$$EC_{peat} = \rho_d\ V_{peat} \times (1/F) \times (OC/100) \times (C_{lost}/100) \times (44/12) \qquad \textbf{Equation 7.2}$$

Table 7.5 demonstrates why it is plausible that 100% of the peat's carbon may be released over the road's 120-year life cycle. According to this analysis, peat will have released all its carbon as CO_2 in 61–67 years at an emission rate of 20 $tCO_2eq\ ha^{-1}\ yr^{-1}$ (D. Wilson & Farrell, 2007), or, as calculated similarly, in 123–134 years at an emission rate of 10 $tCO_2eq\ ha^{-1}\ yr^{-1}$, which is typical of a drained peatland (Sundh et al., 2000). Had the removed peat from the road and associated drainage systems not been disturbed, it would have produced emissions. This has to be factored into net direct emissions because the focus is the environmental impact of the road, not the natural emissions that would have occurred in the absence of construction. Therefore, after subtracting the CO_2 from these excavated peat areas, the total net direct emissions were 10,885 tCO_2eq (Table 7.6 and Section 7.2.2.4).

Table 7.5 - Calculating the time it takes the excavated peat in the peat disposal areas (PDAs) to release all their carbon as CO_2 at an emission rate of 20 $tCO_2eq\ ha^{-1}\ yr^{-1}$

	PDA1	PDA2	PDA3	Total
Area (m^2)	51000	14805	27500	93305
Max. Vol. of peat (m^3)	94080	29610	50422	174112
Vol. of peat (m^3)	73040	22988	39145	135173
EC of peat (tCO_2eq)	6306	1985	3379	11670
Rate (tCO_2eq/yr)	102	29.6	55	
Duration to emit (yrs)	61.8	67.0	61.4	

7.2.2.4 Indirect emissions

Indirect emissions are related to emissions from land construction activities. These include ponds, ditches, peat disposal areas and the roadway itself. As outlined in Section 7.1.2.2, the three main types of lands existing in the area surrounding the road are cutover bog, wet fields (grassland) and former bogland reclaimed for agriculture, along with other land types of small area, including broadleaf plantation and made ground. Due to the various land-use types surrounding the Pollboy section, it was decided to divide the road section into two land type classifications to simplify calculations. The surrounding land was assumed to be all drained peatland grassland, except from Ch. 52,930 to 53,530, which was considered to be a cutover raised bog. Limited gas studies on emission factors from land types have been performed in Ireland, so Tier 2 country-specific emission factors were used where applicable. However, in cases where there were insufficient studies on a particular land type, emissions factors were taken from the IPCC (Table 7.7).

Although the water table lay below the peat layer (Figure 7.2), there were some pools on the cutover bog. Post construction, it was expected that a small amount of further peat drainage would occur in this area as a result of the road's drainage system, which may cause these pools to disappear. Had the surrounding peatland been undisturbed and not drained, the road's drainage system would have had a much higher impact on indirect emissions, and the peat would have lost its ability to store carbon due to peat drainage. The amount of carbon that could have been sequestered over the life cycle had the road not been built is called the carbon-fixing potential; in this study, it was zero as the site was already drained.

As a restoration technique, birch/willow woodlands were planted on peat disposal areas to blend in with the surrounding area. These woodlands have a low-yield class; consequently, soil emissions are greater than the CO_2 uptake by the woodland. Soil emissions are accounted for to an extent in direct emissions; but once all the CO_2 in the excavated peat is emitted, the peat underneath the peat disposal areas will begin to release CO_2 for the remainder of the life cycle and is accounted for in indirect emissions (Table 7.8). Reported

CO_2 soil emission losses and CO_2 uptake from naturally regenerated woodlands range from 15 $tCO_2eq\ ha^{-1}\ yr^{-1}$ and -6 $tCO_2eq\ ha^{-1}\ yr^{-1}$ at a drained peatland site in Sweden (von Arnold et al., 2005) to 26 $tCO_2eq\ ha^{-1}\ yr^{-1}$ and -8 $tCO_2eq\ ha^{-1}\ yr^{-1}$ at a woody, minertrophic fen site in Ireland (D. Wilson & Farrell, 2007). Soil emissions from fens tend to be higher than from ombrotrophic bogs because the residual peat may be more decomposable (Wilson & Farrell, 2007). Therefore, an average emission factor for soil of 20 $tCO_2eq\ ha^{-1}\ yr^{-1}$ and an average carbon uptake of -7 $tCO_2eq\ ha^{-1}\ yr^{-1}$ were assumed in this study as there were some fen species at Pollboy. A breakdown in calculating the EC for restoration is shown in Table 7.8, which is then used to estimate the total indirect emissions (Table 7.6).

Table 7.6 - Breakdown of indirect emissions for Scenario ER.

	Area (m^2)	**% comprising drained peatland grassland**	**Cutover bog (%)**	**Emissions (tCO_2eq) with the road built**	**Emissions had the road not been built (tCO_2eq)**	**Indirect Emissions (tCO_2eq)**
Ponds	1656	0	100	397	-28[2]	397
Ditches	3890	32	68	934	-58[2]	934
Peat disposal areas	93305	0	100	2886[1]	-1552	-1552
Road	55640	72	28	0	-699[2]	0
Total				1331	-1552	**-221**

[1] Restoration Emissions—figure will go into restoration category.
[2] Already accounted for in direct emissions; otherwise there is double counting of this figure (11670-699-28-58 = 10885 tCO_2eq).

Table 7.7 - Emission factors for various land types

Land type	**Tier**	**CO_2 uptake ($tCO_2eq\ ha^{-1}\ yr^{-1}$)**	**CO_2 loss ($tCO_2eq\ ha^{-1}\ yr^{-1}$)**	**References**
Ditches/Ponds	2		20	Table 7.4
Cutover raised bog	1		1.39	IPCC (2006), IPCC, (1997)
Rewetted Industrial Cutaway	2	-0.5		Kiely et al. (2009), Koehler et al. (2011)
Drained peatland grassland	1		0.917	IPCC (2003)
Forest peatland (Sitka Spruce)	2	-30	20	Wilson & Farrell, (2007), Black & Farrell, (2006)
Naturally regenerated birch/willow woodland	2	-7	20	von Arnold et al. (2005), Wilson & Farrell, (2007)

Another loss of CO_2 not accounted for in this study comes from dissolved organic carbon (DOC) and particulate organic carbon (POC) leaching from the peatland (fluvial outputs), which will increase due to ditch construction and further drainage (Worrall et al., 2003). However, this is difficult to quantify and varies dramatically from site to site. Limited

studies have been performed, although no emission factors have been published by the IPCC.

Table 7.8 - Net CO_2eq broken down for restoration emissions

	PDA1	PDA2	PDA3	Total
Remaining Years (yrs)	58.2	53	58.6	
Soil Emissions (tCO_2eq)	5934	1569	3220	10723
Uptake over 120 years (tCO_2eq)	-4284	-1244	-2310	-7838
Net (tCO_2eq)	1650	325	910	**2886**

7.2.2.5 Forest and vegetation

No significant forest felling or clearance of vegetation occurred. However, if the amount of felling is known, the EC for these clearfelled trees should be calculated. Undoubtedly, some vegetation clearance took place, which also has an EC factor, but was not included (Duggan, et al., 2012).

7.2.2.6 Slope stability

A slope stability risk assessment was deemed unnecessary in this study. The site had an average annual rainfall for the west of Ireland, a slope angle of less than 0.5° and is in an area not known for peat failures. Therefore, a factor of safety on indirect CO_2 emissions was not needed, which would have, if employed, accounted for peat debris from peat failures drying and releasing CO_2 (Dykes & Warburton, 2007).

Peat failures along the sides of the peat excavation prior to backfill and in peat disposal areas are assumed to be included in the total CO_2 emissions in the excavated peat EC figure. The extent of side collapse can, in general, be limited by experienced contractors who maintain the backfill close to the face.

7.2.3 Scenario S: peat stabilisation

7.2.3.1 Materials, transport, machinery

In Scenario S, stabilisation of the peat to support a road embankment (Figure 7.5(a)) is examined as an alternative ground improvement technique to excavate-and-replace. The peat on the mainline was considered to be stabilised with a total binder content of 250 kg/m^3, consisting of 75% cement and 25% GGBS, proportions commonly adopted in practice. A polyester geotextile of sufficient tensile strength was placed on the stabilised platform, with the embankment placed on the geotextile. It is assumed that peat stabilisation was carried out in two sections. A surcharge 0.5 m in height was incorporated over the stabilised area (as is standard practice to maximise strength gain); once it had

gained adequate strength, it was placed on the second section. The surcharge was retained as part of the embankment.

Table 7.9 details the materials required, together with their relevant transport distances. Fuel consumption rates for the machinery are shown in Table 7.10, which also includes stabilising machinery for dry soil-mixing.

7.2.3.2 Drainage and drainage systems

Total EC for drainage and drainage systems were calculated using the same methodology as in Section 7.2.2.2. Scenario S required only one peat disposal area (PDA 2 (Figure 7.2)), and consequently required fewer retention ponds and ditches than Scenario ER.

7.2.3.3 Direct emissions

In Scenario S, direct emissions, if any, come from the stabilised peat, However, the stabilised peat examined in this body of work not only proved to retain its carbon for at least the first 228 days after peat stabilisation but also acted as a net carbon sink (see Chapter 4). This section explains how the results of Chapters 4, 5 and 6 were incorporated into the life cycle inventory for Scenario S.

The moisture content of the peat prior to mixing was between 500% and 1000% but after mixing could be lower than 200%. Even though the water content of the peat reduces significantly due to hydration, stabilised peat has been proven to retain its carbon after soil-mixing (Chapter 4). The binder in the stabilised peat does this through carbonation, taking in CO_2 from not only CO_2 released by the oxidised peat but also from atmospheric CO_2. Depending on the organic content of the peat and the binder type and amount, some or all of the carbon in the peat carbon sink switches to the cement carbon sink due to peat oxidation and carbonation (Section 4.4). The carbonation potential (C_p) of the binder in Scenario S is assumed to have the same C_p as specimens A6 from Experiment A as they had the same binder type and content. Using Equation 2.14 with the CaO content of the cement and GGBS, C_p was calculated to be 84.8 $kgCO_2/m^3$, which represents 98.6% of the peat's carbon per m^3 (Figure 2.23 can be used as a guide to estimate this percentage). However, because carbon is neither being taken in from nor released into the atmosphere, the carbon sink switch is not accounted for in the LCA.

Table 7.9 - Properties, quantities and distances for materials needed for Scenario S

Materials	Density (kg/m^3)	EC intensity ($kgCO_2eq/kg$)	EE intensity (MJ/kg)	Distance on land (km)	Transport Vehicle	% Weight Laden	Distance by sea (km)	One or two-way transport	Volume dealt with (m^3)
Binder (75:25)	250	0.7357	4.61	92.5 - CEM 1 167-GGBS	Rigid[1]	100, 0	0	Two	115000
Aggregate	2240	0.0052	0.083	15	Rigid[1]	100, 0	0	Two	41090
Surcharge	2240	0.0052	0.083	15	Rigid[1]	100, 0	0	Two	13910
Rockfill	2240	0.0052	0.083	15	Rigid[1]	100, 0	0	Two	176
	(kg/m^2)								**(m^2)**
Geotextile (PE)	0.3	2.54	83.1	204	Articulated	62	226	One	80447
Geocomposite (LLDPE)	0.939	2.08	78.1	204	Articulated	62	226	One	728

[1] The trucks were 100% loaded from quarry to site and returned to the quarry empty.

Table 7.10 - Fuel consumption rates and rates of work for Scenario S

Machinery (Scenario S)	Fuel consumption (l/hr)	Rate (m^3/hr)	Volume of peat (m^3)
Stabilising machinery	40	41.67	115000
21 tonne excavator	16	100	15206

Nevertheless, it is important to quantify the amount of carbon that has switched from the peat to the cement so that it is known how much carbon cannot be released into the atmosphere by peat oxidation after the stabilised peat is 100% carbonated. Firstly, the depth of carbonation (X_c) was calculated using both the k-rate factors presented in Table 6.3, and Equation 5.3 developed by multiple linear regression analysis. After the road's 120-year lifecycle, it was assumed that up to X_c, the binder in the stabilised peat was 100% carbonated. Since there was no k-rate factor available for the stabilised peat in Scenario S, which had a surcharge of greater than 12 kPa and a binder content of 250 kg/m^3 with a cement to GGBS ratio of 3:1, the k-rate factor (33 mm/yr) for a stabilised peat with 250 kg/m^3 of cement binder and 12 kPa of surcharge was used (Table 6.3). This was considered a conservative approach as k-rate factors for unsurcharged specimens increased with GGBS content, a phenomenon also found in concrete (Section 2.7.1.5). X_c was calculated as 0.36 m using the k-rate factor and 0.32 m using Equation 5.3. Assuming the k-rate factor gives the correct X_c, a total of 1706 tCOeq is taken in by the binder over 120 years, the majority of which comes from CO_2 released by the oxidised peat.

The initial carbonation witnessed in the supposedly uncarbonated stabilised peat in Experiments A and B, described in Section 5.3.4.4, can be used by way of the initial percentage carbonated (D_{c0}) to estimate the initial carbonation in the stabilised peat in Scenario S. The average D_{c0} from Experiment A for the specimens a6(c) and A6 with the same binder type and content as in Scenario S was 28 ± 0.8%. With the average depth of the stabilised peat being 2.07 m (115,000 m^3/55640 m^2), a switch in carbon sinks of 2728 tCO_2eq was calculated. If it is assumed that 100% of the CO_2 taken in by the cement in the carbonated region is from CO_2 released by oxidised peat, a total carbon sink switch of 3957 tCO_2 occurred. Again, these figures have no impact on total EC for Scenario S. Table 7.11 is a summary of some of the results that are important in quantifying the environmental impact of stabilised peat.

Table 7.11 - Values for X_c and CO_2 intake for stabilised peat in the case study

Carbonation properties of stabilised peat	Value
Percentage of the peats carbon is the C_p of binder (%)	98.6
Average depth of stabilised peat (m)	2.07
X_c using k-rate factor (33 mm/year) (m)	0.36
X_c using Equation 5.3 (m)	0.32
D_{c0} for stabilised peat (%)	28 ± 0.8
Switch between carbon sinks (tCO_2eq)	3957
ΣCO_2 flux over 179 days (Equation 4.5) (tCO_2eq)	-15.209

The stabilised peat in Scenario S has aggregate on top, something not examined in the experiments; however, it is assumed that both CO_2 and O_2 will diffuse into the stabilised

peat at the same speed as in the experiments. To incorporate the CO_2 flux results of Chapter 4 into the LCA, two scenarios were examined, Scenario S1 and Scenario S2.

Scenario S1: It was assumed that any CO_2 released from peat was absorbed by the cement in the life cycle; consequently, net emissions from stabilised peat were assumed to be zero. No intake from atmospheric CO_2 was taken into account to balance the notion that the stabilised peat is likely to change from a carbon sink to a carbon source at some point over the road's lifecycle as X_c increases and the release of CO_2 from the oxidised peat surpasses the intake of CO_2 due to carbonation. This assumption was considered conservative.

Scenario S2: This scenario is considered less conservative than Scenario S1. Using Equation 4.5 from the CO_2 flux analysis study to calculate the CO_2 flux values for the first 179 days, the amount of CO_2 taken in over this period is incorporated as a negative value into the materials category of the LCA. The CO_2 intake on each day from 55640 m^2 of stabilised peat was calculated for the 179 days ($\Sigma\ CO_{2\ cd,h}$), the summation of which was 15.209 tCO_2eq. After this period, net emissions like Scenario S1 are assumed to be zero. The direct CO_2 intake is classified under the direct emissions category as it happens on-site. However, it is not the peat that is taking in CO_2 but the cement. This CO_2 intake is therefore subtracted from the EC of the binder under the materials category.

7.2.3.4 Indirect emissions

Total EC for indirect emissions for Scenarios S1 and S2 were calculated using the same methodology presented in Section 7.2.2.4.

7.2.4 Scenario ER + P: combination of excavate-and-replace and piling

7.2.4.1 Materials, transport and machinery

For this scenario, a piled embankment was envisaged over a 300 m section as mentioned in Section 7.2.1. This consisted of driven precast C32/40 concrete piles, 8 m long with a cross section of 0.4 m^2 piles and 80 kg/m^3 of reinforcement. The reinforcement was imported from the UK and had an EU-27 market 3-year average recycled content of 59% (G. Hammond & Jones, 2011). Cast-in-situ 0.5 m^3 pile caps containing 80 kg/m^3 of steel reinforcement imported from the UK were considered and installed at a centre-to-centre spacing of 1.5 m. Above the pile caps, there is a 0.9 m thick piling platform to support machinery and a 2 m thick load transfer platform. A polypropylene geotextile was laid in the piling platform and a polyester geotextile in the load transfer platform. It is well established (Adams & Hanna, 1970; Cooke & Price, 1973) that piling has an impact on the intervening soil; ideally, any effect on indirect emissions would be captured in an analysis. However, the impact is unknown at this stage and was not included in this study.

Table 7.12 details the materials required along with their relevant transport distances. Fuel consumption rates for the machinery used, including a piling rig, are shown in Table 7.13. The concrete mixer truck was assumed to transport the concrete for the pile caps a distance of 53 km at a speed of 50 kph. This is the maximum distance it can travel as the total time between the beginning of mixing the concrete and its final pouring should not exceed 90 minutes (Goggins et al., 2010).

7.2.4.2 Drainage and drainage systems

Total EC for drainage and drainage systems in Scenario ER + P was calculated using the same methodology as in Section 7.2.2.2. Scenario ER + P required only two peat disposal areas (PDA 1 and PDA 2 (Figure 7.2)) and consequently fewer retention ponds and ditches than Scenario ER.

7.2.4.3 Direct and indirect emissions

Direct emissions, indirect emissions and restoration emissions for Scenarios ER + P were calculated using the same methodology as in Sections 7.2.2.3 and 7.2.2.4.

7.2.5 Summary

The novel LCA methodology to calculate EC and EE for ground improvement and foundation techniques for road construction on peat was presented, with EC and EE intensity values produced for each factor affecting the carbon and energy calculations. The LCA inventories for the Scenarios ER, S and ER + P were then compiled and the LCA performed. The results of this LCA are presented in the next section.

Table 7.12 - Properties, quantities and distances for materials needed for Scenario ER + P

Materials	Density (kg/m^3)	EC intensity ($kgCO_2eq/kg$)	EE intensity (MJ/kg)	Distance on land (km)	Transport Vehicle	% Weight Laden	Distance by sea (km)	One or two-way transport	Volume dealt with (m^3)
Aggregate	2240	0.0052	0.083	15	Rigid[1]	100, 0	0	Two	120000
Rockfill	2240	0.0052	0.083	15	Rigid[1]	100, 0	0	Two	277
Piles (RC 32/40)	2480	0.2226	2.162	129[3] 60[3]	Articulated[1] Articulated[1,2]	100,0 100,0	0 226	Two Two/One	6784
Load transfer platform	2240	0.0052	0.083	15	Rigid[1]	100, 0	0	Two	24000
Piling platform	2240	0.0052	0.083	15	Rigid[1]	100, 0	0	Two	10800
Pile caps (Concrete) (32/40 MPa) (Steel)	2400 80	0.132 1.4	0.88 17.4	53 165	Mixer[1] Articulated[1,2]	100,0 100,0	0 226	Two/One	663
	(kg/m^2)								**(m^2)**
Geogrid (PP)	0.4	3.43	99.2	204	Articulated	62	226	One	68000
Geotextile (PP)	0.4	3.43	99.2	204	Articulated	62	226	One	12000
Geotextile (PE)	0.3	2.54	83.1	204	Articulated	62	226	One	12000
Geocomposite (LLDPE)	0.939	2.08	78.1	204	Articulated	62	226	One	728
Vertical drain	1	3.43	99.2	486	Articulated	62	626	One	8572

[1] The trucks were 100% loaded from quarry to site and returned to the quarry empty.
[2] Both transport of piles and pile caps include two-way transport, except for the return boat journey for the imported steel.
[3] Precast piles were transported 129 km from the piling production plant to site while the steel needed to produce the piles was transported 60 km from the steel producer to the piling plant.

Table 7.13 - Fuel consumption rates and rates of work for Scenario ER + P

Machinery (Scenario ER + P)	Fuel consumption (l/hr)	Rate (m/hr)	Total length (m)
Piling rig	23	40	42400
		(m^3/hr)	**Volume of peat (m^3)**
21 tonne excavator	16	100	72918
		(drains/hr)	**Number (drains)**
Band drain rig	45	87.5	14287

7.3 Environmental impact assessment in the LCA

7.3.1 Introduction

The results of the environmental LCA are presented in this section, the results of Scenario ER in Section 7.3.2.1 and the results of the alternative scenarios, Scenario S (S1, S2) and Scenario ER + P in Section 7.3.2.2.

7.3.2 Results

7.3.2.1 Case study (Scenario ER)

As a result of the excavate-and-replace (Scenario ER) ground improvement method used at Pollboy, the section's EC and EE totalled 8047 tCO_2eq/km and 25,487 GJ/km, respectively (Table 7.14). If the whole 56 km of the scheme were built on similar depths of peat, the total EC would represent 0.74% of Ireland's GHG emissions in 2010 (61.31 $MtCO_2eq$), emphasising the importance of these summations as part of design (EPA, 2011).

Table 7.14 - Breakdown of total EC and EE for Scenario ER

Factor	EC (tCO_2eq)	(%)	EE (GJ)	(%)
Materials	2132	12.1	35962	65.9
Transport	1458	8.25	17612	32.3
Machinery	80	0.45	968	1.77
Carbon Fixing Potential	0	0		
Direct emissions	10885	61.6		
Indirect emissions	-221	1.25		
Vegetation/Forest	0	0		
DOC and POC leaching	0	0		
Slope stability	0	0		
Restoration	2886	16.3		
Total	**17220**	**100**	**54541**	**100**
Total (per km)	**8047**		**25487**	

Of the total EC, 62% came from CO_2 released from the excavated peat (Figure 7.8), highlighting the significance of how excavated peat is managed. The restoration measure undertaken also showed a big loss at 16%, which could have been reduced substantially had alternative measures been taken. Materials at 66% accounted for the bulk of energy consumed, followed by transport at 32% and machinery at 1.8%. The order of EE

contributions calculated are in agreement with other studies such as Chau et al. (2012), which was based on a rail tunnel construction where EE of materials for one construction scenario was also the highest contributor at 82%, followed by transport and machinery at 10% and 8% respectively.

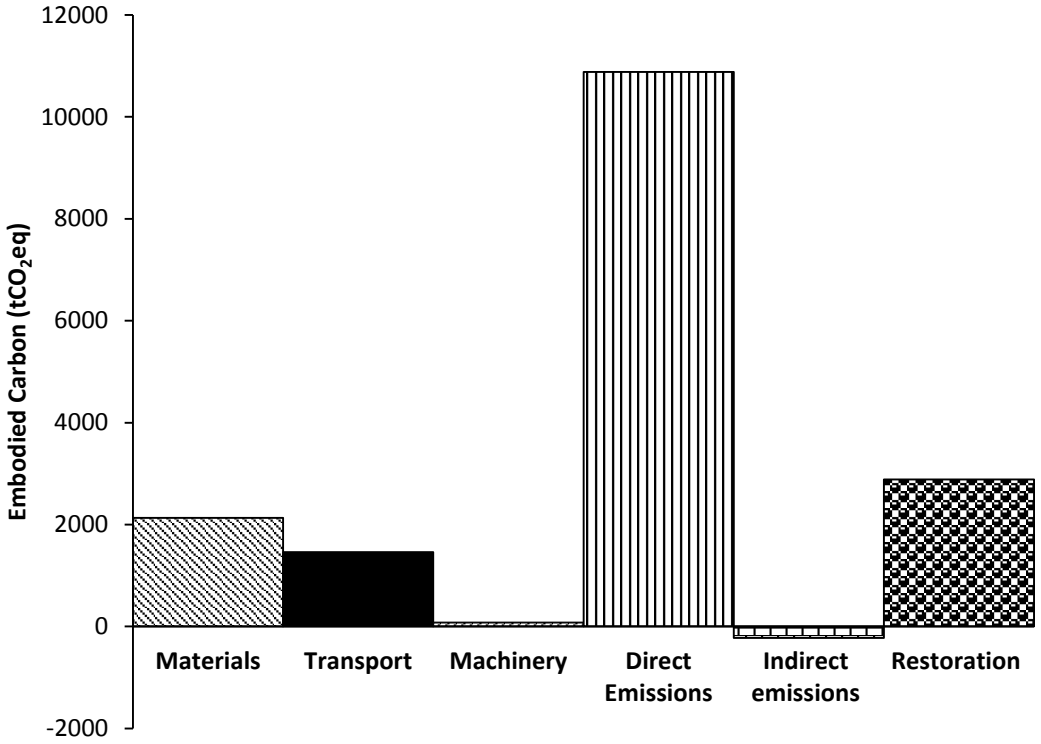

Figure 7.8 - Breakdown of total EC for Scenario ER

7.3.2.2 Alternative scenarios (Scenarios S1, S2 and ER + P)

Scenario S1, defined in Section 7.2.3.3, had a total EC and EE of 25,306 tCO_2eq (11,825 tCO_2eq/km) and 164,364 GJ (76,806 GJ/km). Table 7.15 and Figure 7.9 detail the EC and EE for Scenario S1. As small amounts of peat were excavated, materials in Scenario S1 accounted for 86% of the total EC. The only difference in Scenario S2, defined in Section 7.2.3.3, was a reduction of 15 tCO_2eq in the EC of the binder, which in turn, reduced the EC of materials from 21857 tCO_2eq to 21842 tCO_2eq. Thus, only Scenario S1 is considered in the interpretation of the LCA results presented in Section 7.4.

Table 7.15 - Breakdown of total EC and EE for Scenario S1

Factor	EC (tCO_2eq)	(%)	EE (GJ)	(%)
Materials	21857	86.4	144855	88.1
Transport	1257	4.97	15192	9.24
Machinery	357	1.41	4317	2.63
Carbon Fixing Potential	0	0		
Direct emissions	581	2.30		
Indirect emissions	256	1.01		
Veg/Forest	0	0		
DOC + POC	0	0		
Peat stability	0	0		
Restoration	997	3.94		
Total	**25306**	**100**	**164364**	**100**
Total per km	**11825**		**76806**	

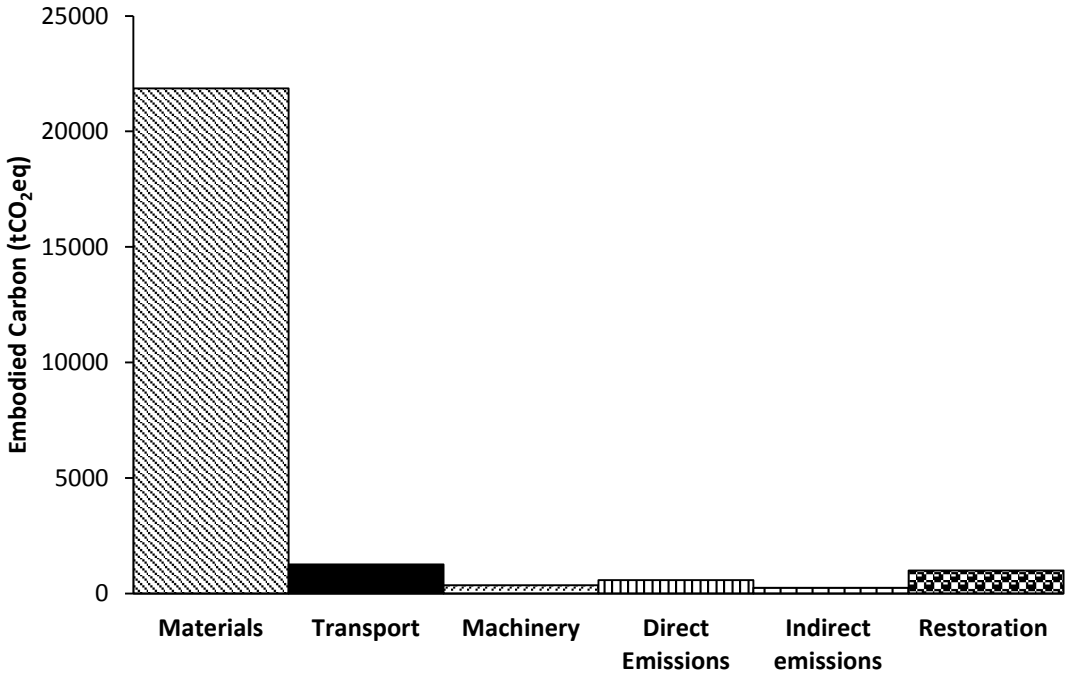

Figure 7.9 - Breakdown of total EC for Scenario S1

Scenario ER + P amounted to a total EC and EE of 17,048 tCO_2eq (7966 tCO_2eq/km) and 92,706 GJ (43,320 GJ/km), detailed further in Table 7.16 and Figure 7.10. The biggest contributors of EC in this case were materials at 34% due to the high EC intensity of the piles and direct emissions at 32% from the relatively high volume of peat excavated.

Table 7.16 - Breakdown of total EC and EE for Scenario ER + P

Factor	EC (tCO_2eq)	(%)	EE (GJ)	(%)
Materials	5986	34.4	71933	77.6
Transport	1595	9.18	19275	20.8
Machinery	124	0.71	1498	1.62
Carbon Fixing Potential	0	0		
Direct emissions	5537	31.9		
Indirect emissions	-165	0.95		
Veg/Forest	0	0		
DOC + POC	0	0		
Peat stability	0	0		
Restoration	3970	22.8		
Total	**17048**	**100**	**92706**	**100**
Total per km	**7966**		**43320**	

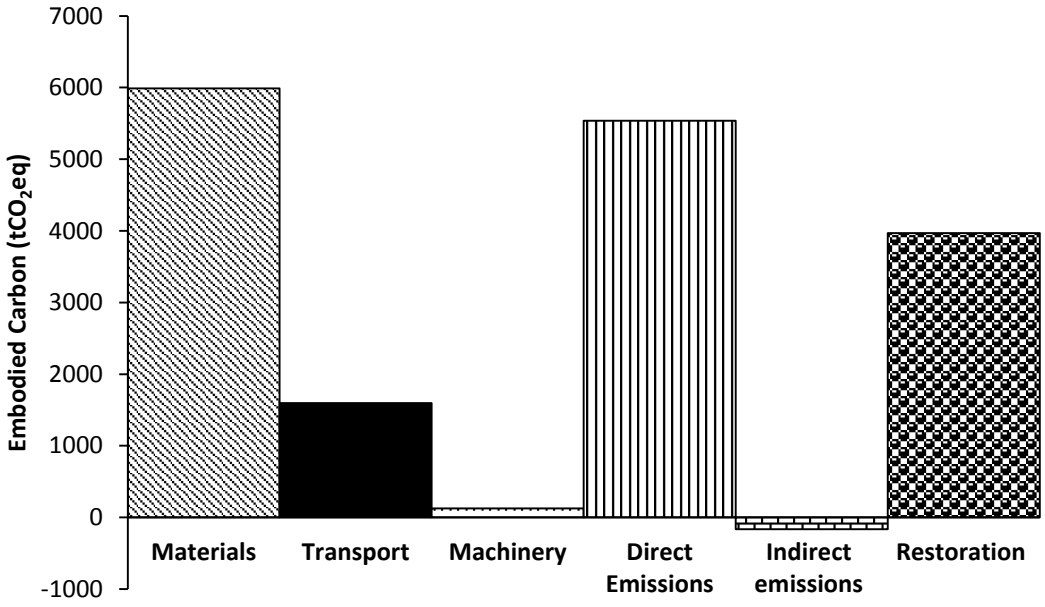

Figure 7.10 - Breakdown of total EC for Scenario ER + P

7.4 Interpretation and discussion of results

7.4.1 Introduction

LCA results are discussed and interpreted in this section. The relative importance of the EC and EE indicators is first assessed before comparing the total EC and EE results of the ground improvement scenarios. Comparisons are also made between the EC and EE of the individual LCA factors from each ground improvement scenario. The significance of the binder type in terms of EC, EE, CO_2 intake and carbonation potential is explained in Section 7.4.4.

Comparisons of total EC are investigated under various management practices and restoration techniques for peatlands, assessing their strength in terms of hydrology and carbon storage potential. The method of converting this carbon storage potential into

carbon credits is discussed briefly. Section 7.4.7 shows the increased environmental impact, quantified in terms of EC, had the drained peatland where the section of road was built been an undisturbed peatland.

The cost of an environmental LCA study and the volume of information needed to perform such a study are explained in Section 7.4.8. Discussed in Section 7.4.9 are ancillary details such as the effect of climate change on road construction and total EC and the added environmental impact had the organic content of the peat been higher.

7.4.2 The relative importance of the EC and EE indicators

It is important to distinguish between EC and EE in the context of road construction. For the LCA factors for materials, transport and machinery, a high EE figure gives rise to a high EC figure due to the typical use of fossil fuels as primary energy sources for these processes. This would be the case had the road not been built in peatlands. However, in the Pollboy case study, the road is built in peatlands; consequently, peat-related factors increase EC substantially while having no effect on EE. Additional contributions to EC include emissions from land construction activities, such as excavated peat, drainage systems, ponds and peat disposal areas. The higher the EC, the greater the on-site environmental impact, hence the greater the effect on global warming. In summary, EC is more important than EE when determining the ground improvement technique to use in construction on peat.

However, EC and EE results are both calculated in this LCA as the EE value may be used as a distinguishing factor when EC results are similar for two ground improvement methods. Furthermore, if EE results are also similar, the on-site impact could then be examined in terms of land area required as well as direct, indirect and restoration emissions. Cost is obviously also a major factor in design but is not examined in this study. When EC values are similar, caution is advised in ranking the methods as the accuracy of carbon emissions is more difficult to estimate and subject to more variability than EE results due to the variability in peat and the uncertainty of emission factors. Consequently, it is for the consulting engineer to determine the accuracy of the EC figures as any total EC figure calculated depends on the comprehensiveness of the LCA study (see Section 7.4.8).

7.4.3 Comparison of ground improvement techniques

Comparisons of total EC and EE for the three scenarios investigated in this study are illustrated in Figure 7.11. Scenario ER and ER + P had similar EC values (17,220 tCO_2eq and 17,048 tCO_2eq respectively), whereas Scenario S1 had an EC value of 25,306 tCO_2eq.

However, Scenario ER had the lowest EE (54,541 GJ) compared to Scenario ER + P (92,706 GJ) and Scenario S1 (164,364 GJ). Scenario ER was, therefore, the preferred technique. The main advantages and disadvantages of each scenario are summarised in Table 7.17.

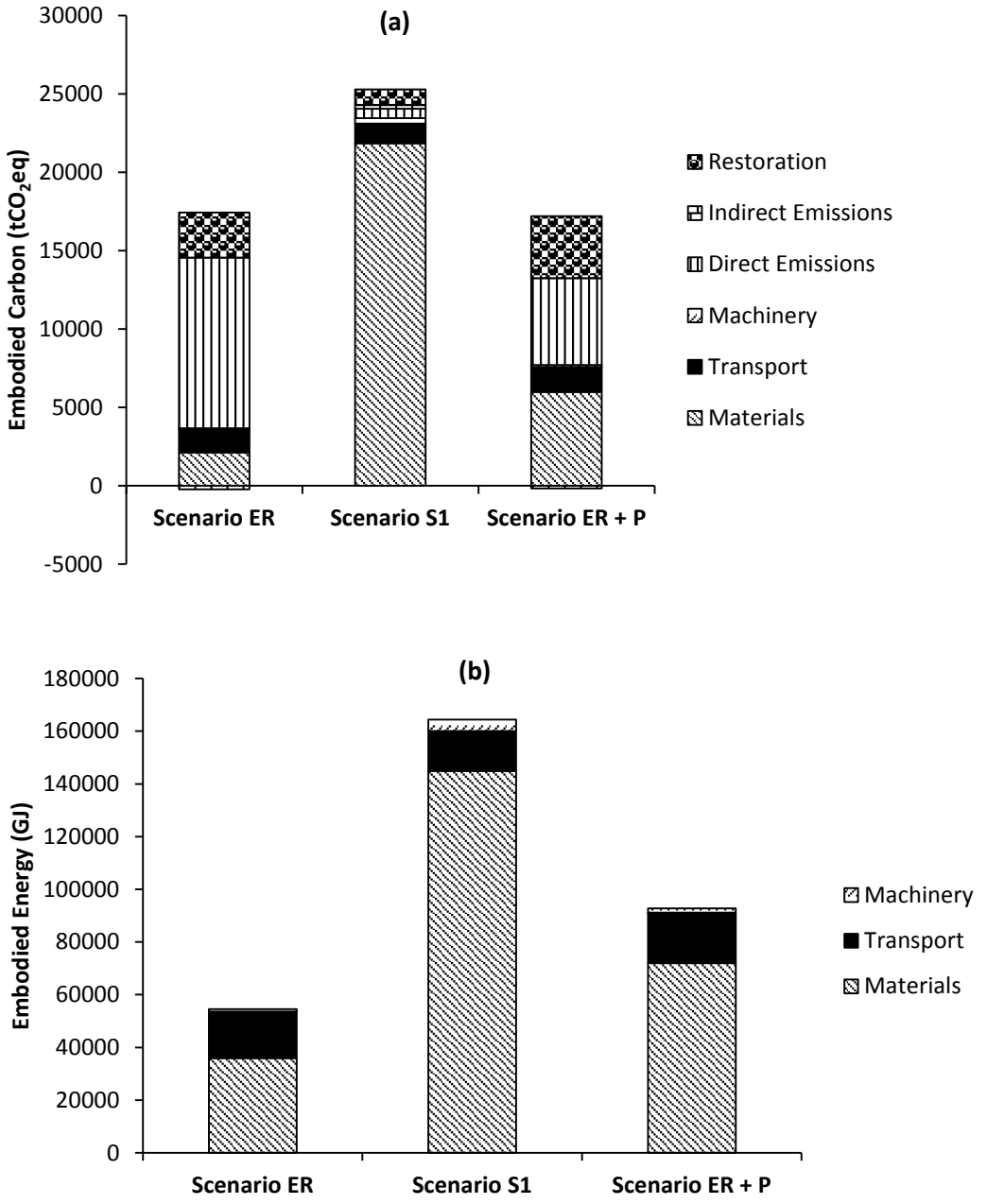

Figure 7.11 - (a) Comparison of total EC of the three scenarios investigated in this study and (b) comparison of total EE of the three scenarios

Table 7.17 - Main advantages and disadvantages of each scenario

Scenario	Advantages	Disadvantages
ER	• Materials were of low EC and EE intensity • Emissions from transport were low as quarries were nearby • Low machinery emissions	• High on-site impact • Depending on organic content, carbon emissions from excavated peat may be high
S1	• Low on-site impact due to peat remaining *in situ*. • Alternative binder combinations have the potential to have low EC and EE intensities	• Binder had a high EC and EE intensity due to high levels of cement used • Stabilising machinery is environmentally intensive
ER + P	• Where sections were piled, peat remained *in situ*—smaller environmental impact • Some materials such as aggregate were locally sourced and were of low EC and EE intensity	• High EC and EE intensity for piles due to concrete and imported steel • Piling machinery is environmentally intensive

The EC and EE of construction materials were the predominant contributors to the overall EC and EE of Scenario S1 at 86.4% (i.e. 21,857 tCO_2eq) and 88.1% (i.e.144,855 GJ) respectively (Figure 7.11). This was due principally to the use of a blend of 75% CEM 1 and 25% GGBS as a stabiliser. The effect of an alternative binder combination is discussed in Section 7.4.4. On the other hand, no cementitious material was used in Scenario ER, hence the contribution of materials to total EC and EE for Scenario ER was lower at 12.1% (i.e. 2132 tCO_2eq) and 65.9% (i.e. 35,962 GJ) respectively.

The construction of a piled embankment section in Scenario ER + P was an energy-intensive procedure attributable to the relatively high EC and EE cost of reinforced concrete piles and pile caps. The contribution of materials to overall EC and EE for Scenario ER + P was therefore 34.4% (5986 tCO_2eq) and 77.6% (71,933 GJ) respectively. Shipment of steel reinforcement from the UK to the site in Ireland for the pile caps and piles as well as the requisite aggregate from local quarries caused Scenario ER + P to have the highest EC (1595 tCO_2eq) and EE (19,275 GJ) for transport. Scenario S1 necessitated a lower volume of materials (binder) than the other scenarios; and as the binder was sourced in Ireland, it had the lowest EC (1257 tCO_2eq) and EE (15,192 GJ) for transport. The EC of operating machinery, however, was highest in Scenario S1 (357 tCO_2eq), primarily due to the stabilising machinery (350 tCO_2eq). In Scenario ER + P, the piling machinery had a relatively high EC value (77 tCO_2eq) compared to the excavator (37 tCO_2eq), which was used extensively in Scenario ER.

While the optimal method will always depend on the site and construction scenario, the least preferred technique for this study was Scenario S1 as it had the highest EC and EE on account of the high EE and EC intensities of the binder. It also had the lowest on-site and environmental impact on local surroundings of the three scenarios as the majority of the peat remained *in situ*. Scenario ER had the highest on-site and negative environmental impact on local surroundings due to high levels of peat excavation, which is reflected in the high direct and restoration emissions. These emissions were responsible for 61.6% (10,885 tCO_2eq) and 16.3% (2886 tCO_2eq) of the total EC respectively, as more land was required for peat disposal areas, drainage ditches and ponds than either of the other scenarios (Figure 7.11(a)) (Table 7.18). In Scenario ER + P and Scenario S1, direct emissions accounted for only 31.9% (5537 tCO_2eq) and 2.3% (581 tCO_2eq) respectively, as less land was needed. Restoration emissions for Scenario ER + P and Scenario S1 were 22.8% (3970 tCO_2eq) and 3.9% (997 tCO_2eq) of the total EC respectively. The management of peat during and after construction is discussed in Sections 7.4.5 and 7.4.7.

Table 7.18 - Land area required for some features required for the three ground improvement scenarios where the restoration scenario is a naturally regenerated woodland

Scenario Name	PDAs (m^2)	Drainage ditches (m^2)	Ponds (m^2)
Scenario ER	93305	3890	1656
Scenario S1	14805	1730	362
Scenario ER + P	65805	2945	927

7.4.4 Materials—binder

7.4.4.1 EC and EE of binder

Materials can represent a high environmental cost in a road construction project. In Scenario S1, they amounted to 86% of total EC, with the binder accounting for 97% of this figure. Timoney et al. (2012) showed that 1:3 cement to GGBS mixes can produce high stabilised peat strengths; therefore, it may have been possible to use less energy-intensive binders to give sufficiently high strengths. Ordinary Portland cement (OPC) has an EE intensity of three times greater than that of GGBS and an EC intensity of approximately 11 times more than GGBS (G. Hammond & Jones, 2011). Ratios of 1:1 and 1:3 cement to GGBS were examined for the Pollboy section. Results show that EC costs can be reduced considerably to a level where the total EC in Scenario S1 is lower than the other scenarios (Figure 7.12(a)). However, EE costs are still higher than the other two ground improvement scenarios (Figure 7.12(b)), though in recent years cement has a decreasing clinker content, which would further reduce EC and EE costs.

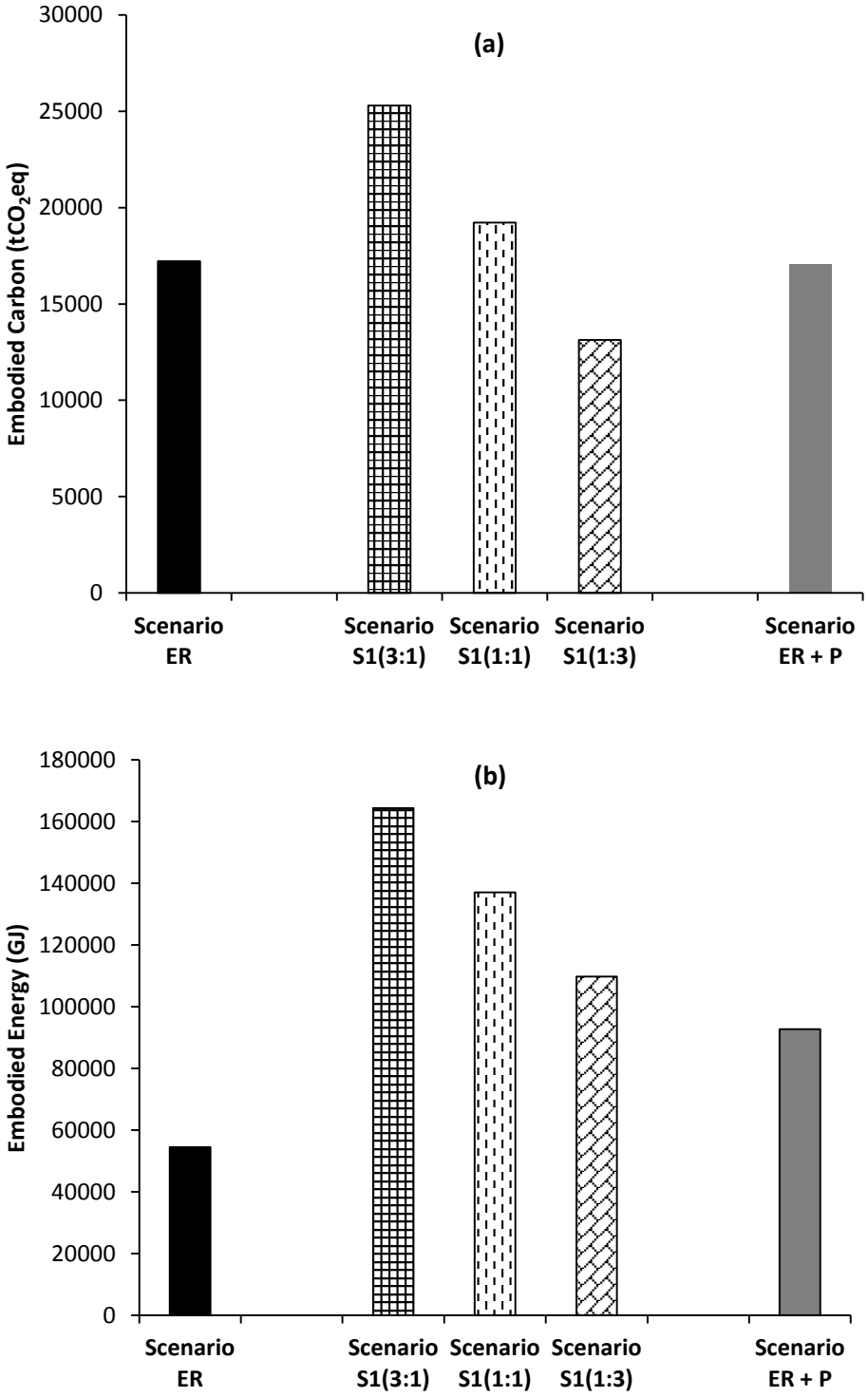

Figure 7.12 - (a) Bar chart showing how different binders compare with total EC and (b) bar chart showing how different binders compare with total EE

7.4.4.2 Carbonation and CO_2 flux

While in Section 7.4.4.1 it was found that changing the binder type from a 3:1 (Scenario S1(3:1)) to 1:3 (Scenario S1(1:3)) cement to GGBS ratio impacts largely on EC, the change makes only a small difference to the CO_2 intake flux over the first 179 days

(only accounted for in Scenario S2) and to the carbon sink switch (Table 7.19). The two binder type scenarios are compared in this section.

Using Equation 2.14 and the CaO content of cement and GGBS, C_p is calculated to be 70.3 $kgCO_2/m^3$ for Scenario S1(1:3), representing only 81.8% of the peat's carbon per m^3 compared to 98.6% for Scenario S1(3:1). The initial carbonation percentage (D_{c0}) is also less in Scenario S1(1:3) as the average D_{c0} from Experiment A for the specimens (a7(c) and A7) with the same binder type and content as in Scenario S1(1:3) is 18 ± 2.24% (Table 7.19). This denotes an initial carbon sink switch from peat to cement of 1472 tCO_2eq, 46% less than the switch in Scenario S1(3:1).

Table 7.19 - Carbonation properties of stabilised peat for Scenario S1(3:1) and Scenario S1(1:3)

Carbonation properties of stabilised peat	**Scenario S1(3:1)**	**Scenario S1(1:3)**
Total EC of binder (tCO_2eq)	25306	13127
Carbonation potential of binder ($kgCO_2eq/m^3$)	84.8	70.3
Percentage of the peats carbon is the C_p of binder (%)	98.6	81.8
D_{c0} for stabilised peat (%)	28 ± 0.8	18 ± 2.2
Switch between carbon sinks (tCO_2eq)	3957	2629
	Scenario S2(3:1)	**Scenario S2(1:3)**
ΣCO_2 flux over 179 days (Equation 4.5) (tCO_2eq)	-15.209	-12.867

The same k-rate factor is used for the two binder types, resulting in the same X_c value of 0.36 m. In the carbonated zone after 120 years, 17% less CO_2 is taken in by the binder in Scenario S1(1:3) (1414 tCOeq) than in Scenario S1(3:1) (1706 tCOeq). If it is assumed that 100% of the CO_2 taken in by the binder in the carbonated region is from CO_2 released by oxidised peat, and taking into account the initial carbonation in the uncarbonated zone, a total carbon sink switch of 2629 tCO_2 occurs in Scenario S1(1:3), 34% less than in Scenario S1(3:1). Again, these figures have no impact on total EC for Scenario S1.

Using Equation 4.5, the CO_2 intake over the first 179 days, accounted for in Scenario S2, reduces from only -15.209 tCO_2eq in Scenario S2(3:1) to -12.867 tCO_2eq in Scenario S2(1:3), making little difference to the overall EC. The 12179 tCO_2eq difference in the EC of the binder between Scenario S1(3:1) and Scenario S1(1:3) dwarfs the differences in CO_2 intake flux and carbon sinks. Even though a binder with more cement has a greater C_p value, carbon sink and CO_2 intake flux, a binder with less cement and accordingly lower EC should be used, if possible, to achieve the lowest total EC.

7.4.5 Management of excavated peat

Around 600,000 m^3 of peat was excavated along the 56 km route, 115,000 m^3 from the Pollboy section. Scenario ER and Scenario ER + P had much higher levels of excavated peat and greater on-site impacts than Scenario S1. For example, the largest EC component of Scenario ER was direct emissions at 62% (10,885 tCO_2eq) while restoration emissions

accounted for 16% (2886 tCO_2eq). By using other restoration techniques, it is possible to reduce these percentages significantly. Rather than growing birch/willow woodland on the peat disposal areas, which was a major contributor of CO_2, afforestation with Sitka spruce or peatland restoration could be undertaken.

Substantial amounts of CO_2 can be sequestered in the 120-year life cycle by growing Sitka spruce, a tree species that has a yield class ranging from 10 m^3 ha^{-1} yr^{-1} to 24 m^3 ha^{-1} yr^{-1} and is a source of income when thinned and harvested (Black & Farrell, 2006). For this study, a carbon uptake emission factor of -30 tCO_2eq ha^{-1} yr^{-1} was used (Figure 7.13). The figure is based on an average of studies undertaken on Sitka spruce forests on organic soils in Ireland (-29 tCO_2eq ha^{-1} yr^{-1} (Wilson & Farrell, 2007) to -32 tCO_2eq ha^{-1} yr^{-1}, (Black & Farrell, 2006)). Losses due to soil emissions were assumed to be at the same rate as soil emissions from birch/willow woodlands; that is, 20 tCO_2eq ha^{-1} yr^{-1} (Table 7.7). Losses due to harvesting and thinning were not accounted for.

In Ireland's current climate, there is a high probability that peatland restoration will serve as a small sink. Uptake by undisturbed peatlands in Ireland has been reported from between -0.47 tCO_2eq ha^{-1} yr^{-1} by Kiely et al. (2009) and -1.1 tCO_2eq ha^{-1} yr^{-1} by Koehler et al. (2011). For the current study, a lower bound long-term emission factor of -0.5 tCO_2eq ha^{-1} yr^{-1} was used to account for climate change, which will have a negative impact on carbon uptake. In this restoration technique, it was assumed that 50% of the carbon in the excavated peat was released as CO_2 due to the agitation (breakup) of peat during transport and, more importantly, to the time it takes to restore a peatland, estimated at 20 years by the IPCC (2003).

Depending on groundwater vulnerability, another option for dealing with removed peat is to dump and bury it in decommissioned quarries and borrow pits. Two cases and two assumptions for each scenario were examined for this site where excavated peat was placed at depth and under the water table, therefore retaining much of its carbon. In the first instance, it was assumed that if the peat were kept below the water table for 120 years, 90% of the carbon would remain intact. In the second case, only 50% of the carbon in the peat would remain because the disposed peat is over and under the water table at different periods. In both cases, indirect emissions were assumed to be zero because it was assumed that emissions would be zero had the peat not been disposed of in these areas. Also included in the aforementioned cases was the fact that due to the lack of peat disposal areas, ponds were not constructed and fewer drainage ditches were required.

The options described above to cater for the excavated peat were examined in terms of EC (Figure 7.13). Results show that afforestation with Sitka spruce seems to be the most promising and rewarding in terms of EC, with total EC ranging from -8532 tCO_2eq in Scenario ER to 21,220 tCO_2eq in Scenario S1. Burying the peat permanently under the water table and peatland restoration were also quite positive for Scenario ER, with EC totalling 4359 tCO_2eq and 7939 tCO_2eq respectively. Figure 7.13 shows that EC is heavily influenced by the extent of excavation of peat. When examining restoration options, it is important to use the emission factors presented as guidelines only. Further work is required to define country-specific emission factors more accurately.

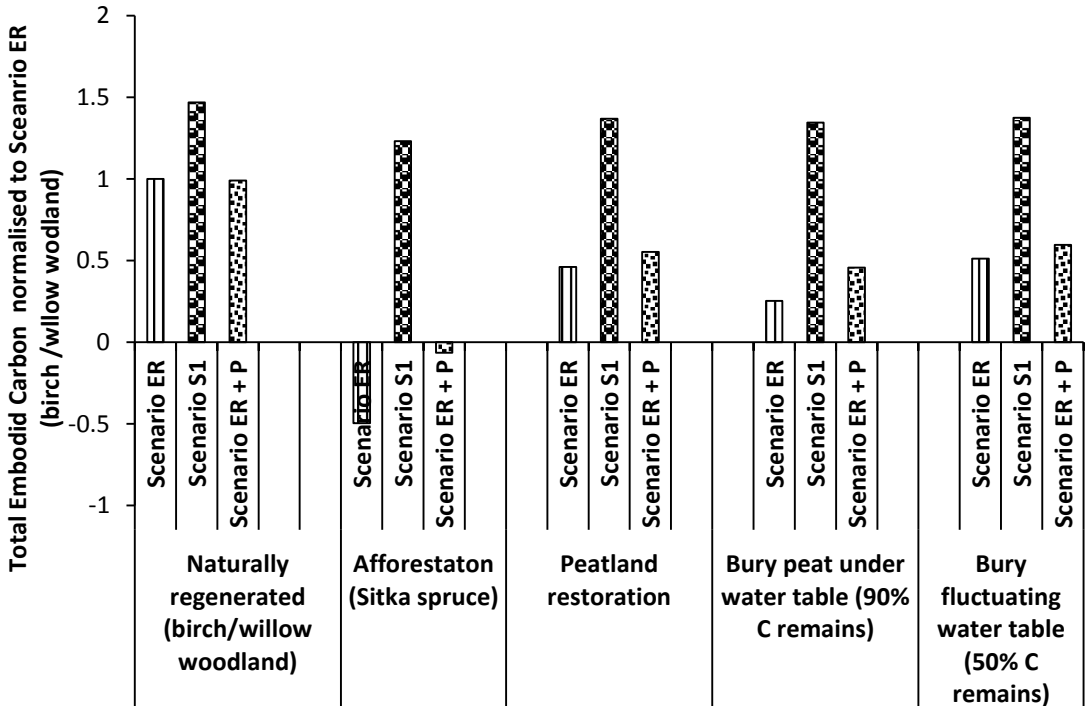

Figure 7.13 - Total EC showing various restoration scenarios normalised to Scenario ER (birch/willow woodland) over the 120-year life cycle

7.4.6 Carbon credits

As discussed in Section 2.2.3, afforestation and peatland restoration can be carried out in conjunction with a road construction project, thereby accumulating carbon credits. A study was undertaken on Irish peatland restoration by Wilson et al. (2012) where a carbon credit price of €20 was assumed. At this value, if a peatland had been restored at the Pollboy section as part of the construction process and the peatland had a sink of 0.5 $tCO_2eq\ ha^{-1}\ yr^{-1}$ for the 120-year life cycle, €1200 per hectare could have been earned.

7.4.7 Construction on undisturbed peatland

Had the peatland at Pollboy been undisturbed and not drained, Scenarios ER would have had a higher environmental impact due to construction, resulting in an increase in total EC. The peatland directly affected by excavation would have continued sequestering CO_2

over the 120 years had the road and drainage system not been built. The peatland would also have changed from a sink to a source of CO_2 caused by the extent of drainage. The drainage system along the road and around peat disposal areas is vast, making it problematic to estimate the area affected by drainage. In essence, had there been a drain either side of the road in the peat excavate-and-replace scenario, an area of 6.25 ha would have been damaged, releasing 1040 tCO_2eq over the road's lifetime at an emission rate of 1.39 $tCO_2eq\ ha^{-1}\ yr^{-1}$. Furthermore, had the peatland not been disturbed, the carbon-fixing potential would have been 375 tCO_2eq. Together, the added EC cost of indirect emissions and the carbon-fixing potential represent an additional 8% of the overall EC total of Scenario ER in this LCA.

7.4.8 The cost of performing a study

A key consideration for a company wishing to perform this specific type of environmental LCA is the time and skill required and the accessibility of data. The more information a company has on a project, the more comprehensive an LCA calculation it can undertake. Once the site investigation documents are completed and the geotechnical issues are brought forward in the design stage, the data needed for this calculation will be readily available in these documents and will help in deciding which ground improvement scenario to use.

The basic components needed for the materials, transport, and machinery factors should be the most straightforward to obtain. Finding EC and EE intensities for fuel and materials, such as aggregate and cement can be sourced from databases, such as the Inventory of Carbon and Energy Version 2.0 (ICE V2.0) (G. Hammond & Jones, 2011) and Guidelines to Defra/DECC's GHG Conversion Factors for Company Reporting (DECC & Defra, 2012). For the peat-related factors, the following information is needed: the volume of peat excavated, the size and number of peat disposal areas required, the size of drainage systems (ponds and drainage ditches), the proposed restoration techniques and the peatland type (drained or undisturbed). Using the emission factors, extent of drainage equation and the methodology presented, an EC value for direct, indirect and restoration emissions for each scenario can be obtained. Although a user-friendly tool/calculator to quantify the main peat-related factors for construction of roads on peatlands would be useful, this body of work outlines ways of tackling each factor, which can be subsequently assimilated in a spreadsheet.

7.4.9 Other factors

Additional carbon costs not considered in this LCA include: maintenance, fencing, road markings and signs, asphalt concrete and pavement layers, subgrade preparation

(compaction) and work on link and side roads and structures such as the overpass bridge at Ch. 52,900. Another factor not examined was the number of workers needed for each ground improvement technique. Soil-mixing would probably have required fewer personnel than peat excavate-and-replace or piling methods but would have a minimal influence on the method chosen from an EE/EC perspective. With reference specifically to peat-related factors, direct emissions would have been 23,408 tCO_2eq, 2.2 times higher had the peat, for example, an average organic content of 85%, showing it to be a high-sensitivity variable.

While climate change was beyond the scope of this study, it should be accounted for as it is likely to have a negative impact on the environment and to increase EC. As temperatures rise, CO_2 emissions from peatlands will increase (Strack et al., 2004); Scenario ER + P and Scenario ER will be most affected as both deal with more excavated peat and have a greater on-site impact than Scenario S1. The binder in the stabilised peat in Scenario S1 will carbonate quicker due to increased temperatures, leading to full carbonation occurring in a shorter period of time (Section 2.7.1.4).

7.5 Summary and conclusions

By examining all construction and peat-related factors, the LCA methodology presented has clear potential to reduce the EE and EC of a road construction project on peat. Three ground improvement technique scenarios were assessed in terms of EE and EC, allowing the major contributions to be highlighted. Restoration techniques and other methods of reducing these factors were then examined. From the calculations presented, the main conclusions are:

- The method adopted for the Pollboy contract amounted to an EC of 8047 tCO_2eq/km and an EE of 25,487 GJ/ km. This is over 6 times greater in EC and 1.6 times greater in EE than the cost of building an asphalt pavement for a 26 m wide two-lane motorway whose EC and EE were 1300 tCO_2eq/ km and 15,600 GJ respectively (Chappat & Bilal, 2003). In context, it is also over 5 times greater than the cost of building an asphalt pavement for a 28 m wide two-lane motorway (1574 tCO_2eq/km) (Milachowski et al., 2011) and 119 times more than building a 3 m wide greenway (67.6 tCO_2eq/km) (Manton et al., 2014).

- The predominant EC component in peat excavate-and-replace was direct emissions from excavated peat, signalling the importance of how excavated peat should be managed.

- Scenario ER was the favoured technique for this project as it had similar EC to Scenario ER + P and the lowest EE. Scenario ER + P ranked second, with an EE of 1.7 times greater than Scenario ER due to the energy intensive procedure of building a piled embankment. Scenario S1, on the other hand, had both the highest EC and EE and was, therefore, the least desirable solution. The EE total of materials in Scenario S1 was twice as high in Scenario ER + P and 4 times greater than Scenario ER due to the EE intensity of cement.

- Employing a variety of restoration techniques can substantially reduce restoration, direct and indirect emissions and provide an income from the sale of carbon credits.

- Indirect emissions can fluctuate according to the type of peatland on which the road is built whether, for example, it is an undisturbed peatland, drained peatland, drained grassland peatland or forest peatland.

- Soil-mixing in Scenario S1 had the lowest on-site and environmental impact on the local surroundings in terms of direct and indirect emissions, but the binder used in stabilising the peat represented 86% of the EC total. As a result, the total EC was 1.47 and 1.48 times larger than in Scenario ER and Scenario ER + P respectively, and the total EE was 3.01 and 1.77 times higher than Scenario ER and Scenario ER + P respectively. However, the use of an alternative 1:3 cement to GGBS binder split, if appropriate from a strength perspective, reduces total EC by 48% and total EE by 33% even though the carbonation potential, CO_2 gas intake flux and carbon sink switch is lower for a binder with less cement and more GGBS.

When the potential greenhouse gases released from peat are factored in, building on peat and organic soils increases the EC cost substantially compared to building a road on mineral soils. Each ground improvement technique employed has advantages and disadvantages. By carrying out various scenarios of EC calculations on a peatland site where one of the three techniques is used or where combinations of techniques are applied, optimum EC and EE solutions can be achieved in construction on peat. It is only by analysing these outcomes that the most appropriate solution can be produced as the preferred technique will change according to the project and site location

Chapter 8: Conclusions

8.1 Introduction

The primary objective of this thesis was to evaluate the on-site carbon impact of peat stabilisation (soil-mixing) by establishing whether stabilised peat was a net source or sink of carbon. This was achieved by studying the carbonation process in stabilised peat through laboratory experiments. A broader objective was to incorporate the results of these experiments in a comparison of embodied energy (EE) and embodied carbon (EC) (also known as global warming potential) associated with various ground improvement/foundation options, including peat stabilisation for road construction in highly organic soils such as peatlands.

One preliminary and two extensive sets of experiments were carried out on stabilised peat with varying binder types, binder contents, and environmental conditions to examine (i) the CO_2 gas flux and (ii) the depth and level of carbonation. A closed chamber method employed extensively in environmental applications to quantify CO_2 fluxes between the soil and the atmosphere was applied to stabilised peat. Several carbonation depth techniques generally associated with concrete were also applied to stabilised peat to ascertain the depth and level of carbonation. In particular, the following techniques were employed: phenolphthalein indicator, X-ray diffraction analysis (XRD), Fourier transform infrared spectroscopy (FTIR), loss on ignition (LOI), pH of stabilised peat slurries, and the water evaporation method.

A novel LCA methodology was developed to quantify EC and EE for ground improvement/foundation techniques employed in road construction in peatlands, and the methodology was initially applied to an Irish case study in which excavate-and-replace was used. An alternative peat stabilisation solution was also analysed that incorporated the outcomes of the carbonation experiments. This chapter reviews the key findings of the thesis and makes recommendations for future work.

8.2 Research findings

8.2.1 Novelty of the research

The experiments used to assess carbonation in stabilised peat described in this thesis are believed to be the first of their kind for this material. Arising from these experiments, the following original experimental procedures were developed:

(i) Successful construction of stabilised peat columns with an air space specifically designed to allow gas fluxes to be measured using a gas chamber method.

(ii) Application of carbonation depth techniques to stabilised peat.

(iii) An alternative method to thermogravimetric analysis (TGA); namely, the LOI technique to calculate the mass loss due to $CaCO_3$ decomposition and the percentage carbonated value (D_c) at each depth to produce a carbonation front depth (X_c) value.

From the experimental results, a hypothesis was outlined to show why CO_2 flux results and carbonation depth results in stabilised peat vary with binder content, binder type(s) and environmental conditions.

A novel LCA methodology to quantify the EC and EE for various ground improvement/foundation techniques for road construction on peat was developed. In addition to the standard factors considered in LCA, this methodology also encompassed relevant factors such as emissions from drainage ditches, ponds and various restoration techniques, as well as the effect of carbonation in the case of stabilised peat.

8.2.2 CO_2 gas flux in stabilised peat

CO_2 fluxes were measured from: 9 columns in Experiment P (3 stabilised peat) over 228 days; 24 columns in Experiment A (21 stabilised peat) over 180 days; and 24 columns in Experiment B (15 stabilised peat) over 180 days. From the CO_2 flux results, the following conclusions were drawn:

(i) While the raw peat was found to be a net source of carbon, stabilised peat proved to be a net sink of carbon, taking in CO_2 from both the atmosphere and oxidised peat.

(ii) The variable that had the greatest influence on the CO_2 fluxes in stabilised peat was time, with the CO_2 flux decreasing logarithmically with time.

(iii) As well as time, the best-fit statistical models in Experiments A and B included cement, surcharge, and an interaction variable surcharge*time (where * denotes an interaction). While cement content and surcharge increased the CO_2 intake rate, the surcharge*time variable had a negative effect on the CO_2 intake rate due to the smaller effect surcharge had on the CO_2 flux over time.

(iv) The best-fit statistical model in Experiment A also contained initial CO_2 concentration in the headspace and an interaction variable, cement*GGBS. The CO_2 intake rate declined when a decrease in initial CO_2 concentration occurred, and the replacement of cement with GGBS had a negative effect on the CO_2 intake rate due its lower carbonation potential.

(v) When low and high water tables were examined in Experiment B, it was found to be significant in predicting CO_2 fluxes, with the presence of a high water table decreasing the CO_2 intake rate and a low water table increasing this rate.

CO_2 intake rates were generally higher in Experiment B, and it was thought that this difference was due to the higher CaO content of the cement used in Experiment B, which had, as a result, a greater carbonation potential and was capable of taking in more CO_2 due to carbonation.

8.2.3 Use of carbonation depth techniques in stabilised peat

Six techniques were examined in detail to verify their suitability for finding the depth and level of carbonation in stabilised peat; namely, XRD, FTIR, LOI, pH of stabilised peat slurries, the phenolphthalein indicator, and the water evaporation method. The use of these techniques revealed the following:

(i) The XRD, FTIR and LOI techniques gave similar X_c values ($p > 0.05$), but the pH of stabilised peat slurries technique produced significantly greater X_c values than the other techniques ($p < 0.05$), while the phenolphthalein indicator technique gave significantly lower X_c values than the others ($p < 0.05$). The pH of stabilised peat slurries technique was found not to give a carbonation depth; instead, it gave the depth at which leaching of $Ca(OH)_2$ and Ca^{2+} occurs.

(ii) In Experiment B for some of the small and large specimens, the LOI technique produced significantly greater carbonation depth results than XRD and FTIR. It is suggested that the reason for this difference is the higher average pH in the stabilised peat in Experiment B. The higher pH may have inhibited the ability of XRD and FTIR to detect small changes in $CaCO_3$ concentrations, especially at the carbonation front. LOI, on the other hand, records the $CaCO_3$ concentration difference directly by measuring the extra mass CO_2 loss due to carbonation.

(iii) For the LOI technique, it was difficult to pinpoint the temperature range at which $CaCO_3$ decomposes in stabilised peat. The more conservative option of using only the mass loss between 650 and 850ºC is recommended for calculating D_c, and thus X_c. However, if other techniques such as FTIR and XRD are used in tandem with LOI, combining the mass loss between 520 and 650ºC with the mass loss between 650 and 850ºC to calculate X_c is recommended but only if two of the three criteria outlined in Section 5.3.4.3 are met.

(iv) The depth of the pH front (X_{pH}) was hard to recognise in stabilised peat whose binder had a high GGBS content. Due to the smaller pH value of GGBS than cement, a

smaller range of pH existed between carbonated and uncarbonated stabilised peat with high GGBS content, which rendered it more difficult to distinguish between the carbonated and uncarbonated stabilised peat. Unsurcharged specimens with a binder content of ≤ 200 kg/m^3 in Experiment A also made it increasingly challenging to locate X_{pH}, as lower cement content produces stabilised peat with a lower pH.

(v) Due to the colour of stabilised peat, differentiating between colour changes at the carbonation front was sometimes problematic when using the phenolphthalein indicator, making it difficult to pinpoint the carbonation front.

(vi) While the porosity readings in stabilised peat showed a significant decrease ($p < 0.05$) over the duration of experiments, the highest was in the surcharged specimens with the greatest X_c. This technique needs to be adjusted to produce an X_c value (see Section 8.3.2).

8.2.4 Carbonation depth in stabilised peat

Carbonation depth was analysed in Experiments A and B by using the various carbonation depth techniques discussed in Section 8.2.3. In Experiment A, 90 specimens were tested, and in Experiment B, 96 specimens were tested. The results can be summarised as follows:

(i) In each experiment, time and surcharge were shown to be highly significant variables ($p < 0.01$) in predicting X_c, with time and surcharge increasing X_c in the best-fit statiscal models. In Experiment B, cement and water table were also significant in the best-fit statiscal models. Cement content and a high water table decreased X_c.

(ii) Small specimens were used to calculate the rate of carbonation (as defined by k-rate factors) due to the availability of more data points over time than in the large specimens. The highest k-rate factors measured for the small specimens were for the surcharged specimens with 278 kg/m^3 of cement binder and 12 kPa of surcharge at a value of 50 mm/√yr and the lowest at a value of 10 mm/√yr for the unsurcharged specimens with 148 kg/m^3 of cement binder. These values indicate that carbonation rates in stabilised peat are higher than in concrete with Portland cement, where k ranges from 0.5 mm/√yr in wet/submerged concrete (> 35 MPa) to 15 mm/√yr in concrete indoors (< 15 MPa).

(iii) For the large specimens, a highly significant relationship ($p < 0.001$) exists between X_c as measured by LOI and the depth at which the organic content becomes constant (X_{oc}). X_{oc} was on average $0.68X_c$ for Experiment A and $0.63X_c$ for Experiment B.

(iv) The results showed that the percentage carbonated in the supposedly uncarbonated zone (D_{c0}) for the cement-only stabilised peat columns was on average 36 ± 3% for the large specimens in Experiment A and 39 ± 4% in Experiment B. In contrast, D_{c0} in concrete is on average a much smaller percentage; for instance, one study showed it to be 12.5%.

(v) There were some strong relationships between X_c values and CO_2 fluxes. For example, there was a significant relationship ($p = 0.003$) between X_c as measured by FTIR and CO_2 fluxes for the specimens with a cement content of 250 kg/m^3 or more. There was also a highly significant correlation ($p < 0.001$) between X_c and D_c at the surface.

8.2.5 Novel LCA methodology and LCA case study

A novel life cycle assessment (LCA) methodology was outlined that allows a quantitative comparison of EC and EE of various ground improvement/foundation options for road construction on peat, including peat stabilisation. In addition to accounting for construction related factors, the methodology incorporates some peat-related factors not examined previously in this type of environmental assessment. Some of these include:

(i) Emissions from drainage systems (i.e. drainage ditches and ponds) associated with the road and peat disposal areas.

(ii) Restoration techniques such as afforestation, peatland restoration and natural woodland regeneration that can be carried out on peat disposal areas and drained peatlands and may decrease the total EC (or global warming potential) of a road construction project.

(iii) The on-site impact of stabilising peat in terms of EC. The experimental results from stabilised peat were incorporated into the methodology and have huge positive ramifications for stabilised peat scenarios as stabilised peat can now be modelled as a carbon sink. The best-fit models for CO_2 fluxes and X_c, as well as the k-rate factors and D_{c0} values, were integrated into the methodology.

The methodology was applied to a case study on a section of a recent Irish motorway project for which the excavation and replacement of peaty soil was the chosen solution (Scenario ER, as detailed in Chapter 7). The results of the case study show that:

(i) The total EC for road construction to the sub-base level (and implications thereof) of the 2.14 km section of the M6 showed carbon loss from excavated peat accounted for 62% of the total EC, signalling the importance of the management of excavated peat. Emissions from peat would have been, for example, 2.2 times higher had its

organic content been 85% instead of 41%, showing excavated peat to be a high-sensitivity variable. When the potential GHGs released from peat are factored in, building on peat increases EC substantially compared to building on mineral soils.

(ii) Two other ground improvement method scenarios for constructing this section of road were also considered: Scenario S, dry soil-mixing and Scenario ER + P, an appropriate combination of excavate-and-replace and piling. Based on the experimental results, stabilised peat was modelled as a carbon sink, consequently Scenario S had the lowest on-site carbon impact on the local surroundings in terms of direct and indirect emissions, but the binder used in stabilising the peat represented 86% of the overall EC total for Scenario S.

(iii) Scenario ER was the overall favoured technique for this project as it had the lowest EC and EE. Scenario S was the least favourable due to the high EC and EE of the binder. However, the EC and EE of Scenario S could have been decreased dramatically by changing the binder proportions from 3:1 cement to GGBS binder split to a 1:3 cement to GGBS binder split, if appropriate from a strength perspective. This change reduces total EC by 48% and total EE by 33%, giving Scenario S the lowest EC.

(iv) Employing a variety of restoration techniques, such as peatland restoration and afforestation on peat disposal areas and drained peatlands, can play a large part in reducing total EC. Furthermore, the EC of Scenarios ER and ER + P can be dramatically reduced if these techniques are employed for excavated peat.

8.3 Recommendations

8.3.1 Experimental testing

In the application of the gas chamber method and carbonation techniques to stabilised peat in this body of work, a framework of procedures and interpretation methods for future work in this area has been created. From the knowledge garnered from performing the experiments, some modifications to the carbonation techniques that would enhance the quality of the data obtained in future tests are suggested:

(i) When using the phenolphthalein indicator, it is proposed that to remove the effect of non-horizontal, uneven carbonation fronts displayed by 13% of the specimens tested, weighted averages for stabilised peat should be used, which would account for the different carbonation front depths and the different widths of the front at these depths and would, consequently, enhance the representation of the carbonation depth.

(ii) The small amount of sample required for XRD and FTIR analysis may incorrectly identify the position of the carbonation front as it may not be horizontal. It is advisable, therefore, in future stabilised peat studies to analyse at least three samples from positions evenly spaced across the carbonation front to guarantee a more comprehensive examination of the front.

(iii) A period of time greater than 10 minutes, but not exceeding 40 minutes, should be used to calculate the CO_2 flux for stabilised peat for a 180-day study. These recommendations stem from the examination of the linearity of the fluxes, the error of the GC and the underestimation of the true flux (see Section 4.7).

(iv) If the stabilised peat is older than in the experiments in this thesis, TGA analyses may be required to identify the $CaCO_3$ decomposition temperature range so that the LOI technique can be applied. It is recommended to test the most and least carbonated samples to identify this range.

(v) On a smaller scale, porosity could be used to show X_c if specimens were cut in 10 or 20 mm sections before being used in the water evaporation method. A difference in porosity with depth would indicate a carbonation front. This may work better in older stabilised peat where a large X_c is anticipated; otherwise, the water evaporation method can be used only as an indicator of carbonation over time.

8.3.2 Additional lab and field testing

While this thesis contributes substantially to the knowledge of the carbonation process in stabilised peat, the following suggestions for future research are recommended:

(i) In this study, eleven different stabilised peat scenarios were investigated. The next step in studying CO_2 fluxes and X_c in stabilised peat should be to explore different combinations of various binder type and content and environmental conditions; for example, the effect of surcharge and water table on stabilised peat with a 1:1 cement to GGBS binder split. Other variables requiring closer examination include CO_2 concentration and the effect of temperature and climate.

(ii) In order to expand on the current understanding of the carbonation process in stabilised peat described in this body of work, the carbonation behaviour of other stabilised soils should also be studied, including peat from fens and raised bogs and organic silts/clays.

(iii) While X_c shows the depth at which CO_2 is being taken in by the binder, another aspect of studying X_c would be to examine the change in strength properties of the stabilised peat (if any) as a result of carbonation. Porosity decreases and dry

densities increase due to carbonation which is likely to increase the strength, impermeability and stiffness properties of the stabilised peat and would, therefore, be of interest to geotechnical engineers for design and modelling purposes.

(iv) With further laboratory testing, a carbonation diffusion model could be developed that would account for several diffusion processes and for changes in stabilised peat properties that occur over time due to hydration and carbonation.

(v) CO_2 fluxes and X_c should be studied in the field. Comparative studies of field and laboratory carbonation behaviour should be undertaken to improve the prediction of CO_2 flux and carbonation depth in the field; for instance, correlations between laboratory and field should be examined.

If doubts about the on-site impact of carbon emissions from the stabilised peat were addressed, geotechnical engineers could make more informed decisions on the suitability of this technique for road construction and other infrastructure projects.

8.3.3 Factors affecting embodied carbon (EC)

The LCA methodology presented has potential to reduce the environmental impact of construction projects on peat when considering embodied energy (EE) and embodied carbon (EC) or global warming potential as indicators. Nevertheless, there are aspects of the methodology that could be improved. As well as incorporating more information on the carbonation process in stabilised peat into the methodology, two other avenues could be explored:

(i) Combine a drained peatland model such as the one developed by Ballard et al. (2011) that estimates water table depth at any point in time with equations developed by Nayak et al. (2008) that calculate emissions based on variables that include water table depth. Emissions from drained peatlands could then be estimated more precisely.

(ii) Investigate the peat emission rate of surcharging peat as a ground improvement technique. The availability of oxygen in surcharged peat may decrease due to a lower porosity, which makes it harder for oxygen to diffuse through the peat, hence CO_2 emissions may reduce.

References

Acquaye, A., & Duffy, A. (2010). Input-output Analysis of Irish Construction Sector Greenhouse Gas Emissions. *Building and Environment*, *45*(3), 784–791.

Adams, J. I., & Hanna, T. H. (1970). Ground improvements due to pile driving. In *Proceedings of a conference on the behaviour of piles.* (pp. 127–133). London, UK: Institution of Civil Engineers.

Åhnberg, H. (2006). *Strength of Stabilised Soils – A laboratory study on clays and organic soils stabilised with different types of binder*. Lunds Tekniska Högskola, Lund University.

AI-Khaiat, H., Haque, M. N., & Fattuhi, N. (2004). Concrete carbonation in arid climate. In *29th conference on our world in concrete & structures* (pp. 161–167). Singapore.

Ali, F. H., Sing, W. L., & Hashim, R. (2010). Engineering properties of improved fibrous peat. *Scientific Research and Essay*, *5*(2), 154–169.

Allott, T. E., Evans, M. G., Lindsay, J. B., Agnew, C. T., Freer, J. E., Jones, A. & Parnell, M. (2009). *Water table in peak district blanket peatlands. Moors for the future partnership. Moors for the future Report No. 17.* The Moorland Centre, Derbyshire, UK.

Allu. (2007). *Mass stabilisation manual*. Orimattila, Finland.

Alm, J., Saarnio, S., Nykänen, H., Silvola, J. & Martikainen, P. J. (1999). Winter CO_2, CH_4 and N_2O fluxes on some natural and drained boreal peatlands. Biogeochemistry, 44(2), 163–186.

Alm, J., Shurpali, N. J., Tuittila, E., Laurila, T., Maljanen, M., Saarnio, S., & Minkkinen, K. (2007). Methods for determining emission factors for the use of peat and peatlands — flux measurements and modelling. *Boreal Env. Res.*, *12*, 85–100.

Anstice, D. J., Page, C. L., & Page, M. M. (2005). The pore solution phase of carbonated cement pastes. *Cement and Concrete Research*, *35*(2), 377–383.

Anthony, W. H., Hutchinson, G. L., & Livingston, G. P. (1995). Chamber Measurement of Soil-Atmosphere Gas Exchange: Linear vs. Diffusion-Based Flux Models. *Soil Science Society of America Journal*, *59*(5), 1308.

Appelo, C. A. ., & Postmas, D. (1993). *Geochemistry, groundwater and pollution*. Rotterdam: A.A Balkema.

ASTM. (2007). *ASTM Standard D2974, Standard Test Methods for Moisture, Ash and Organic Matter of Peat and Other Organic Soils.* ASTM International, United States.

ASTM. (2008). *ASTM Standard D4531. Standard Test Methods for Bulk Density of Peat and Peat Products*. ASTM International, United States.

ASTM. (2010). *Designation: D2980 – 04 (Reapproved 2010): Standard Test Method for Volume Mass, Moisture-Holding Capacity, and Porocity of Saturated Peat Materials.* ASTM International, United States.

AWWA. (2011). *Internal Corrosion Control in Water Distribution Systems: Awwa Manual M58* (1st ed.). Denver, CO.: American Water Works Association.

Axelsson, K., Johansson, S.-E., & Andersson, R. (2002). *Stabilization of Organic Soils by Cement and Puzzolanic Reactions - Feasibility study; Report 3*. Swedish Deep Stabilization Research Centre c/o Swedish Geotechnical Institute, Linkoping.

Ballard, C. E., McIntyre, N., Wheater, H. S., Holden, J., & Wallage, Z. E. (2011). Hydrological modelling of drained blanket peatland. *Journal of Hydrology*, *407*(1–4), 81–93.

Barthelmy, D. (2014). Mineralogy Database. Retrieved December 5, 2014, from http://webmineral.com/

Bary, B., & Sellier, A. (2004). Coupled moisture—carbon dioxide–calcium transfer model for carbonation of concrete. *Cement and Concrete Research*, *34*(10), 1859–1872.

Beuving, J., & van den Akker, J. (1996). *SC-DLO Rapport 377 - Maaiveldsdaling van veengrasland bij twee polderpeilen in de polder Zegvelderbroek; vijfentwintig jaar zakkingsmetingen op het ROC Zegveld.* SC-DLO, Wageningen, the Netherlands.

Bier, T. A. (1987). Influence of type of cement and curing on carbonation progress and pore structure

of hydrated cement pastes. In *Microstructural development during hydration of cement* (pp. 123–134). Boston.

Bier, T. A., Kropp, J., & Hilsdorf, H. K. (1989). Formation of Silica gel During Carbonation of Cementitious Systems Containing Slag Cements. *ACI Special Publications*, *SP-114*, 1413–28.

Birnie, R., Clayton, P., Griffiths, P., Hulme, P., Roberston, R., Soane, B., & Ward, S. (1991). *Scottish Peat Resources and Their Energy Potential. Contract report for ETSU, E/5A/CON/1204/1676*. Energy Technology Support Unit, Scotland.

Black, K. G., & Farrell, E. P. (2006). *Carbon sequestration and Irish forest ecosystems*. COFORD, Dublin.

Black, K., & Gallagher, G. (2010). *The greenhouse gas balance of peatland forest*. COFORD, Dublin.

Boelter, D. H. (1972). Water table drawdown around an open ditch in organic soils. Journal of Hydrology, 15(4), 329–340.

Bord Na Mona. (2015). Peatlands in Ireland. Retrieved May 10, 2015, from http://www.heartland.ie/articles/peatlands-ireland

Bord na Móna. (2005). *Srahmore Waste Licence W199-1. Appendix 9.1 Annual Environmental Report*. Bord na Móna, Tullamore, Ireland.

Bouikni, A., Swamy, R., & Bali, A. (2009). Durability properties of concrete containing 50% and 65% slag. *Constr Build Mater*, *23*, 2836–45.

Boylan, N., Jennings, P., & Long, M. (2008). Peat slope failure in Ireland. *Quarterly Journal of Engineering Geology and Hydrogeology*, *41*(1), 93–108.

Bozkurt, S., Lucisano, M., Moreno, L., & Neretnieks, I. (2001). Peat as a potential analogue for the long-term evolution in landfills. *Earth-Science Reviews*, *53*(1–2), 95–147.

Brasseur, G.P., Orlando, J.J. and Tyndall, G. S. (1999). *Atmospheric Chemistry and Global Change*. New York: Oxford University Press.

Broomfield, J. P. (2007). *Corrosion of Steel in Concrete: Understanding, Investigation and Repair* (2nd ed.). London and New York: Taylor & Francis.

BSI. (1996). *BS 1377-3:1990 Methods of test for soils for civil engineering purposes. Part 3: Chemical and electro-chemical tests.* London, UK.

BSI. (2006a). *BS EN ISO 14040:2006. Environmental management — Life cycle assessment — Principles and framework*. European Committee for Standardization, Brussels, Belgium.

BSI. (2006b). *BS EN ISO 14044:2006. Environmental management — Life cycle assessment — Requirements and guidelines*. European Committee for Standardization, Brussels, Belgium.

BSI. (2006c). *BS ISO 14025:2006. Environmental labels and declarations — Type III environmental declarations — Principles and procedures*. European Committee for Standardization, Brussels, Belgium.

Buggy, F., & Farrell, E. R. (2012). Geotechnical challenges in road construction in Ireland: 2000–2010. In *Proceedings of a conference on geotechnics on Irish roads, 2000–2010 – a decade of achievement* (pp. 1–15). Portlaoise, Ireland: Engineers Ireland.

Burke, W. (1961). Drainage investigations on bogland: the effects of drain spacing on ground water levels. *Irish J Agric Res*, 1(1), 31–34.

Chambers, F. M., Beilman, D. W., & Yu, Z. (2011). Methods for determining peat humification and for quantifying peat bulk density, organic matter and carbon content for palaeostudies of climate and peatland carbon dynamics. *Mires and Peat*, *7*, 1–10.

Chang, C.-F., & Chen, J.-W. (2006). The experimental investigation of concrete carbonation depth. *Cement and Concrete Research*, *36*(9), 1760–1767.

Chappat, M., & Bilal, J. (2003). *The environmental road of the future*. COLAS group, France.

Chau, C., Soga, K., O'Riordan, N., & Nicholson, D. (2012). Embodied energy evaluation for sections of the UK Channel Tunnel rail link. *Proceedings of the ICE - Geotechnical Engineering*, *165*(2), 65–81.

Chen, H., & Wang, Q. (2006). The behaviour of organic matter in the process of soft soil stabilization

using cement. *Bull Eng Geol Env*, *65*, 445–448.

Chen, J. J., Thomas, J. J., Taylor, H. W. F., & Jennings, H. M. (2004). Solubility and structure of calcium silicate hydrate,. *Cem. Conc. Res.*, *34*, 1499–1521.

Clymo, R. S. (1984). The limits to peat bog growth. *Philosophical Transactions of Royal Society of London Series B*, *303*, 605–654.

Cole, W. F., & Kroone, B. (1959). Carbonate Minerals in Hydrated Portland Cement. *Nature*, *184*(57).

Connolly, J., Holden, N. M., & Ward, S. M. (2007). Mapping Peatlands in Ireland using a Rule-Based Methodology and Digital Data. *Soil Science Society of America Journal*, *71*(2), 492.

Cooke, R., & Price, G. (1973). Strains and displacements around friction piles. In *Proceeding of the 8th international conference on soil mechanics and foundation engineering*, (p. vol. 2.1., 53-60). Moscow.

Coulson, J. C., Butterfield, J. E. L. & Henderson, E. (1990). The Effect of Open Drainage Ditches on the Plant and Invertebrate Communities of Moorland and on the Decomposition of Peat. *Journal of Applied Ecology*, 27(2), 549–61.

Couwenberg, J. (2009). *Methane emissions from peat soils (organic soils, histosols)*. Greifswald University, Wetlands International.

Crill, P., Hargreaves, K. & Korhola, A. (2000). *The Role of Peat in Finnish Greenhouse Gas Balances*. Ministry of Trade and Industry, Helsinki, Finland.

Dapkus, G., & Stankevičius, V. (1985). Cellular Concrete Carbonation. *Batiment International, Building Research and Practice*, *13*(2), 184–187.

DECC, & Defra. (2012). *Guidelines to Defra/DECC's GHG conversion factors for company reporting. : Defra; 2012.* London, UK.

Duggan, A. R., McCabe, B. A., Clifford, E., & Goggins, J. (2015). Carbonation in stabilised peat: an accelerated pilot study. In *16th European Conference on Soil Mechanics and Geotechnical Engineering* (Vol. 5, pp. 2383–2388). Edinburgh.

Duggan, A. R., McCabe, B. A., Goggins, J., & Clifford, E. (2015). An embodied carbon and embodied energy appraisal of a section of Irish motorway constructed in peatlands. *Construction and Building Materials*, *79*, 402–419.

Duggan, A. R., McCabe, B. A., Goggins, J. M., & Clifford, E. (2012). Factors affecting Embodied Carbon / Embodied Energy associated with ground improvements techniques for construction on peat. In *Proceedings of the Bridge & Concrete Research in Ireland Conference* (pp. 147–152). Dublin Institute of Technology, Ireland.

Dweck, J., Buchler, P. M., Coelho, A. C. V., & Cartledge, F. K. (2000). Hydration of a Portland cement blended with calcium carbonate. *Thermochimica Acta*, *346*(1–2), 105–113.

Dykes, A. P., & Warburton, J. (2007). Mass movements in peat: A formal classification scheme. *Geomorphology*, *86*(1–2), 73–93.

Ecocem. (2015). About ggbs. Retrieved August 17, 2015, from http://www.ecocem.ie/technical,ggbs,properties.htm

EFFC, & DFI. (2013). EFFC Carbon Calculator. Retrieved from http://www.geotechnicalcarboncalculator.com/en/

Egan, D., & Slocombe, B. C. (2010). Demonstrating environmental benefits of ground improvement. *Proceedings of the ICE - Ground Improvement*, *163*(1), 63–69.

Eireann, M. (2015a). No Title. Retrieved from http://www.met.ie/climate/monthly-data.asp?Num=1175

Eireann, M. (2015b). No Title. Retrieved January 15, 2015, from http://www.met.ie/climate-ireland/rainfall.asp

Engelson, C. J., Mehus, J., Pade, C., & Saether, D. H. (2005). *Carbon dioxide uptake in demolished and crushed concrete*. Norwegian Building Research Institute, Oslo, Norway.

EPA. (2008). *Ireland's National Greenhouse Gas Emissions Projections to 2020*. Environmental

Protection Agency, Johnstown Castle, Co. Wexford, Ireland.

EPA. (2010a). Atmospheric Carbon Dioxide -Mace Head, Galway, Ireland. Retrieved June 18, 2015, from http://www.epa.ie/media/Atmospheric Carbon Dioxide.xls

EPA. (2010b). *Ireland's greenhouse gas emissions in 2009*. Environmental Protection Agency, Johnstown Castle, Co. Wexford, Ireland.

EPA. (2011). *Ireland's Greenhouse Gas Emissions in 2010.* Environmental Protection Agency, Johnstown Castle, Co. Wexford, Ireland.

EPA. (2012). *Ireland's greenhouse gas emissions projections 2011–2020.* Environmental Protection Agency, Johnstown Castle, Co. Wexford, Ireland.

EPA. (2014). *Ireland's greenhouse gas emissions in 2012*. Environmental Protection Agency, Johnstown Castle, Co. Wexford, Ireland.

EPA. (2015). *Ireland's Greenhouse Gas Emission Projections 2014 - 2035*. Environmental Protection Agency, Johnstown Castle, Co. Wexford, Ireland.

European Commission. (2003). *Establishing a scheme for GHG allowance trading within the community. 2003/87/EC.* European Commission Official Journal L 275.

European Commission. (2009a). *Directive 2009/29/EC of the European Parliament and of the Council*. European Commission Official Journal L 140.

European Commission. (2009b). *Promotion of the use of energy from renewable sources*. European Commission Official Journal L140.

EuroSoilStab. (2002). *Development of Design and Construction Methods to Stabilize Soft Organic Soils: Design Guide Soft Soil Stabilization. CT97-0351. Project No. BE 96-3177*. BREPress.

Fasihnikoutalab, M. H., Asadi, A., Kim Huat, B., Westgate, P., Ball, R. J., & Pourakbar, S. (2016). Laboratory-scale model of carbon dioxide deposition for soil stabilisation. *Journal of Rock Mechanics and Geotechnical Engineering*, *8*(2), 178–186.

Fernández Bertos, M., Simons, S. J. R., Hills, C. D., & Carey, P. J. (2004). A review of accelerated carbonation technology in the treatment of cement-based materials and sequestration of CO_2. *Journal of Hazardous Materials*, *112*(3), 193–205.

Forbrich, I., Kutzbach, L., Hormann, A., & Wilmking, M. (2010). A comparison of linear and exponential regression for estimating diffusive CH_4 fluxes by closed-chambers in peatlands. *Soil Biology and Biochemistry*, *42*(3), 507–515.

Forsman, J., Jyrävä, H., Lahtinen, P., Niemelin, T., & Hyvönen, I. (2015). *Mass stabilization manual*. Finland.

Forster, P., Ramaswamy, V., Artaxo, P., Berntsen, T., Betts, R., Fahey, D. W., … Dorland, R. V. (2007). Changes in Atmospheric Constituents and in Radiative Forcing. In M. T. and H. L. M. [Solomon, S., D. Qin, M. Manning, Z. Chen, M. Marquis, K.B. Averyt (Ed.), *Climate Change 2007: The Physical Science Basis. Contribution of Working Group I to the Fourth Assessment Report of the Intergovernmental Panel on Climate Change*. UK and USA: Cambridge University Press.

Frost, J. (2013). Multiple Regression Analysis: Use Adjusted R-Squared and Predicted R-Squared to Include the Correct Number of Variables. Retrieved October 3, 2015, from http://blog.minitab.com/blog/adventures-in-statistics/multiple-regession-analysis-use-adjusted-r-squared-and-predicted-r-squared-to-include-the-correct-number-of-variables

Frost, J. (2014). How Important Are Normal Residuals in Regression Analysis? Retrieved November 26, 2015, from http://blog.minitab.com/blog/adventures-in-statistics/how-important-are-normal-residuals-in-regression-analysis

Frost, J. (2015). Choosing Between a Nonparametric Test and a Parametric Test. Retrieved November 27, 2015, from http://blog.minitab.com/blog/adventures-in-statistics/choosing-between-a-nonparametric-test-and-a-parametric-test

Fukushima, T. (1988). *Theoretical investigation on the influence of various factors on carbonation of concrete, BRI Research Paper No 127 (ISSN 0453-4972)*. Building research Institute, Japan).

Fukushima, T., Yoshizaki, Y., Tomosawa, F., & Takahashi, K. (1998). Relationship Between

Neutralization Depth and Concentration Distribution of $CaCO_3$ -$Ca(OH)_2$ in Carbonated Concrete. *Advances in Concrete Technology, ACI SP-179*, 347–363.

Gemite Products Inc. (2005). *Technical Memorandum: Corrosion of Steel in Concrete due to Carbonation*. Gemite Group of Companies, USA and Canada.

GGBS Review Group. (2009). Frequently asked questions (FAQs) about Ground Granulated Blastfurnace Slag (GGBS). Retrieved from http://ggbsreviewgroup.blogspot.ie/

Gill, M. (2010). *Peatland Hydrology Impact Assessment, Corrib Onshore Pipeline*. Hydro-Environmental Services (HES), Ireland.

Gilman, K. (1994). *Hydrology and wetland conservation*. London, UK: Wiley.

Girardello, F., Guégan, R., Esteves, V. I., Baumvol, I. J. R., Sierra, M. M. D., Crespo, J. S., … Giovanela, M. (2013). Characterization of Brazilian peat samples by applying a multi-method approach. *Spectroscopy Letters: An International Journal for Rapid Communication*, *46*(3), 201–210.

Glass, G. K. (2003). Reinforcement Corrosion. In J. Newman & B. S. Choo (Eds.), *Advanced Concrete Technology 2: Concrete Properties* (p. 97). Great Britain: Elsevier Ltd.

Glatzel, S., Basiliko, N. & Moore, T. (2004). Carbon dioxide and methane production potentials of peats from natural, harvested and restored sites, eastern Québec, Canada. Wetlands, 24(2), 261–267.

Glatzel, S., Forbrich, I., Lemke, S. & Gerold, G. (2008). Environmental controls of greenhouse gas release in a restoring peat bog in NW Germany. *Biogeosciences, 5*, 213–242.

Goggins, J., Keane, T., & Kelly, A. (2010). The assessment of embodied energy in typical reinforced concrete building structures in Ireland. *Energy & Buildings*, *42*(5), 735–744.

HA. (1991). *Design manual for road and bridges (DMRB), volume 4, geotechnics and drainage, section 1 earthworks, geotechnical considerations and techniques for widening highway earthworks HA 43/91*. The Highways Agency, UK.

Haan, E. J. Den. (1996). A compression model for non-brittle soft clays and peat. *Géotechnique*, *46*(1), 1–16.

Häkkinen, T. (1993). *Influence of High Slag Content on the Basic Mechanical Properties and Carbonation of Concrete*. VTT publications No.141, Finland.

Hammond, G., & Jones, C. (2011). *Inventory of Carbon & Energy Version 2.0 (ICE V2.0)*. University of Bath, UK.

Hammond, R. F. (1981). *Soil Survery Bulletin No. 35, The Peatlands of Ireland* (2nd ed.). An Foras Taluntais, Dublin.

Hanrahan, E. T. (1954). An investigation of physical properties of peat. *Geotechnique*, *4*, 108–121.

Hargreaves, K. J., Milne, R., & Cannell, M. G. R. (2003). Carbon balance of afforested peatland in Scotland. *Forestry*, *76*(3), 299–317.

Hassanein. (1997). T*he application of neural networks to service life prediction of concrete structures*. Department of Civil Engineering, Imperial College London.

Heathwaite, A. L. (1990). Solute transfer from drained fen peat. *Water Air Soil Pollut*, 55(3–4), 379–95.

Hebib, S., & Farrell, E. R. (2003). Some experiences on the stabilization of Irish peats. *Can. Geotech. J.*, *120*, 107–120.

Helenlund, K. V. (1980). Geotechnical properties and behaviour of Finnish peats. In *Valtion Teknillinen Tutkimuskeskus, VTT Symposium* (p. 8, reprint, 85–107.). Finland.

Hendriks, D. M. D., Huissteden, J. Van, Dolman, A. J., Molen, M. K. Van Der, & Amsterdam, V. U. (2007). The full greenhouse gas balance of an abandoned peat meadow. *Biogeosciences*, *4*(3), 411–424.

Herrera, R. (2011). *Comparison of methods to determine the carbonation depth in fly ash blended cement mortars*. Thunder Bay, Ontario, Canada.

Higgins, D. (2007). Briefing: GGBS and sustainability. *Proceedings of the ICE - Construction Materials, 160*(3), 99–101.

Hillman, G. R. (1992). Some hydrological effects of peatland drainage in Alberta's boreal forest. *Canadian Journal of Forest Research*, 22(11), 1588–96.

Hobbs, N. B. (1986). Mire morphology and the properties and behaviour of some British and foreign peats. *Quarterly Journal of Engineering Geology and Hydrogeology*, *19*(1), 7–80.

Holden, J. & Burt, T. P. (2003). Hydrological studies on blanket peat: the significance of the acrotelm-catotelm model. *Journal of Ecology*, 91(1), 86–102.

Holden, J. (2009). Flow through macropores of different size classes in blanket peat. *Journal of Hydrology*, *364*(3-4), 342–348.

Holden, N. M., Brereton, A. J., Fealy, R. & Sweeney, J. (2003). Possible change in Irish climate and its impact on barley and potato yields. *Agricultural and Forest Meteorology*, *116*(3-4), 181–196.

Houst, Y. F. (1996). *The Role of Moisture in the Carbonation of Cementitious Materials*. Federal Institute of Technology, EPF Lausanne, Switzerland.

Houst, Y. F. (2002). Depth profiles of carbonates formed during natural carbonation. *Cement and Concrete Research*, *32*(12), 1923–1930.

Hudson, J. & Roberts, G. (1982). The effect of a tile drain on the soil moisture content of peat. J Agric Eng Res, 27(6), 495–500.

Huntzinger, D. N., Gierke, J. S., Kawatra, S. K., Eisele, T. C., & Sutter, L. L. (2009). Carbon dioxide sequestration in cement kiln dust through mineral carbonation. *Environmental Science & Technology*, *43*(6), 1986–92.

Huntzinger, D. N., Gierke, J. S., Sutter, L. L., Kawatra, S. K., & Eisele, T. C. (2009). Mineral carbonation for carbon sequestration in cement kiln dust from waste piles. *Journal of Hazardous Materials*, *168*(1), 31–7.

Hutchinson, G. L., & Mosier, A. R. (1981). Improved Soil Cover Method for Field Measurement of Nitrous Oxide Fluxes. *Soil Science Society of America Journal*, *45*(2), 311.

Huttunen, E., & Kujala, K. (1996). On the stabilization of organic soils. In *Proceedings of the 2nd International Conference on Ground Improvement Geosystems* (Vol. 1, pp. 411–414). IS-Tokyo 96.

Iiyama, I., & Hasegawa, S. (2010). Gas Diffusion Coefficient of Undisturbed Peat Soils, Soil Science and Plant Nutrition, *51*(3), 431–435.

IMCES. (2011). *Mass loss and nutrient release during litter decay in oligotrophic peatland*. Institute of monitoring of climatic and ecological systems, Russia.

Inui, T., Chau, C., Soga, K., Nicolson, D., & O'Riordan, N. (2011). Embodied energy and gas emissions of retaining wall structures. *Journal of Geotechnical and Geoenvironmental Engineering*, *137*(10), 958–967.

IPCC. (1997). *Revised 1996 IPCC guidelines for national greenhouse gas inventories.* Intergovernmental Panel on Climate Change, Bracknell, UK.

IPCC. (2001). *Climate Change 2001. The Scientific Basis. Contribution of Working Group 1 to the Third Assessment Report of the Inter-Governmental Panel on Climate Change.* Cambridge University Press, Cambridge, United Kingdom.

IPCC. (2003). *Good practice guidance for land use, land-use change and forestry*. (Penman, J., Gytarsky, M., Hiraishi, T., Krug, T., Kruger, D., Pipatti, R.,… Wagner, F., Eds.). The Intergovernmental Panel on Climate Change, Japan: Institute for Global Environmental Strategies.

IPCC. (2006). *2006 IPCC Guidelines for National Greenhouse Gas Inventories, Vol. 4, Ch. 7*. Institute for Global Environmental Strategies, Japan.

IPCC. (2007). *Summary for Policymakers. In: Climate Change 2007: The Physical Science Basis. Contribution of Working Group I to the Fourth Assessment Report of the Intergovernmental Panel on Climate Change*. Cambridge University Press, Cambridge, United Kingdom and New York, NY, USA,.

IPCC. (2015a). Blanket bogs. Retrieved from http://www.ipcc.ie/a-to-z-peatlands/blanket-bogs/

IPCC. (2015b). Raised bogs. Retrieved from http://www.ipcc.ie/a-to-z-peatlands/raised-bogs/

Irish Cement. (2010). *Safety Data Sheet for Cement*. Irish Cement Ltd., Drogheda, Co. Louth, Ireland.

Iwasaki, M., & Tada, S. (1985). Carbonation of aerated concrete. In *Proceedings of 1985 Beijing International Symposium on Cement and Concrete (Volume 3)* (pp. 414–423). Beijing, China.

Jansen, E. (2008). *The effects of land use, temperature and water level fluctuations on the emission of nitrous oxide (N_2O), carbon dioxide (CO_2) and methane (CH_4) from organic soil cores in Iceland*. University of Iceland, Iceland.

Janz, M., & Johansson, S.-E. (2002). *The Function of Different Binding Agents in Deep Stabilization*. Swedish Deep Stabilization Research Centre, Sweden.

Jelisic, N., & Leppänen, M. (1999). Mass stabilization of peat in road and railway construction. In H. & B. Bredenber (Ed.), *Dry mix methods for deep soil stabiilization*. International Society for Rock Mechanics.

Joosten, H., & Clarke, D. (2002). *Wise Use of Mires and Peatlands - Background and Principles Including a Framework for Decision-Making*. International Mire Conservation Group and International Peat Society, Finland.

Kazemian, S., Huat, B. B. K., Prasad, A., & Barghchi, M. (2011). Effect of peat media on stabilization of peat by traditional binders. *International Journal of the Physical Sciences*, *6*(3), 476–481.

Kennedy, D. (2000). *Chemistry Live!* (1st edition). Dublin: Folens Publishers.

Khunthongkeaw, J., Tangtermsirikul, S., & Leelawat, T. (2006). A study on carbonation depth prediction for fly ash concrete. *Construction and Building Materials*, *20*(9), 744–753.

Kiely, G., Leahy, P., Sottocornola, M., & et al. (2009). *Celticflux: measurement and modelling of greenhouse gas fluxes from grasslands and a peatland in Ireland.* Environmental Protection Agency, Co. Wexford, Ireland.

Klemedtsson, L., Von Arnold, K., Weslien, P., & Gundersen, P. (2005). Soil CN ratio as a scalar parameter to predict nitrous oxide emissions. *Global Change Biology*, *11*(7), 1142–1147.

Klug, H. P., & Alexander, L. E. (1974). *X-Ray Diffraction Procedures: For Polycrystalline and Amorphous Materials* (2nd ed.). New York: John Wiley & Sons.

Koehler, A.-K., Sottocornola, M., & Kiely, G. (2011). How strong is the current carbon sequestration of an Atlantic blanket bog? *Global Change Biology*, *17*(1), 309–319.

Kosmatka, S. H., Kerkhoff, B., & Panarese, W. C. (2002). *Design and Control of Concrete Mixtures* (14th ed.). Portland Cement Association, Skokie, IL.

Kutzbach, L., Schneider, J., Sachs, T., Giebels, M., Nykanen, H., Shurpali, N. J., … Wilmking, M. (2007). CO_2 flux determination by closed-chamber methods can be seriously biased by inappropriate application of linear regression. *Biogeosciences*, *4*, 1005–1025.

Lagerblad, B. (2001). *Leaching performance of concrete based on samples from old concrete constructions, SKB TR-01-27*. Report series of Swedish Nuclear Fuel and Waste Management CO, Stockholm, Sweden.

Lagerblad, B. (2005). *Carbon dioxide uptake during concrete life cycle – State of the art*. Swedish Cement and Concrete Research Institute, Stockholm, Sweden.

Laine, A. (2006). *Carbon gas fluxes in an irish lowland blanket bog*. National University of Ireland, Cork.

Laine, A., Wilson, D., Kiely, G., & Byrne, K. a. (2007). Methane flux dynamics in an Irish lowland blanket bog. *Plant and Soil*, *299*(1–2), 181–193.

Lamers, L. P. M., Bobbink, R., & Roelofs, J. G. M. (2000). Natural nitrogen filter fails in polluted raised bogs. *Global Change Biology*, 6(5), 583–586.

Landva, A., Pheeney, P. and Mersereau, D. (1983). *Undisturbed Sampling of Peat. In: Testing of Peats & Organic Soils ASTM STP 820.* (P. M. Jarrett, Ed.). West Conshohocken, PA: American Society of Testing and Materials.

Lange, L. C., Hills, C. D., & Poole, A. B. (1996). The effect of accelerated carbonation on the properties of cement-solidified waste forms. *Waste Management*, *16*(8), 757–763.

Lee, H. J., Kim, D. G., Lee, J. H., & Cho, M. S. (2012). A Study for Carbonation Degree on Concrete

using a Phenolphthalein Indicator and Fourier-Transform Infrared Spectroscopy. *World Academy of Science, Engineering and Technology*, *62*, 184–190.

Lindsay, R. (2010). *Peatbogs and Carbon, a critical synthesis*. University of East London: Environmental Research Group (ERG), UK.

Livingston, G. P., & Hutchinson, G. L. (1995). Enclosure-based measurement of trace gas exchange: Applications and sources of error. In P. A. Matson & R. C. Harriss (Eds.), *Biogenic Trace Gases: Measuring Emissions from Soil and Water. Methods in Ecology* (pp. 14–51). Blackwell Science/Cambridge Univ. Press, Cambridge, UK.

Livingston, G. P., Hutchinson, G. L., & Spartalian, K. (2005). Diffusion theory improves chamber-based measurements of trace gas emissions. *Geophysical Research Letters*, *32*(24), L24817.

Lo, Y., & Lee, H. M. (2002). Curing effects on carbonation of concrete using a phenolphthalein indicator and Fourier-transform infrared spectroscopy. *Building and Environment*, *37*(5), 507–514.

Long, M. (2005). Review of Peat Strength , Peat Characterisation and Constitutive Modelling of Peat With Reference To Landslides. *Studia Geotechnica et Mechanica*, *27*(3), 67–90.

Loo, Y. H., Chin, M. S., Tam, C. T., & Ong, K. C. . (1994). A carbonation prediction model for acclerated carbonation testing of concrete. *Magazine of Concrete Research*, *46*(168), 191–200.

Lowry, C. S. (2008). *Controls on Groundwater Flow in a Peat Dominated Wetland/stream Complex, allequash wetland, northern Wisconsin*. University of Wisconsin-Madison.

MacCulloch, F. (2006). *Guidelines for the risk management of peat slips on the construction of low volume/low cost roads over peat*. Forestry Commission, Scotland.

MacFarlane, I. C., & Radworth, M. W. (1964). A study of the physical behaviour of peat derivatives under compression. In *Proceedings of the 10th Muskeg Conference, Technical Memorandum 85, Ottawa*. Ottawa, Canada.

Manton, R., Duggan, A., Goggins, J., & Clifford, E. (2014). Carbon costs and savings of Greenways: creating a balance sheet for the sustainable design and construction of cycling routes. *International Journal of Environment and Sustainable Development*, *13*(1), 3.

Martikainen, P., Nykänen, H., Crill, P., & Silvola, J. (1993). Effect of a lowered water table on nitrous oxide fluxes from northern peatlands. *Nature*, *366*, 51–53.

Martz, E. (2013). Enough Is Enough! Handling Multicollinearity in Regression Analysis. Retrieved November 25, 2015, from http://blog.minitab.com/blog/understanding-statistics/handling-multicollinearity-in-regression-analysis

Matsushita, F., Aono, Y., & Shibata, S. (2000). Carbonation degree of autoclaved aerated concrete. *Cem. Conc. Res.*, *30*(11), 1741–1745.

Matthews, A. (2015). Including LULUCF in the EU's 2030 climate policy target. Retrieved June 24, 2015, from http://capreform.eu/including-lulucf-in-the-eus-2030-climate-policy-target/

Matthews, J. (1984). Carbonation of ten years old concretes with and without PFA. In *Conference proceedings of Ashtech' 84 second international conference on ash technology and marketing* (p. 398A). London.

Matthews, S. (2012). *Structural Concrete Textbook on behaviour design and performance, vol. 5* (2nd Editon). International Federation for structural concrete.

Matthias, A. D., Yarger, D. N., & Weinbeck, R. S. (1978). A numerical evaluation of chamber methods for determining gas fluxes. *Geophysical Research Letters*, *5*(9), 765–768.

Matthiesen, H., Dunlop, R., Jann, A. J., & Christensson, A. (2004). *Monitoring of cultural deposits below Bryggen in Bergen, Norway*. Nationalmuseet ; NIKU ; Multiconsult ; Riksantikvaren.

McCaffrey, M. (2011). *An I-O hybrid methodology for environmental LCA of embodied energy and carbon in Irish products and services - A study of reinforced concrete*. National University of Ireland, Galway.

McPolin, D., Basheer, P., Long, A., Grattan, K., & Sun, T. (2007). New test method to obtain pH profiles due to carbonation of concretes containing supplementary cementitious materials. *Journal of Materials in Civil Engineering*, *19*(11), 936–946.

Meland, I. (1985). *Karbonatisering i flygaskecement og standard portland sement med og utan silika, SINTEF Rapport, STF A85049*. Trondheim, Norge.

Mesri, G., & Ajlouni, M. (2007). Engineering Properties of Fibrous Peats. *Journal of Geotechnical and Geoenvironmental Engineering*, *133*(7), 850–866.

Mesri, G., Stark, T. D., Ajlouni, M. A., & Chen, C. S. (1997). Secondary compression of peat with or without surcharging. *Journal of Geotechnical and Geoenvironmental Engineering*, *123*(5), 411–421.

Milachowski, C., Stengel, T., & Gehlen, C. (2011). *Life cycle assessment for road construction and use*. Centre for Building Materials, Germany.

Minitab. (2016a). Lack-of-fit and lack-of-fit tests. Retrieved February 2, 2016, from http://support.minitab.com/en-us/minitab/17/topic-library/modeling-statistics/regression-and-correlation/regression-models/lack-of-fit-and-lack-of-fit-tests/

Minitab. (2016b). What is a variance inflation factor (VIF)? Retrieved from http://support.minitab.com/en-us/minitab/17/topic-library/modeling-statistics/regression-and-correlation/model-assumptions/what-is-a-variance-inflation-factor-vif/

Minkkinen, K., & Laine, J. (2006). Vegetation heterogeneity and ditches create spatial variability in methane fluxes from peatlands drained for forestry. *Plant and Soil*, *285*(1–2), 289–304.

Moncaster, A. M., & Symons, K. E. (2013). A method and tool for "cradle to grave" embodied carbon and energy impacts of UK buildings in compliance with the new TC350 standards. *Energy and Buildings*, *66*, 514–523.

Montanarella, L., Jones, R. J. ., & Hiederer, R. (2006). The distribution of peatland in Europe. *Mires and Peat*, *1*, 1–10.

Moore, T. R., & Dalva, M. (1993). The influence of temperature and water table position on carbon dioxide and methane emissions from laboratory columns of peatland soils. *Journal of Soil Science*, *44*, 651–664.

Munro, R. (2004). *Dealing with bearing capacity problems on low volume roads constructed on peat*. The Highland Council, Scotland.

Nagataki, S., Ohga, H., & Kim, E. (1986). Effect of Curing Conditions on the Carbonation of Concrete with Fly Ash and the Corrosion of Reinforcement in Long-Term Tests. In *ACI SP-91 Madrid, Proc* (pp. 521–540).

Nakamoto, J., & Togawa, K. (1995). A Study of Strength Development and Carbonation of Concrete Incorporating High Volume Blast Furnace Slag. In *International Conference on the use of fly ash, silica fume, slag and other mineral by-products in concrete* (p. 1121–1140 (SP 153)).

Nakanoa, T., Sawamotob, T., Morishitac, T., Inoued, G., & Hatano, R. (2004). A comparison of regression methods for estimating soil–atmosphere diffusion gas fluxes by a closed-chamber technique. *Soil Biology and Biochemistry*, *36*(1), 107–113.

Nayak, R., Miller, D., Nolan, A., Smith, P., & Smith, J. (2008). *Calculating carbon savings from wind farms on Scottish peat lands—a new approach*. University of Aberdeen and Macaulay Land Use Research Institute, London, UK.

Ngala, V. T. (1997). Effect of carobonation on pore structure and diffusional properties of hydrated cement pastes. *Cement and Concrete Research*, *27*(7), 995–1007.

NRA. (2010). *NRA annual report 2010*. National Roads Authority, Dublin, Ireland.

NRA. (2013). *NRA manual of contract documents for roadworks, vol. 4*. National Roads Authority, Dublin, Ireland.

O'Loughlin, C., & Lehane, B. (2003). A study of the link between composition and compressibility of peat and organic soils. In *Proceedings of the Second Conference on Advances in Soft Soil Engineering and Technology* (pp. 135–152). Malaysia: Universiti Putra Malaysia Press.

Orsmond, W. (2012). Piled Embankments – Recent Experiences. In *Proceedings of a conference on geotechnics on Irish roads, 2000–2010 – a decade of achievement* (pp. 36–46). Portlaoise, Ireland.

Pantelidou, H., Nicholson, D., Hughes, L., Jukes, A., & Wellappili, L. (2012). Earthworks emissions

in construction of a highway. *Geological Society, London, Engineering Geology Special Publications*, *26*(1), 175–180.

Papadakis, V. G., Fardis, M. N., & Vayenas, C. G. (1992). Hydration and carbonation of pozzolanic cements. *Materials*, *89*(2), 119–130.

Papadakis, V. G., Vayenas, C. G., & Fardis, M. N. (1991a). Experimental investigation and mathematical modeling of the concrete carbonation problem. *Chemical Engineering Science*, *46*(5/6), 1333–1338.

Papadakis, V. G., Vayenas, C. G., & Fardis, M. N. (1991b). Fundamental modeling and experimental investigation of concrete carbonation. *ACI Material Journal*, *88*(4), 363–373.

Parish, F., Sirin, A., Charman, D., Joosten, H., Minayeva, T., & Silvius, M. (2007). *Assessment on peatlands, biodiversity and climate change: Executive summary*. Global Environment Centre, Kuala Lumper and Wetlands International, Wageningen.

Park, G. (1995). Durability and carbonation of concrete. *Mag Korean Concr Inst*, *7*, 74–81.

Parkin, T.B. and Venterea, R. T. (2010). *Sampling Protocols. Chapter 3. Chamber-Based Trace Gas Flux Measurements. IN Sampling Protocols* (Vol. 2010).

Parrot, L. J. (1987). *A reveiw of carbonation in reinforced concrete*. Cement and Concrete Association, Slough, UK.

Parrott, L. J., & Killoh, D. C. (1989). Carbonation in a 36 year old, in-situ concrete. *Cement and Concrete Research*, *19*(4), 649–656.

Pedersen, A. R. (2000). Estimating the Nitrous Oxide Emission Rate from the Soil Surface by Means of a Diffusion Model. *Scandinavian Journal of Statistics*, *27*(3), 385–403.

Pedersen, A. R., Petersen, S. O., & Schelde, K. (2010). A comprehensive approach to soil-atmosphere trace-gas flux estimation with static chambers. *European Journal of Soil Science*, *61*(6), 888–902.

Pedersen, A. R., Petersen, S. O., & Vinther, F. P. (2001). Stochastic Diffusion Model for Estimating Trace Gas Emissions with Static Chambers. *Soil Science Society of America Journal*, *65*(1), 49.

Petit, J. R. et al. (1999). Climate and atmospheric history of the past 420,000 years from the Vostok ice core, Antarctica. *Nature*, *399*, 429–436.

Pichan, S. P., & O'Kelly, B. . (2012). Stimulated decomposition in peat for engineering applications. *Proceedings of the ICE-Ground Improvement*, *166*(3), 168–176.

Pousette, K., Mácsik, J., Jacobsson, A., Andersson, R., & Lahtinen, P. (1999). Peat soil samples in laboratory - Experiences from manufacturing and testing. In H. Bredenberg, G. Holm, & B. B. Broms (Eds.), *Dry Mix Methods for Deep Soil Stabilization* (pp. 85–92). Stockholm.

PRé Sustainability. (2015). SimaPro. Retrieved June 5, 2015, from https://www.pre-sustainability.com/simapro.

Preston, M. D., Smemo, K. A., McLaughlin, J. W. & Basiliko, N. (2012). Peatland microbial communities and decomposition processes in the james bay lowlands, Canada. *Frontiers in Microbiology*, 3, 70.

Prevost, M., Belleau, P. & Plamondon, A. P. (1997). Substrate conditions in a treed peatland: responses to drainage. *Ecoscience*, 4(4), 543–54.

Rahman, A. A., & Glasser, F. P. (1989). Comparative studies of the carbonation of hydrated cements. *Advances in Cement Research*, *2*(6), 49–54.

Regan, S., & Johnston, P. (2010). Consequences of marginal drainage from a raised bog and understanding the hydrogeological dynamics as a basis for restoration. *Geophysical Research Abstracts*, *12*.

Regina, K., Nykänen, H., Silvola, J., & Martikainen, P. J. (1996). Fluxes of nitrous oxide from boreal peatlands as affected by peatland type, water table level and nitrification capacity. *Biogeochemistry*, *35*(3), 401–418.

Regina, K., Silvola, J., & Martikainen, P. J. (1999). Short-term effects of changing water table on N_2O fluxes from peat monoliths from natural and drained boreal peatlands. *Global Change Biology*, *5*(2), 183–189.

Renou-wilson, F., Bolger, T., Bullock, C., Convery, F., Curry, J., Ward, S., … Müller, C. (2013). *BOGLAND : Sustainable Management of Peatlands in Ireland*. Environmental Protection Agency, Johnstown Castle, Co. Wexford, Ireland.

Rezagholilou, A., & Nikraz, H. (2012). Analytical method in carbonation of cement treated base material. In *25th ARRB Conference*. Perth, Australia.

RPS Group. (2004). *Environmental impact statement (EIS) N6 Galway to East Ballinasloe. Galway, Ireland, vol. 1*. RPS, Galway, Ireland.

Rückauf, U., Augustina, J., Russowb, R., & Merbach, W. (2004). Nitrate removal from drained and reflooded fen soils affected by soil N transformation processes and plant uptake. *Soil Biology and Biochemistry*, *36*(1), 77–90.

Ryan, M. G. (1991). Effects of Climate Change on Plant Respiration. *Ecological Applications*, *1*(2), 157–167.

Saarnio, S., Alm, J., Silvola, J., Lohila, A., Nykänen, H., & Martikainen, P. J. (1997). Seasonal variation in CH_4 emissions and production and oxidation potentials at microsites on an oligotrophic pine fen. *Oecologia*, *110*(3), 414–422.

Safiuddin, M., & Hearn, N. (2005). Comparison of ASTM saturation techniques for measuring the permeable porosity of concrete. *Cement and Concrete Research*, *35*(5), 1008–1013.

Sanders, J. P., & Gallagher, P. K. (2002). Kinetic analyses using simultaneous TG/DSC measurements. *Thermochimica Acta*, *388*(1–2), 115–128.

Sauman, Z. (1971). Carbonization of porous concrete and its main binding components. *Cement and Concrete Research*, *1*(6), 645–662.

Schiller, C. L., & Hastie, D. R. (1996). Nitrous oxide and methane fluxes from perturbed and unperturbed boreal. *Journal of Geophysical Research*, *101*(D17), 22767–22774.

Schrier-Uijl, A. P., Veenendaal, E. M., Leffelaar, P. A., van Huissteden, J. C., & Berendse, F. (2008). Spatial and temporal variation of methane emissions in drained eutrophic peat agro-ecosystems: drainage ditches as emission hotspots. *Biogeosciences Discussions*, *5*(2), 1237–1261.

Schrier-Uijl, a. P., Veraart, a. J., Leffelaar, P. a., Berendse, F., & Veenendaal, E. M. (2011). Release of CO_2 and CH_4 from lakes and drainage ditches in temperate wetlands. *Biogeochemistry*, *102*(1), 265–279.

Schubert, P. (1987). Carbonation behaviour of mortars and concrete made with fly ash. *ACI Special Publications, SP-100*, 1945–62.

Schumacher, B. A. (2002). *Methods for the determination of total organic carbon (TOC) in soils and sediments*. U.S. Environmental Protection Agency, Washington, US.

Scottish Executive. (2006). *Peat landslide hazard and risk assessment*. Scottish Executive, Edinburgh, Scotland.

Sear, L., & Coombs, R. (2001). The use of PFA as a fill material and the environment. In R. Yong & H. Thomas (Eds.), *Geoenvironmental Engineering: Geoenvironmental impact management* (pp. 33–38). Edinburgh: Thomas Telford.

Segers, R. (1998). Methane production and methane consumption: a review of processes underlying wetland methane fluxes. *Biogeochemistry*, *41*, 23–51.

Sethuraman, D., Pearson, N. O., & Kwiatkowski, A. (2011). Carbon credits becoming "Junk" before 2013 ban closes door: energy markets. Retrieved January 6, 2013, from http://www.bloomberg.com/news/articles/2011-12-06/carbon-credits-becoming-junk-before-2013-ban-closes-door-energy-markets

Shillaber, C. M., Asce, S. M., Mitchell, J. K., Asce, D. M., Dove, J. E., & Asce, M. (2015). Energy and Carbon Assessment of Ground Improvement Works . I : Definitions and Background. *J. Geotech. Geoenviron. Eng*, *142*(3), 1–9.

Shui, K., Yuan, K., Sun, T., Li, Q., & Zeng, W. (2015). Calcined Clays for Sustainable Concrete: Proceedings of the 1st International Conference on Calcined Clays for Sustainable Concrete. In K. Scrivener & A. Favier (Eds.), *Design and preparation of metakaolin-based mineral based admixture and its effects on the durability of concrete* (pp. 229–236). Springer.

Silins, U. & Rothwell, R. (1998). Forest peatland drainage and subsidence affect soil water retention and transport properties in an Alberta peatland. Soil Sci Soc Am J, 62(4), 1048–56.

Silvan, N., Tuittila, E.-S., Kitunen, V., Vasander, H., & Laine, J. (2005). Nitrate uptake by Eriophorum vaginatum controls N_2O production in a restored peatland. *Soil Biology and Biochemistry*, *37*(8), 1519–1526.

Singh, N. B., & Singh, N. P. (2007). Formation of CaO from thermal decomposition of calcium carbonate in the presence of carboxylic acids. *Journal of Thermal Analysis and Calorimetry*, *89*(1), 159–162.

Slegers, P. A., & Rouxhet, P. G. (1976). Carbonation of the hydration products of tricalcium silicate. *Cement and Concrete Research*, *6*(3), 381–388.

SNH. (2000). *Windfarms and carbon savings. Technical guidance note*. Scottish Natural Heritage, Inverness, UK.

Soga, K., Kidd, A., Hughes, L., Guthrie, P., Fraser, N., Phear, A., … Pantelidou, H. (2011). Carbon dioxide from earthworks: a bottom-up approach. *Proceedings of the ICE - Civil Engineering*, *164*(2), 66–72.

Sottocornola, M., & Kiely, G. (2005). An Atlantic blanket bog is a modest CO_2 sink. *Geophysical Research Letters*, *32*(December), 1–4.

Speakman, S. A. (n.d.). Basics of X-Ray Powder Diffraction. Retrieved April 4, 2014, from http://prism.mit.edu/xray/oldsite/Basics of X-Ray Powder Diffraction.pdf

Stark, J., & Ludwig, H.-M. (1997). Freeze-thaw-deiceing salt resistance of concrete containing cement rich in granulated blast furnace slag. *ACI Materials Journal*, *94*(1).

Stevenson, F. J. (1994). *Humus chemistry* (2nd ed.). New York: John Wiley & Sons, Inc.

Ševula, L., Madej, J., Kozánková, J., & Madejová, J. (1994). Hydration products at the blastfurnace slag aggregate - cement paste interface. *Cement and Concrete Research*, *24*(3), 413–423.

Stewart, A. & Lance, A. (1983). Moor draining: a review of impacts on land use. *Journal of Environmental Management*, 17(1), 81–99.

Stewart, A. & Lance, A. (1991). Effects of moor-draining on the hydrology and vegetation of Northern Pennine blanket bog. *Journal of Applied Ecology*, 28(3), 1105–17.

Strack, M., Waddington, J. M., & Tuittila, E.-S. (2004). Effect of water table drawdown on northern peatland methane dynamics: Implications for climate change. *Global Biogeochemical Cycles*, *18*(4), 1–7.

Stronach, S. A., & Glasser, F. P. (1997). Modelling of the impact of abundant geochemical components on the phase stability and solubility of the CaO-SiO_2-H_2O system at 25 ºC. *Advances in Cement Research*, *9*(36), 167–181.

Stutzman, P. E. (1996). *NISTIR 5755 - Guide for x-ray powder diffraction analysis of portland cement and clinker*. U.S. Department of Commerce.

Sundh, I., Nilsson, M., Mikkelä, C., Granberg, G., & Svensson, B. H. (2000). Fluxes of Methane and Carbon Dioxide on Peat-Mining Areas in Sweden. *Ambio*, *29*(8), 499–503.

Taylor, H. F. W. (1997). *Cement Chemistry* (2nd ed.). Thomas Telford.

Teh, Y. A., Silver, W. L., Sonnentag, O., Detto, M., Kelly, M., & Baldocchi, D. D. (2011). Large Greenhouse Gas Emissions from a Temperate Peatland Pasture. *Ecosystems*, *14*(2), 311–325.

Thiery, M., Villain, G., Dangla, P., & Platret, G. (2007). Investigation of the carbonation front shape on cementitious materials: Effects of the chemical kinetics. *Cement and Concrete Research*, *37*(7), 1047–1058.

Thinkstep. (2015). GaBi software. Retrieved July 6, 2015, from https://www.thinkstep.com/software/gabi-lca/

Timoney, M. J. (2015). *Strength Verification Methods for Stabilised Soil-Cement Columns: A Laboratory Investigation of PORT and PIRT*.

Timoney, M. J., Bell, A. L., & Mccabe, B. A. (2011). Experiences of dry soil mixing in highly organic soils. *Proceedings of the ICE - Ground Improvement*, *164*(GI1), 1–12.

Timoney, M., Quigley, P., & McCabe, B. A. (2012). Some laboratory soil mixing trials of Irish peats. In *ISSMGE - TC 211 International Symposium on Ground Improvement IS-GI* (p. Volume 2). Brussels.

Torgal, F. P., Miraldo, S., Labrincha, J. A., & De Brito, J. (2012). An overview on concrete carbonation in the context of eco-efficient construction: Evaluation, use of SCMs and/or RAC. *Construction and Building Materials*, *36*, 141–150.

Torii, K., & Kawamura, M. (1992). Pore structure and chloride permeability of concretes containing fly ash, blast furnace slag and silica fume. *Fly Ash, Silica Fume, Slag and Natural Pozzolans in Concrete*, *vols. SP-1*, 135–50.

Treloar, G. J. (1997). Extracting Embodied Energy Paths from Input-Output Tables: Towards an Input-Output-Based Hybrid Energy Analysis Method. *Economic Systems Research*, *9*(4), 375–391.

Treloar, G. J., Love, P. E. D., & Crawford, R. H. (2004). Hybrid Life-Cycle Inventory for Road Construction and Use. *Journal of Construction Engineering and Management*, *130*(1), 43–49.

Tremblay, H., Duchesne, J., Locat, J., & Leroueil, S. (2002). Influence of the nature of organic compounds on fine soil stabilization with cement. *Canadian Geotechnical Journal*, *39*(3), 535–546.

Tucker, S. N., Tharumarajah, A., May, B., England, J., Paul, K., Hall, M., … Syme, M. (2009). *Life Cycle Inventory of Australian Forestry and Wood Products*. Forest & Wood Products Australia, Australia.

Tuittila, E.-S., Komulainen, V.-M., Vasander, H., Nykanen, H., Martikainen, P. J., & Laine, J. (2000). Methane dynamics of a restored cut-away peatland. *Global Change Biology*, *6*, 569–581.

UNFCCC. (1998). *Kyoto Protocol to the United Nations Framework Convention on Climate Change*. United Nations.

UNFCCC. (2011). The United Nations Framework Convention on Climate Change, Conference of the Parties 17 (COP17), Conference of the Parties 17 (COP17), Durban, South Africa - November/December 2011. Retrieved October 14, 2015, from http://unfccc.int/meetings/durban_nov_2011/meeting/6245.php

Unosson, J. E., Persson, C., & Engqvist, H. (2015). An evaluation of methods to determine the porosity of calcium phosphate cements. *J Biomed Mater Res*, *103*(1), 62–71.

Utgenant, P. (2004). *The influence of ageing on the salt-frost resistance of concrete*. Lund Institute of Technology.

Villain, G., & Platret, G. (2006). Two experimental methods to determine carbonation profile in concrete. *ACI Material Journal*, *103*(4), 265–271.

Villain, G., Thiery, M., & Platret, G. (2007). Measurement methods of carbonation profiles in concrete: Thermogravimetry, chemical analysis and gammadensimetry. *Cement and Concrete Research*, *37*(8), 1182–1192.

Vitelli, A. (2013). EU carbon permits pare early losses, tracking German 2014 power. Retrieved January 6, 2013, from http://www.bloomberg.com/news/articles/2013-01-03/european-union-carbon-dioxide-permits-decline-to-one-month-low

von Arnold, K., Nilsson, M., Hånell, B., Weslien, P., & Klemedtsson, L. (2005). Fluxes of CO_2, CH_4 and N_2O from drained organic soils in deciduous forests. *Soil Biology and Biochemistry*, *37*(6), 1059–1071.

von Post, L. (1922). *Sveriges Geologiska Undersøknings torvinventering och nogra av dess hittils vunna resultat (SGU peat inventory and some preliminary results)* (Vol. 36). Svenska Mosskulturføreningens Tidskrift, Jønkøping, Sweden.

Wagner, S. W., Reicosky, D. C., & Alessi, R. S. (1997). Regression Models for Calculating Gas Fluxes Measured with a Closed Chamber. *Agronomy Journal*, *89*(2), 279.

Walczak, R., Rovdan, E., & Witkowska-Walczak, B. (2002). Water retention characteristics of peat and sand mixtures. *International Agrophysics*, *16*(2), 161–165.

Wang, C. (2010). *Simultaneous Analysis of Greenhouse Gases by Gas Chromatography*. Agilent Technologies, Shanghai. Retrieved from http://www.agilent.com/cs/library/applications/5990-

5129EN.pdf

Warburton, J., Holden, J., & Mills, A. J. (2004). Hydrological controls of surficial mass movements in peat. *Earth-Science Reviews*, *67*(1–2), 139–156.

Ward, S., Connolly, J., Walsh, J., Dahlman, L., & Holden, N. M. (2006). *Climate Change – Modelling Carbon Fluxes from Irish Peatlands : Towards the Development of a National Carbon Fluxes Inventory for Irish Peatlands*. Bioresources Research Centre (BRC), University College Dublin, Dublin, Ireland.

Wardwell, R. E., Charlie, W. A., & Doxtader, K. A. (1983). *Test method for determining the potential for decomposition in organic soils. In Testing of Peats and Organic Soils*. ASTM STP 820 (Jarrett PM (ed.)), ASTM International, West Conshohocken, PA, USA.

Whalen, S. C. (2005). Biogeochemistry of methane exchange between natural wetlands and the atmosphere. *Environmental Engineering Science*, *22*, *22*(1), 73–94.

Wiedmann, T. (2010). *Frequently Asked Questions about Input-Output Analysis*. Centre for Sustainability Accounting, United Kingdom.

Williams, R. & Crawford, R. (1984). Methane production in Minnesota Peatlands. *Applied and Environmental Microbiology*, 47, 1266– 1271.

Wilson, D., Alm, J., Laine, J., Byrne, K. a., Farrell, E. P., & Tuittila, E.-S. (2009). Rewetting of Cutaway Peatlands: Are We Re-Creating Hot Spots of Methane Emissions? *Restoration Ecology*, *17*(6), 796–806.

Wilson, D., & Farrell, E. P. (2007). *Carbal: Carbon gas balances in industrial cutaway peatlands in Ireland*. Forest Ecosystem Research Group, University College Dublin, Duiblin, Ireland.

Wilson, D., Müller, C., & Renou-Wilson, F. (2013). Carbon emissions and removals from Irish peatlands: present trends and future mitigation measures. *Irish Geography*, *46*(1), 1–23.

Wilson, D., Renou-Wilson, F., Farrell, C., Bullock, C., & Müller, C. (2012). *Carbon restore – the potential of restored Irish peatlands for carbon uptake and storage.* EPA, Co. Wexford, Ireland.

Wilson, P., & Hegarty, C. (1993). Morphology and causes of recent peat slides on Skerry Hill, Co. Antrim, Northern Ireland. *Earth Surface Processes and Landforms*, *18*(7), 593–601.

Wojtasik, A. T., Łecki, P., Troc, M., & Dojcz, P. (2006). Geotechnical conditions and soil improvment techniques applied in construction of the A2 motorway in Poland. In *2nd International Conference on Problematic Soils*. Selangor, Malaysia.

Woodward, J. (2005). *An introduction to geotectnical processes*. Glasgow, Scotland: Spon Press.

Worrall, F., Reed, M., Warburton, J., & Burt, T. (2003). Carbon budget for a British upland peat catchment. *The Science of the Total Environment*, *312*(1–3), 133–46.

Ylmén, R., & Jäglid, U. (2013). Carbonation of Portland Cement Studied by Diffuse Reflection Fourier Transform Infrared Spectroscopy. *International Journal of Concrete Structures and Materials*, *7*(2), 119–125.

Appendices

Appendix A - Review of the effect of some variables on emissions from ombrotrophic raised/blanket bog in a temperate climate

		Carbon dioxide		Methane		Nitrous Oxide (low emissions)		
		Uptake	**Release**	**Release**	**Negligible**	**Uptake**	**Release**	**Negligible**
Water table	**Undrained**	Couwenberg, 2009 Tuitilla et al., 2000 Crill et al., 2000		Crill et al., 2000 Whalen, 2005 Glatzel et al., 2008		Martikainen et al., 1993		Couwenberg, 2009
	Drained		Couwenberg, 2009 Tuitilla et al., 2000 Crill et al., 2000		Glatzel et al., 2008 Segers, 1998 Couwenberg, 2009		Martikainen et al., 1993 Regina et al., 1996	
Temperature	**High**		Hobbs, 1986	Laine et al., 2007			Martikainen et al., 1993	
	Low (< 0)				Couwenberg, 2009 Laine et al., 2007			Martikainen et al., 1993
pH	**High**		Hobbs, 1986 Preston et al., 2012	Williams & Crawford, 1984				
	Low				Laine et al., 2007			Martikainen et al., 1993
Von Post scale	**High**						Alm et al., 1999	
	Low		Glatzel et al., 2004	Glatzel et al., 2004				
Weather	**Dry**							
	Wet	Koehler et al., 2011			Glatzel et al., 2008			Rückauf et al., 2004
Season	**Winter**		Sottocornola & Kiely, 2005		Laine et al., 2007			Martikainen et al., 1993
	Summer	Sottocornola & Kiely, 2005		Glatzel et al., 2008 Laine et al., 2007			Martikainen et al., 1993	Silvan et al., 2005 Glatzel et al. 2008
Vegetation	**Not vascular**		Glatzel et al., 2004	Couwenberg, 2009	Laine et al., 2007		Glatzel et al., 2008 Lamers et al., 2000	
	None							Glatzel et al., 2008
	Vascular			Whalen, 2005 Laine et al., 2007 Couwenberg, 2009				

Note: Negligible means zero to low release except for nitrous oxide where negligible is close to zero.
Release means medium to high release except for nitrous oxide where release is small.

Appendix B - Notation for small and large specimens in Experiments P, A and B showing also the characteristics of the peat and stabilised peat specimens

Note:

- c: Cement
- g: GGBS
- Similar non-white colours represent similar mixes and conditions

Table B1 - Notation for large specimens in Experiment P

Experiment P					
Specimen Type	Specimen name	Binder content (kg/m³)	Water table	Surcharge (kPa)	Binder type
P1	P1(1)	0	top	0	
	P1(2)	0	top	0	
	P1(3)	0	top	0	
P2	P2(1)	0	bottom	0	
	P2(2)	0	bottom	0	
	P2(3)	0	bottom	0	
P3	P3(1)	250	bottom	0	100c
	P3(2)	250	bottom	0	100c
	P3(3)	250	bottom	0	100c

Table B2 - Notation for small and large specimens in Experiment A

Experiment A						
Specimen Type	Large Specimen name	Binder content (kg/m³)	Water table	Surcharge (kPa)	Binder type	Small specimen name
A1	A1(1)	148	bottom	0	100c	a1(1a), a1(1b), a1(1c)
	A1(2)	148	bottom	0	100c	a1(2a), a1(2b), a1(2c)
	A1(3)	148	bottom	0	100c	a1(3a), a1(3b)
A2	A2(1)	200	bottom	0	100c	a2(1a), a2(1b), a2(1c)
	A2(2)	200	bottom	0	100c	a2(2a), a2(2b)
	A2(3)	200	bottom	0	100c	a2(3a), a2(3b), a2(3c)
A3	A3(1)	250	bottom	0	100c	a3(1a), a3(1b)
	A3(2)	250	bottom	0	100c	a3(2a), a3(2b), a3(2c)
	A3(3)	250	bottom	0	100c	a3(3a), a3(3b), a3(3c)
A4	A4(1)	250	bottom	6	100c	a4(1a), a4(1b), a4(1c)
	A4(2)	250	bottom	6	100c	a4(2a), a4(2b), a4(2c)
	A4(3)	250	bottom	6	100c	a4(3a)
A5	A5(1)	278	bottom	12	100c	a5(1a), a5(1b)
	A5(2)	278	bottom	12	100c	a5(2a), a5(2b), a5(2c)
	A5(3)	278	bottom	12	100c	a5(3a), a5(3b), a5(3c)
A6	A6(1)	250	bottom	0	75c:25g	a6(1a), a6(1b), a6(1c)
	A6(2)	250	bottom	0	75c:25g	a6(2a), a6(2b), a6(2c)
	A6(3)	250	bottom	0	75c:25g	a6(3a), a6(3b), a6(3c)
A7	A7(1)	250	bottom	0	25c:75g	a7(1a), a7(1b), a7(1c)
	A7(2)	250	bottom	0	25c:75g	a7(2a), a7(2b), a7(2c)
	A7(3)	250	bottom	0	25c:75g	a7(3a), a7(3b), a7(3c)
A8	A8(1)	0	bottom	0		a8(1a), a8(1b), a8(1c)
	A8(2)	0	bottom	0		a8(2a), a8(2b), a8(2c)
	A8(3)	0	bottom	0		a8(3a), a8(3b), a8(3c)

Table B3 - Notation for small and large specimens in Experiment B

Experiment B						
Specimen Type	**Large Specimen name**	**Binder content (kg/m³)**	**Water table**	**Surcharge (kPa)**	**Binder type**	**Small specimen name**
B1	B1(1)	150	bottom	6	100c	b1(1a), b1(1b), b1(1c)
	B1(2)	150	bottom	6	100c	b1(2a), b1(2b), b1(2c)
	B1(3)	150	bottom	6	100c	b1(3a), b1(3b), b1(3c)
B2	B2(1)	200	bottom	6	100c	b2(1a), b2(1b),b2(1c)
	B2(2)	200	bottom	6	100c	b2(2a), b2(2b), b2(2c)
	B2(3)	200	bottom	6	100c	b2(3a), b2(3b), b2(3c)
B3	B3(1)	250	bottom	6	100c	b3(1a), b3(1b), b3(1c)
	B3(2)	250	bottom	6	100c	b3(2a), b3(2b), b3(2c)
	B3(3)	250	bottom	6	100c	b3(3a), b3(3b), b3(3c)
B4	B4(1)	250	bottom	0	100c	b4(1a), b4(1b), b4(1c)
	B4(2)	250	bottom	0	100c	b4(2a), b4(2b), b4(2c)
	B4(3)	250	bottom	0	100c	b4(3a), b4(3b), b4(3c)
B5	B5(1)	250	top	0	100c	b5(1a), b5(1b), b5(1c)
	B5(2)	250	top	0	100c	b5(2a), b5(2b), b5(2c)
	B5(3)	250	top	0	100c	b5(3a), b5(3b), b5(3c)
B6	B6(1)	0	top	0		b6(1a), b6(1b), b6(1c)
	B6(2)	0	top	0		b6(2a), b6(2b), b6(2c)
	B6(3)	0	top	0		b6(3a), b6(3b), b6(3c)
B7	B7(1)	0	bottom	0		b7(1a), b7(1b), b7(1c)
	B7(2)	0	bottom	0		b7(2a), b7(2b), b7(2c)
	B7(3)	0	bottom	0		b7(3a), b7(3b), b7(3c)
B8	B8(1)	250	bottom	12	100c	b8(1a), b8(1b),b8(1c)
	B8(2)	250	bottom	12	100c	b8(2a), b8(2b),b8(2c)
	B8(3)	250	bottom	12	100c	b8(3a), b8(3b), b8(3c)

Note:

- c: Cement
- g: GGBS
- Similar non-white colours represent similar mixes and conditions

Appendix C - Reference plots for XRD and FTIR

Appendix C1 - Reference plots for XRD

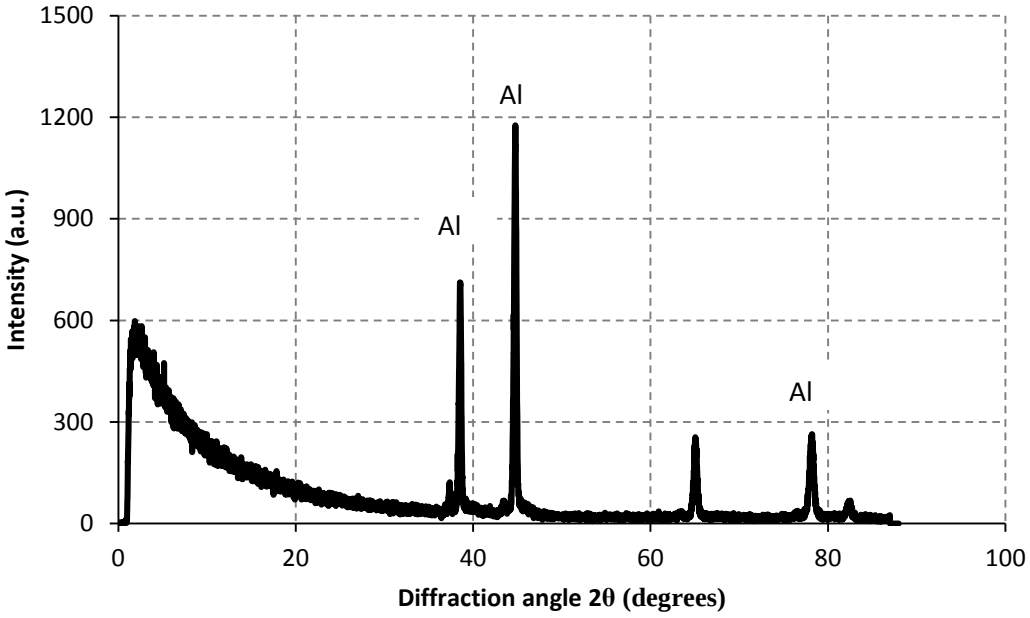

Figure C1 - Reference XRD graph for aluminium (Al)

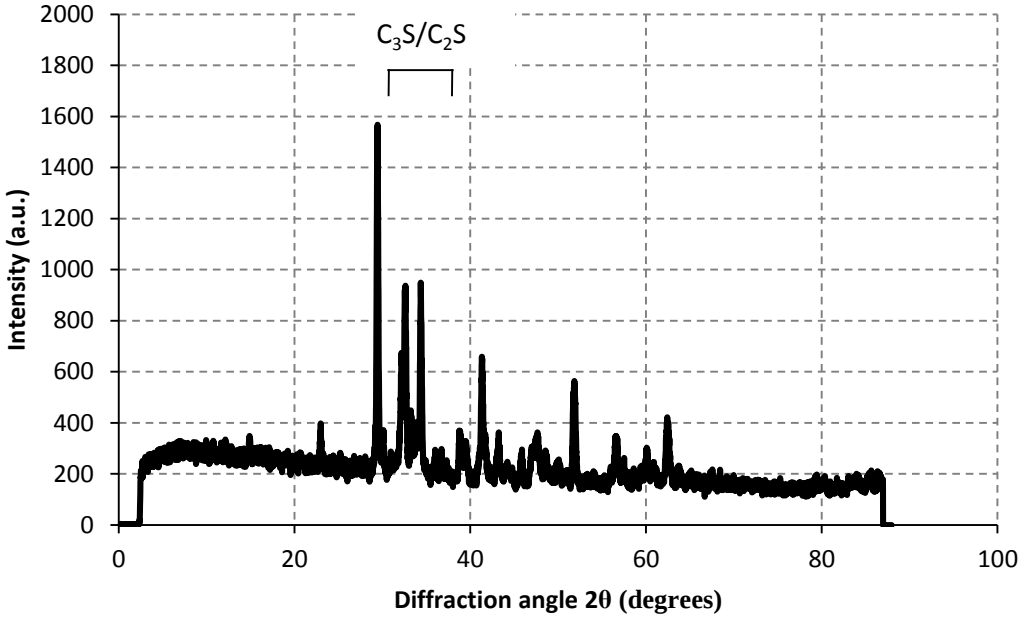

Figure C2 - Reference XRD graph for Ordinary Portland Cement

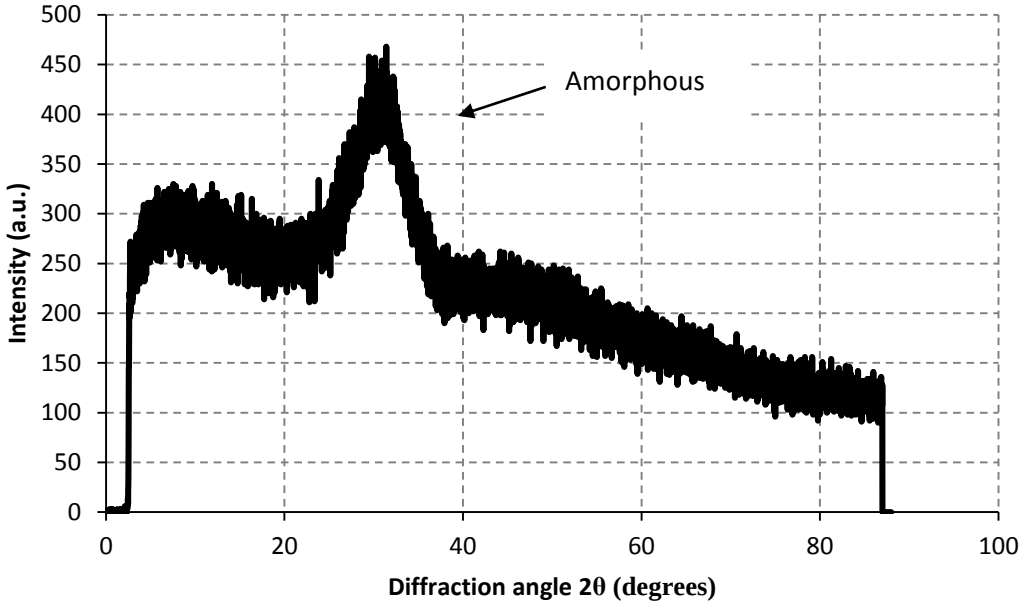

Figure C3 - Reference XRD graph for GGBS

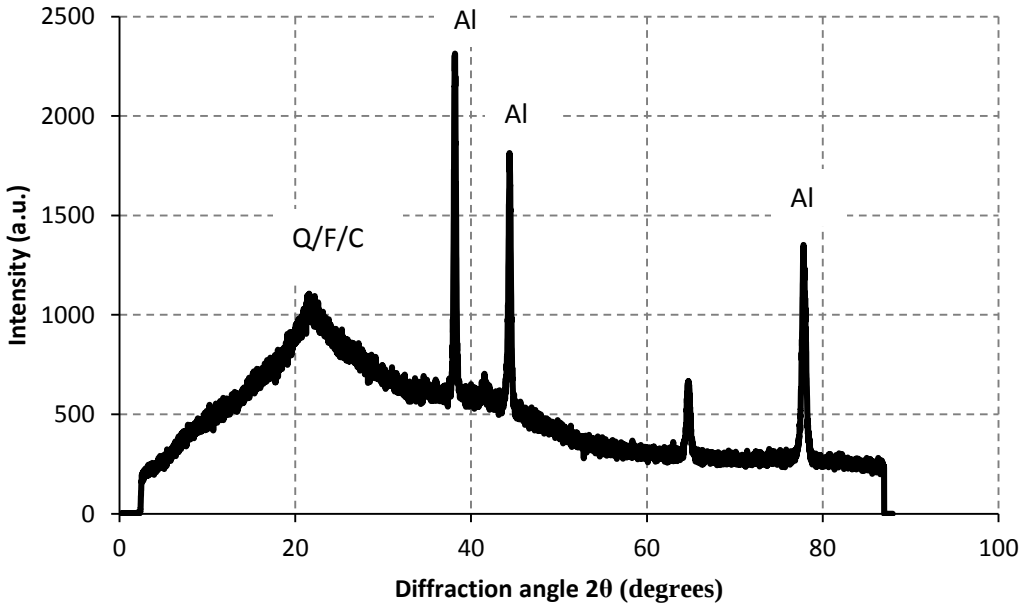

Figure C4 - Reference XRD graph for peat overlapping aluminium (C = Clay, F = feldspar and Q = quartz).

Note: Wide hump between 10° and 30° highlights the amorphous matter that includes vitreous phases and gels (Girardello et al., 2013)

Appendix C2 - Reference plots for FTIR

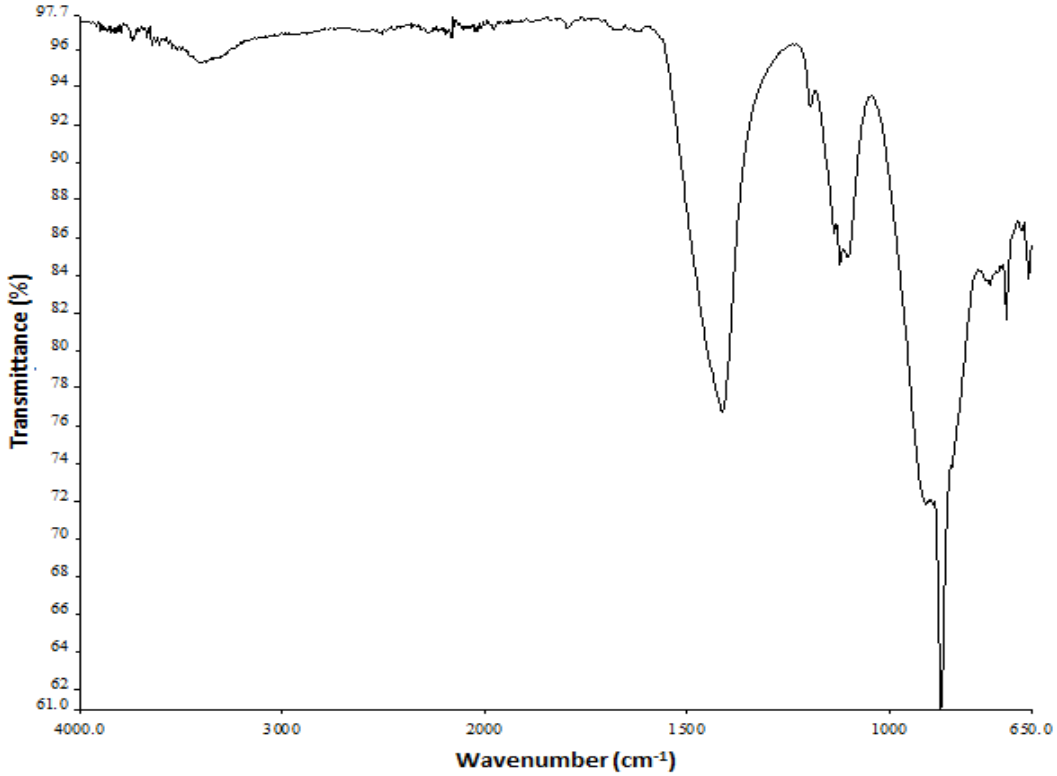

Figure C5 - FTIR of cement

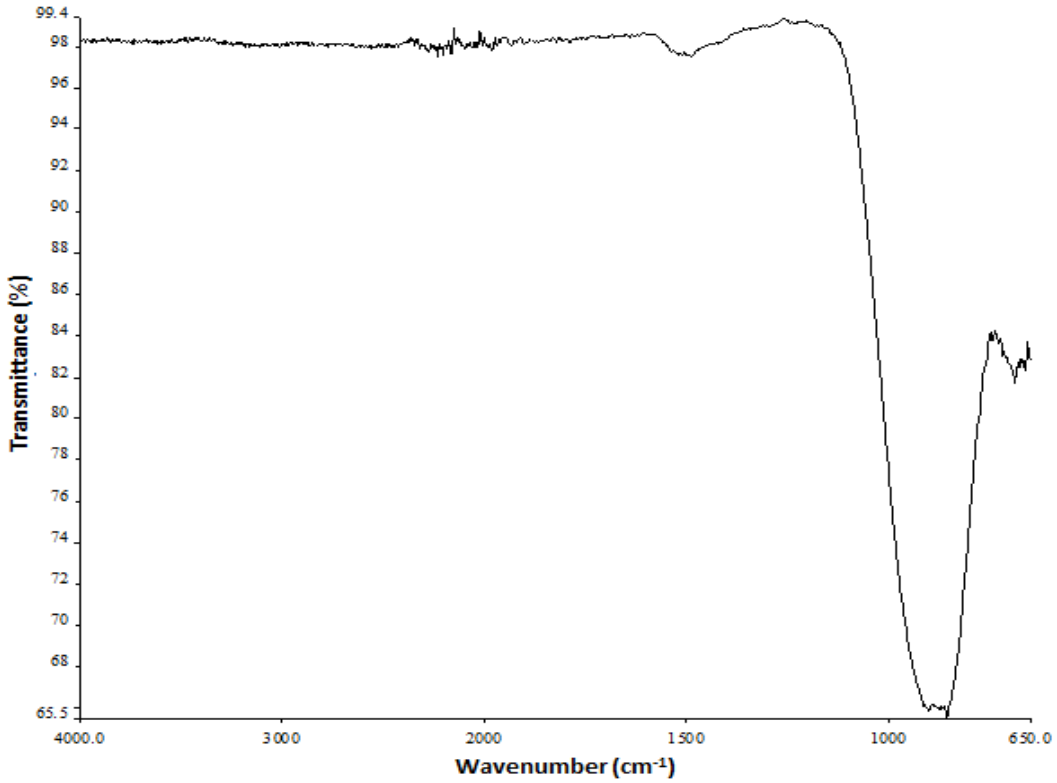

Figure C6 - FTIR graph of GGBS

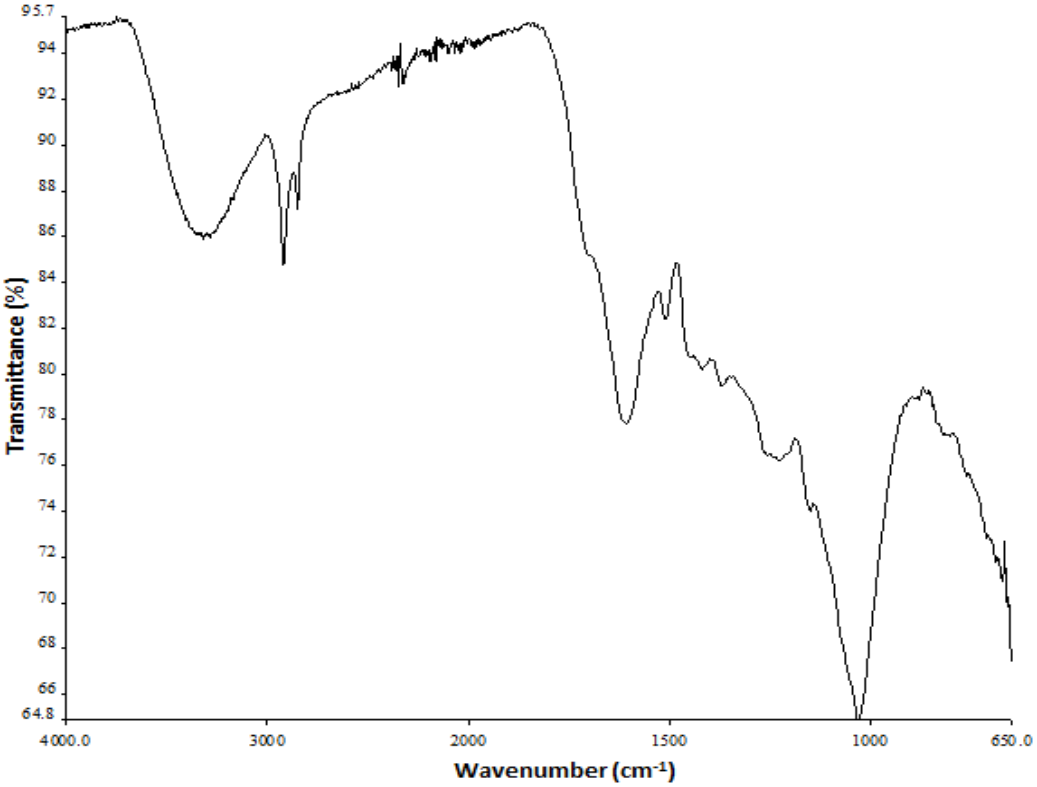

Figure C7 - FTIR graph of peat

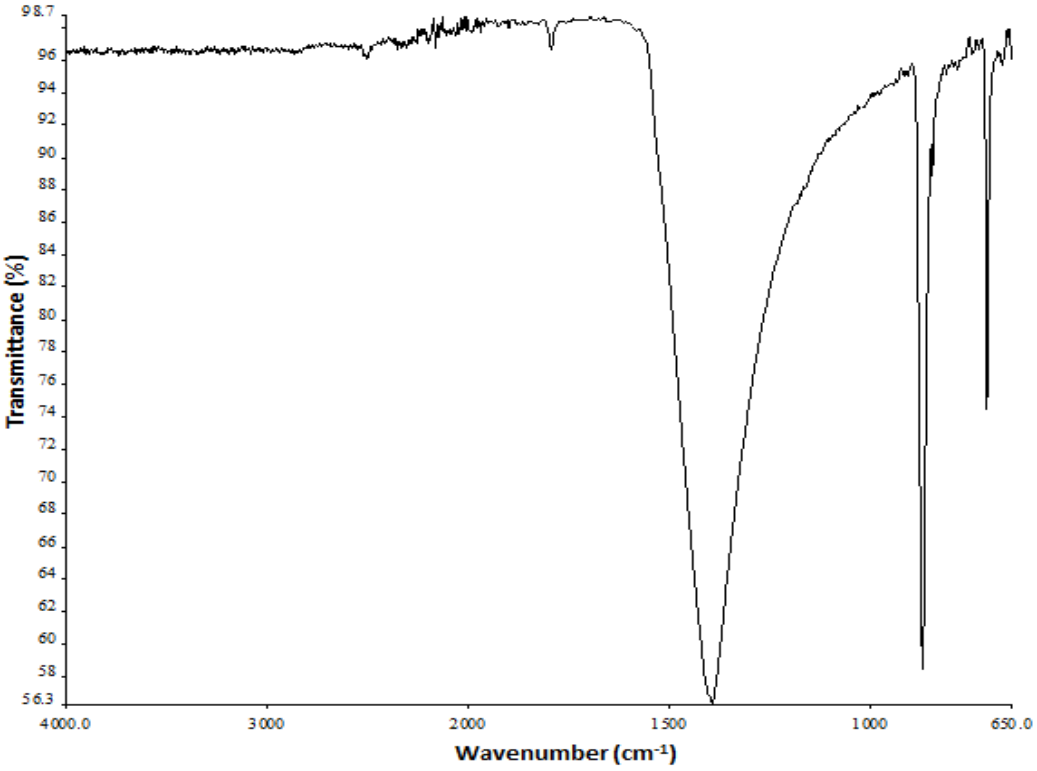

Figure C8 - FTIR graph of pure $CaCO_3$

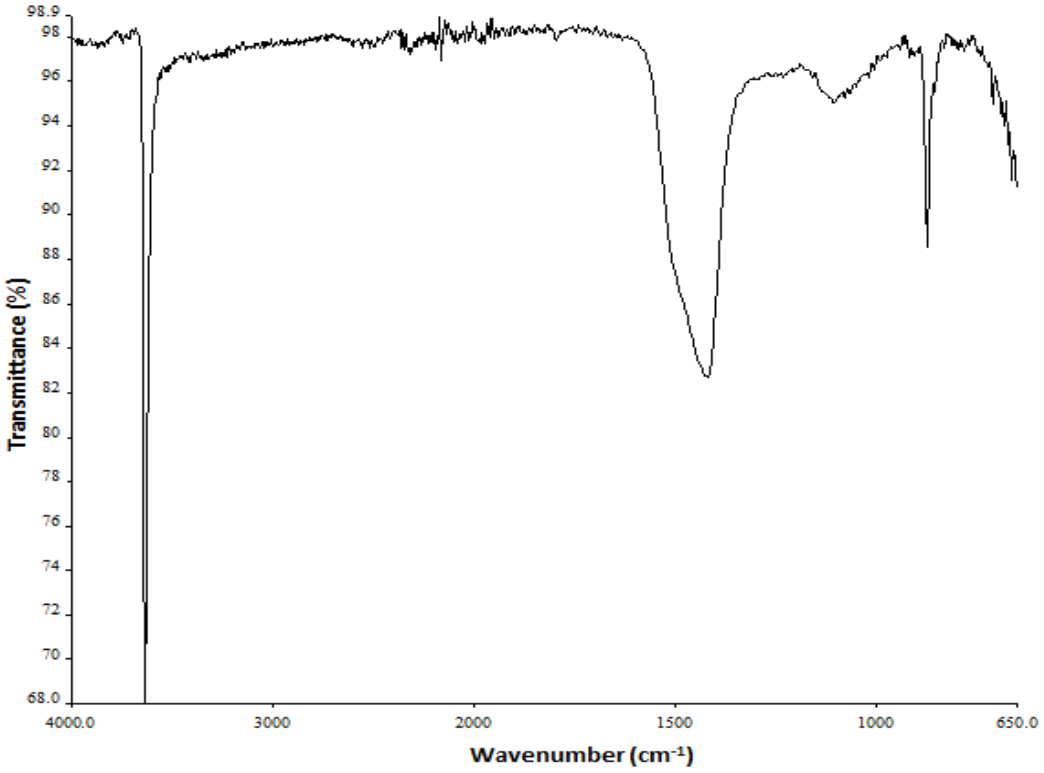

Figure C9 - FTIR graph of pure $Ca(OH)_2$ (peak at about 1390 cm^{-1} to C-0 is related to a calcium carbonate impurity)

Appendix D - Some results from Chapter 4, including some of the output from the Minitab statistical analyses for the CO_2 flux studies

Appendix D1 - Final moisture content versus initial moisture content in Experiments A and B

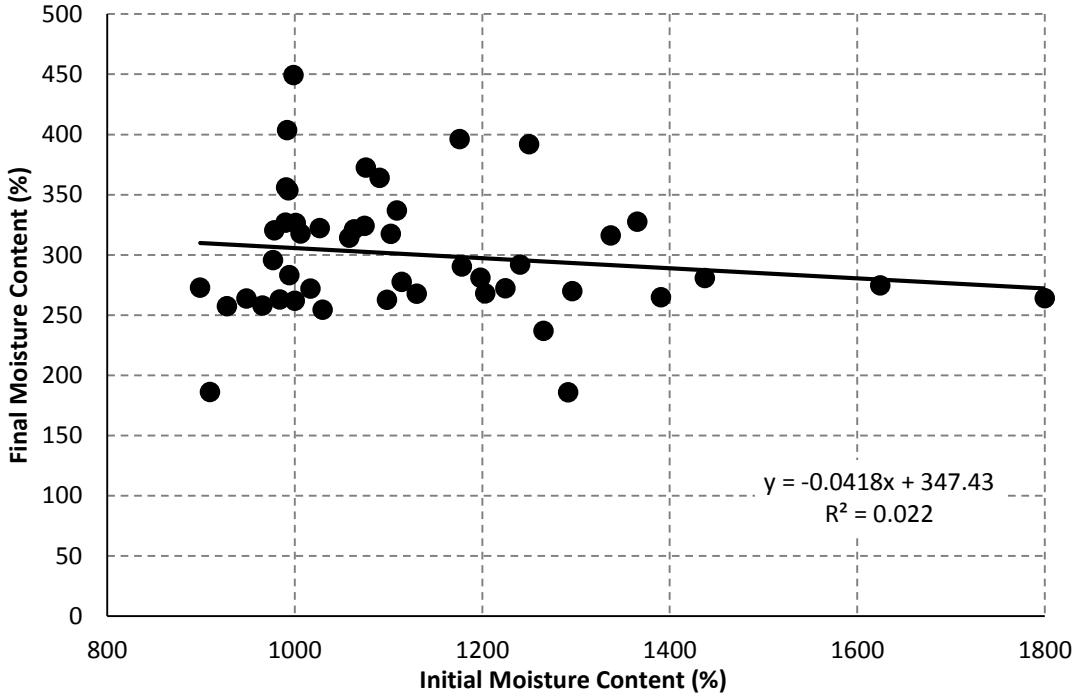

Figure D1 - Final moisture content versus initial moisture content in Experiments A and B

Appendix D2 - Gas flux results for P1 and P2 in Experiment P

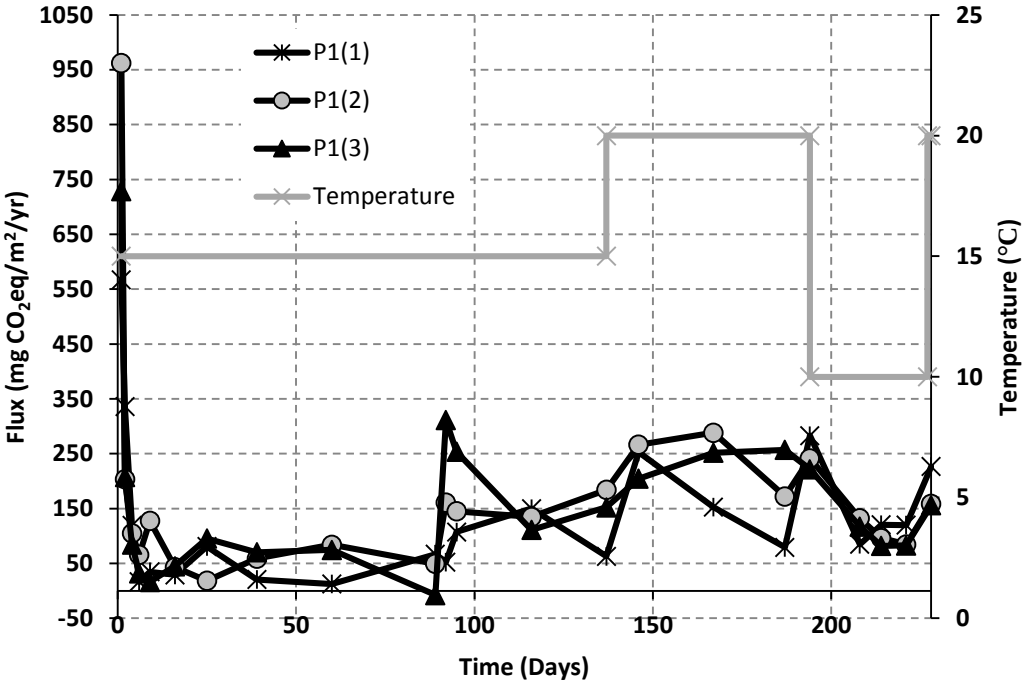

Figure D2 - 60-minute CO_2 fluxes for P1(1)–P1(3)

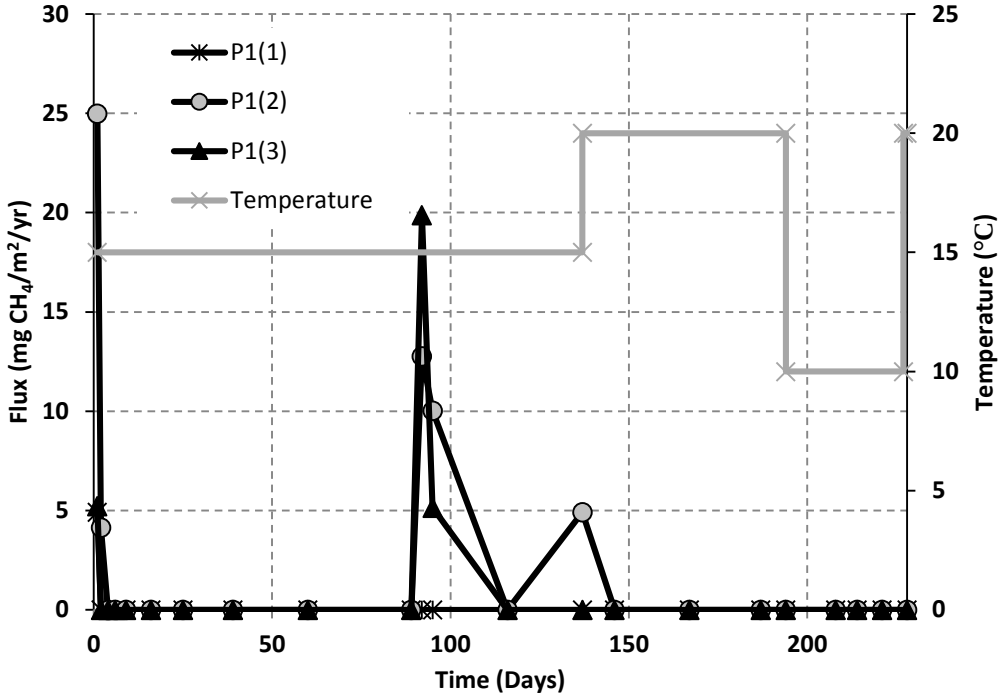

Figure D3 - 60-minute CH_4 fluxes for P1(1)–P1(3)

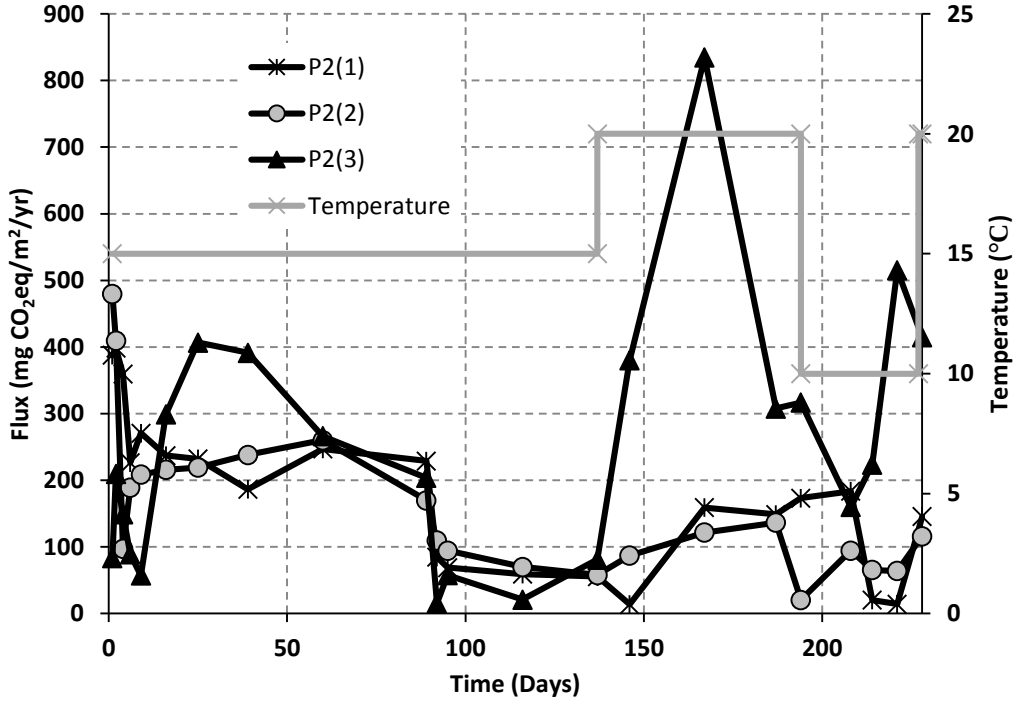

Figure D4 - 60-minute CO_2 fluxes for P1(1)–P1(3)

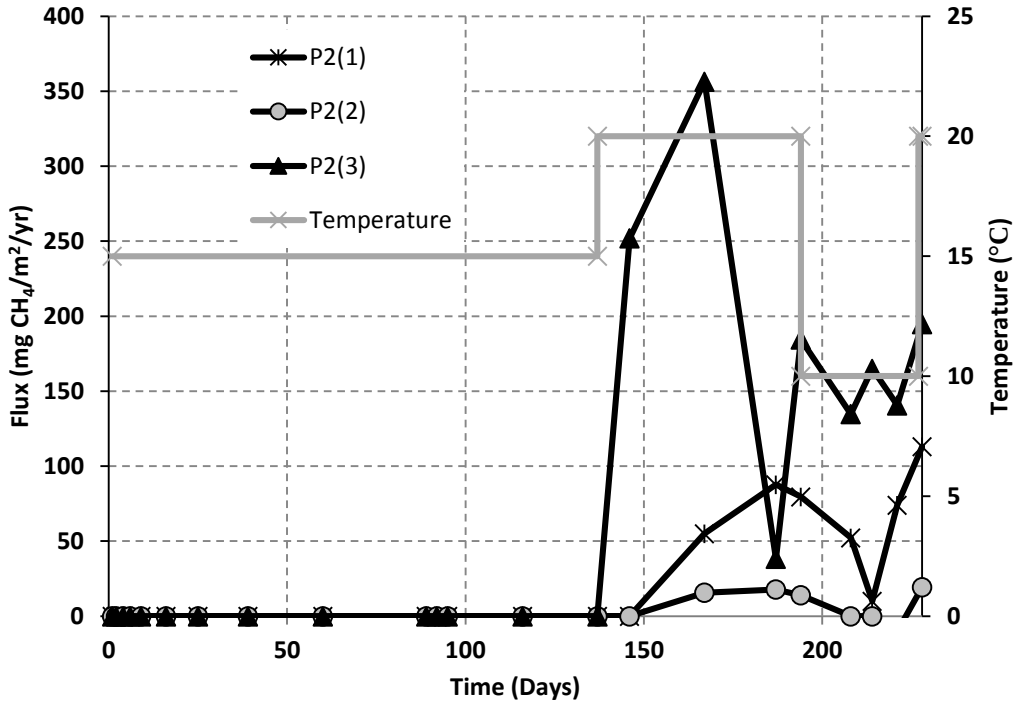

Figure D5 - 60-minute CH_4 fluxes for P1(1)–P1(3)

Appendix D3 - Definitions of some statistical terms and regression model parameters

The lack-of-fit value determines whether the model accurately fits the data. It is good practice after deriving a regression equation from data to use a subset of the data to create equations to check if similar equations/models are produced. This approach gives a realistic indication of the reliability of the regression relationship. A high lack-of-fit value shows that the model accurately fits the data while a value lower than the significance level of 0.05 means the model does not fit the data well. However, care must be taken when using this vale as the lack-of-fit value is zero if your data contains replicates (multiple observations with identical x-value). Replicates represent 'pure errors' because only random variation can cause differences between the observed response values (Minitab, 2016a).

The adjusted R^2 value is used to compare models with different numbers of predictors and is a version of R^2 adjusted for the number of predictors in the model. The adjusted R^2 increases only if the new term improves the model more than would be expected by chance.

The predicted R^2 value is a form of cross validation that does not require a separate sample to be collected. It determines how well the model predicts new observations and whether the model is overfitted. Minitab calculates predicted R^2 by systematically removing each observation from the data set, estimating the regression equation and

determining how well the model predicts the removed observation (Frost, 2013). To avoid overfitting, a large number of gas samples were collected.

Variance inflation factor (VIF): VIF values show how much the variance of the regression coefficient is larger than it would otherwise have been if the variable had been completely uncorrelated with all the other variables in the model (Table D1).

Table D1 - Correlation strength based on VIF values (Minitab, 2016b)

VIF	Status of predictors
VIF = 1	Not correlated
1 < VIF < 0.5	Moderately correlated
VIF > 5 to 10	Highly correlated

Multicollinearity is a phenomenon in which two or more predictor variables in a multiple regression model are highly correlated, meaning that one can be linearly predicted from the others with a substantial degree of accuracy. Multicollinearity increases the standard errors of the coefficients; by overinflating the standard errors, multicollinearity makes some variables statistically insignificant when they should be significant (Martz, 2013).

Table D2 - Explanation of regression model parameters

Parameters	Coefficient	Standard error[2]	p-value[3]
b_0 (constant)[1]	-32.2	48.7	0.511
b_1 (initial CO_2)[1]	-1278.5	390.4	0.002
b_2 (ln(time))[1]	19.71	4.855	0.000
R^2 (adj.)[4]	0.698		
R^2 (pred.)[5]	0.671		
SE[6]	36.6869		
d.f (reg, res)[7]	2,63		
F-value[8]	76.08		
P-value[9]	0.000		

[1] b_0,b_1,b_2 = regression coefficients
[2] Standard error = standard error of the regression coefficients
[3] p-value = significance of the variable
[4] R^2 adj. = R^2 adjusted (see Appendix D2)
[5] R^2 pred. = R^2 predicted (see Appendix D2)
[6] SE = Standard error of statistical model
[7] d.f. = degrees of freedom (regression (number of parameters - 1 = k (predictor variables)), residuals (n(number of data points)-k-1))
[8] F value = overall significance of entire model
[9] P-value = overall significance of entire model

Appendix D4 - Multiple regression analysis for Experiment P (Best-fit model results)

Analysis of Variance

Source	DF	Adj SS	Adj MC	F-value	p-value
Regression	2	204809	102405	76.08	0.000
Initial CO_2	1	14437	14437	10.73	0.002
Ln(time)	1	22186	22186	16.48	0.000
Error	63	84793	1346		
Lack-of-Fit	62	84317	1360	2.86	0.444
Pure Error	1	476	476		
Total	65	289603			

Model Summary

S	R-sq	R-sq(adj)	R-sq(pred)
36.6869	70.72%	69.79%	67.06%

Coefficients

Term	Coef	SE Coef	T-Value	P-Value	VIF
Constant	-32.2	48.7	-0.66	0.511	
Initial CO_2	-1278	390	-3.28	0.002	3.10
Ln(time)	19.71	4.85	4.06	0.000	3.10

Regression Equation

60-minute gas flux = -32.2 - 1278 initial CO_2 concentration + 19.71 ln(time).

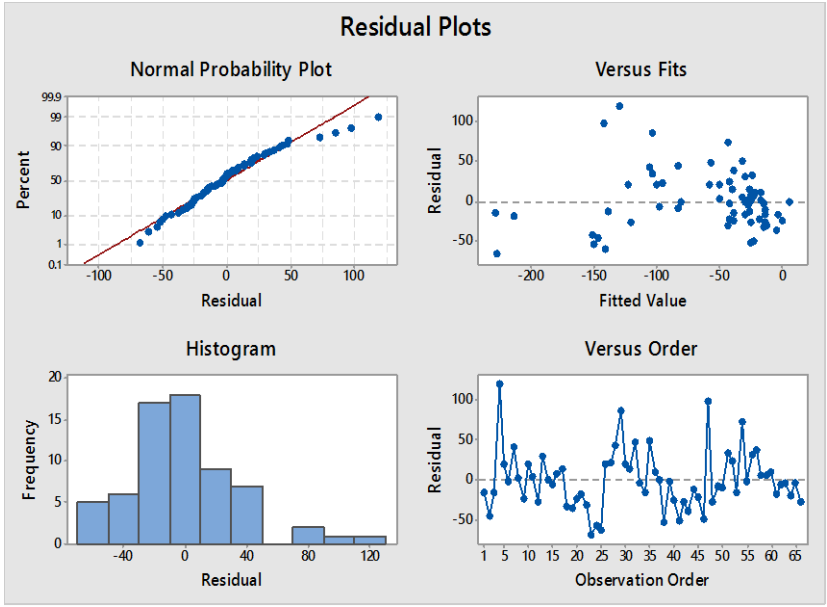

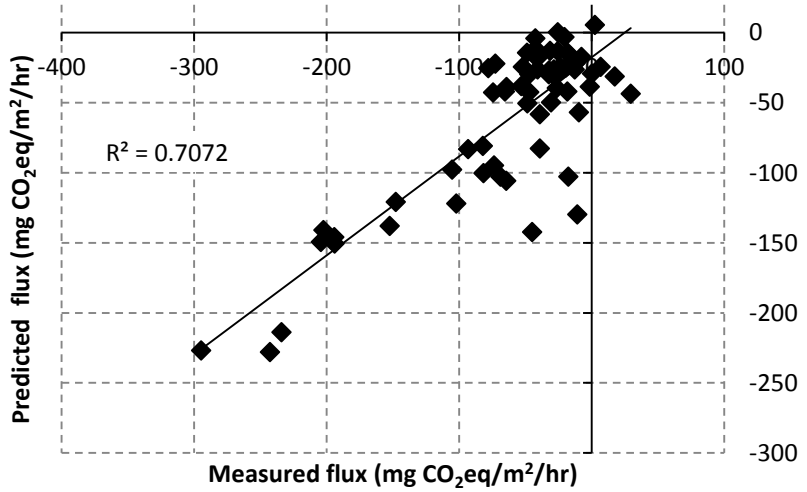

Appendix D5 - Difference between using 0 and 50 ppm for undetectable gas samples for Experiments A and B

Table D3 - Difference in mg CO_2eq/m^2/hr between using 0 and 50 ppm for undetectable gas samples for Experiment A

Column	Measurement period over which regression model was applied (minutes)			
	0–60	**0–40**	**0–20**	**0–10**
A1(1)	0.00 ± 0.00	0.00 ± 0.00	0.00 ± 0.00	0.00 ± 0.00
A1(2)	0.00 ± 0.00	0.00 ± 0.00	0.00 ± 0.00	0.00 ± 0.00
A1(3)	0.00 ± 0.00	0.00 ± 0.00	0.00 ± 0.00	0.00 ± 0.00
A2(1)	0.00 ± 0.00	0.00 ± 0.00	0.00 ± 0.00	0.00 ± 0.00
A2(2)	0.00 ± 0.00	0.00 ± 0.00	0.00 ± 0.00	0.00 ± 0.00
A2(3)	**-0.21 ± 0.89**	**-0.34 ± 1.12**	0.00 ± 0.00	0.00 ± 0.00
A3(1)	0.00 ± 0.00	0.00 ± 0.00	0.00 ± 0.00	0.00 ± 0.00
A3(2)	0.00 ± 0.00	0.00 ± 0.00	0.00 ± 0.00	0.00 ± 0.00
A3(3)	0.00 ± 0.00	**-0.41 ± 2.26**	0.00 ± 0.00	0.00 ± 0.00
A4(1)	0.00 ± 0.00	0.00 ± 0.00	0.00 ± 0.00	0.00 ± 0.00
A4(2)	**-1.40 ± 2.11**	**-1.01 ± 2.67**	**-1.35 ± 4.00**	0.00 ± 0.00
A4(3)	**-1.26 ± 1.61**	**-0.70 ± 1.37**	**-0.70 ± 1.73**	**-0.70 ± 1.36**
A5(1)	**-2.06 ± 2.11**	**-0.91 ± 1.78**	**-0.65 ± 2.21**	**-0.64 ± 1.37**
A5(2)	**-0.49 ± 1.23**	**-0.37 ± 0.96**	**-0.74 ± 2.48**	**-0.74 ± 1.36**
A5(3)	**-3.94 ± 4.48**	**-0.31 ± 0.29**	**-0.76 ± 2.19**	**-0.77 ± 1.43**
A6(1)	0.00 ± 0.00	**-0.40 ± 2.35**	0.00 ± 0.00	0.00 ± 0.00
A6(2)	0.00 ± 0.00	0.00 ± 0.00	0.00 ± 0.00	0.00 ± 0.00
A6(3)	0.00 ± 0.00	0.00 ± 0.00	0.00 ± 0.00	0.00 ± 0.00
A7(1)	0.00 ± 0.00	0.00 ± 0.00	0.00 ± 0.00	0.00 ± 0.00
A7(2)	0.00 ± 0.00	0.00 ± 0.00	0.00 ± 0.00	0.00 ± 0.00
A7(3)	0.00 ± 0.00	0.00 ± 0.00	0.00 ± 0.00	0.00 ± 0.00
A8(1)	0.00 ± 0.00	0.00 ± 0.00	0.00 ± 0.00	0.00 ± 0.00
A8(2)	0.00 ± 0.00	0.00 ± 0.00	0.00 ± 0.00	0.00 ± 0.00
A8(3)	0.00 ± 0.00	0.00 ± 0.00	0.00 ± 0.00	0.00 ± 0.00

Table D4 - Difference in mg CO_2eq/m^2/hr between using 0 and 50 ppm for undetectable gas samples for Experiment B

Column	Measurement period over which regression model was applied (min)		
	0–40	**0-20**	**0–10**
B1(1)	**-2.01 ± 4.39**	**-2.31 ± 6.14**	**0.00 ± 0.00**
B1(2)	**-4.32 ± 7.16**	**-5.99 ± 11.70**	**-3.31 ± 8.45**
B1(3)	**-1.53 ± 3.74**	**-3.06 ± 7.50**	**-3.37 ± 9.70**
B2(1)	**-2.54 ± 5.09**	**-6.80 ± 13.55**	**-3.43 ± 8.75**
B2(2)	**-2.35 ± 5.21**	**-4.71 ± 10.05**	**-4.93 ± 12.40**
B2(3)	**-2.75 ± 4.82**	**-5.66 ± 10.87**	**-4.49 ± 11.57**
B3(1)	**-3.75 ± 6.30**	**-7.66 ± 13.78**	**-4.90 ± 11.22**
B3(2)	**-4.16 ± 6.27**	**-6.21 ± 10.93**	**-8.17 ± 17.54**
B3(3)	**-3.48 ± 5.69**	**-6.08 ± 10.97**	**-9.51 ± 21.56**
B4(1)	**-0.87 ± 2.81**	0.00 ± 0.00	0.00 ± 0.00
B4(2)	**-0.67 ± 1.61**	0.00 ± 0.00	0.00 ± 0.00
B4(3)	**-0.41 ± 1.41**	0.00 ± 0.00	0.00 ± 0.00
B5(1)	**-0.34 ± 1.04**	**-0.69 ± 2.69**	0.00 ± 0.00
B5(2)	**-0.69 ± 1.53**	**-0.69 ± 1.92**	0.00 ± 0.00
B5(3)	**-0.84 ± 1.86**	0.00 ± 0.00	0.00 ± 0.00
B6(1)	0.00 ± 0.00	0.00 ± 0.00	0.00 ± 0.00
B6(2)	0.00 ± 0.00	0.00 ± 0.00	0.00 ± 0.00
B6(3)	0.00 ± 0.00	0.00 ± 0.00	0.00 ± 0.00
B7(1)	0.00 ± 0.00	0.00 ± 0.00	0.00 ± 0.00
B7(2)	0.00 ± 0.00	0.00 ± 0.00	0.00 ± 0.00
B7(3)	0.00 ± 0.00	0.00 ± 0.00	0.00 ± 0.00
B8(1)	**-2.99 ± 4.99**	**-2.15 ± 4.73**	**-1.43 ± 4.24**
B8(2)	**-2.48 ± 4.90**	**-2.21 ± 5.65**	**-1.68 ± 6.78**
B8(3)	**-4.02 ± 6.04**	**-4.02 ± 8.08**	**-2.68 ± 7.04**

Appendix D6 - Summary reports for 0–60, 0–40 and 0–20 and 0–10 minute fluxes in Experiments A and B

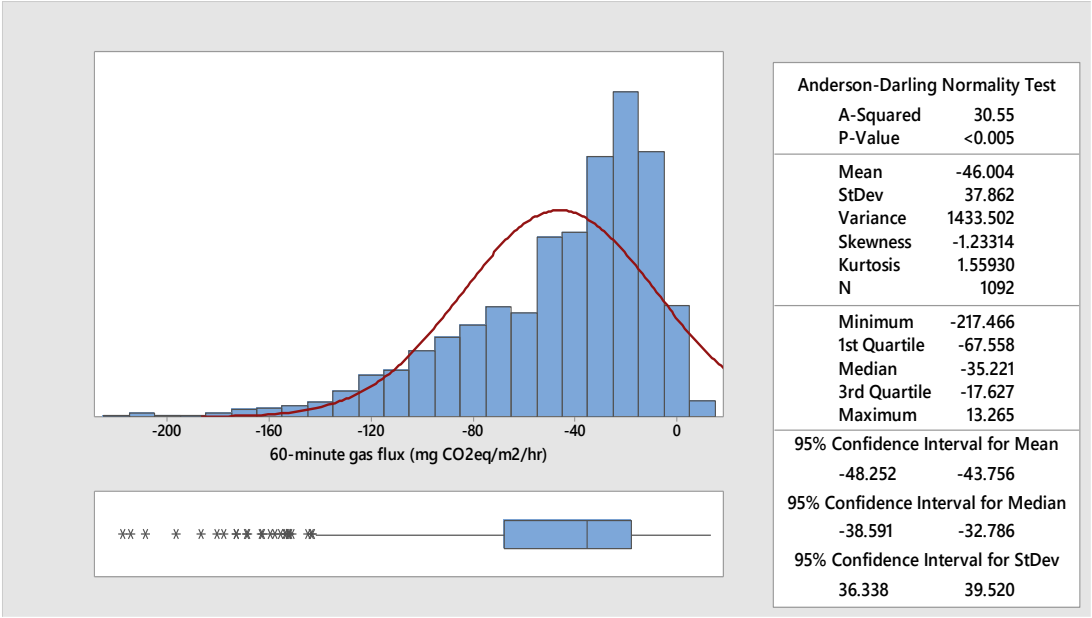

Figure D6 - Summary reports for 0–60 minute fluxes in Experiment A

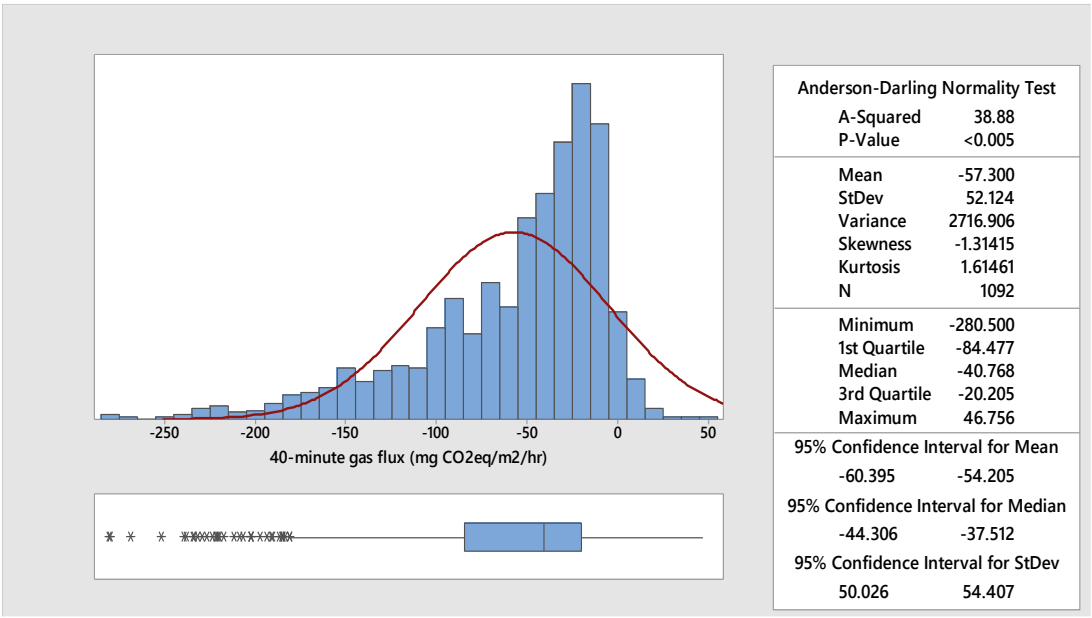

Figure D7 - Summary reports for 0–40 minute fluxes in Experiment A

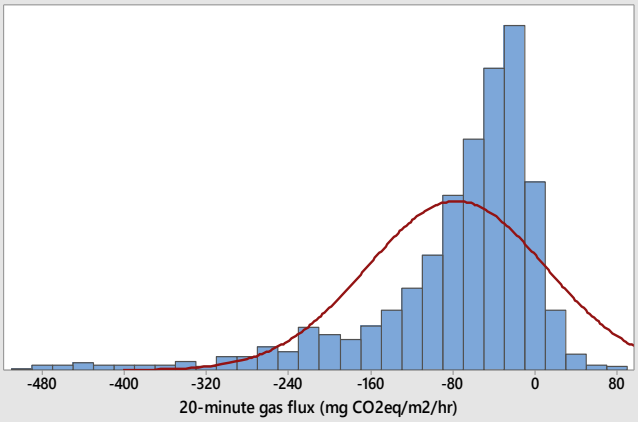

Anderson-Darling Normality Test	
A-Squared	58.33
P-Value	<0.005
Mean	-76.458
StDev	87.464
Variance	7650.016
Skewness	-1.95013
Kurtosis	4.61693
N	1092
Minimum	-498.471
1st Quartile	-101.793
Median	-50.681
3rd Quartile	-21.614
Maximum	81.420
95% Confidence Interval for Mean	
-81.651	-71.264
95% Confidence Interval for Median	
-54.625	-46.979
95% Confidence Interval for StDev	
83.944	91.296

Figure D8 - Summary reports for 0–20 minute fluxes in Experiment A

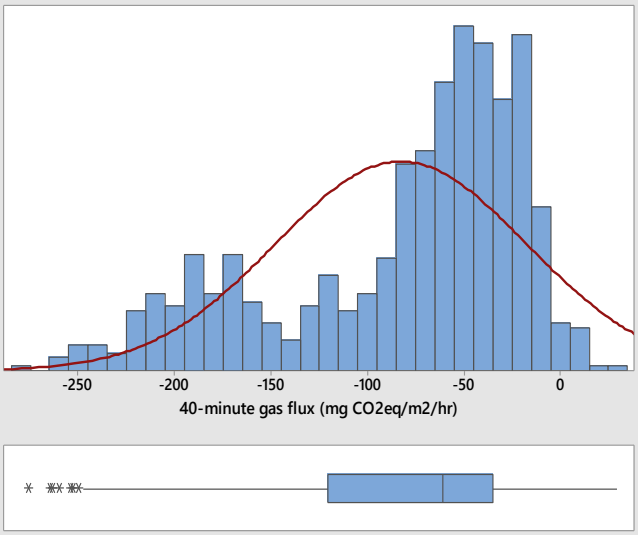

Anderson-Darling Normality Test	
A-Squared	32.46
P-Value	<0.005
Mean	-82.693
StDev	65.069
Variance	4234.040
Skewness	-0.923337
Kurtosis	-0.203724
N	792
Minimum	-276.148
1st Quartile	-120.619
Median	-60.918
3rd Quartile	-34.753
Maximum	29.736
95% Confidence Interval for Mean	
-87.231	-78.154
95% Confidence Interval for Median	
-64.798	-56.471
95% Confidence Interval for StDev	
62.015	68.443

Figure D9 - Summary reports for 0–40 minute fluxes in Experiment B

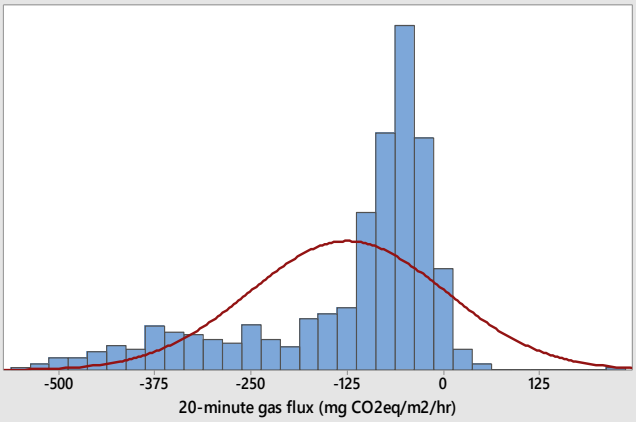

Anderson-Darling Normality Test	
A-Squared	56.22
P-Value	<0.005
Mean	-124.23
StDev	127.13
Variance	16162.96
Skewness	-1.32734
Kurtosis	0.87897
N	792
Minimum	-552.30
1st Quartile	-168.49
Median	-73.42
3rd Quartile	-40.91
Maximum	221.04
95% Confidence Interval for Mean	
-133.10	-115.36
95% Confidence Interval for Median	
-78.38	-66.96
95% Confidence Interval for StDev	
121.17	133.72

Figure D10 - Summary reports for 0–20 minute fluxes in Experiment B

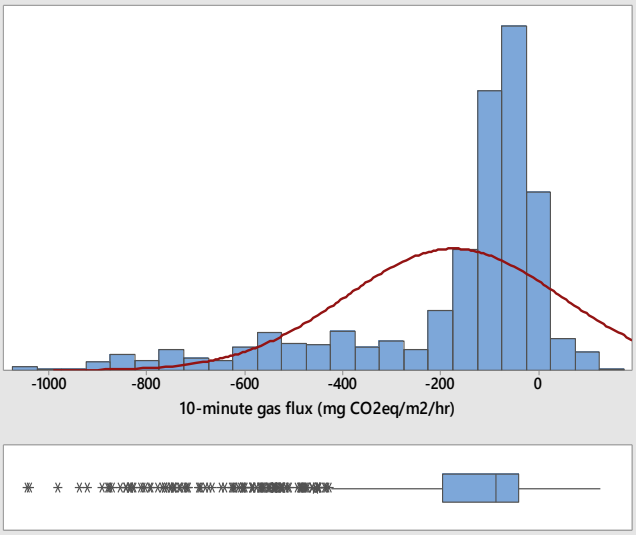

Anderson-Darling Normality Test	
A-Squared	70.87
P-Value	<0.005
Mean	-173.54
StDev	220.36
Variance	48557.80
Skewness	-1.69970
Kurtosis	2.19658
N	792
Minimum	-1045.93
1st Quartile	-195.16
Median	-87.43
3rd Quartile	-40.99
Maximum	125.60
95% Confidence Interval for Mean	
-188.91	-158.17
95% Confidence Interval for Median	
-93.36	-82.27
95% Confidence Interval for StDev	
210.02	231.78

Figure D11 - Summary reports for 0–10 minute fluxes in Experiment B

Appendix D7 - Interval plots for CO_2 flux results from Experiments A and B

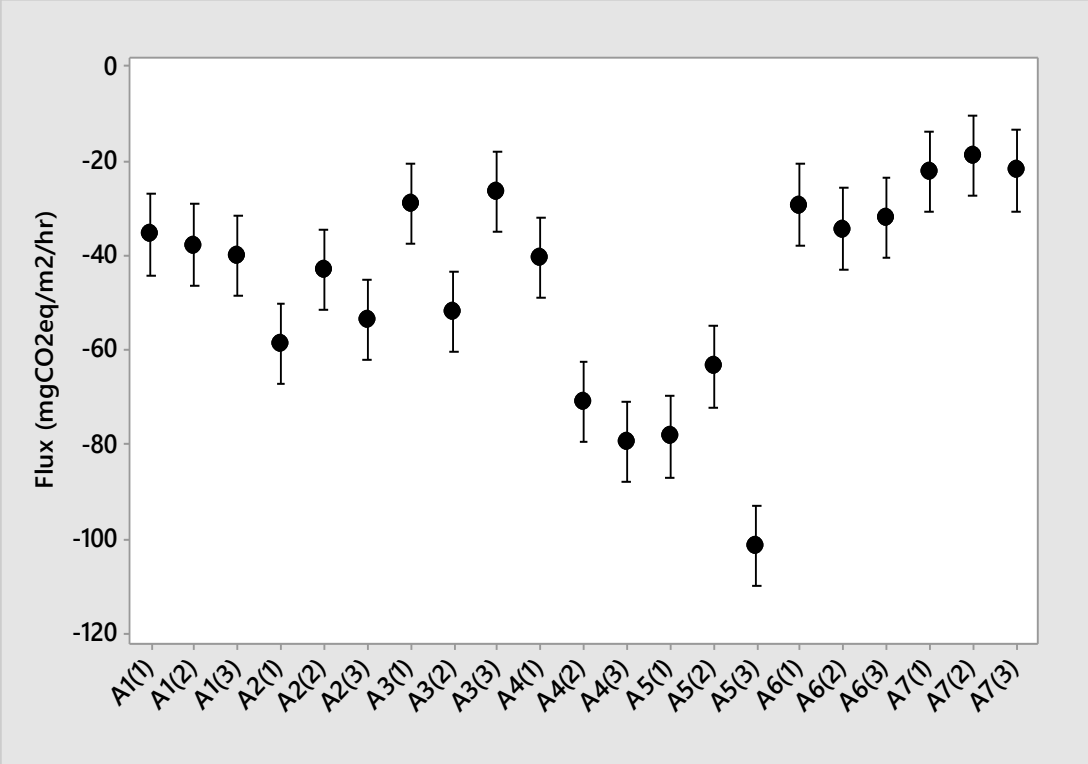

Figure D12 - Interval plot showing mean 60-minute flux for A1(1)–A7(3) over 180 days with 95% confidence interval bars for the mean, based on a pooled standard deviation

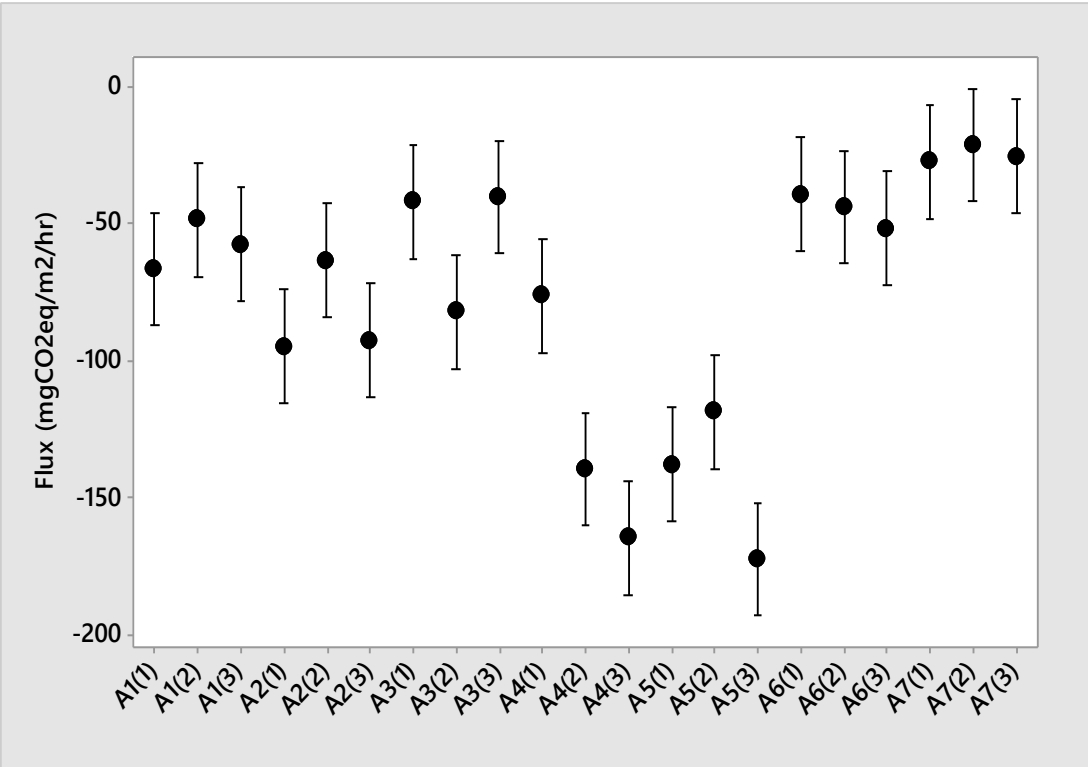

Figure D13 - Interval plot showing mean 20-minute flux for A1(1)–A7(3) over 180 days with 95% confidence interval bars for the mean, based on a pooled standard deviation

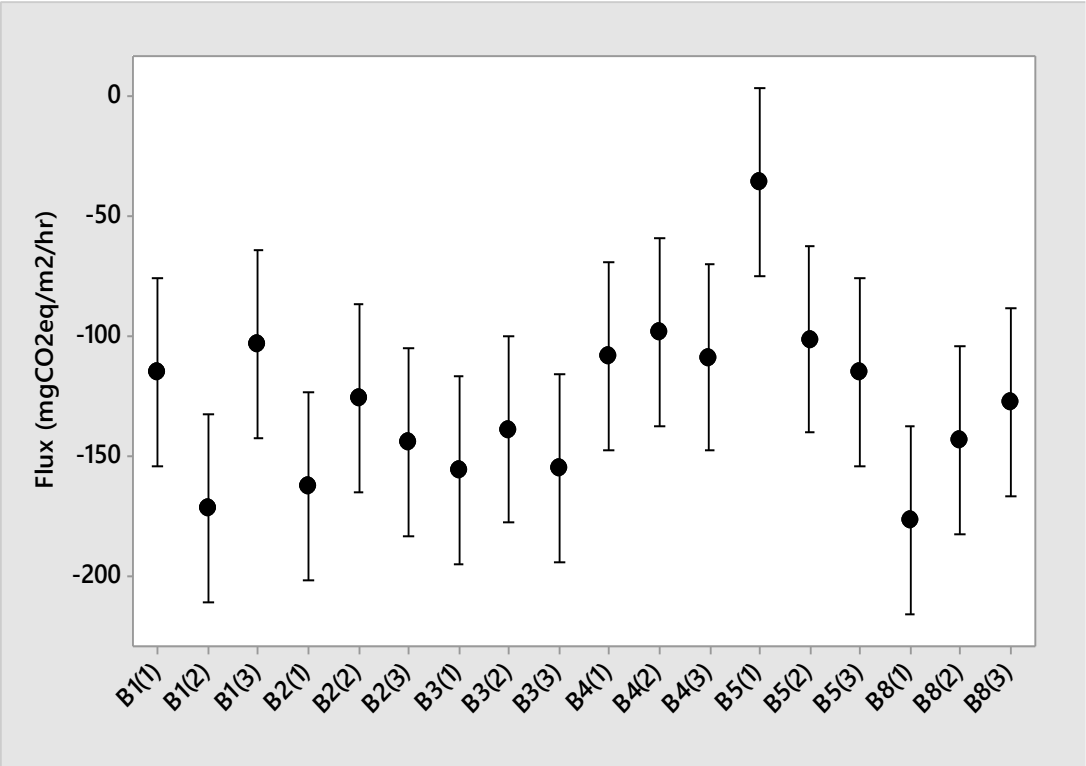

Figure D14 - Interval plot showing mean 20-minute flux for B1(1)–B5(3), B8(1)–B8(3) over 180 days with 95% confidence interval bars for the mean, based on a pooled standard deviation

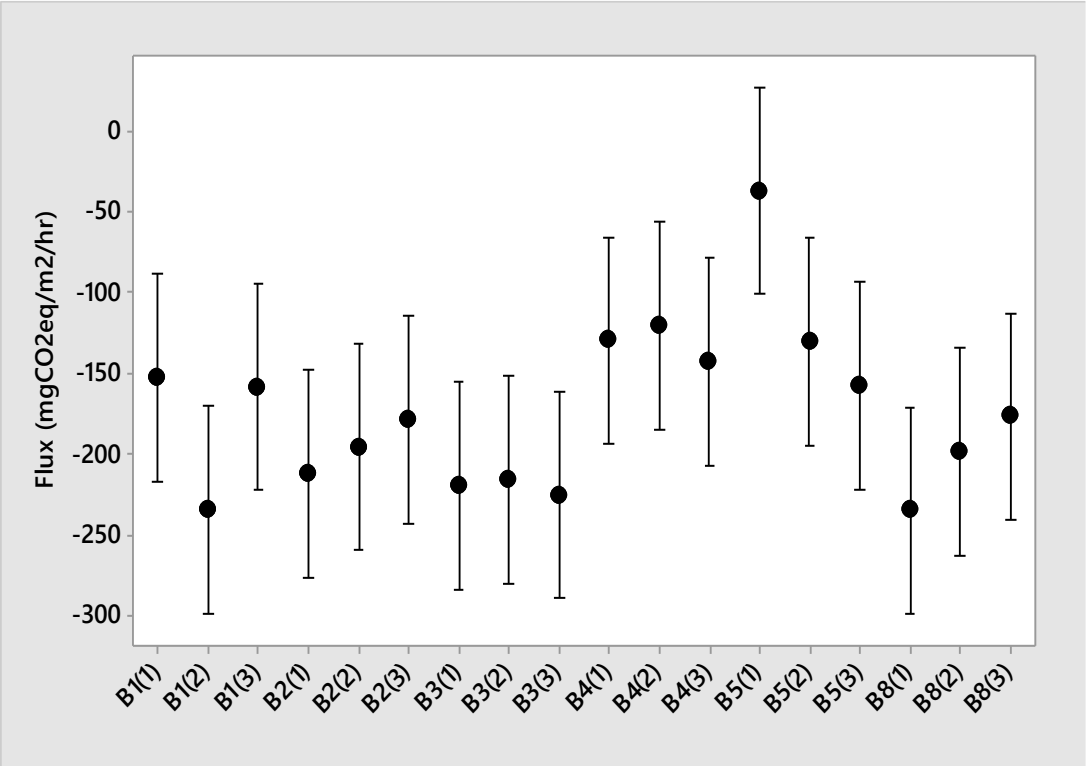

Figure D15 - Interval plot showing mean 10-minute flux for B1(1)–B5(3), B8(1–-B8(3) over 180 days with 95% confidence interval bars for the mean, based on a pooled standard deviation

Appendix D8 - CO_2 flux results from Experiments A and B

Table D5 - Mean CO_2 fluxes values (mg CO_2eq/m^2/hr) with standard error for a chamber deployment period of 10, 20, 40 and 60 minutes for Experiment A

Column	Measurement period over which regression model was applied			
	0-60	**0-40**	**0-20**	**0-10**
A1(1)	-36 ± 34	-45 ± 51	-67 ± 76	-85 ± 78
A1(2)	-38 ± 30	-42 ± 41	-48 ± 54	-61 ± 69
A1(3)	-40 ± 45	-50 ± 61	-58 ± 86	-62 ± 93
A2(1)	-59 ± 32	-67 ± 41	-95 ± 73	-93 ± 79
A2(2)	-43 ± 28	-51 ± 42	-63 ± 61	-58 ± 70
A2(3)	-54 ± 30	-72 ± 45	-92 ± 58	-86 ± 71
A3(1)	-29 ± 24	-35±35	-42 ± 51	-41 ± 73
A3(2)	-52 ± 29	-62 ± 42	-82 ± 66	-94 ± 72
A3(3)	-26 ± 26	-32 ± 47	-40 ± 64	-36 ± 71
A4(1)	-40 ± 30	-57 ± 43	-76 ± 73	-98 ± 107
A4(2)	-71 ± 36	-90 ± 56	-139 ± 112	-157 ± 160
A4(3)	-79 ± 31	-108 ± 50	-164 ± 121	-184 ± 145
A5(1)	-78 ± 28	-104 ± 47	-138 ± 84	-155 ± 128
A5(2)	-63 ± 48	-82 ± 60	-119 ± 107	-152 ± 177
A5(3)	-101 ± 45	-117 ± 51	-172 ± 119	-204 ± 166
A6(1)	-29 ± 26	-33 ± 44	-39 ± 63	-36 ± 73
A6(2)	-34 ± 26	-39 ± 32	-44 ± 43	-44 ± 71
A6(3)	-32 ± 27	-46 ± 43	-52 ± 68	-50 ± 77
A7(1)	-22 ± 25	-26 ± 30	-28 ± 57	-25 ± 62
A7(2)	-19 ± 21	-20 ± 25	-21 ± 35	-12 ± 55
A7(3)	-22 ± 20	-26 ± 28	-26 ± 34	-30 ± 41
A8(1)	113 ± 41	110 ± 46	110 ± 51	101 ± 54
A8(2)	44 ± 23	38 ± 25	38 ± 39	42 ± 42
A8(3)	135 ± 47	129 ± 46	127 ± 53	152 ± 73
Pooled StDev	**32.31**	**43.96**	**72.97**	**95.45**

Table D6 - Mean CO_2 fluxes values (mg CO_2eq/m^2/hr) with standard error for a chamber deployment period of 10, 20 and 40 minutes for Experiment B

Column	Measurement period over which regression model was applied		
	0–40	**0–20**	**0–10**
B1(1)	-72 ± 65	-113 ± 121	-153 ± 208
B1(2)	-104 ± 75	-166 ± 149	-235 ± 254
B1(3)	-64 ± 55	-101 ± 120	-158 ± 236
B2(1)	-95 ± 70	-156 ± 159	-212 ± 275
B2(2)	-87 ± 58	-122 ± 146	-196 ± 262
B2(3)	-85 ± 61	-139 ± 134	-179 ± 256
B3(1)	-86 ± 86	-149 ± 181	-220 ± 301
B3(2)	-79 ± 73	-133 ± 143	-216 ± 259
B3(3)	-86 ± 72	-149 ± 148	-225 ± 289
B4(1)	-91 ± 49	-109 ± 77	-130 ± 115
B4(2)	-80 ± 44	-99 ± 66	-121 ± 88
B4(3)	-85 ± 40	-109 ± 59	-143 ± 98
B5(1)	-28 ± 50	-35 ± 82	-37 ± 120
B5(2)	-72 ± 56	-101 ± 96	-131 ± 144
B5(3)	-81 ± 75	-116 ± 125	-158 ± 191
B6(1)	439 ± 776	832 ± 1487	1421 ± 2743
B6(2)	632 ± 1007	1038 ± 1766	1589 ± 2952
B6(3)	52 ± 98	35 ± 30	61 ± 110
B7(1)	84 ± 48	89 ± 54	84 ± 62
B7(2)	161 ± 22	179 ± 35	197 ± 48
B7(3)	174 ± 305	184 ± 384	177 ± 418
B8(1)	-118 ± 56	-175 ± 104	-235 ± 175
B8(2)	-92 ± 62	-141 ± 121	-199 ± 220
B8(3)	-84 ± 72	-124 ± 134	-177 ± 229

Appendix D9 - Interval plots for CO_2 flux results for each column type in Experiments A and B

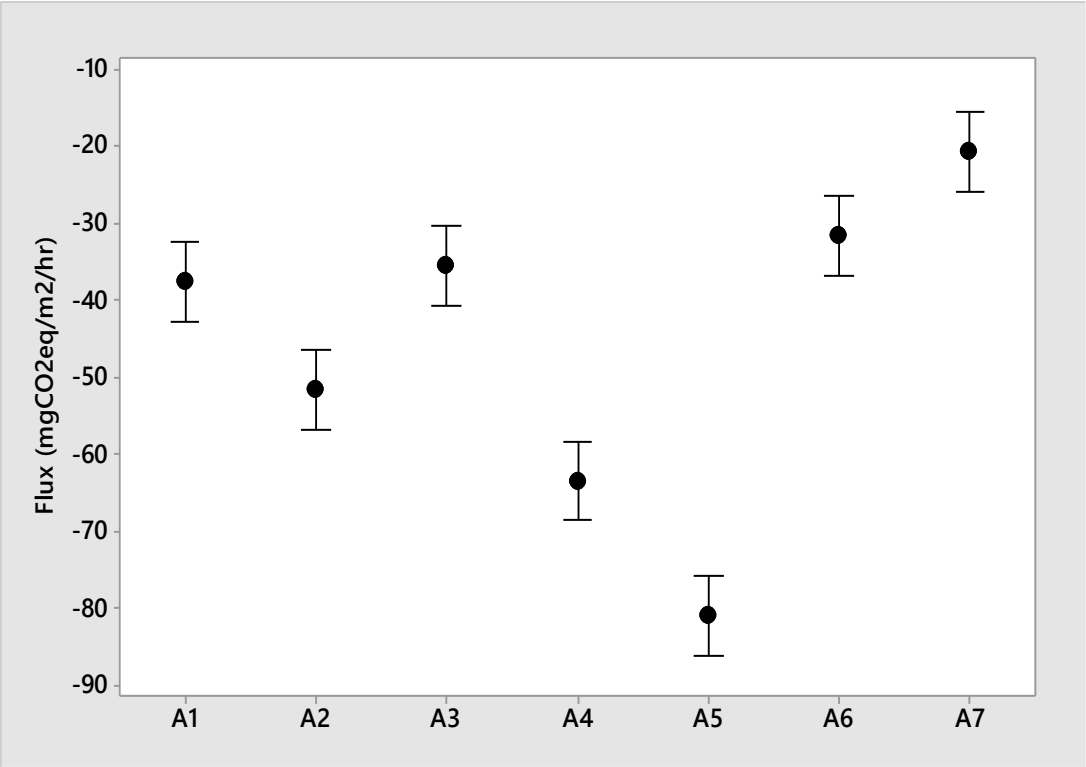

Figure D16 - Interval plot showing mean 60-minute flux for each column type in Experiment A with 95% confidence interval bars for the mean, based on a pooled standard deviation

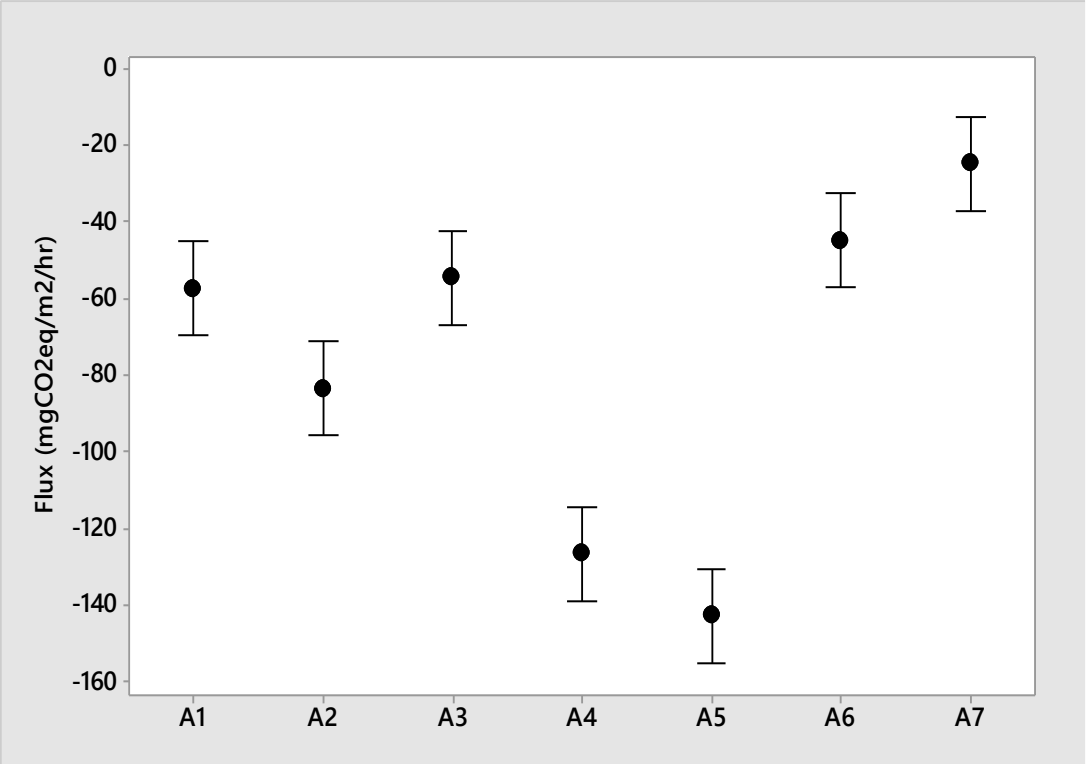

Figure D17 - Interval plot showing mean 20-minute flux for each column type in Experiment A with 95% confidence interval bars for the mean, based on a pooled standard deviation

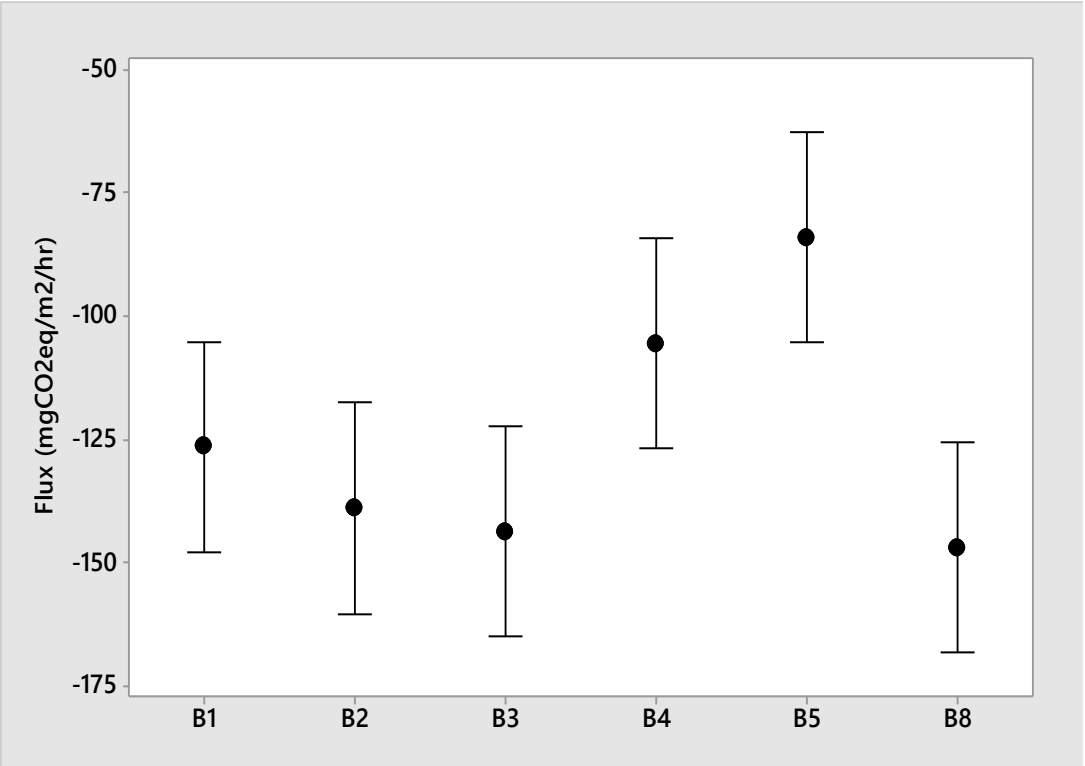

Figure D18 - Interval plot showing mean 20-minute flux for each column type in Experiment B with 95% confidence interval bars for the mean, based on a pooled standard deviation

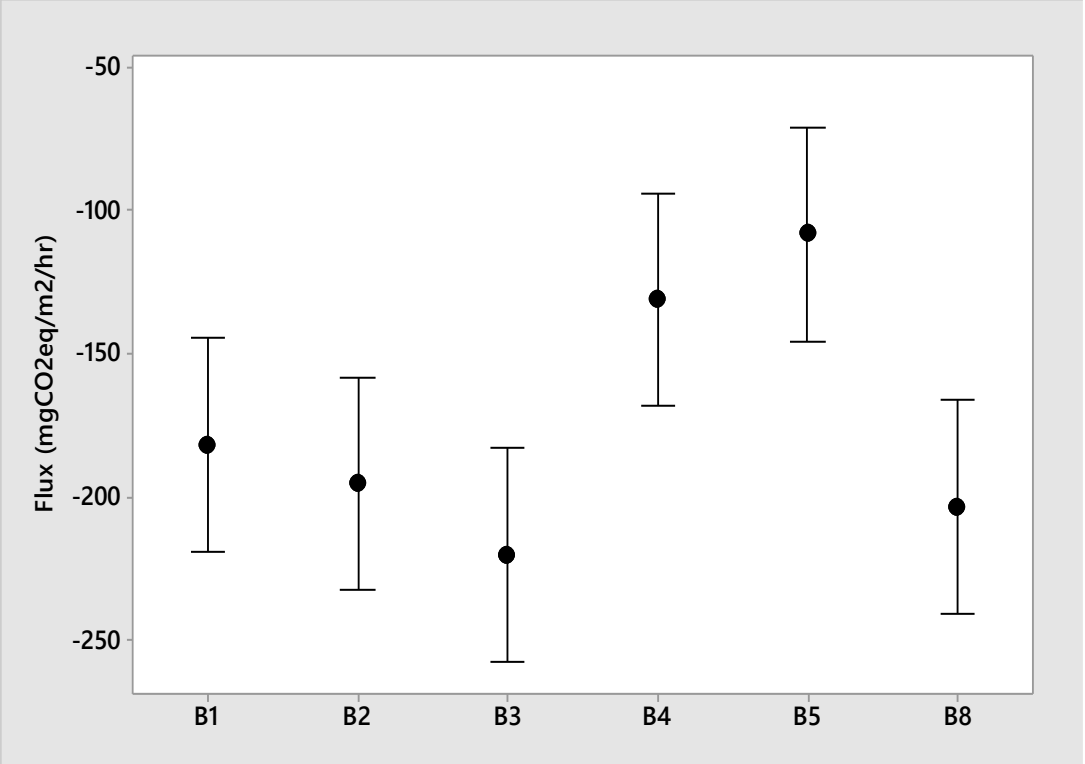

Figure D19 - Interval plot showing mean 10-minute flux for each column type in Experiment B with 95% confidence interval bars for the mean, based on a pooled standard deviation

Appendix D10 - Multiple regression analysis for Experiments A and B

Table D7 - Multiple regression analysis for the 60-minute flux in Experiment A

	60-minute flux					
Analysis	1	2	3	4	5	6
R^2 (adj)	58.58	62.05	61	62.3	62.15	62.3
Lack-of-fit	0.528	0.56	0.55	0.562	0.561	0.562
Variables	**p-values**					
Intercept	**0.021**	0.923	**0.001**	0.915	0.059	0.853
Time	**0.000**	-	-	-	-	-
Ln (time)	-	**0.000**	**0.000**	**0.000**	**0.000**	**0.000**
Initial CO_2 conc.	**0.000**	**0.000**	**0.000**	**0.000**	**0.000**	**0.000**
Cement	0.722	-	**0.000**	-	**0.000**	-
GGBS	**0.000**	**0.000**	-	**0.000**	-	**0.000**
Surcharge	**0.000**	**0.000**	**0.000**	**0.000**	**0.000**	**0.000**
Surcharge*time	-	-	-	**0.005**	**0.005**	**0.005**
Cement*GGBS	-	-	-	0.271	**0.000**	-

Table D8 - Multiple regression analysis for the 20-minute flux in Experiment A

	20-minute flux					
Analysis	1	2	3	4	5	6
R^2 (adj)	50.68	59.17	58.4	62.42	62.39	62.37
Lack-of-fit	0.054	0.065	0.064	0.071	0.071	0.071
Variables	**p-values**					
Intercept	0.314	**0.000**	0.367	**0.000**	0.106	**0.001**
Time	**0.000**	-	-	-	-	-
Ln (time)	-	**0.000**	**0.000**	**0.000**	**0.000**	**0.000**
Initial CO_2 conc.	**0.000**	**0.000**	**0.000**	**0.000**	**0.000**	**0.000**
Cement	0.623	-	**0.000**	-	-	-
GGBS	**0.000**	**0.000**	-	**0.000**	**0.000**	**0.000**
Surcharge	**0.000**	**0.000**	**0.000**	**0.000**	**0.000**	**0.000**
Surcharge*time	-	-	-	**0.000**	**0.000**	**0.000**
Cement*GGBS	-	-	-	0.122	**0.000**	-

Table D9 - Multiple regression analysis for the 10-minute flux in Experiment B

	10-minute flux					
Analysis	1	2	3	4	5	6
R^2 (adj)	46.25	61.85	64.77	63.42	63.47	63.47
Lack-of-fit	0.582	0.663	0.683	0.674	0.503	0.000
Variables	**p-values**					
Intercept	**0.000**	**0.000**	**0.000**	**0.000**	**0.000**	**0.000**
Time	**0.000**	-	-	-	-	-
Ln (Time)	-	**0.000**	**0.000**	**0.000**	**0.000**	**0.000**
Initial CO_2 conc.	0.414	0.304	0.301	0.335	0.336	-
Cement	0.956	0.944	0.013	0.948	-	-
Water table	**0.028**	**0.009**	0.088	**0.008**	**0.006**	**0.006**
Surcharge	**0.000**	**0.000**	**0.000**	**0.000**	**0.000**	**0.000**
Surcharge*time	-	-	**0.000**	**0.000**	**0.000**	**0.000**
Water table*time	-	-	0.830	-	-	-
Cement*time	-	-	**0.000**	-	-	-

Table D10 - Multiple regression analysis for the 20-minute flux in Experiment B

	20-minute flux					
Analysis	1	2	3	4	5	6
R^2 (adj)	53.76	65.2	67.33	67.22	67.26	67.26
Lack-of-fit	0.801	0.862	0.874	0.873	0.890	0.000
Variables	**p-values**					
Intercept	**0.000**	**0.000**	**0.000**	**0.000**	**0.000**	**0.000**
Time	**0.000**					
Ln (Time)		**0.000**	**0.000**	**0.000**	**0.000**	**0.000**
Initial CO_2 conc.	0.421	0.399	0.324	0.333	0.318	
Cement	0.764	0.735	0.449	0.722		
Water table	**0.005**	**0.001**	0.165	**0.001**	**0.001**	**0.001**
Surcharge	**0.000**	**0.000**	**0.000**	**0.000**	**0.000**	**0.000**
Surcharge*time			**0.000**	**0.000**	**0.000**	**0.000**
Water table*time			0.552			
Cement*time			**0.041**			

Appendix D11 - Best-fit models for Experiments A and B

Model 1- Best-fit model for Experiment A

Analysis of Variance

Source	DF	Adj SS	Adj MC	F-value	p-value
Regression	6	1964739	327456	355.50	0.000
Initial CO_2	1	152507	152507	165.57	0.000
Ln(time)	1	314536	314536	341.47	0.000
Cement	1	18550	18550	20.14	0.000
Surcharge	1	190887	190887	207.24	0.000
Surcharge*time	1	31668	31668	34.38	0.000
GGBS*cement	1	22721	22721	24.67	0.000
Error	1085	999406	921		
Lack-of-Fit	1083	998208	922	1.54	0.478
Pure Error	2	1198	599		
Total	1091	2964145			

Model Summary

S	R-sq	R-sq(adj)	R-sq(pred)
30.3498	66.28%	66.10%	65.68%

Coefficients

Term	Coef	SE Coef	T-Value	p-value	VIF
Constant	-11.0	11.4	-0.96	0.337	
Initial CO_2	-1488	116	-12.87	0.000	1.46
Ln(time)	18.87	1.02	18.48	0.000	1.64
Cement	-0.0957	0.0213	-4.49	0.000	2.52
Surcharge	-5.751	0.399	-14.40	0.000	3.61
Surcharge*time	0.02157	0.00368	5.86	0.000	3.24
GGBS*cement	0.001152	0.000232	4.97	0.000	1.79

Regression Equation

40-minute flux = - 11.0 - 1488 initial CO_2 concentration + 18.87 ln(time)
- 0.0957 cement - 5.751 surcharge + 0.02157 surcharge*time
+ 0.001152 GGBS*cement

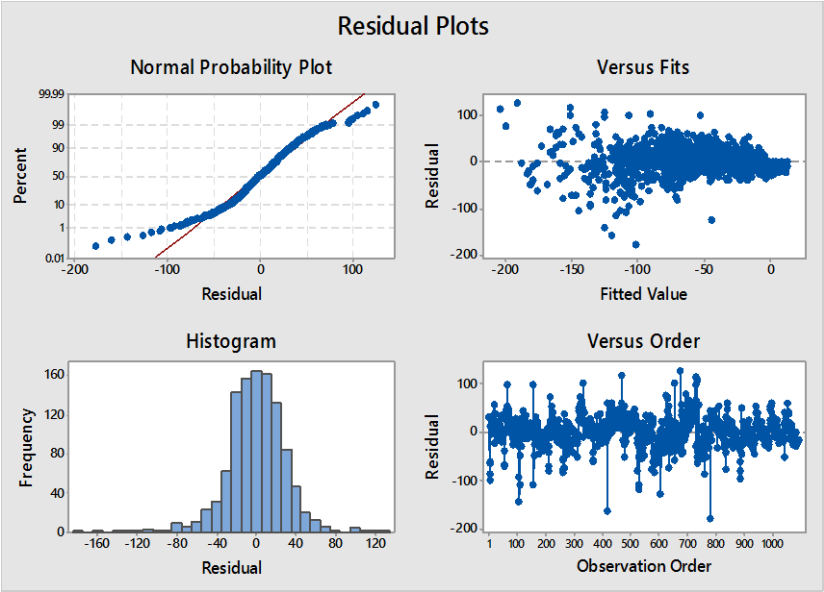

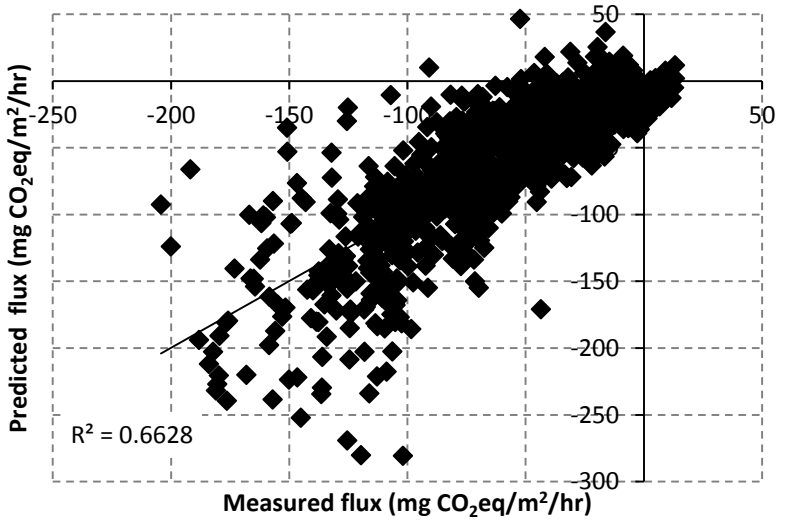

Model 2 - Best-fit model for Experiment B

Analysis of Variance

Source	DF	Adj SS	Adj MC	F-value	p-value
Regression	5	2298078	459616	343.71	0.000
Ln(time)	1	768072	768072	574.38	0.000
Cement	1	6254	6254	4.68	0.031
Surcharge	1	78952	78952	59.04	0.000
Surcharge*time	1	82237	82237	61.50	0.000
Water table	1	37532	37532	28.07	0.000
Error	786	1051048	1337		
Lack-of-Fit	258	604764	2344	2.77	0.000
Pure Error	528	446283	845		
Total	791	3349125			

Model Summary

S	R-sq	R-sq(adj)	R-sq(pred)
36.5679	68.62%	68.42%	68.04%

Coefficients

Term	Coef	SE Coef	T-Value	p-value	VIF
Constant	-202.7	10.1	-20.07	0.000	
Ln(time)	35.03	1.46	23.97	0.000	1.85
Cement	-0.0770	0.0356	-2.16	0.031	1.09
Surcharge	-4.209	0.548	-7.68	0.000	3.02
Surcharge*time	0.03770	0.00481	7.84	0.000	3.45
Water table	22.70	4.29	5.30	0.000	1.51

Regression Equation

40-minute flux = - 202.7 + 35.03 ln(time) - 0.0770 cement - 4.209 surcharge + 0.03770 surcharge*time + 22.70 water table

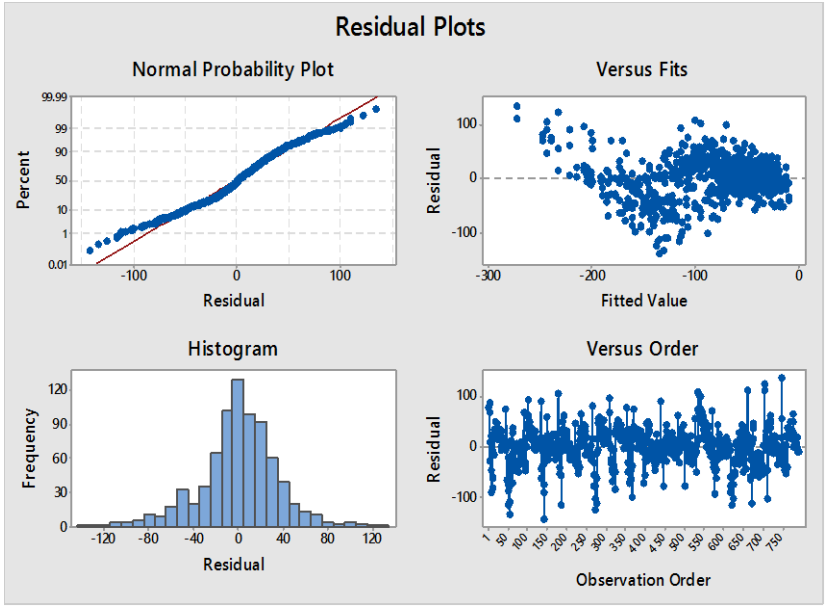

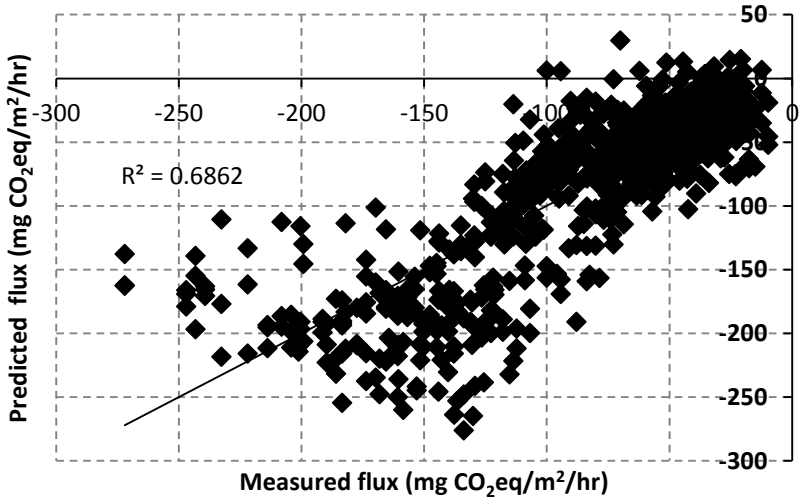

Appendix D12 - Slopes and R^2 values for plots of predicted versus observed fluxes for the individual columns

Table D11 - Slopes and R^2 values for plots of predicted versus observed fluxes for the individual columns A1(1) to A7(3)

Column No.	Slope	R^2 value
A1(1)	1.20	0.70
A1(2)	0.87	0.53
A1(3)	1.51	0.79
A2(1)	0.92	0.63
A2(2)	1.00	0.65
A2(3)	1.18	0.76
A3(1)	0.83	0.57
A3(2)	1.08	0.83
A3(3)	1.17	0.61
A4(1)	0.99	0.68
A4(2)	1.33	0.75
A4(3)	1.08	0.66
A5(1)	0.80	0.55
A5(2)	1.23	0.79
A5(3)	0.76	0.42
A6(1)	0.99	0.49
A6(2)	0.75	0.45
A6(3)	1.23	0.71
A7(1)	0.75	0.65
A7(2)	0.56	0.50
A7(3)	0.63	0.53
Average	0.99	0.63
Std.	0.24	0.12
Max	1.51	0.83
Min	0.56	0.42

Tables D12 - Slopes and R^2 values for plots of predicted versus observed fluxes for the individual columns B1(1) to B5(3) and B8(1) to B8(3)

Column No.	Slope	R^2 value
B1(1)	0.99	0.69
B1(2)	1.16	0.71
B1(3)	0.87	0.76
B2(1)	1.11	0.74
B2(2)	0.87	0.67
B2(3)	1.01	0.81
B3(1)	1.35	0.74
B3(2)	1.15	0.75
B3(3)	1.15	0.76
B4(1)	0.98	0.73
B4(2)	0.89	0.75
B4(3)	0.81	0.73
B5(1)	0.88	0.57
B5(2)	1.14	0.77
B5(3)	1.61	0.84
B8(1)	0.71	0.71
B8(2)	0.77	0.69
B8(3)	0.96	0.79
Average	1.02	0.73
Std.	0.22	0.06
Max	1.61	0.84
Min	0.71	0.57

Appendix D13 - Examination of surcharge*time variable

Table D13 - Slopes and R^2 values for plots of predicted versus observed fluxes for the surcharged columns A4(1) to A5(3) for model which includes surcharge*time variable and model that excludes the variable

	With surcharge*time variable		Without surcharge*time variable	
	Slope	**R^2 value**	**Slope**	**R^2 value**
A4(1)	0.99	0.68	1.09	0.65
A4(2)	1.33	0.75	1.48	0.74
A4(3)	1.08	0.66	1.18	0.66
A5(1)	0.80	0.55	1.05	0.53
A5(2)	1.23	0.79	1.63	0.78
A5(3)	0.76	0.42	1.00	0.41
Average	1.03	0.64	1.24	0.63
Std	0.23	0.14	0.26	0.14

Appendix D14 - Cross-validation models for Experiments A and B

Table D14 - Cross-validation model for Scenario 2 using data from Experiment A

Parameters	Coefficient	Standard error	p-value
b_0 (constant)	-7.5	14.2	0.595
b_1 (initial CO_2 conc.)	-1552	146	0.000
b_2 (ln(time))	19.18	1.21	0.000
b_3 (cement)	-0.1032	0.0268	0.000
b_4 (surcharge)	-5.875	0.497	0.000
b_5 (surcharge*time)	0.02213	0.00459	0.000
b_6 (GGBS*cement)	0.001105	0.000291	0.000
R^2 (adj)	66.64		
R^2 (pred)	66.04		
SE	31.2883		
d.f (reg, res)	6,728		
F-value	245.38		
P-value	0.000		

Table D15 - Cross-validation model for Scenario 2 using data from Experiment B

Parameters	Coefficient	Standard error	p-value
b_0 (constant)	-192.3	11.9	0.000
b_2 (ln(time))	33.23	1.66	0.000
b_3 (cement)	-0.0894	0.0427	0.037
b_4 (surcharge)	-4.389	0.648	0.000
b_5 (surcharge*time)	0.03951	0.00576	0.000
b_7 (water table)	21.82	5.14	0.000
R^2 (adj)	66.92		
R^2 (pred)	66.40		
SE	37.9929		
d.f (reg, res)	5,588		
F-value	240.88		
P-value	0.000		

Table D16 - Best-fit model using 0 ppm assumption for 40-minute flux for Experiment A data

Parameters	Coefficient	Standard error	p-value
b_0 (constant)	-13.7	11.7	0.243
b_1 (initial CO_2 conc.)	-1466	118	0.000
b_2 (ln(time))	19.21	1.05	0.000
b_3 (cement)	-0.1137	0.0286	0.000
b_4 (surcharge)	-5.809	0.409	0.000
b_5 (GGBS*cement)	0.001150	0.000238	0.000
b_6 (surcharge*time)	0.02188	0.00377	0.000
R^2 (adj)	65.37		
R^2 (pred)	64.93		
SE	31.0801		
d.f (reg, res)	6,1085		
F-value	344.18		
P-value	0.000		

Table D17 - Best-fit model using 0 ppm assumption for 40-minute flux for Experiment B data

Parameters	Coefficient	Standard error	p-value
b_0 (constant)	-210.2	10.9	0.000
b_2 (ln(time))	36.57	1.58	0.000
b_3 (cement)	-0.0792	0.0385	0.048
b_4 (surcharge)	-4.766	0.593	0.000
b_5 (surcharge*time)	0.04189	0.00521	0.000
b_7 (water table)	23.35	4.64	0.000
R^2 (adj)	67.44		
R^2 (pred)	67.04		
SE	39.6074		
d.f (reg, res)	5,786		
F-value	328.67		
P-value	0.000		

Appendix D15 - Interval plots showing gas fluxes for Experiments A and B together

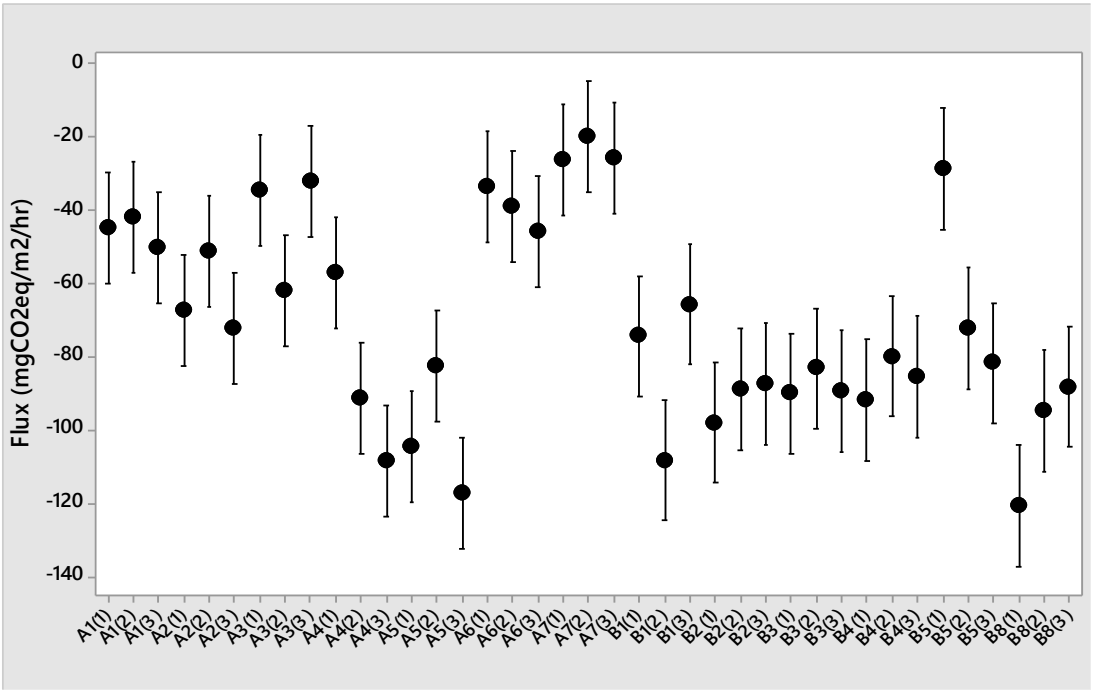

Figure D20 - Interval plots of mean 40-minute fluxes for stabilised peat in Experiments A and B with 95% confidence interval bars for the mean, based on a pooled standard deviation

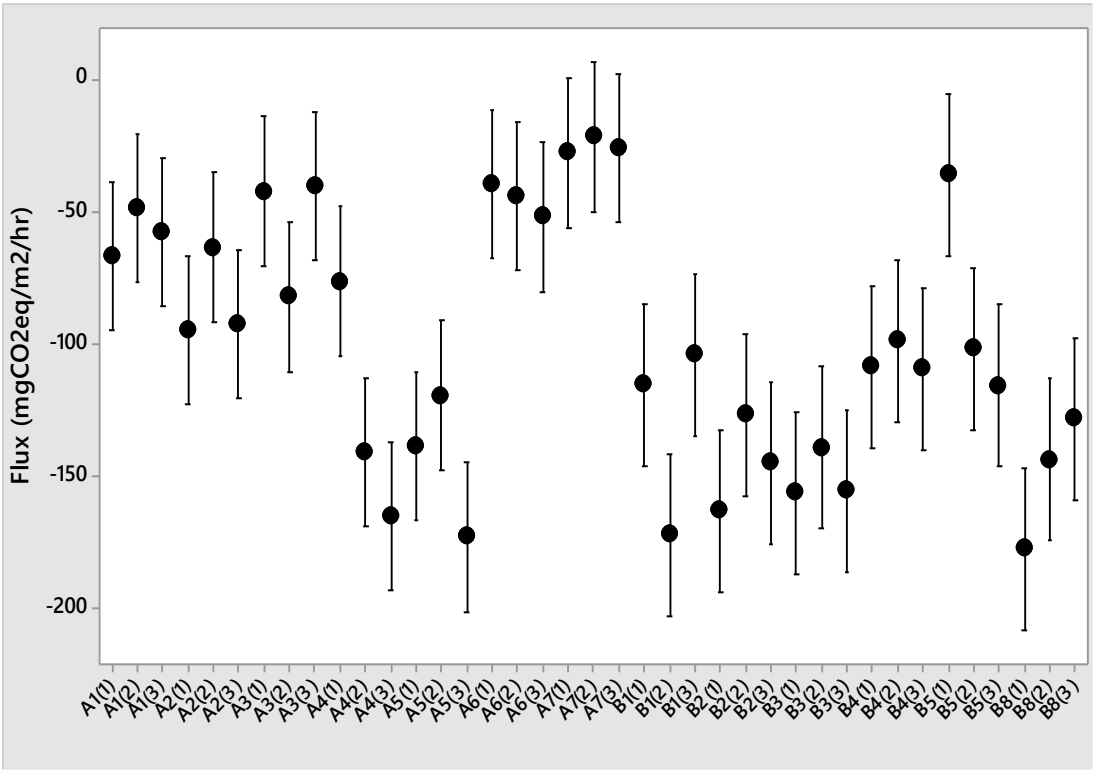

Figure D21 - Interval plots of mean 20-minute fluxes for stabilised peat in Experiments A and B with 95% confidence interval bars for the mean, based on a pooled standard deviation

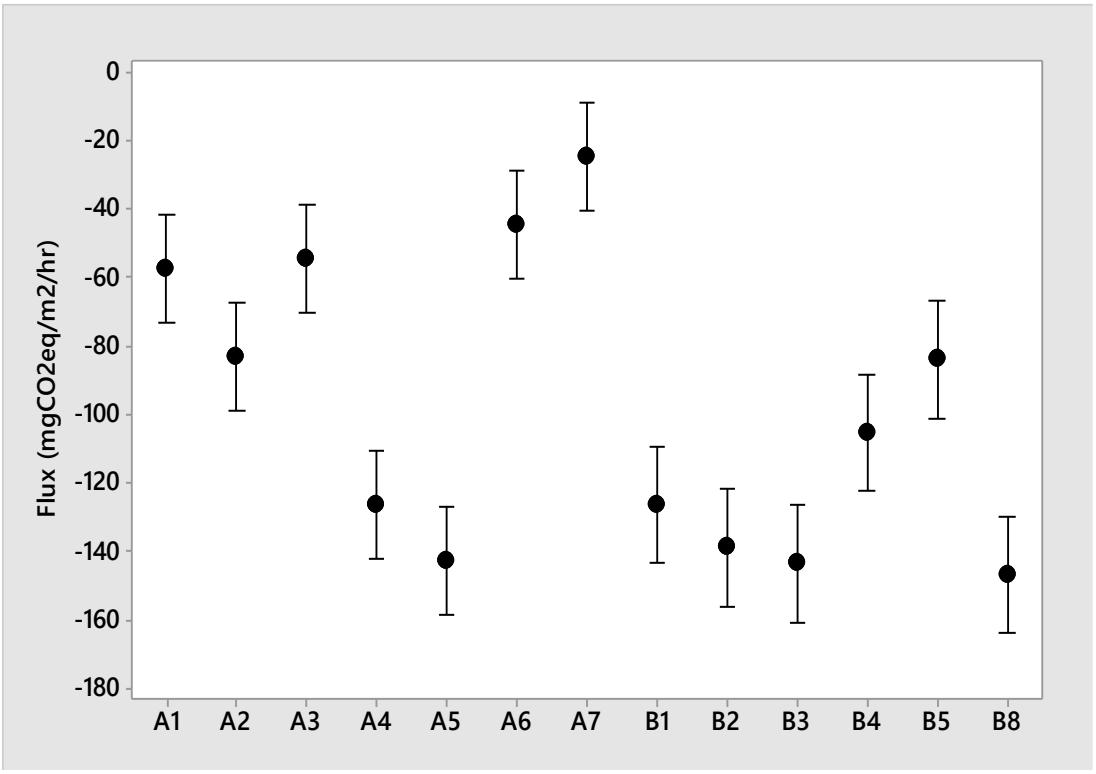

Figure D22 - Interval plot of mean 20-minute fluxes for each stabilised peat column type in Experiments A and B with 95% confidence interval bars for the mean, based on a pooled standard deviation

Appendix D16 - Best-fit models for meta-analysis

Analysis of Variance

Source	DF	Adj SS	Adj MC	F-value	P-value
Regression	6	4220165	703361	552.59	0.000
Initial CO_2	1	13618	13618	10.70	0.001
Ln(time)	1	1458669	1458669	1146.00	0.000
Cement	1	22784	22784	17.90	0.000
Surcharge	1	467761	467761	367.50	0.000
Surcharge*time	1	172299	172299	135.37	0.000
Cement*GGBS		70797	70797	55.62	0.000
Error	1877	2389109	1273		
Lack-of-Fit	1872	2380003	1271	0.70	0.791
Pure Error	5	9106	1821		
Total	1883	6609273			

Model Summary

S	R-sq	R-sq(adj)	R-sq(pred)
35.6768	63.85%	63.74%	63.18%

Coefficients

Term	Coef	SE Coef	T-Value	P-Value	VIF
Constant	-149.11	5.98	-24.95	0.000	
Initial CO_2	-121.5	37.1	-3.27	0.001	1.02
Ln(time)	28.719	0.848	33.85	0.000	1.47
Cement	-0.0784	0.0185	-4.23	0.000	1.79
Surcharge	-6.287	0.328	-19.17	0.000	3.13
Surcharge*time	0.03607	0.00310	11.63	0.000	3.32
Cement*GGBS	0.001821	0.000244	7.46	0.000	1.67

Regression Equation

40-minute flux = - 149.11 - 121.5 initial CO_2 + 28.719 ln(time) - 0.0784 cement - 6.287 surcharge + 0.03607 surcharge*time + 0.001821 cement*GGBS

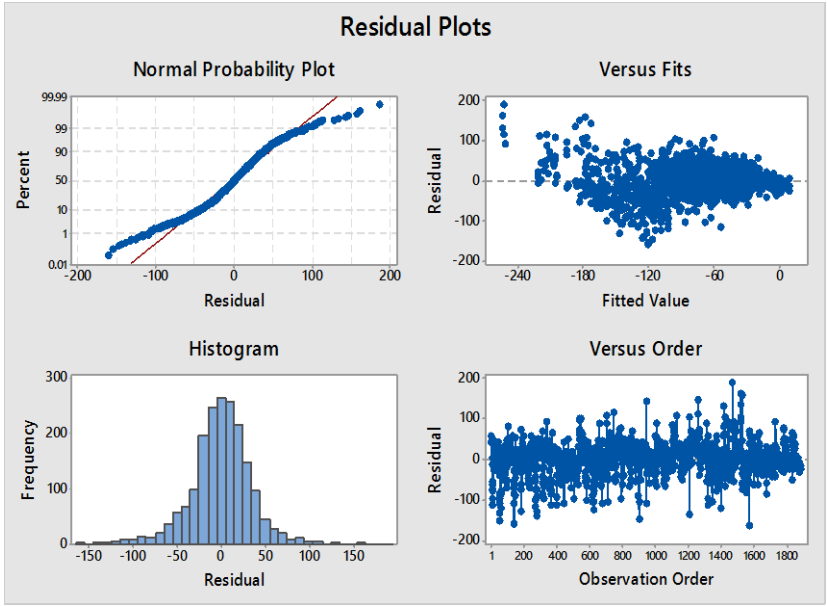

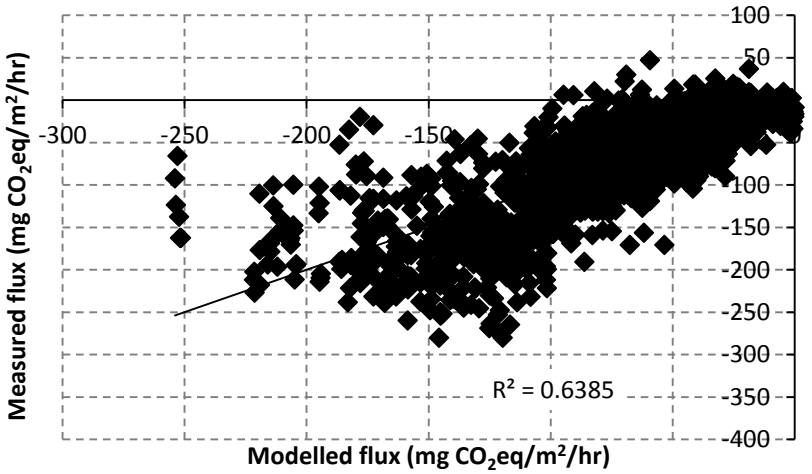

Appendix D17 - Slopes and R^2 values for plots of predicted versus observed fluxes for the individual stabilised peat columns A1(1) to A7(3), B1(1) to B5(3) and B8(1) to B8(3)

Table D18 - Slopes and R^2 values for plots of predicted versus observed fluxes for the individual stabilised peat columns A1(1) to A7(3), B1(1) to B5(3) and B8(1) to B8(3)

Column No.	40-min. flux		Column No.	40-min. flux	
	Slope	R^2 value		Slope	R^2 value
A1(1)	1.25	0.72	**B1(1)**	1.16	0.69
A1(2)	0.92	0.60	**B1(2)**	1.37	0.72
A1(3)	1.55	0.77	**B1(3)**	1.02	0.75
A2(1)	0.87	0.52	**B2(1)**	1.30	0.74
A2(2)	0.96	0.63	**B2(2)**	1.02	0.67
A2(3)	1.18	0.81	**B2(3)**	1.18	0.81
A3(1)	0.81	0.63	**B3(1)**	1.58	0.74
A3(2)	1.09	0.81	**B3(2)**	1.29	0.70
A3(3)	1.08	0.62	**B3(3)**	1.35	0.76
A4(1)	0.72	0.57	**B4(1)**	1.18	0.74
A4(2)	0.96	0.58	**B4(2)**	1.01	0.70
A4(3)	0.87	0.62	**B4(3)**	0.98	0.74
A5(1)	0.58	0.48	**B5(1)**	1.08	0.58
A5(2)	0.87	0.66	**B5(2)**	1.39	0.78
A5(3)	0.46	0.26	**B5(3)**	1.96	0.84
A6(1)	0.87	0.46	**B8(1)**	0.82	0.72
A6(2)	0.68	0.53	**B8(2)**	0.89	0.70
A6(3)	1.13	0.78	**B8(3)**	1.10	0.80
A7(1)	0.71	0.64			
A7(2)	0.52	0.49			
A7(3)	0.56	0.48			
Average	0.89	0.60		1.20	0.73
Std	0.27	0.14		0.27	0.06
Max	1.55	0.81		1.96	0.84
Min	0.46	0.26		0.82	0.58

Appendix D18 - Cross-validation model for Scenario 2 for combined data from Experiments A and B

Table D19 - Slopes and R^2 values for plots of predicted versus observed fluxes for the individual stabilised peat columns A1(1) to A7(3), B1(1) to B5(3) and B8(1) to B8(3)

Parameters	Coefficient	Standard error	p-value
b_0 (constant)	-70.3	12.1	0.000
b_1 (initial CO_2)	-1115	136	0.000
b_2 (ln(time)))	25.52	1.03	0.000
b_3 (cement)	-0.0919	0.0223	0.000
b_4 (surcharge)	-6.454	0.387	0.000
b_5 (surcharge*time)	0.03777	0.00369	0.000
b_6 (cement*ggbs)	0.001751	0.000297	0.000
R^2 (adj)	65.34		
R^2 (pred)	65.07		
SE	35.8975		
d.f (reg, res)	6,1322		
F-value	418.25		
P-value	0.000		

Appendix D19 - Underestimating the true gas flux

Table D20 - Slope and R^2 values of plots of fluxes against each other for stabilised peat in Experiment A

Flux		0–60	0–40	0–20
0–40	**R^2**	0.8354		
	Slope	1.2583		
0–20	**R^2**	0.7425	0.8709	
	Slope	1.9906	1.5659	
0–10	**R^2**	0.618	0.7123	0.8281
	Slope	2.3419	1.8262	1.1735

Table D21 - Slope and R^2 values of plots of fluxes against each other for stabilised peat in Experiment B

Flux		0–40	0–20
0–20	**R^2**	0.9034	
	Slope	1.7897	
0–10	**R^2**	0.8012	0.9206
	Slope	2.8645	1.6306

Appendix E - Some results from the carbonation depth technique studies

Appendix E1 - Some relative intensity with depth plots from Experiments A and B

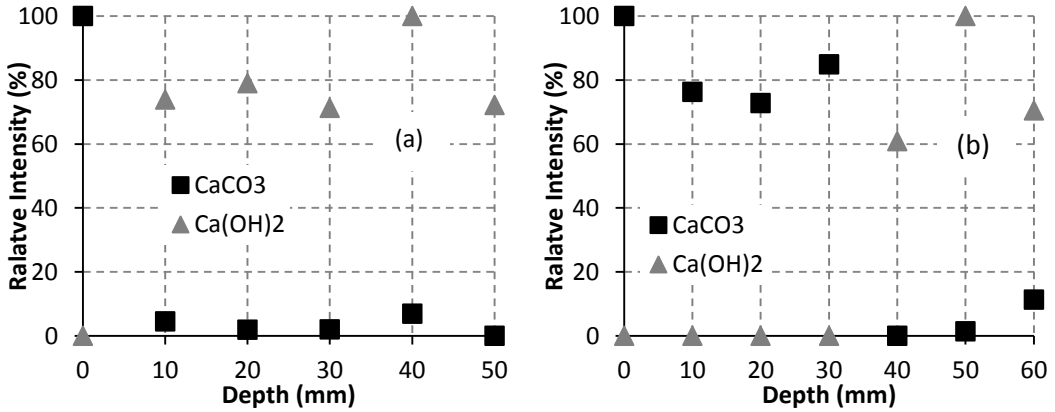

Figure E1 - Relative intensity plots for (a) a1(1c) and (b) a5(3c)

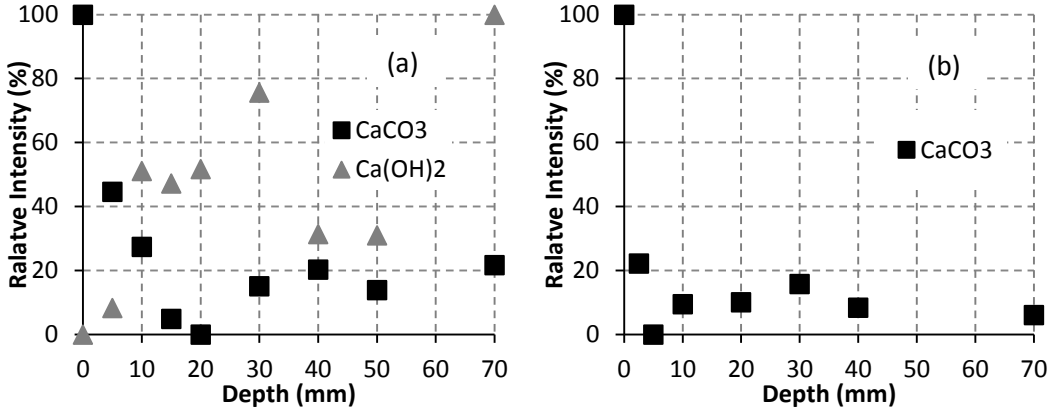

Figure E2 - Relative intensity plots for (a) A3(3) and (b) A7(3)

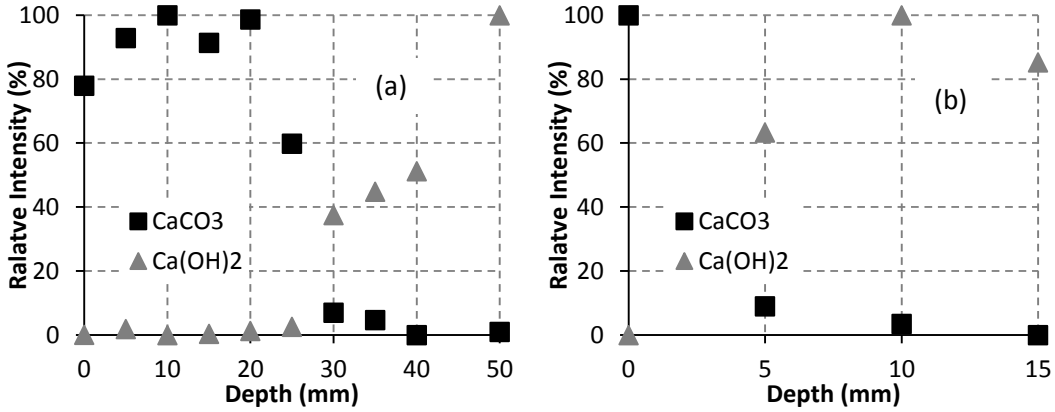

Figure E3 - Relative intensity plots for (a) b2(2c) and (b) b4(1c)

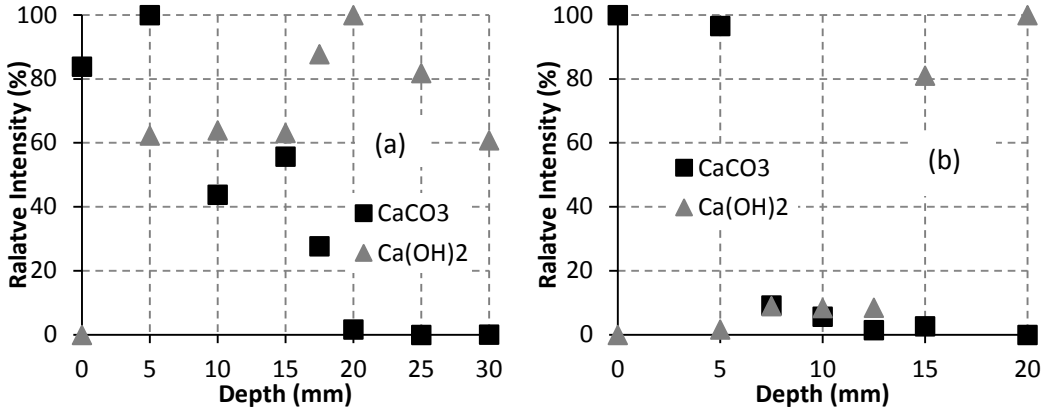

Figure E4 - Relative intensity plots for (a) B1(2) and (b) B4(2)

Appendix E2 - XRD plots for A7(2) d = 40 mm for (a) NUIG (b) UL

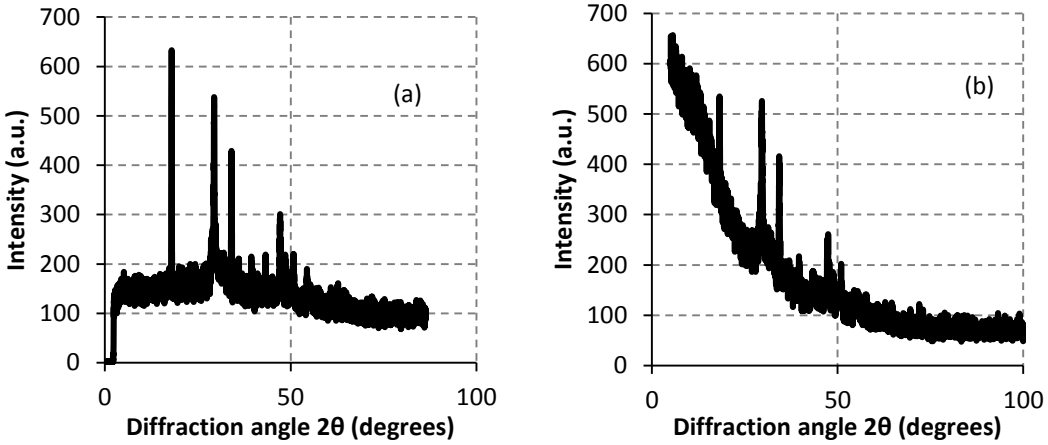

Figure E5 - XRD plots for A7(2) d = 40 mm for (a) NUIG and (b) UL

Appendix E3 - Some calcite/portlandite ratio with depth plots from Experiments A and B

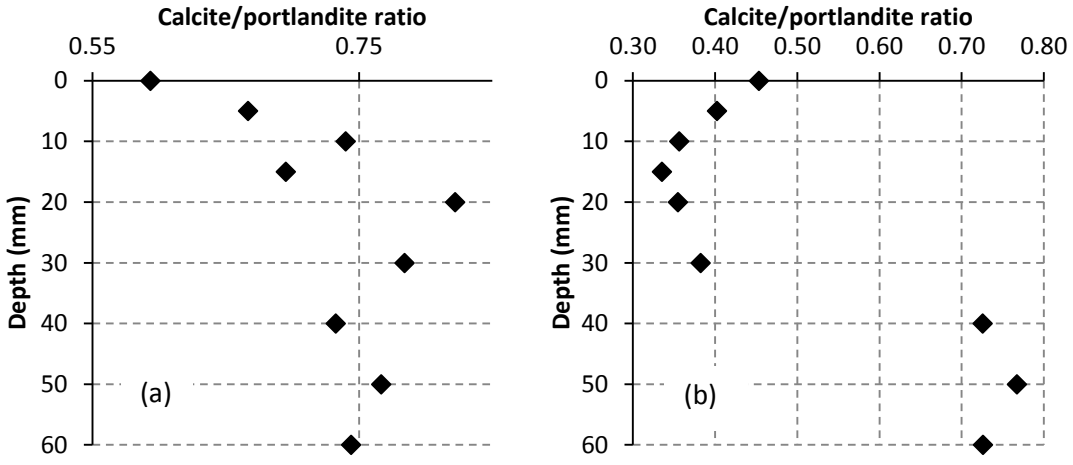

Figure E6 - Calcite/portlandite ratio with depth plots (a) a2(1c) and (b) a5(3c)

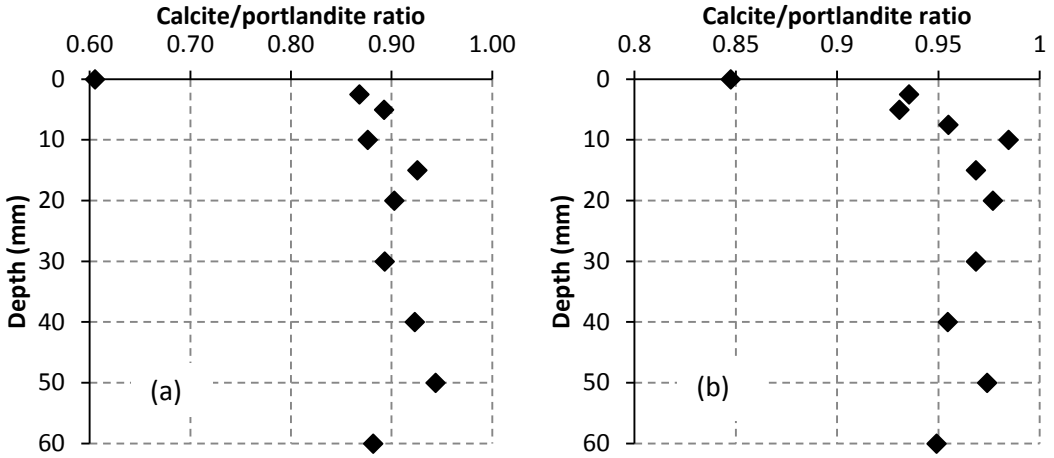

Figure E7 - Calcite/portlandite ratio with depth plots (a) A3(1) and (b) A7(2)

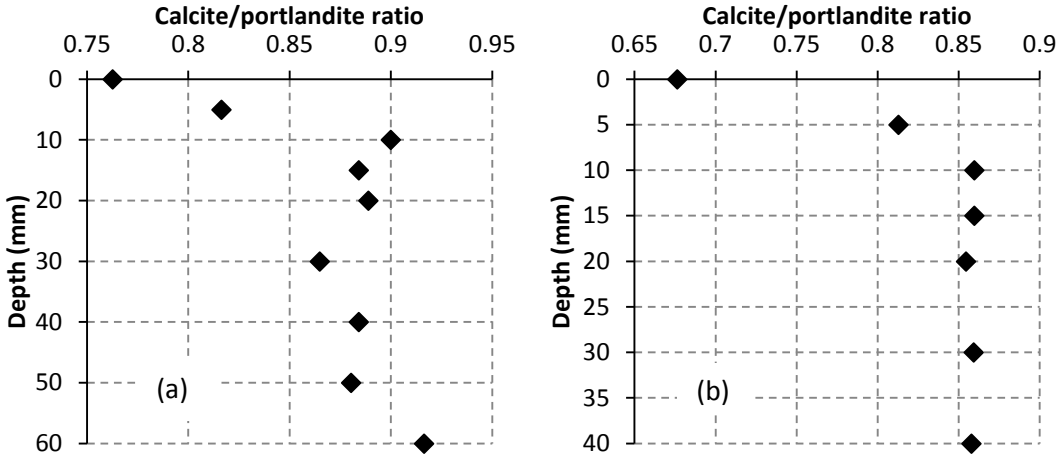

Figure E8 - Calcite/portlandite ratio with depth plots (a) b1(3c) and (b) b4(1c)

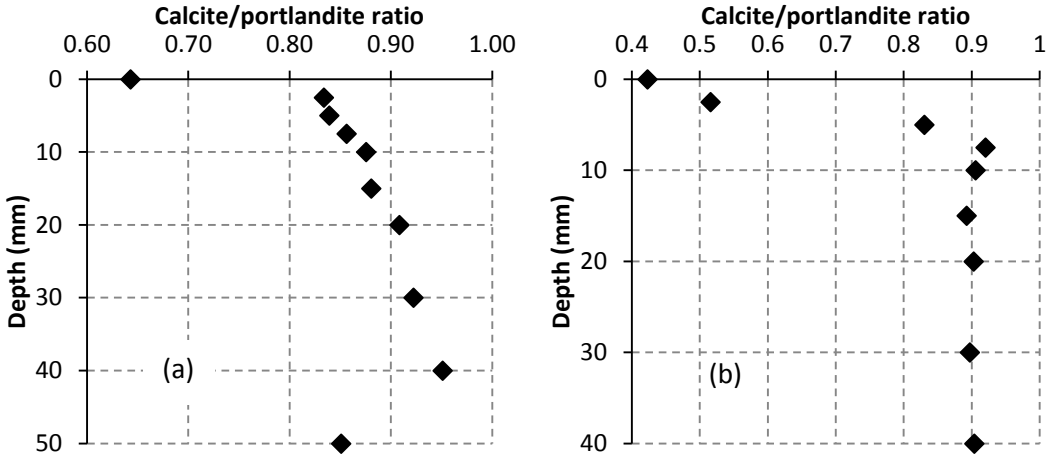

Figure E9 - Calcite/portlandite ratio with depth plots (a) B5(1) and (b) B8(1)

Appendix E4 - Some LOI plots from Experiments A and B

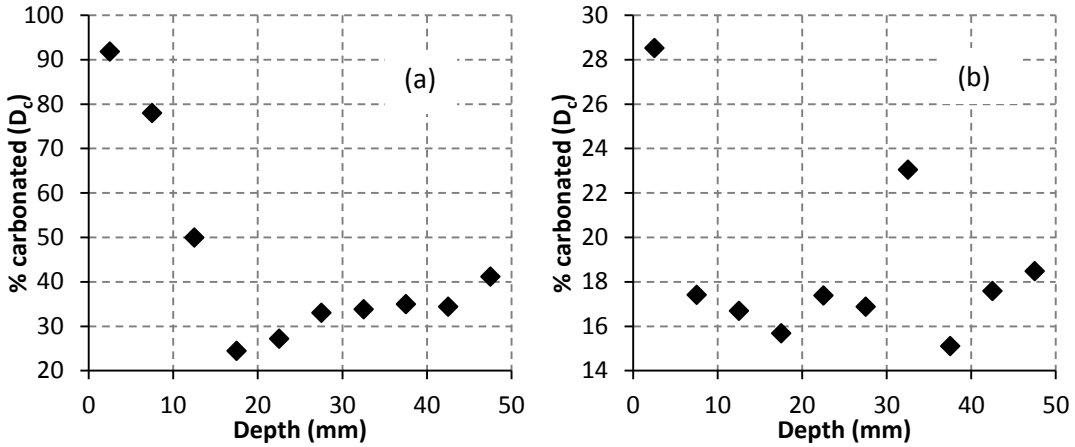

Figure E10 - LOI plots for (a) A5(3) and (b) A7(1)

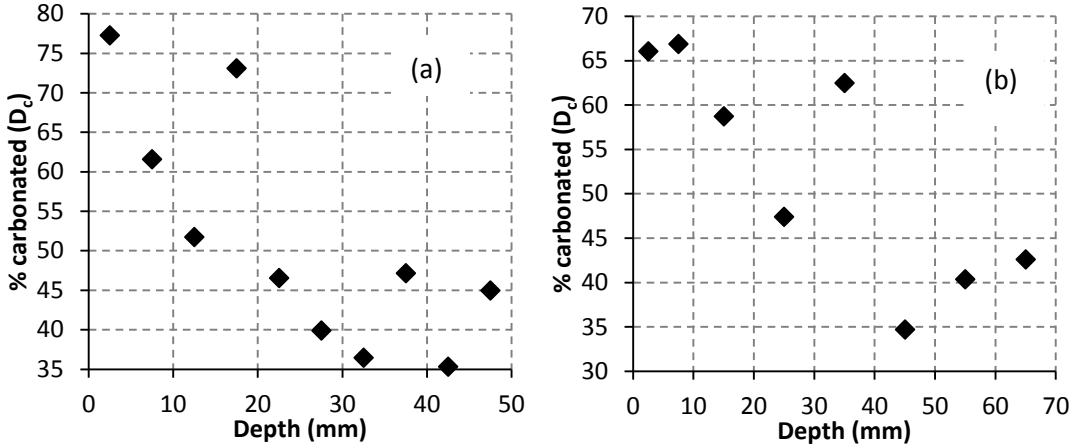

Figure E11 - LOI plots for (a) a2(3c) and (b) a5(3c)

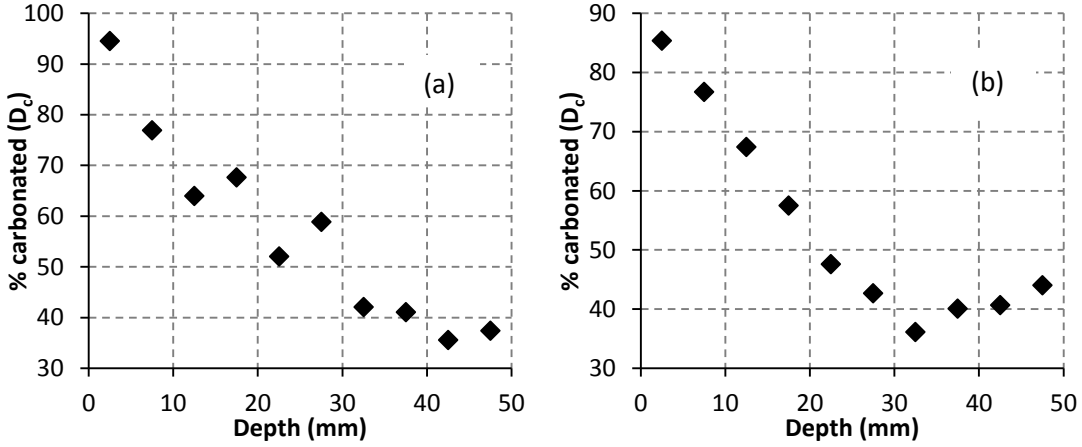

Figure E12 - LOI plots for (a) b1(1c) and (b) b8(2c)

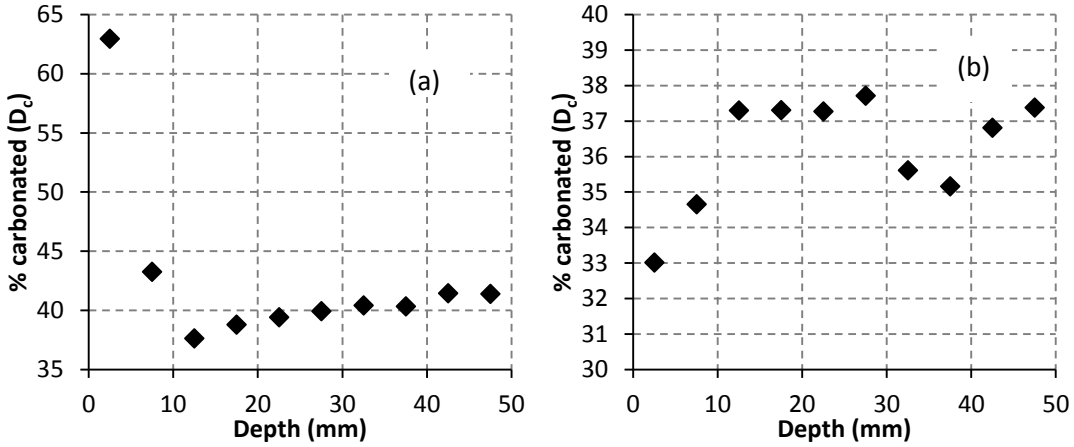

Figure E13 - LOI plots for (a) B4(1) and (b) B5(1)

Appendix E5 - Results from LOI study on B1(1) to B5(3), B8(1) to B8(3)

Table E1 - Results from LOI study on B1(1) to B5(3), B8(1) to B8(3)

Specimen	C_0 (g)	C_p (g)	D_{c0} (%)	$D_{c,max}$ (%)	$D_{CSH,0}$ (%)	$D_{CSH,max}$ (%)
B1(1)	0.63	1.94	32	70	49	84
B1(2)	0.73	1.94	38	130	51	146
B1(3)	0.65	1.94	33	78	46	92
B2(1)	0.85	2.59	33	73	50	92
B2(2)	1.08	2.59	42	71	62	87
B2(3)	0.99	2.59	38	89	54	103
B3(1)	1.18	3.24	37	92	51	108
B3(2)	1.32	3.24	41	89	55	105
B3(3)	1.20	3.24	37	81	48	94
B4(1)	1.29	3.24	40	63	46	70
B4(2)	1.60	3.24	49	63	64	81
B4(3)*	0.16	3.24	5	14	54	71
B5(1)	1.17	3.24	36	38	47	48
B5(2)	1.28	3.24	40	66	47	75
B5(3)*	0.25	3.24	8	23	45	64
B8(1)	1.25	3.24	38	76	43	80
B8(2)	1.41	3.24	44	77	54	88
B8(3)	1.27	3.24	39	78	51	89

* Specimens left in oven for more than an hour at 520 to 650°C.

Appendix E6 - pH plots for large specimens from Experiments A and B

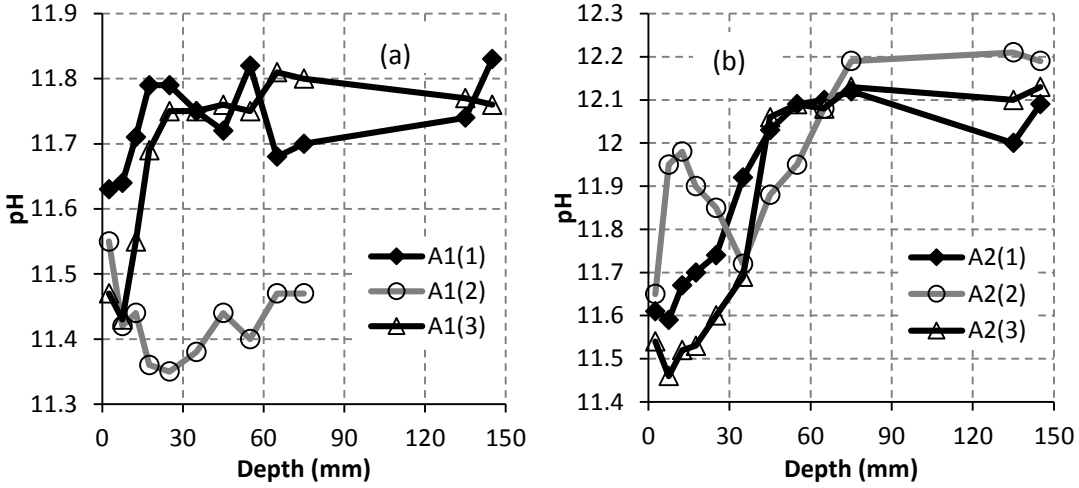

Figure E14 - pH plots for (a) A1(1)–A1(3) and (b) A2(1)–A2(3)

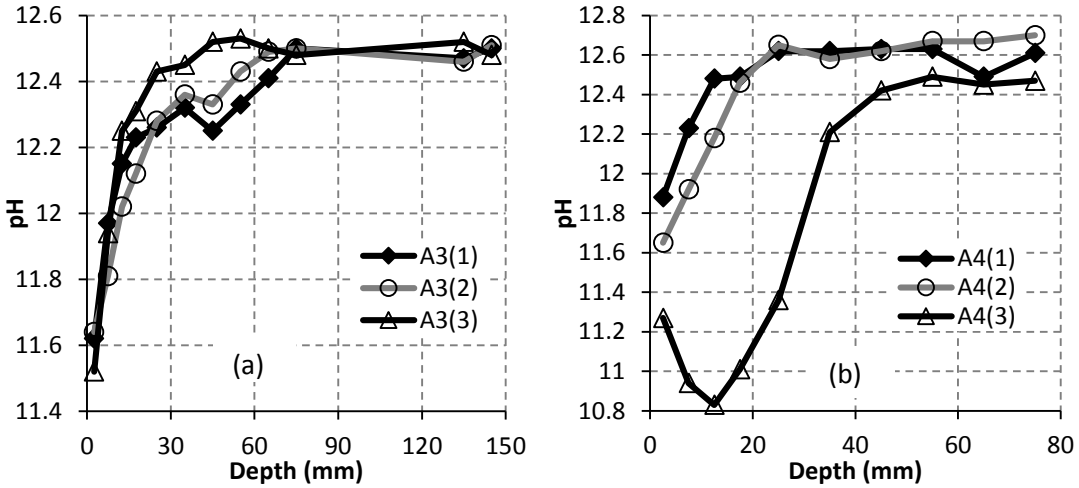

Figure E15 - pH plots for (a) A3(1)–A3(3) and (b) A4(1)–A4(3)

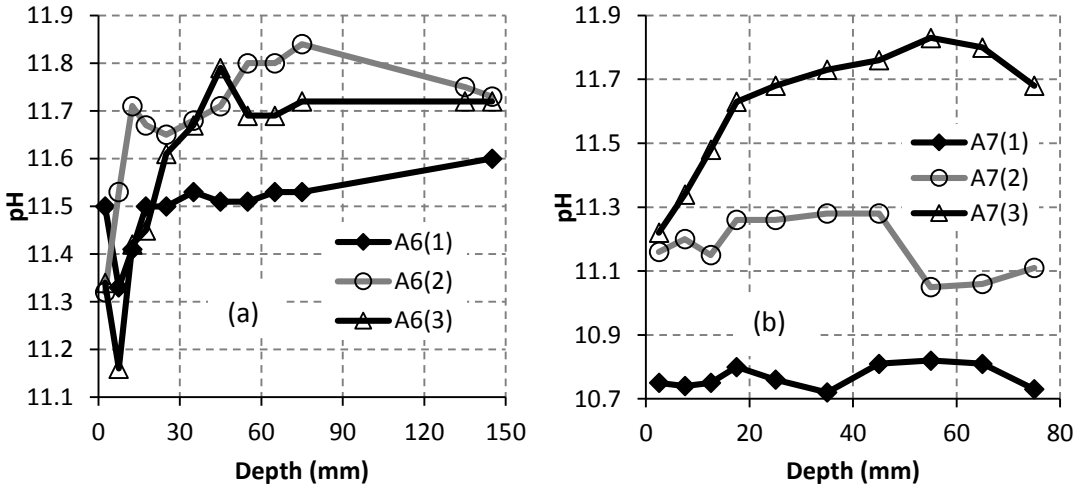

Figure E16 - pH plots for (a) A6(1)–A6(3) and (b) A7(1)–A7(3)

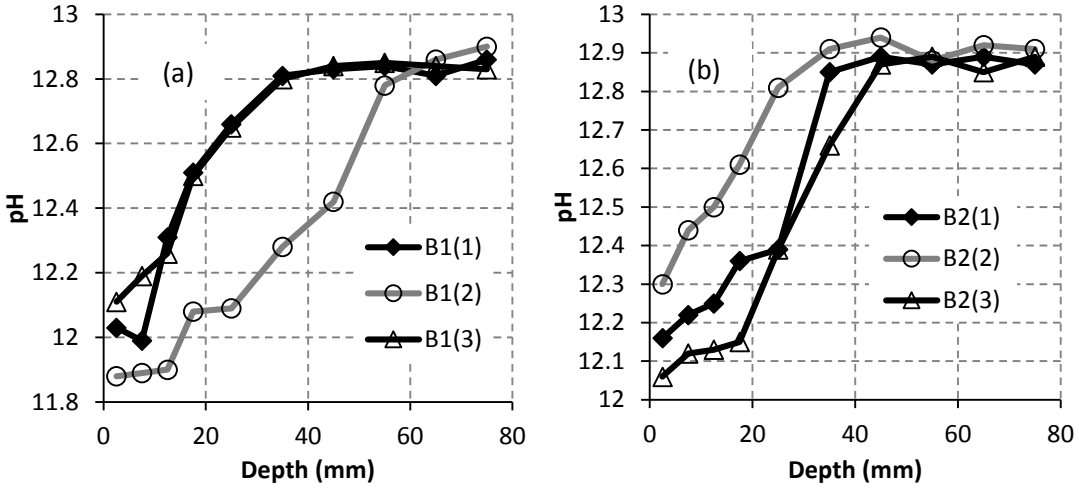

Figure E17 - pH plots for (a) B1(1)–B1(3) and (b) B2(1)–B2(3)

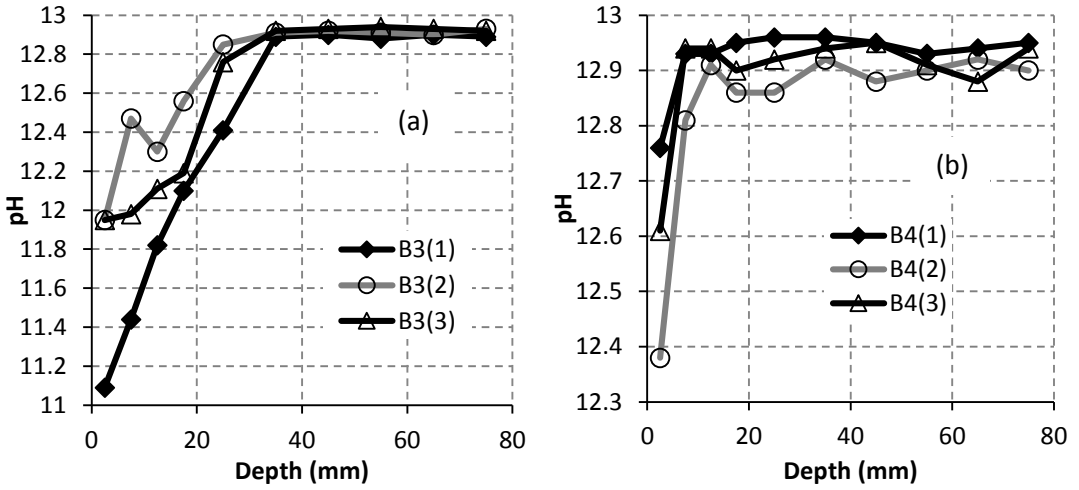

Figure E18 - pH plots for (a) B3(1)–B3(3) and (b) B4(1)–B4(3)

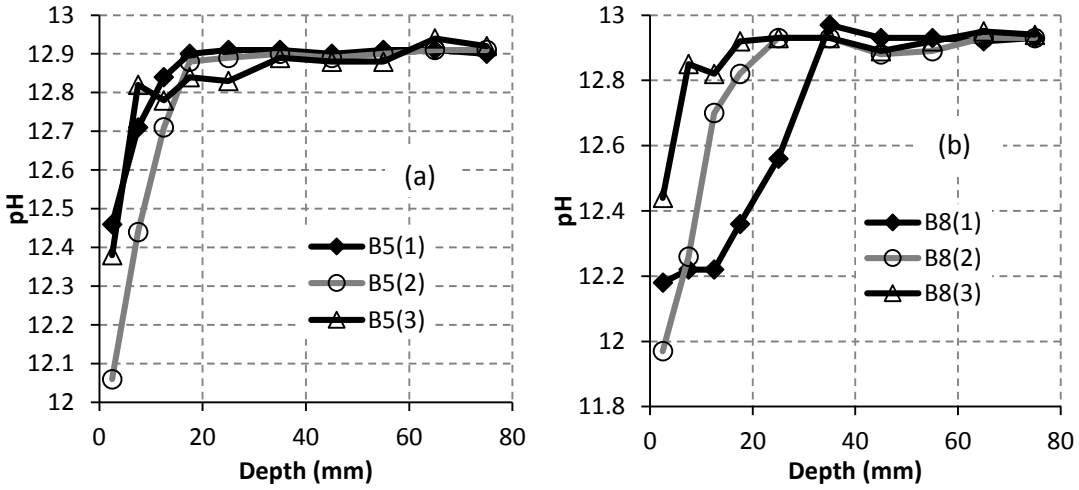

Figure E19 - pH plots for (a) B5(1)–B5(3) and (b) B8(1)–B8(3)

Appendix E7 - Average pH (± one standard deviation) for the large specimens in Experiments A and B

Table E2 - Average pH (± one standard deviation) for the large specimens in Experiments A and B

Specimen No.	pH	Specimen No.	pH
A1(1)	11.72 ± 0.07	B1(1)	12.57 ± 0.34
A1(2)	11.43 ± 0.06	B1(2)	12.31 ± 0.41
A1(3)	11.68 ± 0.13	B1(3)	12.59 ± 0.30
A2(1)	11.86 ± 0.21	B2(1)	12.58 ± 0.32
A2(2)	11.92 ± 0.18	B2(2)	12.72 ± 0.24
A2(3)	11.77 ± 0.29	B2(3)	12.50 ± 0.36
A3(1)	12.20 ± 0.25	B3(1)	12.33 ± 0.69
A3(2)	12.20 ± 0.29	B3(2)	12.67 ± 0.34
A3(3)	12.29 ± 0.31	B3(3)	12.56 ± 0.44
A4(1)	12.47 ± 0.24	B4(1)	12.93 ± 0.06
A4(2)	12.41 ± 0.37	B4(2)	12.83 ± 0.16
A4(3)	11.75 ± 0.72	B4(3)	12.89 ± 0.10
A5(1)	12.21 ± 0.54	B5(1)	12.84 ± 0.15
A5(2)	12.31 ± 0.31	B5(2)	12.75 ± 0.28
A5(3)	12.02 ± 0.66	B5(3)	12.82 ± 0.16
A6(1)	11.49 ± 0.07	B6(1)	4.60 ± 0.00
A6(2)	11.67 ± 0.14	B6(2)	4.49 ± 0.00
A6(3)	11.55 ± 0.19	B6(3)	5.59 ± 0.00
A7(1)	10.77 ± 0.04	B7(1)	4.45 ± 0.00
A7(2)	11.18 ± 0.09	B7(2)	5.24 ± 0.00
A7(3)	11.62 ± 0.20	B7(3)	5.58 ±0.00
A8(1)	5.74 ± 0.53	B8(1)	12.62 ± 0.35
A8(2)	4.48 ± 0.02	B8(2)	12.72 ± 0.34
A8(3)	4.47 ± 0.17	B8(3)	12.86 ± 0.15

Appendix E8 - Results from water evaporation method

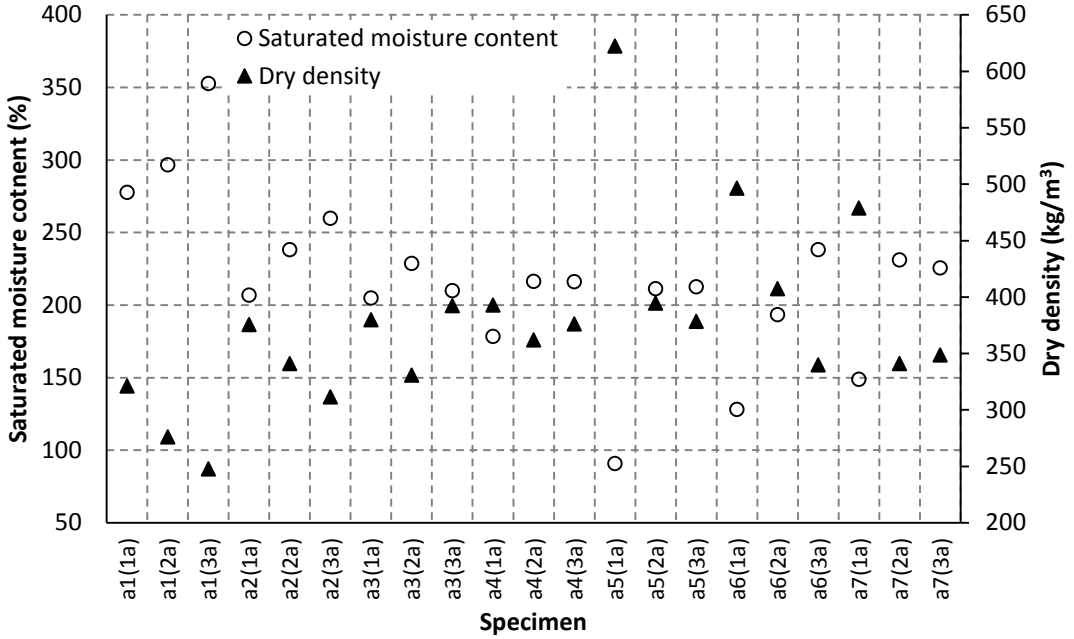

Figure E20 - Saturated moisture contents and dry densities in Experiment A for specimens a

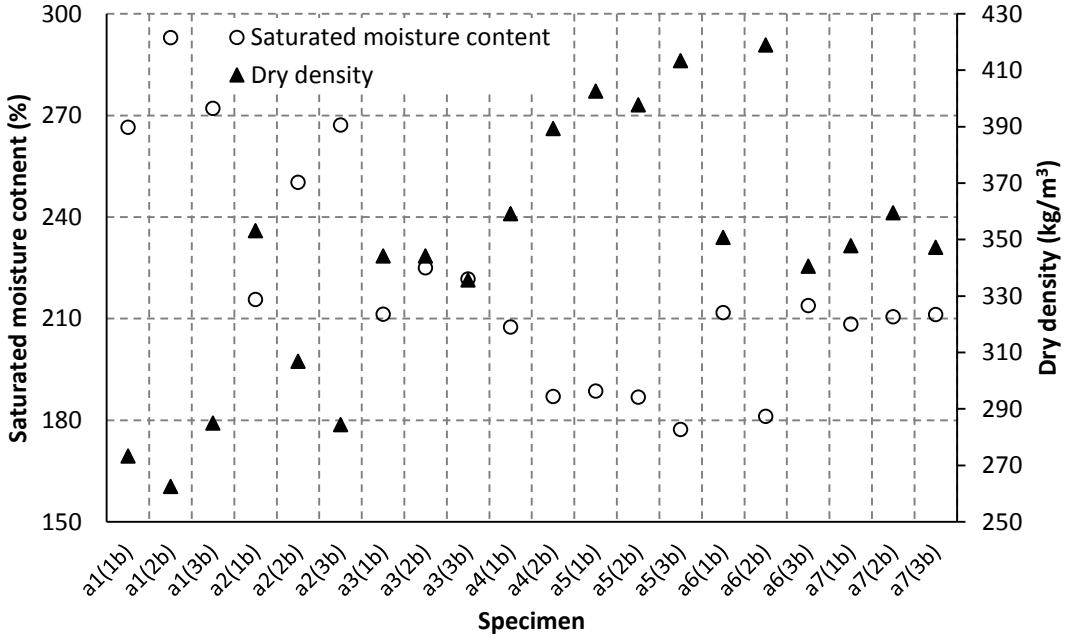

Figure E21 - Saturated moisture contents and dry densities in Experiment A for specimens b

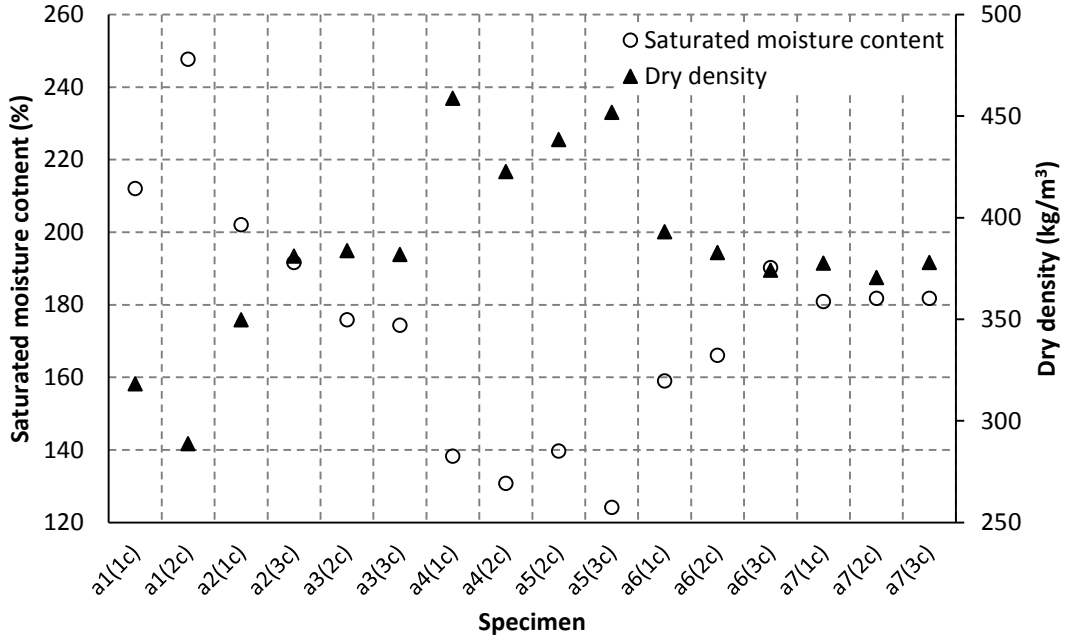

Figure E22 - Saturated moisture contents and dry densities in Experiment A for specimens c

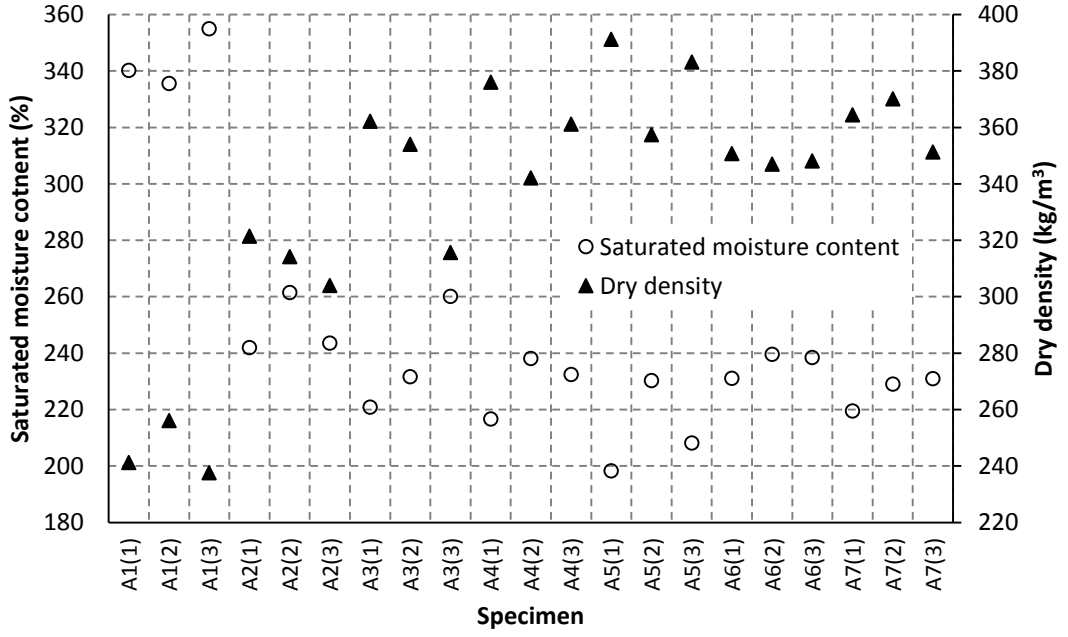

Figure E23 - Saturated moisture contents and dry densities in Experiment A for large specimens

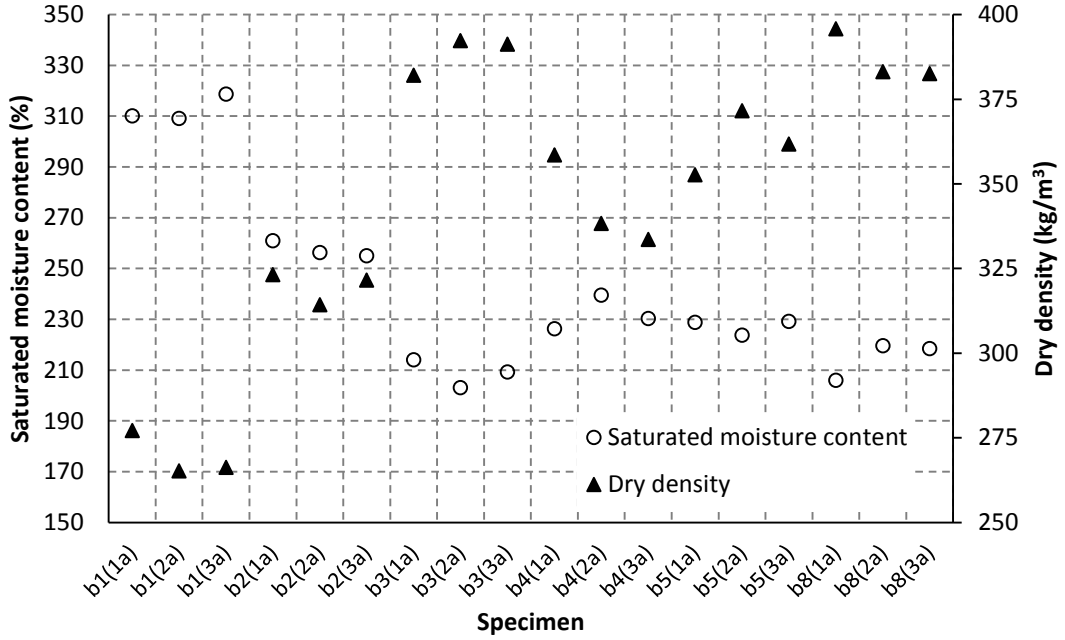

Figure E24 - Saturated moisture contents and dry densities in Experiment B for small specimens a

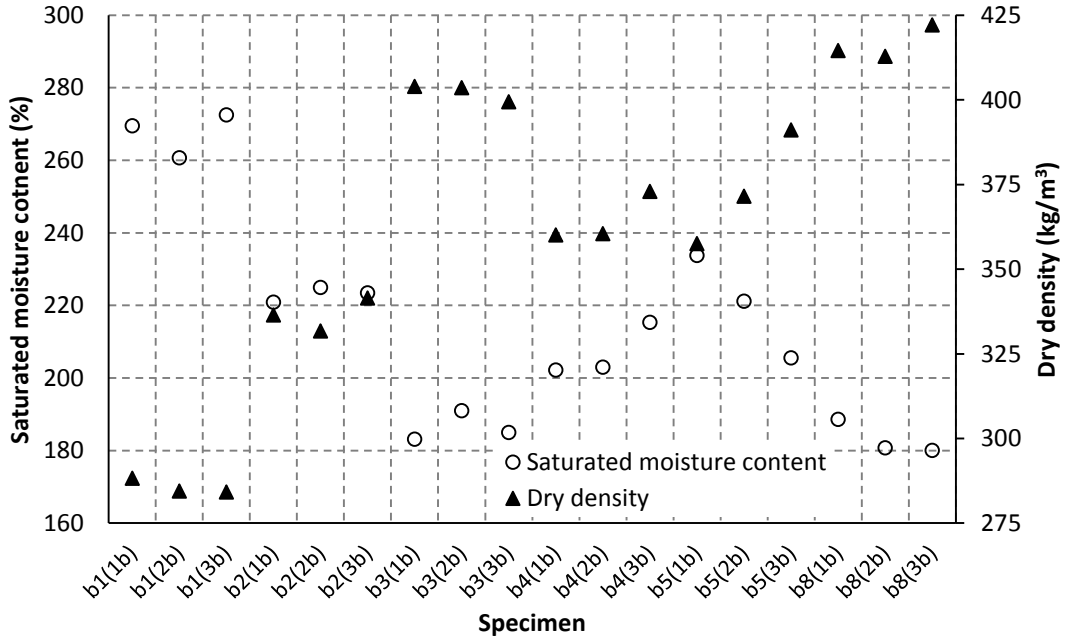

Figure E25 - Saturated moisture contents and dry densities in Experiment B for small specimens b

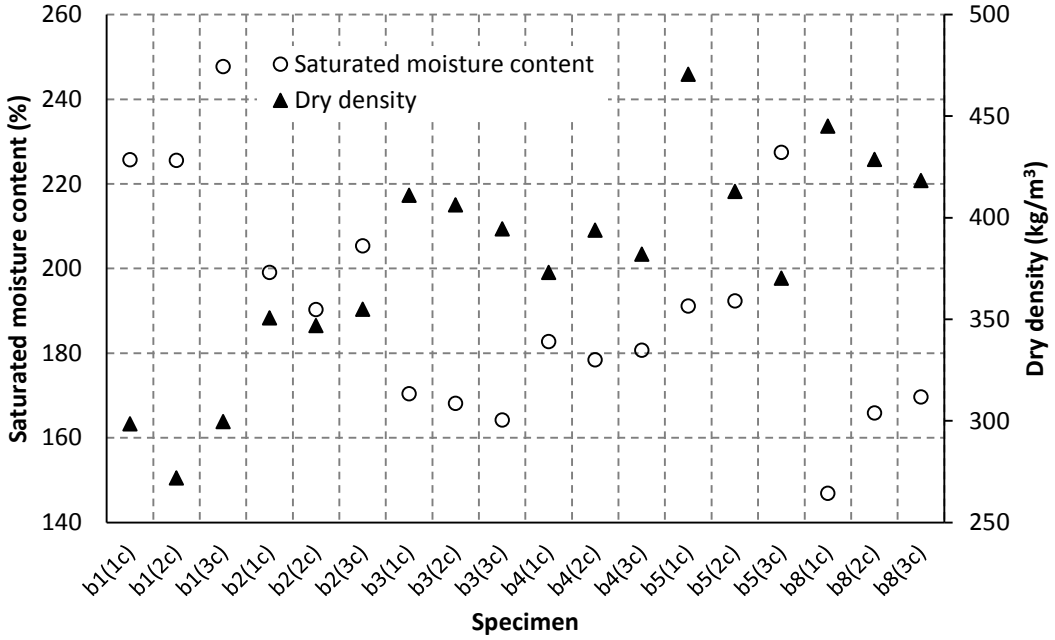

Figure E26 - Saturated moisture contents and dry densities in Experiment B for small specimens c

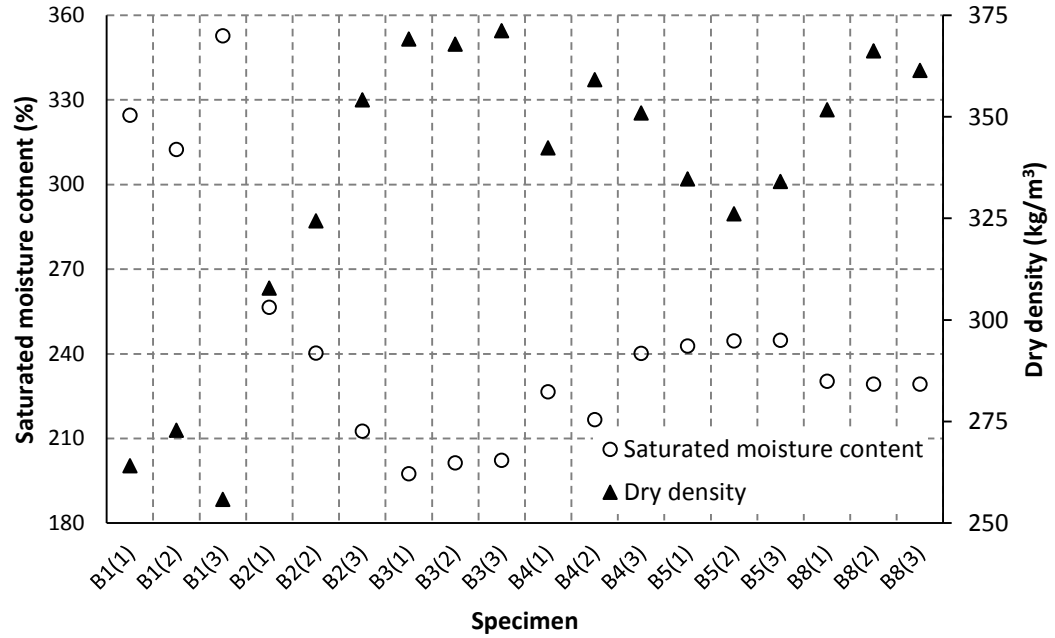

Figure E27 - Saturated moisture contents and dry densities in Experiment B for large specimens

Appendix E9 - Elemental composition of large specimens in Experiment A (Weight percentages)

Table E3 - Elemental composition of large specimens in Experiment A (Weight percentages)

Specimen No.	No. of samples	Elemental composition (%)					
		Ca	C	Si	Mg	Al	O
A1(1)	11	23.0±3.7	24.0±3.7	5.3±0.7	0.7±0.3	1.3±0.2	45.3±2.0
A2(1)	14	23.3±2.2	24.5±1.8	4.5±1.2	0.2±0.1	0.9±0.3	46.2±2.3
A2(2)	17	24.2±4.3	22.6±3.6	5.0±1.4	0.1±0.1	0.9±0.2	46.0±2.4
A3(2)	16	25.3±1.0	19.7±3.0	5.5±1.8	0.3±0.1	1.1±0.3	47.8±2.0
A3(3)	16	24.4±3.6	22.3±0.4	4.4±1.7	0.5±0.3	1.2±0.7	46.8±2.1
A4(1)	18	26.2±3.1	18.8±1.4	5.2±0.9	0.8±0.9	1.5±0.7	46.4±2.4
A4(3)	17	24.9±4.5	22.3±3.3	3.9±1.4	0.3±0.2	1.1±0.6	46.5±3.4
A5(1)	15	20.2±2.4	22.3±1.7	4.6±2.1	0.7±0.2	1.3±0.6	49.8±2.7
A5(3)	18	24.5±1.4	21.9±3.1	3.3±1.7	0.4±0.1	0.9±0.4	48.2±3.4
A6(3)	13	24.2±0.1	19.6±2.1	7.3±1.5	1.4±0.3	1.7±0.1	45.9±0.7
A7(3)	13	20.3±2.0	19.9±3.6	8.0±2.9	1.9±0.1	2.6±0.2	47.2±1.2

Appendix F - Some of the output from the Minitab statistical analyses for the carbonation depth technique studies

Appendix F1 - Comparing carbonation depths using various techniques

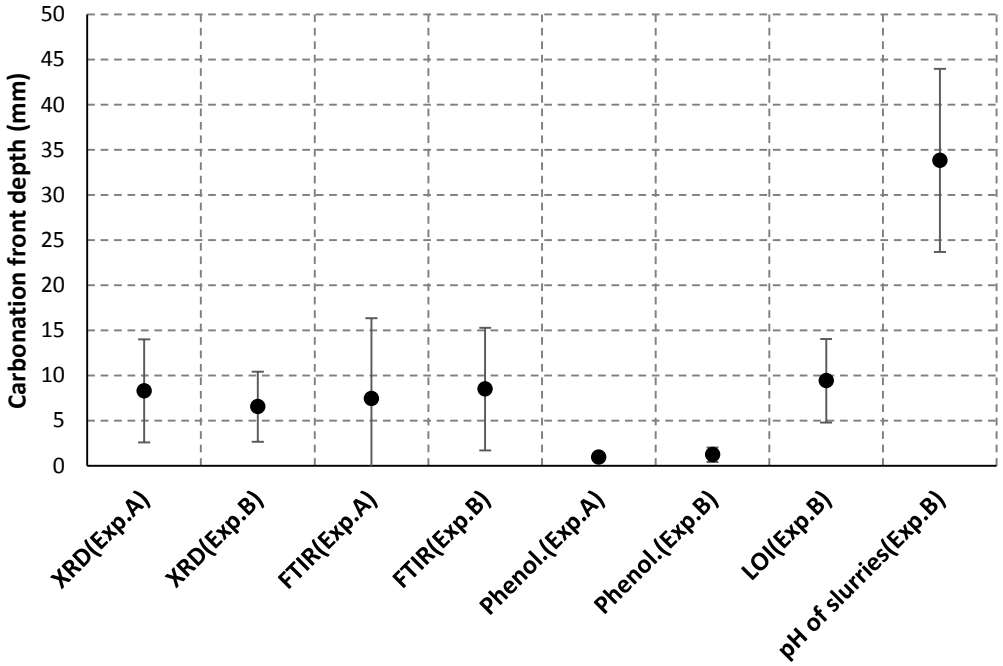

Figure F1 - Average X_c, X_p and X_{pH} values with standard deviation bars for the small specimens b in Experiments A and B

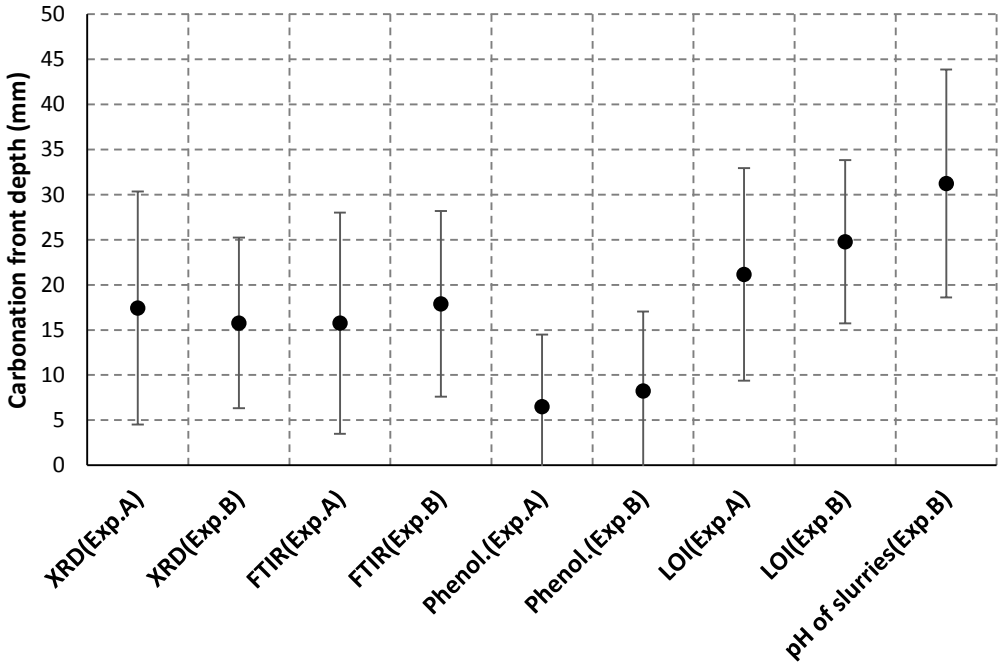

Figure F2 - Average X_c, X_p and X_{pH} values with standard deviation bars for the small specimens c in Experiments A and B

Table F1 - One-way ANOVA table showing p-values for X_c, X_p and X_{pH} values obtained using carbonation depth techniques for small specimens b in Experiment A

	XRD	FTIR
FTIR	0.721	
Phenol.	**0.000**	**0.002**

Table F2 - One-way ANOVA table showing p-values for X_c, X_p and X_{pH} values obtained using carbonation depth techniques for small specimens b in Experiment B

	XRD	FTIR	LOI	Phenol.
FTIR	0.299			
LOI	0.053	0.639		
Phenol.	**0.000**	**0.000**	**0.000**	
pH	**0.000**	**0.000**	**0.000**	**0.000**

Table F3 - One-way ANOVA table showing p-values for X_c, X_p and X_{pH} values obtained using carbonation depth techniques for small specimens c in Experiment B

	XRD	FTIR	LOI	Phenol.
FTIR	0.526			
LOI	**0.006**	**0.040**		
Phenol.	**0.019**	**0.005**	**0.000**	
pH	**0.000**	**0.001**	0.087	**0.000**

Table F4 - One-way ANOVA table showing p-values for X_c, X_p and X_{pH} values obtained using carbonation depth techniques for large specimens in Experiment B

	XRD	FTIR	LOI	Phenol.
FTIR	0.831			
LOI	**0.001**	**0.001**		
Phenol.	**0.000**	**0.000**	**0.000**	
pH	**0.000**	**0.000**	**0.001**	**0.000**

Appendix F2 - Multiple linear regression analyses for carbonation depths for the small specimens in Experiments A and B modelled using XRD, FTIR and LOI results combined

Model 1 - Best-fit model for Experiment A using XRD, FTIR and LOI results combined

Analysis of Variance

Source	DF	Adj SS	Adj MC	F-value	p-value
Regression	2	7538	3768.98	71.13	0.000
Surcharge	1	3188	3188.50	60.18	0.000
Time	1	4578	4577.90	86.40	0.000
Error	127	6729	52.99		
Lack-of-Fit	6	2927	487.85	15.53	0.000
Pure Error	121	3802	31.42		
Total	129	14267			

Model Summary

S	R-sq	R-sq(adj)	R-sq(pred)
7.27922	52.83%	52.09%	49.64%

Coefficients

Term	Coef	SE Coef	T-Value	p-value	VIF
Constant	-1.27	1.23	-1.04	0.301	
Surcharge	1.149	0.148	7.76	0.000	1.00
Time	0.08912	0.00959	9.29	0.000	1.00

Regression Equation

X_c = - 1.27 + 1.149 surcharge + 0.08912 time

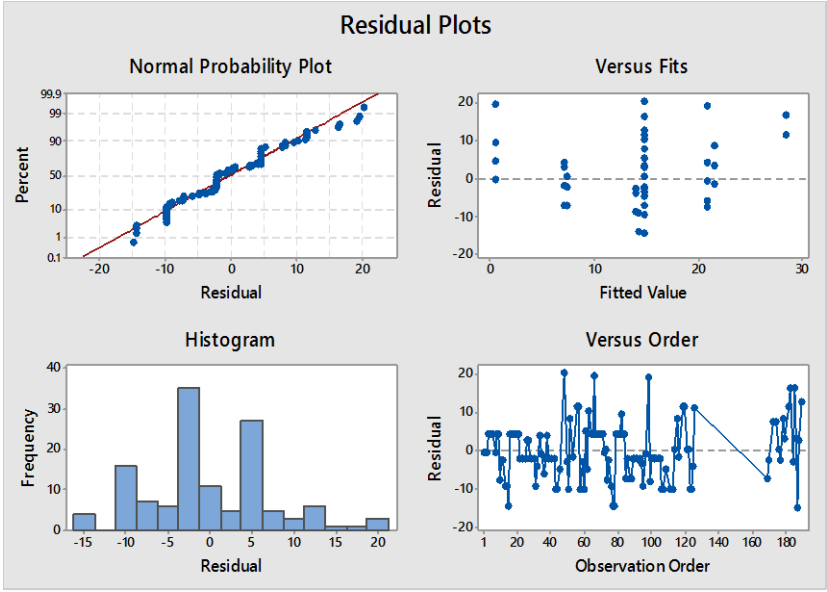

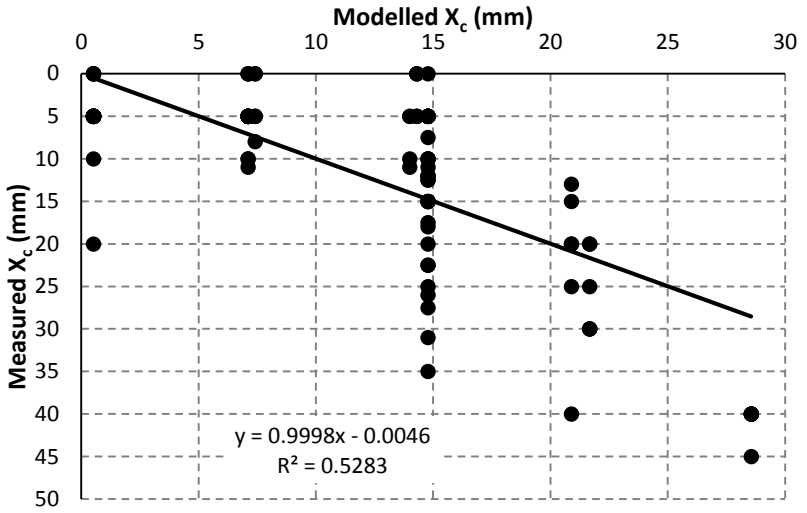

Model 2 - Best-fit model in Experiment B using XRD, FTIR and LOI results combined

Analysis of Variance

Source	DF	Adj SS	Adj MC	F-value	p-value
Regression	3	7234.1	2411.37	51.21	0.000
Cement	1	215.5	215.46	4.58	0.034
Surcharge	1	1214.2	1214.19	25.79	0.000
Time	1	5600.9	5600.85	118.94	0.000
Error	158	7439.9	47.09		
Lack-of-Fit	11	2338.3	212.57	6.13	0.000
Pure Error	147	5101.6	34.70		
Total	161	14674.0			

Model Summary

S	R-sq	R-sq(adj)	R-sq(pred)
6.86206	49.30%	48.34%	46.53%

Coefficients

Term	Coef	SE Coef	T-Value	p-value	VIF
Constant	5.85	3.52	1.66	0.098	
Cement	-0.0306	0.0143	-2.14	0.034	1.03
Surcharge	0.673	0.132	5.08	0.000	1.03
Time	0.08978	0.00823	10.91	0.000	1.00

Regression Equation

$X_c = 5.85 - 0.0306 \text{ cement} + 0.673 \text{ surcharge} + 0.08978 \text{ time}$

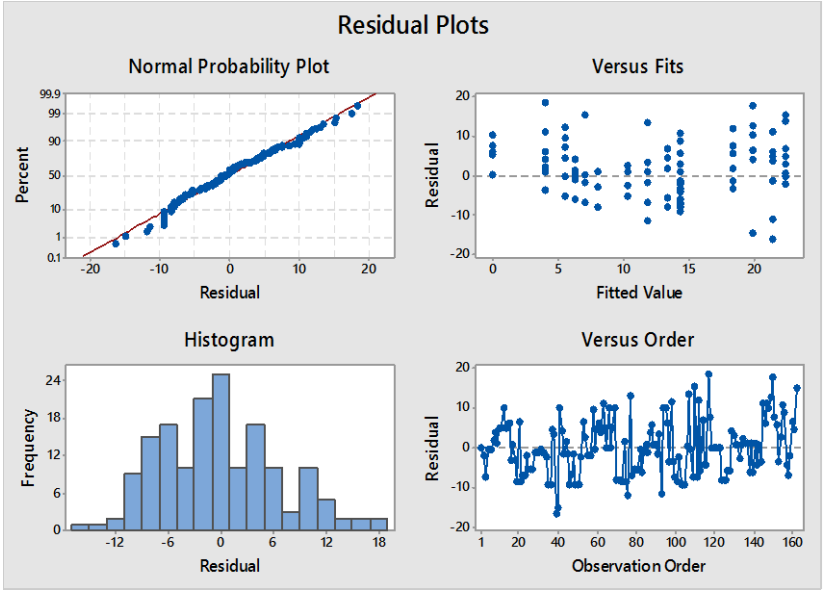

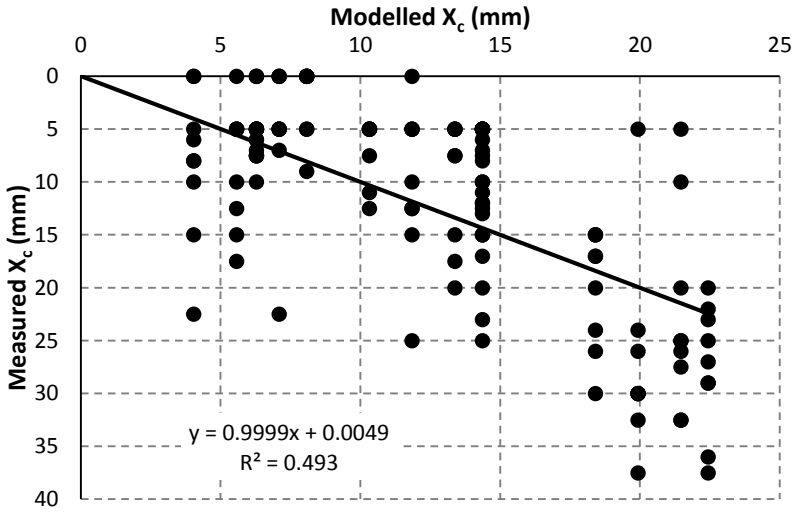

Appendix F3 - Variables controlling carbonation depths for the large specimens in Experiments A and B

Table F5 - Variables controlling carbonation depths for the large specimens in Experiment A

	XRD		FTIR			LOI		Phenol.	
Analysis	1	2	1	2	3	1	2	1	2
R^2 (adj)	29.92	31.72	29.28	5.58	13.94	9.45	18.14	6.63	7.49
Lack-of-fit	0.491	0.519	0.928	0.228	0.430	0.049	0.765	0.611	0.530
Variables					p-values				
Intercept	0.131	**0.000**	**0.008**	0.221	**0.001**	0.294	**0.000**	0.420	**0.000**
Cement	0.474	-	**0.041**	0.994	-	0.962	-	0.821	-
GGBS	0.165	0.141	**0.017**	-	0.203	0.790	-	0.593	-
Surcharge	**0.040**	**0.031**	**0.020**	0.177	0.195	0.148	**0.031**	0.123	0.122

Table F6 - Variables controlling carbonation depths for the large specimens in Experiment B

	XRD		FTIR		LOI		Phenol		pH	
Analysis	1	2	1	2	1	2	1	2	1	2
R^2 (adj)	1.41	2.69	17.18	14.41	33.55	27.78	34.65	22.08	33.42	31.24
Lack-of-fit	0.164	0.152	0.552	0.112	0.225	-	0.056	-	0.062	0.369
Variables					p-values					
Intercept	0.133	0.053	**0.034**	**0.005**	**0.014**	**0.000**	0.865	**0.000**	**0.001**	**0.000**
Cement	0.328	0.243	0.150	-	0.195	-	0.161	-	**0.012**	**0.009**
Water table	0.896	-	0.945	-	0.202	**0.014**	**0.004**	**0.028**	0.404	-
Surcharge	0.436	-	0.176	0.067	0.235	-	0.111	-	0.135	-

Table F7 - Variables controlling carbonation depths for the large specimens in Experiments A and B (XRD, FTIR and LOI combined)

	Experiment A XRD, FTIR and LOI		Experiment B XRD, FTIR and LOI	
Analysis	1	2	1	2
R^2 (adj)	27.15	24.23	14.00	14.89
Lack-of-fit	0.438	0.100	0.239	0.187
Variables		p-values		
Intercept	**0.001**	**0.000**	**0.003**	**0.002**
Cement	0.070	-	0.079	**0.046**
GGBS	**0.009**	**0.045**	-	-
Surcharge	**0.000**	**0.002**	0.118	**0.025**
Water table	-	-	0.493	-

Appendix F4 - Meta-analysis for carbonation depths for the small specimens in Experiments A and B measured using XRD, FTIR and LOI results combined

Model 1 - Best-fit model

Analysis of Variance

Source	DF	Adj SS	Adj MC	F-value	p-value
Regression	2	14189	7094.5	138.84	0.000
Surcharge	1	4287	4286.6	83.89	0.000
Time	1	10225	10224.7	200.10	0.000
Error	289	14767	51.1		
Lack-of-Fit	9	4650	516.6	14.30	0.000
Pure Error	280	10117	36.1		
Total	291	28956			

Model Summary

S	R-sq	R-sq(adj)	R-sq(pred)
7.14823	49.00%	48.65%	47.74%

Coefficients

Term	Coef	SE Coef	T-Value	p-value	VIF
Constant	-1.405	0.844	-1.66	0.097	
Surcharge	0.8705	0.0950	9.16	0.000	1.00
Time	0.08962	0.00634	14.15	0.000	1.00

Regression Equation

X_c = - 1.405 + 0.8705 surcharge + 0.08962 time

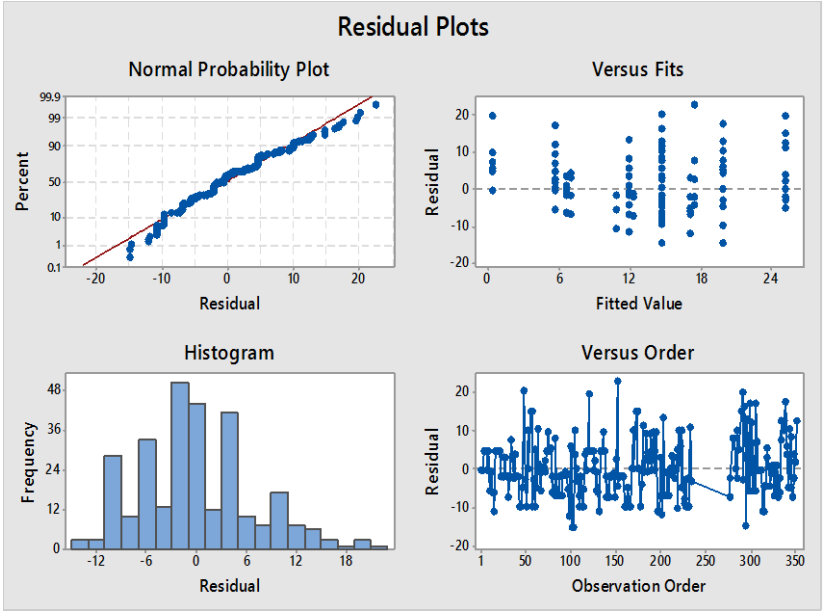

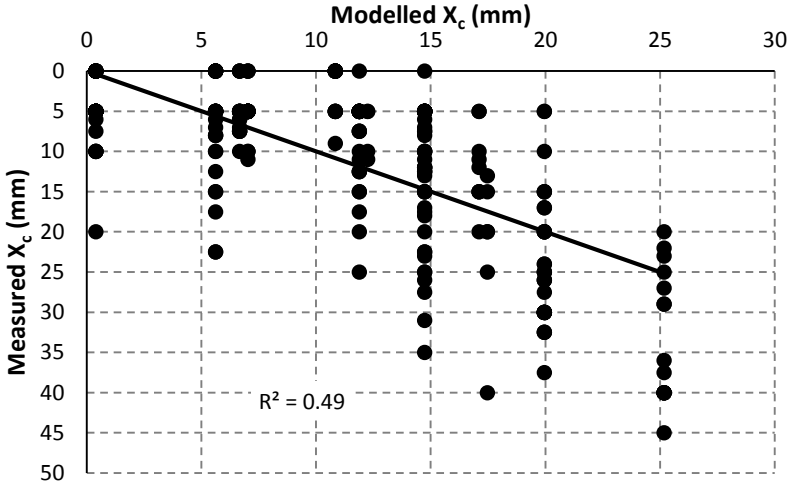

Model 2 - Best-fit model with square root of time variable

Analysis of Variance

Source	DF	Adj SS	Adj MC	F-value	p-value
Regression	2	13296	6647.78	122.68	0.000
Surcharge	1	4256	4255.99	78.54	0.000
√Time	1	9331	9331.14	172.20	0.000
Error	289	15661	54.19		
Lack-of-Fit	9	5543	615.91	17.05	0.000
Pure Error	280	10117	36.13		
Total	291	28956			

Model Summary

S	R-sq	R-sq(adj)	R-sq(pred)
7.36132	45.92%	45.54%	44.62%

Coefficients

Term	Coef	SE Coef	T-Value	p-value	VIF
Constant	-6.69	1.23	-5.44	0.000	
Surcharge	0.8673	0.0979	8.86	0.000	1.00
√Time	1.533	0.117	13.12	0.000	1.00

Regression Equation

X_c = - 6.69 + 0.8673 surcharge + 1.533 √time

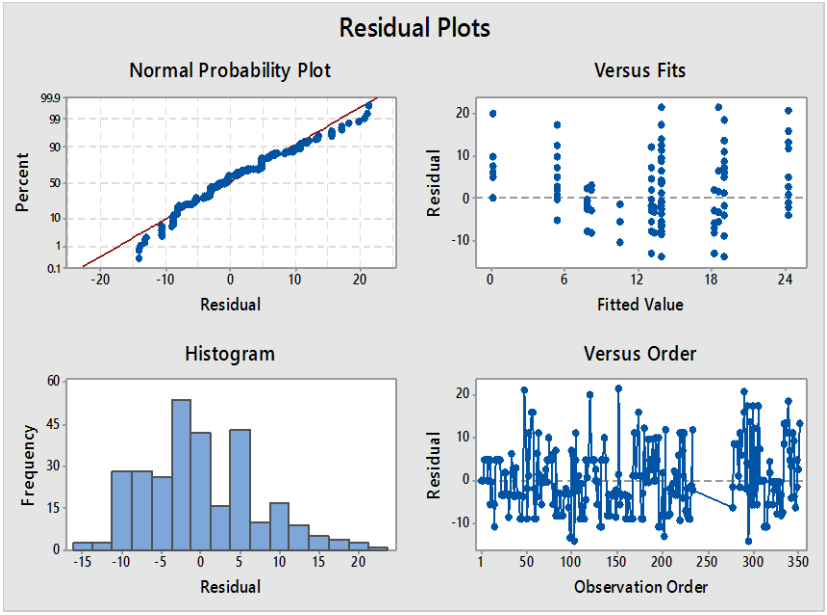

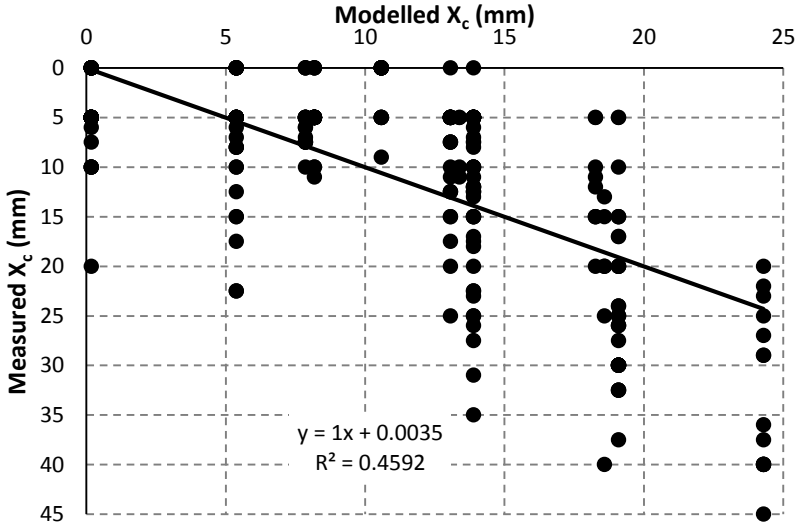

Appendix F5 - Meta-analysis for carbonation depths for the large specimens in Experiments A and B

Meta-analyses showing the effects of the variables examined on X_c (XRD, FTIR and LOI combined), X_p and X_{pH}

	XRD, FTIR and LOI		Phenol.		pH	
Analysis	1	2	1	2	1	2
R^2 (adj)	18.80	18.81	18.41	9.01	3.21	7.96
Lack-of-fit	0.105	0.085	0.715	-	0.093	0.591
Variables			p-values			
Intercept	**0.000**	**0.000**	0.259	**0.000**	0.052	**0.000**
GGBS	**0.009**	**0.007**	0.500		0.111	**0.045**
Cement	**0.071**	**0.031**	0.412		0.915	
Water table	0.325		**0.004**	**0.036**	0.342	
Surcharge	**0.000**	**0.000**	**0.017**		0.602	

Best-fit meta-analysis model for X_c values using XRD, FTIR and LOI results combined

Analysis of Variance

Source	DF	Adj SS	Adj MC	F-value	P-value
Regression	3	910.1	303.36	9.96	0.000
Cement	1	146.1	146.14	4.80	0.031
GGBS	1	228.9	228.85	7.51	0.007
Surcharge	1	591.9	591.86	19.43	0.000
Error	113	3442.0	30.46		
Lack-of-Fit	6	333.6	55.59	1.91	0.085
Pure Error	107	3108.4	29.05		
Total	116	4352.1			

Model Summary

S	R-sq	R-sq(adj)	R-sq(pred)
5.51906	20.91%	18.81%	15.64%

Coefficients

Term	Coef	SE Coef	T-Value	p-value	VIF
Constant	13.31	3.04	4.38	0.000	
Cement	-0.0300	0.0137	-2.19	0.031	2.44
GGBS	-0.0409	0.0149	-2.74	0.007	2.25
Surcharge	0.557	0.126	4.41	0.000	1.20

Regression Equation

$X_c = 13.31 - 0.0300\ \text{Cement} - 0.0409\ \text{GGBS} + 0.557\ \text{Surcharge}$